AD-A087 704 ADVISORY GROUP FOR AEROSPACE RESEARCH AND DEVELOPMENT--ETC F/G 20/4
A CRITICAL COMMENTARY ON MEAN FLOW DATA FOR TWO-DIMENSIONAL COM--ETC(U)
MAY 80 H H FERNHOLZ, P J FINLEY

UNCLASSIFIED AGARD-AG-253 NL

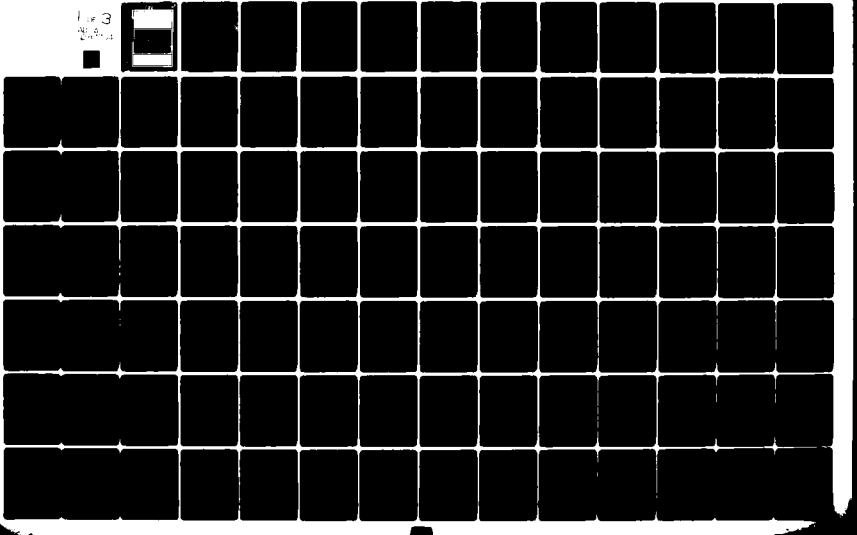

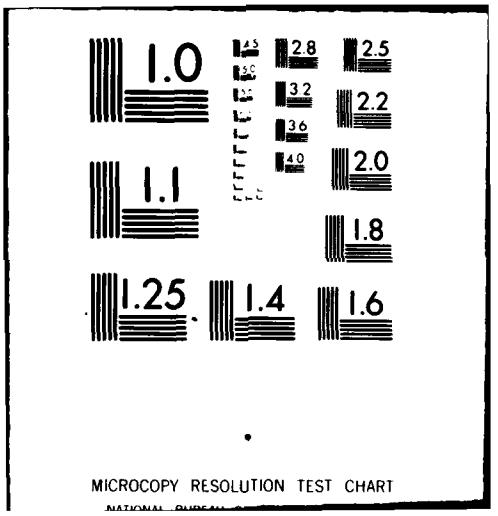
1.0
1.1
1.25
1.4
1.6
1.8
2.0
2.2
2.5
2.8
3.2
3.6
4.0
MICROCOPY RESOLUTION TEST CHART

ADVISORY GROUP FOR AEROSPACE RESEARCH & DEVELOPMENT

AGARDograph No. 253

A Critical Commentary on Mean Flow Data for Two-Dimensional Compressible Turbulent Boundary Layers

NORTH ATLANTIC TREATY ORGANIZATION

NORTH ATLANTIC TREATY ORGANIZATION

ADVISORY GROUP FOR AEROSPACE RESEARCH AND DEVELOPMENT

(ORGANISATION DU TRAITE DE L'ATLANTIQUE NORD)

AGARDograph No.253

A CRITICAL COMMENTARY ON MEAN FLOW DATA FOR TWO-DIMENSIONAL COMPRESSIBLE TURBULENT BOUNDARY LAYERS

by

(10)

[redacted]g. H.H.Fernholz
[redacted]für
Thermo-und-Fluiddynamik
Technische Universität Berlin
D-1000 Berlin 12
Strasse des 17. Juni 135
BRD Germany

and

P.J.Finley [redacted]Ph.D.
Department of Aeronautics
Imperial College of
Science and Technology
Prince Consort Road
London SW7 2BY
Great Britain

This AGARDograph was prepared at the request of the Fluid Dynamics Panel of AGARD.

THE MISSION OF AGARD

The mission of AGARD is to bring together the leading personalities of the NATO nations in the fields of science and technology relating to aerospace for the following purposes:

- Exchanging of scientific and technical information;
- Continuously stimulating advances in the aerospace sciences relevant to strengthening the common defence posture;
- Improving the co-operation among member nations in aerospace research and development;
- Providing scientific and technical advice and assistance to the North Atlantic Military Committee in the field of aerospace research and development;
- Rendering scientific and technical assistance, as requested, to other NATO bodies and to member nations in connection with research and development problems in the aerospace field;
- Providing assistance to member nations for the purpose of increasing their scientific and technical potential;
- Recommending effective ways for the member nations to use their research and development capabilities for the common benefit of the NATO community.

The highest authority within AGARD is the National Delegates Board consisting of officially appointed senior representatives from each member nation. The mission of AGARD is carried out through the Panels which are composed of experts appointed by the National Delegates, the Consultant and Exchange Programme and the Aerospace Applications Studies Programme. The results of AGARD work are reported to the member nations and the NATO Authorities through the AGARD series of publications of which this is one.

Participation in AGARD activities is by invitation only and is normally limited to citizens of the NATO nations.

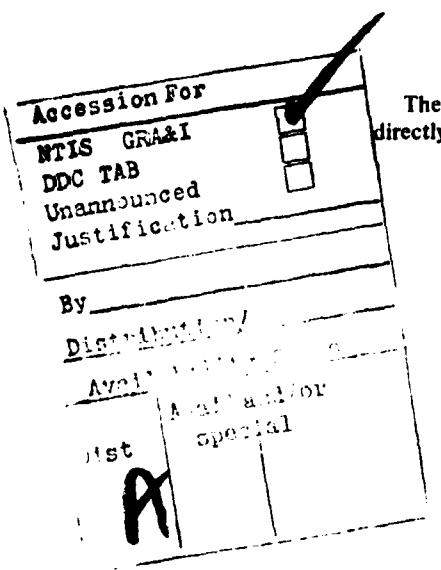

Published May 1980

ISBN 92-835-1362-2

Printed by Technical Editing and Reproduction Ltd
Harford House, 7–9 Charlotte St, London, W1P 1HD

CONTENTS

i. PREFACE - THE AGARD-EUROVISC CATALOGUE

This is the second of three proposed volumes presenting and discussing two dimensional compressible turbulent boundary layer data. The first volume, AGARDograph 223, contained tabulated data, in complete form on microfiche, and in abbreviated form as printed tables, for 59 experimental boundary layer studies. The experiments were also described in a standardised manner, and a certain amount of introductory material was provided so as to assist readers wishing to make use of the data. So far as possible, comment and discussion was reserved for this second, commentary, volume. We have, in the main, restricted our discussion here to the time-mean data presented in AGARDograph 223, but have felt free to supplement them with data from experimental studies which we have processed since the completion of that volume. Entries in AGARDograph 223 are indicated by a reference number such as CAT 7201, while supplementary data to be presented in the third volume are labeled with a distinguishing "S" - as for example, CAT 7802S. In addition to these supplementary entries, about twelve in number, the third volume will contain a discussion of the available fluctuation data, and a "source catalogue" which will provide an annotated bibliography of the many papers which we have consulted in the course of this enterprise.

The data presented in AGARDograph 223 are also available on magnetic tape. Our original tape output has been modified, mainly for the greater convenience of FORTRAN users, by P. Bradshaw of Imperial College, and copies may be obtained from the centres listed in the foreword to AGARDograph 223.

The project arose from a suggestion made to the first author by the late Dietrich Küchemann, and has continued under the auspices of EUROVISC, principally through the assistance of an informal guidance panel. The data collection and computation have throughout been funded by the German Research Council (DFG) and the Technical University, Berlin (TUB). The Fluid Dynamics Panel of AGARD have supported the editorial work and arranged publication.

Both for our own correction, and as a reminder to the many workers in the field, we would recall* that "It is a capital mistake to theorise before one has data". We hope that the publication of the first volume provides a sufficient justification for the modest level of theoretical appreciation presented here.

---

* A scandal in Bohemia, Sir Arthur Conan Doyle.

ii. ACKNOWLEDGEMENTS

Preeminence amongst all those to whom we owe thanks must be given to Miss C. Mohr, who has handled all the computational work associated with the project. We also thank Mrs. H. Geib and Miss J. Barritt for preparing the text, Miss A. Behlow for collating and typing the references, and Mrs. I. Gereke for making all our drawings.

We must thank the DFG and TUB for funding the research work, while the second author must thank the TUB and the Hermann-Föttinger-Institut for the many occasions on which he has been welcomed as a guest. The publication is funded by AGARD, and we must thank successive executives of the Fluid Dynamics Panel, J. Lawford, M. Fischer and R.H. Rollins for their help and encouragement.

We have throughout benefited from the support and advice of Professors T. Fanneløp (Trondheim) and K. Gersten (Ruhr-Universitat Bochum) as successive AGARD editors, and much informal assistance from Professor A.D. Young. We have continued to receive help and guidance from the EUROVISC advisory panel, L.C. Squire (Cambridge), J.L. Stollery (Cranfield) and K.G. Winter (R.A.E. Bedford). We are particularly indebted to Professors P. Bradshaw and D. Coles for detailed criticism of the text, and much helpful general advice. Since this last has not always been taken, they and the many other colleagues who have assisted in this way are not to be blamed for errors of fact or phrasing, which remain our own.

iii. GRAPHICAL PRESENTATION OF PROFILE DATA: LIST OF SOURCES REPRESENTED IN FIGURES

For the sources below a selection of the profile information may be found in the figures listed.

Source		Profiles		
		Temperature	Velocity	
			"Inner"	"Outer"
5301	Coles	-	3.3.11,4.2.5	4.2.6
5501	Shutts et al.	-	3.3.9,4.2.7	4.2.8
5502	Shutts & Fenter	-	4.6.2,4.6.4	4.6.5
5801	Naleid	-	5.3.8	-
5802	Stalmach	-	3.3.8,4.2.9	4.2.10
5805	Moore (Step)	-	4.5.1	4.5.2
5901	Hill	5.1.7	5.2.11	5.2.12
6502	Moore & Harkness	-	4.2.7,4.2.15	4.2.8,4.2.16
6505	Jackson et al.	-	3.3.10,4.2.13	4.2.14
6506	Young	-	3.3.8,4.3.1,4.6.4,4.6.6	4.3.2,4.6.5
6602	Jeromin	2.5.8	-	-
6701	Samuels et al.	2.5.15	-	-
6702	Danberg	2.5.10-13	-	-
6801	Perry & East	5.1.8	5.2.13,5.2.14	5.2.15
6903	Thomke	-	3.3.10,4.2.17	4.2.18
7003	Meier	2.5.9	-	-
7004	Winter et al.	-	5.3.18,5.3.19	5.3.20,5.3.21
7006	Hastings & Sawyer	2.5.5	3.3.8,4.4.12	4.4.11
7007	Zwarts	-	5.3.13	5.3.14
7101	Sturek & Danberg	5.1.5	5.3.15,5.3.16	5.3.17
7102	Peake et al.	-	3.3.12,5.3.1,5.3.2	5.3.3
7103	Fischer & Maddalon	4.4.7	-	.
7104	Waltrup & Schetz	5.1.4	5.3.10	5.3.9
7105	Beckwith et al.	5.1.9	5.2.18	5.2.19
7201	Lewis et al.	-	5.1.2,5.2.1,5.3.4	5.1.3,5.2.2,5.3.5
7202	Voisinet & Lee	2.5.17,2.5.18	3.3.13,4.2.19,4.3.9/10/13	4.2.20,4.3.11/12/14
7203	Hopkins & Keener	-	4.3.7	4.3.8
7204	Kenner & Hopkins	2.5.14	4.3.1	4.3.2
7205	Horstman & Owen	2.5.13,4.3.6	3.3.0/1,4.3.5	4.3.6
7206	Kemp & Owen	5.1.10	5.2.17	5.2.16
7301	Gates	2.5.6,4.5.6	4.5.4,4.5.5	-
7302	Winter & Gaudet	-	3.3.10,4.2.11	4.2.12
7304	Voisinet & Lee	5.1.6	5.2.5,5.2.7,5.2.9	5.2.6,5.2.8,5.2.10
7305	Watson et al.	2.5.7,4.4.3	4.4.4,4.4.5	4.4.6
7401	Thomas	-	5.2.3,5.3.11	5.2.4
7402	Mabey et al.	2.5.1-4	3.3.0/1/8/9,4.2.1/2	4.2.3,4.2.4
7601	Vas et al.	-	4.2.15	4.2.16
6002S	Danberg	2.5.21	4.4.8,4.4.10	4.4.9
7404S	Voisinet et al	2.5.19,2.5.20	-	-
7701S	Mabey	3.3.8	4.4.13-16	4.4.15,4.4.17
7702S	Laderman & Demetriades	2.5.16	4.3.3	4.3.4
7802S	Kussoy et al.	-	5.3.6	5.3.7

iv. **AGARDograph 223 - CORRIGENDA**

page vi - Abbreviations: STP - stagnation temperature probe.

page 13 - § 3.6, para. 2, last line: ρ' not p'.

page 25 - eqn. 5.13: $\delta_1 = -R_z[1 - (1+2\delta_n/R_z)^{\frac{1}{2}}]$.

page 27 - 5.6, para. 2, line 4: "---, so that p_{or} was set equal to ---".

5503-A-1: § DATA: 55030101 - 0113.

7006-B-2: First profile numbered 70060406 should be 70060405.

7105-A-3, Table 1: Table heading; P INF at X = 2.083 m.

: Last line, X = 2.083, -RZ = 197.5.

7209-A-1, para. 2, line 3: "--- at X = 25 mm ---".

7303-A-1, footnote: "--- values about 10% lower".

7305-A-1, Identification panel: $9 < RE/m \times 10^{-6} < 50$.

7401-A-1, para 2: "--- here. The plates were 0.1 m wide ---".

para 4: Reference to Smith et al. should be "1962".

7402-B-4, run 1702: X = 0.623.

R-3 References: Fenter (1960) DRL 468 should be Fenter (1959) DRL 437.

1. INTRODUCTION

The quantity of compressible turbulent boundary layer data which is available in the open literature is very great. In AGARDograph 223 (Fernholz & Finley, 1977), the predecessor of this volume, we presented a selection of data, restricting our choice to nominally two dimensional flows for which, with one exception, mean flow profile data were available in tabular form. In that data compilation we kept to a minimum any discussion of the quality or significance of the data, as our primary concern was to make it available in standard form without, so far as possible, introducing any particular pattern to which it should be expected to conform. Where we did make comments based on our own ideas or prejudices, we endeavoured to keep them as distinct as might be from the data proper, and the description of the experiment in which they had been obtained. Individual experiments - "entries" - which are described in AGARDograph 223 are referred to in this volume by the identification used in the data compilation as, for example, CAT 7205 (Horstman & Owen, 1972) - where the first two digits (72) refer to the year of publication of the experiment and the second two (05) were arbitrarily assigned by us during data processing. Four succeeding digits, as in 7205 0102, refer to the series and the individual boundary layer profile concerned. We also hope to provide a supplementary volume, and possible entries in this are indicated by four digits and an S. Some of these data are used in the present volume - e.g. 7802S (Kussoy et al, 1978).

In general we will not discuss practical details of the individual experiments here, presuming that the published account and our standardised description in AGARDograph 223 or its successor give any information which is desired - or at least, which is available. We will however describe and discuss the data themselves in close detail, for the greater part by comparing the mean velocity profiles to the basic pattern suggested by the so-called inner and outer 'laws' as used to describe the incompressible zero-pressure-gradient boundary layer. This procedure is at first sight rather simple minded. The theoretical background is discussed in §§ 2,3 however, and leads to the expectation that a suitable transformation of the profiles will allow the data to be compared directly to an accepted 'incompressible norm' (§ 3) for the zero pressure gradient case (§ 4) and that, as at low speeds, the differences from this standard case will be informative in pressure gradient flow (§ 5) and in flows which have not achieved equilibrium for other causes (§ 4.5). The main body of this paper therefore contains, in §§ 4,5, a graphical presentation of a great number of transformed velocity profiles in relation to the accepted semi-logarithmic inner law and a semi-empirical, also semi-logarithmic, outer law (Fernholz 1969, 1971).

In preparing the data compilation we originally found some difficulty, evidently often shared by the original experimental worker, in handling data from experiments displaying a significant pressure gradient normal to the wall. This led us to undertake a thorough investigation of the causes of such normal pressure gradients, the results of which are reported in § 6, while some of the resulting effects are considered as part of a general assessment of boundary layer thicknesses in § 7.

Whatever the topic being discussed, the illustrations here used are in every case drawn from experiments reported in AGARDograph 223 or the proposed supplement. Their validity therefore depends on the general validity of experimental data and we commence with an assessment of the data needed and the extent to which it is possible to hope for accurate measurement.

1.1 Requirement for profile data

Aeronautical boundary layer studies have their technological justification in the provision of usable data or calculation methods for the accurate prediction of skin friction, heat transfer, boundary layer separation and, to a lesser extent, displacement effect. While, in principle, any prototype situation could be modelled in an experiment, in practice it is virtually impossible to obtain complete dynamic similitude, if only because the prototype Reynolds numbers are usually so high that they cannot be reproduced economically in laboratory experiments. There is therefore a need to develop rational correlations of data which will allow engineers to predict, or extrapolate, from a limited range of experimental geometries and governing dimensionless parameters, the likely values of the technically important quantities in markedly differing prototype situations.

The practical requirement is for good values of the "wall data" - principally skin friction, and in high speed flows, heat transfer - but laboratory measurements of these alone do not provide adequate information as any mode of extrapolation, whether by the use of a refined and complex field calculation method or by a grossly simplified empirical formula, will depend also on details of the flow field in the boundary layer. This essentially results from experimental difficulties in modelling transition, as even flat plate results cannot be properly correlated against values of Re_x, while some measure of success has been achieved when the reference length used is a boundary layer thickness. All rational prediction methods therefore depend finally on some kind of mean flow, and possibly turbulence, profile information. The more refined calculation methods attempt to use a limited amount of very generalised fundamental data, while empirical projections tend to use a very large pool of data from situations which are often more variously distributed in their original range of application than one would wish when applying the results - e.g. the 'parametric approach' of § 2.1.2(1). Whatever the approach, profile information is required - rarely for its own sake, since it has no direct technical application - but for use in the development of prediction methods.

This volume presents a discussion of the mean flow profile data of compressible boundary layers. A natural approach is to compare the data with, in some way equivalent, incompressible boundary layers, and this is indeed the general method used in the detailed profile analysis of §§ 4,5. The comparison is, however, with the simplest possible case - a 'standard' flat plate boundary layer - and cannot yet be extended other than in qualitative terms to more general cases. Indeed, it is wise to express caution about any assumption that the low speed layer itself is fully understood. A good, if now slightly dated, appreciation may be obtained by a study of the proceedings of the 1968 Stanford conference on the calculation of incompressible turbulent boundary layers (Kline et al., 1969, Coles & Hirst, 1969, or briefly, with particular reference to compressible flows, Morkovin & Kline, 1968). A valuable result of this meeting was that many of the basic problem areas were identified. Recent experimental work aimed at elucidating some of the individual features of 'complex' two dimensional flows is exemplified by Smits et al. (1979, a,b) while a more general review may be found in Bradshaw (1976, Ed.). Whether the 'incompressible base' can be treated as known or not, it remains difficult to think of incompressible analogues for some features of compressible flows. In particular there is the possibility of concentrated pressure changes in distances comparable to the boundary layer thickness, even if shock-wave boundary-layer interactions are excluded. High heat transfer rates are common, and certainly of technical importance to a greater extent than at low speeds, so that heat transfer enters as a principal variable. The data base required for study is therefore extended by at least two 'dimensions' - heat transfer, and of course, Mach number.

1.2 The nature of experimental observations

For the reasons stated above, the original data compilation presented as AGARDograph 223 concentrated on cases for which profile information was available, while this volume discusses the features of the mean flow profiles which were presented there, with some additions. Before embarking on this detailed study however, we consider some of the general factors which determine the availability of data.

An ideal data set would consist of a series of measurements at successive streamwise stations. The data presented would include

(a) Wall pressure and temperature at close intervals.

(b) Skin friction and heat transfer at close intervals.

(c) At a number of succeeding profile stations, self-sufficient sets of three independent mean flow properties.

(d) Turbulence measurements giving, as a minimum, profiles of the mean-square velocity fluctuation components and of shear stress.

(e) Properly conducted investigations of the experimental environment, such as checks on two-dimensionality, free-stream uniformity and turbulence level as a function of frequency, noise levels, and where appropriate, the state of tunnel sidewall boundary layers.

The length of the list is enough to suggest that the ideal is not readily attainable, but the difficulties involved in obtaining each item vary widely, and occasionally present conflicting experimental requirements.

1.2.1 Long- and short-run facilities

The most significant classification of experimental facilities is into "short-run" and "long-" or "continuous-running" tunnels. In practice this means that "short-run" devices have a typical test duration of 10 ms or less, while "long-run" tunnels range from about 10 s to the effectively unlimited. The significance of the distinction is that the technically important measurement of heat transfer is very straightforward in a "short-run" test, and difficult in a "long-run" facility. On the other hand it is very difficult indeed to measure profile data in a "short-run" tunnel, and relatively straightforward when given enough time. In compiling data for the development of prediction methods there is therefore a basic problem in linking heat transfer data simply, and fairly reliably, obtained from short-run tests to the profile and skin friction data obtained in the very different environment of a continuous, or at least "long", running wind tunnel. The profile-based nature of our own compilation has therefore led us to request G.T. Coleman & J.L. Stollery to prepare a short appreciation of data from short-run facilities which appears as § 1.3 below.

1.2.2 Wall measurements

Of the 'ideal data set' wall measurements, static pressure and wall temperature are easily measured, though the latter is often not recorded by experimental workers who believe their walls to be adiabatic, or nearly so. Heat transfer rates are, as stated above, readily determined in short-run facilities, but can present considerable problems in continuous run tunnels since most techniques then require some form of steady state calorimetry, with the associated difficulties of assessing leakage fluxes (mostly due to lateral conduction) or of arranging a complex set of buffer rings. Many of the techniques require the actual heat flux meter surface, or part of it, to be at a different temperature from the surrounding wall, and this can cause serious distortion of the results. (See Winter, 1976, for a review of heat transfer measurement techniques). An interesting hybrid technique, which in principle evades these difficulties, is the use of an 'isolated mass calorimeter' (Westkaemper, 1959). It is perhaps significant however that the vast majority of writers on heat transfer techniques for long-run facilities find it necessary to devote a substantial part of their text to techniques for correcting the inherent errors of the method.

Skin friction is perhaps the most difficult quantity of all to measure directly (see the review paper by Winter, 1977). There is a long history of 'direct' measurement of wall shear stress using floating element balances, but unless the balance is very large, when, however, the value obtained will not be truly local (e.g. Winter & Gaudet 1973, CAT 7302) it is very difficult to be certain that various forms of systematic edge-flow-induced errors are not present (Allen, 1976, 1977a) however repeatable the static calibration may have been.

A vital step in the development of experimental techniques is the extension of skin friction measurements to provide a Preston tube calibration. Balances are expensive, require a relatively large space for installation even when the element is small, and are very difficult to use. Further, the edge-induced errors are likely to become even larger when complicated by inflow and outflow due to pressure gradients, while "moment sensing" balances are affected directly by the pressure gradient (e.g. the NOL design, Bruno et al., 1969). Unfortunately, even for adiabatic wall boundary layers, there is as yet no final agreement on the Preston tube calibration (Fenter & Stalmach, 1957; Hopkins & Keener 1966; Allen, 1973, 1974 revised, Allen 1977b; Bradshaw & Unsworth, 1974, and revised, Bradshaw 1977b), so that research workers often present several different values and leave it to the reader to choose (e.g. Peake et al., 1971, CAT 7102). It may or may not be possible to extend the calibration to severe heat transfer cases (it is not uncommon to find a 30%-50% difference in values depending on the calibration chosen - Bartlett et al., 1979a), but if this is done it is most important that calibrations are made against balances which have the floating element at the same temperature as the surrounding test surface. This is clearly a formidable design problem, but an uncooled floating element in a cooled wall may give unrealistically low shear stress values (Westkaemper, 1963). A difference of order 20% was found by Voisinet & Lee with

T_w/T_r = 0.22 (CAT 7202, and corrected data, private communication). We would however encourage experimental workers to take Preston tube readings whenever possible, since it is relatively straightforward and cheap to do so, while disregarding the apparent discouragements above, as if the raw Preston data are presented it will always be possible to reduce the data using the calibration of the reader's choice - or the final definitive calibration if that is ever achieved.

1.2.3 Mean flow profile data

Mean flow data in the boundary layer are with very rare exceptions (LDV, Electron beam, hot-wire probes in use for turbulence measurements) deduced from measured Pitot (p_{t2}) profiles and measured or assumed total temperature(T_o) and static pressure (p) profiles. The question of static pressure variation is fully discussed in § 6 below, and so will not be considered further here, other than by remarking that on a straight wall with not too severe longtiudinal pressure gradients it is usually reasonable to assume that p is a function of x only. The measurements, if made, are likely to prove difficult, especially at high Mach numbers (see Beckwith et al., 1971).

Usually total temperature profiles are, in practice, measured nowadays, and in severe heat transfer cases this is absolutely necessary. A general appreciation of the extent to which available theories predict the temperature profile may be found in § 2.5.6 below, and may serve as a guide to the requirement for a measured profile. Three basic types of probe can be distinguished, each with its own advantages and disadvantages. Historically the first of these, and conceptually the simplest, is the vented Pitot type referred to in AGARDograph 223 as a stagnation temperature probe (STP). The earlier designs (Winkler 1954) appeared successful, but later users sometimes obtained anomalous results. This was almost certainly a consequence of insufficient attention to the details of the flow within the probe and inadequate care in designing the vents (Bartlett et al., 1979). The advantage of a probe of this type is that it is relatively robust and, when properly designed, the calibration factor is very close to one. The disadvantage is that the probes are comparatively large, because of relatively complex construction, and that the good calibration characteristics begin to fail below probe Reynolds numbers based on outside diameter of about 50.

Dissatisfaction with the STP led to the development of the equilibrium cone probe (ECP) by Danberg (1961). The aim here is to achieve, as closely as possible, the laminar flow recovery temperature on a cone which is in principle thermally isolated from its support. In use the probe seems very satisfactory, but it requires a relatively long settling time. It also appears to be difficult to construct a very small probe with satisfactory characteristics (see Fig. 2.1.3 below, from Meier, 1976, and Figs. 2.5.17,18) as the achievement of a constant calibration factor implies a requirement for effectively conical flow, so that there is again a minimum Reynolds number limit. Effective thermal isolation is also difficult to achieve.

Unshielded fine wire probes (FWP), whether thermocouple probes or resistance wires, can be made very small (Fig. 2.1.3) but usually have very variable calibration characteristics. They operate in a sensitive low Reynolds number regime and, since they are not shielded, cannot have very long supports. Since the supports are the electrical leads themselves, there are usually also large conduction corrections. They obviously have an advantage in high resolution and the possibility of getting close to the wall, though wall proximity corrections might be significant, but because of the fundamentally unattractive calibration characteristics should perhaps be avoided unless small size and rapid response are the dominating requirements.

Finally, there is the possibility of constructing a combined Pitot/total temperature probe (Meier, 1968). Considered as a T_o probe, this is a vented STP with the vents outside the wind tunnel. An advantage is that the flow rate in the probe can be controlled, which however introduces a further variable into the calibration procedure. The combined probe does give a 'single point' p_{t2}, T_o determination at the expense of relatively complicated calibration equipment and procedures. The construction is also difficult, and may give rise to unrepeatable conduction errors (Mabey & Sawyer, 1976).

The pitot profile is the fundamental boundary layer measurement, and is, by comparison with total temperature or static pressure measurement, relatively straightforward. The probes themselves are very simple and so can be made, in flattened form, with a very small vertical dimension. The limits are set by settling time and at high Mach numbers, by low Reynolds number and rarefaction effects on the calibration (e.g. Beckwith et al., 1971, at M = 20 where the probe height Reynolds number was about 3 at the innermost measuring points, and the associated calibration factor about 2:1). At more modest Mach numbers (less than about 10) the restriction is however more a matter of difficulty of construction and settling time.

Probe size limitations and calibration procedures do not significantly affect the quality of data in the greater part of the boundary layer, but result in serious restrictions as the wall is approached. There are virtually no experiments for which it is possible to place confidence in wall shear stress and heat flux values obtained from the slope of the velocity and total temperature profiles, and except in hypersonic flows with very thick sublayers it is unusual for observations to extend into the sublayer (say $yu_\tau/\nu < 20$) without extrapolation of total temperature data. It is therefore not possible to check wall measurements against profile data unless it can be assumed that the profile as a whole obeys a general similarity relationship as discussed in §§ 3, 4 below, when a curve-fitting procedure as suggested by Coles (1964), Coles & Hirst (1968) will give a statistically determined shear stress value.

1.2.4 Turbulence profile measurements

We hope in a succeeding volume, to consider the available turbulence profile data, and so will be examining the possibilities of measuring various quantities there. There are three main approaches. The classic route is to use hot-wire (or hot-wire related) devices, much as for low speed flow, which with the separation of variables achieved by mode analysis (Kovasznay, 1950, 1953a, Morkovin, 1956, 1967) provide velocity and total temperature fluctuation profiles. Cross-wires (Laderman, 1976) or analogous devices (Mikulla & Horstman, 1976) may be used to give shear stress values. Reduction of data must however remain problematic for the immediate future (see the effects of 'response restoration' and changes in modal analysis in Laderman & Demetriades, 1979). Spatial resolution is good, but accuracy not very high. Recently the non-intrusive techniques have started to give usable data. These, the laser-doppler-velocimeter and the electron beam fluorescent technique (for ρ') are of the highest importance as they give both mean and fluctuation data by means which are quite unrelated to the hot-wire techniques, and so in principle may provide a direct check on the calibration and reduction procedures of the classic technique. (See the comparisons between hot-wire and laser derived values in Johnson & Rose 1975, 1976). For optical reasons it can be difficult to make measurements very close to the wall, and the results, particularly from the electron beam technique, may not be very precise. It does seem likely, however, that well established turbulence profiles may become available in the near future when all three techniques are combined.

1.2.5 Availability of data from 'long run' facilities - a summary

The greater part of the 'complete data set' specified at the start of § 1.2 can be measured with reasonable success. The principal areas of difficulty in mean flow measurements remain the determination of the shear stress and heat transfer at the wall, the static pressure profiles and of all profile data very close to the wall. Values found from measurements in the wall itself are probably more reliable than values deduced from profile measurements, but even so not of sufficient accuracy to allow confident prediction at the 10% level. This is particularly the case with shear stress measurements in flows with pressure gradients, or in any flow with substantial heat transfer. Mean profile data outside the sublayer are reasonably reliable, but are not, unfortunately, good enough near the wall to allow a proper comparison with wall measurements. The available turbulence data are valuable but as yet relatively imprecise, with some uncertainty remaining in the accuracy of data reduction procedures.

1.3 Data from short-run facilities (by G.T. Coleman* & J.L. Stollery†)

The use of short duration (intermittent) facilities for hypersonic research is relatively common for two reasons. Firstly such facilities, which are often derivatives of shock tubes (e.g. Shock Tunnel, Longshot Tunnel) can be built at a relatively low cost, and secondly the energy released in the running

* Aerodynamics Department, RAE Farnborough - †Aerodynamics Division, College of Aeronautics, Cranfield, Bedford

time (usually measured in tens of milliseconds) is stored up over a longer period (usually measured in minutes) so that the required power input is low. The Reynolds numbers obtainable in tunnels of this type are now high enough for flat plate turbulent layers to be studied under both natural and forced transition conditions if long models are used. A problem is that such tunnels are frequently of an open-jet configuration with a fairly small nozzle, necessitating the use of low aspect ratio models which immediately throws some doubt on the two-dimensionality of the results.

The great advantage of short duration facilities is the ability to measure easily the heat transfer rate to the wall using well-developed transient techniques (for reviews see Schultz & Jones, 1973, Winter, 1976). The measurements are made at constant wall temperature, without any requirement for control, and most frequently under cold wall conditions. In this context of heat transfer measurement it is worth making a brief mention of other facilities which, although not strictly short duration, do share both some of the problems and some features of techniques and analysis. They usually run at lower Mach numbers with relatively long running times (seconds), and use transient techniques (either injection of the model into the established free-stream or fast removal of a shroud from the model) for measurement of heat transfer. Examples are given in the work of Eaton et al. (1968) and Hughes (1973).

In short-run facilities pressure measurements are invariably more difficult to make because the filling time of tubes is a parameter to be considered by the experimenter. This response time becomes longer as the pressure to be measured becomes lower. Wall static pressure, although low, is usually measured easily and accurately because the orifice itself can be of a relatively large diameter. However, the ability to measure pitot pressure profiles is limited, thick boundary layers can be generated but the probes themselves are, of necessity, large. The comments in the report by Allen (1974a) are particularly relevant here. He shows that small probes ($d/\delta < 0.05$) are needed to avoid distorting as well as dis-displacing the true profile. He also shows that the displacement correction increases strongly with Mach number rising from the low speed value of 0.15 d to around 1.0 d at M = 4. This leads to difficulty of interpretation, particularly close to the wall where the probe records some average value in a region where large gradients are present. Combined with this problem is the present inability, not restricted solely to this type of facility, to measure the boundary layer temperature profile. Numerous attempts have been and are currently being made to develop a reliable fast response temperature probe (East & Perry, 1967; Bartlett et al., 1979) but the fact is that no definitive temperature profile data exist. Calculation of velocity profiles invariably depends on an assumed temperature relation (usually Crocco, § 2.5). This combination of problems encountered with profile measurements results in the inability to reliably estimate the skin friction coefficient from profile data in short duration facilities (see for example Coleman et al., 1973, or Coleman, 1973a,b).

Most theoretical approaches to compressible turbulent boundary layers predict C_f as a function of a Reynolds number, a Mach number and a heat transfer parameter and this has to be related to Stanton number by the use of an assumed Reynolds analogy factor. The large amount of heat transfer data available from the short duration facilities would provide a good test of any theory if the theories themselves could predict the relevant quantities. The measurement of skin friction coefficient is arguably the most difficult task at present. The use of surface pitot tubes, in particular the Preston tube, is feasible but the validity of the interpretation formulae at high Mach numbers and cold wall conditions is not yet satis-factorily established (Coleman et al., 1973) despite the recent findings of Allen (1974, 1977b). There have been attempts to develop new techniques for measuring wall shear stress under such conditions; for example Green and Coleman (1973) tried to relate small pressure differences across inclined surface slots to τ_w. Unfortunately the experiments showed that geometric considerations and pressure gradient effects dominated the results, and hence these tests further emphasised the difficulty of c_f measurement. The data of Holden (1972), taken from the Calspan Shock Tunnel are unique in this field since he measured c_f using a floating surface element balance. He was also able to make simultaneous measurements of heat transfer and hence could evaluate the Reynolds analogy factor directly. Even so the values varied between 0.95 and 1.2. To summarise the situation with respect to measurements from short duration facilities, they are characterised by a reliance on wall pressure and heat transfer data, with only rare profile surveys and wall shear stress measurements. Such tunnels have the unique ability of providing accurate heat transfer measurements under isothermal, cold-wall conditions.

2. THEORETICAL BASIS FOR THE INTERPRETATION OF MEASUREMENTS

2.1 Introduction

2.1.1 State of the art

In forming their analysis for boundary layers in compressible fluids Karman & Tsien (1938) were compelled to assume that the greater part of the boundary layer was laminar. Such a restriction was necessary "because of the lamentable state of knowledge concerning the laws of turbulent flow of compressible fluids at high speeds". This statement is still true as far as analytical and numerical solutions are concerned. On the other hand one must concede that over the years a considerable measure of success has been achieved by those who set out to provide a description of the two-dimensional incompressible turbulent boundary layer. It remains true, however, that what has been accomplished is a description rather than a theory and it is certainly not possible, as yet, to predict the behaviour of a boundary layer beginning from a general descriptive theory of turbulence as such. To round off the picture, one should add to this Willmarth's statement (1975) that our basic experimental knowledge of the structure of turbulence in low speed flow is only rudimentary at present. Knowing that the state of the art is even worse for compressible turbulent boundary layers, one can only admire the ingenuity and audacity of scientists and engineers who have sent men to the moon and space probes to other planets. There is no doubt that it is the wish and the need to fly at supersonic speeds which started and has kept going research on high speed boundary layers. We have attempted to collect and present some of the experimental data gained in many windtunnels and on many geometrical configurations in AGARDograph 223, and we hope to discuss, briefly, an even greater number of experiments in a "source catalogue" as part of a succeeding volume. The availability of this bulk of data has been too tempting for us not to at least attempt an interpretative survey of some aspects of the two-dimensional compressible turbulent boundary layer. Theoretical results with a sound physical basis will be used wherever possible so to impose some order on the vast amount of experimental data.

2.1.2 Classification of calculation methods

We shall not try to discuss calculation methods here, nor evaluate their underlying semi-empirical input, nor shall we compare their success or failure with respect to experiments. This, we hope, will be done by others in connection with or after a "Stanford type" conference on compressible turbulent boundary layers (see Kline et al. 1968). It seems useful, however, to point out connections between the experimental results and physical concepts discussed below on the one hand and the different types of prediction methods on the other hand by referring to a classification given by Laufer (1969):

(1) Parametric approach. This technique does not tackle the complete boundary layer problem; that is, the question of the velocity and temperature distributions, but concentrates on the technologically important question of prediction of the skin friction and of the heat-transfer coefficient. It introduces new parameters (such as the wall-to-freestream temperature ratio, Mach number and Reynolds number), with the help of which it seeks an empirical correlation of the experimental data.

(2) Direct approach. Here the flow parameters such as the mean velocity and the mean temperature are computed from the equations for compressible boundary layers after some necessary assumptions have been made concerning the turbulent transport and correlation terms.

(3) Transformation method. Here a mathematical transformation is sought that would reduce the compressible equations to their incompressible form. It is then possible to use the extensive and well documented empirical information available for the incompressible case and apply it to the compressible case by means of the transformation. Obviously, such a scheme can work only if the transformation correctly reflects all of the differences exhibited by the turbulent mechanism in a compressible flow as contrasted with one in an incompressible flow.

All three approaches need boundary conditions both at the free-stream edge of the boundary layer and at the wall. These are readily available for the cases collected in AGARDograph 223.
The parametric approach needs in addition a Reynolds number formed with a characteristic length of the boundary layer, e.g. the momentum loss thickness δ_2 (eqn. 2.3.4) for the determination of which density and velocity profiles at a position x in the boundary layer must be known. The direct approach makes use

of starting profiles for temperature and velocity but needs measured profiles for comparison with the theoretical results at various stations x downstream, since closure assumptions known so far are tentative only. Lastly the transformation method needs both measurements in the domain of the compressible boundary layer and in the transformed domain where the latter can - in the most favourable case - be a boundary layer comparable with the one in the subsonic case (Coles 1964). Though we do not deal in this investigation with calculation methods for compressible turbulent boundary layers, we thought it to be convenient to give a few references, especially for those readers who are new to the field. Apart from an early survey by Hornung (1966) the conference at Langley Research Center in 1968 (Compressible turbulent boundary layers, NASA SP-216, 1968) gave the first general review on compressible turbulent boundary layers both from a theoretical and from an experimental point of view. Some of the knowledge available at NASA Langley was presented at a Von Karman Institute Short Course in 1976 by Bushnell et al. (1976). This was followed by three investigations: On compressible turbulent shear layers (Bradshaw 1977), a critique of some recent second order closure models for compressible boundary layers (Rubesin et al. 1977), and by turbulence modeling for compressible flows (Marvin 1977). Finally it may suffice to show the bold aim of those who intend to calculate compressible boundary layers by quoting the title of an investigation by Adams & Hodge (1977) - "The calculation of compressible, transitional, turbulent, and relaminarizational boundary layers over smooth and rough surfaces using an extended mixing length hypothesis" - which contains a large number of further references. We agree with Marvin's (1977) statement that "if progress in modeling for compressible flows is to be made, it will come through combining a broad experimental effort with developments in computational techniques and modeling ideas".

2.1.3 Restrictions for the present discussion

Before we set out, we should state - as was done in AGARDograph 223 - what flows we have considered and under what conditions:
We have restricted ourselves to the study of nominally two-dimensional turbulent boundary layers (some of them transitional) formed on rigid impermeable walls, and have excluded cases in which it would be necessary to take account of chemical reactions or ionization. In fact we have assumed throughout that the test gas was a perfect gas, with constant specific heats, although in a few cases the temperature range is such that the relationship between reservoir conditions and test station conditions is detectably falsified as a result of vibrational excitation. Boundary layers with suction or injection through the wall were excluded. In the region of interest flows had to be free of discontinuities (e.g. shockwaves), and the boundary layers under investigation had to be steady. No viscous-inviscid interaction at the free-stream boundary of the boundary layer is considered here.

With these assumptions the equations for compressible laminar boundary layers can be solved by computers of the size available in most universities, aerospace companies, and government establishments. In the case of a turbulent boundary layer, however, the problem is not solely a numerical one: Calculation methods still depend on some form of empirical correlation or a simplified model of turbulence which again requires an empirical - mostly experimental - input in order to cope with the closure problem. When the turbulent fields to be considered are further complicated by three-dimensionality and/or property variation the problems of calculation or rational description become so complex that successful predictions - in contrast to "postdictions" (Saffman 1978)-are still extremely rare. As stated above, the mean flow is assumed two-dimensional with mean velocities denoted by $\bar{u}$ and $\bar{v}$ in the x and y directions respectively, where x is the coordinate parallel to and y normal to the wall. Fluctuating quantities are indicated by a dash as u', v', p', ρ' and T'.

2.1.4 Characteristics of compressible boundary layers

The flow in a compressible boundary layer is characterized by large changes in density and temperature (Fig. 2.1.1) which again influence such transport properties as the viscosity μ and the heat conductivity λ. The density and temperature changes are a result of compressibility, viscous dissipation and/or heat transfer at the wall. In turbulent flows the transport mechanisms associated with fluctuation quantities such as velocity, temperature, and pressure increase the exchange of momentum and heat considerably as compared to that in a laminar boundary layer. Fig. 2.1.1 shows two sets of boundary layer profiles at

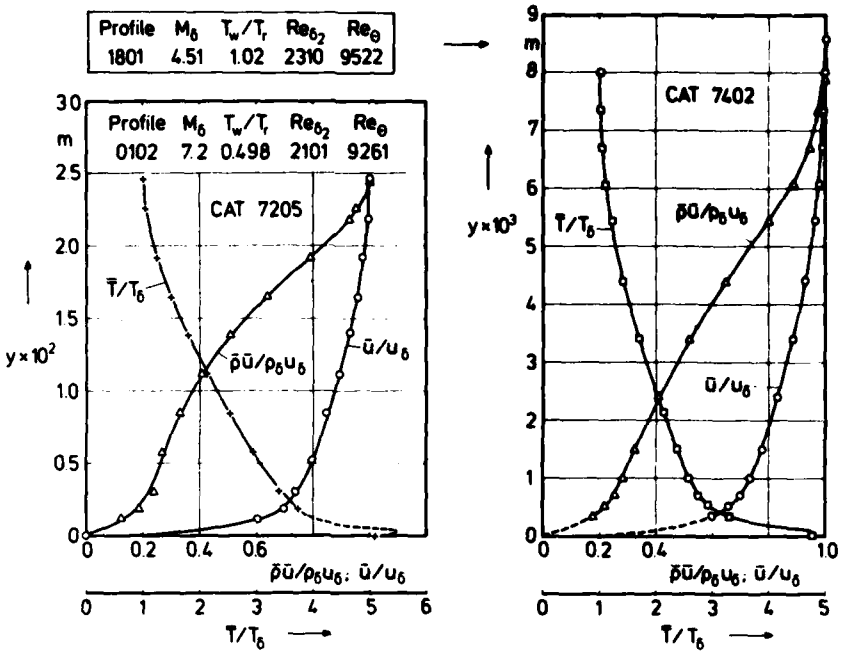

Fig. 2.1.1 Velocity-, temperature-, and mass flow profiles in a zero pressure gradient boundary layer along an isothermal and adiabatic wall (air).

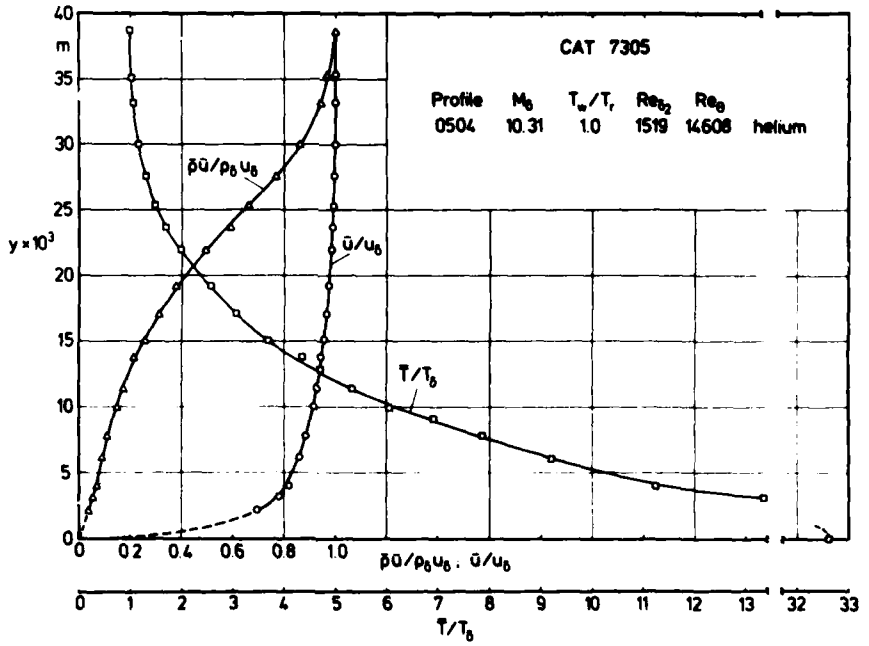

Fig. 2.1.2 Velocity-, temperature-, and mass flow profiles in a zero pressure gradient boundary layer along an adiabatic wall (Watson et al. 1973).

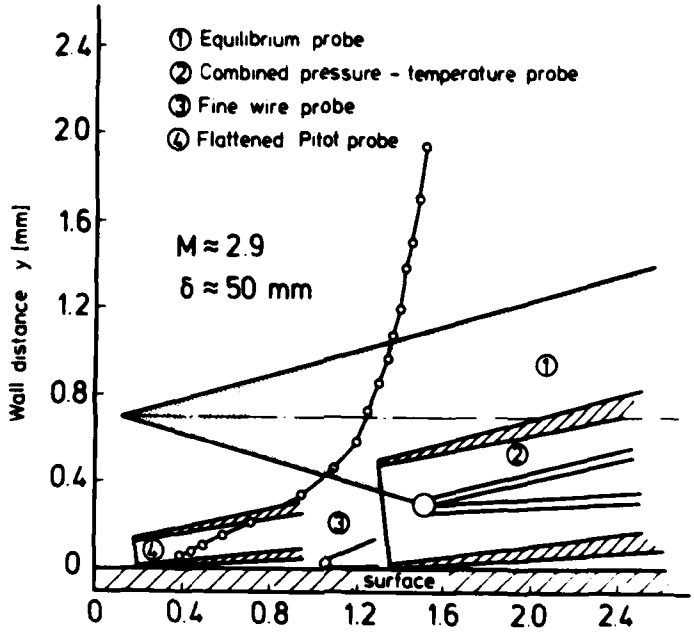

Fig. 2.1.3 Typical dimensions of temperature and pressure boundary layer probes (courtesy H.U. Meier 1976).

about the same Reynolds number ($Re_{\delta_2} \approx 2200$), one set measured on an adiabatic wall, the other on an isothermal wall. Though the boundary conditions, Mach number and heat transfer parameter, differ considerably, the respective velocity, temperature, and mass flow profiles look very much the same. The reader should note that neither of the measured profiles can provide such information as the velocity and temperature gradient at the wall, necessary to determine skin friction and heat flux. What is evident, however, is the fact that the bulk of the mass flow is increasingly found toward the outer edge of the boundary layer with rising Mach number. This effect is emphasised even more in Fig. 2.1.2, where the Mach number was 10 in a helium flow on an adiabatic wall. Here the temperature ratio between the wall and the boundary layer edge is about 30! In this context it is also of interest to note the size of total temperature and pressure probes in comparison with a typical boundary layer (Fig. 2.1.3).

2.2 Fundamental equations for two-dimensional compressible turbulent boundary layers

2.2.1 Background

As far as the authors are aware, these equations were first derived in detail in 1951 independently by Young - published by Howarth (1953) - and by Van Driest (1951). A later version was given by Schubauer & Tchen - published by C.C. Lin (1959). We shall follow here those versions of the basic equations containing time averaged variables and not Favre's suggestion (1965), (1971) to use "mass-weighted" variables, whereby density fluctuations are removed from the equations of motion, continuity and energy. For a further discussion of these equations the reader is referred to Laufer (1969), Rubesin & Rose (1973) and Cebeci & Smith (1974), for example.

It appears necessary to state explicitly which assumptions for the derivation of the conservation equation for compressible turbulent boundary layers were made, so that the order of magnitude of the terms neglected can be re-assessed as new data - mainly fluctuation measurements - become available. This is even more important for compressible than for incompressible boundary layers, since supersonic flows offer more opportunities than subsonic ones for violent changes in pressure gradient or geometry (Bradshaw, 1974a). Turbulence intensity, shear stress and heat transfer rate rise through a shock wave and fall through an expansion. This can diminish the reliability of estimates for the order of magnitude of turbulence terms in the conservation equations for compressible flow as compared with those for incompressible flow. Furthermore we find additional turbulence terms in compressible boundary layers due to density and temperature fluctuation. In addition the pressure fluctuations - this holds mainly for the transport equations where they appear explicitly - become thermodynamic variables and could, in fact, attain the same order of magnitude as the other fluctuating quantities. Clearly, this is the situation in a random sound field (Laufer, 1969).

We shall not consider here terms containing viscosity fluctuations, since it is reasonable to assume that these terms are negligibly small (Laufer, 1969).

For steady, two-dimensional boundary layers the usual assumptions are: $(\delta/x) = 0\ (\varepsilon)$, where $\varepsilon << 1$ and δ is the boundary layer thickness, $x/L = 0\ (1)$; $(\tilde{u}/u_\delta) = 0\ (1)$; $\bar{T}/T_\delta = 0\ (1)$; $\tilde{\rho}/\rho_\delta = 0\ (1)$ where L is a characteristic length of a body in x-direction and δ denotes the edge of the boundary layer.

For a discussion of δ see § 7.

Double correlations of fluctuating quantities are at most of the order of ε, while triple correlations will be at most of the order of ε^2 (Schubauer & Tchen, 1959).

2.2.2 The conservation equations

For the sake of simplicity we shall write the conservation equations in a cartesian coordinate system where x denotes the main flow direction parallel to the wall and where y is the coordinate normal to the wall. We have also assumed throughout this chapter that the effects of normal pressure gradients due to curvature are negligible. This is not always the case. The conditions under which normal pressure gradients are significant will be discussed in § 6. We thought it helpful to deal with this question separately since the more general question of the effects of compressibility on turbulence can then be dealt with here with the equations retaining a general likeness to those with which readers are accustomed when dealing with low-speed flow.

The continuity equation then reads

$$\frac{\partial}{\partial x}\ (\bar{\rho}\bar{u}) + \frac{\partial}{\partial y}\ (\bar{\rho}\bar{v} + \overline{\rho' v'}) + \frac{\partial}{\partial x}\ (\overline{\rho' u'}) = 0. \tag{2.2.1}$$

The last term in eqn. (2.2.1) will be considered as of order ε, i.e. small, being the derivative in the direction parallel to the wall and in addition that of a double correlation which in itself is assumed to be of order ε. The equation of motion in x-direction can be written:

$$\begin{aligned}\bar{\rho}\bar{u}\ \frac{\partial \bar{u}}{\partial x} + (\bar{\rho}\bar{v} + \overline{\rho' v'})\ \frac{\partial \bar{u}}{\partial y} = &- \frac{\partial \bar{p}}{\partial x} + \frac{\partial}{\partial y}\ (\bar{\mu}\ \frac{\partial \bar{u}}{\partial y} - \bar{\rho}\ \overline{u' v'} - \overline{\rho' u' v'}) \\ &- 2\ \overline{\rho' u'}\ \frac{\partial \bar{u}}{\partial x} - \frac{\partial}{\partial x}\ (\bar{\rho}\ \overline{u'^2} + \overline{\rho' u'}\ \bar{u}) + \frac{\partial}{\partial y}\ \overline{[\mu'\ (\frac{\partial u'}{\partial y} + \frac{\partial v'}{\partial x})]} \\ &- \frac{\partial}{\partial x}\ [\frac{2}{3}\ \overline{\mu'\ (\frac{\partial u'}{\partial x} + \frac{\partial v'}{\partial y} + \frac{\partial w'}{\partial z})} - 2\ \overline{\mu'\ \frac{\partial u'}{\partial x}}\ ].\end{aligned} \tag{2.2.2}$$

Assuming that the terms

$$\frac{\partial}{\partial y}\ (\overline{\rho' u' v'})\ ,\ 2\ \overline{\rho' u'}\ \frac{\partial u}{\partial x}\ ,\ \frac{\partial}{\partial x}\ (\bar{\rho}\ \overline{u'^2} + \overline{\rho' u'}\ \bar{u})\ ,\ \frac{\partial}{\partial y}\ \overline{[\mu'\ (\frac{\partial u'}{\partial y} + \frac{\partial v'}{\partial x})]},$$

$$\frac{\partial}{\partial x}\ \overline{[\frac{2}{3}\ \mu'\ (\frac{\partial u'}{\partial x} + \frac{\partial v'}{\partial y} + \frac{\partial w'}{\partial z})]} - 2\ \overline{\mu'\ \frac{\partial u'}{\partial x}}]$$

are one order of magnitude smaller than the remaining ones, that is, of order ε, eqn. (2.2.2) becomes

$$\bar{\rho}\ \bar{u}\ \frac{\partial \bar{u}}{\partial x} + (\bar{\rho}\ \bar{v} + \overline{\rho' v'})\ \frac{\partial \bar{u}}{\partial y} = - \frac{\partial \bar{p}}{\partial x} + \frac{\partial}{\partial y}\ (\bar{\mu}\ \frac{\partial \bar{u}}{\partial y} - \bar{\rho}\ \overline{u' v'}). \tag{2.2.3}$$

We cannot rule out the possibility that the equation of motion normal to the wall (y-direction) may become important in a reduced form

$$\frac{\partial \bar{p}}{\partial y} + \frac{\partial}{\partial y}\ (\bar{\rho}\ \overline{v'^2}) = 0 \tag{2.2.4}$$

resulting in a variation of the mean static pressure across the boundary layer due to the increasing importance of the Reynolds stress contribution as the Mach number rises (e.g. Finley 1977). The magnitude of the normal pressure variation can be evaluated from eqn. (2.2.4) which yields after integration:

$$\bar{p} = p_w - \bar{\rho}\ \overline{v'^2}\ . \tag{2.2.5}$$

Beckwith (1970) relates $\overline{v'^2}$ and $-\ \bar{\rho}\ \overline{u' v'}$ by relations holding for incompressible turbulent boundary layers and obtains

$$\frac{\bar{p}}{\bar{p}_w} = 1 + \frac{5}{3}\ \frac{\bar{\rho}\ \overline{u' v'}}{\bar{p}_w}\ . \tag{2.2.6}$$

If one integrates eqn. (2.2.4) from y to the boundary layer edge one gets

$$\bar{p} = \bar{p}_\delta - \bar{\rho}\ \overline{v'^2} \tag{2.2.7}$$

and by substituting for $\bar{p}_\delta$ by $\rho_\delta\ u^2_\delta/(\gamma\ M^2_\delta)$

$$\bar{p} = \bar{p}_\delta\ (1 - \gamma\ M^2_\delta\ \frac{\bar{\rho}\ \overline{v'^2}}{\rho_\delta\ u^2_\delta})\ . \tag{2.2.7a}$$

This relationship is given incorrectly by Schubauer & Tchen (Lin 1959 p.90)
The energy equation reads:

$$\bar{\rho}\,\bar{u}\,\frac{\partial \bar{h}}{\partial x} + (\bar{\rho}\,\bar{v} + \overline{\rho' v'})\,\frac{\partial \bar{h}}{\partial y} = \frac{\partial}{\partial y}\left(\frac{\lambda}{c_p}\,\frac{\partial \bar{h}}{\partial y} - c_p\,\bar{\rho}\,\overline{v'T'}\right)$$

$$+ \bar{u}\,\frac{\partial \bar{p}}{\partial x} + \left(\mu\,\frac{\partial \bar{u}}{\partial y} - \bar{\rho}\,\overline{u'v'}\right)\frac{\partial \bar{u}}{\partial y} \qquad (2.2.8)$$

Here we have assumed that the terms

$$\frac{\partial}{\partial x}\left[c_p\left(\bar{T}\,\overline{\rho' u'} + \bar{u}\,\overline{\rho' T'} + \bar{\rho}\,\overline{u'T'} + \overline{\rho' u' T'}\right)\right] \;;\; \frac{\partial}{\partial y}\left[c_p\left(\bar{v}\,\overline{\rho' T'} + \overline{\rho' v' T'}\right)\right]$$

can be neglected as at most of order ε compared with the remaining terms in eqn. (2.2.8). Here $\bar{h} = c_p\bar{T}$ is the mean specific enthalpy.

A further necessary relationship is the equation of state which becomes, after the introduction of mean and fluctuating quantities,

$$\bar{p} = R\left(\bar{\rho}\,\bar{T} + \overline{\rho' T'}\right) \qquad (2.2.9)$$

where in many cases $\overline{\rho' T'}$ is assumed small compared with $\bar{\rho}\,\bar{T}$.

The equation of state provides a relationship which is needed below in connection with Morkovin's hypothesis between the fluctuating components of pressure, density and temperature:

$$\frac{p'}{\bar{p}} = \frac{\rho'}{\bar{\rho}} + \frac{T'}{\bar{T}} + \frac{\rho' T'}{\bar{\rho}\,\bar{T}} \qquad (2.2.10)$$

Under the conditions set above the system of conservation equations has the following boundary conditions:

At $y = 0$:

$\bar{u} = 0$ (where $\bar{u}$ is the relative mean velocity between the wall and the fluid)

$\bar{v} = 0$ (impermeable wall)

$u' = v' = w' = 0$

$\bar{T} = T_w$

$\bar{\rho} = \rho_w$

At $y = \delta$:

$\bar{u} = u_\delta$

$\bar{T} = T_\delta$

$\bar{\rho} = \rho_\delta$

$\overline{u'v'} = \overline{v'T'} = 0$ (alternatively, for high free-stream turbulence these values must be known).

2.2.3 Momentum and energy transport terms

The system of conservation equations and state equations (which include those for the transport properties μ, λ etc.) contains more unknowns than equations. The essential difficulty is that described as the closure problem, in which one attempts to relate turbulence quantities, such as the double correlations $\overline{u'v'}$ and $\overline{v'T'}$ to the mean flow field.
Such a closure can in principle be achieved by using the transport equations for turbulence quantities such as Reynolds stresses, turbulent kinetic energy or heat flow $\bar{\rho}c_p\overline{v'T'}$ but again we need a much wider knowledge of the behaviour of turbulence under the influence of compressibility and heat transfer before such a general closure of the system of conservation equations will be possible. Nevertheless, attempts in this

direction have been undertaken (see references in section 2.1.2).
A second way of coping with the closure problem consists of using empirical correlations for the eddy viscosity ε_μ, defined by

$$\varepsilon_\mu = - \bar{\rho}\, \overline{u'v'}/(\partial\bar{u}/\partial y) \tag{2.2.11}$$

and for the eddy coefficient of heat transfer ε_λ, where

$$\varepsilon_\lambda = - c_p\, \bar{\rho}\, \overline{v'T'}/(\partial\bar{T}/\partial y) \ . \tag{2.2.12}$$

It is obvious that a transfer of knowledge from incompressible to compressible flow is attempted here which appears to be reasonable at first sight but may contain serious danger when one considers the different turbulence structure in subsonic and supersonic flows. Also, ε_μ and ε_λ being relations between turbulence and mean field quantities, may in principle be affected by the influence of density changes on the mean fields of $\bar{u}$ and $\bar{T}$. Indeed, this turns out to be the main complication in practice. A relationship between the two eddy coefficients is given by the definition of the turbulent Prandtl number Pr_t

$$Pr_t = \frac{\varepsilon_\mu \cdot c_p}{\varepsilon_\lambda} = \frac{\overline{u'v'}}{\overline{v'T'}} \ \frac{\partial\bar{u}/\partial y}{\partial\bar{T}/\partial y} \tag{2.2.13}$$

which has the advantage of being free from the direct influence of the mean densitiy $\bar{\rho}$. The Prandtl number will be discussed below in more detail. For laminar flow the Prandtl number is defined by

$$Pr_l = \frac{\mu c_p}{\lambda} \tag{2.2.14}$$

and the ratio γ of the specific heats c_p and c_v is a further necessary quantity specifying the properties of the fluid. For practical purposes these quantities can be treated as virtually invariant for the diatomic gases in which we are most interested.
There were only three gases used in the experiments described in AGARDograph 223 - air, nitrogen and helium. Unless specifically stated we have treated the working fluid as a perfect gas with constant specific heats. The perfect gas properties assumed are:

Gas	air	nitrogen	helium
Gas constant R in m^2/s^2 K:	287.1387	296.50	2078.739
Ratio of specific heats :	1.40	1.40	1.667

The transport properties were calculated after Keyes (1952) for the diatomic gases (minor constituents of air being ignored) and Neubert (1974) for helium.
For the diatomic gases the expression

$$\mu = \frac{10^{-6}\, a_o\, T^{1/2}}{1 + a\, T^{-1}\, 10^{-a_1/T}} \ Ns/m^2 \tag{2.2.15}$$

was used, where the constants and the range of validity are given as

	a_o	a	a_1	range of validity
air:	1.488	122.1	5	$79 < T/K < 1845$
nitrogen:	1.418	116.4	5	$81 < T/K < 1695.$

These relations were used also at lower temperatures down to 50 K for lack of better information. For helium the expression

$$\mu = \left[\frac{50.23\ T^{0.647}}{1+ T^{0.5}\ (T-0.3)\ e^{-T/\ (T-0.3)}} + e^{-T}\ (61.2730T^3 - 199.1754T^2 + 179.1353T - 59.05466\right]$$

$$\times\ 10^{-8}\ Ns/m^2 \qquad (2.2.16)$$

was used, and the range of validity is $0.4 < T/K < 400$.

2.3 Principal parameters for compressible boundary layers

2.3.1 Identification of parameters

The relevant dimensionless quantities for compressible turbulent boundary layers can be obtained by a formal scaling of the equation of motion (2.2.3) and the energy equation (2.2.8). Scaling is done by using quantities of the undisturbed free stream, such as velocity, density, temperature and transport coefficients. Here we have used

$$x = \hat{x}\ L \qquad \bar{u} = \hat{u}\ U_\infty \qquad \bar{p} = \hat{p}\ \rho_\infty\ U^2_\infty \qquad \bar{h} = \hat{h}\ h_\infty \qquad y = \hat{y}\ L$$

$$v = \hat{v}\ U_\infty \qquad \bar{\rho} = \hat{\rho}\ \rho_\infty \qquad \mu = \hat{\mu}\ \mu_\infty \qquad c_p = \hat{c}_p\ c_{p_\infty} \qquad \lambda = \hat{\lambda}\ \lambda_\infty\ .$$

If the dimensionless quantities are denoted by $\hat{}$ the equations read:

$$\hat{\bar{\rho}}\ \hat{\bar{u}}\ \frac{\partial \hat{\bar{u}}}{\partial \hat{x}} + (\hat{\bar{\rho}}\ \hat{\bar{v}} + \widehat{\overline{\rho' v'}})\ \frac{\partial \hat{\bar{u}}}{\partial y} = -\frac{\partial \hat{\bar{p}}}{\partial x} + \frac{1}{Re_\infty}\ \frac{\partial}{\partial y}\ (\hat{\mu}\ \frac{\partial \hat{\bar{u}}}{\partial y}) - \frac{\partial}{\partial y}\ (\hat{\bar{\rho}}\ \widehat{\overline{u'v'}}) \qquad (2.3.1)$$

$$\hat{\bar{\rho}}\ \hat{\bar{u}}\ \frac{\partial \hat{\bar{h}}}{\partial x} + (\hat{\bar{\rho}}\ \hat{\bar{v}} + \widehat{\overline{\rho' v'}})\ \frac{\partial \hat{\bar{h}}}{\partial y} = (Pr_\infty\ Re_\infty)^{-1}\ \frac{\partial}{\partial y}\ (\frac{\hat{\lambda}}{c_p}\ \frac{\partial \hat{\bar{h}}}{\partial y}) - \frac{\partial}{\partial y}\ (\hat{\bar{\rho}}\ \widehat{\overline{v'T'}})$$

$$+ (\gamma-1)\ M^2_\infty\ \hat{\bar{u}}\ \frac{\partial \hat{\bar{p}}}{\partial x} + (\gamma-1)\ M^2_\infty\ [\hat{\mu}(\frac{\partial \hat{\bar{u}}}{\partial y})^2\ \ Re^{-1}_\infty - \hat{\bar{\rho}}\ \widehat{\overline{u'v'}}\ \frac{\partial \hat{\bar{u}}}{\partial \hat{y}}\ ] \qquad (2.3.2)$$

(note that as a result of assuming the fluid to be a perfect gas, $\hat{c}_p$ equals one).

The Reynolds number appears explicitly in those terms which denote viscous effects or heat conduction. The Mach number is found in combination with both "pressure work" and viscous dissipation, i. e. with terms indicating the changes in the mean flow which result from compressibility and dissipation effects which are of much greater importance in supersonic than in subsonic boundary layer flow.

Taking into account variable transport properties causes a further difficulty, in that it is no longer obvious at which position in the boundary layer the transport properties should be defined. Values are required for the formation of the characteristic parameters of the boundary layer problem, mainly in the Reynolds and Prandtl numbers. One rather unscientific way out of this difficulty is the definition of a "reference temperature", at which the transport properties are determined. For the purposes of this discussion we will assume that experimental results may be treated as though the test wall is either adiabatic or isothermal. Under these circumstances the recovery temperature T_r, at which there would be no heat transfer, can be reasonably defined (see eqn. 2.5.38) and a simple heat transfer parameter is obtained as the ratio T_w/T_r. For a discussion of other possibilities see Walz (1966).

A constant pressure compressible boundary layer will therefore be specified by the following parameters

Reynolds number Re (specification still open), heat transfer parameter Tw/Tr, and
Mach number $M_\delta = u_\delta/a_\delta$

(where δ denotes the free-stream edge of the boundary layer) as variables of the first importance, and by Prandtl number and the ratio of the specific heats as specific properties of the fluid.

2.3.2 Reynolds number

So far we have used a definition for the Reynolds number based on quantities of the free-stream or, more precisely, on the undisturbed free-stream and on the "body" length scale L. A Reynolds number so defined is clearly not characteristic of a boundary layer which should at least contain a characteristic boundary layer thickness δ'. As mentioned above a problem also occurs in deciding at what position in the boundary layer density and viscosity should be determined. This specification is made difficult by the large variations in the fluid properties and by the much increased influence of the thermal boundary condition. The physical explanation of the Reynolds number as the ratio of momentum flux to shear stress, might be interpreted as the ratio of the maximum values, which are, to a first approximation, the momentum flux at the outer edge of the boundary layer $\rho_\delta u^2_\delta$ and the shear stress at the wall τ_w. Substituting τ_w by $\mu_w (\partial\bar{u}/\partial y)_w$ and the gradient by u_δ/δ', where δ' is some characteristic boundary layer thickness, yields:

$$\frac{\rho_\delta u^2}{\tau_w} = \frac{\rho_\delta u^2_\delta}{\mu_w (\partial\bar{u}/\partial y)_w} \qquad \frac{\rho_\delta u^2_\delta}{\mu_w u_\delta/\delta'} = \frac{\rho_\delta u_\delta \delta'}{\mu_w} \tag{2.3.3}$$

When δ' is specified for example by the momentum loss thickness δ_2

$$\delta_2 = \int_0^\delta \frac{\bar{\rho}\,\bar{u}}{\rho_\delta u_\delta} \left(1 - \frac{\bar{u}}{u_\delta}\right) dy \tag{2.3.4}$$

then we arrive at, as a definition for the Reynolds number in a boundary layer

$$Re_{\delta_2} = \rho_\delta u_\delta \delta_2 / \mu_w \,. \tag{2.3.5}$$

This formulation - not a derivation - of a characteristic Reynolds number was first advocated by Walz (1966) in a formal arrangement of the skin friction coefficient. The use of the wall shear stress, and hence the viscosity at the wall, in forming the Reynolds number, would also seem to follow from the fact that τ_w is the characteristic shear stress throughout the viscous sublayer. As the Mach number rises, this region increases in relative thickness and gains in importance. In contrast to the subsonic case where the sublayer is mostly of negligible thickness, it may even be expected (Morkovin 1960) "that with continued increase in Mach number, the low-density, low-mass flux "wall layer" would occupy most of the boundary layer thickness and would be topped by a thinner turbulent region of sufficiently high Reynolds number per unit length to maintain itself". This tendency for the low Reynolds number characteristics of the wall region to encroach on and dominate the layer as a whole is very apparent in the experimental results - in §§ 3, 4 we will frequently remark on the apparent low Reynolds number behaviour of boundary layers which to the experimenter were fully turbulent. Indeed, although the specification of Re_{δ_2} in eqn. (2.3.5) is not definitive and can finally only be justified by empirical success as a correlating parameter, there is, as discussed above, some physical justification for hoping that it will so serve. This cannot be said for the conventional, widespread definition of momentum thickness Reynolds number

$$Re_\Theta = \rho_\delta u_\delta \delta_2 / \mu_\delta \tag{2.3.6}$$

which demonstrably ceases to be an effective specifying parameter in compressible flows.
The reader of pre-1966 papers (and some later authors) should be especially careful, as often the Reynolds number is formed using property values for either an intermediate temperature or for an intermediate position in the boundary layer, and these arbitrary definitions are not infrequently used without a proper declaration. The difference between Re_{δ_2} and Re_Θ steadily increases with Mach number - the variation with both Mach number and heat transfer parameter Tw/Tr is shown in figures 6.1 - 6.3 of AG 223 - and we have chosen here and in AG 223 to give both values, Re_{δ_2} as the most representative parameter, and Re_Θ as the value in most general use. The distinction is of course specially important when considering phenomena at low or transitional Reynolds numbers.

2.3.3 Pressure gradient

We also require some form of a pressure gradient parameter. This does not emerge explicitly from the conservation equations. Such a parameter can, however, be derived in several ways. One form is obtained by comparing the pressure gradient to the shear stress times a characteristic boundary layer thickness:

$$\frac{dp/dx}{\tau_w} \cdot \delta' = -\frac{\rho_\delta u_\delta}{\tau_w} \frac{du_\delta}{dx} \delta' = \frac{\rho_\delta u_\delta \delta'}{\mu_w} \frac{du_\delta/dx}{(\partial \bar{u}/\partial y)_w} \simeq Re_{\delta'} \cdot \frac{-du_\delta/dx}{u_\delta/\delta'}$$

When the characteristic thickness δ' is taken as δ_2 one obtains the pressure gradient parameter which has for a long time been used for incompressible turbulent boundary layers,

$$\Pi_2 = -\frac{\rho_\delta u_\delta \delta_2}{\tau_w} \frac{du_\delta}{dx} = \frac{\delta_2}{\tau_w} \frac{dp}{dx} \tag{2.3.7}$$

In a few catalogue entries Π_2 was calculated but very often the distances between the free-stream velocity measurements were too large to permit an accurate determination of the gradient du_δ/dx.

Clauser (1956) in his work on constant density equilibrium boundary layers was possibly the first to show that a parameter of this type, Π_1, using δ_1, as the characteristic length, provided an adequate pressure gradient parameter for this restricted class of flows. Π_1 is also suggested by the raw form of the boundary layer integral equation

$$\frac{d}{dx}(\rho_\delta u^2_\delta \delta_2) = \tau_w + \delta_1 \frac{dp}{dx}$$

though the strict conditions for similarity cannot be satisfied. In a variable density flow where

$$\delta_1 = \int_0^\delta (1 - \frac{\bar{\rho}\bar{u}}{\rho_\delta u_\delta}) \, dy \tag{2.3.8}$$

we doubt that a general correlation can be achieved with Π_1 as parameter since cases can occur for which δ_1 becomes negative. As an example, see the flow with strong acceleration and wall cooling studied by Back & Cuffel (1972 - CAT 7207 series 01).

Π_2 has one disadvantage which it shares with Π_1 in that it tends toward infinity in the case of flow separation. This can be avoided by using the alternative second definition

$$\Pi_2^* = -\frac{du_\delta/dx}{u_\delta/\delta_2} \cdot Re_{\delta_2} \tag{2.3.9}$$

In supersonic flow, the pressure field is not adequately described by its streamwise derivative alone. Principally as a result of the large ratio between dynamic head and static pressure, substantial pressure variations may occur normal to the wall on which a boundary layer grows. An outline of the factors involved is given in § 5, while a detailed consideration of the pressure field in the boundary layer is given in § 6. Here we note that a parameter is required to express the likely importance of the normal pressure gradient and we propose the quantity

$$SW = (\partial\Theta/\partial x) \,/\, (\partial\nu/\partial x) \tag{2.3.10}$$

which represents the degree to which a change in Prandtl-Meyer angle (ν), and so Mach number, is associated with a change in flow direction (Θ), or streamwise curvature.

2.3.4 The hypersonic regime

We have not, in this section, made any attempt to draw a distinction between the "supersonic" and the "hypersonic" regime - and consider any such attempt unrewarding. As M_δ increases, there is no possible simplification of the equation of motion in the boundary layer as a result of being able to assume

$M^2 >> 1$ - as in many gasdynamic applications. If any such distinction is to be made, it would for this purpose, be related to some basic change in the relative importance of the turbulent terms, for example by defining a "hypersonic turbulent flow" as one for which Morkovin's hypothesis (§ 2.4) has demonstrably broken down,or where chemical reactions have to be taken into account due to the high total enthalpy of the high Mach number flow. It is not possible to say that this occurs for M larger than any particular value.

2.4 Morkovin's hypothesis

It is difficult to perceive how strongly the terms $\overline{u'v'}$, $\overline{v'T'}$, and $\overline{\rho'v'}$ are influenced by compressibility by direct inspection of eqns. (2.3.1) and (2.3.2). The Mach number appears explicitly only in the dissipation term of the energy equation which contains $\overline{u'v'} \cdot \partial\bar{u}/\partial y$. As $\partial\bar{u}/\partial y$ tends to zero in the outer layer and $\overline{u'v'}$ towards the wall, the product of the two may be smaller than the first term containing $(\partial\bar{u}/\partial y)^2$ only. The term $\overline{\rho'v'}$ need not be considered here since it can be eliminated by means of the continuity equation (2.2.1).
In order to obtain an estimate of the importance of the fluctuating quantities we examine the definition of total enthalpy H in a boundary layer. For instantaneous quantities H is defined:

$$H = c_p T_o = c_p T + 1/2\ (u^2 + v^2 + w^2)\ . \tag{2.4.1}$$

After the introduction of mean and fluctuating quantities this equation can be written for a two-dimensional flow as

$$\frac{T_o'}{\bar{T}_o} = \frac{T'}{\bar{T}_o} + \frac{\bar{u}^2}{c_p \bar{T}_o}\,\frac{u'}{\bar{u}} + \frac{1}{c_p \bar{T}_o}\,\frac{1}{2}\,[u'^2 + 2\,\bar{v}\,v' + \bar{v}^2 + v'^2 + w'^2]\ . \tag{2.4.2}$$

When fluctuation terms are sufficiently small for second order terms to be neglected (a condition which embraces the region of validity of the hot-wire anemometer at high speeds) one can write with some rearrangement (Morkovin 1960)

$$\frac{T_o'}{\bar{T}_o} = \frac{T'}{\bar{T}}\,\left(1 + \frac{\gamma-1}{2}\,\bar{M}^2\right)^{-1} + \frac{u'}{\bar{u}}\,\frac{(\gamma-1)\,\bar{M}^2}{1+\frac{\gamma-1}{2}\,\bar{M}^2}\ . \tag{2.4.3}$$

Under the additional assumption that $T_o'/\bar{T}_o$ is an order smaller than the two remaining terms (confirmed by measurements e.g. Kistler (1959) in boundary layers along adiabatic walls) - this is called the "strong Reynolds analogy" statement by Morkovin (1960) - we can write

$$\frac{T'}{\bar{T}} = -\,(\gamma-1)\,\bar{M}^2\,\frac{u'}{\bar{u}}\ . \tag{2.4.4}$$

Using eqn. (2.2.10) yields for $T'/\bar{T}$

$$\frac{T'}{\bar{T}} = -\,\frac{\rho'}{\bar{\rho}} - \frac{\rho'T'}{\bar{\rho}\,\bar{T}} + \frac{P'}{\bar{P}} \tag{2.4.5}$$

and neglecting pressure fluctuations and second order terms one obtains

$$\frac{T'}{\bar{T}} = -\,\frac{\rho'}{\bar{\rho}} = -\,(\gamma-1)\,\bar{M}^2\,\frac{u'}{\bar{u}}\ . \tag{2.4.6}$$

Eqn. (2.4.6) was given by Morkovin (1960, eqn. 8). Bradshaw & Ferris (1971) deduced from this equation that if $\rho'/\bar{\rho}$ is small the turbulence structure is not affected by compressibility effects and called this **Morkovin's hypothesis.**

As in the outer region of a boundary layer the velocity fluctuations are usually small and the Mach number large, $(\overline{T'^2})^{1/2}/\bar{T}$ is nowhere larger than 0.1 even at a Mach number 5. Under the above assumptions temperature and density fluctuations do not influence the turbulence field significantly up to at least a Mach number of 5. This means that the knowledge of the turbulence structure gained in subsonic flow can be extended to supersonic flow.

2.5 Analytical solutions of the energy equation

2.5.1 The total enthalpy equation

Further insight into the relation between the mean velocity and the mean temperature field can be gained by deriving an equation for the mean total enthalpy. This can be achieved by multiplying eqn. (2.2.3) by $\bar{u}$ and adding this equation for the mechanical energy to the thermal energy equation (2.2.8). After some rearrangement and writing

$$\bar{H} = \bar{h} + \bar{u}^2/2 \quad \text{(mean total enthalpy per unit mass)} \tag{2.5.1}$$

one obtains

$$\bar{\rho}\,\bar{u}\,\frac{\partial \bar{H}}{\partial x} + (\bar{\rho}\,\bar{v} + \overline{\rho' v'})\,\frac{\partial \bar{H}}{\partial y} = \frac{\partial}{\partial y}\left(\frac{\bar{\mu}}{Pr}\frac{\partial \bar{H}}{\partial y}\right) + \frac{\partial}{\partial y}\left[\bar{u}\,\frac{Pr-1}{Pr}\,\bar{\mu}\,\frac{\partial \bar{u}}{\partial y}\right]$$

$$- \frac{\partial}{\partial y}\left[\bar{u}\,\bar{\rho}\,\overline{u'v'} + c_p\,\bar{\rho}\,\overline{v'T'}\right]. \tag{2.5.2}$$

This equation is identical with eqn. (155) of Howarth (1953) if due account is taken of eqn. (2.4.2), ignoring the terms in square brackets in the latter equation. Eqn. (2.5.2) has the following boundary conditions:

$y = 0$:

$\bar{u} = \bar{v} = 0; \quad \overline{u'v'} = \overline{v'T'} = \overline{\rho'v'} = 0; \quad \bar{H} = c_p T_w;$

$y = \delta$:

$\bar{u} = u_\delta; \quad \overline{u'v'} = \overline{v'T'} = 0; \quad \bar{H} = c_p T_\delta + u^2_\delta/2.$

Under the special conditions Pr = 1 and $(\bar{u}\,\bar{\rho}\,\overline{u'v'} + c_p\,\bar{\rho}\,\overline{v'T'})$ independent of y or zero, eqn. (2.5.2) has a particular solution, H = constant, which was first published by Busemann (1931) for laminar boundary layers. This solution will be discussed and extended for values of the Prandtl number smaller but close to one in § 2.5.4. While the assumption Pr ≃ 1 needs little justification for the technically important gases, it is less obvious under which conditions $(\bar{u}\,\bar{\rho}\,\overline{u'v'} + c_p\,\bar{\rho}\,\overline{v'T'})$ may be assumed to be independent of the coordinate y or even be zero. Neglecting second order terms in eqn. (2.4.2), multiplying the remaining terms by $\bar{\rho}\,v'$ and taking the temporal mean, yields

$$\bar{\rho}\,c_p\,\overline{v'T'_o} = \bar{\rho}\,c_p\,\overline{v'T'} + \bar{\rho}\,\bar{u}\,\overline{u'v'}. \tag{2.5.3}$$

Now for adiabatic flow Morkovin (1960) has shown that

$(\overline{v'T'_o})/\overline{v'T'}) \ll 1$ which, inserted into eqn. (2.5.3)

leaves us with

$$\bar{\rho}\,c_p\,\overline{v'T'} + \bar{\rho}\,\bar{u}\,\overline{u'v'} \simeq 0. \tag{2.5.4}$$

Eqn. (2.5.4) shows further that subject to the above condition $c_p\,\overline{v'T'}$ must be of the same order as $\bar{u}\,\overline{u'v'}$.

Another possible line of argument starts from the energy equation for instantaneous quantities. Comparing this equation for H with the equation for $\bar{H}$, in which the temporal mean was taken, allows the conclusion that if $\partial\bar{H}/\partial y = 0$, for the particular solution giving $\bar{H}$ = constant, then $\partial H/\partial y$ is very likely to be zero,

implying that $\partial H'/\partial y$ must be zero also. This reasoning leads to

$$\frac{\partial}{\partial y}\left(\bar{\rho}\, c_p\, \overline{v'T'} + \bar{\rho}\, \bar{u}\, \overline{u'v'}\right) = 0 \,. \tag{2.5.5}$$

The case for accepting this result is further developed in Howarth (1953).

2.5.2 The total enthalpy integral

The special case of adiabatic flow is clearly of the greatest interest both experimentally and theoretically. It is difficult to ensure that a test wall is in fact truly adiabatic, and one of the most important experimental criteria available is that there be a zero streamwise growth rate of the total enthalpy integral across the boundary layer. If we integrate eqn. (2.5.2) with respect to y from zero to a "D-state" well outside the boundary layer, we obtain

$$\int_0^D \left[\bar{\rho}\,\bar{u}\,\frac{\partial \bar{H}}{\partial x} + \left(\bar{\rho}\bar{v} + \overline{\rho' v'}\right)\frac{\partial \bar{H}}{\partial y}\right] dy - \left[\frac{\bar{\mu}}{Pr}\,\frac{\partial \bar{H}}{\partial y} + \frac{Pr-1}{Pr}\,\bar{u}\,\mu\,\frac{\partial \bar{u}}{\partial y}\right]_0^D + \left[\bar{u}\bar{\rho}\,\overline{u'v'} + c_p\,\bar{\rho}\,\overline{v'T'}\right]_0^D = 0 \,. \tag{2.5.6}$$

An evaluation of the second and third term in connection with the boundary conditions of eqn. (2.5.2) yields

$$\int_0^D \left[\bar{\rho}\,\bar{u}\,\frac{\partial \bar{H}}{\partial x} + \left(\bar{\rho}\,\bar{v} + \overline{\rho' v'}\right)\frac{\partial \bar{H}}{\partial y}\right] dy + \lambda_w \left(\frac{\partial \bar{T}}{\partial y}\right)_w = 0 \,. \tag{2.5.7}$$

It should be noted here that a number of the "conventional" assumptions at the boundary layer edge have been made. For instance, assuming that $(\partial \bar{u}/\partial y)_D = 0$ and $(\partial \bar{T}/\partial y)_D = 0$ implies, probably correctly, that molecular transfer terms at the boundary layer edge are negligible. Less satisfactory in a windtunnel flow is the assumption that the term $(\bar{u}\,\bar{\rho}\,\overline{u'v'})_D$ does not contribute to the energy balance as although $\overline{u'v'}$ does fall off, many experimental facilities have a strongly turbulent freestream flow, and $\bar{u}\,\bar{\rho}$ is a large term at the D-point.

Generally, particularly in high Mach number facilities, both the choice of the D-point (see § 7 below) and the free-stream turbulence rate require a careful assessment. Otherwise one is easily led to erroneous estimates of the total energy content of the boundary layer and to wrong conclusions about the existence and/or magnitude of the so-called overshoot (see § 2.5.6 below).

After differentiation, rearrangement and taking account of the continuity equation (2.2.1), eqn. (2.5.7) yields:

$$\frac{d}{dx}\int_0^D \bar{\rho}\,\bar{u}\,(\bar{H} - H_D)\, d y + \lambda_w \left(\frac{\partial \bar{T}}{\partial y}\right)_w = 0$$

and after integration between two streamwise positions x_1 and x_2

$$\left[\int_0^D \bar{\rho}\,\bar{u}\,(\bar{H} - H_D)\, dy\right]_{x_1}^{x_2} = -\int_{x_1}^{x_2} \lambda_w \left(\frac{\partial \bar{T}}{\partial y}\right)_w dx \,. \tag{2.5.8}$$

On the left-hand side we have the difference in the rate of flux of total enthalpy, integrated across the boundary layer, between the fixed positions x_1 and x_2 and on the right-hand side the heat flux at the wall between the same fixed positions x_1 and x_2.

For an adiabatic wall the right-hand side of eqn. (2.5.8) is zero and, by assuming that at $x = 0$ $\bar{H} = H_D$, one obtains

$$H_D = \left(\int_0^D \bar{\rho}\,\bar{u}\,\bar{H}\, dy\right)\Big/\left(\int_0^D \bar{\rho}\,\bar{u}\, dy\right). \tag{2.5.9}$$

This latter equation is often used as a check as to whether a flow is truly adiabatic when both total pressure and total temperature profiles across the boundary layer are available.
Equations (2.5.8) and (2.5.9) are formally the same as those for compressible laminar boundary layers which can be found in Howarth (1953 p. 397).

2.5.3 The mean temperature distribution

Since it is impossible to determine the mean velocity profile in a compressible turbulent boundary layer without knowing the temperature distribution across the boundary layer, Morkovin (1960) is certainly correct in stating that "the second cornerstone of analytical and empirical evaluations of skin friction and heat transfer lies in the correct determination of the mean static or stagnation temperature profiles". It is therefore extremely fortunate that we know of two exact solutions giving relations between the mean static enthalpy $\bar{h}$ or the mean static temperature $\bar{T}$ and the mean velocity $\bar{u}$ in which the parameters are the Mach number, the ratio of the specific heats, and a heat transfer parameter. We shall first discuss these particular solutions of the energy equation for Prandtl number equal to one and then extend the discussion to a Prandtl number range $0.70 \leq Pr \leq 1$.

2.5.3.1 The mean temperature distribution for Pr = 1 in a boundary layer along an adiabatic wall

As already mentioned in § 2.5.1 the equation for the mean total enthalpy (2.5.2) has the particular solution $\bar{H}$ equals constant under the conditions that the Prandtl number is unity and that the term $(\bar{u}\,\bar{\rho}\,\overline{u'v'} + \bar{\rho}\,c_p\,\overline{v'T'})$ is zero or independent of y. A justification for this latter condition was given in § 2.5.1. The solution $\bar{H}$ = constant satisfies the boundary conditions of eqn. (2.5.2) only if one requires that $(\partial\bar{H}/\partial y)_w = 0$, i.e. according to eqn. (2.5.1) that $(\partial\bar{T}/\partial y)_w$ be zero. This implies that the heat transfer between the fluid and the wall must be zero. Now if $\bar{H}$ is constant across the boundary layer, then the following relationship holds

$$c_p\,\bar{T} + \bar{u}/2 = c_p\,T_\delta + u^2{}_\delta/2 \tag{2.5.10}$$

and noting that (e.g. Busemann in Wien, Harms 1931)

$$(u^2{}_\delta/2)/c_p\,T_\delta = (\gamma-1)\,M^2{}_\delta/2 \tag{2.5.11}$$

one obtains

$$\frac{\bar{T}}{T_\delta} = 1 + \frac{\gamma-1}{2}\,M^2{}_\delta\,\left[1 - \left(\frac{\bar{u}}{u_\delta}\right)^2\right]. \tag{2.5.12}$$

Eqn. (2.5.12) holds for both laminar and turbulent boundary layers for all pressure gradients dp/dx under the condition Prandtl number unity and zero heat transfer at the wall.
The reader should note that this solution cannot describe correctly the temperature distribution at the outer edge of an adiabatic boundary layer due to the limitation that the Prandtl number has been assumed to be unity (see § 2.5.4.1).

For the boundary condition y = 0 and $\bar{u}$ = 0 eqn. (2.5.12) yields a relationship for the so called adiabatic wall temperature (again for Pr = 1),

$$(T_w)_{ad} = T_\delta\,\left(1 + \frac{\gamma-1}{2}\,M^2{}_\delta\right). \tag{2.5.13}$$

The temperature difference $(T_w)_{ad} - T_\delta$ denotes the temperature increase of an adiabatic wall due to compressibility effects.
If eqn. (2.5.12) is re-written in terms of the total temperature it reduces to

$$\frac{T_{o\delta}}{(T_w)_{ad}} = \frac{T_{o\delta}}{T_o} = 1 \tag{2.5.14}$$

The temperature-velocity relationship expressed by eqn. (2.5.12) was given for laminar boundary layers by Busemann (1935) and Crocco (1932).

2.5.3.2 The mean temperature distribution for a boundary layer with zero pressure gradient along an isothermal wall. In this paragraph we discuss the second analytical solution of the energy equation. For this purpose we need the assumptions that the pressure gradient dp/dx is zero and that the temperature of the wall is constant. Furthermore the Prandtl number range will be restricted.

The following equations were derived in principle by van Driest (in Lin 1959) who, however, used the concepts of the eddy coefficients of friction ε_μ and heat transfer ε_λ resulting in a mixed Prandtl number Pr_m

$$Pr_M = \frac{c_p\,(\mu + \varepsilon_\mu)}{\lambda + \varepsilon_\lambda} \tag{2.5.15}$$

We think it more advantageous to keep the molecular Prandtl number $Pr = \mu c_p/\lambda$ and the turbulent Prandtl number Pr_t (cf. eqn. 2.5.18) apart in the terms of the following equations and present therefore a slightly different derivation for the $\bar{T} - \bar{u}$ relationship. For this it is convenient to substitute the term $(\bar{\rho}\,\bar{v} + \overline{\rho' v'})$ in the energy equation (2.2.5) by means of the equation of motion (2.2.3) and to introduce $\tau_l = \mu \partial\bar{u}/\partial y$ resulting in

$$\bar{\rho}\,\bar{u}\,\frac{\partial \bar{h}}{\partial x} + \frac{\mu}{\tau}\frac{\partial \bar{h}}{\partial y}\left[\frac{\partial \tau_l}{\partial y} - \frac{\partial}{\partial y}\left(\bar{\rho}\,\overline{u'v'}\right) - \bar{\rho}\,\bar{u}\,\frac{\partial \bar{u}}{\partial x} - \frac{d\bar{p}}{dx}\right] - \bar{u}\,\frac{d\bar{p}}{dx}$$

$$= \frac{\partial}{\partial y}\left(\frac{\mu}{Pr}\frac{\partial \bar{h}}{\partial y}\right) - \frac{\partial}{\partial y}\left(\bar{\rho}\,c_p\,\overline{v'T'}\right) + \frac{\tau_l^2}{\mu} - \frac{\bar{\rho}}{\mu}\tau_l\,\overline{u'v'}\,. \tag{2.5.16}$$

The independent variables x and y are now replaced by ξ and $\bar{u}$ using the Crocco transformation $\bar{u} = \bar{u}(\xi, y)$ and $x = \xi$. Hence eqn. (2.5.16) becomes

$$\tau_l^2\left[1 + \frac{\partial}{\partial \bar{u}}\left(\frac{1}{Pr}\frac{\partial \bar{h}}{\partial \bar{u}}\right)\right] + \frac{\tau_l}{Pr}\frac{\partial \bar{h}}{\partial \bar{u}}\frac{\partial \tau}{\partial \bar{u}}(1-Pr) - \mu\,\bar{\rho}\,\bar{u}\,\frac{\partial \bar{h}}{\partial \xi} + \mu\,\frac{d\bar{p}}{d\xi}\left(\bar{u} + \frac{\partial \bar{h}}{\partial \bar{u}}\right)$$

$$+ \left[\frac{\tau_l}{Pr_t}\frac{\partial \bar{h}}{\partial \bar{u}}\frac{\partial}{\partial \bar{u}}\left(\bar{\rho}\,\overline{u'v'}\right)\right](Pr_t - 1) - \bar{\rho}\,\overline{u'v'}\,\tau_l\left[1 + \frac{\partial}{\partial \bar{u}}\left(\frac{1}{Pr_t}\frac{\partial \bar{h}}{\partial \bar{u}}\right)\right] = 0 \tag{2.5.17}$$

where the Prandtl number for turbulent flows is defined as

$$Pr_t = \frac{\overline{u'v'}}{\overline{v'T'}}\,\frac{\partial \bar{T}/\partial y}{\partial \bar{u}/\partial y} = \frac{\overline{u'v'}}{\overline{v'h'}}\,\frac{\partial \bar{h}/\partial y}{\partial \bar{u}/\partial y}\,. \tag{2.5.18}$$

So far we do not have an analytical solution for eqn. (2.5.17) and it is necessary to introduce further simplifications. One possible assumption is that the pressure gradient in the streamwise direction, $d\bar{p}/d\xi = d\bar{p}/dx$, be zero which implies that $\partial \bar{h}/\partial \xi = 0$. Eqn. (2.5.17) then reduces to

$$\tau_l\left[1 + \frac{\partial}{\partial \bar{u}}\left(\frac{1}{Pr}\frac{\partial \bar{h}}{\partial \bar{u}}\right)\right] + \frac{\partial \bar{h}}{\partial \bar{u}}\left[\frac{1-Pr}{Pr}\frac{\partial \tau_l}{\partial \bar{u}} - \frac{1-Pr_t}{Pr_t}\frac{\partial}{\partial \bar{u}}\left(\bar{\rho}\,\overline{u'v'}\right)\right]$$

$$- \bar{\rho}\,\overline{u'v'}\left[1 + \frac{\partial}{\partial \bar{u}}\left(\frac{1}{Pr_t}\frac{\partial \bar{h}}{\partial \bar{u}}\right)\right] = 0\,. \tag{2.5.19}$$

A simple solution for eqn. (2.5.19) can be given for laminar boundary layers where $\overline{u'v'}$ is zero and if it is further assumed that the Prandtl number is unity. The resulting relationship was - though derived in a different manner - published independently by Crocco (1932)[+)] and Busemann (1935).

+) This date is given by Schlichting (1965). The original source has not been consulted.

Under these assumptions eqn. (2.5.19) yields

$$\frac{\partial^2 \bar{h}}{\partial \bar{u}^2} = -1 \tag{2.5.20}$$

which with eqn. (2.5.11) and the boundary conditions

$$\left.\begin{aligned} y = 0 &: \bar{u} = 0; \quad T_w = \text{constant} \\ y = \delta &: \bar{u} = u_\delta; \quad \bar{T} = T_\delta \end{aligned}\right\} \tag{2.5.21}$$

gives

$$\frac{\bar{T}}{T_\delta} = \frac{T_w}{T_\delta} + \left(1 - \frac{T_w}{T_\delta}\right)\frac{\bar{u}}{u_\delta} + \frac{\gamma-1}{2} M_\delta^2 \left(1 - \frac{\bar{u}}{u_\delta}\right)\frac{\bar{u}}{u_\delta} . \tag{2.5.22}$$

If the adiabatic wall temperature, eqn. (2.5.13), is introduced one obtains the alternative form:

$$\frac{\bar{T}}{T_\delta} = \frac{T_w}{T_\delta} + \frac{(T_w)_{ad} - T_w}{T_\delta}\frac{\bar{u}}{u_\delta} - \frac{\gamma-1}{2} M_\delta^2 \left(\frac{\bar{u}}{u_\delta}\right)^2 . \tag{2.5.22a}$$

Eqn. (2.5.22) is strictly valid only for laminar boundary layers with zero pressure gradient, constant wall temperature and Prandtl number unity. It is commonly referred to as the Crocco-relationship (e.g. Rotta 1964).

For a discussion of the solutions which are obtained from eqn. (2.5.20) when boundary conditions, different from (2.5.21) are used, the reader is referred to Rotta (1964).
In the case of an adiabatic wall, when $(T_w)_{ad} = T_w$, eqn. (2.5.22a) becomes identical with eqn. (2.5.12).

Another form of eqn. (2.5.22) which is often used for comparison with measurements follows after some rearrangement

$$\frac{\bar{T}_o - T_w}{T_{o_\delta} - T_w} = \frac{\bar{H}_o - H_w}{\bar{H}_{o_\delta} - H_w} = \frac{\bar{u}}{u_\delta} \tag{2.5.22b}$$

and is sometimes called the "linear" temperature-velocity relationship.

The range of validity of these two equations can be extended to turbulent boundary layers if one assumes that both Prandtl numbers, Pr and Pr_t, are one. The pressure gradient dp/dx must, of course, be zero and the wall temperature constant. Under these conditions eqn. (2.5.19) yields formally the same solution, i.e. eqn. (2.5.22). The difference in the temperature profile for laminar and turbulent flows with the same boundary conditions will then be caused only by the different velocity profiles.

Before we proceed to further analytical solutions of the energy equation which hold also for a Prandtl number in the range $0.70 \leq Pr \leq 1$, van Driest's (1955) form of the energy equation will be given which is essentially identical with eqn. (2.5.19).

$$\tau\left[\frac{\partial}{\partial \bar{u}}\left(\frac{1}{Pr_M}\frac{\partial \bar{h}}{\partial \bar{u}}\right) + 1\right] + \frac{1-Pr_M}{Pr_M}\frac{\partial \bar{h}}{\partial \bar{u}}\frac{\partial \tau}{\partial \bar{u}} = 0 \tag{2.5.23}$$

where $\tau = \mu \, \partial\bar{u}/\partial y - \bar{\rho}\,\overline{u'v'}$ and the mixed Prandtl number Pr_M is defined by eqn. (2.5.15).
Eqn. (2.5.23) is easier to handle than eqn. (2.5.19) though one cannot distinguish any longer between the development of the molecular and the turbulent Prandtl number across the boundary layer. For ease of handling we shall henceforth use eqn. (2.5.23) while retaining eqn. (2.5.19) briefly for discussion in § 2.5.4.2 below.

2.5.4 A semi-empirical temperature distribution for $Pr \neq 1$

Van Driest extended Crocco's (1946) analysis for an arbitrary but constant Prandtl number to a "variable Prandtl number theory" for both laminar (1954) and turbulent (1955) compressible boundary layers. The aim of van Driest's investigation was largely to determine theoretically the Reynolds analogy and recovery factors for compressible boundary layers with zero pressure and wall temperature gradients in streamwise direction ($dp/dx = 0$ and T_w = constant). Walz (1956, 1959) has further developed van Driest's work to arrive at an extended form of the Crocco temperature velocity relationship (2.5.22). His version (eqn. 2.5.37) allows for constant Prandtl numbers in the range $0.7 \leq Pr \leq 1$ which covers all technically important gases. The modification becomes the more significant as the Mach number of the flow is increased. The van Driest-Walz approach is outlined below.

2.5.4.1 Solutions of equation (2.5.23). Following Crocco, or, for a turbulent boundary layer, Van Driest (1955) a rearrangement of eqn. (2.5.23) leads to the following dimensionless equation

$$\left(\frac{\bar{h}_*}{Pr_M}\right)' + (1-Pr_M)\,\frac{\tau'}{\tau}\,\left(\frac{\bar{h}_*}{Pr_M}\right) = -(\gamma-1)\,M_\delta^2 \qquad (2.5.24)$$

which is a linear, first-order differential equation in $(\bar{h}'/Pr_M)$ as a function of $\bar{u}_*$ at constant x. The symbols $\bar{h}_*$ and $\bar{u}_*$ denote $\bar{h}/h_\delta$ and $\bar{u}/u_\delta$ respectively, and the primes indicate differentiation with respect to $\bar{u}_*$ alone.
After integration - for details see van Driest (in Lin 1959) - eqn. (2.5.24) becomes

$$\bar{h}_*(\bar{u}_*) = \bar{h}_*(0) + [1-\bar{h}(0)]\,\frac{S^*(\bar{u}_*)}{S^*(1)} + (\gamma-1)\,M_\delta^2\,\left[\frac{S^*(\bar{u}_*)}{S^*(1)}\,R^*(1) - R^*(\bar{u})\right]. \qquad (2.5.25)$$

Eqn. (2.5.25) gives the enthalpy distribution for a turbulent boundary layer from the wall to the outer edge under the conditions $dp/dx = 0$ and constant wall temperature and was first given in this form by van Driest (1955).

The integrals $S^*(\bar{u}_*)$ and $R^*(\bar{u}_*)$ are defined by

$$S^*(\bar{u}_*) = \int_0^1 Pr_M \exp\left(-\int_{\tau_w}^{\tau} \frac{(1-Pr_M)}{\tau}\,d\tau\right) d\bar{u}_* \qquad (2.5.26)$$

and

$$R^*(\bar{u}_*) = \int_0^1 Pr_M \exp\left\{-\int_{\tau_w}^{\tau} \frac{1-Pr_M}{\tau}\,d\tau\right\}\left[\int_0^{\bar{u}_*} \exp\left(\int_{\tau_w}^{\tau} \frac{1-Pr_M}{\tau}\,d\tau\right) d\bar{u}\right] d\bar{u}_* . \qquad (2.5.27)$$

S (1) is a general expression for the Reynolds-analogy factor

$$S^*(1) \equiv s^* = \int_0^1 Pr_M \exp\left(-\int_{\tau_w}^{\tau} (1-Pr_M)\,\frac{d\tau}{\tau}\right) d\bar{u}_* \qquad (2.5.28)$$

and $R^*(1)$ a general expression for the recovery factor

$$2\,R^*(1) \equiv r^* = 2\int_0^1 Pr_M \exp\left[-\int_{\tau_w}^{\tau} (1-Pr_M)\,\frac{d\tau}{\tau}\right]$$

$$\left\{\int_0^1 \exp\left[\int_{\tau_w}^{\tau} (1-Pr_M)\,\frac{d\tau}{\tau}\right] d\bar{u}_*\right\} d\bar{u}_* . \qquad (2.5.29)$$

Now, eqn. (2.5.25) can only be solved if the Prandtl number and the shear stress distributions are known in order to evaluate integrals (2.5.26) to (2.5.29). Under the assumption that the Prandtl number is constant but may assume values different from unity eqns. (2.5.26) to (2.5.29) can be written (for laminar flows these equations were originally given by Crocco):

$$S^*_{Pr_M}(\bar{u}_*) = Pr_M \int_0^{\bar{u}_*} \left[\frac{\tau}{\tau_w}\right]^{Pr_M-1} d\bar{u}_* = Pr_M \cdot S(\bar{u}_*), \tag{2.5.30}$$

$$R_{Pr_M}(\bar{u}_*) = Pr_M \int_0^{\bar{u}_*} \left\{\left[\frac{\tau}{\tau_w}\right]^{Pr_M-1} \int_0^{\bar{u}_*} \left[\frac{\tau}{\tau_w}\right]^{1-Pr_M} d\bar{u}_*\right\} d\bar{u}_* = Pr_M \; R(\bar{u}_*), \tag{2.5.31}$$

$$S^*_{Pr_M}(1) = Pr_M \int_0^{1} \left[\frac{\tau}{\tau_w}\right]^{Pr_M-1} d\bar{u}_* = s, \tag{2.5.32}$$

and

$$2R^*_{Pr_M}(1) = 2 \int_0^{1} \left\{\left[\frac{\tau}{\tau_w}\right]^{Pr_M-1} \int_0^{1} \left[\frac{\tau}{\tau_w}\right]^{1-Pr_M} d\bar{u}_*\right\} d\bar{u}_* = r. \tag{2.5.33}$$

For a constant mixed Prandtl number Pr_M eqn. (2.5.25) then yields

$$\bar{h}_*(\bar{u}_*) = \bar{h}_*(0) + [1-\bar{h}_*(0)] \frac{Pr_M S(\bar{u}_*)}{s} + \frac{\gamma-1}{2} r M_\delta^2 \left[\frac{Pr_M S(\bar{u}_*)}{s} - \frac{2 Pr_M R(\bar{u}_*)}{r}\right]. \tag{2.5.34}$$

Eqn. (2.5.34) was first given by Walz (1956, published 1959) who introduced a further assumption, namely

$$\frac{Pr_M S(\bar{u}_*)}{s} \simeq \bar{u}_* \quad \text{and} \quad \frac{2 Pr_M R(\bar{u}_*)}{r} \simeq \bar{u}_*^2 \tag{2.5.35}$$

As an inspection of eqns. (2.5.30) and (2.5.31) shows, these relationships can hold only if the Prandtl number is close to unity, say in the range $0.7 \leq Pr_M \leq 1$, which is the case for technically important gases. Introducing the relationships (2.5.35) into eqn. (2.5.34) yields

$$\bar{h}(\bar{u}_*) = \bar{h}_*(0) + [1-\bar{h}_*(0)] \; \bar{u}_* + r \frac{\gamma-1}{2} M_\delta^2 [\bar{u}_* - \bar{u}_*^2] \tag{2.5.36}$$

or for constant specific heat c_p

$$\bar{T}/T_\delta = (T_w/T_\delta) + [1 + r \frac{\gamma-1}{2} M_\delta^2 - T_w/T_\delta] (\bar{u}/u_\delta) - r \frac{\gamma-1}{2} M_\delta^2 (\bar{u}/u_\delta)^2. \tag{2.5.37}$$

Differentiating eqn. (2.5.36) with respect to y and assuming zero heat transfer at the wall, which results in $(\partial\bar{h}/\partial y)_{y=0} = 0$, one obtains for the temperature at the wall, now called the recovery temperature T_r

$$T_r = T_\delta (1+r \frac{\gamma-1}{2} M_\delta^2). \tag{2.5.38}$$

Eqn. (2.5.38) was originally derived by van Driest (1955) using eqn. (2.5.25) and given empirically by Ackermann (1942) and H.B. Squire (1942). Both authors, however, used a function dependent on the Prandtl number instead of the recovery factor as defined by eqn. (2.5.33) (see Schubauer & Tchen in Lin 1959). Since all the quantities in eqn. (2.5.38) can be determined from measurements when the wall is adiabatic, this equation is often used for an experimental determination of the recovery factor as

$$r = \frac{T_r - T_\delta}{T_0 - T_\delta}. \tag{2.5.38a}$$

If the recovery temperature is introduced into eqn. (2.5.37), the temperature velocity relationship reads

$$\frac{\bar{T}}{T_\delta} = 1 + \frac{T_r - T_w}{T_\delta}\left(\frac{\bar{u}}{u_\delta} - 1\right) + r\,\frac{\gamma-1}{2}\,M_\delta^2\,\left[1 - \left(\frac{\bar{u}}{u_\delta}\right)^2\right] \tag{2.5.37a}$$

or

$$\frac{\bar{T}}{T_\delta} = \frac{T_w}{T_\delta} + \frac{T_r - T_w}{T_\delta}\,\frac{\bar{u}}{u_\delta} - r\,\frac{\gamma-1}{2}\,M_\delta^2\,\left(\frac{\bar{u}}{u_\delta}\right)^2 . \tag{2.5.37b}$$

When r = 1 eqn. (2.5.37b) is identical with eqn. (2.5.22a), as derived for Pr = 1.
The equations listed under (2.5.37) have been called Walz's equations (e.g. Voisinet & Lee 1973).
Likewise, after some rearrangement, another form of eqn. (2.5.37) is

$$\frac{\bar{T}_o - T_w}{T_{o\delta} - T_w} = \frac{T_r - T_w}{T_{o\delta} - T_w}\,\frac{\bar{u}}{u_\delta} + \frac{T_{o\delta} - T_r}{T_{o\delta} - T_w}\left(\frac{\bar{u}}{u_\delta}\right)^2 \tag{2.5.37c}$$

which may again be compared with eqn. (2.5.22b) derived for Pr = 1.
Eqn. (2.5.37c) may also be written

$$\frac{\bar{T}_o - T_w}{T_{o\delta} - T_w} = \beta\,\frac{\bar{u}}{u_\delta} + (1-\beta)\left(\frac{\bar{u}}{u_\delta}\right)^2 \tag{2.5.37d}$$

where $\beta = \dfrac{T_r - T_w}{T_{o\delta} - T_w}$ (see Danberg 1971).

Danberg calls eqn. (2.5.37d) "a well known modification of the Crocco temperature velocity relationship".
Still another form of eqn. (2.5.37) is mentioned by Rotta (1965) and called case I or Crocco's solution:

$$\frac{\bar{T}_o}{T_{o\delta}} = \frac{T_w}{T_{o\delta}} + \frac{T_r - T_w}{T_{o\delta}}\,\frac{\bar{u}}{u_\delta} + \left[1 - \frac{T_r}{T_{o\delta}}\right]\left(\frac{\bar{u}}{u_\delta}\right)^2 \tag{2.5.37e}$$

For Prandtl number unity equation (2.5.37e) becomes identical with eqn. (2.5.22b) since $T_r \to T_{o\delta}$.

A special case of this temperature-velocity relationship is obtained for zero heat transfer at the wall, i.e. for an adiabatic wall. Then eqn. (2.5.37a) for example reduces to

$$\left(\frac{\bar{T}}{T_\delta}\right)_{(q_w=0)} = 1 + r\,\frac{\gamma-1}{2}\,M_\delta^2\,\left[1 - \left(\frac{\bar{u}}{u_\delta}\right)^2\right] \tag{2.5.39}$$

which again is equivalent to eqn. (2.5.12) for Prandtl number unity. Another form of eqn. (2.5.39) - sometimes called the modified Crocco equation - follows immediately from eqn. (2.5.37c) for $T_w = T_r$, i.e. for zero heat transfer:

$$\frac{T_o - T_r}{T_{o\delta} - T_r} = \left(\frac{\bar{u}}{u_\delta}\right)^2 \tag{2.5.40}$$

Probably because of the similar form of eqn. (2.5.39) and (2.5.12) the validity range of the former equations is sometimes extended to flows with pressure gradients in the main stream direction along adiabatic walls. Since no analytical solution for these boundary conditions is known, eqn. (2.5.39) may represent a reasonable first order approximation for the temperature distribution where the Prandtl number differs from unity and lies in the range $0.7 \leq Pr_M \leq 1$. Eqn. (2.5.40) is recommended as being especially suitable for boundary layers in wind tunnel nozzles by many authors, irrespective of upstream and local temperature conditions at the wall or upstream and local pressure gradients in the main stream direction or normal to the wall.
Eqn. (2.5.40) is sometimes called the "quadratic" temperature velocity relationship in comparison to the

"linear" temperature-velocity relationship eqn. (2.5.22b) derived for Prandtl number unity.
If "linear" and "quadratic" relationships are used in the same figure for a comparison with measured data, then the pairs of comparable equations (2.5.14 & 2.5.22b) and (2.5.40 & 2.5.37c) should be taken. Unfortunately this simple rule is neglected by many authors.
Table (2.5.1) gives a summary of the temperature velocity relationships derived so far and their status and restrictions.

Table 2.5.1 Temperature-velocity relationships for compressible turbulent boundary layers

Number	Equation	Status	Restrictions
(2.5.12)	$\bar{T}/T_\delta = 1 + [(\gamma-1)/2]\, M_\delta^2\, [1-(\bar{u}/u_\delta)^2]$	exact	Pr = 1; adiabatic wall ;
(2.5.14)	$H_\delta/H_w = 1$	exact	$(\bar{u}\,\bar{\rho}\,\overline{u'v'} + \bar{\rho}\, c_p\, \overline{v'T'}) \neq f(y)$
(2.5.22)	$\bar{T}/T_\delta = (T_w/T_\delta) + [1-(T_w/T_\delta)]\,(\bar{u}/u_\delta) + [(\gamma-1)/2]\, M_\delta^2\, [(\bar{u}/u_\delta) - (\bar{u}/u_\delta)^2]$	exact	Pr = 1; Pr_t = 0; dp/dx = 0;
(2.5.22b)	$(T_o-T_w)/(T_{oD}-T_w) = (\bar{H}_o-H_w)/(\bar{H}_{o_\delta}-H_w) = \bar{u}/u_\delta$	exact	T_w = constant
(2.5.39)	$\bar{T}/T_\delta = 1 + r\,[(\gamma-1)/2]\, M_\delta^2\, [1-(\bar{u}/u_\delta)^2]$	based on eqn. (2.5.25)	Pr_M = constant and $0.7 \leq Pr_M \leq 1$;
(2.5.40)	$(\bar{T}_o-T_r)/(T_{o\delta}-T_r) = (\bar{u}/u_\delta)^2$		dp/dx = 0; adiabatic wall
(2.5.39) (2.5.40)	These equations are used for flows with pressure gradients in mainstream direction along adiabatic walls because of their form which is similar to eqns. (2.5.12) and (2.5.14).	semi-empirical	Pr_M = constant and $0.7 \leq Pr_M \leq 1$; adiabatic wall
(2.5.37a)	$\bar{T}/T_\delta = (T_w/T_\delta) + [1+r[(\gamma-1)/2]M_\delta^2 - (T_w/T_\delta)]\,(\bar{u}/u_\delta) - r\,[(\gamma-1)/2]\, M_\delta^2\, (\bar{u}/u_\delta)^2$	based on eqn. (2.5.25)	Pr_M = constant and $0.7 \leq Pr_M \leq 1$;
(2.5.37d)	$(\bar{T}_o-T_w)/(T_{o\delta}-T_w) = [(T_r-T_w)/(T_{o\delta}-T_w)](\bar{u}/u_\delta) + [(T_{o\delta}-T_r)/(T_{o\delta}-T_w)]\,(\bar{u}/u_\delta)^2$		dp/dx = 0; T_w = constant
(2.5.37e)	$\bar{T}_o/T_{o\delta} = (T_w/T_{o\delta}) + [(T_r-T_w)/T_{o\delta}]\,(\bar{u}/u_\delta) + [1-(T_r/T_{o\delta})]\,(\bar{u}/u_\delta)^2$		

2.5.4.2 A discussion of equation (2.5.19). If the boundary layer is divided into a viscous sublayer where the influence of viscosity dominates over that of the turbulence terms and into an outer region where the turbulence terms dominate over the viscous shear stress, then eqn. (2.5.19) can be simplified and reduces to

$$\tau_1\, [1 + \frac{\partial}{\partial\bar{u}}\,(\frac{1}{Pr}\,\frac{\partial\bar{h}}{\partial\bar{u}})] + \frac{\partial\bar{h}}{\partial\bar{u}}\,[\frac{1-Pr}{Pr}\,\frac{\partial\tau_1}{\partial\bar{u}}] \simeq 0 \qquad (2.5.41)$$

and

$$\bar{\rho}\,\overline{u'v'}\,[1 + \frac{\partial}{\partial\bar{u}}\,(\frac{1}{Pr_t}\,\frac{\partial\bar{h}}{\partial\bar{u}})] + \frac{\partial\bar{h}}{\partial\bar{u}}\,[\frac{1-Pr_t}{Pr_t}\,\frac{\partial}{\partial\bar{u}}\,(\bar{\rho}\,\overline{u'v'})] \simeq 0 \qquad (2.5.42)$$

respectively.
For constant but non-unity Prandtl number the respective solution for eqns. (2.5.41) and (2.5.42) is formally given by eqn. (2.5.34) where the mixed Prandtl number Pr_M must be substituted by the molecular Prandtl number Pr or the turbulent Prandtl number Pr_t respectively. Since Pr ≃ 0.72 and Pr_t ≃ 0.90 (e.g. Lin 1959), it remains to match the two solutions somehow in the buffer layer. This could be achieved by a straight line to a first order approximation. We shall comment again on Prandtl number distributions in § 2.6.4.

2.5.5 Other semi-empirical temperature distributions

Numerous attempts have been made to find analytical expressions for temperature distributions in turbulent boundary layers. Among those which have come to our attention we have chosen a few, none of which appears to us in any way better than the relations derived in § 2.5.4. This may be due to the fact that the authors of these semi-empirical relationships were short of measurements which could be used for a comparison or did not care to present comparisons over a wider range of data. For a survey of pre-1958 attempts to find relationships between the static temperature and the mean velocity $\bar{u}$ the reader is referred to Schubauer & Tchen in Lin (1959).

2.5.5.1 Zero pressure gradient and adiabatic wall. Schubauer & Tchen (Lin 1959) suggested a semi-empirical temperature-velocity relation with "variable recovery factor", starting from the following equation written in a form similar to eqn. (2.5.10)

$$c_p \bar{T} + \frac{1}{2} r\,(y)\,\bar{u}^2 = c_p T_\delta + \frac{1}{2} r_\delta\, u_\delta^2 = (c_p T_w)_{q_w=0}.$$

This yields

$$\frac{\bar{T}_o}{T_{o\delta}} = \frac{T_w}{T_{o\delta}} + \alpha\,(1 - \frac{T_w}{T_{o\delta}})\,(\frac{\bar{u}}{u})^2 \qquad (2.5.43)$$

where

$$\alpha = \frac{r\,(y) - 1}{r\,(\delta) - 1}.$$

If the distribution of the recovery factor is chosen suitably, eqn. (2.5.43) can represent a total temperature distribution with an overshoot.
A further analytical expression for the temperature as a function of the velocity was given by Whitfield & High (1977) in adiabatic or constant wall temperature boundary layers with constant but non-unity Prandtl numbers. Here the Reynolds stress was assumed to be proportional to the local turbulent kinetic energy in the boundary layer

$$\tau = u_\tau^2\, \rho\, \exp\,(-4\eta^{5/2})$$

where $\eta = y/\delta$ was approximated by $(\bar{u}/u_\delta)^m$ and inserted into eqn. (2.5.23).
This results in a second-order, non-linear ordinary differential equation for which zeroth and first-order perturbation solutions were obtained in terms of the small parameter $\epsilon = 1 - Pr_M$. For the adiabatic wall case the solution permits the calculation of the total temperature overshoot and is apparently used at AEDC for data reduction. Comparisons with measurements were performed for data given by Gates (1973), Danberg (1964), Hopkins & Keener (1972), and Bertram & Neal (1965). Some of these data, however, do not show an overshoot (the reader is also referred to Laderman (1977) who found good agreement with the theoretical prediction suggested by Whitfield & High). Finally Hopkins & Keener (1972) presented an empirical relation

$$\frac{\bar{T}_o - T_w}{T_{o\delta} - T_w} = (\bar{u}/u)^{1.66}$$

which was found to fit their data and was used to determine total temperatures in the region between the innermost probe measurement and the wall. This relationship comes close to eqn. (2.5.40) which is valid for zero heat transfer.

2.5.5.2 Zero pressure gradient and isothermal wall. Rotta (1960) presented a more sophisticated model for the temperature distribution. In our notation this semi-empirical relationship reads for the log-law region

$$\frac{\bar{T}}{T_w} = Pr_t \left[\beta_q \frac{\bar{u}}{u_\tau} - \frac{\gamma-1}{2} M_\tau \left(\frac{\bar{u}}{u_\tau}\right)^2 \right] + C_1 \qquad (2.5.44)$$

where M_τ and β_q are defined by eqns. (3.2.8) and (3.2.9) respectively and the "constant" of integration C_1 is determined from experiments as

$$C_1 = 1 - 3.4 \beta_q - 0.2 M_\tau \ . \qquad (2.5.45a)$$

Bradshaw (1976, 1977b) gives another relationship for C_1

$$C_1 = 5.2 + 95 M_\tau^2 - 30.7 \beta_q - 226 \beta_q^2 \ . \qquad (2.5.45b)$$

Bradshaw states "that the trends of the two equations (2.5.45 a and b) are quite different except for the rise in C_1 with M_τ" but he concludes "the present evidence, though inconclusive, suggests that changes in C_1 need be considered only if accuracies better than 5 to 10 % are being aimed at".

For the outer region of the boundary layer Rotta found

$$\frac{\bar{T}}{T_\delta} = \frac{T_R^*}{T_\delta} - Pr_t \frac{\gamma-1}{2} M_\delta^2 \left(\frac{\bar{u}}{u_\delta} - \frac{\bar{u}^*}{u_\delta}\right)^2 \qquad (2.5.46)$$

where

$$\bar{u}^* = (u_\tau \beta_q) / [(\gamma-1) M_\tau^2] \text{ and}$$

$$T_R^* = T_w \left\{ Pr_t \beta_q^2 \left[2 (\gamma-1) M_\tau^2\right]^{-1} \right\} + C_1 T_w$$

u^* and T_R^* are here the velocity and temperature at "a point of virtual maximum temperature".

The data used for comparison by Rotta were those of Lobb et al. (1955) and Winkler & Cha (1959) for which the important skin friction values were deduced from the slope of the velocity profile. Therefore such a comparison cannot be conclusive.

Without giving any proof, Danberg (1971) states that "for the high heat transfer or high Mach number situation, the deviation of experimental data from the Crocco relationship is known to be significant". He therefore suggests a better method of correlating temperature profile data by introducing a length scale Δ being a characteristic thermal boundary layer thickness and a characteristic enthalpy scale H_s. The non-dimensional total enthalpy H^{++} is then expressed as

$$H^{++} = \frac{1}{H_s} \int_0^H \left(\frac{\bar{\rho}}{\rho_w}\right)^{1/2} d (H-H_w) = \ln \frac{y (H_s)^{1/2}}{a_w} + C_H + 2\Pi_H \omega_H \qquad (2.5.47)$$

where $\omega_H = \sin^2 \frac{\pi}{2} \frac{y}{\Delta}$.

H_s, Δ and the two profile constants C_H and Π_H are obtained from measured temperature data by a least square method. This suggestion of an improved temperature relation cannot be regarded as established since the author has provided too little experimental evidence for comparison. Beyond this it is well known that four adjustable constants allow almost any curve fit. Since a comparison with measurements was performed in one case only (Sturek 1970) it is too early to judge how this correlation will appear when applied to other cases.

2.5.5.3 Variable pressure gradient and variable wall-temperature. Küster (1972) extended a suggestion by Cohen (1959) and Walz (in Favre 1964) to introduce the influence of the pressure and the temperature gradients, dp/dx and dT_w/dx, via two free functions c_j - with $j = 1$ and 2 - in a semi-empirical relationship which contains the exact solutions derived in § 2.5.4. The following relationship was suggested

$$\frac{H_o}{H_{o\delta}} = \frac{H_w}{H_{o\delta}} + (1-\frac{H_w}{H_{o\delta}}) [\frac{\bar{u}}{u_\delta} + \sum_{j=1}^{n} c_j (\frac{\bar{u}}{u_\delta})^j (\frac{\bar{u}}{u_\delta} -1)] - \frac{m_\delta(1-r)}{1+m_\delta} [\frac{\bar{u}}{u_\delta} - (\frac{\bar{u}}{u_\delta})^2] \qquad (2.5.48)$$

where $m_\delta = (\gamma-1) M_\delta^2/2$.
The difficulty lies in the problem of how one should determine the functions c_1 nd c_2. Küster used t'e first and second compatibility conditions but agreement with measurements was not satisfactory, judged from the few comparisons with measurements published in Küster's thesis. Nevertheless, we feel that there may be a possibility of improvement.

2.5.6 Comparison with measurements and conclusions

There exist two major comparisons between measured and theoretically predicted temperature profiles, one by Walz (Favre 1964) and the other by Rotta (1964) and both investigations share the same problems. Firstly very few reliable data were available at the time - Walz used the measurements by Lobb et al. (1955) and by Winkler & Cha (1959), Rotta those by Lobb et al., Winkler & Cha, Hill (1959), and Nothwang (1957) - and secondly neither Walz nor Rotta were aware of possible transition effects on the boundary layer profiles they had investigated. Rotta's paper (1964) - better known as Rotta (1965) - has had a widespread effect on the literature up to the present and so it seems worthwhile to repeat his main conclusions:

"(a) The measured temperature distributions in turbulent boundary layers with zero heat transfer satisfy the requirement of vanishing energy loss thickness with sufficient accuracy. ... The Crocco relation (eqn. 2.5.37) provides a good approximation to the actual temperature distribution.

(b) The temperature distributions of boundary layers on nozzle walls are not representative of those on flat plates. Obviously the temperature distributions on nozzle walls are severely affected by the upstream history. The measured temperature distributions differ greatly from the Crocco-relation.

(c) The available temperature distributions of flat plate boundary layers with heat transfer are found to be only in moderate or poor agreement with the modified Reynolds analogy. ... The measured temperature distributions display unexpected deviations from the Crocco solution.

(d) There is no evidence that the Crocco relation provides a satisfactory approximation to the temperature distribution in supersonic turbulent boundary layers with heat transfer.

(e) Obvious shortcomings of the available experimental results shed doubts on the reliability of the conclusions drawn."

Unfortunately many later authors have overlooked Rotta's important statement (e) and have happily copied (a) to (d) only.
In the meantime Rotta's plea for more experiments has been fulfilled and the survey which follows, accompanied by figures (2.5.1) to (2.5.19) and further ones in section 5 should allow a check and possibly an extension of Rotta's conclusions.

The comparison between measured temperature distributions and theoretical predictions is confined to the following boundary conditions:
Zero pressure gradient, adiabatic or isothermal wall, while the Prandtl number of the flow is assumed constant and must lie in the range $0.7 \leq Pr_M \leq 1$. If the origin of the boundary layer is defined, for instance by the known position of the leading edge of a flat plate, equations (2.5.37) to (2.5.40) can be applied and suggest three different plots: $\bar{T}_o/T_{o\delta}$, $\bar{T}/T_\delta$, nd $(\bar{T}_o-T_w)/(T_{o\delta}-T_w)$ versus $\bar{u}/u_\delta$. Though Rotta chose $\bar{T}_o/To_\delta$ versus $\bar{u}/u_\delta$ we prefer the latter two combinations. In a few cases we have also plotted $\bar{T}_o/T_{o\delta}$ for comparison.
Since there follows a rather extensive discussion of mean temperature profiles we wish to define our aims clearly. Firstly, we want to find out whether eqn. (2.5.37) provides a correct description of the temperature profile $\bar{T}/T_\delta$ as a function of $\bar{u}/u_\delta$, γ, r, and M_δ; secondly, many investigators have chosen to plot

$(\bar{T}_o-T_w)/(T_{o\delta}-T_w)$ versus $\bar{u}/u_\delta$, a version of the temperature profile plot which requires very accurate wall temperature and total temperature measurements, especially in the vicinity of the wall. Such accurate measurements do not seem to be feasible in the inner region of the boundary layer at present, and for this reason such a plot can lead to conclusions about physical effects which are - to put it mildly - at least dubious. We also wish to issue a warning here to those readers who intend to compare their theories with temperature measurements close to a wall. There are several cases where experimentalists - probably because their temperature probes were much larger than their pressure probes - extrapolated their temperature distributions towards the wall by assuming a priori the validity of certain relationships $\bar{T}=\bar{T}(\bar{u})$. Such a procedure can easily be detected if the wall distance of a measuring station is compared with the dimensions of the temperature probe in the y-direction. We have commented on such extrapolations in the "Editors' Comment" of the entries in AGARDograph 223, e.g. Jeromin (6602), Samuels et al. (CAT 6701), Voisinet & Lee (CAT 7202), Gates (CAT 7301), and Laderman & Demetriades (CAT 7403). For a comment on the latter measurements the reader is referred to Meier (1977, p. 20). In this context we should also mention that total temperature probes have been much improved over the past fifteen years. The reader is referred to the investigations of Winkler (1954), Danberg (1961), Meier (1968, 1969b), Meier et al. (1974a), Voisinet et al. (1974), Maurer & Petersen (1975), Meier (1977) and Hovstadius (1977b).

The comparisons presented here are intended to show that only the version $\bar{T}/T_\delta$ versus $\bar{u}/u_\delta$ presents a readily assessable picture from which conclusions about the validity of eqn. (2.5.37) may be drawn. The investigation is divided into two parts, the first deals with boundary layers along adiabatic walls and the second with boundary layers along isothermal walls. In both sections we shall distinguish between flows with and without upstream effects. Further details of the cases discussed are given in table 2.5.2.

Table 2.5.2 Selected temperature profile measurements

CAT	M_δ	Tw/Tr	Re_{δ_2} x 10^{-3}	Type of probe
	(i) Adiabatic wall, defined origin			
7006	4	1	0.7 - 2	ECP +)
7301	4.9	0.9-1	2.6 - 7	ECP
7305	10	1	0.2 - 1.6	STP ++)
7402	2.5-4.5	1	1.1 - 9.1	STP
	(ii) Adiabatic wall, origin not defined			
6602	2.5-3.5	1	4.3 - 9.6	ECP
7003	1.7-3.0	0.9-1	1.9 - 7.2	STP
	(iii) Isothermal wall, defined origin			
6701	6	0.4-0.5	0.9 - 3.5	STP
6702	6.5	0.5-0.9	0.3 - 1.9	ECP
7204	6.3	0.3-0.5	1.1 - 2.3	STP
7205	7.2	0.5	1.4 - 3.0	STP+FWP ++++)
7702S	3.0	0.57-1	1.4 - 2.8	BWP +++)
	(iv) Isothermal wall, origin not defined			
7202	4.9	0.2-1	1.6 - 38	ECP+FWP

+) ECP = equilibrium cone probe
++) STP = shielded temperature probe
+++) BWP = bare wire probe
++++) FWP = fine wire probe

2.5.6.1 Temperature profiles (zero-pressure gradient, adiabatic wall). Among the measurements in compressible turbulent boundary layers with zero pressure gradient along an adiabatic wall with a defined origin those of Mabey et al. (1974) seem to us very reliable, and we shall therefore make extensive use of them (see also sections 3 and 4).

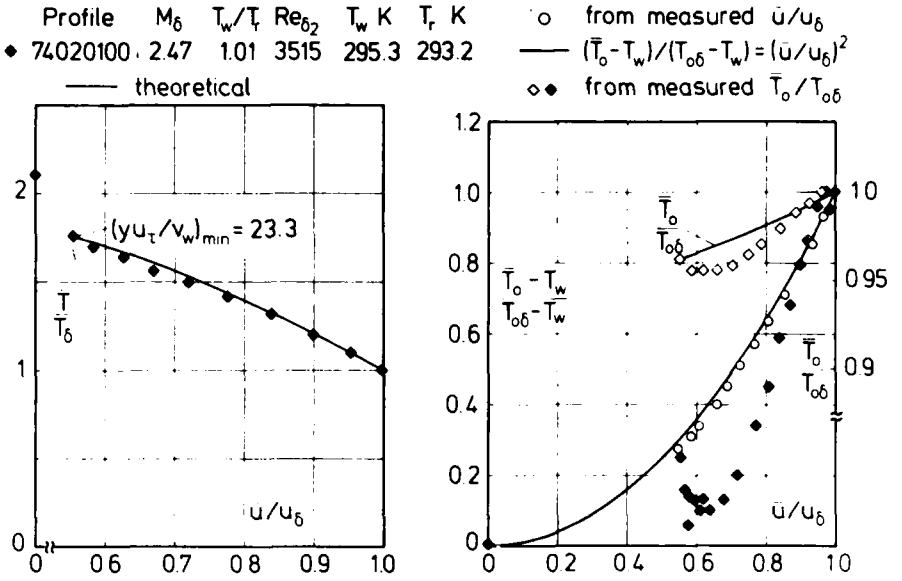

Fig. 2.5.1 Comparison between measured and theoretical temperature profiles in a boundary layer (zero pressure gradient, adiabatic wall, defined origin) Mabey et al. (1974)

Figure 2.5.1 shows a sample from their data and will be used as an example for the method of discussion of all data in this connection. The left hand graph shows a comparison of $\bar{T}/T_\delta$ as measured with the prediction of eqn. (2.5.37a). The curve shown is obtained by using as input the measured values of $\bar{u}/u_\delta$, T_w, T_δ and M_δ. γ was assumed to be 1.40, and the recovery factor r was taken to be 0.896. The measured temperature values are shown as filled diamonds, and it can be seen that agreement with the prediction of eqn. (2.5.37a) is good - the maximum deviation is less than 5 %.

The right hand graph displays firstly the data plotted in a manner designed to show how well it fits the "quadratic" relationship of eqn. (2.5.40). This relation is shown as the lower solid line. Adjacent to this are open circles which represent values of $T^* = (\bar{T}_o-T_w)/(T_{o\delta}-T_w)$ calculated from eqn. (2.5.37d) using as input the experimental values of $\bar{u}/u_\delta$. As might be expected, the two 'theoretical' values agree very closely, as any difference between them arises only from uncertainties in the selection of the recovery factor r and from lack of confidence that the wall is truly adiabatic - eqn. (2.5.40) of course here assumes that $T_w = T_r$ while eqn. (2.5.37d) does not. The directly measured data, shown as solid diamonds, apparently differ radically from the predicted curve, but as seen below, this difference is in fact illusory. A more profitable comparison is between the predicted relationship of $\bar{T}_o/T_{o_\delta}$ to $\bar{u}/u_\delta$ shown by the upper line [here calculated from eqn. (2.5.37e)] and the measured values of $\bar{T}_o/T_{o_\delta}$ and $\bar{u}/u_\delta$ shown as open diamonds. The differences in $\bar{T}_o$ do not exceed 1 % and it becomes apparent that the seemingly large differences observed in the plot of T^* against $\bar{u}/u_\delta$ arise from the fact that the ordinate represents a difference of two comparable relatively large and uncertainly determined quantities. The differences observed, in other words, arise from the sensitivity of the plotting method chosen rather than from any real physical phenomenon. This sensitivity is not necessarily undesirable - what is to be regretted is the tendency of workers in the field to emphasize differences observed in this presentation as being technically significant.

The sensitivity of the plot is further underlined in Fig.2.5.2 which shows data from two other profiles in Mabey et al. (CAT 7402). The left hand graph shows that on the $\bar{T}/T_\delta$ against $\bar{u}/u_\delta$ axes there are only very small differences between the profiles and that they are in good agreement with the theoretical curve of

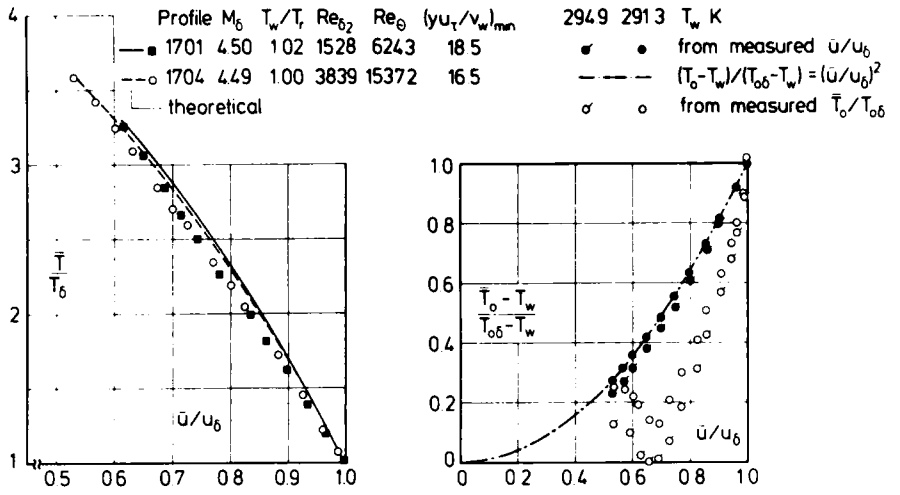

Fig. 2.5.2 Comparison between measured and theoretical temperature profiles in a boundary layer (zero pressure gradient, adiabatic wall, defined origin). Mabey et al. (1974)

eqn. (2.5.37a). For the right hand graph the data for profile 74021704 are plotted twice, using two slightly differing values for the wall temperature, both of which were given by the authors as experimental values in different stages of their work. The only difference between the experimental values (open symbols) is the small difference in T_w, but the plot apparently shows large systematic differences between the two sets, especially in the vicinity of the wall. Also shown adjacent to the line representing eqn. (2.5.40) are T^* values (filled circles) calculated from eqn. (2.5.37d) with the experimental $\bar{u}/u_\delta$ and the different values for T_w as input. The differences are again small.

The sensitivity of the plot is greatest when the flow is near-adiabatic, and we are of the opinion that those who conclude, on the basis of the popular T^* agains $\bar{u}/u_\delta$ plot, that agreement between theory and experiment is bad, have been misled by the particular characteristics of the plotting method. It is also probable that the apparent increase in T^* (and so $\bar{T}_o$) near the wall is not very important and could indeed be related to small systematic imperfections in the experimental measurement techniques.

Confidence in the theoretical relations based on eqn. (2.5.37) is of great importance, as without some temperature-velocity correlation a very great part of the data available, for which there are no temperature measurements (see AGARDograph 223, table 7.1), must be regarded as of very restricted use. We therefore propose to examine further the extent to which relations such as eqn. (2.5.37) predict the temperature satisfactorily. In the figures which follow, measured data points are indexed to their profile number in AGARDograph 223 and compared to the predictions of eqns. (2.5.37a) and (2.5.40).

Fig. (2.5.3) shows T^*-data for which we have calculated the recovery temperature T_r and have evaluated T^* with both T_r and the measured wall temperature T_w. Again the differences between the T^* data are of a magnitude which cannot have been caused by a physical effect, especially since agreement between theoretical and measured $\bar{T}/T_\delta$ -profiles is good (left hand graph). But since the increase of T^* after the sharp fall in the wall region was found to be smaller than in the measurements shown in Fig. (2.5.2), we looked for data which do not show such an increase at all (Fig. 2.5.4). For a comparison with Fig. (2.5.1) we have also plotted the $\bar{T}_o/T_{o\delta}$-profile which shows the same small deviation from the theoretical curve. The experiments described so far cover a Mach number range $2.5 \leq M_\delta \leq 4.5$ and a Reynolds number range $1500 \leq Re_{\delta_2} \leq 7600$. Earlier measurements, on the same flat plate but with an equilibrium cone probe instead of a combined temperature-pressure probe, were performed by Hastings & Sawyer (1970). These data show a very similar behaviour - good agreement for the $\bar{T}/T_\delta$-profiles and deviation in the T^*-profiles in the near wall region - however, they lack the increase of T^* near the wall, though data were taken at y^+ values as low as 18 (Fig. 2.5.5).

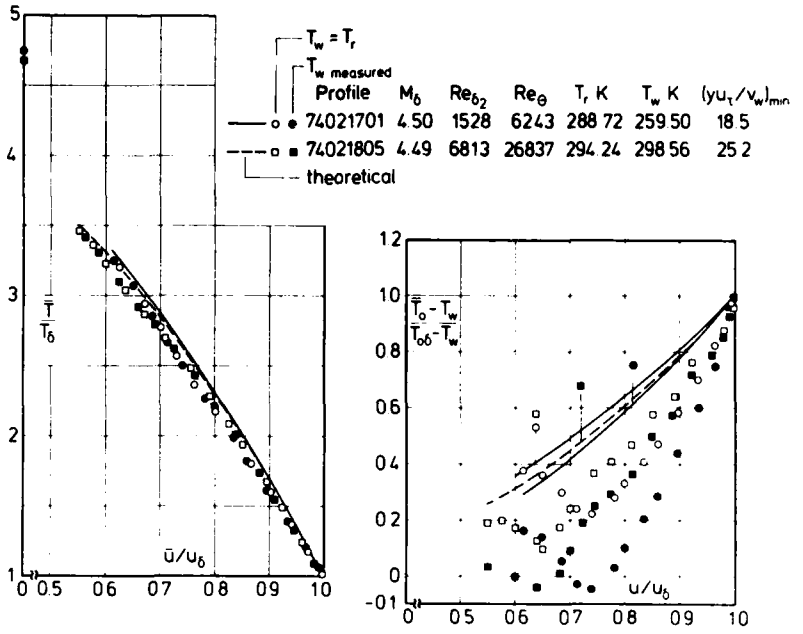

Fig. 2.5.3 Comparison between measured and theoretical temperature profiles in a boundary layer (zero pressure gradient, adiabatic wall, defined origin). Mabey et al. (1974)

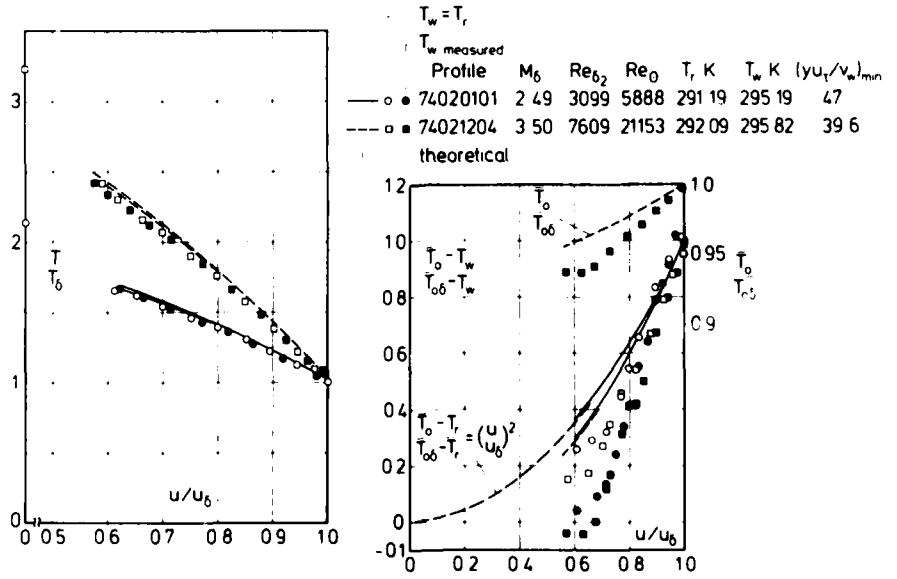

Fig. 2.5.4 Comparison between measured and theoretical temperature profiles in a boundary layer (zero pressure gradient, adiabatic wall, defined origin). Mabey et al. (1974)

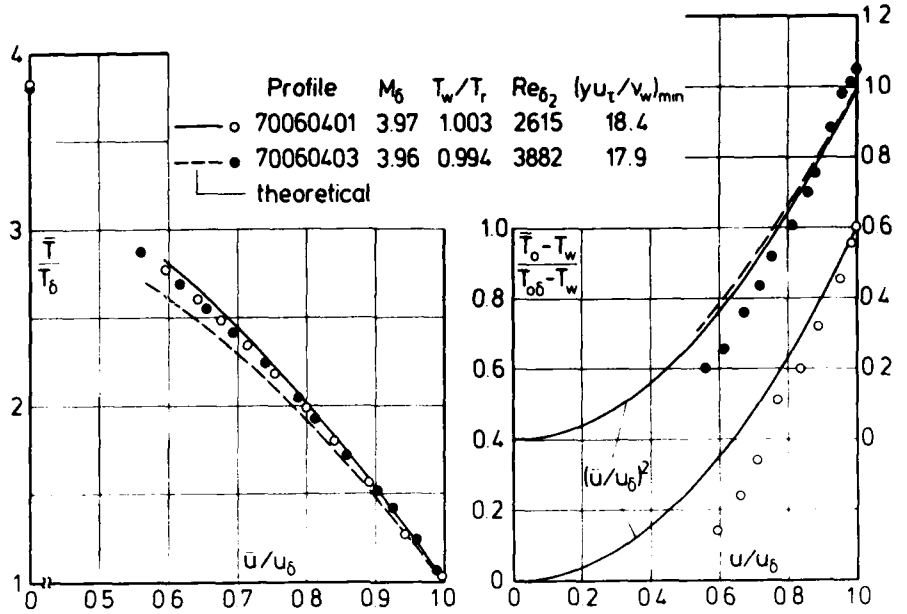

Fig. 2.5.5 Comparison between measured and theoretical temperature profiles in a boundary layer (zero pressure gradient, adiabatic wall, defined origin). Hastings & Sawyer (1970)

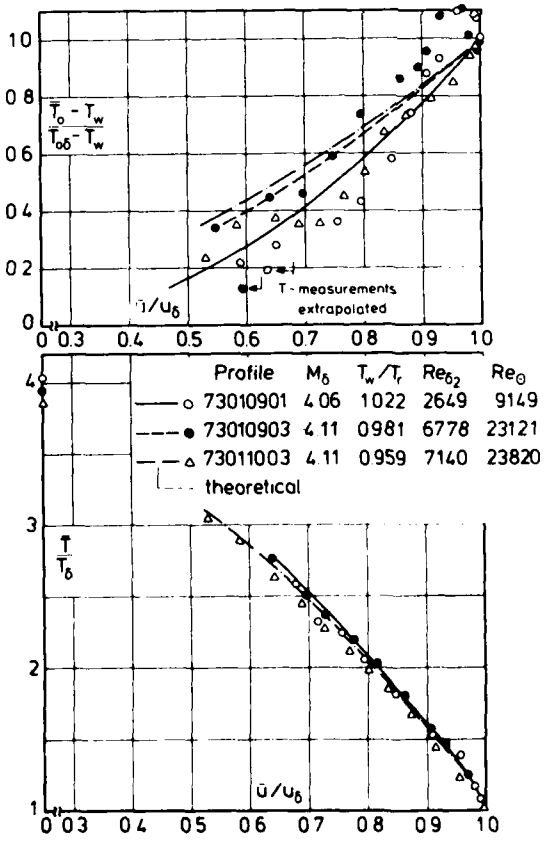

Fig. 2.5.6 Comparison between measured and theoretical temperature profiles (zero pressure gradient, adiabatic and isothermal wall, defined origin). Gates (1973)

As with the "Mabey data" some profiles show an overshoot of the total temperature profile (see § 2.5.2) but some do not. Mabey et al. (1974) investigated their temperature probe very carefully and found "that the measured temperature profiles were slightly in error (appendix C of their paper) and that an increase in total temperature of only 3^oC towards the edge of the boundary layer would be sufficient to correct the enthalpy balance". A very pronounced overshoot occurs in profile 7702 S 0103 (Fig. 2.5.16 , Laderman & Demetriades 1977), in profiles 73010901/ 0903 (Fig. 2.5.6 Gates), and in the profile plotted in Fig. (2.5.15) where we show measurements on an isothermal wall with cooling (Samuels et al. 1967). For these profiles the temperature overshoot is large enough to cause a false velocity overshoot.

Gates (1973) investigated boundary layers with different upstream histories the effect of which will be discussed later. In Fig. (2.5.6) we have plotted three temperature profiles in an approximately adiabatic boundary layer with defined origin. The leading edge region of the flat plate was uncooled for series 09 and cooled for series 10.

Since no discrepancies are discernible which go beyond the normal measuring inaccuracies, one may conclude that the upstream temperature effect was either too small to affect the downstream velocity profiles or that the temperature profiles are already back to equilibrium as they agree well with the temperature-velocity relationship (see also section 4.5). The overshoot apparently decreases with decreasing heat transfer parameter T_w/T_r. Agreement between measured and theoretical values for $\bar{T}/T_\delta$ is very good but less satisfactory for T^*, with measurements lying above and below the theoretical curve - the measurements shown so far lay all below the theoretical curve.

In Fig. (2.5.6) we draw the reader's attention to extrapolated temperature data. Such data occur in several publications but the authors' remark that some wall data were in fact extrapolated has sometimes been overlooked by theoreticians who happily compare their theoretical results with "imaginary" measurements (e.g. Shang 1973 brought to our attention by H.U. Meier). Watson et al. (1973) extended the Mach number range for boundary layers along adiabatic walls to $M_\delta = 10$ by performing measurements in helium. Agreement between measured and theoretical temperature profiles $\bar{T}/T_\delta$ is very good (Fig. 2.5.7) whereas deviations between the T^*-profiles are again large.

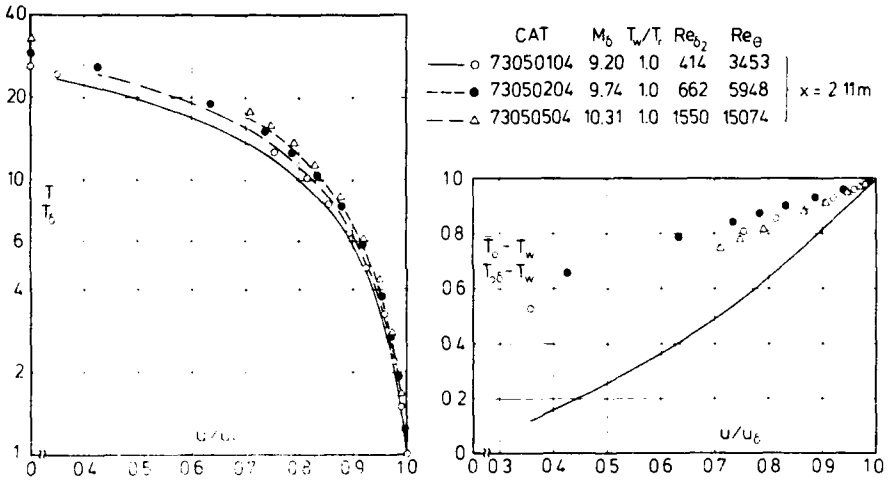

Fig. 2.5.7 Comparison between measured and theoretical temperature profiles in a boundary layer (zero pressure gradient, adiabatic wall, defined origin, helium). Watson et al. (1973)

So far we have examined only those temperature profiles where the origin of the boundary layer was clearly defined, in most cases by the leading edge of the flat plate. Apart from Winter & Gaudet (1973) who measured boundary layers with Mach numbers smaller than 3 there are only two further cases where the temperature distribution was actually measured in a boundary layer along an adiabatic wall. Jeromin (1966) measured temperature profiles on a nozzle wall at Mach numbers 2.55 and 3.58, two of which are plotted in Fig. (2.5.8). The temperature profile $\bar{T}/T_\delta$ confirms Jeromin's statement that "the Crocco-van Driest temperature-velocity relationship - here eqn. (2.5.37a) - with a recovery factor $r = 0.89$ was indistinguishable from the experimental temperature data". We find, however, a discrepancy between eqn. (2.5.40) on the one hand and

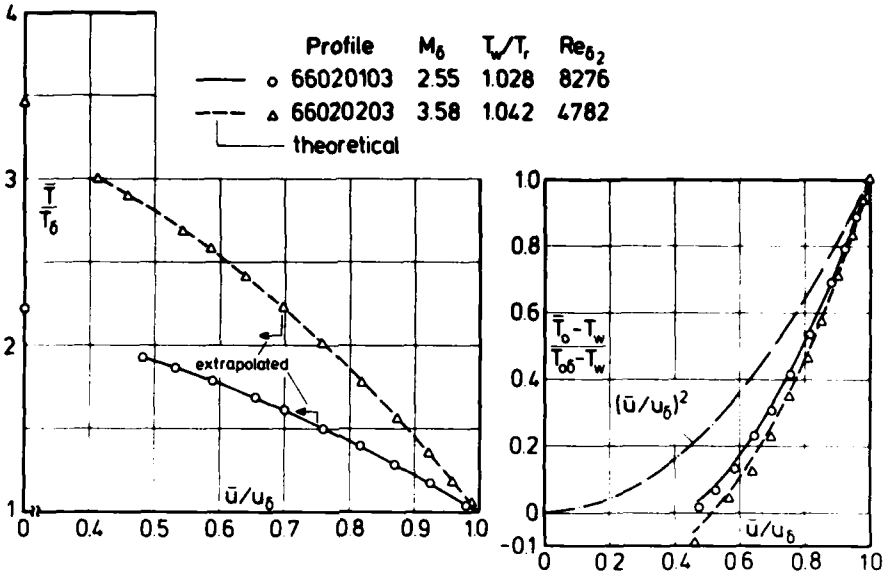

Fig. 2.5.8 Comparison between measured and theoretical temperature profiles (zero pressure gradient, adiabatic wall, origin not defined). Jeromin (1966)

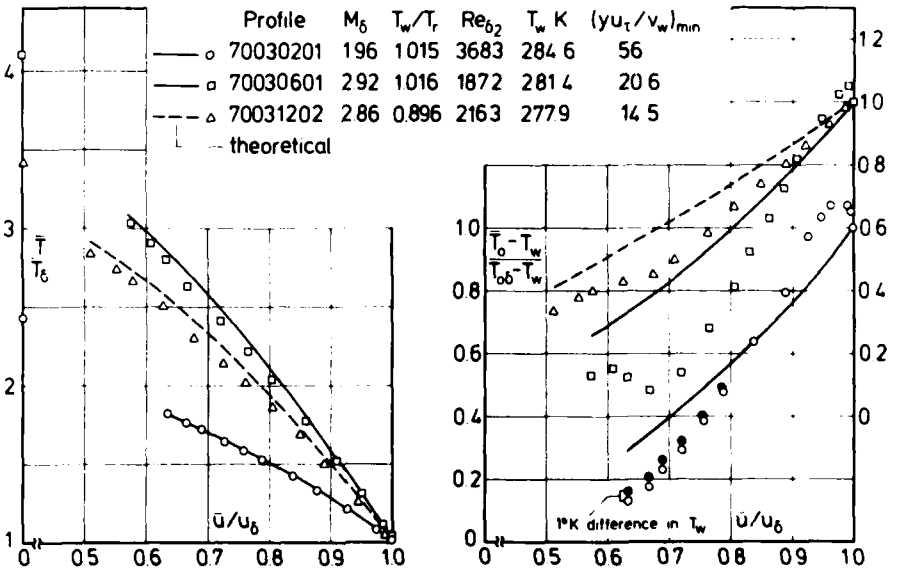

Fig. 2.5.9 Comparison between measured and theoretical temperature profiles (zero pressure gradient, adiabatic and slightly cooled wall, origin not defined). Meier (1970)

eqn. (2.5.37d) and the measured data on the other hand. This could again have been caused by small inaccuracies in the temperature measurements or because the wall is slightly heated. The measurements show no overshoot. It is interesting to compare Jeromin's measurements with those of Meier (1970) which were also performed on a flat nozzle wall (Fig. 2.5.9). From the large number of measurements two profiles were selected with zero heat transfer at the wall and one with slight cooling. For all three temperature profiles agreement between measured and theoretical $\bar{T}/T_\delta$ profiles is good but again

disagreement between the T^* data occurs. One of the measured T^*- profiles with zero heat transfer shows an increase of T^* in the wall region whereas the other does not. Both have, however, an overshoot which then disappears for the profile with slight cooling, as one might expect.

2.5.6.2 Temperature profiles (zero pressure gradient, isothermal wall). Among the measurements along isothermal walls with defined origin we have chosen those by Danberg (1967) for a detailed discussion because they seem to have been very carefully performed and exploit technique and knowledge gained in the earlier investigations by Lobb et al. (1955) and Winkler & Cha (1959). Beginning with a near-adiabatic flat plate case (Fig. 2.5.10) we find good agreement between the measured and the theoretical temperature distribution $\bar{T}/T_\delta$ and again differences in the T^* profiles, with the measurements lying this time above the theoretical curve (cf. Figs. 2.5.6 and 2.5.7). Since the Danberg temperature probe was an equilibrium cone probe (ECP) we will discuss later (Fig. 2.5.19) measurements performed with both types of probes (ECP and STP), in order to investigate whether probe effects could have caused these discrepancies. Fig. (2.5.11) shows temperature profiles with a heat transfer parameter $T_w/T_r \approx 0.55$ which agree well with the theoretical curves, both for static temperature $\bar{T}/T_\delta$ and total temperature, i.e. T^*-profiles. The same investigation contains also measurements where agreement between measured and theoretical profiles in the near wall region is less good (Fig. 2.5.12). These discrepancies become even more marked in the temperature profiles 67020104 and 0201 (Danberg) which are plotted in Fig. (2.5.13). Since the Reynolds numbers $Re_{\delta 2}$ are rather low (< 2000) we first thought of Reynolds number effects - though difficult to account for - but this argument had to be discarded when we remembered that good agreement between measurements and theory had been found for temperature profiles at much lower Reynolds numbers, such as in Fig. (2.5.10) than those presented in Fig. (2.5.12). There was, of course, the possibility that these discrepancies were specific to this experiment and other measurements in a comparable parameter range would show better agreement between measured and theoretical data. Fortunately the measurements of Horstman & Owen (1972) lie in the same parameter range though the Reynolds numbers were slightly higher (profiles 72050102 and 0103 in Fig. 2.5.13). These measurements confirm the trend of the temperature distribution predicted by the theory though deviations exist of up to 8 % between measured and theoretical data as the wall is approached. A further set of measurements, again in the same parameter range (Keener & Hopkins 1972) is shown in Fig. (2.5.14) and gives good agreement with the theoretical data though the y^+ values are bigger than those of the profiles shown in Fig. (2.5.13).

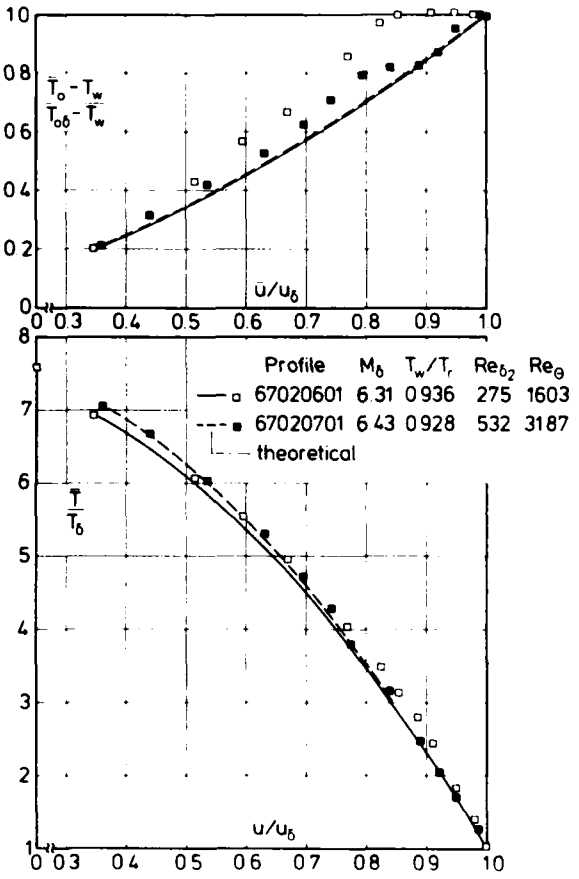

Fig. 2.5.10 Comparison between measured and theoretical temperature profiles in a boundary layer (zero pressure gradient, isothermal wall, defined origin) Danberg (1967)

We may conclude therefore that the deviations in the vicinity of the wall are specific for Danberg's measurements only.

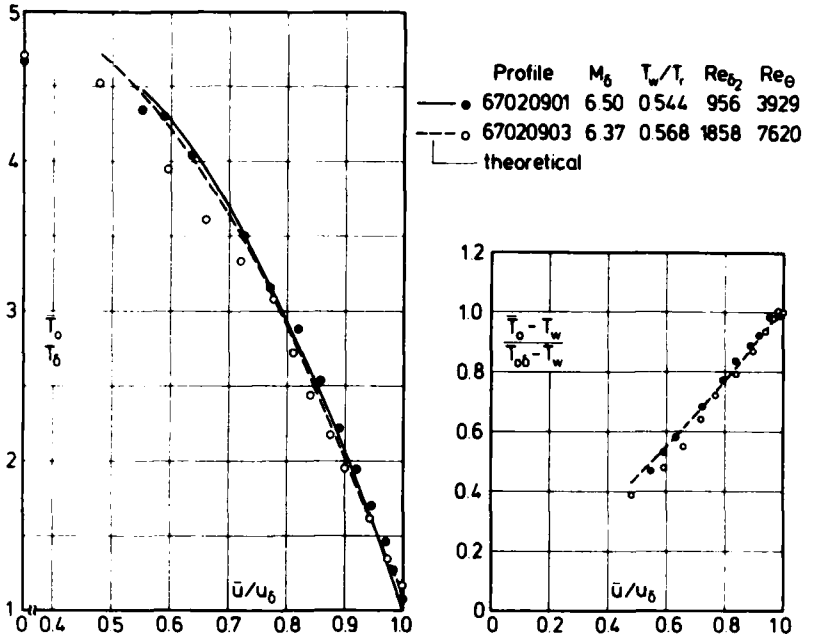

Fig. 2.5.11 Comparison between measured and theoretical temperature profiles in a boundary layer (zero pressure gradient, isothermal wall, defined origin). Danberg (1967)

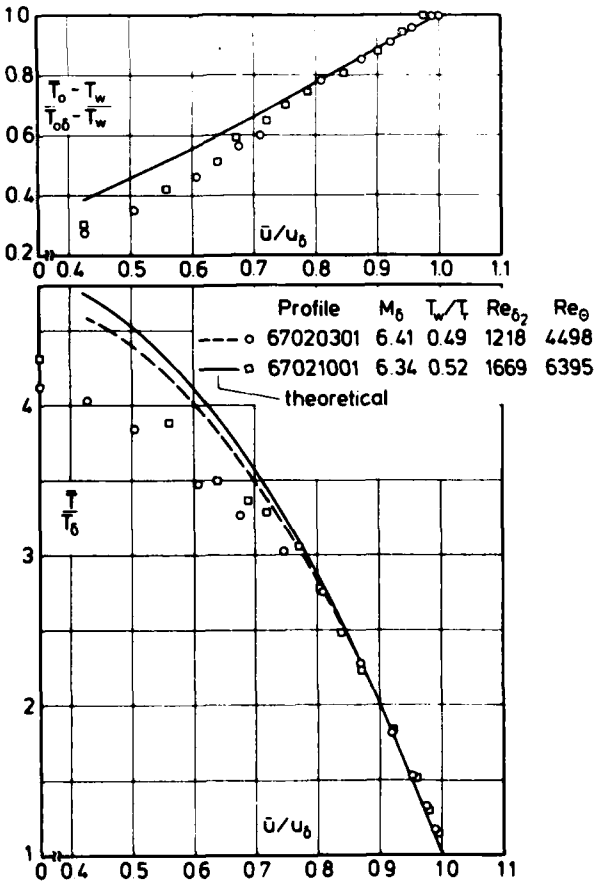

Fig. 2.5.12 Comparison between measured and theoretical temperature profiles (zero pressure gradient, isothermal wall, defined origin). Danberg (1967)

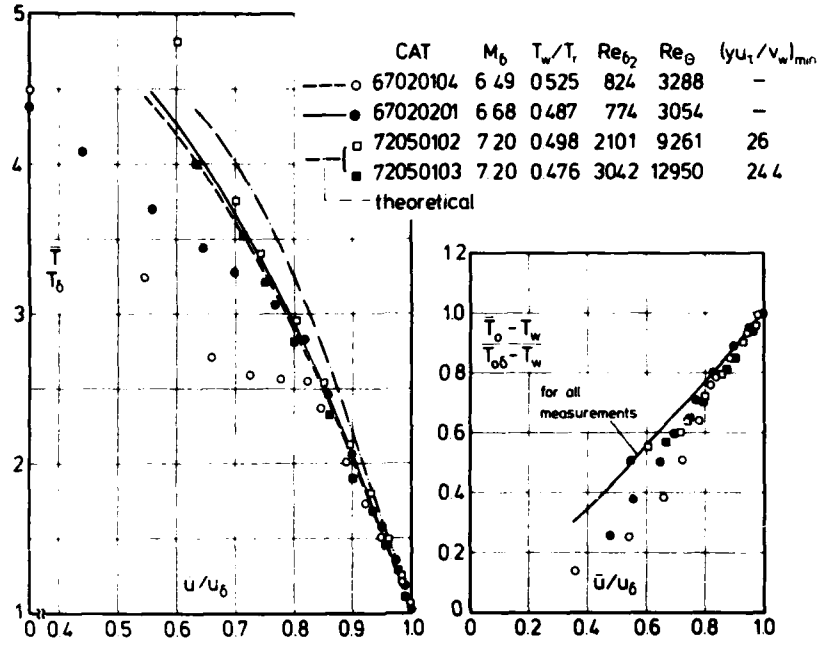

Fig. 2.5.13 Comparison between measured and theoretical temperature profiles in a boundary layer (zero pressure gradient, isothermal wall, defined origin). Danberg (1967), Horstman & Owen (1972)

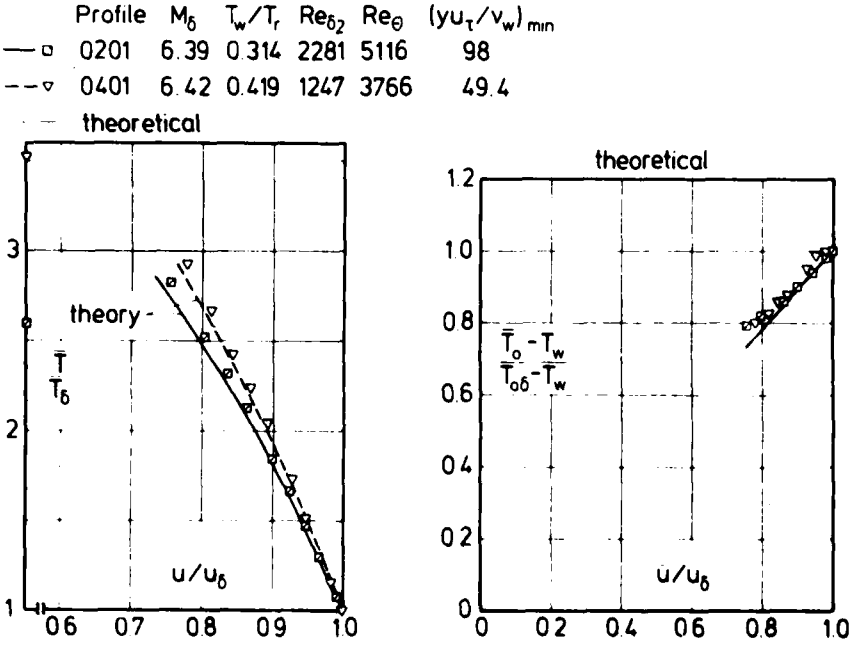

Fig. 2.5.14 Comparison between measured and theoretical temperature profiles in a boundary layer (zero pressure gradient, isothermal wall, defined origin). Keener & Hopkins (1972)

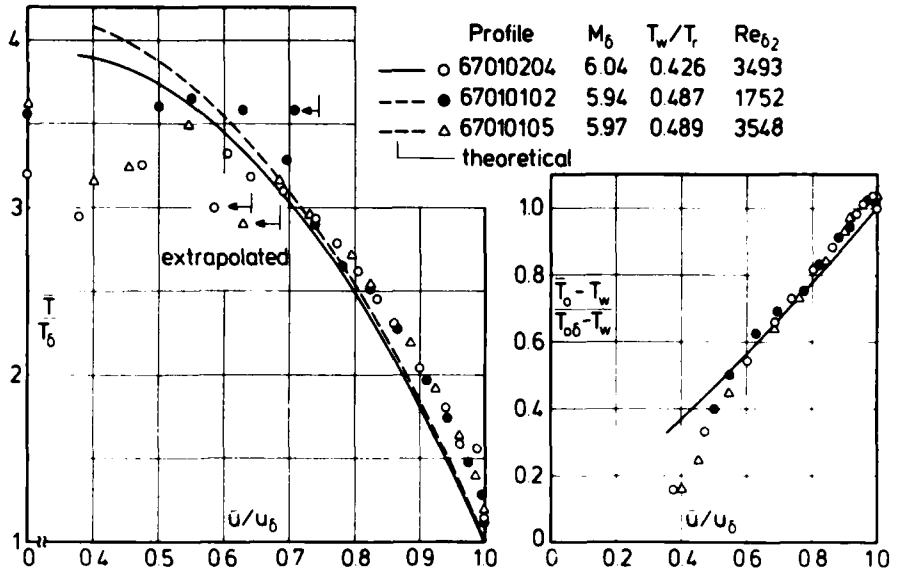

Fig. 2.5.15 Comparison between measured and theoretical temperature profiles (zero pressure gradient, isothermal wall, defined origin). Samuels et al. (1967).

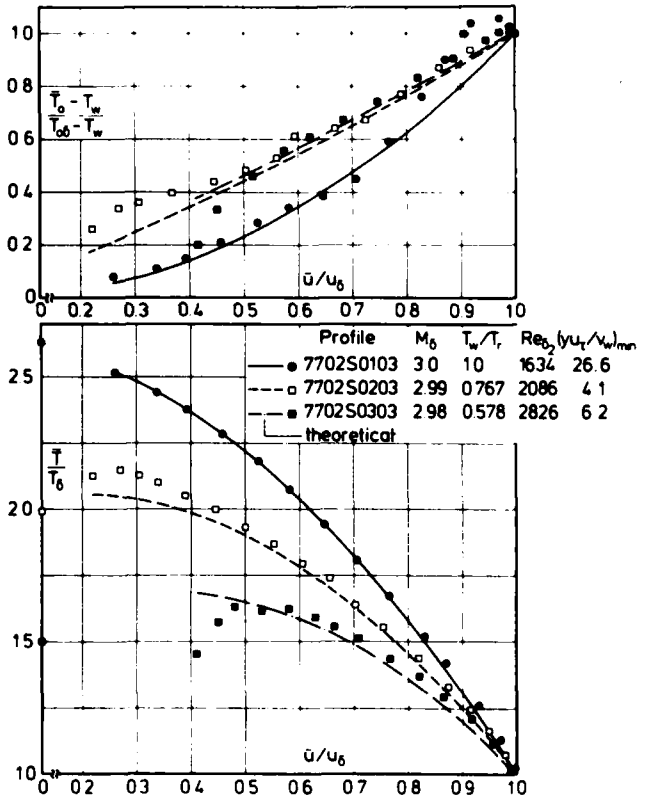

Fig. 2.5.16 Comparison between measured and theoretical temperature profiles (zero pressure gradient, adiabatic and isothermal wall, defined origin). Laderman & Demetriades (1977)

In Fig. (2.5.15) we present measurements which were performed by Samuels et al. (1967) in a boundary layer on the exterior of a hollow cylinder. They found an unexpectedly large overshoot in the T_o-profiles which causes an apparent associated overshoot in the velocity profiles. These temperature measurements must therefore be treated with reserve. Furthermore the innermost T_o values (sometimes up to 5 points) are extrapolations. The position from which extrapolations were used is indicated in Fig. (2.5.15) for each temperature profile. Apart from the differences between the measured and theoretical temperature profiles in the vicinity of the wall the trend of the theory is, however, confirmed also by these measurements.

Finally, recent measurements on a flat plate carried out by Laderman & Demetriades (1977) are shown in Fig. (2.5.16). The heat transfer parameter is varied in a range $0.58 \leq T_w/T_r \leq 1$, and agreement between both types of profiles, $\bar{T}/T_\delta$ and T, and the theoretical values is good if some measured data close to the wall of profile 7702S0303 are not considered. It is interesting to note that Laderman (1978) comes to the same conclusion about the use of the T^* versus $\bar{u}/u_\delta$ plot as we are trying to bring to our readers' attention. Laderman states "that in the adiabatic case the Crocco parameter T^* is extremely sensitive to uncertainties in the total temperature and that the Crocco relation, cast in its usual form T^* versus $\bar{u}/u_\delta$, cannot be used to judge the quality of the boundary layer flow".

Experiments in a boundary layer along an isothermal nozzle wall with no defined origin have been performed by Voisinet & Lee (1972). These measurements are shown in Fig. (2.5.17) and (2.5.18) for a Mach number 4.80 and a range of the heat transfer parameter $0.22 < T_w/T_r < 0.91$. The measured $\bar{T}/T$ -profiles agree very well with the theoretical profiles though the large amount of extrapolated data is noteworthy. The T*-data disagree with the theoretical curves - except for profiles 1103 and 1203 - and the measured data lie below the theoretical ones. In the same test section Voisinet et al. (1974) undertook a comparative experiment with an equilibrium cone probe (ECP) and a shielded temperature-pressure probe (STP) which had also been previously used by Meier (1970) and by Mabey et al. (1974). As can be seen from Fig. (2.5.19) agreement between the two temperature probes is very good except for the region close to the wall where the ST-probe gives higher temperatures than the EC-probe (about 2 % according to the authors). In Fig. (2.5.21) we finally show a comparison between theory and measurements performed with the original "Danberg probe" (1961). This comparison agrees well with the results obtained so far and shows no shortcomings in the temperature measurements as sometimes suggested. A further comparison between velocity profile data obtained by an ST-probe (Meier 1970) and by a Laser-Doppler technique was performed by Maurer et al. (1975) who found discrepancies between the two measuring techniques both at the outer edge and in the wall region of the boundary layer. The explanation of the differences between the measurements is not yet conclusive but the phenomena are of sufficient interest to need further clarification. In Fig. (2.5.20) we plotted some velocity profiles given by Voisinet et al. (1974) where skin friction was determined according to Fernholz (1971). No differences between the velocity profiles occur which could be due to the different temperature profiles used for the determination of the transformed velocity profiles.

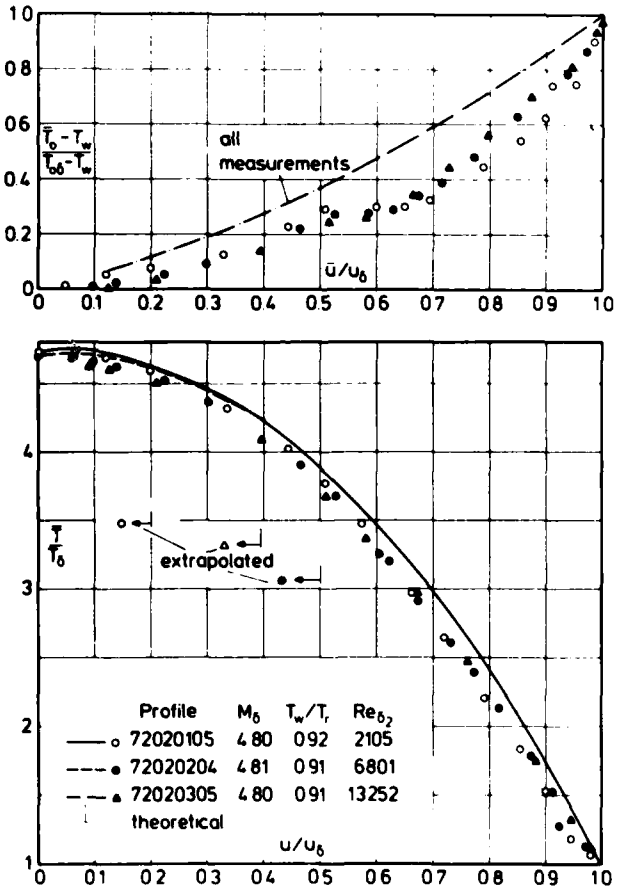

Fig. 2.5.17 Comparison between measured and theoretical temperature profiles (zero pressure gradient, slightly cooled wall, origin not defined) Voisinet & Lee (1972)

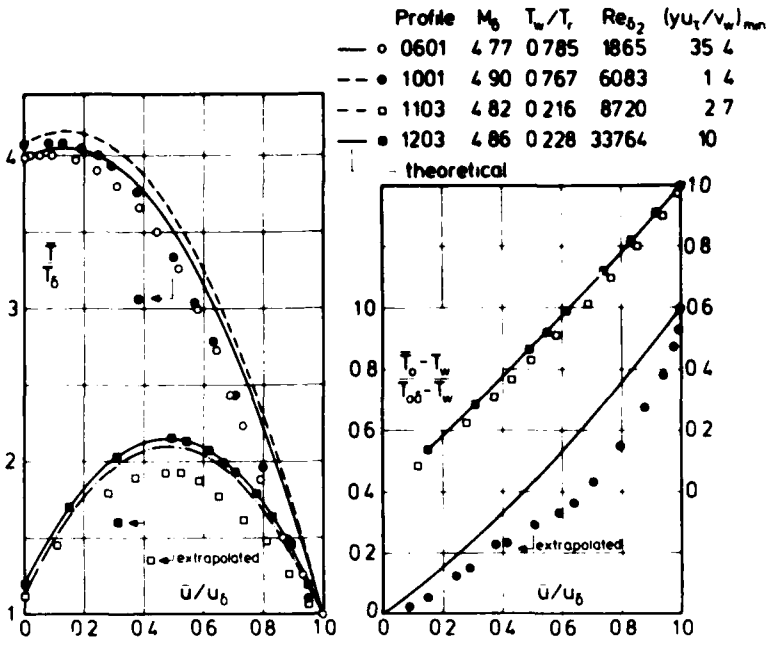

Fig. 2.5.18 Comparison between measured and theoretical temperature profiles in a boundary layer along an isothermal wall with probable upstream effects. Voisinet & Lee (1972)

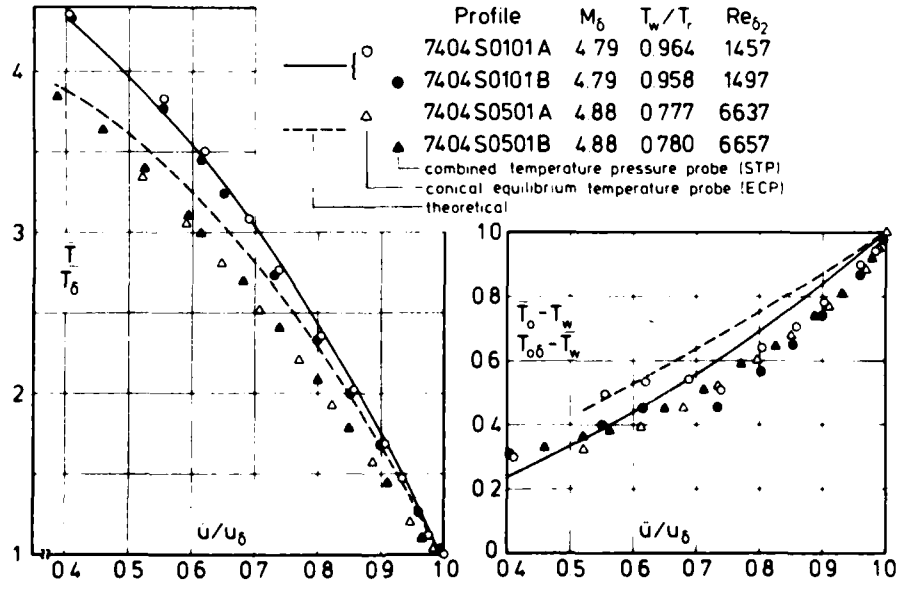

Fig. 2.5.19 Comparison between measured - two different probes - and theoretical temperature profiles in a boundary layer (zero pressure gradient, isothermal wall, origin not defined). Voisinet et al. (1974)

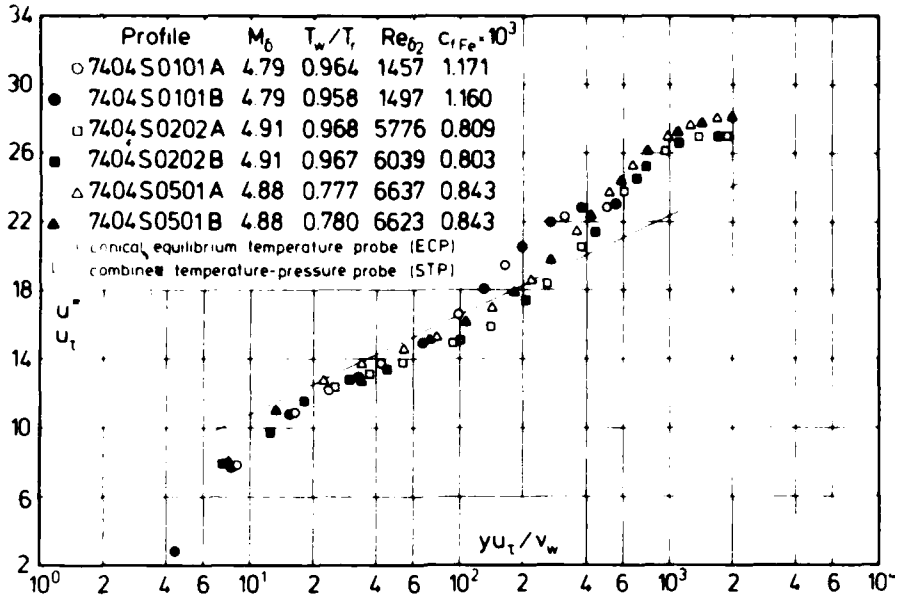

Fig. 2.5.20 Law of the wall for a compressible turbulent boundary layer (adiabatic and isothermal wall, zero pressure gradient, origin not defined). Voisinet et al. (1974)

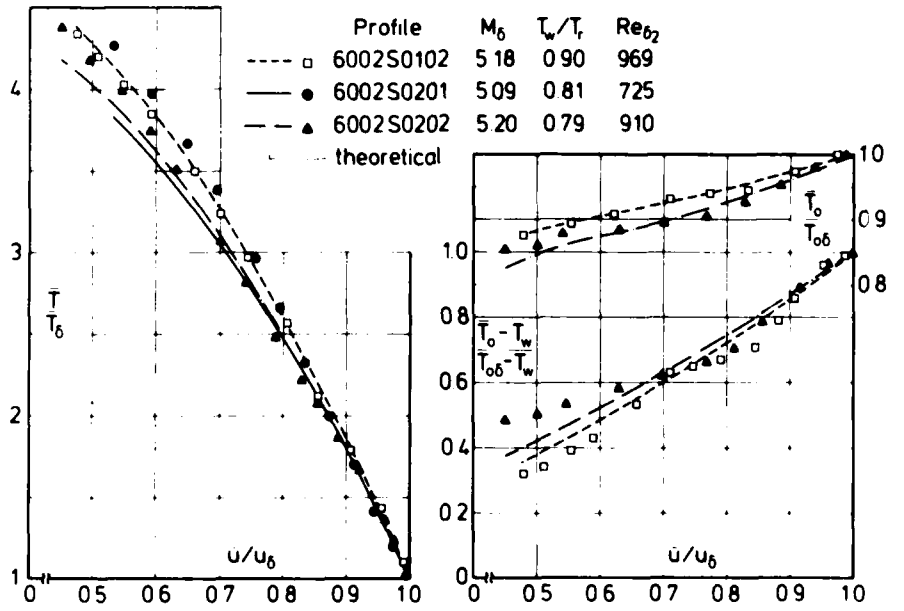

Fig. 2.5.21 Comparison between measured and theoretical temperature profiles in a transitional compressible boundary layer (isothermal wall, zero pressure gradient, defined origin). Danberg (1960)

2.5.6.3 Conclusions. After this survey of measured and theoretical temperature profiles, based on a wide variety of measurements in compressible turbulent boundary layers with zero pressure gradient along adiabatic and isothermal walls where (a) the origin is defined and where (b) upstream effects cannot absolutely be excluded, the following conclusions may be drawn. They hold for the parameter range investigated which is approximately: $M_\delta < 10$, $0.2 < T_w/T_r < 1$, $275 < Re_{\delta 2} < 33000$.

(1) Eqns. (2.5.37a) with $T_r=T_w$ and (2.5.40) hold for compressible turbulent boundary layers along adiabatic walls. It need not be repeated that these temperature-velocity relationships cannot describe the temperature overshoot at the boundary layer edge. This overshoot is consistent and essentially implied by the total enthalpy integral presented in eqn. (2.5.9). Though this deficiency may be deplorable, it appears to be of little importance if only the mean temperature distribution is needed. The plot $(\bar{T}_0/T_w)/(T_{0e} - T_w) = T^*$ versus $\bar{u}/u_\delta$ is so sensitive to small errors in $\bar{T}_0$ or T_w that it should not be used as a test for the validity of eqn. (2.5.40). An increase of T^* in the wall region is physically not plausible and is due to small measuring errors and does not represent a physical effect of any importance. It is highly improbable that there exists any such strong relationship between the T^*-distribution and the Prandtl number distribution which might be used to explain the temperature increase (see section 2.5.8) as claimed by Meier & Rotta (1971).

(2) Eqns. (2.5.37a), (2.5.37d) and (2.5.37e) hold for compressible turbulent boundary layers along isothermal walls with moderate and high cooling rates. There are so few measurements in the viscous sublayer that it is impossible to judge whether these equations can predict the wall slope of the temperature profile $(\partial T/\partial y)_w$ which would be desirable in order to determine the heat transfer rate at the wall. Eqn. (2.5.37a) can predict the mean temperature profile in a boundary layer within an accuracy range of 10 %.

(3) Failure of the equations derived in § 2.5.4 to agree with measurements is probably due to their application to flow cases which go beyond their range of validity or because local equilibrium of the boundary layer had not been reached or there were unresolved measuring problems in the wall regions.

(4) We still lack relations for the mean temperature profile when the wall temperature varies with x and/or if there exists a pressure gradient dp/dx in streamwise direction. Boundary layers along isothermal walls with pressure gradients in the streamwise direction are dealt with in section 5.

(5) This survey should end once and for all speculations that the Crocco parameter T^* is adequately represented by a linear relationship between T^* and the velocity profile, such as eqn. (2.5.22b), for boundary layers of the "flat-plate" type and that it follows a quadratic relation, such as eqn. (2.5.40), for boundary layers in nozzle flows. For flows with pressure gradients the reader is referred to § 5.

2.5.7 Recovery factor and Reynolds analogy factor

2.5.7.1 General remarks. In § 2.5.4 we presented an analysis largely due to Van Driest (1955) which permits a prediction of the temperature-velocity relationship restricted to flows with zero pressure gradient along isothermal walls. The solution used also required the assumption of constant laminar and turbulent Prandtl numbers close to one and as presented implied a knowledge of the recovery factor, defined within these restrictions by eqn. (2.5.33).

In general the recovery factor is treated as an empirical constant (we have used the value 0.896 throughout) but the Van Driest analysis does allow of an assessment of the sensitivity of the recovery factor to changes in the laminar and turbulent Prandtl numbers. This is a matter of considerable potential importance, as with

the same restrictions the analysis predicts a value for the Reynolds analogy factor s (eqn. (2.5.32) which relates skin friction to wall heat flux.

The relationships of eqns. (2.5.32) and (2.5.33) give r and s as functions of the velocity and shear stress distributions through the layer with the "combined Prandtl number" Pr_M (eqn. 2.5.15) as parameter and are special cases of the more general relations of eqns. (2.5.28) and (2.5.29) in which this also varies through the layer. To evaluate the integrals it is necessary to provide as input either a theoretical or empirical relationship. Van Driest in fact used the imcompressible pipe flow data of Nikuradse (1932) so that in principle the results should apply to incompressible flow.

The empirical input consists firstly of a velocity profile the key features of which are the velocity at the outer edges of the viscous sublayer $\bar{u}_{sl}$, and the buffer layer, $\bar{u}_{bl}$. These are taken to be given by

$$(\bar{u}_{sl}/u_\delta) = 5\ (c_f/2)^{1/2} \text{ and } (\bar{u}_{bl}/u_\delta) = 5\ (1+\ln 6)\ (c_f/2)^{1/2} . \tag{2.5.48}$$

The shear-stress / velocity relationship assumes that $\tau = \tau_w$ in the sublayer and buffer layer and that elsewhere it is adequately described by

$$(\tau/\tau_w) = 1 - \exp\ \left[-\frac{K_1}{(c_f/2)^{1/2}}\ (1-\frac{\bar{u}}{u_\delta})\right] \tag{2.5.49}$$

which is effectively the semi-log law. After much numerical work, eqns. (2.5.32) and (2.5.33) then give

$$s = Pr_t\ \{1 + 2.50\ (c_f/2)^{1/2}\ (1-Pr_t)\ [\frac{\Pi^2}{6} + \frac{3}{2}\ (1-Pr_t)]$$

$$+ 5\ (c_f/2)^{1/2}\ [(\frac{Pr_1}{Pr_t} - 1) + \ln\ [1 + \frac{5}{6}\ (\frac{Pr_1}{Pr_t} - 1)]]\} \tag{2.5.50}$$

$$r = Pr_t\ \{1 + 5\ (c_f/2)^{1/2}\ (1-Pr_t)\ [\frac{\Pi^2}{6} + \frac{3}{2}\ (1-Pr_t)] + 25\ (c_f/2)^{1/2}$$

$$[(\frac{Pr_1}{Pr_t} - 1) + 2\ \ln\ [1 + \frac{5}{6}\ (\frac{Pr_1}{Pr_t} + 1)]\ + \ln 6 \cdot \ln\ [1 + \frac{7}{8}\ (\frac{Pr_1}{Pr_t} - 1)]$$

$$- \ln 6 \cdot \ln\ [1 + \frac{1}{4}\ (\frac{Pr_1}{Pr_t} - 1)]]\} \tag{2.5.51}$$

as accurate representations of the result.

The effects of compressibility and temperature changes on these expressions are represented by replacing $c_f/2$ in the above expressions by the product $(c_f/2)(T_w/T_\delta)$ which for an adiabatic wall implies an iterative approach as (T_w/T_δ) then equals $(1 + r\ \frac{\gamma-1}{2}\ M_\delta^2)$, though Van Driest also used Coles'(1953) experimental values for some of the analysis. The very large number of arbitrary assumptions required is unfortunate, but the analysis is instructive as the results are very insensitive to variations in the input. For a wide range of c_f corresponding to Re_x values from 3×10^5 to 10^8 at $M_\delta = 0$,

with $Pr_t = 0.86$, $Pr_1 = 0.71$ r = const = 0.88; $0.82 \leq s \leq 0.83$ while

with $Pr_t = 1.0$, $Pr_1 = 0.71$ $0.88 \leq s \leq 0.92$.

For a fixed Re_x of 10^7 on an adiabatic wall as the Mach number varies from 0 to 3, with $Pr_t = 0.86$, $Pr_1 = 0.71$

$$r = 0.88 \pm 0.005, \quad 0.828 \leq s \leq 0.829 .$$

The influence of the temperature upstream-history on the recovery factor was investigated by Gates (1973) - see also § 4.5 where the effects are summarized.

2.5.7.2 Recovery factor. The analytic expression of eqn. (2.5.51) requires as input a value of Pr_t, assumed constant through the layer. Van Driest adopted a circular argument, choosing a value of Pr_t (= 0.86) which leads to a constant value of r (= 0.88) which was in agreement with the experimental data available to him (data from BRL, NACA and MIT, the last probably Shoulberg et al. (1953/54)). Experimental determination of the recovery factor is in principle fairly straight-forward, residual uncertainties arising from the fact that no experimental boundary layer can be turbulent from the leading edge and heat transfer from one face of a model to the other. The early values cited by Van Driest were close to 0.88, and were supported by the results of Mack (1954) at M_δ = 4.4. More recent measurements at Mach numbers up to 6.9 in helium are reported by Rudy & Weinstein (1973). In contrast to the early results they found an increase in the recovery factor from 0.88 to approximately 0.91 at M_δ = 7. In the transitional regime Shoulberg et al. (1954) found that the recovery factor in a laminar boundary layer decreased slightly with Reynolds number from 0.885 to 0.866 and increased to 0.90 during transition falling sharply to the constant value 0.88 in the turbulent boundary layer.
The experimental and theoretical values are discussed here as a constant value of r should at least give a reasonable hope that the range of values for s should not be too great.

2.5.7.3 Reynolds analogy factor. The quantity s, in principle determined from eqn. (2.5.32) or, more generally, eqn. (2.5.28), is within the assumptions leading to eqn. (2.5.25) the "Reynolds analogy factor" relating skin friction and heat transfer by

$$s = c_f / (2\,St) \qquad (2.5.52).$$

Since, especially in short duration facilities, heat transfer measurements are relatively easily performed, while skin friction measurements are always difficult, it would be of great value to have a reliable value for s.
Analyses of the available experimental information have been given by, among others, Wilson (1969), Cary (1970), and Cary & Bertram (1974). No calculation method for s may be considered as established, so that we must rely on experiments in which both τ_w and q_w were measured. Cary (1970) evaluated measurements by Fallis (1952), Heronimus (1966), Neal (1966), Bertram et al. (1968), and Wallace (1967) for which there was little or no associated profile data, and by Young (1965), Lee et al. (1968) and Hopkins et al. (1969). These last three sets of data, or later updated versions, are in AGARDograph 223 as CAT 6505, 7202, 7203, and 7204 and include full profile tabulations. Over the ranges $2 \leq M_\delta \leq 12$ and $0.1 \leq H_w/H_o$ Cary found a scatter

$$0.9 \leq s \leq 1.3$$

in s-values on flat plates, for which Reynolds analogy should be applicable, and gave as his conclusions: "For Mach numbers less than 4 or 5 with other than near-adiabatic wall conditions and for Mach numbers greater than 4 or 5, there are insufficient data and too much scatter in the available data to empirically define the Reynolds analogy factor within desirable accuracy limits".
A more recent survey by Bradshaw (1977) suggests that in constant pressure flows $0.75 \leq s \leq 1.0$.
Keener & Polek (1972) performed measurements of both skin friction and heat transfer in a zero-pressure gradient boundary layer for the parameter range $5.9 \leq M_\delta \leq 7.7$, $0.3 \leq T_w/T_r \leq 0.5$, and $2 \times 10^3 \leq Re$ 2×10^4. They did not find any distinct Mach number effect on the Reynolds analogy factor, and most of their results fall within 4 % of s = 1 with a maximum scatter of $\pm$ 9 %.

Results from experiments with pressure gradients need careful interpretation as Reynolds analogy does not strictly apply, so that variations may be observed as a result either of the effect of pressure gradient or as a change in the circumstances of some ill defined equivalent zero pressure value. This does not, however, prevent workers in the field from presenting so called Reynolds analogy factors even without proper measurements of CF or CQ. For instance Pasiuk et al. (1965) made some measurements in a mild favourable pressure gradient on a straight wall and found s-values well described by the empirical relation $s = Pr_l^{2/3}$ suggested by Colburn (1933). The authors deduce these values by comparison with mean CF values estimated from the momentum integral equation so that they cannot be assumed to be in any way accurate.

The only pressure gradient cases in AGARDograph 223 for which both CF and CQ were directly measured are those of Voisinet & Lee (CAT 7304) and of Kemp & Owen (CAT 7206). The Voisinet & Lee measurements were made on a flat tunnel wall. The Mach number rose steadily from 3.8 to 4.5 and for the cases with both CF and CQ values T_w/T_r was about 0.75. The apparent s-values range from 1.19 to 1.66 with a mean of 1.45 if T_r is calculated assuming a flat plate value for r = 0.896. As remarked elsewhere, it is difficult to assign a meaning or value to "recovery temperature" in a flow affected by upstream history, and the authors found "true experimental adiabatic wall temperatures" for which T_w/T_r was about 0.93. If these temperatures were used instead of the "flat plate" T_r when defining the Stanton number the mean value of s would be about 1.03. Such a finding is, however, superseded if one considers the corrected CF values published recently by Voisinet (1977). The influence of the correction on the logarithmic law of the wall is shown in Fig. (4.3.13). It would also be very unwise to draw precise conclusions from the measurements of Kemp & Owen (1972) who measured τ_w and q_w on a curved nozzle wall in a favourable pressure gradient. The range covered was $20 \leq M_\delta \leq 50$, $0.35 \leq T_w/T_r \leq 0.85$, and $9 \times 10^2 \leq Re_\theta \leq 6 \times 10^3$, giving apparent s-values from 1.06 to 1.8 with a mean of about 1.4 (even higher values up to 2.5 appear not to have been presented explicitly in the report). These results are also, possibly, uncharacteristic as a consequence of low Reynolds number effects (see also the discussion in context with Figs. (5.2.13 and 5.2.14)).

The available experimental data, then, do not permit any conclusion which might be relied upon to agree with new experimental evidence. Any new data must be based on skin friction and heat transfer measurements of a very high standard associated with a careful - and honest - error analysis so that genuine physical changes in the value of s can be distinguished from the unavoidably large scatter of the skin friction and heat transfer measurements.

2.6 Heat transfer at the wall

2.6.1 General remarks

This paragraph is suitably begun with the statement made by Van Driest (see Lin 1959): "Any discussion of convective heat transfer in gases is essentially a discussion of the characteristics of the boundary layer in a compressible real fluid subjected to arbitrary wall temperature ... . The heat transfer to or from the boundary layer takes place by molecular conduction at the wall, whether the flow is laminar or turbulent; thus the transfer of heat per unit area from a wall to a flowing fluid, or vice versa, is the product of the thermal conductivity and temperature gradient in the fluid at the surface of contact of fluid and wall".
This is a reiteration of Fourier's law of heat conduction, here

$$q_w = - \lambda_w \, (\partial \bar{T}/\partial y)_w \qquad (2.6.1)$$

The principal objects of boundary layer theory must be to predict firstly skin friction and secondly - and perhaps the more important at very high speeds - the heat transfer at the wall, or the temperature profile gradient at the wall. This requires, in general, the solution of the coupled system of momentum and energy equations, which, for turbulent boundary layers, can be achieved for only a few special cases. There is a double closure problem in that $\overline{u'v'}$ and $\overline{v'T'}$ must somehow be related to the mean velocity and temperature field. The problem is of such complexity that no full solution for boundary layers in a pressure gradient and flowing over a wall with arbitrary temperature distribution can be expected in the near future.

There are a few numerical solutions for selected boundary conditions, and even fewer analytical solutions. In fact it is probably proper to describe as such only one - the form of "Reynolds Analogy" based on the Van Driest solution for isothermal wall boundary layers in zero pressure gradient. It is only fair to remark that there is very little experimental information for the more complex cases which could be used to check any theoretical or numerical solution. The experiment of Gran et al. (1974) includes an account of the constant pressure flow over a wall with a step change in temperature, and a varied pressure gradient flow including quite strong adverse gradients over a cooled wall of roughly constant temperature. Unfortunately detailed data were not available to us. Voisinet & Lee (1973) describe an accelerated flow over a cooled wall, the data for which is available as CAT 7304, but some caution is called for interpretation as there are probably substantial upstream history effects present (see the discussion of Figs. (4.2.19/20) and (4.3.9-14) below, where the favourable pressure gradient case and the "control" zero pressure gradient case (CAT 7202) is described). Further results from properly instrumented test cases of this type would be highly desirable.

2.6.2 Reynolds analogy

Reynolds, in 1874, remarked on the close analogy which exists between heat transfer and momentum transfer. Since that time a very wide range of analytical expressions relating the wall shear stress to the heat flux have been developed for a variety of boundary conditions by a multitude of authors. These relations are commonly referred to as "Reynolds analogy".
Because of this variety, it is always needful to enquire what an author in fact means by Reynolds analogy in a given context, and to determine what expression he is using, and what may be its range of validity. For surveys of "ordinary", "modified", "weak" and "strong" Reynolds analogies, the reader is referred to Schubauer & Tchen (in Lin 1959), Morkovin (in Favre 1964) and Rotta (1964).
As discussed in § 2.5.7.3 above, there are relatively few fully documented sets of data available which would allow a check on the various, mostly semi-empirical, relationships which go by the name of "Reynolds analogy". We do not consider it useful therefore, at present, to list these varied relationships and attempt a comparison with experiment. Rather we will briefly discuss a single relationship based on eqn. (2.5.25) which is due to Van Driest (1955). If the Crocco transformation is applied to eqn. (2.6.1) and q_w is made dimensionless by $\rho_\delta u_\delta^3$ eqn. (2.6.1) yields

$$\frac{q_w}{\rho_\delta u_\delta^3} = - \frac{2\tau_w}{\rho_\delta u_\delta^2} \, \frac{1}{Pr_w} \, \frac{h_\delta}{2u_\delta^2} \, \left(\frac{\partial(\bar{h}/h_\delta)}{\partial(\bar{u}/u_\delta)}\right)_w \qquad (2.6.2).$$

Apart from τ_w the only unknown of the problem is the dimensionless derivative at the wall. A value can be obtained if one differentiates eqn. (2.5.25) and inserts the boundary conditions at the wall to give

$$\frac{q_w}{\rho_\delta u^3_\delta} = - c_f \frac{1}{s} \frac{h_\delta}{2u^2_\delta} \left(\frac{h_r}{h_\delta} - \frac{h_w}{h_\delta}\right) , \tag{2.6.3}$$

where, for constant specific heat, $h_r = c_p T_r$ and s is the Reynolds analogy factor as defined by eqn. (2.5.32) with $(Pr_M)_w = Pr_w$. Substitution of the Stanton number

$$St = \frac{/q_w/}{\rho_\delta u_\delta (h_r - h_w)} \tag{2.6.4}$$

into eqn. (2.6.3) then gives

$$St = c_f/(2s) . \tag{2.6.5}$$

In the text below the name "Reynolds analogy" implies eqn. (2.6.5).
The range of validity of this definition is determined by that of eqn. (2.5.25) and thus it holds for boundary layers with zero pressure gradient (dp/dx = 0) and with constant wall temperature where the Prandtl number lies in the range $0.7 \leq Pr \leq 1$.
Eqn. (2.6.5) offers, in principle, an elegant means for determining the skin friction coefficient from heat transfer measurements with of course the necessary precondition that the Reynolds analogy factor s is known. It seems wisest to accept Cary's comment (1970) that - so far - heat transfer data cannot in general be used to validate c_f formulas because of the uncertainty in the Reynolds analogy factor (see also § 2.5.7.3).

2.6.3 Stanton number and recovery factor

Partly as a consequence of the common use of Reynolds analogy, and partly as, often, the most convenient form in which boundary layer calculations predict heat transfer, the Stanton number is perhaps the usually preferred form of presentation for heat transfer data. Data in this form implies that the wall temperature and recovery temperature are known. If measurements are made in near adiabatic conditions, the Stanton number, if not the heat flux measurement, becomes unduly sensitive to errors in the measurement of T_w, and more importantly in the estimation of T_r. This can lead to considerable difficulty in processing data, as authors are not always punctilious in stating what values of the recovery factor or directly, T_r, they have used. The possible importance of the selection of T_r or T_{ad} is well shown in the discussion of possible s-values deduced from the data of Voisinet & Lee (CAT 7304) in § 2.5.7.3. For this reason we follow a suggestion by J.E. Green (private communication) and recommend that data be presented as values of

$$CQ = q_w/\rho_\delta H_\delta u_\delta \tag{2.6.6}$$

and have done so in AGARDograph 223. Workers using the data can then convert them into values of St according to their own ideas as to what T_r is, so long as T_w is also stated.

3. CONCEPTS FROM LOW-SPEED STUDIES

3.1 Introduction

Over the years a considerable measure of success has been attained by those who set out to provide a description of the two-dimensional incompressible turbulent boundary layer. The complications in the compressible case are such that rather than make a direct attack on the actual compressible flow field, a great part of the effort has been,and probably will be,devoted to the relation of observations in compressible flow to those in incompressible flow. Before we attempt this, at least for some aspects of compressible turbulent boundary layer behaviour, it seems reasonable to discuss briefly the basis for such a comparison. The discussion will of itself make clear why any such framework for description cannot be generally valid, and, indeed, we must hope that the procedure will eventually be superseded by a more complete theoretical treatment. The probable reason why it is possible to transfer knowledge from the incompressible to the compressible case is the validity of the Morkovin hypothesis (see § 2.4) which can be interpreted as stating that the turbulence structure in boundary layers at $M_\delta < 5$ - possibly < 7 - is virtually the same as at low speeds. This is good luck for the fluid dynamicist but cannot yet be proved rigorously in the mathematical sense. If a mathematical justification were possible then a compressibility transformation should exist which transforms the conservation equations for a compressible flow into those for a flow of constant density but variable transport coefficients. We do not wish to discuss the topic of the general validity of a transformation for the conservation equations here and refer the reader to a brief review in § 3.4. We will only remark here that it seems impossible to transform the turbulence characteristics pointwise.

There are more obvious gross physical phenomena present in compressible flows which have no direct analogue in the incompressible case, so we can only be surprised by the success of a description based on the "laws" of the wall and the wake. To what low speed flow, for instance, should one compare a case such as that of Sturek & Danberg (1971 - CAT 7101) in which a boundary layer is compressed on a curved "isentropic" ramp? There are strong normal pressure gradients present ($\partial p/\partial y \sim 0.4\, p/\delta$) and the boundary layer is rapidly compressed so as to become thinner (- in an adverse pressure gradient! -) while the shear stress both at the wall and in the body of the flow rises again. As an extreme example of a flow differing radically from any low speed analogue, we may cite the shock-boundary layer interaction (e.g. Rose, 1973 - CAT 7306 S) in which a near step change in pressure occurs, often leading to immediate separation (see also Bradshaw 1974a).

Nevertheless, low speed ideas developed for "modest" pressure gradients still provide a useful starting point for compressible flows (see § 5). Thus it is convenient to carry over certain of the concepts which have proved successful in incompressible flows, and apply them to compressible cases. This is permissable so long as the underlying assumptions are borne in mind and their essentially semi-empirical basis is recognised. It is very unlikely that there will be any substantial theoretical (as opposed to computational) advance in the near future, so that the extension of these concepts to compressible flow can only be justified by experimental evidence of their success. At low speeds, for a given geometry, the behaviour of the turbulent boundary layer is specified by the value of the Reynolds number which in a constant transport property fluid is fixed by a representative velocity and length and the kinematic viscosity. Any attempt to extend the principle of similarity to boundary layers on bodies of different shapes rapidly founders, except for some cases of affine transformations (almost exclusively in laminar boundary layers) or for certain very restricted ranges of self-similar flows. A large measure of success has, however, been achieved qualitatively, and within limits, quantitatively,by appeal to the concept of "local similarity". The presumption is that the features of a boundary layer at a point will at least primarily, if not completely, be determined by the mean flow boundary conditions at that point. We shall deal with modifications of this concept in § 4.3.3 where upstream influences or history effects will be discussed. Thus the velocity profile in a turbulent boundary layer at a point may be expected to depend on the values of a locally defined Reynolds number and pressure gradient parameter, together with a sufficient number of streamwise derivatives of these quantities. The derivatives effectively define the upstream history of the boundary layer, which physically is of very great importance.

3.2 Similarity laws and their description

Leaving aside history effects at present, the similarity concept assumes that there is local equilibrium as between the production and dissipation of turbulent energy (Townsend 1960). The further assumption of dual "wall" and "wake" similarity, confirmed for large enough Reynolds number by experiment, leads to the well known statement of a "wall" law for the inner region of a turbulent boundary layer

$$\bar{u}/u_\tau = f_1 (y\, u_\tau/\nu) \tag{3.2.1}$$

and a "wake" law for the outer region

$$(u_\delta/u_\tau) - (\bar{u}/u_\tau) = f_2 (y/\delta') \tag{3.2.2}$$

which are individually independent of Reynolds number and where δ' is some characteristic length of the boundary layer, such as, though not necessarily, a boundary layer thickness δ.
Eqn. (3.2.2) has been found to depend heavily on some as yet unexpressed pressure gradient parameter, whereas f_1 in eqn. (3.2.1) is effectively invariant also for boundary layers with adverse and slightly favourable pressure gradients (see Patel 1965), though the extent of the region within which the relation holds may be found to shrink considerably. Since we have not defined what we mean by "large enough Reynolds number" low Reynolds number effects will be dealt with in § 4.4. Functional arguments, or appeal to dimensional analysis of the turbulent structure in the inner region of the boundary layer lead to the so called universal logarithmic wall law which forms a part of both f_1 and f_2

$$\bar{u}/u_\tau = K_1^{-1} \ln (y\, u_\tau/\nu_w) + C_1 \tag{3.2.3}$$

while a useful description of the outer region, for zero pressure gradient, has been given by Rotta (1962) as

$$(u_\delta/u_\tau) - (\bar{u}/u_\tau) = K_2 \ln (y/\delta') + f_3 (u_\tau/u_\delta) \tag{3.2.4}.$$

This description is essentially empirical, and the choice of any one expression for f_2 rather than another must be based on a balance between convenience and accuracy of description.
A relation of this general type will be shown below (eqn. 3.2.25 and Fernholz 1971) to provide with certain conditions, a good description for the compressible zero pressure gradient boundary layer also.
An alternative method of describing the log-law region (i.e. the larger part of the inner region) and the outer region is to adopt the principle of Coles (1956) and to use a combination of eqns. (3.2.3) and (3.2.4) where the influence of an adverse pressure gradient is included by adding a function of (y/δ') to f_1 to give

$$\bar{u}/u_\tau = K_1^{-1} \ln (y\, u_\tau/\nu_w) + C_1 + K^{-1}\, \Pi\, (x)\, w\, (y/\delta') \tag{3.2.5}$$

$w\,(y/\delta')$ is the wake function which is assumed to be effectively universal. Changes in the pressure gradient, and to a lesser extent in Reynolds number, make themselves felt by changes in the value of the parameter Π, found experimentally by inserting the boundary conditions at the outer edge of the boundary layer - the conventionally used description of w being chosen so that $w\,(1) = 2$. Hinze (1959) suggested that the wake function could be adequately described by

$$w\,(\eta) = 1 + \sin \frac{\pi}{2} (2\eta - 1). \tag{3.2.6a}$$

and it is this simple form which was chosen for the data description at the Stanford Conference (Coles & Hirst 1969). There have been various attempts at increasing the accuracy of description, typical of which is the polynominal form proposed by Rotta (1964a)

$$w = 39\eta^2 - 125\eta^4 + 138\eta^5 - 133\eta^6 + 38\eta^7 \tag{3.2.6b}$$

where $\eta = y/\delta$. The apparent increased precision of any of these descriptions is probably not justified by

the accuracy of the experimental data. The various expressions usually used for w also have in common the defect that they are formulated not only to give w (1) = 2 but also $(\partial w/\partial n)_1 = 0$. In consequence they cannot satisfy $(\partial \bar{u}/\partial y)_\delta = 0$. This does not introduce significant falsification except at low values of Π - the effect on results for zero pressure gradient is discussed in some detail by Finley (1966) and Bull (1969). The difficulty can be circumvented, at the cost of losing a "universal shape" for the wake profile by replacing the whole wake term in eqn. (3.2.5) by a divergence function g expressing the difference between the mean velocity and the wall law

$$\bar{u}/u_\tau = K_1^{-1} \ln (y u_\tau/\nu_w) + C_1 + g\,(y/\delta'). \tag{3.2.5a}$$

The function g is then constrained to satisfy the wall law at low values of y and

$$\bar{u} = u_\delta, \qquad \partial \bar{u}/\partial y = 0$$

at $y = \delta'$. A simple form satisfying the minimum number of constraints is that proposed by Finley (1966):

$$g = g_\delta\, \eta^2\,(3-2\eta) \;+\; \frac{i}{K_1}\;\; \eta^2\,(1-\eta) \tag{3.2.6c}$$

where g_δ is the value of g at $\eta = 1$ and corresponds closely to the "wake strength" $\Delta\,(\bar{u}/u_\tau)$ discussed in 3.3.3 below. This description, in common with the "wake law" descriptions, suffers from the defect that the characteristic thickness δ' must either be left as a free variable in a curve fitting procedure or identified with a boundary layer thickness which, experimentally, is very ill defined (§ 7).

The question then arises as to how this low speed concept may be transferred to supersonic boundary layers. Coles (1953 pt. I) gives an extensive survey (table III of his report) of the generalizations of Prandtl's mixing length-theory, of von Kármán's similarity theory to the compressible case, and of various other generalizations of incompressible flow models for the log-law and for skin-friction laws. Part of this investigation resulted in the now "classic" graph by Chapman & Kester (1953) showing skin friction versus Mach number and revealing differences up to 140 %.
Among the later attempts to extend the logarithmic law of the wall to compressible turbulent boundary layers we mention only Rotta's (1959, 1960) suggestion that one should write the "law of the wall" in the following form

$$\bar{u}/u_\tau = f_3\;\; [y\, u_\tau/\nu_w\;;\; M_\tau\;;\; B_q\;;\; \gamma\;,\; Pr]\;, \tag{3.2.7}$$

where M_τ is a Mach number parameter

$$M_\tau = \left(\frac{\tau_w}{\gamma p_w}\right)^{1/2} = \frac{u_\tau}{a_w} = M_\delta\,(c_f/2)^{1/2}, \tag{3.2.8}$$

B_q a dimensionless heat flux parameter

$$B_q = \frac{q_w}{\rho_w c_p T_w u_\tau} \tag{3.2.9}$$

and a_w and q_w are the speed of sound and the rate of heat transfer at the wall.
For a detailed discussion and the complete formulation of the logarithmic law (3.2.3), the outer law (3.2.4), and Coles' combined law (3.2.5) the reader is referred to the original paper (Rotta 1959). Unfortunately no comparison with reliable measurements was or could be made then in order to test this model. It has recently been taken up again by Bradshaw (1977b) in a slightly modified version.

3.3 Similarity laws and their extension to compressible flow

If we transfer the similarity concept to supersonic turbulent boundary layers, it is only reasonable to continue using the same multilayer concept of the boundary layer since it successfully provided a reasonable account of the structure of the mean velocity profile in the subsonic case. The boundary layer is therefore again divided into an "inner region" formed successively by the viscous sublayer, the buffer layer, and the log-law region, and an "outer region" formed by the outer layer and a superlayer.

3.3.1 *The inner region*

The usual derivation of the velocity distribution in the inner region is based on the assumptions (1) that the convection term $\partial/\partial x$ in the equation of motion is small compared with the viscous term, (2) that the pressure gradient term can be ignored so as to simplify the discussion and (3) that τ_{total} where

$$\tau_{total} = \mu \, \partial\bar{u}/\partial y \; - \; \bar{\rho} \; \overline{u'v'} \tag{3.3.1}$$

is constant in the inner region and equals τ_w. This model as taken from the theory of incompressible turbulent boundary layers is complemented by Morkovin's hypothesis that the structure of the turbulence does not change significantly due to compressibility effects up to about a Mach number $M_\delta \approx 5$ in the outer flow. "The dominating factor in the compressible turbulent-boundary-layer problem is apparently then the effect of high temperature on the velocity profile near the wall and therefore on the shear stress. This latter observation was first advanced by von Kármán in 1935 but has been somewhat neglected in favour of interpolation formulae or of elaborate generalizations of the mixing length hypothesis" (Coles 1953 part I). The increased dissipation rate in the viscous sublayer has the effect that with increasing Mach number at a fixed Reynolds number the sublayer thickness increases. The same effect is of course responsible for the observed increase in the thickness of the laminar boundary layer at high Mach numbers (see for example Van Driest 1951).

The viscous sublayer

If one assumes that in the viscous sublayer the molecular shear stress $\mu\partial\bar{u}/\partial y$ is large compared with the Reynolds shear stress $\bar{\rho}\,\overline{u'v'}$ and equal to the skin friction τ_w, then one obtains for the velocity gradient

$$\frac{\partial\bar{u}}{\partial y} = \frac{u_\tau^2}{\nu_w} \left(\frac{T_w}{\bar{T}}\right)^\omega \; , \tag{3.3.2}$$

in which the variation of the viscosity with temperature is taken to be given adequately by

$$\mu = \mu_w \, (\bar{T}/T_w)^\omega \tag{3.3.3}.$$

Using eqn. (2.5.37) for the temperature distribution (valid under the assumptions $dp/dx = 0$ and T_w = constant) eqn. (3.3.2) yields, with $\omega = 1$

$$\frac{\bar{u}_{s.l.}}{u_\tau} = \frac{u_\tau y}{\nu_w} \tag{3.3.4}$$

where the transformed mean velocity in the sublayer $\bar{u}_{s.l.}$ is defined by

$$\bar{u}_{s.l.} = \bar{u} \left[1 + \frac{1}{2} a^* \frac{\bar{u}}{u_\delta} \; - \; \frac{1}{3} b^{*2} \left(\frac{\bar{u}}{u_\delta}\right)^2\right] \tag{3.3.5}$$

in which

$$a^* = \frac{T_\delta}{T_w} \left(1 + r \, \frac{\gamma-1}{2} \, M_\delta^2\right) - 1 \text{ and} \tag{3.3.6}$$

$$b^{*2} = r \, \frac{\gamma-1}{2} \, M_\delta^2 \, \frac{T_\delta}{T_w} \tag{3.3.7}$$

When the transformed velocity $\bar{u}_{s.l.}$ is used, eqn. (3.3.4) is formally identical with the linear velocity distribution in the incompressible turbulent boundary layer to which it reduces for $\bar{T} = T_w$ and $M_\delta \to 0$.

The log-law region

Between the viscous sublayer and the outer layer there exists a region where the Reynolds shear stress $\bar{\rho}\,\overline{u'v'}$ is dominant and is assumed equal to the skin friction τ_w. If one assumes further that Prandtl's mixing length theory is also valid for compressible turbulent boundary layers, one obtains from $\tau_w = -\bar{\rho}\,\overline{u'v'} = \ell^2\,\bar{\rho}\,(\partial\bar{u}/\partial y)^2$

$$\frac{\partial\bar{u}}{\partial y} = \frac{1}{K_1\,y}\;u_\tau\;\left(\frac{\bar{T}}{T_w}\right)^{1/2} \tag{3.3.8}$$

where $K_1 = 0.40$ is von Kármán's constant and ℓ Prandtl's mixing length.
Again one can use eqn. (2.5.37) to substitute for the temperature ratio and obtain (Fernholz 1969)

$$\frac{\bar{u}^*}{u_\tau} = \frac{1}{K_1}\;\ln\;\frac{y\,u_\tau}{\nu_w} + C_1^* \tag{3.3.9}$$

where

$$\bar{u}^* = \frac{u_\delta}{b^*}\;\sin^{-1}\;\left[\frac{2b^{*2}\;\frac{\bar{u}}{u_\delta} - a^*}{(a^{*2} + 4b^{*2})^{1/2}}\right] \tag{3.3.10}$$

a^* and b^{*2} are given by eqns. (3.3.6) and (3.3.7) and

$$C_1^* = -\frac{1}{K_1}\;\ln\;\frac{u_\tau y_1}{\nu_w} + \frac{u_\delta}{u_\tau}\;b^{*-1}\;\sin^{-1}\left[\frac{2b^{*2}\;\frac{\bar{u}_1}{u_\delta} - a^*}{(a^{*2} + 4b^{*2})^{1/2}}\right] .$$

The suffix 1 - except for K - here denotes a boundary condition at the lower end of the validity range of the log-law which can in principle only be found by experiment.
For an adiabatic wall T_w becomes the recovery temperature T_r (eqn. 2.5.38) and $a^* = 0$. In this case experiments show that $\bar{u}_1/u_\delta$ lies in the range $0.3 \leq \bar{u}_1/u_\delta \leq 0.6$. With a value for $\bar{u}_1/u_\delta \approx 0.5$ one can show that arc sin [] can be replaced by the expression in the square bracket for Mach numbers up to 8 with a relative error of - 4 % or less only. Then C_1^* reduces to

$$C_{1_{ad}}^* \approx \frac{\bar{u}_1}{u_\tau} - \frac{1}{K_1}\;\ln\;\frac{y_1 u_\tau}{\nu_w} \approx 5.10 \tag{3.3.11}$$

which is the same value as for the incompressible case.*) This result was also confirmed by the measurements discussed in this report and by general computational experience (Bushnell et al. 1976).

---

*)
A comparison of measurements with the logarithmic law of the wall and the determination of the wake strength $\Delta(\bar{u}^*/u_\tau)$ (see section 3.3.3) are obviously affected by the choice of the "log-law constants" ($K_1 = 0.40$ and $C_1^* = 5.10$). One of our (otherwise exceedingly helpful) commentators has remarked that it is a pity we are using these "relatively old fashioned" values. Since the constants are experimentally determined we feel that it is not possible to state that one set of values is correct and have stayed with the values used here. Firstly, because we relied on Coles' (1956) thorough investigation and secondly, because a visual comparison of this log-law with a large quantity of the data presented in raw form, in AGARDograph 223, suggests that it provides a good description which would not be materially improved by changing to any of the other pairs of values given in table (3.3.1), which presents a selection taken from four of the most thorough investigations.

- continued next page

The first approach to this type of transformation was suggested by Van Driest (1951) who derived a relationship similar to eqn. (3.3.9) also using the mixing length concept. He assumed Prandtl number unity and so a recovery factor equal to one and determined the constant C_1 so that for the limit $M_\delta \to 0$ and $(T_w/T_\delta) \to 1$ the well established relationship for the incompressible case should result. Van Driest's equation for the logarithmic law then reads:

$$\frac{\bar{u}^{**}}{u_\tau} = \frac{1}{K} \ln \frac{u_\tau y}{\nu_w} + F_1 \tag{3.3.12}$$

where

$$\bar{u}^{**} = \frac{u_\delta}{A} \sin^{-1} \left(\frac{2A^2 \frac{\bar{u}}{u_\delta} - B}{(B^2+4A^2)^{1/2}} \right) + \frac{u_\delta}{A} \sin^{-1} \left(\frac{B^2}{(B^2+4A^2)^{1/2}} \right) , \tag{3.3.13a}$$

where

$$A^2 = \frac{\gamma-1}{2} M_\delta^2 \frac{T_\delta}{T_w} ; \quad B = (1 + \frac{\gamma-1}{2} M_\delta^2) \frac{T_\delta}{T_w} - 1 \tag{3.3.13b}$$

and where F_1 is a constant.

Comparisons between measurements and the logarithmic law of the wall are made in this survey only with the relationship given by eqn. (3.3.9). Without attempting a true statistical survey, routine plotting of most of the profiles in AGARDograph 223 has convinced us that velocity profiles in compressible turbulent boundary layers are well represented by eqn. (3.3.9) within the limits set by the assumptions. A comparison between measurements in transformed and un-transformed coordinates is given in Fig. (3.3.0). There is little need to make any further comment about the necessity to take into account the effects caused by Mach number and heat transfer on the velocity profile.

The differences likely to appear if the alternative transformation is used can be seen in Fig. (3.3.1). Here three sets of profile data are plotted using firstly eqn. (3.3.10) with r = 0.896 and secondly eqn. (3.3.10) with r = 1.0 which then reduces to eqn. (3.3.13a). The differences, although systematic, are small when compared to experimental error, particularly in the determination of c_f. (These data are further discussed in connection with figures 4.2.1 - 4.2.4,4.3.5 and 4.3.6.)

Table 3.3.1

Author	K_1	C_1
Coles (1956)	0.40	5.10
Coles (1962)	0.41	5.0
Patel (1965, 1969)	0.418	5.45
Huffmann & Bradshaw (1972)	0.41	5.0
Bradshaw (1976)	0.41	5.20

For a discussion of the various experiments considered by these authors when recommending particular values, the reader is referred to the original papers.

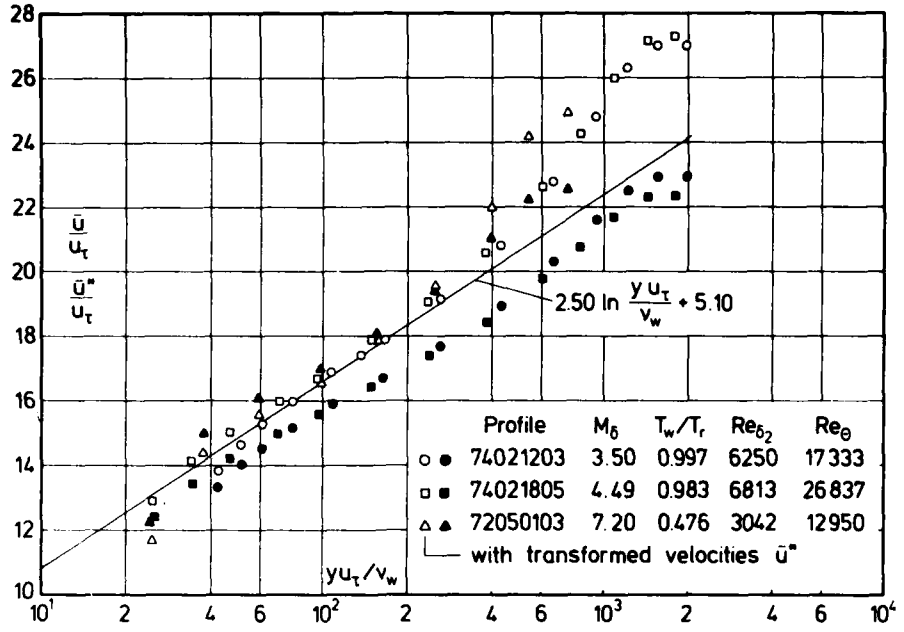

Fig. 3.3.0 Law of the wall for a compressible turbulent boundary layer with zero pressure gradient. Natural and transformed velocities. CAT 7205 & 7402.

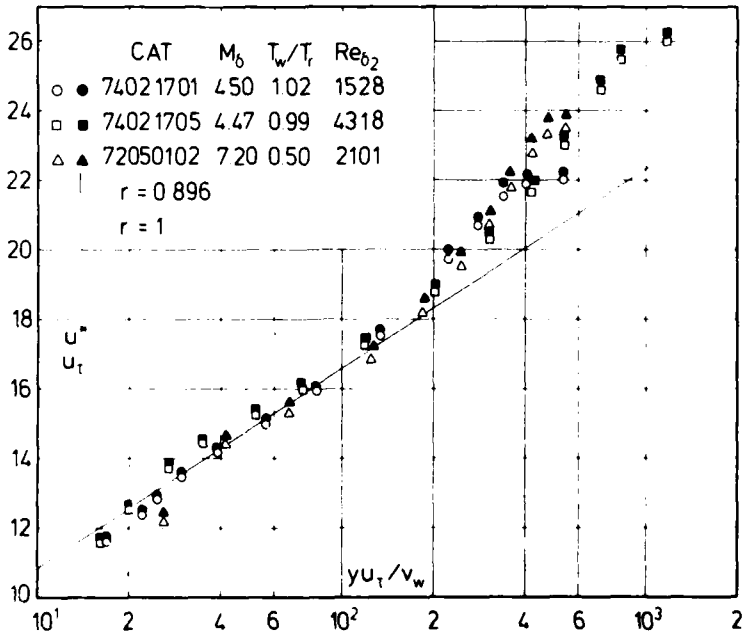

Fig. 3.3.1 Comparison of velocity profiles transformed by using recovery factors 1 and 0.896. Mabey et al. (1974), Horstman & Owen (1972).

3.3.2 The outer region

The existence of the postulated similarity of the velocity profile in the outer region of a compressible turbulent boundary layer can be verified by plotting the velocity defect $(u_\delta^* - \bar{u}^*)/u_\tau$ over y/δ' where the transformation of the velocities u_δ^*, $\bar{u}^*$ and the characteristic length δ' have yet to be determined. Since the mean velocity approaches the velocity u_δ in the free-stream asymptotically the boundary layer thickness is an ill-defined quantity, and it is sensible to use instead an integral length Δ as suggested by Rotta (1950) for incompressible boundary layers:

$$\Delta = \int_0^\delta \frac{u_\delta - \bar{u}}{u_\tau}\, dy = \frac{\delta_{1K}\, u_\delta}{u_\tau} \tag{3.3.14}$$

δ_{1K} is defined by setting the density constant in eqn. (2.3.8). The only difficulty in using the reference length Δ is that both the velocity profile and the skin friction must be known which, unfortunately, is not always the case for the published measurements. If both are available then both the velocity defect distribution and the integral length scale can be transformed and applied to compressible turbulent boundary layers. It is then hoped that the dimensionless velocity defect will be described by a function

$$\frac{u_\delta^* - \bar{u}^*}{u_\tau} = f_4\left(\frac{y}{\Delta^*}\text{ , some pressure gradient parameter}\right) \tag{3.3.15}$$

where

$$\Delta^*/\delta = \int_0^1 \frac{u_\delta^* - \bar{u}^*}{u_\tau}\, d\,(y/\delta)\ . \tag{3.3.16}$$

The transformed velocities u_δ^* and $\bar{u}^*$ are defined by eqn. (3.3.10). There is no justification for the simple relationship of eqn. (3.3.15) other than verification by experiment. An evaluation of a large number of experiments in zero-pressure gradient boundary layers, mainly along adiabatic walls has led to the following semi-empirical relation (Fernholz 1971)

$$\frac{u_\delta^* - \bar{u}^*}{u_\tau} = -\,M\ \ln\frac{y}{\Delta^*} - N \tag{3.3.17}$$

with $M = 4.70$ and $N = 6.74$ $(1.5 \times 10^3 \leq Re_{\delta 2} \leq 4 \times 10^4)$.
While eqn. (3.3.17) may well represent an oversimplification, it will be found that this semilogarithmic defect law serves as an effective benchmark when we examine various secondary influences on the boundary layer (e.g. low Reynolds number effects in § 4.4 and pressure gradient effects in § 5).
More elaborate semi-empirical relationships of the type

$$\frac{u_\delta^+ - u^+}{u_\tau} = -\frac{1}{K_1}\ \ln\frac{y}{\delta} + K_1\, f_5\left(\frac{y}{\delta}\right) \tag{3.3.18}$$

were suggested by Coles (1953), by Stalmach (1958) and by Maise & McDonald (1968), the latter two authors using Van Driest's velocity transformation according to eqn. (3.3.12), i.e. with Prandtl number one.
Due to the different methods applied in specifying the boundary layer thickness δ, the authors of the semi-empirical relations mentioned above do not agree with each other nor do they agree with measurements if these are plotted using values as given by the experimentalists.
Fig. (3.3.2) shows this comparison. Since the figure is meant only to illustrate the problem, the reader is referred to an earlier paper (Fernholz 1969) for the identification of the experimental data.
Libby & Visich (1959), Mathews & Childs (1970) and Sun & Childs (1973) extended Coles' (1956) wall-wake velocity profile (eqn. 3.2.5) to compressible turbulent boundary layers (a) for adiabatic flows with pressure gradient and (b) for isothermal wall and zero pressure gradient, using in the 1973 paper the transformed velocity $\bar{u}^*$ as given by eqn. (3.3.12). Sun & Childs (1976) modified Coles' relationship to avoid the shortcoming basic to this formulation that the velocity gradient at the boundary edge has a

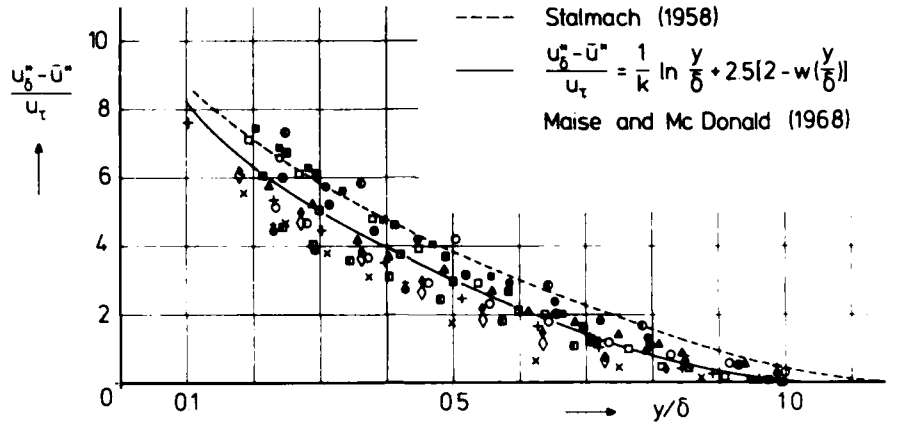

Fig. 3.3.2 Velocity distribution in a compressible turbulent boundary layer with zero pressure gradient. (For legend see Fernholz 1969)

non-zero value. Though the basic elements of this "amalgamated" velocity profile look promising, no sufficient comparisons with experiments are available as yet. We do not see, however, how the authors can solve the problem of determining the boundary layer thickness δ in a generally valid way other than by leaving it as a free variable in a curve-fitting operation and so essentially begging the question. Transformed velocities according to Van Driest (eqn. 3.3.12) were also used by Lewis, Gran & Kubota (1972) for a semi-empirical description of the velocity distribution in the inner and outer region.

3.3.3 The strength of the wake component

The velocity profile in the outer region generally departs quite noticeably from the semi-logarithmic profile of the inner region. Coles (1964) denoted the maximum difference between the profile and the logarithmic law

$$\frac{\bar{u}}{u_\tau} = \frac{1}{K_1} \ln \frac{u_\tau y}{\nu} + C_1 \qquad (3.3.19)$$

for subsonic boundary layers ($K = 0.40$ and $C_1 = 5.10$) by $\Delta\,(\bar{u}/u_\tau)$ and referred to it as the strength of the wake component for boundary layer flow. The quantity $\Delta\,(\bar{u}/u_\tau)$ was found by Coles "to be distinguished by an almost exquisite sensitivity to the history and environment of a particular flow". It can thus be of assistance in assessing boundary layer data more precisely and achieve the tentative identification of a normal state for tne turbulent boundary layer at constant pressure .

As can be seen from Fig. (3.3.3) - for the references see Coles' paper - the strength of the wake component of a subsonic zero-pressure-gradient turbulent velocity profile is a function of the Reynolds number $Re_{\delta 2}$, ranging from a constant value of approximately 2.75 in the range $4 \leq Re_{\delta 2} \times 10^{-3} \leq 15$ to zero at about $Re_{\delta 2} = 500$. For Reynolds numbers in the range $25 \times 10^3 \leq Re_{\delta 2} \leq 60 \times 10^3$ Coles noticed that measurements disagree both with each other and with experimental data at lower Reynolds numbers. He left the issue open, noting only that it seems to be necessary to choose between two alternatives: (1) either some of the experimental data at large Reynolds numbers must be questioned on grounds that are at present obscure; (2) or the similarity laws for the mean profile, particularly the defect law, are not valid at the high level of precision attempted in Coles' survey. He estimated the accuracy with which $\Delta\,(\bar{u}/u_\tau)$ can be determined as being no better than 5 to 10 %, given a typical uncertainty of perhaps 0.01 in $\bar{u}/u_\delta$. This seems to be an optimistic estimate for compressible boundary layers, because skin friction measurements

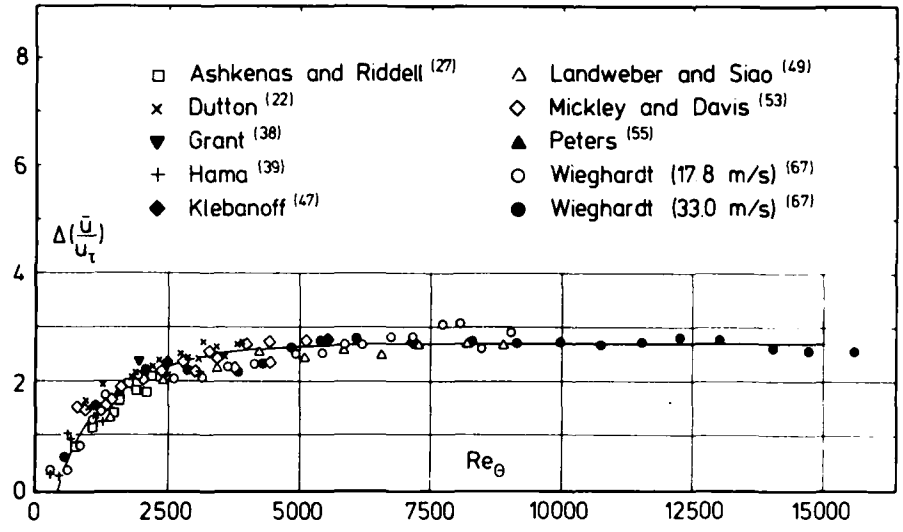

Fig. 3.3.3 Strength of the wake component in equilibrium subsonic turbulent flow (zero pressure gradient). From Coles (1962).

alone show a greater range of uncertainty than in the subsonic case.
Nevertheless it seems to be worthwhile to transfer the evaluation of such a wake-strength model to compressible boundary layers. First attempts were presented by Squire and Fernholz (Euromech 21, Toulouse 1970) and published in 1971 and 1972, respectively. In both cases the strength of the wake component $\Delta(\bar{u}/u_\tau)$ was evaluated from transformed velocities with eqn. (3.3.9) as the base line. For the determination of $\bar{u}^*$ Squire (1971) used the original Van Driest transformation with recovery factor unity and Re_ζ as the abscissa whereas Fernholz (1972) used eqn. (3.3.10) with recovery factor 0.896 and $Re_{\delta 2}$ (eqn.2.3.5) as correlation parameter (see also Mabey 1977).
In the subsonic case the choice of the Reynolds number - defined as $\delta_{2K}\, \rho_\delta\, u_\delta/\mu_\delta$ - does not pose a problem. This is not so in supersonic boundary layers where there exist many more possible combinations of ρ_δ, ρ_w, μ_δ, μ_w, δ_2 and δ_{2K}.
This is well illustrated by a comparison of Figs. (3.3.4 a & b). For this initial discussion of the wake-strength we have restricted the test cases to those where the boundary layer on an adiabatic wall has grown from a well defined origin - the leading edge of a flat plate, for example, - under constant pressure conditions throughout.

Fig. (3.3.4a) shows the development of the strength of the wake component with Reynolds number $Re_{\delta 2}$. There is a decrease of the wake component similar to that observed in the subsonic case, with $\Delta(\bar{u}^*/u_\tau)$ tending towards zero as $Re_{\delta 2}$ becomes smaller than about 500; furthermore there is an overshoot beyond the subsonic line (taken from Coles (1962) Rand Report) with a peak at about $Re_{\delta 2} = 6 \times 10^3$, and perhaps a subsequent decay to the subsonic line. Overshoot and peak are, however, almost entirely formed by measurements carried out in a single experimental facility by Hastings & Sawyer (1970) and Mabey et al. (1974). It would therefore be unwise to place too much emphasis on this group alone without further evidence from other experiments. Compared with this group of high data, recent measurements of velocity profiles at low Reynolds numbers by Mabey (1977) reveal a much smaller wake strength. They are in fact lower than Coles' (1953) velocity profiles in about the same Mach number range.
The scatter of the data is such that we could not discover any explicit influence of the Mach number on the strength of the wake component (see also Squire 1971). Any attempt to do so would have to be in statistical terms.

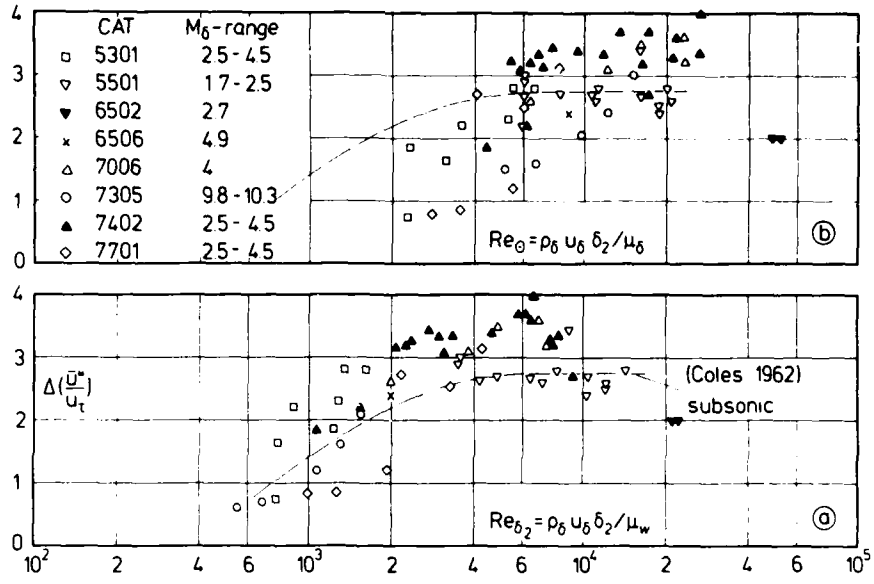

Fig. 3.3.4 Strength of the wake component in a compressible turbulent boundary layer (adiabatic wall, zero pressure gradient, defined origin)

As will be evident from the log-law plots below, measurements did not always agree with eqn. (3.3.9). In these cases the wake strength $\Delta\ (\bar{u}^*/u_\tau)$ was determined as the maximum vertical distance between the measurements in the outer region and a line with the same slope as eqn. (3.3.9) but with a constant C_1^* adapted to the measurements of the specific velocity profile, sometimes larger and sometimes smaller than 5.10. Such a procedure inevitably introduces a personal factor and thus contains a further uncertainty.

In Fig. (3.3.4b) the wake strength is plotted versus $Re_\Theta = \rho_\delta u_\delta\ \delta_2/\mu_\delta$. One might argue that a quantity characteristic of the outer region of a boundary layer such as the strength of the wake component should be a function of outer-edge quantities only and should therefore be a function of Re_Θ rather than Re_{δ_2}. An empirical reason for not accepting this argument is that the decay of the wake component to zero at Reynolds numbers at about 500 would not then be transformed correctly on to the subsonic data collected by Coles (1962).

Fig. (3.3.3) leads to the suggestion that the strength of the wake component and the wake parameter Π in eqn. (3.2.5) of Coles' wall-wake law are correlated for at least a subsonic boundary layer with zero pressure gradient by

$$\Pi = \frac{K_1}{2}\ \Delta(\bar{u}/u_\tau) \qquad (3.3.19).$$

This relation can be extended to compressible boundary layers when $\Delta\ (\bar{u}/u_\tau)$ is replaced by $\Delta\ (\bar{u}^*/u_\tau)$. If such a correlation exists then it should be possible to transform eqn. (3.2.5) by using $\bar{u}^*$ and the integral length Δ^* defined by eqn. (3.3.16) and to calculate Π^* from a suitably transformed relationship, such as eqn. (3.3.20).

$$\Pi^* = \frac{K_1}{2}\left[\frac{\bar{u}_\delta^*}{u_\tau} - \frac{1}{K_1}\ \ln\left(\frac{u_\tau \Delta^*}{\nu_w}\ \frac{\delta}{\Delta^*}\right) - C_1\right] \qquad (3.3.20).$$

It is interesting to note that for zero pressure gradient boundary layers on adiabatic walls the expression $(u_\tau\ \Delta^*/\nu_w)$ is to a good approximation a function of the Reynolds number Re_{δ_2} only (Fernholz 1969) and that this statement can be extended to boundary layers along isothermal walls as can be seen in Fig. (3.3.5).

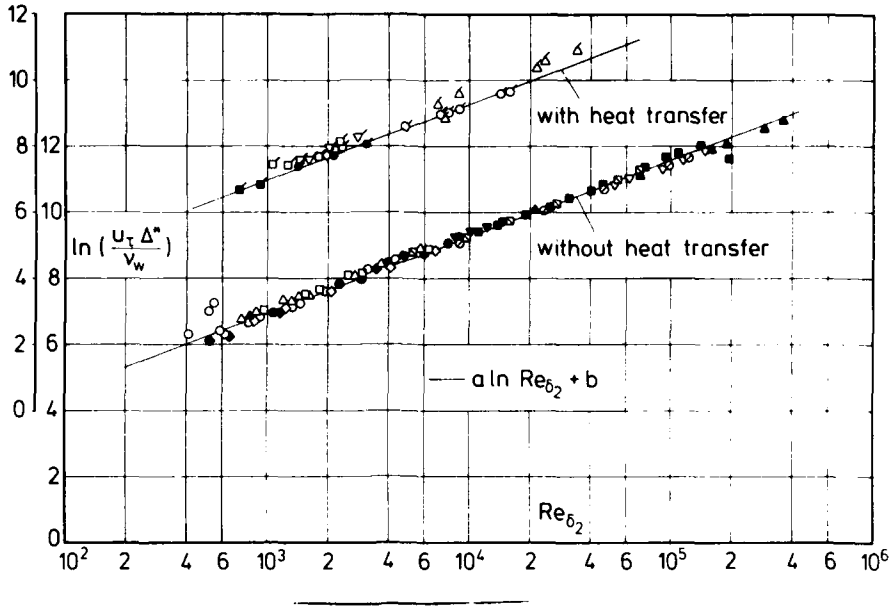

Fig. 3.3.5 Relationship between the characteristic Reynolds numbers $u_\tau \Delta^* / \upsilon_w$ and $u_\delta \rho_\delta \delta_2 / \mu_w$ for compressible turbulent boundary layers (isothermal and adiabatic walls, zero pressure gradient)

The symbols in Fig.(3.3.5)are explained in Table 3.3.2.

	CAT		M_δ	$Re_{\delta_2} \times 10^{-3}$	T_w/T_r
○	7701 S	Mabey	2.5 - 4.5	0.4 - 4.3	1
◆	7305	Watson	9.0 - 10	0.5 - 1.5	1
△	5301	Coles	2.0 - 4.5	0.7 - 5.8	1
□	5802	Stalmach	1.7 - 3.7	0.9 - 5.8	1
●	7402	Mabey et al.	2.5 - 4.5	2.2 - 9.1	1
◇	7006	Hastings & Sawyer	4	0.8 - 6.7	1
▼	5501	Shutts	1.7 - 2.5	3.5 - 14.3	1
⊠	6505	Jackson	1.6 - 2.2	8.9 - 71.1	1
⊘	7601	Vas	3	9.1 - 121	1
■	7302	Winter & Gaudet	0.2 - 2.2	10.8 - 196	1
▲	6502	Moore & Harkness	2.7 - 2.9	21.6 - 359.3	1
▽	6903	Thomke	3.0 - 4.4	62.0 - 115	1
◪	6002 S	Danberg	5.2	0.7 - 1.0	0.80 - 0.90
◱	7204	Keener & Hopkins	2.0 - 6.5	1.0 - 2.3	0.33 - 0.50
◩	7205	Horstman & Owen	7.2	1.4 - 3.0	0.50
▽	7702 S	Laderman & Demetriades	3	1.3 - 2.8	0.57 - 1.00
◇	6506	Young	4.9	2.0	0.50 - 1.00
◎	7303	Hopkins & Keener	7.5	4.5 - 15.5	0.31 - 0.46
△	7202	Voisinet & Lee	4.9	6.9 - 33.0	0.22

Table 3.3.2

Furthermore one can easily verify that the following identity holds

$$\frac{u_\tau \Delta^*}{\nu_w} = \frac{u_\delta \, \delta_1^*}{\nu_w} \tag{3.3.21}$$

where

$$\delta_1^* = \int_0^\delta \left(1 - \frac{\bar{u}^*}{u_\delta^*}\right) dy \tag{3.3.22}$$

Eqn. (3.3.21) reduces to the equivalent relation for incompressible flow suggested by Rotta (1962). The measurements plotted in Fig. (3.3.5) can be approximated by

$$\ln \left(u_\tau \Delta^* / \nu_w\right) \simeq 0.964 \ln Re_{\delta_2} + 0.04 \tag{3.3.23}$$

The strength of the wake component at higher Reynolds numbers - up to 3.6×10^5 - can be investigated only if one is prepared to evaluate measurements where the origin of the boundary layer is not defined (Fig. 3.3.6) such as on wind tunnel wall or a wall forming a continuation of a wind tunnel nozzle. The scatter of the data in relation to the line for subsonic equilibrium flat plate data is even larger than in Fig. (3.2.4). A second peak, formed by noticeably "high" data at about $Re_{\delta 2} = 7 \times 10^4$, is again formed by measurements from a single experiment (Thomke 1969).

The measurements of Jackson et al. (CAT 6505) contain both profiles with large and with small wake strength, the latter at $Re_{\delta 2} > 6 \times 10^3$ supported by the measurements of Vas et al. (CAT 7601). Two velocity profiles with a similarly small wake strength at moderately high Reynolds numbers were measured by Moore & Harkness (CAT 6502) but the majority of their velocity profiles showed the almost "normal" scatter about the line $\Delta(\bar{u}^*/u_\tau) = 2.75$.

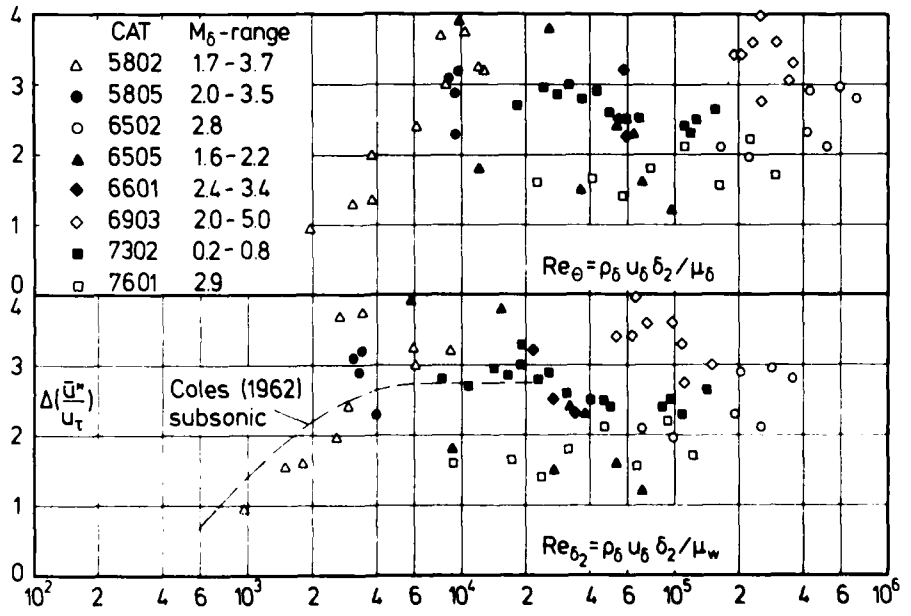

Fig. 3.3.6 Strength of the wake component in a compressible turbulent boundary layer (adiabatic wall, zero pressure gradient, origin not defined)

If one allows scatter of the wake strength within a band of ± 15% then one can conclude that similarity exists even for high Reynolds numbers, but we have no explanation yet for the consistent lower or higher data from CAT 6505 and 7601 or 6903 (Thomke), respectively.
An even less satisfactory picture is obtained from a plot of the wake strength in boundary layers with heat transfer (Fig. 3.3.7). There are very few measurements available and no trend can be recognised. An exceptionally large value of the wake strength (of about 7) occurs in a velocity profile measured by Laderman & Demetriades (1974) (see § 4.3) and some similarly high values in measurements of Voisinet & Lee (1972) (see Fig. 4.3.9). Neither of these data was plotted in Fig. (3.3.7), however.

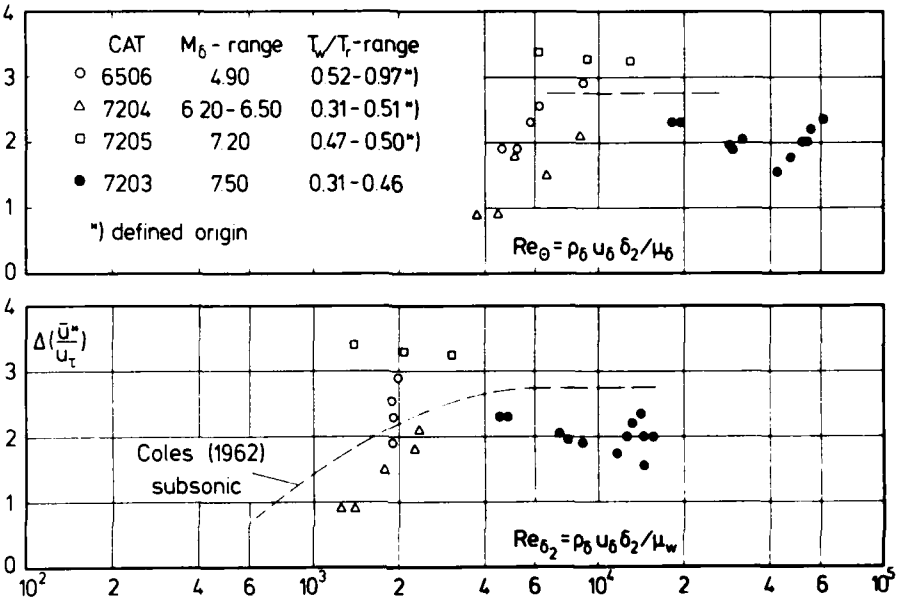

Fig. 3.3.7 Strength of the wake component in a compressible turbulent boundary layer (isothermal wall, zero pressure gradient)

Since this more general discussion of the development of the wake strength in a compressible turbulent boundary layer does not lead to a clear conclusion, velocity profiles with approximately the same Reynolds number were selected from among the large number of measurements and plotted as $\bar{u}^*/u_\tau$ versus yu_τ/ν_w in groups with approximately common Reynolds numbers $Re\delta_2$ of 2×10^3; 2.7×10^3; 8×10^3; 71×10^3 and 34×10^3.
Beginning at the low Reynolds numbers (Fig. 3.3.8) we find velocity profiles with little scatter about the logarithmic law - note the scale - but with a variation in wake strength in the range $1.60 \leq \Delta(\bar{u}^*/u_\tau) \leq 3.70$. For the upper group all measurements were taken from one experiment (CAT 5302), while for the lower the data were selected from four different experiments. No systematic differences are found though higher values of the wake strength seem to be linked more often to the higher Mach numbers. Fig. (3.3.9) shows measurements with different upstream conditions (CAT 5501) on a flat plate: Transition trip upstream of profile 0102, no transition trip (profile 0401) and extra screens in the settling chamber upstream of profile 0603 (skin friction was measured, however, without the extra screens). Also shown is profile 74021505, for which transition was forced. Apart from the disturbed lower part of profile 0401 the behaviour of the other profiles is normal and it is not possible - taking into account Fig. (3.3.8) - to say whether the variation in wake strength $2.20 \leq \Delta(\bar{u}^*/u_\tau) \leq 3.20$ is due to the changed upstream conditions or due to "normal" scatter.

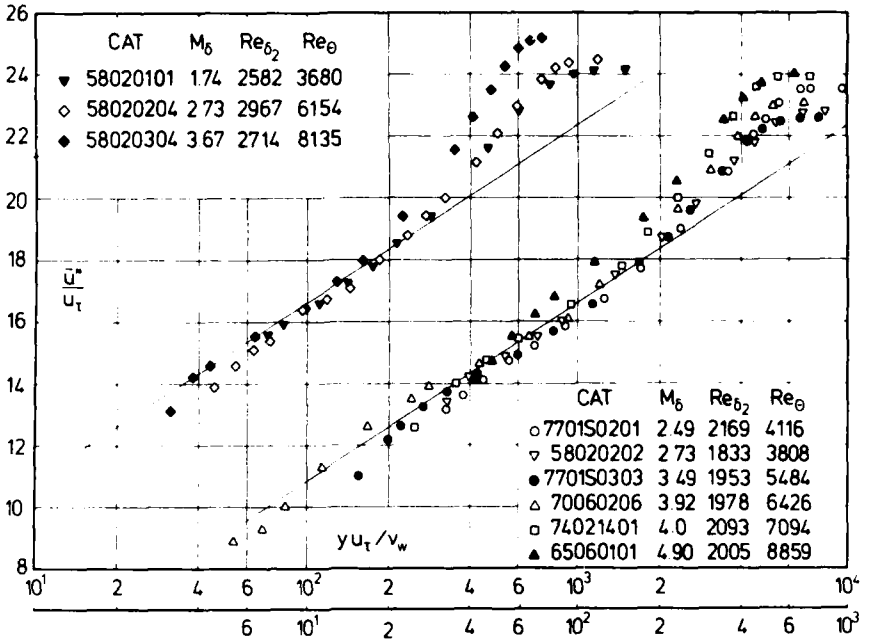

Fig. 3.3.8 Variable wake strength in a compressible boundary layer at constant Reynolds number $Re_{\delta 2}$ (adiabatic wall, zero pressure gradient)

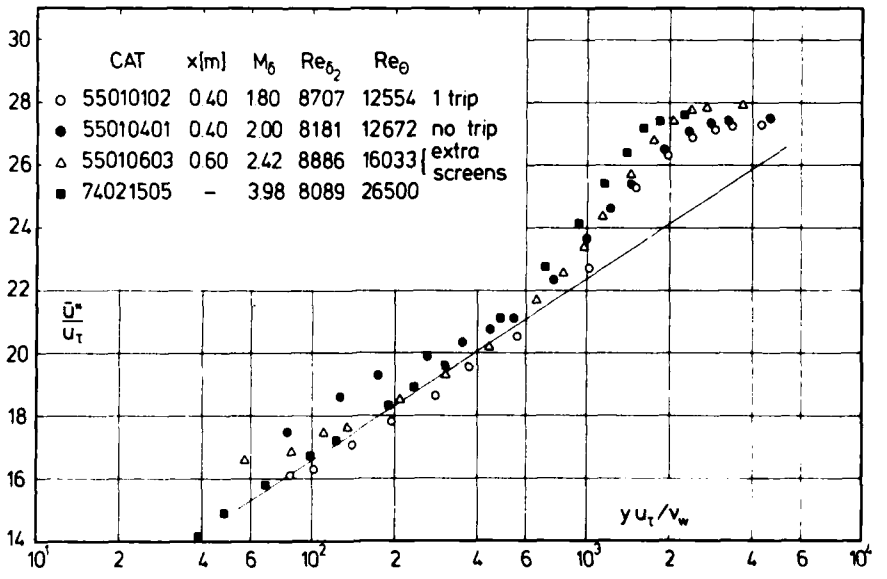

Fig. 3.3.9 Variable wake strength in a compressible boundary layer with variable upstream conditions (adiabatic wall, zero pressure gradient)

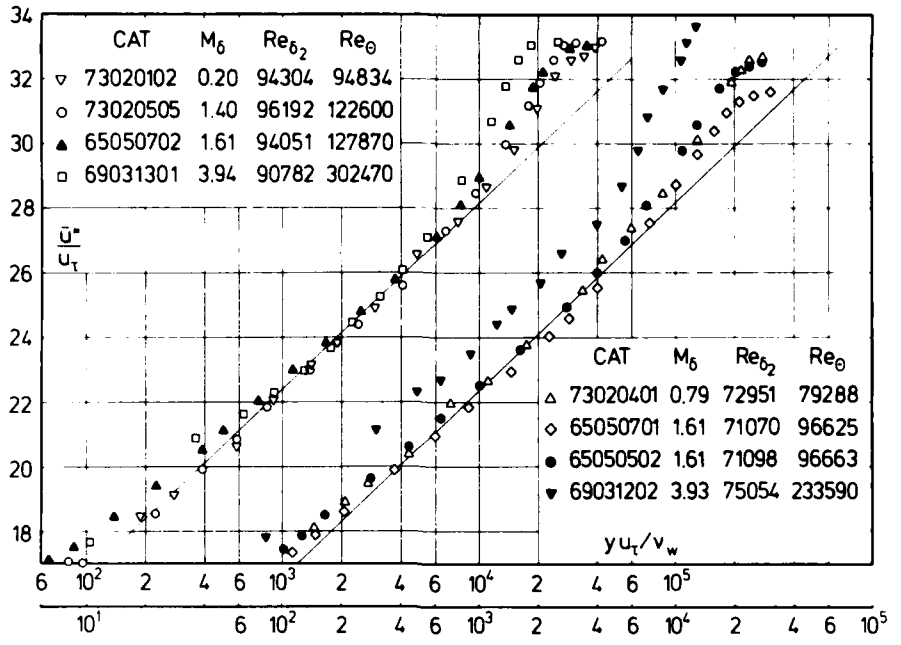

Fig. 3.3.10 Variable wake strength in a compressible boundary layer at constant Reynolds number Re_{δ_2} (adiabatic wall, zero pressure gradient)

This wide variation of $\Delta(\bar{u}^*/u_\tau)$ is found again at still higher Reynolds numbers (Fig. 3.3.10), and no clear cut reason can be found for these differences in terms of the information given in the description of the experiments. Profile 69031202 (Thomke) shows definitely an odd behaviour but this is not characteristic of this experiment if one takes into account profile 69031301 or other profiles in Fig. (4.2.17).

3.3.4 Factors influencing the wake component

In an attempt to account for the observed discrepancies in supersonic boundary layers we should perhaps look first at the main effects which were considered to be the cause of anomalies in the wake strength in subsonic boundary layers. Coles (1962) found that three-dimensionality in the mean flow, free-stream turbulence level and tripping devices were such causes. "Except possibly at very low Reynolds numbers, the effect of increased free-stream turbulence is to decrease the strength of the wake component. The amount of the decrease may also depend on Reynolds number and on the scale of the turbulence. As for boundary layers with tripping devices it was found that the strength of the wake component sometimes dropped below the normal or equilibrium value following a strong disturbance". We now comment on each factor in turn:

Three-dimensionality of the flow

In principle all measurements in boundary layers are likely to be influenced by three-dimensional effects if they were obtained in the downstream part of a wind tunnel the width to length ratio of which is small. Unfortunately it is impossible to prove or qualify such a deficiency since in general we do not have enough information about the flow field, and sufficiently closely spaced velocity profiles are not available to allow a check of the momentum integral equation. We can only accept - or not - the authors' word that all is well. A first attempt to estimate the effects of convergence or divergence of the flow for center-line velocity profiles in square-duct type wind tunnels was made by Brederode & Bradshaw (1978) for subsonic flow. They suggest a ratio of $\delta/b = 0.25$ as an upper limit for the boundary layer along the center-line to be still two-dimensional.

Free-stream turbulence level

We know of only one case where an attempt was made to influence the free-stream turbulence level deliberately (CAT 5501) and the velocity profiles are plotted in Fig. (3.3.9). If the extra screens in the settling chamber have reduced the turbulence level - which was not explicitly stated by Shutts et al. (1955)- then the increase of the wake strength from $\Delta\ (\bar{u}^+/u_\tau) = 2.70$ for no extra screens (profile 55010102) to 3.20 would agree with the finding of Coles for subsonic boundary layers. But even this rather weak conclusion must be treated with caution since only the Reynolds numbers have a common value, the Mach number was changed from 1.80 to 2.42, and the skin friction was measured only without the extra screens. This is a good example of how difficult it can be to draw definite conclusions from the measurements in AGARDograph 223.

There is no experiment where the free-stream turbulence level is explicitly stated in any of our documented entries. If its influence on the wake strength and on the skin friction were to be strong then this lack of information would be extremely unfortunate. Systematic experiments are urgently required and could well explain some of the scatter found in the wake strength of velocity profiles in supersonic boundary layers.

Tripping devices

Tripping devices are used for several purposes in boundary layer investigations, mainly for promoting transition and for artificially thickening the boundary layer. Tripping the boundary layer automatically introduces disturbances and this must be done with great care since a boundary layer may recover very slowly from the effects of such a disturbance. Though a tripped boundary layer is thicker and so more convenient for the insertion of measuring probes, it may exhibit features which are by no means characteristic of the equilibrium or normal boundary layer which was the original aim of an investigation. As can be seen from tables 4.2.1, 4.3.1 and 4.3.2 most of the boundary layers which are well documented have undergone forced transition and have thus been disturbed in one way or another.

Coles (CAT 1953) investigated the effect of different types of tripping devices on a boundary layer (Fig. 3.3.11) - fence trip (53011101), sand strip (53011201) and air-jet trip (53011302) - at the same Mach number (4.54) and about the same Reynolds number Re_{δ_2} (1288 to 1603). The small differences between the velocity profiles - measured about 0.5 m downstream from the trips - cannot be attributed to the tripping devices but more probably to values of the skin friction which, for example, seem to be too high for velocity profiles 0801 and 1101 as is suggested by the visible discrepancies in the semi-log region.

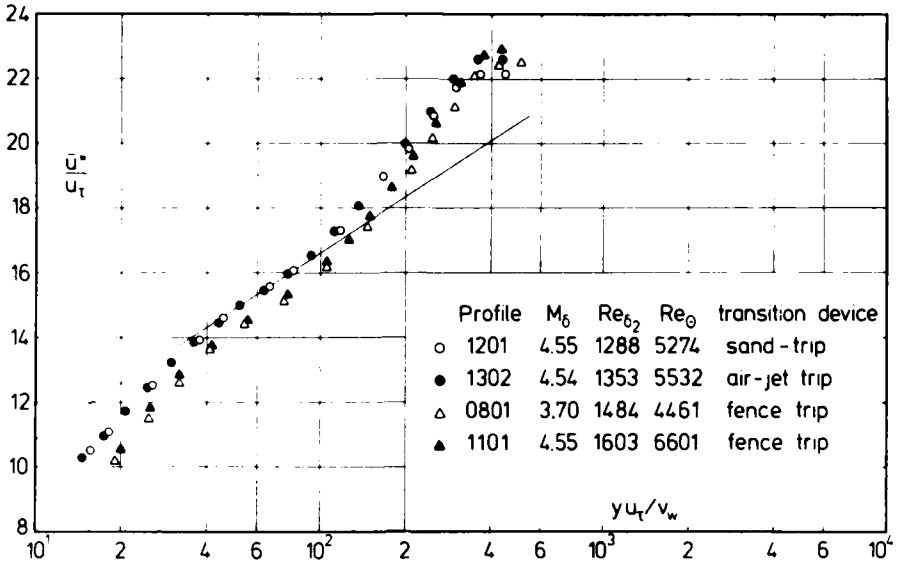

Fig. 3.3.11 Law of the wall for a compressible boundary layer (adiabatic wall, zero pressure gradient, different transition devices). Coles (CAT 5301)

Investigations into the effectiveness of air jets were extended by Korkegi (1954, 1956) but unfortunately no tabulated data are available. Stone & Cary (1972) present profiles downstream of very violent trips - airjets and rows of relatively large balls near the leading edge of a flat plate. We find less distortion introduced by the trips than is reported by the authors, and in general the interesting result is that the trips, at least at the downstream station of the two, do not seem to leave any special mark on the mean profile characteristics. On a transformed log-law plot, no effect can be seen which could not be accounted for by the general experimental scatter. Peake et al. (1971) investigated a boundary layer recovering in nearly constant pressure from the disturbance of flowing up and down a step (height 3.8 and length 12.3 mm at a station for which δ would have been 4 - 6 mm with no trip). The velocity profiles are shown in Fig. (3.3.12). Except for the first velocity profile (71020301), measured 36 mm behind the ring, the velocity profiles further downstream seem to have recovered completely from the disturbance if one accepts that the scatter may well not be due to physical effects but to uncertainties in the skin friction measurements. Scatter larger than normal is found in the measurements as a whole. In Fig. (3.3.12) we have also plotted for comparison profile 71020101 measured at the same position as profile 71020301 but without the ring. If one assumes the boundary layer thickness of this undisturbed velocity profile as a scale then the last measured velocity profile (0305) is about 63 boundary layer thicknesses downstream, and the normal behaviour of the velocity profiles downstream of a step with a height of about 60 % of the undisturbed boundary layer thickness is almost surprising.
As can be seen from Fig. (3.3.12) the measurements - except for 71020303 - do not agree well with eqn. (3.3.9), both gradient and constant being different. Such profiles are rare among the data presented in AGARDograph 223. If the wake strength is evaluated on the basis of individual straight lines through the data, one finds that $(\bar{u}^*/u_\tau)$ varies with the distance downstream falling to a value of 1.55 at $x = 0.66$ m (data not given in Fig. 3.3.12).

Upstream history effects

To the three physical effects discussed by Coles (1962) we would like to add at least one more, i.e. the influence of the upstream history on the strength of the wake component other than by tripping devices. Since there is no full systematic investigation of upstream history effects on the boundary layer - the experiment of Gates (CAT 7301) lacks skin friction information - we would like to draw attention to an experiment where there is a probable downstream heat-transfer history effect in addition to a downstream

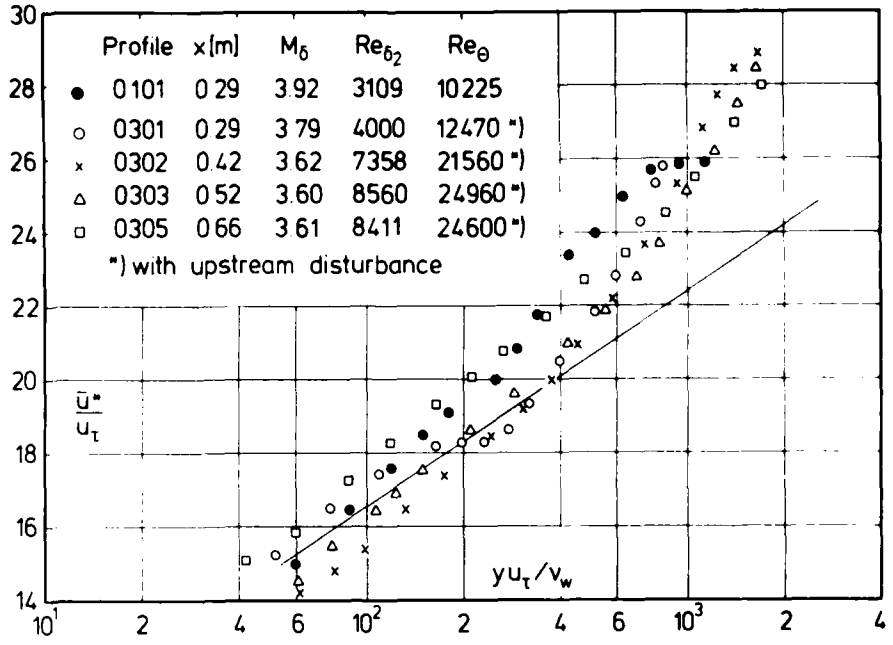

Fig. 3.3.12 Development of a compressible turbulent boundary layer downstream from a disturbance (adiabatic wall, zero pressure gradient). Peake et al. (CAT 7102).

effect of the nozzle pressure gradient (CAT 7202). These experiments, which cover the adiabatic wall and the isothermal wall cases, contain velocity profiles showing a different behaviour from any we have observed before. The wake strength in the adiabatic wall zero pressure gradient boundary layer reaches values of $\Delta (\bar{u}^*/u_\tau)$ ranging from 5.4 to 8.0 (Fig. 3.3.13). Other velocity profiles in the same Reynolds number range show a transitional behaviour (not plotted here) and velocity profiles with very high cooling rates show a behaviour which differs completely from the normal logarithmic law (Fig. 4.3.10) and which is due to uncorrected skin friction measurements (Voisinet 1977).

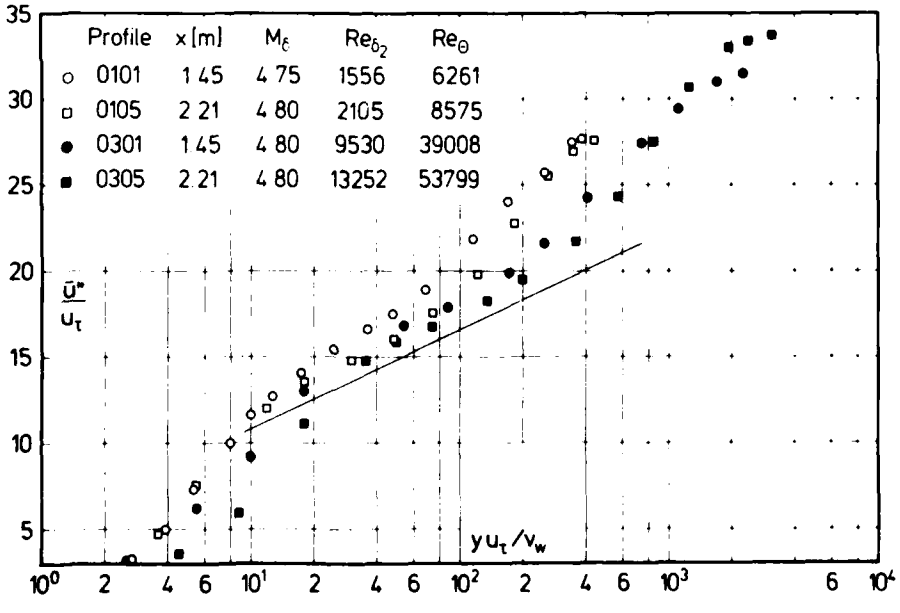

Fig. 3.3.13 Law of the wall for a compressible boundary layer (adiabatic wall, zero pressure gradient, origin not defined). Voisinet & Lee (CAT 7202).

3.3.5 Conclusions as to the strength of the wake component

Tentatively one could draw the following conclusions:

1) More systematic measurements with well defined boundary conditions and a well known wind tunnel environment are necessary.

2) The strength of the wake component decays at low Reynolds numbers both in subsonic and supersonic boundary layers tending to zero below a Reynolds number $Re_{\delta_2} < 500$. This behaviour appears to be independent of Mach number and heat transfer in the parameter range discussed in this report.

3) The apparent maxima of the wake strength at Reynolds numbers $Re_{\delta_2} \approx 6 \times 10^3$ and 7×10^4 must be treated with caution since they are in each case formed by measurements from a single experiment.

4) If a scatter of about $\pm$ 20 % of the wake strength is accepted then an average value of the wake strength of 2.75 can be assumed to exist for supersonic boundary layers at $Re_{\delta_2} > 6 \times 10^3$. This agrees with the wake strength for subsonic flow found by Coles (1962) in the range $6 \times 10^3 \leq Re_{\delta_2} \leq 15 \times 10^3$.

5) A determination of the wake strength cannot be very precise, but the amount of scatter found is too great to be accounted for by simple random error. No definite explanation can be given yet. Discrepancies in the wake strength could be due to the three-dimensionality of the flow, free-stream turbulence, upstream history effects or other as yet unknown environmental conditions. This deficiency prevents us as yet from using the wake strength as a means of classification for compressible turbulent boundary layers as suggested by Coles (1962) for subsonic zero-pressure gradient boundary layers.

3.4 Transformation concepts

We have just advocated rather strongly van Driest's transformation and this will be used throughout the remainder of sections 4 and 5, where we compare measurements with each other and with semi-empirical relations. Therefore it seems necessary to make a few more general remarks about transformation concepts in boundary layer theory. The motivation behind all transformations is to convert the mathematically difficult coupled system of partial differential equations describing compressible boundary layers into a form which can be solved more easily, for example into a system which is mathematically similar to the equations for boundary layers with constant density. A mathematically correct transformation then makes it possible to transform the solutions of the "simpler" system to the complex system in order to predict the behaviour of the compressible flow. The Stewartson-Illingworth transformation provides such a relationship between a high Mach number laminar boundary layer and a subsonic flow (see for example Stewartson 1964). The difference in the turbulent case has been stated by Crocco (1963) as follows: "since the mechanism determining the distribution of the turbulent shearing stress is unknown, one cannot be assured of the physical validity of the transformation, even if this correctly transforms the inertia and pressure terms of the equations". On this point Crocco differs from Coles (1962) who points out that: "if a transformation can be found to treat the acceleration and pressure terms in the equations, and if this transformation is required to be physically realistic, then it must follow without reference to any special definition of the shearing stresses that these stresses can also be treated by the transformation". There have been many attempts to take into account the arguments given by Coles and Crocco for their respective views, but the problem of a point to point transformation of a high speed turbulence field to a low speed one remains unsolved. All transformation concepts for turbulent flows need assumptions based on experimental input. We hope it will suffice here to say that Coles' transformation connects the full set of equations in both planes of the transformation, considers the physics of the turbulent motion via three functions and needs a minimum of semi-empirical information. For a survey of empirical relations used in transformation concepts the reader is referred to Economos (1970), Economos & Boccio (1970) and Küster (1972). Van Driest's transformation as applied in this investigation circumvents the problem inherent in transformations for turbulent flows by shifting the difficulties into the acceptance of a mixing length hypothesis used to connect the turbulent shear stress and the mean velocity. Before considering any further development of transformation concepts for compressible turbulent boundary layers the reader should take note of the argument brought forward by Beckwith (1970) to illustrate the lack of correspondence in the transformed incompressible flow:

"(1) When streamwise pressure gradients are large in a hypersonic boundary layer, then the <u>normal</u> pressure gradients are also large because of the inherent Mach wave structure of the flow (see § 6 where it will be seen that this is not necessarily the case).

(2) When the heat transfer is large in the compressible flow, $\partial\bar{T}/\partial y$ is large both in the compressible flow and in the corresponding incompressible flow which is, however, restricted by the condition that $\partial\bar{p}/\partial y = 0$ and that $\bar{\rho}$ is constant. Hence, for any reasonable equation of state for gases, the requirements for correspondence between the two flows cannot be satisfied.

(3) If the turbulent correlation terms containing ρ' are significant (e.g. in low-density compressible flows), then the transformation again breaks down because of the constant-density limitation in the low-speed flow."

Two further remarks concern the energy equation which must be retained in full also in the case of the low-speed flow. Terms which can usually be omitted if the Mach number tends to zero - as the last two terms in square brackets of eqn. (2.3.2) - may become important near the wall where the temperature and viscosity on the one hand and the turbulent dissipation term $\bar{u}\,\bar{\rho}\,\overline{u'v'}$ on the other hand are large.

4. INTERPRETATION OF MEAN FLOW MEASUREMENTS FOR ZERO PRESSURE GRADIENT

4.1 General remarks

4.1.1 Basis of presentation

Since this section will consist of a discussion of mean flow measurements in compressible turbulent boundary layers and a comparison of the measured data with theoretically or semi-empirically derived solutions, we start by quoting a remark of Coles' (1953): "In the area of compressible turbulent boundary layers a comparison of experimental results does not involve the measurements so much as their interpretation". We have presented here only "raw" data or at most measurements corrected by the experimentalist whom we have assumed to be the person who is most familiar with the peculiarities of his equipment and his specific experimental conditions. We decided therefore not to follow Coles (1962) or Coles & Hirst (1968) who fitted the profiles to the logarithmic law of the wall before discussing them any further, since we could not be sure that by such a procedure some information inherent in the measurements - though possibly not yet recognizable - might get lost. Sometimes the "obviously" erroneous data point has indicated the direction to future progress.

Unfortunately, we do not know the environmental conditions, such as the noise level or the freestream-turbulence level in the tunnel, for any of the experiments documented in AGARDograph 223 (Fernholz & Finley 1977), and for only a few are we fortunate enough to know something about the upstream history. We also point out here that we do not think that the boundary layer thickness δ should be used in the interpretation of compressible boundary layer data but a better defined integral length, such as δ_2 or Δ^*. Here we recognize that we are prejudiced and discuss the reasons in § 7.

4.1.2 Classification of experiments

The experiments available for comparison suggest an order of presentation which was given in § 6 and 7 of AGARDograph 223 and which will also be used here.
More than half of the available data describe tests made in nominally constant-pressure boundary layers (group I) which we have subdivided firstly into cases in which the boundary layer has grown from a well defined origin under constant pressure conditions throughout (IA) and secondly into cases (IB) where the boundary layer is formed on a tunnel wall or the continuation of the nozzle wall after having passed through the nozzle expansion upstream. In two cases (CAT 7202 and 7301) this history is in some measure described and in one (CAT 7302) the development is so long and gradual that the boundary layer is probably fully "relaxed" so as to have the same characteristics as a fully developed flat plate boundary layer. Cases with substantial heat transfer are relatively rare. There is in addition a small group (IC) of cases describing the recovery of a severely disturbed layer, under local zero-pressure-gradient conditions. Unless otherwise stated, we have chosen for comparison only those measurements for which at least both the velocity profile and the skin friction were measured.

4.1.3 The standard case

A discussion of the different velocity profiles belonging to one of these categories would be more logical and informative if a standard velocity profile could be defined. One result of the investigation described in § 3.3.5 has been to show that in compressible boundary layers a criterion based on the wake strength is not definite enough "to make possible not only a precise classification of boundary layer flows but a refinement and rationalization of the similarity laws" (Coles 1962). We are forced therefore to retreat one step and to demand only that the transformed standard velocity profile for a zero pressure gradient compressible turbulent boundary layer along an adiabatic wall obeys the law of the wall (eqn. 3.3.9) and the outer law (eqn. 3.3.17) in their van Driest transformed form. How far both relationships may be extended to hold for boundary layers along isothermal walls with severe heat transfer must be checked by comparison with experiment. As will be shown the law of the wall can also be applied to boundary layers with moderate adverse and favourable pressure gradients for which the outer law in the form of eqn. (3.3.17) does not hold.

The outer profile is, on the contrary, a very sensitive indicator of the presence of pressure gradients or their downstream effects in a relaxing boundary layer.

The "standard" boundary layer (normal, equilibrium, ideal, fully developed, asymptotic are some other possible adjectives proposed by Coles 1962) must be free of upstream history effects and will develop with constant local boundary conditions only. This state can be achieved in practice if the Reynolds number is high and when upstream disturbances have completely abated. Such flows are probably generated best in two ways: (1) On a flat plate positioned in the zero pressure gradient region of the test section with a sharp leading edge, i.e. with a defined origin. Disturbances caused by a leading edge or a tripping device must have died out completely at the measuring station. (2) On a wind-tunnel wall so far downstream from the nozzle that equilibrium has been reached again. The latter set-up which is the only one by which boundary layers with very high Reynolds numbers can be generated has the inherent disadvantage that it is difficult to keep the boundary layer free of flow convergence or divergence, i.e. of three-dimensional effects over a long running distance.

We shall discuss first the "standard" boundary layer velocity profiles and the effects of perturbations on velocity profiles which are due to boundary or upstream conditions. The procedure for each group of the zero-pressure gradient boundary layers is the same, complemented only by necessary amendments which are specific to a particular case.

We have first plotted the velocity profiles in the law of the wall coordinates as specified by eqns. (3.3.9) and (3.3.10) and compared them with the logarithmic law of the wall using the von Kármán constant $K_1 = 0.40$ and $C_1 = 5.10$.

The next step has been to plot the velocity measurements in the outer region in coordinates as specified by eqn. (3.3.17). Though this is a relatively simple way to perform a comparison we will see that a number of conclusions can be drawn from such a plot demonstrating effects due to low Reynolds number flow, transition, pressure gradient or upstream history.

4.2 Zero pressure gradient adiabatic cases

4.2.1 Supposedly "standard" cases (class IA)

Specification of zero pressure gradient and adiabatic wall gives boundary conditions which reduce the number of parameters to a bare minimum, i.e. to Reynolds number and Mach number, and minimize the dependence on stagnation temperature information.
For the following discussion we have chosen the investigations classified as I A 1, i.e. flows with a defined leading edge or origin, developed under zero pressure gradient conditions, with an adiabatic and smooth wall, where both velocity profiles and skin friction were measured. The relevant overall information is given in table 4.2.1.

Table 4.2.1

CAT	Author	M_δ	$Re_{\delta_2} \times 10^{-3}$	Transition
5301	Coles	2 - 4.5	0.7 - 5.7	Forced
5501	Shutts et al.	2 - 2.2	3.5 - 12	Forced
6502	Moore & Harkness	2.9	21.6	Natural
6506	Young	4.9	2.0	Probably natural
7006	Hastings & Sawyer	3.9	0.7 - 7.4	Natural
7305	Watson et al.	10	0.4 - 1.5	Natural
7402	Mabey et al.	2.5 - 4.5	1 - 9	Forced (glass spheres)

After looking at a very large number of data which were compared with the law of the wall and the law of the wake - a by-product of AGARDograph 223 - we feel that the velocity profiles measured by Mabey et al. (1974) are probably the most reliable ones, performed with a great amount of care and professional skill. From among the large number of velocity profiles a few were chosen which are thought to be representative of this experiment and which are shown in Figs. 4.2.1 to 4.2.4.

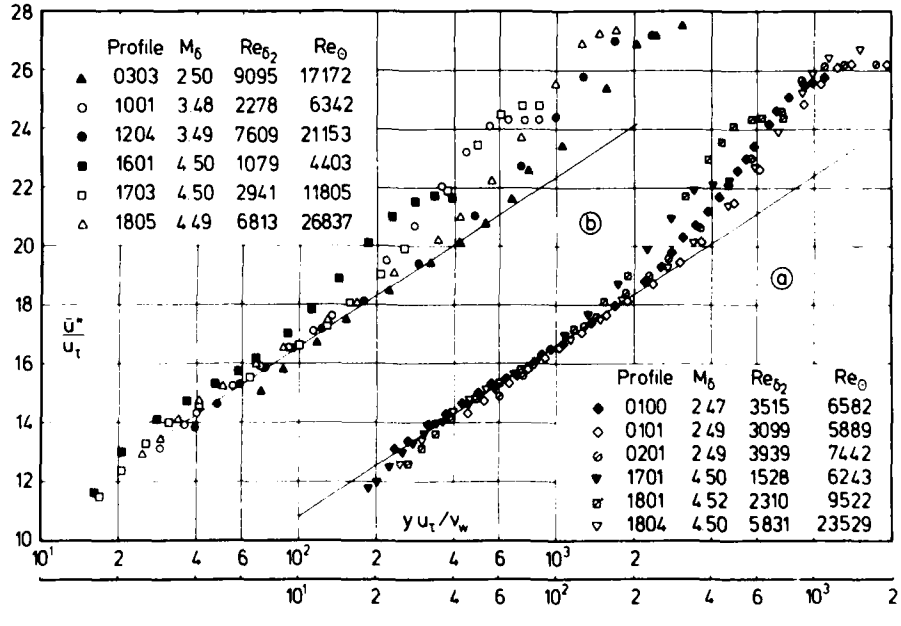

Fig. 4.2.1 Law of the wall for a compressible boundary layer (adiabatic wall, zero pressure gradient, defined origin). Mabey et al. (1974)

In Fig. (4.2.1) velocity profiles are presented which agree very well with the law of the wall (group a) in a Reynolds number range 1500 < $Re_{\delta 2}$ < 6000. Mark the large differences between the two definitions of the Reynolds number $Re_{\delta 2}$ and Re_{Θ}. The velocity profiles plotted in Fig. (4.2.1b) show what is thought to be the normal scatter about the log-law line due to a measuring error in the skin friction τ_w of about ± 4 %. In principle there need not be differences between velocity profiles at low ($Re_{\delta 2}$ < 2000) and moderate to high Reynolds numbers ($Re_{\delta 2}$ > 4500) measured at two positions on the plate if the boundary layer is fully turbulent (Fig. 4.2.2a). All velocity profiles discussed so far exhibit the slope given by the von Kármán constant K = 0.40, only one profile (74020301) having a slightly steeper slope than the others (Fig. 4.2.2b). Similar velocity profiles were measured by Coles (1953) and are presented in Fig. (4.2.5a). Neither of the authors comments on these "odd" profiles, and no explanation could be found from the description of the experiments.

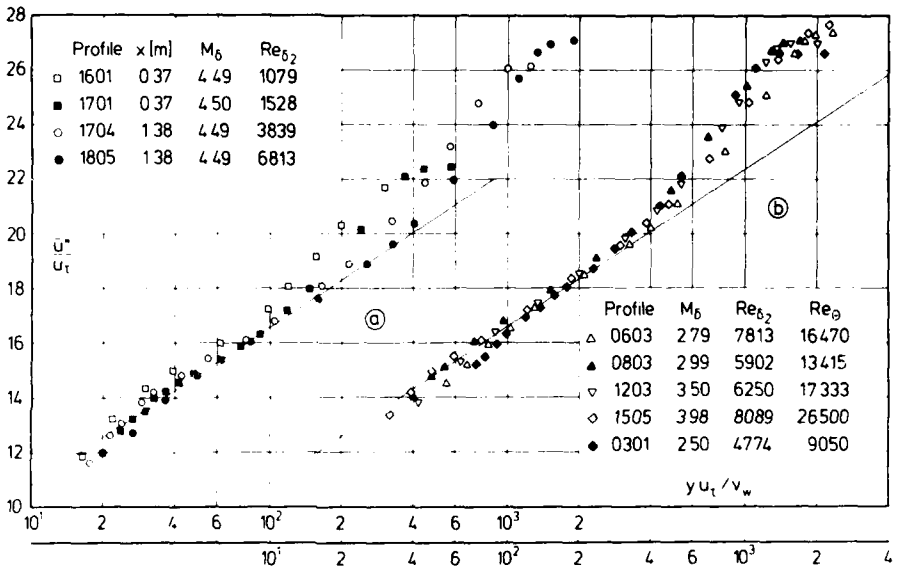

Fig. 4.2.2 Law of the wall for a compressible boundary layer (adiabatic wall, zero pressure gradient, defined origin). Mabey et al. (1974)cf. fig. 4.2.4

Figs. (4.2.3) and (4.2.4) show that the measurements agree well with the outer law in the form of eqn. (3.3.17). The good agreement with both the logarithmic law and the outer law proves that the boundary layer is fully developed in this experiment, even at the low Reynolds numbers. For a discussion of velocity profiles at very low and transition Reynolds numbers, measured in the same test boundary layer by Hastings & Sawyer (1970) and Mabey (1977), the reader is referred to § 4.4.

Coles' (1953) velocity profiles (Fig. 4.2.5) can be divided into two groups, (a) one with a steeper slope than given by the von Kármán constant in eqn. (3.3.11) and the other (group b) where the measurements follow the logarithmic law very well (the two groups of measurements are plotted with a shift by one decade in the abscissa). Different transition devices can not possibly answer for these discrepancies as was shown in Fig. (3.3.11). In the outer law plot this difference in slope does not appear, and here the velocity profiles are preferably grouped according to the Reynolds number range with a rough division at about $Re_{\delta 2} \approx 2000$ (Fig. 4.2.6). For $Re_{\delta 2}$ < 2000 low Reynolds number effects are clearly visible resulting in a departure of the velocity profile from the straight line - at much smaller values of - ln (y/Δ^*) than at higher Reynolds numbers.

Velocity profiles at higher Reynolds numbers were measured by Shutts et al.(1955) and Moore & Harkness (1965). The log-law plot is shown in Fig. (4.2.7) and the outer law in Fig. (4.2.8). Whereas the measurements of Moore & Harkness agree very well with the inner and the outer law (note the small wake strength), those of Shutts et al., while showing the usual amount of scatter for the inner law, agree very well with the outer law.

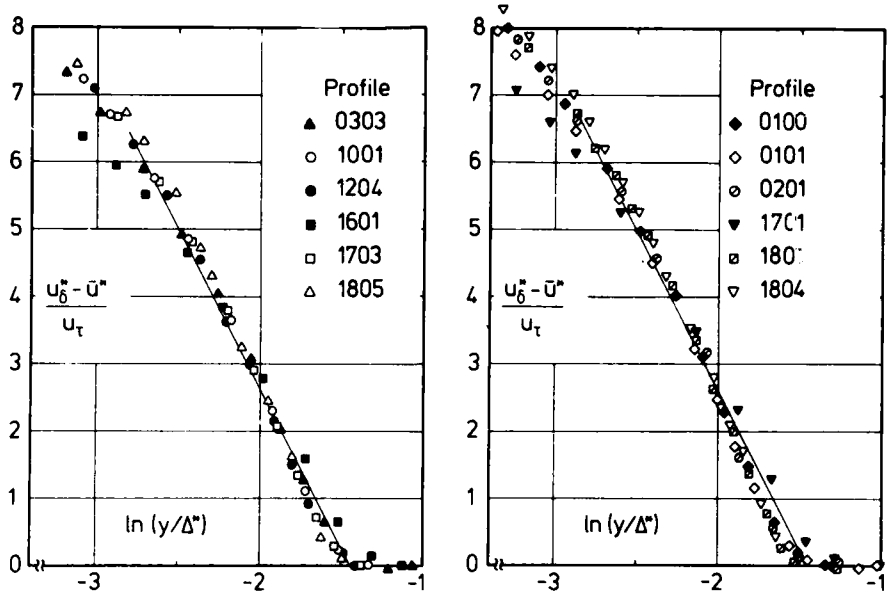

Fig. 4.2.3 Outer law for a compressible boundary layer; Mabey et al. (1974) cf. fig. 4.2.1

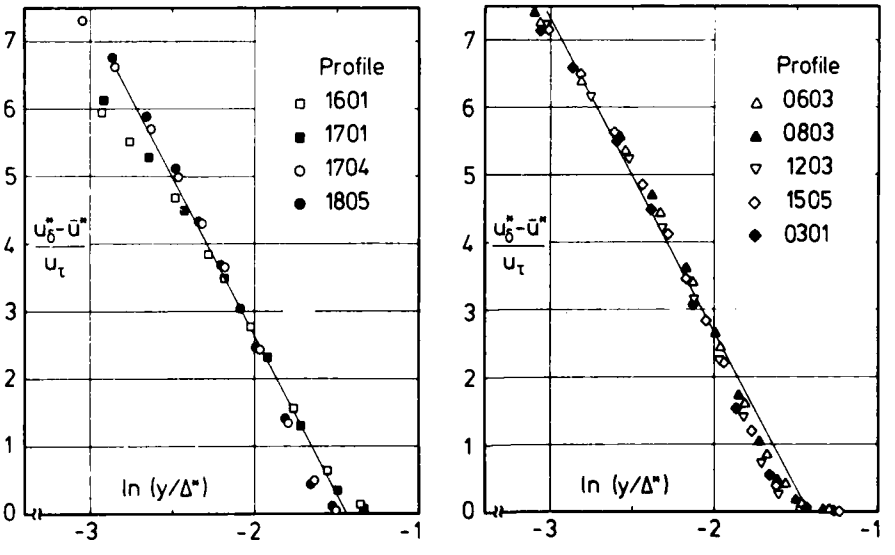

Fig. 4.2.4 Outer law for a compressible boundary layer (adiabatic wall, zero pressure gradient, defined origin). Mabey et al. (1974) cf.fig. 4.2.2

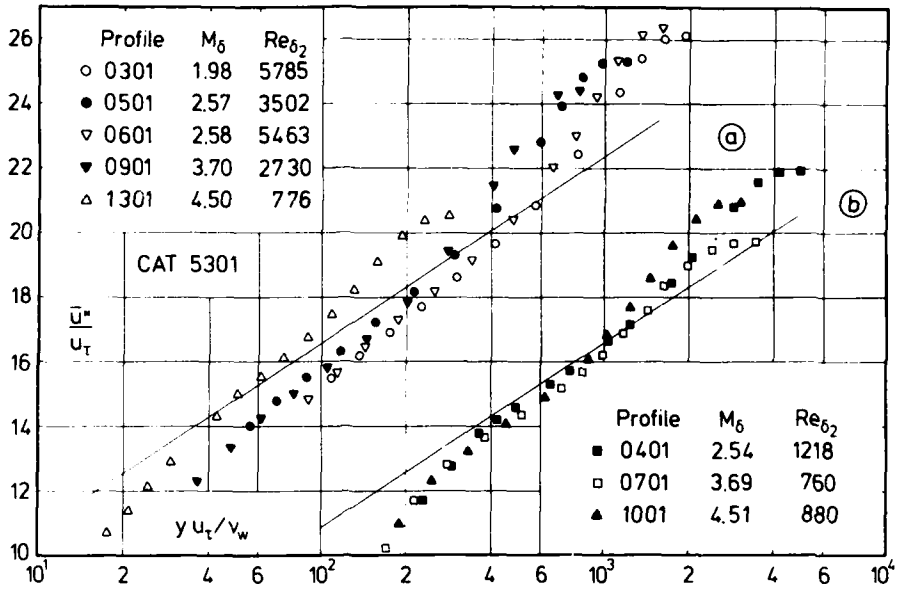

Fig. 4.2.5 Law of the wall for a compressible boundary layer (adiabatic wall, zero pressure gradient, defined origin). Coles (1953)

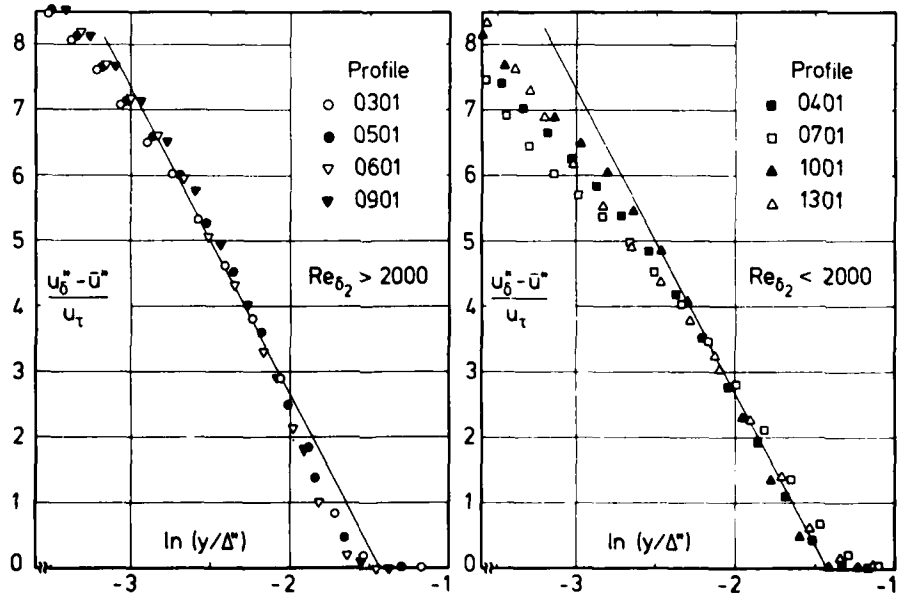

Fig. 4.2.6 Outer law for a compressible boundary layer (adiabatic wall, zero pressure gradient, defined origin). Coles (1953)

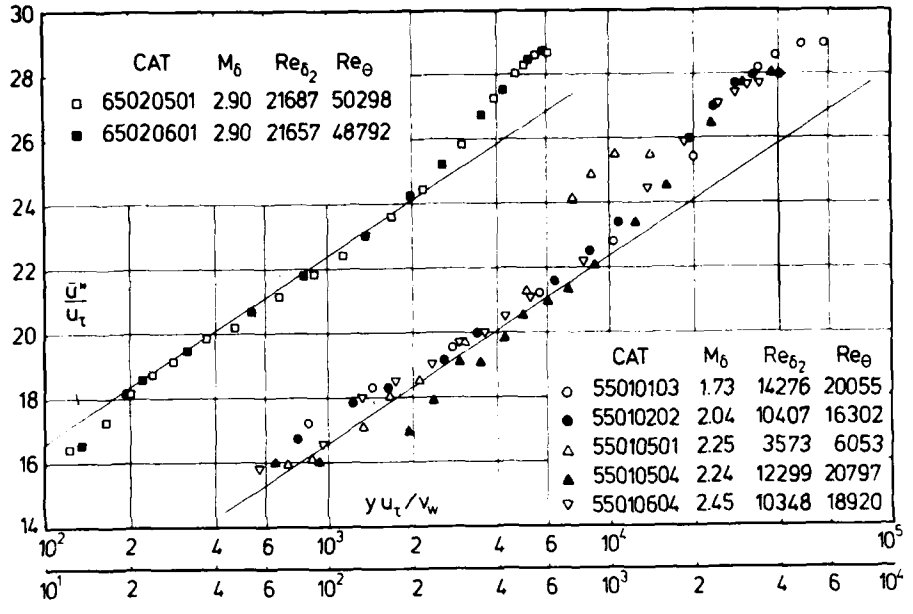

Fig. 4.2.7 Law of the wall fora compressible boundary layer (adiabatic wall, zero pressure gradient, defined origin). Shutts et al. (1955); Moore & Harkness (1965)

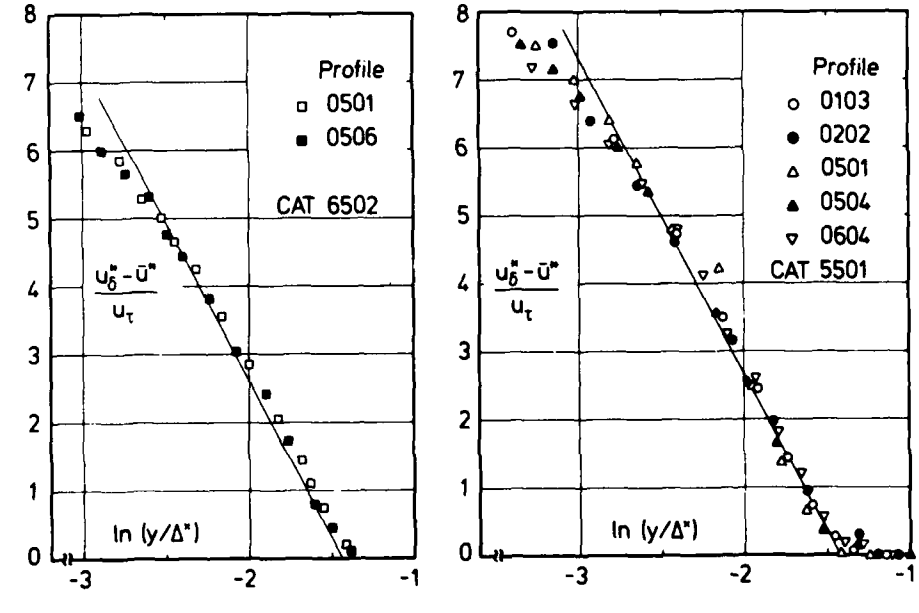

Fig. 4.2.8 Outer law for a compressible boundary layer (adiabatic wall, zero pressure gradient, defined origin). Shutts et al. (1955); Moore & Harkness (1965)

The data of Hastings & Sawyer (1970) were obtained on the same flat plate as those of Mabey et al. (1974). They are superseded by the latter measurements except for the data obtained in the transition region which are discussed in § 4.4 together with the velocity profiles measured by Watson et al. (1973) which also have very low Reynolds numbers.
It is interesting to note that no measurements were taken in the viscous sublayer in any of the experiments presented so far.

4.2.2 Conclusion (class IA)

Unless new and convincing evidence appears it is claimed that the standard turbulent velocity profile in a compressible boundary layer with zero pressure gradient along an adiabatic wall is described satisfactorily by the law of the wall (eqn. 3.3.9) with the constants $K_1 = 0.40$ and $C_1^+ = 5.10$ and by an outer law given by eqn. (3.3.17). All "constants" are truly independent of Mach number, heat transfer parameter and Reynolds number. The range of the validity of the outer law shrinks considerably for $Re_{\delta_2} < 2000$ and finally vanishes completely (see § 4.4).
Assuming this as a basis for a diagnosis of velocity profiles in compressible boundary layers, departures from this standard behaviour must be due to different upstream or boundary conditions, i.e. a departure from local equilibrium in the inner and outer region of the boundary layer respectively.

4.2.3 Other cases with no defined origin (class IB)

We now discuss measurements in boundary layers with zero pressure gradient alorg adiabatic walls with no defined origin (group IB). These cases are listed in table 4.2.2.

Table 4.2.2

CAT	Author	M_δ	$Re_{\delta_2} \times 10^{-3}$	Transition
5802	Stalmach	1.7 - 3.7	0.7 - 8.8	Forced (grit type)
5805	Moore	2 - 3.5	3.4 - 8.5	No information
6502	Moore & Harkness	2.8	70 - 359	Natural
6505	Jackson et al.	1.6 - 2.2	5.8 - 94	No information
6601	Hopkins & Keener	2.4 - 3.4	21 - 34	Natural
6903	Thomke	2 - 5	20 - 150	Natural
7202	Voisinet & Lee	4.9	1.6 - 13	Natural
7302	Winter & Gaudet	0.2 - 2.8	5.4 - 142	Natural
7601	Vas et al.	3	9.1 - 159	Natural

Stalmach's (1958) velocity profiles were measured in a 51 mm wide tunnel with a floating element width of 25.4 mm. It is therefore surprising that the data agree so well with the logarithmic law, at least those of series 02 (Fig. 4.2.9), showing very clearly the increase in wake strength $\Delta(\bar{u}^+/u_\tau)$ from 0.95 to 3.25 with increasing Reynolds number at constant Mach number. The same velocity profiles are compared with the outer law in Fig. (4.2.10) showing the normal behaviour of a fully turbulent boundary layer.
The experiments presented by Moore (1958) do not show anything especially significant except that the skin friction appears to be slightly too high, and they will be discussed in connection with a relaxing boundary layer downstream of a step in § 4.5.
The medium and high Reynolds number range is covered by measurements performed by Winter & Gaudet (Fig. 4.2.11). Velocity profiles at Mach numbers below 2 agree very well with the logarithmic law whereas those at $M_\delta = 2.20$ lie consistently above this line. In the Reynolds number range $11 \times 10^3 \leq Re_{\delta_2} \leq 14 \times 10^4$ presented here, the strength of the wake component is almost constant at 2.70 ± 0.30 which is well within the scatter band mentioned in § 3.3.3. The outer law representation for these measurements is given in Fig. (4.2.12).

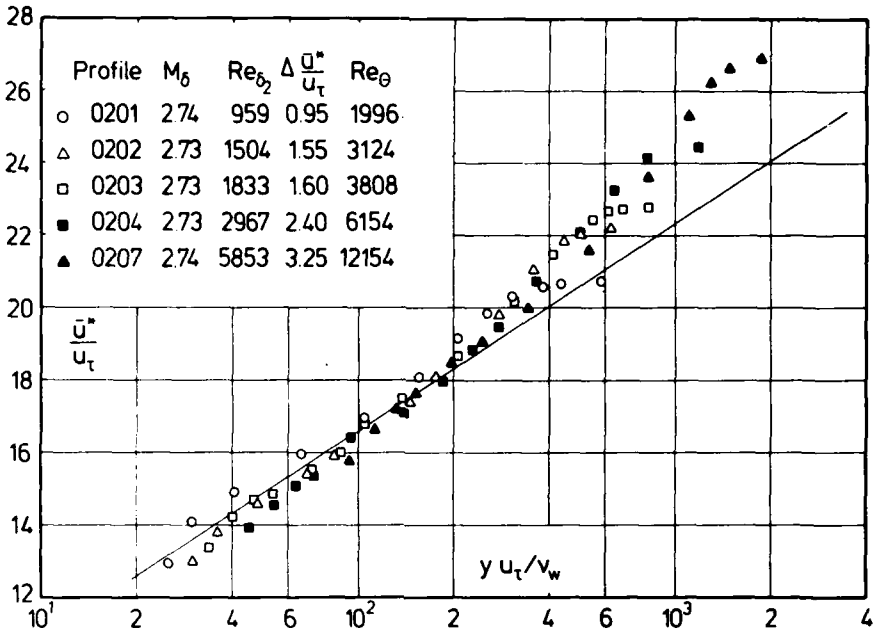

Fig. 4.2.9 Law of the wall for a compressible boundary layer (adiabatic wall, zero pressure gradient, no defined origin). Stalmach (1958)

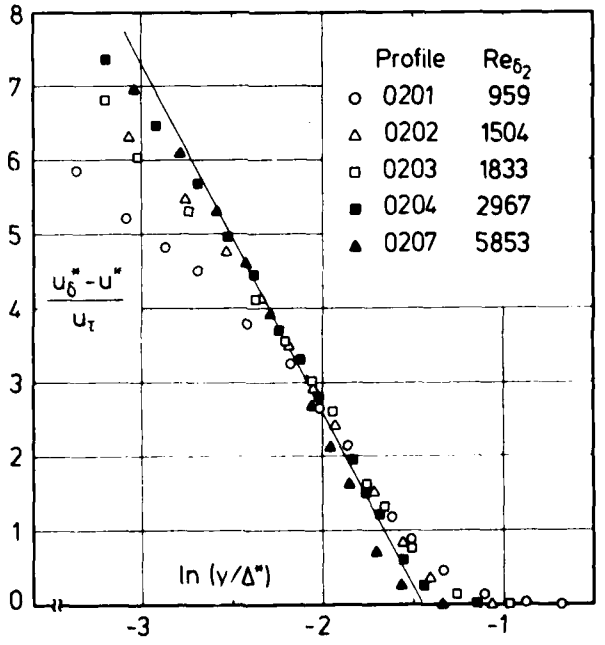

Fig. 4.2.10 Outer law for a compressible boundary layer (adiabatic wall, zero pressure gradient). Stalmach (1958)

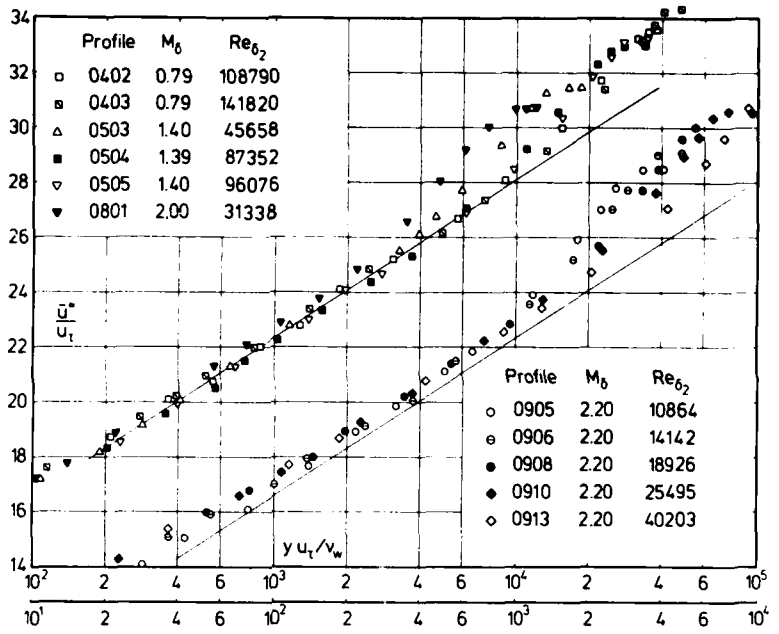

Fig. 4.2.11 Law of the wall for a compressible boundary layer (adiabatic wall, zero pressure gradient). Winter & Gaudet (1973)

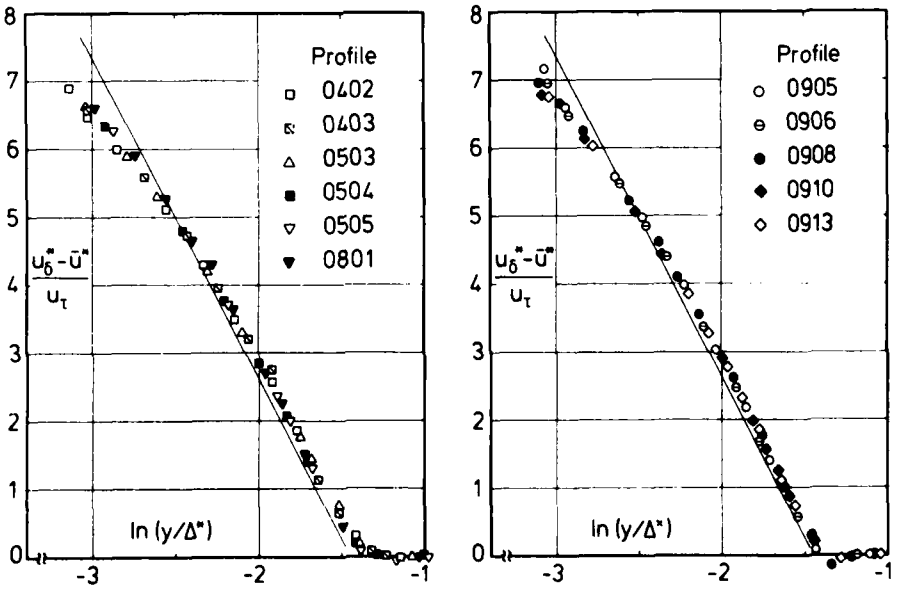

Fig. 4.2.12 Outer law for a compressible boundary layer (adiabatic wall, zero pressure gradient, origin not defined). Winter & Gaudet (1973)

Compared with the velocity profiles of Winter & Gaudet those of Jackson et al. (1965) which are in the same Mach- and Reynolds number range show either a much smaller wake strength $\Delta\ (\bar{u}^*/u_\tau) \approx 1.60$ or a much bigger one, about 3.80 (Fig. 4.2.13). The range overlaps that of the study by Shutts et al. (1955), who used the same balances (cf. data in Fig. 4.2.7). A momentum balance using the experimental c_f-values indicated that the layer was not strictly two-dimensional (authors' comment). It is interesting to note that the velocity profiles which have the larger wake strength agree with the outer law for a much larger distance (Fig. 4.2.14) than those with the smaller wake strength.

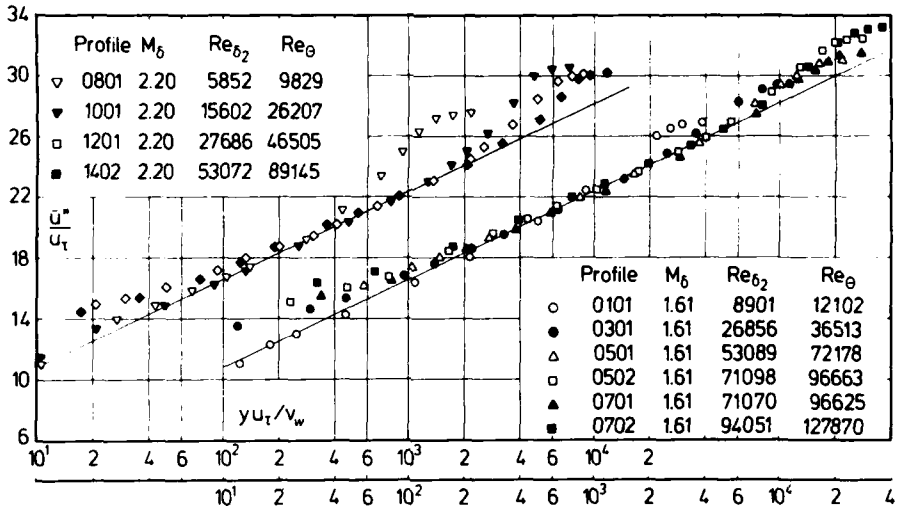

Fig. 4.2.13 Law of the wall for a compressible boundary layer (adiabatic wall, zero pressure gradient, no defined origin). Jackson et al. (1965)

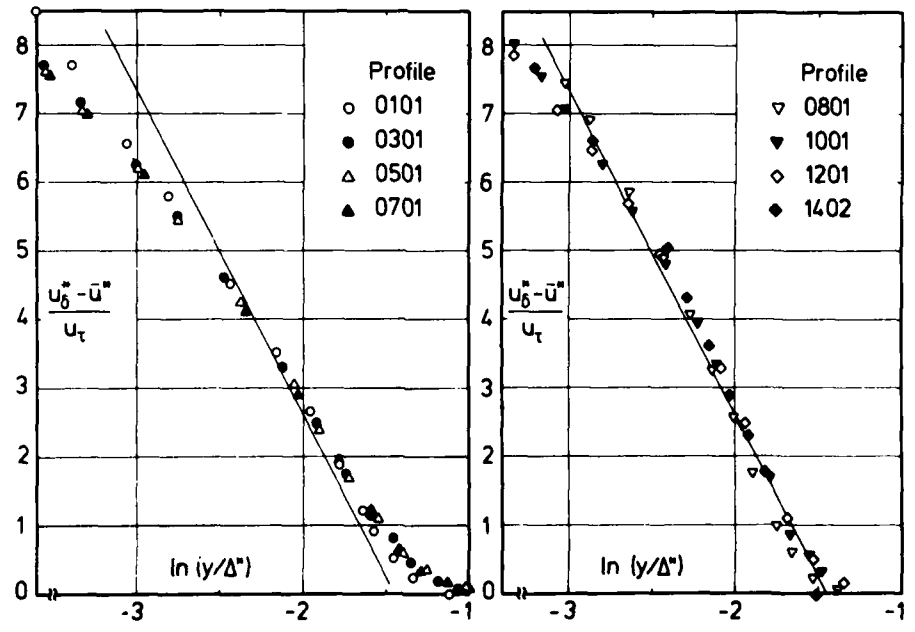

Fig. 4.2.14 Outer law for a compressible boundary layer (adiabatic wall, zero pressure gradient). Jackson et al. (1965)

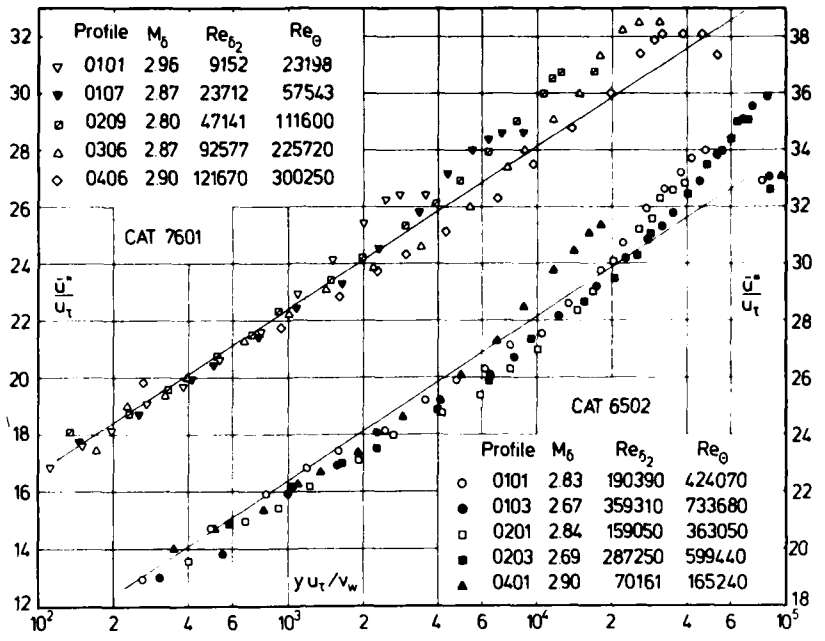

Fig. 4.2.15 Law of the wall for a compressible boundary layer (adiabatic wall, zero pressure gradient). Vas (1976), Moore & Harkness (1965).

Fig. (4.2.15) shows measurements by Vas et al. (1976) and by Moore & Harkness (1965) which were performed at a Mach number 2.90 in a Reynolds number range $9 \times 10^3 \leq Re_{\delta_2} \leq 3.6 \times 10^5$. The velocity profiles presented by Vas et al. again have a rather small wake strength $1.40 \leq \Delta (\bar{u}^+/u_\tau) \leq 2.20$ (see also Fig. 2.7.5) compared with those measured by Moore & Harkness where the strength of the wake component lies in the range 2 to 3. Both cases show the normal amount of scatter below and above the logarithmic law. Apart from the fact that the latter boundary layers reach the highest Reynolds numbers Re_{δ_2} known to the editors of AGARDograph 223, the only obvious difference between the measurements lies in the different size of the test-section, with W = H = 0.232 and L = 2.56 m (CAT 7601) and W = H = 1.22 and L > 14.63 m (CAT 6502) respectively. The outer law shows good agreement with the measurements of both experiments (Fig. 4.2.16).

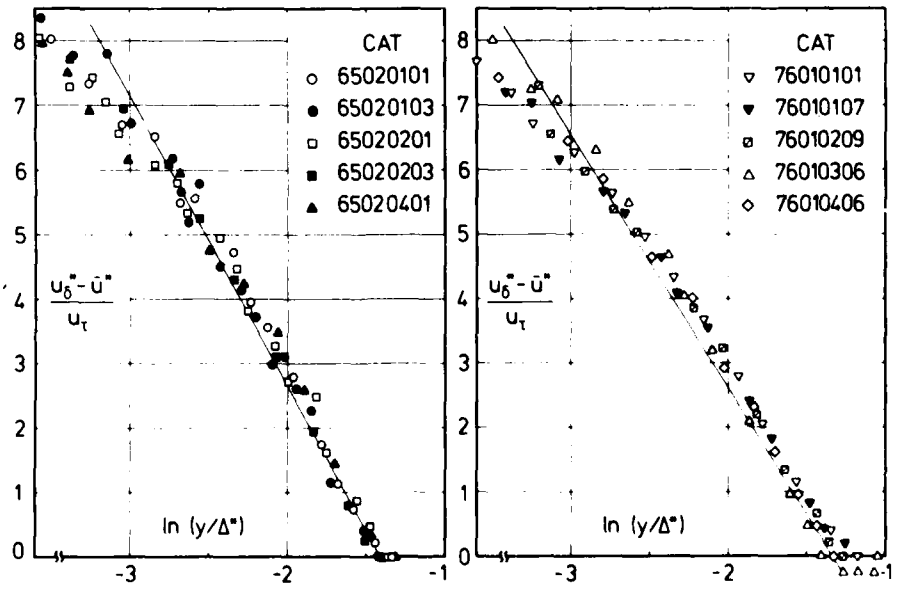

Fig. 4.2.16 Outer law for a compressible boundary layer (adiabatic wall, zero pressure gradient) Moore & Harkness (1965); Vas (1976).

The measurements performed by Thomke (1969) contain velocity profiles in approximately the same Reynolds number range as those of Vas et al. (1976) but at Mach numbers of both 3 and 4. The physical scale of Thomke's experiments is also much greater than that of Vas. For the majority of the data skin friction appears to be slightly low so that the measurements lie above the logarithmic law of the wall (Fig. 4.2.17) but, however assessed, the wake strength is large. In the legend of Fig. (4.2.17) the second additive number in the column with the heading $\Delta(\bar{u}^*/u_\tau)$ denotes the correction due to the shift above or below the standard logarithmic law. Agreement between outer law and measurements is again very good (Fig. 4.2.18).

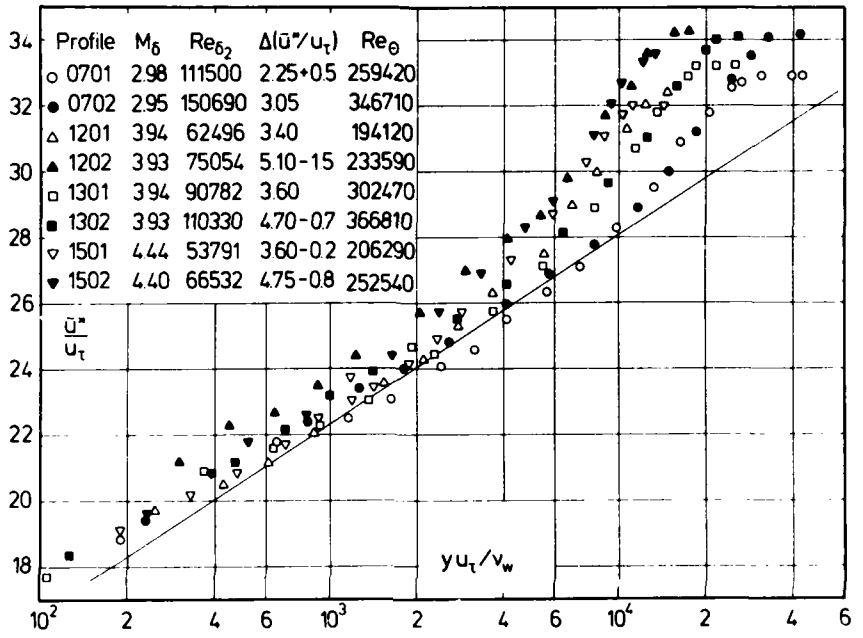

Fig. 4.2.17 Law of the wall for a compressible boundary layer (adiabatic wall, zero pressure gradient). Thomke (1969).

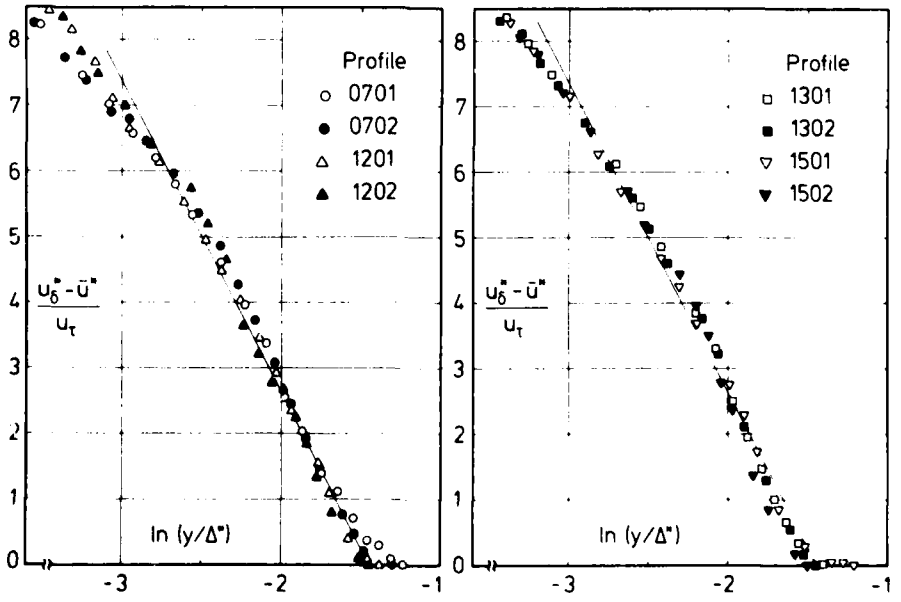

Fig. 4.2.18 Outer law for a compressible boundary layer (adiabatic wall, zero pressure gradient, origin not defined). Thomke (1969).

The three velocity profiles presented by Hopkins & Keener (1966) in the range $21 \leq Re_{\delta_2} \times 10^3 \leq 34$ show a difference in the wake strength between 2.30 and 3.20, and skin friction measured by a balance appears to be low despite the importance given to skin friction measurements in this experiment. Since both Mach number and Reynolds number range are covered by the experiments shown above, the Hopkins & Keener data are not given here in graphical form.

Having discussed measurements over a Mach number range $0.8 \leq M_\delta \leq 4.5$ and a Reynolds number range $1 \times 10^3 \leq Re_{\delta_2} \leq 3.5 \times 10^5$ where the law of the wall and the outer law did agree with the bulk of the data and where discrepancies were very probably due to the normal error which cannot be avoided with skin friction measurements, we have been puzzled all the more by the velocity profiles obtained by Voisinet & Lee (1972) (c.f. Fig. 4.2.19). They lie consistently above the logarithmic law according to eqn. (3.3.9) requiring a constant $C_1 = 6.1$ and they exhibit a wake strength - after correction for disagreement with the standard wall law - in the range $6.30 \leq \Delta(\bar{u}^*/u_\tau) \leq 7.70$. Since otherwise such high values of the wake strength are observed only in boundary layers with high rates of heat transfer (see § 4.3) we can only assume that the upstream thermal history effects have not yet abated at the profile measuring stations. In general there was, for this experiment, substantial heat transfer in the nozzle region, so that there is a downstream history effect in addition to any downstream effect of the nozzle pressure-gradient. After these discrepancies in the log-law plot it is not surprising to find also considerable deviations from the standard outer law (Fig. 4.2.20) which is similar to cases found in boundary layers with adverse pressure gradients (see § 5).

As for a conclusion there is little to add to those given at the end of § 4.2.2 except that the Reynolds number range of the validity of both the law of the wall and the outer law can be extended safely to Reynolds numbers up to 3.5×10^5 for boundary layers with zero pressure gradient along adiabatic walls.

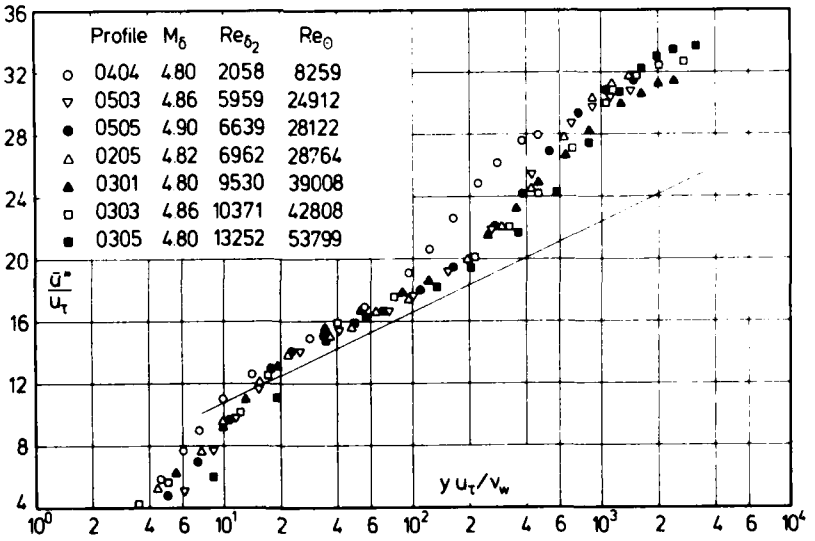

Fig. 4.2.19 Law of the wall for a compressible boundary layer (very slight cooling, zero pressure gradient, upstream history effect). Voisinet & Lee (1972).

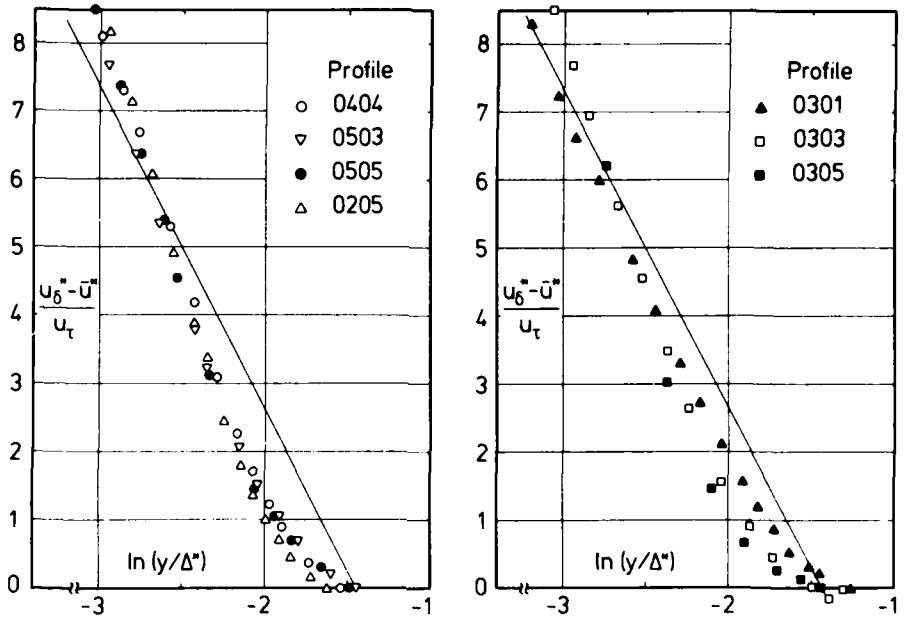

Fig. 4.2.20 Outer law for a compressible boundary layer (adiabatic wall, zero pressure gradient, upstream history effect). Voisinet & Lee (1972).

4.3 Zero-pressure-gradient isothermal wall cases

4.3.1 General remarks

As with compressible turbulent boundary layers along adiabatic walls the validity of the transformed similarity laws for the viscous sublayer, the log-law region, and the outer region rests on the correct representation of the temperature distribution for boundary layers on isothermal walls - here we have used eqn. (2.5.37a) - and on a comparison with measurements.

Experiments in flows with heat transfer are even more laborious and difficult to perform than those on adiabatic walls described above. It is not astonishing therefore to find that the number of cases investigated is small indeed. Since the wall is heated by viscous dissipation in compressible boundary layers, and wall cooling is often essential for the survival of high-speed aircraft, high-speed experiments with heated walls, i.e. $T_w > T_r$, are of little technical interest (little work is available on strongly heated walls even at low speeds, one exception being the investigation by Kelnhofer 1970 who measured velocity and temperature profiles in a turbulent boundary layer with zero pressure gradient). All of the experiments discussed below will therefore belong to the group of the "cooled wall" cases. As experiments in boundary layers with adiabatic walls are limited by the recovery temperature which according to eqn. (2.5.38) is mainly determined by the Mach number, only cooled wall boundary layer experiments permit experiments at higher Mach numbers at all. This extended Mach number range - $5 \leq M_\delta \leq 10$ - is of special interest for experiments concerned with boundary layer flow on the space-shuttle. Another problem which accompanies all high Mach number experiments are low Reynolds number effects. Though a Reynolds number increase is obtained by a decreasing wall temperature reducing the viscosity at the wall, high Mach number flow can only be achieved at bearable costs in small test facilities which have small test sections and can thus only produce flows at relatively low Reynolds numbers. For example at a Mach number $M_\delta = 7.2$ the highest Reynolds number obtained in a published experiment was $Re_{\delta 2} = 3.0 \times 10^3$.

As was mentioned in § 2.2.3 a convenient definition of a heat transfer parameter makes use of the recovery temperature which can be defined for a boundary layer along an isothermal wall. The independent heat transfer parameter used in this investigation is therefore the ratio of the wall temperature T_w to the recovery temperature T_r.

The heat flux is most usually presented in the form of a Stanton number see eqn. (2.6.4), though the difficulty of giving a sensible value to the recovery (or adiabatic wall) temperature when the wall is not isothermal leads us to use $c_q = \dot{q}_w/\rho c_p u_\delta T_{o\delta}$ (see § 2.6.3).

In the experiments discussed below, the heat transfer parameter lies in the range $0.2 \leq T_w/T_r \leq 1.1$, with $T_w/T_r = 1$ characterizing zero heat transfer or the "adiabatic wall" case. $T_w/T_r < 0.50$ will be called high or severe cooling. $T_w/T_r < 0.80$ moderate cooling but this classification was chosen for convenience only.

Since we need the shear stress velocity u_τ for the comparison between the semi-empirical relationships and the measured data, table 4.3.1 contains only experiments where the skin friction was measured. Skin friction was therefore considered a more important quantity than the heat transfer q_w at the wall. This is only due to the poor state of our knowledge concerning the Reynolds analogy factor. Otherwise a version of eqn. (2.6.5) could be used to determine the skin friction for all cases where the Stanton number is known, i. e. where q_w and T_w are available from measurements.

Table 4.3.1

CAT	Author	M_δ	T_w/T_r	$Re_{\delta_2} \times 10^{-3}$	Transition
6506	Young	5.0	0.6 - 1.0	1.7 - 2.5	forced
6702	Danberg	6.5	0.5 - 0.9	0.3 - 1.9	natural
7204	Keener & Hopkins	6.3	0.3 - 0.5	1 - 2.3	natural & forced
7205	Horstman & Owen	7.2	0.5	1.4 - 3.0	natural
7702 S	Laderman & Demetriades	3.0	0.6 - 1.0	1.4 - 2.8	

Table 4.3.2 presents measurements where the origin of the boundary layer is not known (nozzle wall) and where upstream history effects cannot be excluded.

Table 4.3.2

CAT	Author	M_δ	T_w/T_r	$Re_{\delta_2} \times 10^{-3}$	Transition
7202	Voisinet & Lee	4.9	0.25 - 1	1.8 - 38	natural
7203	Hopkins & Keener	7.2	0.3 - 0.5	4.5 - 15.5	natural
7403	Laderman & Demetriades	9.4	0.42	6.5	natural

AGARDograph 223 Fig. (6.3) shows clearly that there exists a great need for more experiments in compressible turbulent boundary layers with heat transfer.

4.3.2 Zero pressure gradient cases with no upstream history effects

Table 4.3.1 lists only five experiments with skin friction measurements where the origin of the zero-pressure-gradient boundary layer was defined by a leading edge and where the wall temperature was constant, so that no upstream history effects should occur. In all cases the wall temperature was below the recovery temperature, i.e. the wall was cooled. Thus all the assumptions were fulfilled which underlie the temperature-velocity relationship given by eqn. (2.5.37a) and which are needed for the transformation of the velocities $\bar{u}^*$ and u_δ^*. Unfortunately these prerequisites are often forgotten when comparisons between theory and experiments are carried out. Except for the Danberg case, where the skin friction was determined from the slope of the velocity profile, the wall shear stress was measured by a floating element balance (CAT 6506, 7204, 7205) or by a Preston tube (CAT 7702 S). Therefore only three sets of data in this group (1 A) can properly be compared directly with the log-law and the outer law plot. It is convenient to begin the discussion with an experiment where the heat transfer parameter T_w/T_r was varied moderately, i.e. with an almost adiabatic case $T_w/T_r = 0.97$ progressing to a value $T_w/T_r = 0.52$ (Young 1965). Some profiles of CAT 6506 are shown in Figs. (4.3.1a) and (4.3.2). Young did not measure temperature profiles, so that the velocities were evaluated from the total pressure distribution by assuming that the temperature distribution was given by eqn. (2.5.37a).

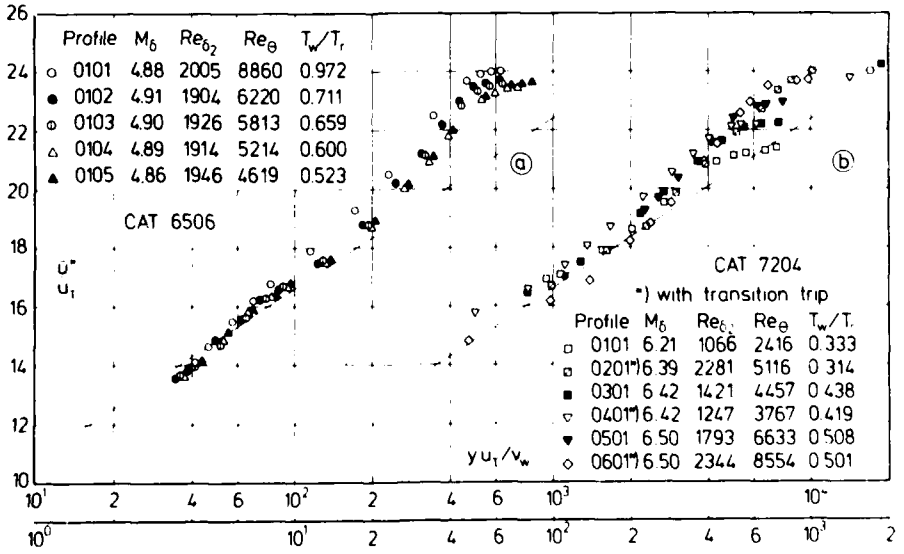

Fig. 4.3.1 Law of the wall for a compressible boundary layer (isothermal wall, zero pressure gradient, defined origin). Young (1965) and Keener & Hopkins (1972).

This assumption is reasonable (see § 2.5.6) if data points close to the temperature peak in the immediate vicinity of the wall are not considered. Fortunately this experiment can be supplemented and extended to higher cooling rates ($0.51 \geq T_w/T_r \geq 0.31$) in about the same Reynolds number range ($1067 \leq Re_{\delta_2} \leq 2347$) with measured temperature profiles by Keener & Hopkins (1972). These velocity profiles are presented in Figs. (4.3.1b) and (4.3.2). Agreement between the log-law (eqn. 3.3.9) and the measurements is very good in the first case and good in the second, if one considers the likely measuring accuracy of a floating element balance in a cooled wall. This comparison suggests that the value of the constant C_1^* in eqn. (3.3.9) remains unchanged from the adiabatic wall case if the wall is cooled and kept isothermal. Three measured temperature profiles are presented in CAT 7204 (0101, 0201, 0401) (see Fig. 2.5.14), so that the uncertainty inherent in Young's experiment is eliminated (see also the comparison between the measured and the calculated temperature profiles in Fig. 4.3.6). In addition the downstream effect of transition on the boundary layer profiles was investigated by introducing a boundary layer trip near the leading edge for profiles 0201, 0401 and 0601, and allowing natural transition to develop for profiles 0101, 0301 and 0501. The profiles with forced transition appear to show a larger strength of the wake component but no generally valid conclusion can be drawn.

The outer law shows good agreement with the measurements (Fig. 4.3.2) for Reynolds numbers $Re_{\delta_2} > 2000$, but deviations occur for profiles with lower Reynolds numbers as already observed in Fig. (4.2.6).

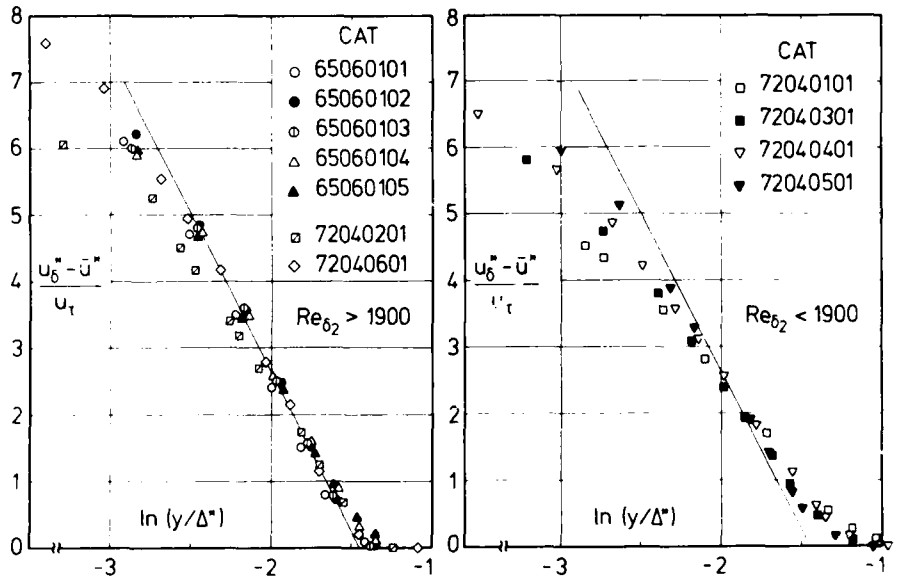

Fig. 4.3.2 Outer law for a compressible boundary layer (isothermal wall, zero pressure gradient, defined origin). Young (1965) and Keener & Hopkins [illegible]

More recent measurements by Laderman & Demetriades (1977) show good agreement both with the [illegible] 4.3.3) and with the outer law (Fig. 4.3.4). Since their skin friction values were determined [illegible] a Preston tube and by using the evaluation method of Hopkins & Inouye (1971)which has been [illegible] by balance measurements in a satisfactory manner, the wall shear stress has also been [illegible] present authors using a semi-empirical method (Fernholz 1971). In both cases measurements [illegible] tatively with the logarithmic law, eqn. (3.3.9). Moreover, while $(\tau_w)_{Fe}$ gives the better [illegible] ment, $(\tau_w)_{H\&I}$ provides the better correlation. The skin friction values are thereby [illegible] (4.3.3) and show differences of up to 20 %. Laderman & Demetriades calculated [illegible] wake correlation (Coles) and found that the $(\tau_w)_{H\&I}$ values were confirmed. The same procedure was applied to the outer law and there are hardly any differences [illegible] There exist so few measurements in boundary layers with defined origin of [illegible] also discuss in this context the axisymmetric boundary layer studied by [illegible] boundary layer may have been affected by a slightly favourable pressure [illegible]

AD-A087 704 ADVISORY GROUP FOR AEROSPACE RESEARCH AND DEVELOPMENT--ETC F/G 20/4
A CRITICAL COMMENTARY ON MEAN FLOW DATA FOR TWO-DIMENSIONAL COM--ETC(U)
MAY 80 H H FERNHOLZ, P J FINLEY

UNCLASSIFIED AGARD-AG-253 NL

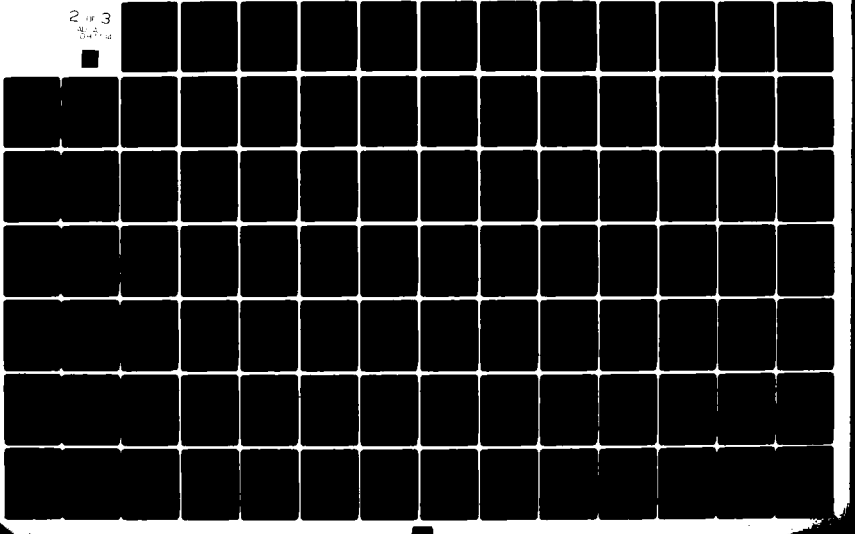

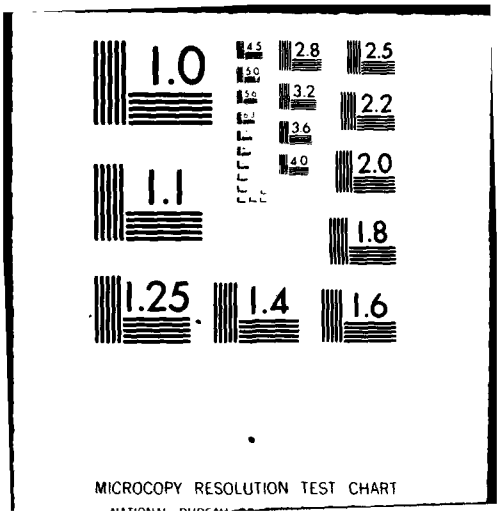
1.0
1.1
1.25
1.4
1.6
1.8
2.0
2.2
2.5
2.8
3.2
3.6
4.0
MICROCOPY RESOLUTION TEST CHART

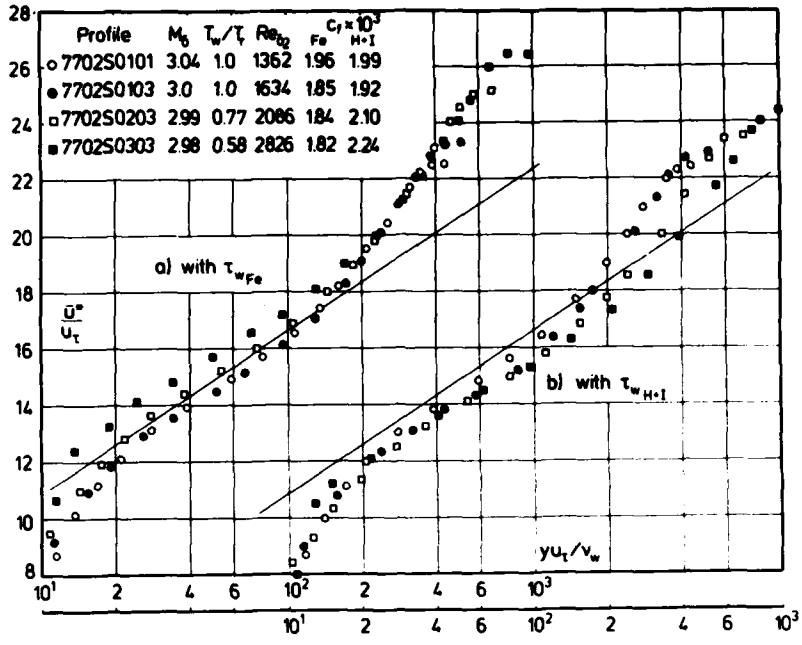

Fig. 4.3.3 Law of the wall for a compressible turbulent boundary layer (zero pressure gradient, isothermal wall, defined origin). Laderman & Demetriades (1977).

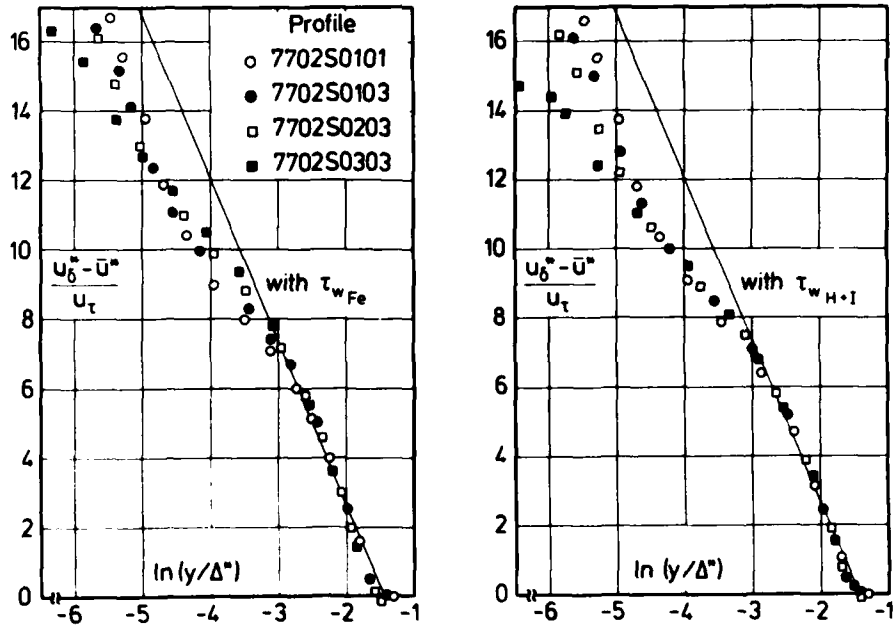

Fig. 4.3.4 Outer law for a compressible turbulent boundary layer (adiabatic wall, zero pressure gradient, defined origin). Laderman & Demetriades (1977).

angle cone-ogive which formed the front part of the 3.30 m long cylinder. It is, however, highly probable that the boundary layer has reached equilibrium at the measuring stations which were in the region 1.15 to 2.37 m downstream. Agreement between measurements and the law of the wall is very good (Fig. 4.3.5), and it is a pity that only three profiles were measured in this carefully designed experiment. Measurements included also skin friction, heat transfer and velocity fluctuations. As can be seen on Fig. (4.3.6) there is good agreement with the outer law, and agreement between measured and theoretical temperature profiles (eqn. 2.5.37a) is satisfactory.

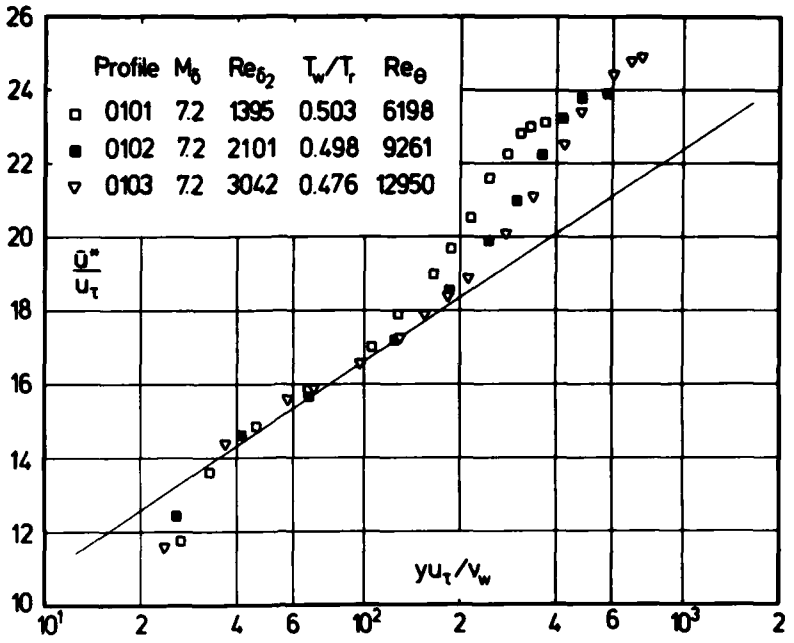

Fig. 4.3.5 Law of the wall for a compressible boundary layer (isothermal wall, zero pressure gradient, axisymmetric). Horstman & Owen (1972).

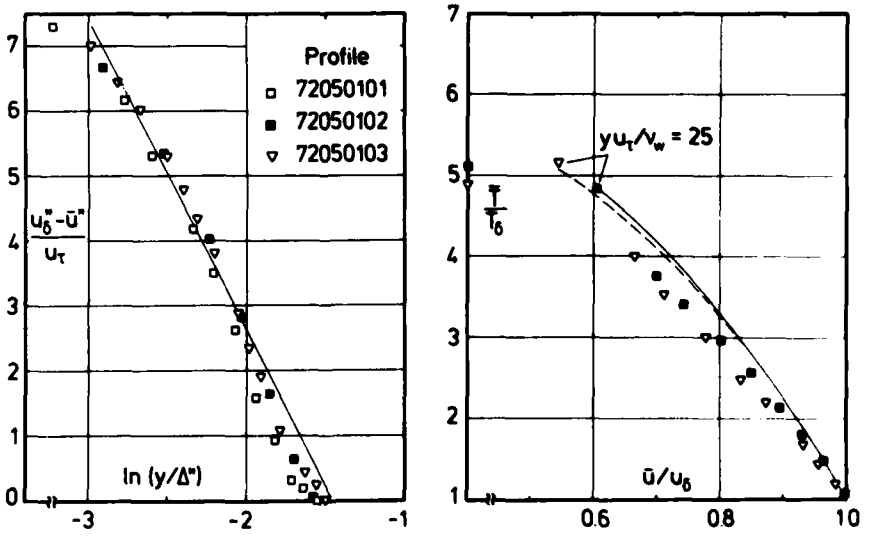

Fig. 4.3.6 Outer law for a compressible boundary layer

Comparison of temperature measurements with theory

(isothermal wall, zero pressure gradient, axisymmetric) Horstman & Owen (1972).

4.3.3 Zero pressure gradient cases with upstream history effects

The next two cases which we deal with are boundary layers along tunnel walls, i.e. with no defined origin, which could be subject to upstream history effects both due to pressure gradient and wall temperature variations. The measurements by Hopkins & Keener (1972) extended the Reynolds number range of the flat plate experiment (CAT 7204) to $Re_{\delta_2} = 15.5 \times 10^3$ at a Mach number $M_\delta = 7.5$ (CAT 7203). The measuring station was 10.13 m downstream of the throat and - as the authors state - the test section flow "was not entirely uniform but relatively so for this type of facility". It would therefore not be too surprising to find more scatter around the law of the wall line than in the cases discussed above (Fig. 4.3.7). All measurements lie consistently low, however, which could be due to a systematic error in the skin friction measurement. As will be seen below in the discussion of the Voisinet et al. (CAT 7202) data, the fact that the floating element of the balance was not cooled could easily have caused the skin friction values to be overestimated. A reduction of around 20 % as in the case of CAT 7202 would bring most of the data into much better agreement with the log-law.

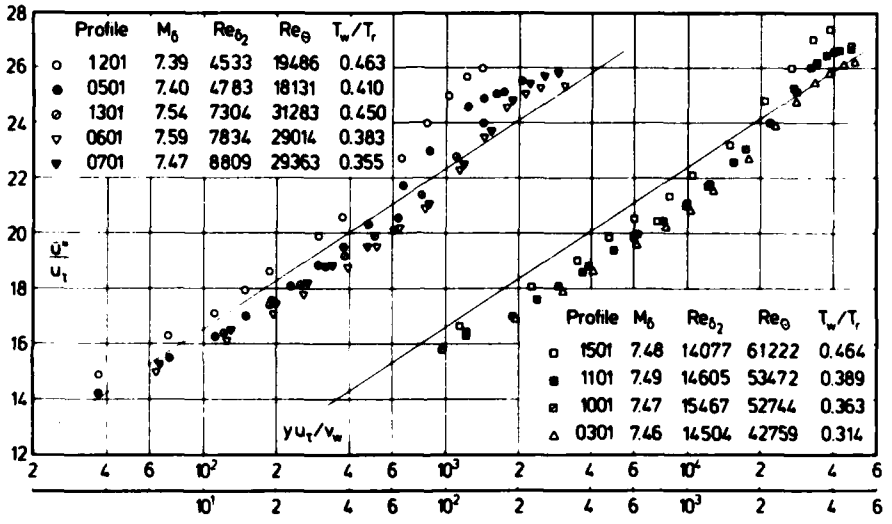

Fig. 4.3.7 Law of the wall for a compressible boundary layer (isothermal wall, zero pressure gradient, no defined origin). Hopkins & Keener (1972).

As for the outer law, the velocity profiles as measured by Hopkins & Keener agree well with eqn. (3.3.17) (see Fig. 4.3.8).

In the nozzle-wall experiment of Voisinet & Lee (CAT 7202) a comparison of the measured data with the logarithmic law of the wall gives a rather confusing result. For moderate wall cooling ($T_w/T_r \approx 0.78$) measurements follow the same slope as the log-law curve but indicate that the constant C_1 is 6.10 instead of 5.10 (Fig. 4.3.9), whereas with severe wall cooling ($T_w/T_r \approx 0.22$) the data do not exhibit a linear behaviour in the log-law region at all and lie consistently lower (Fig. 4.3.10). The velocity profiles in the moderate heat transfer case thus agree qualitatively with the adiabatic wall case both for the log-law region (Figs. 4.3.9 and 4.2.19) and for the outer law (Figs. 4.3.11 and 4.2.20). Compared with the "standard profile" consistent discrepancies occur which seem to be characteristic of the NOL data, however. These deviations from the typical outer law behaviour could be due to upstream history effects. The velocity distribution in the outer layer resembles one in a boundary layer which has been exposed to a slight adverse pressure gradient (Figs. 4.3.11 and 4.3.12).

One reason for faulty skin friction measurements could be the so called "hot-spot-effect" (Westkaemper 1963) which results from an uncooled floating element in an otherwise cooled wall. Experiments with a floating element, the temperature of which was up to 150 K above that of the surrounding wall, revealed that considerable corrections must be applied to the skin friction data (Voisinet 1977). They amount to a reduction of c_f by 20 % according to Reynolds number, Mach number, and the temperature difference between the floating element and the wall.

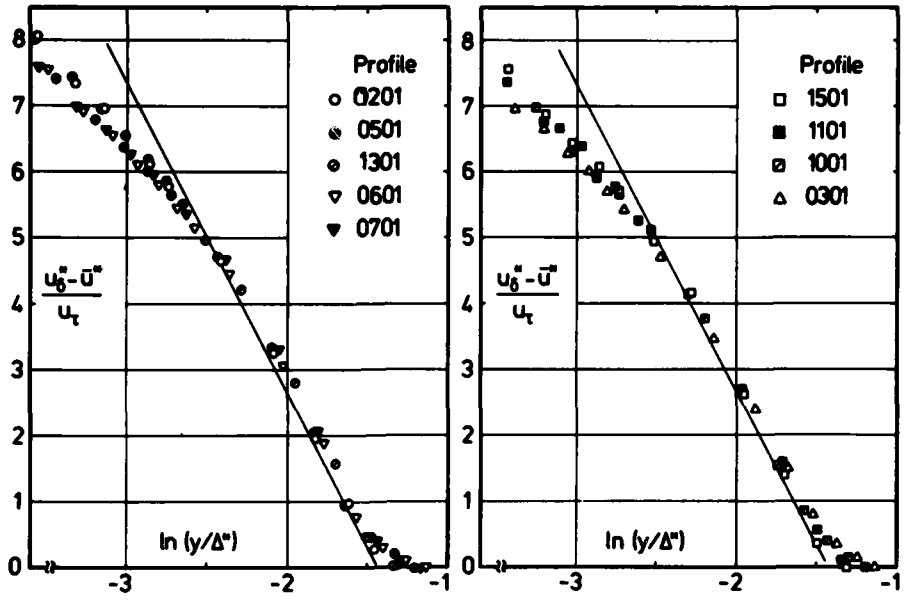

Fig. 4.3.8 Outer law for a compressible boundary layer (isothermal wall, zero pressure gradient). Hopkins & Keener (1972).

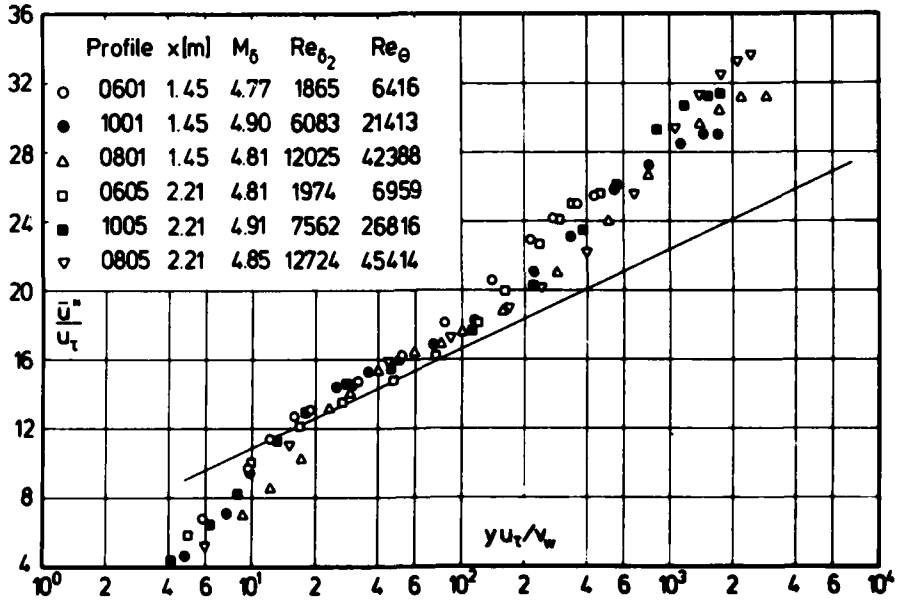

Fig. 4.3.9 Law of the wall for a compressible boundary layer (isothermal wall, T_w/T_r = 0.78, zero pressure gradient). Voisinet & Lee (1972).

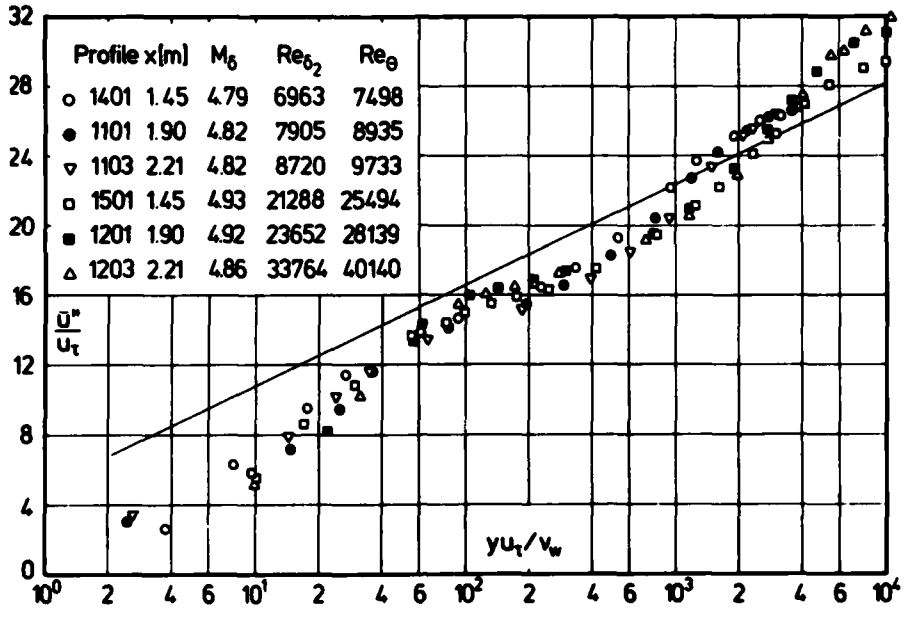

Fig. 4.3.10 Law of the wall for a compressible boundary layer (isothermal wall $(T_w/T_r) = 0.22$; zero pressure gradient, origin not defined). Voisinet & Lee (1972).

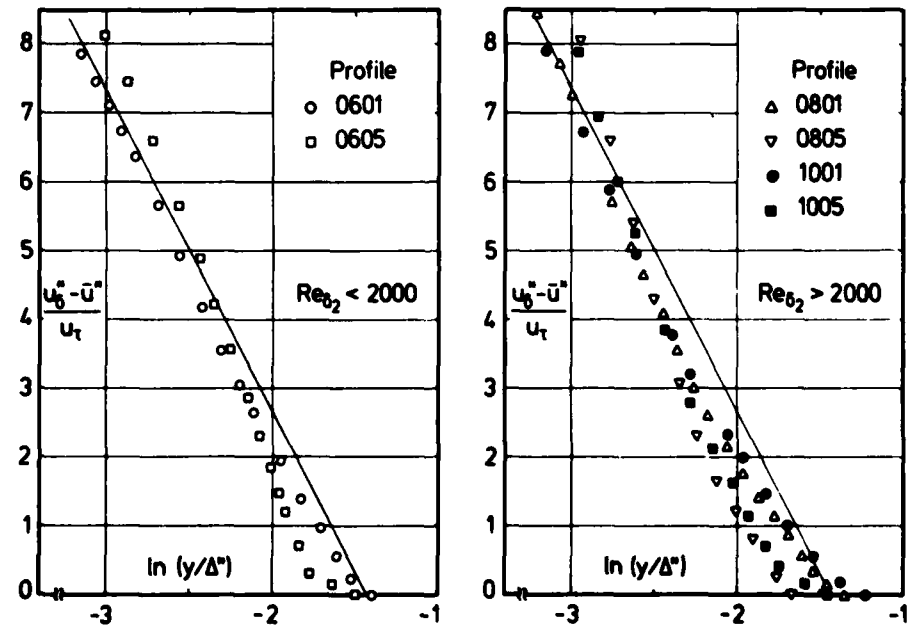

Fig. 4.3.11 Outer law for a compressible boundary layer (isothermal wall, $T_w/T_r = 0.78$, zero pressure gradient). Voisinet & Lee (1972).

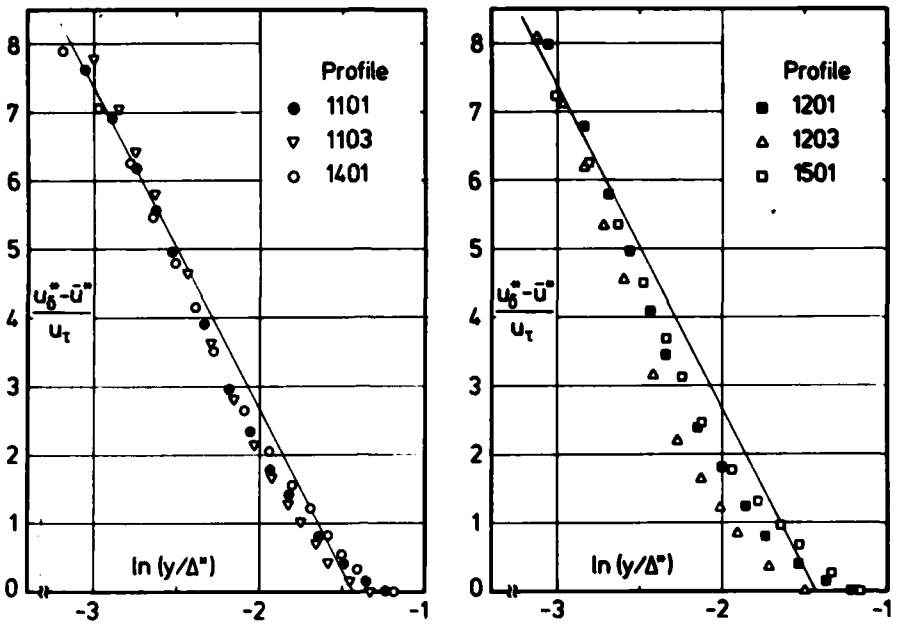

Fig. 4.3.12 Outer law for a compressible boundary layer (isothermal wall $(T_w/T_r) = 0.22$; zero pressure gradient; origin not defined). Voisinet & Lee (1972).

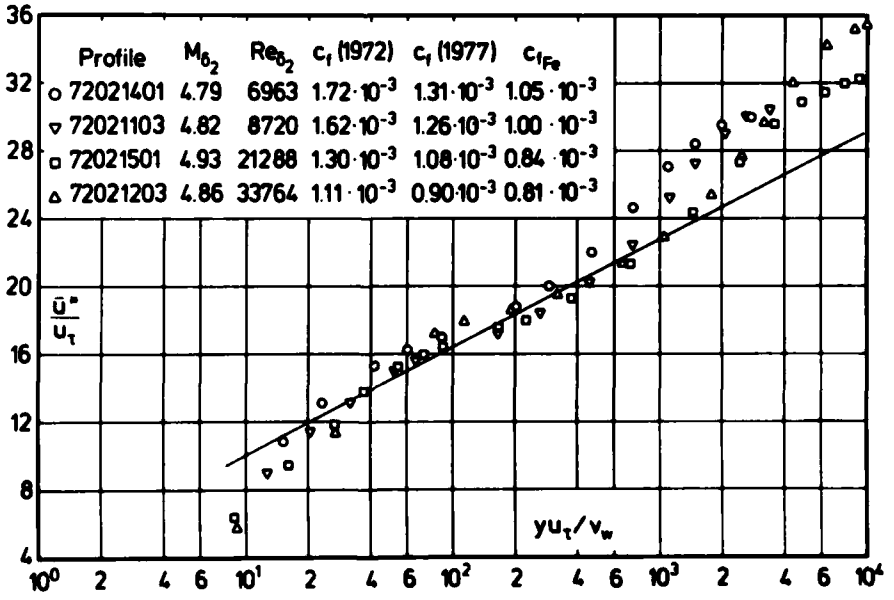

Fig. 4.3.13 Law of the wall for a compressible boundary layer (isothermal wall, $T_w/T_r = 0.22$, zero pressure gradient, origin not defined). Voisinet & Lee (1972). c_f from Voisinet (1977).

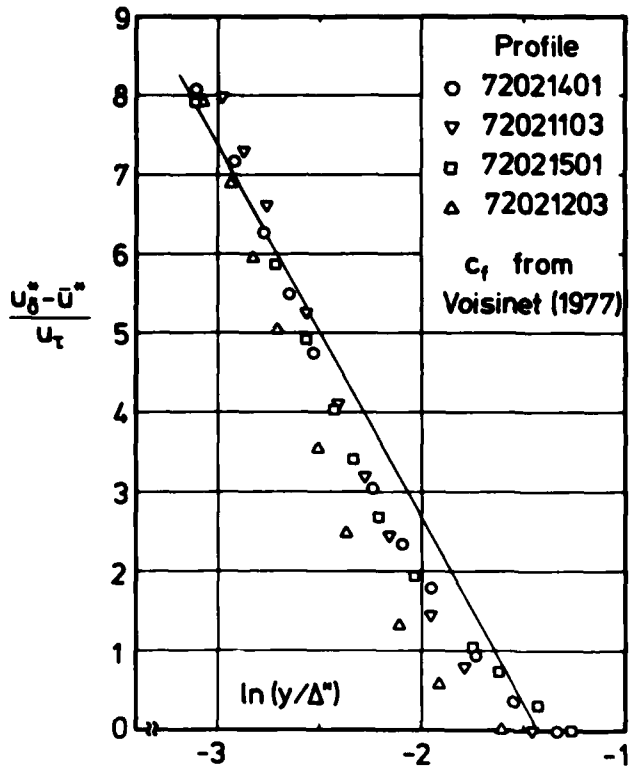

Fig. 4.3.14 Outer law for a compressible boundary layer (isothermal wall, $T_w/T_r \approx 0.22$, zero pressure gradient, origin not defined). Voisinet & Lee (1972).

Since the skin friction measurements in boundary layers with severe cooling (CAT 7203) are affected most by such a correction, we have re-plotted the velocity profiles, shown in Figs. (4.3.10) and (4.3.12) as originally reported. Figs. (4.3.13) and (4.3.14) present the equivalent plots using the revised skin friction values reported by Voisinet (1977). The measurements agree much better with the standard logarithmic wall, though the "velocity dip" below the log-law is still visible. It can be seen that the change in c_f value has little effect on the agreement with the outer law. This is generally the case since changes in u_τ which is contained implicitly in both quantities plotted tend to cancel out.

The velocity and temperature profile measured by Laderman & Demetriades (1974) will not be discussed in detail here though the heat transfer parameter T_w/T_r = 0.42 and Mach number M_δ = 9.37 emphasize the importance and interest of the experiment. Unfortunately skin friction was not measured so that our usual control plots could not be drawn. Measurements furthermore showed a rise in the static pressure of nearly 50 % from the boundary layer edge to the wall which still lacks a satisfactory physical explanation (see § 6.4.2). Probe effects by which an apparent normal pressure distribution could have been caused must be excluded since measurements with a similar static pressure probe (Owen et al. 1975) did not show a static pressure variation in a comparable boundary layer. In any case there is relatively little difficulty in measuring the overall pressure difference across the boundary layer, however difficult it may be to obtain readings within it.

4.3.4 Conclusions

From the evidence presented in § 4.3 we conclude that both the logarithmic law of the wall (eqn. 3.3.9) and the outer law (eqn. 3.3.17) agree satisfactorily with measurements in boundary layers with zero pressure gradient along isothermal walls. The Mach number range investigated is $3 \leq M_\delta \leq 7.2$ and the heat transfer parameter range $0.31 \leq T_w/T_r \leq 1$. Deviations between both the logarithmic law of the wall and the outer law and measurements which occur in the experiments of Voisinet & Lee (1972) are probably due to upstream history effects.

4.4 Transition and low Reynolds number effects

4.4.1 General remarks

We have no intention of adding another and - due to the present state of the art - necessarily inconclusive chapter to the history of transition in compressible boundary layers. For "a critical evaluation of transition from laminar to turbulent shear layers with emphasis on hypersonically traveling bodies" the reader is referred to Morkovin (1969), for more recent basic papers to Kendall (1971 and 1975), Mack (1971 and 1975), Michel (1977) and finally to AGARD CP 224 (1977) (see especially Morkovin's advisory report) on laminar-turbulent transition. In the latter report Reshotko remarks that one of the reasons why the whole picture is so confused is that we have too little information about the disturbance environment (nature and spectrum) in experimental facilities. Though the main sources of the disturbances causing transition have been known for some time, reports of experiments at present do not provide sufficient information about the test conditions, information which would have to encompass both disturbance spectra and amplitudes as well as obliqueness distributions (Morkovin CP 224, Kendall 1975). Since some time must be expected to elapse before a documentation of any experiment will contain all the information necessary for a calculation of the disturbance growth in a boundary layer up to the end of the transition region, it would be helpful if one were able to judge whether the transition process has begun in a boundary layer and how far downstream it has progressed, especially when only mean flow data are available. This is of importance for test models in wind tunnels with flows at high Mach and low Reynolds numbers, a case occurring quite frequently. In this parameter range - especially in pre-1960 investigations - boundary layers were often taken as being turbulent while in fact they were transitional or even still laminar. The Reynolds numbers attained in these boundary layers were necessarily small, and the following discussion will therefore be confined to the phenomena in these low Reynolds number boundary layers and not consider the manifold causes which lead to transition.

As will be shown below, a comparison of measured velocity profiles with the law of the wall and the outer law provides a simple criterion which allows us to distinguish between low-Reynolds number "transitional" and "turbulent" boundary layers. This criterion is so far limited in its range of validity to zero pressure gradient boundary layers along adiabatic or isothermal walls. Accepting these boundary conditions, one can postulate that a compressible boundary layer is considered fully turbulent only when the velocity profile agrees both with the law of the wall in the respective part of the inner layer and with the outer law in the outer region of the boundary layer. The extent of agreement with the outer law, as shown in the many outer region plots (e.g. figures 4.2.3, 4.2.4, 4.2.5 etc.) presented in the preceding sections, increases as the Reynolds number rises. The Reynolds number range within which transitional velocity profiles may be observed is as wide as $300 \leq Re_{\delta_2} \leq 6000$ but equally one may find fully turbulent velocity profiles in this range. The problem which has to be overcome before we can say with certainty that there exists a unique relationship $\Pi = \Pi (Re_{\delta_2})$ is, however, not so much the exclusion of transitional cases but that of profiles strongly influenced by upstream history effects.

Before we look at a few cases and apply the above criterion to transitional boundary layers, some fundamentals of the transition process in compressible boundary layers should be recalled.

The main effect of compressibility on phenomena connected with boundary layer stability is an increase in the wave velocity of the disturbance of self-excited oscillations with Mach number. This has the consequence that the disturbances, although possessing the same dimensionless amplification coefficient as in the incompressible case, have less time (per unit distance) to grow in amplitude. Thus, the adiabatic compressible boundary layer is more stable than the incompressible one (Laufer & Vrebalovich 1960) leading to higher transition Reynolds numbers (Potter & Whitfield 1962).

For boundary layers at Mach numbers of approximately 4.5 and larger, according to the "forcing theory" incoming sound waves are, however, the dominating mechanism which causes transition by inducing fluctuations of all frequencies to grow instead of only selected frequencies as predicted by "simple" stability theory (Mack 1971 and Kendall 1975).

As far as the length of the transition region is concerned, Potter & Whitfield (1962) have found experimentally at Mach numbers from zero to eight that the extent of the transition region increases with increasing transition Reynolds numbers for boundary layers over adiabatic walls. It increases with Mach number if the transition Reynolds number is constant. Thus it is established that we will find higher

transition Reynolds numbers (however defined) and larger transition regions in compressible than in incompressible boundary layers. We must now also consider the local spreading of disturbances through the laminar boundary layer which leads finally to the fully turbulent state. In agreement with other experimental data (Klebanoff & Tidstrom, 1959), Laufer & Vrebalovich (1960), Demetriades (1960) and confirmed by LaGraff (1970) and Owen (1970b) and with theory (Dunn & Lin 1955), Potter & Whitfield found a critical layer of intense fluctuation-energy concentration (mass flow and total temperature) at all Mach numbers. The distance of this layer from the surface increases with Mach number in the case of adiabatic and cooled isothermal walls (e.g. LaGraff 1970). This fluctuation peak is the result of a strong vorticity concentration at points where the local mean velocity is equal to the propagation velocity of the oscillations. The variation of the critical layer height y_c with Mach number is shown in Fig. (4.4.1)

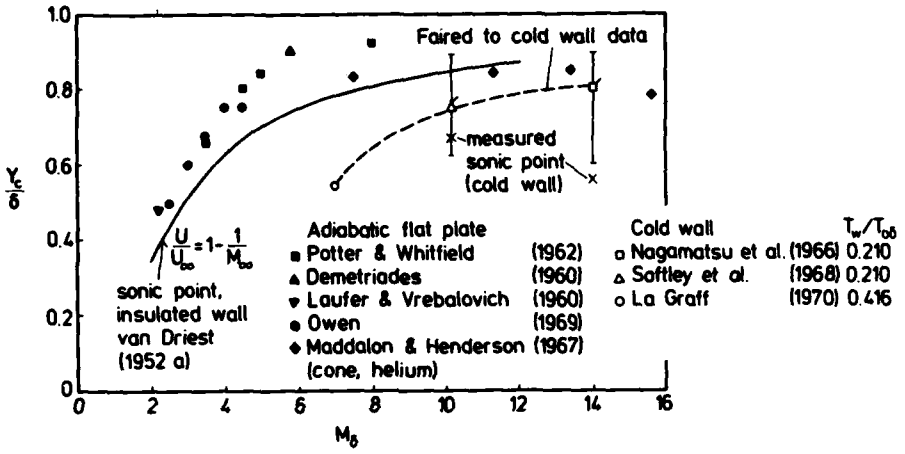

Fig. 4.4.1 Peak fluctuation height in laminar boundary layers from LaGraff (1970). Flagged symbols transitional.

Measurements for both adiabatic and cooled wall boundary layers present a picture of a gradual spreading of fluctuations from this rather narrow critical layer in the outer region of the boundary layer towards the wall with increasing Reynolds number (e.g. LaGraff 1970, 1972) indicating a very gradual growth rate normal to the surface compared to the rapid stretching which must take place in the streamwise direction. Fischer (1972) and Fischer & Weinstein (1972) discussed this spreading of a "turbulent disturbance" and found that the wall spreading angle ($\approx 1^0$) was insensitive to local Mach number. Since, however, the location of the critical layer moves towards the boundary layer edge with increasing Mach number, the relatively constant wall spreading angle (for Mach numbers larger than six) implies a greater downstream lag of wall boundary layer transition as Mach number increases. So it is not surprising to find a high fluctuation level in the outer region of the boundary layer when the Reynolds number is still a factor of two smaller than that which is associated with the onset of transition based on heat transfer measurements at the wall. It thus seems that the wall measurements only detect a change in the laminar conditions when the disturbances have spread to the immediate proximity of the wall. Then transient phenomena become apparent in a surface thin-film gauge output although the mean value is still indicative of a laminar boundary layer (LaGraff 1970). Skin friction measurements performed with a floating element balance seem to be a more reliable means of indicating transition. According to Watson et al. (1973) skin friction values show a departure from the value appropriate for a laminar boundary layer before measured heat transfer coefficients depart from the appropriate laminar coefficient. This finding favours a criterion which uses skin friction as a means of transition detection. Since mean flow profiles deviate also from laminar profiles well upstream of the point where the heat transfer at the wall changes its character from laminar to turbulent (Watson et al. 1973) we have a sound physical background for choosing the law of the wall and the outer law plots as criteria for the state of the velocity profile in a boundary layer in a

compressible fluid. This is certainly a better substantiated procedure than the method which uses the velocity power law exponent n, mentioned for example by Martellucci & Laganelli (1974).

In this context we note an observation related to natural and forced transition made by Owen (1970a), "namely that the fluctuation level in the turbulent boundary layer resulting from forced transition does not approach that of the natural turbulent boundary until some time after complete transition (Fig. 4.4.2).

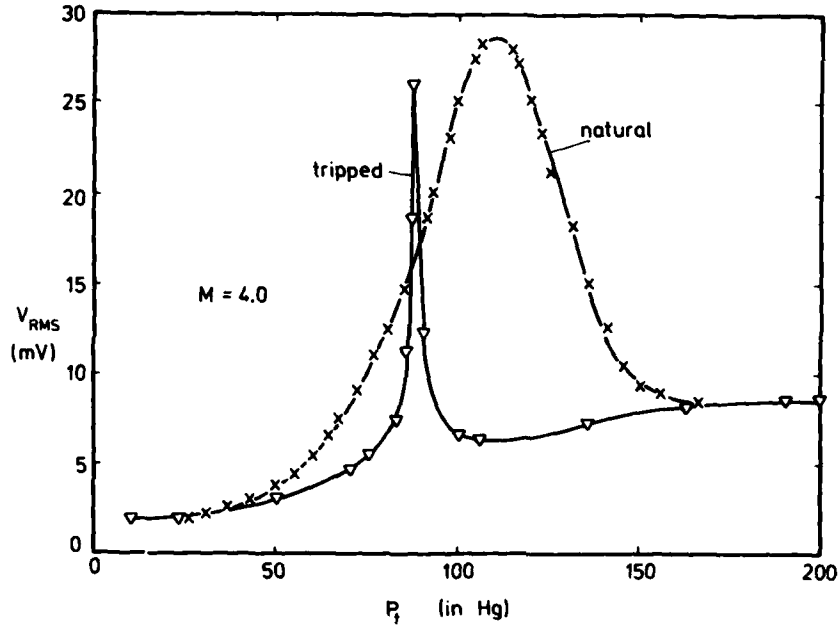

Fig. 4.4.2 Comparison of natural and controlled transition at M=4.0. Reproduced Owen (1970).

This fact suggests that boundary layer measurements should only be made in a region well away from the roughness element if it is desired to simulate turbulent flow due to natural transition. However, since the fluctuation levels in both cases are the same well downstream, it would appear that, in the wall region, no additional disturbances were introduced by the trip although this will not necessarily be the case for the greater roughness heights which would be required to bring transition up close to the trip position". This last remark may lead to an explanation of the slope in the velocity profiles of Fig. 3.3.11 - Coles 1953) which is steeper than the one given by the law of the wall (eqn. 3.3.9) and which is best seen in the velocity profiles downstream of the "fence trip" which seems to have been of a rather "fierce" nature (see also Korkegi 1956).

4.4.2 Analysis of measured velocity profiles

After having discussed some basic features of the transition process it is appropriate to discuss experiments where velocity and temperature profiles as well as wall data have been measured. From among the large number of cases a few are listed here (Table 4.4.1). They were selected because they describe measurements in laminar and transitional boundary layers which were extended into the fully turbulent regime, or because they were thought of as being interesting measurements despite the fact that tabulated data were not always available.

Only of one the listed experiments (Watson et al. 1973), where laminar, transitional and turbulent velocity profiles were measured in sequence, contains skin friction measurements made by a floating element balance. It is therefore appropriate to begin a discussion with these data. In Fig. (4.4.3) typical Mach number, static temperature, and mass flow profiles were plotted for three successive stations, ranging from a profile at the most forward station (which the authors state to be far from laminar by comparison with a profile obtained by a self-similar solution) to a turbulent but not yet fully developed profile at station 4.

Table 4.4.1

Author	Configuration	M_δ	$RE_{\delta_2} \times 10^{-3}$	$RE_\Theta \times 10^{-3}$	$REX/m \times 10^{-6}$	TW/TR	CF	FQ	PG	PO	TO	NX
Korkegi (1956)	Flat plate	5.8	-	0.8-4	$1.07\text{-}2.5 \times 10^5$ per inch	1	F	No	Z	Yes	-	2 (?)
Demetriades (1960)			-	-		1	-	Yes		Yes	-	4
Winkler, Cha (CAT 5902)	Flat plate	5	0.3-0.8	1-4.5	8-16	0.65-0.95	(V)	No	Z	FPP	STP	4
Danberg (CAT 6702)	Flat plate	6.5	0.3-1.8	1.3-6	8-20	0.5-0.9	(V)	No	Z	CPP	ECF	4
Nagamatsu, Graber, Sheer (1965, 1966)	10^0 cone 1,2 and 2.4 m length	9-16	-	0.9-1.4	1-8	$\simeq 0.25$	(V)	No	F	FPP	ECP	2 (1)
Fisher et al. (CAT 7001)	Nozzle wall	19-21.6	0.2-0.3	8-12	45	1.1	(V)	Yes	F/Z	CPP	STP	5
Fisher & Maddalon (CAT 7103)	10^0 wedge	6.5	0.9-4.8	0.5-5.5	6-25	1	-	No	Z	CPP	-	7
LaGraff (1970, 1972)	Flat plate 10^0 cone hollow cylinder	7	-	-	17	$\simeq 0.25$	-	Yes	Z	-	-	3
Owen (1970a, b)	Flat plate	2.5-4.5	-	-	32-45	1	-	Yes	Z	-	-	1
Hastings, Sawyer (CAT 7006)		3.9	7-19	2-25	3.7-29	1	F/P	No	Z	CPP	STP	7
Mabey (CAT 7701S)		2.5-4.5	0.8-4.3	1-8	4-8	1	F	No	Z	CPP	STP	3
Watson et al. (CAT 7305)	Flat plate	9-10	1.7-15	1-12	0.9-5	1	F	No	Z	FPP	STP	4
Martellucci, Laganelli (1974) Laderman (1974) Demetriades (1974)	5^0 cone 1.5 m length	8	-	0.9-5	1-12	$\simeq 1$	-	Yes	-	FPP	STP	1-7

Table 4.4.1 (continued)

Author	Configuration	M_δ	RE_{δ_2} $\times 10^{-3}$	RE_Θ $\times 10^{-3}$	REX/m $\times 10^{-6}$	TW/TR	CF	FQ	PG	PO	TO	NX
Owen & Horstman (1972a) Horstman & Owen (1972) Owen & Horstman (1972b) Owen & Horstman (1974) Owen et al. (1975)	10^o-cone-ogive-cylinder	6.7-7.4	1.3-3	4.9-9.7	10.9	$\simeq$ 0.50	F	Yes	Z	FPP	STP	3
Watson (1977)	4^o-wedge	11	-	2.3-18	47-59	0.3-1	F	No	$\simeq$ Z	CPP	STP	8
Fisher & Weinstein (1972)	5.7^o-cone	$\simeq$ 14	-	-	28-44	$\simeq$ 1	-	No		CPP	-	1

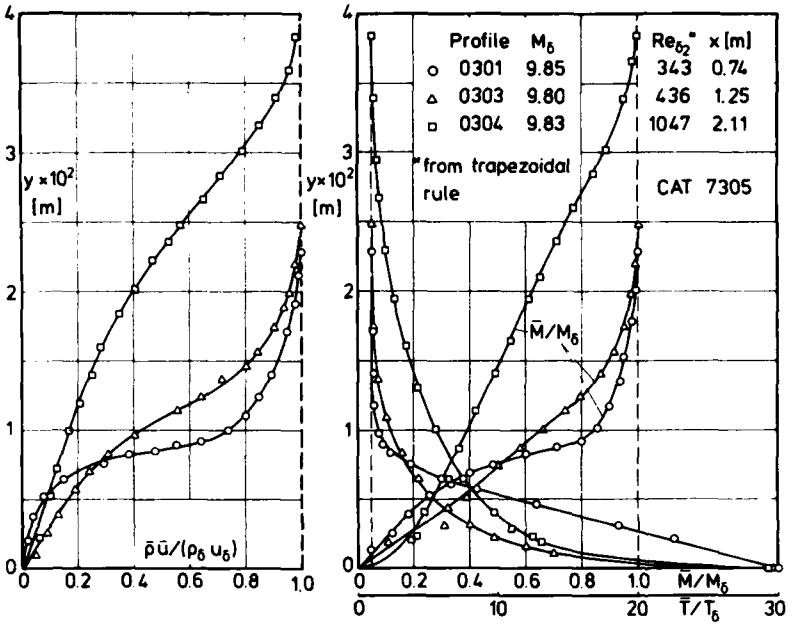

Fig. 4.4.3. Mach number-, temperature- and mass-flow profiles in a transitional / turbulent compressible boundary layer (adiabatic wall, zero pressure gradient). Watson et al. (1973).

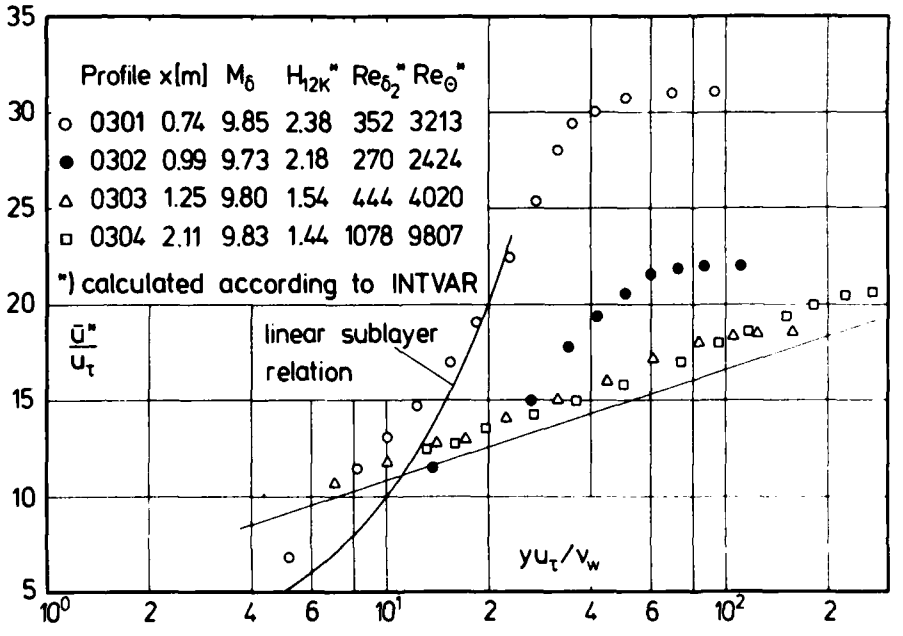

Fig. 4.4.4. Development of transitional velocity profile (adiabatic wall, zero pressure gradient, helium). Watson et al. (1973).

Inspection of Fig. (4.4.4) where the same data are presented in log-law coordinates shows the transitional behaviour of profiles 0301 and 0302 whereas the last two profiles follow the law of the wall as far as the slope is concerned, lying however slightly above the straight line given by eqn. (3.3.9). This latter behaviour is confirmed by the measurements at higher Reynolds numbers given in Fig. (4.4.5). If it is assumed that the parallel shift is not caused by a systematic error in the skin friction measurement (approximately - 10 %), the low value of c_f indicates that the mean skin friction has not reached the value appropriate to the turbulent velocity profile, i.e. the inner region is not yet fully turbulent.

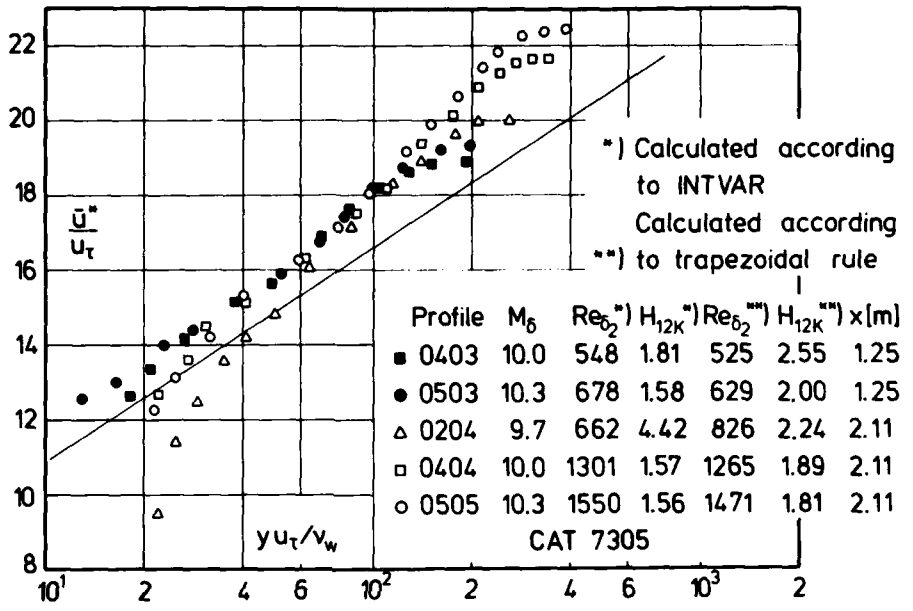

Fig. 4.4.5 Law of the wall for a compressible boundary layer (adiabatic wall, zero pressure gradient, low Reynolds number). Watson et al. (1973).

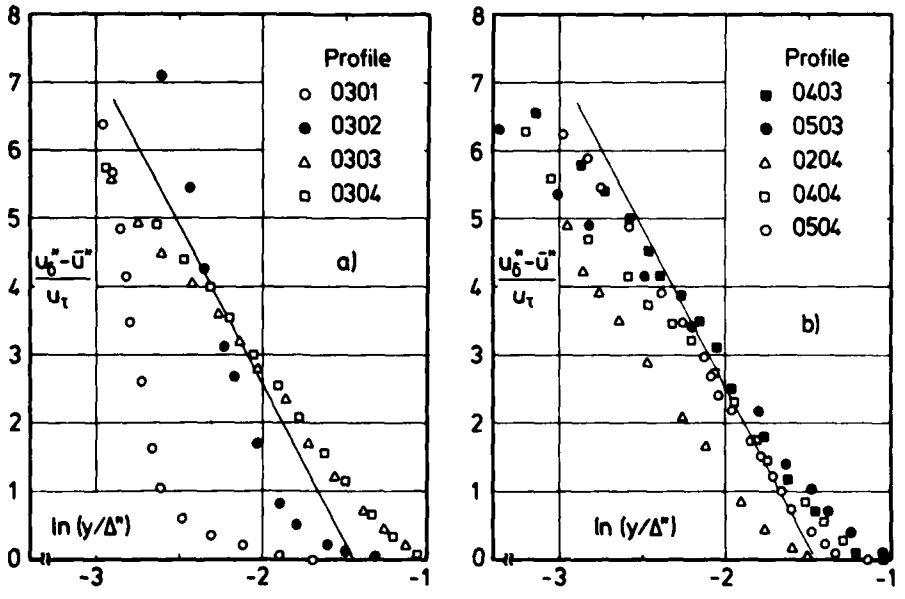

Fig. 4.4.6 Outer law for a compressible boundary layer (adiabatic wall, zero pressure gradient, low Reynolds number). Watson et al. (1973)

The outer law plot in Fig. (4.4.6) shows no agreement with eqn. (3.3.17) for the two clearly transitional velocity profiles (0301, 0302) as is to be expected. Compared with the fully developed velocity profiles described in § 4.2 the low Reynolds number profiles have only short regions where they agree with eqn. (3.3.17), except for profile 0504, but their overall behaviour is clearly distinct from both the transitional and the fully developed velocity profiles.
We now draw attention to the development of the kinematic shape parameter H_{12K} - defined as the ratio of displacement and momentum loss thickness with density set constant - which starts at $H_{12K} = 2.36$ (Fig. 4.4.4) and ends at 1.44. The former value lies not far from 2.60 which corresponds to the appropriate value of the Blasius solution describing the velocity profile in a laminar subsonic boundary layer with zero pressure gradient. H_{12K} which is given in Fig. (4.4.5) for all velocity profiles serves apparently as an excellent indicator for velocity profiles in the laminar or transitional state, as can also be seen from the measurements of Fischer & Maddalon (CAT 7103) plotted in Fig. (4.4.7).

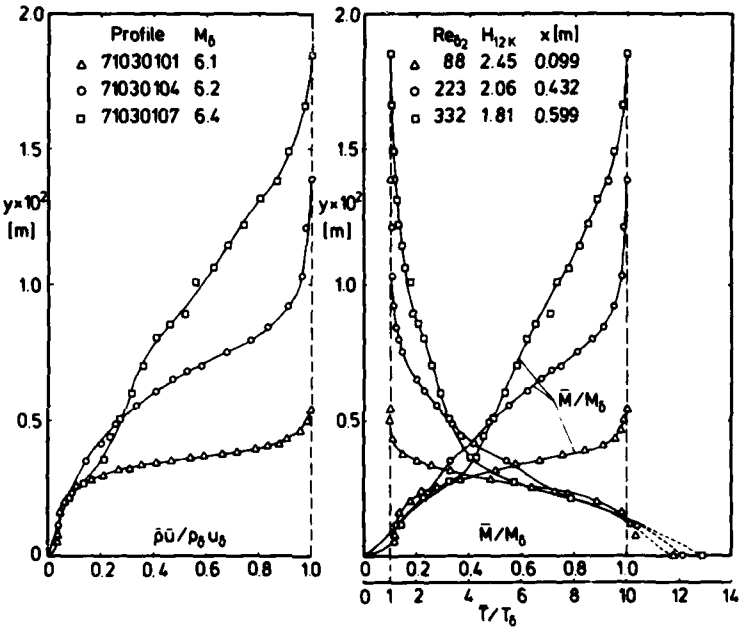

Fig. 4.4.7 Mach number, temperature, and mass-flow profiles in a transitional compressible boundary layer (adiabatic wall, zero pressure gradient, defined origin). Fischer & Maddalon (CAT 7103).

Returning to Figs. (4.4.5) and (4.4.6) one can conclude that the transition process begins and therefore ends first in the outer region of a compressible boundary layer. Due to the very small spreading angle of the disturbances originating in the critical layer the transition process is felt in the inner region further downstream than in the outer region. This phenomenon can be observed (Fernholz 1972) in the measurements performed by Winkler & Cha (1959) and by Danberg (1960) the latter being plotted in Figs. (4.4.8) and (4.4.9). In these experiments the wall was cooled and the skin friction was deduced from the wall slope of the velocity profile. They are less cogent therefore than the data of Watson et al. but show nevertheless the same tendency. It is interesting to note that the outer law is satisfied more closely for Danberg's velocity profiles (Fig. 4.4.9) than for those in Fig. (4.4.6), probably due to the higher Reynolds number and lower Mach number in Danberg's experiment. Since Danberg determined skin friction from the wall slope of the velocity profile, a method which does not guarantee very accurate results, we have calculated c_f from a semi-empirical relationship (Fernholz 1971) assuming that the velocity profile is fully turbulent. The resulting logarithmic-law plot is shown in Fig. (4.4.10) with the respective values of the skin friction coefficient c_f given in the legend. Two groups of velocity profiles can be clearly distinguished differing from each other at the low and the high end of y^+. Even with the higher values of c_f profiles 6002S0101 and 0201 do not behave as fully turbulent velocity profiles should do,

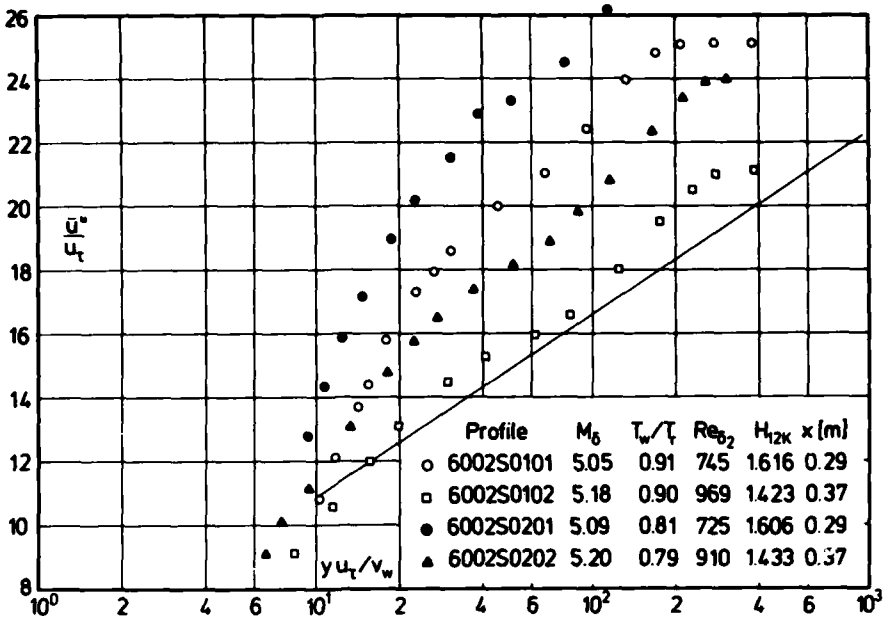

Fig. 4.4.8 Law of the wall for a compressible boundary layer (isothermal wall, zero-pressure gradient, defined origin). Danberg (1960).

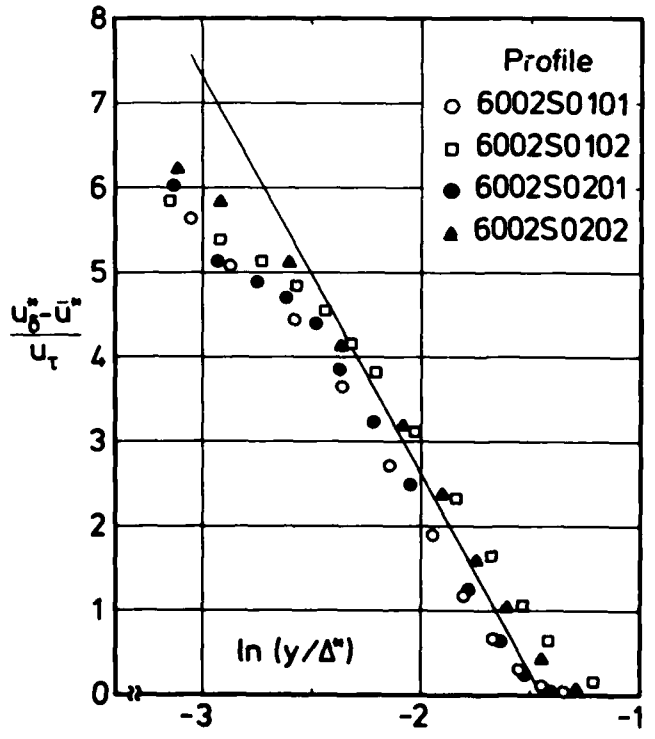

Fig. 4.4.9 Outer law for a compressible boundary layer isothermal wall, zero pressure gradient, defined origin). Danberg (1960).

whereas it would be impossible to distinguish profiles 6002S0102 and 0202 from fully turbulent velocity profiles at low Reynolds numbers. Thus ambiguities arising from an uncertain determination of c_f cannot be wholly excluded.

Hastings & Sawyer (1970) measured turbulent velocity profiles on a flat plate, and the outer law shows very good agreement with the measurements (Fig. 4.4.11), i.e. the outer part of the velocity profile is fully turbulent. The comparison between the law of the wall and profiles 0202, 0203 and 0204 (Fig. 4.4.12) reveals discrepancies which must be attributed to the transitional state of the inner layer and are not necessarily a consequence of difficulties in measuring skin friction at low total pressures in the tunnel.
Mabey (1977) extended earlier measurements (Mabey et al. 1974) to much lower Reynolds numbers ($370 \leq Re_{\delta_2} \leq 4300$). These tests were performed on the same flat plate as those of Hastings & Sawyer (1970). The boundary layer was tripped by means of small glass spheres (ballotini) attached by a thin layer of Araldite in a narrow band (Mabey 1965). "At the low Reynolds

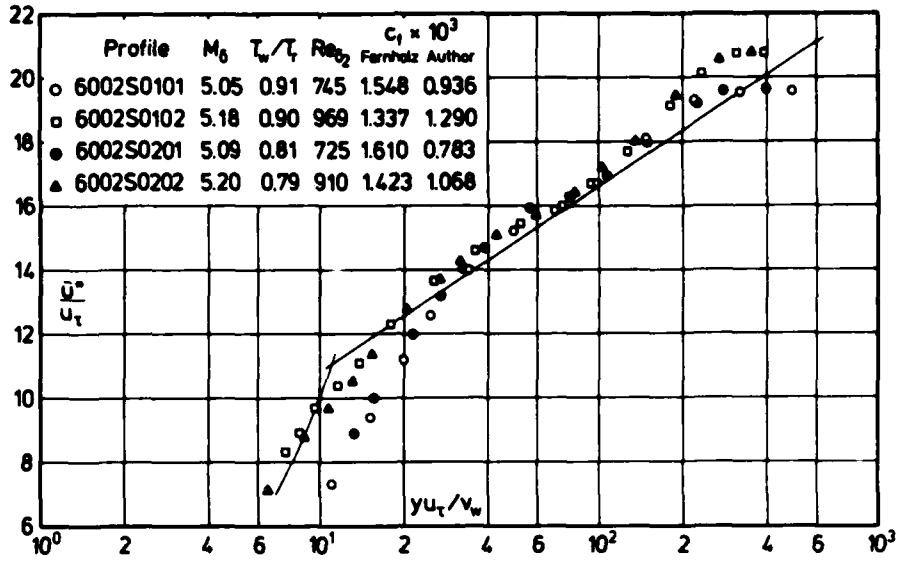

Fig. 4.4.10 Law of the wall for a compressible boundary layer (isothermal wall, zero-pressure gradient, defined origin). Danberg (1960). c_f from Fernholz (1971).

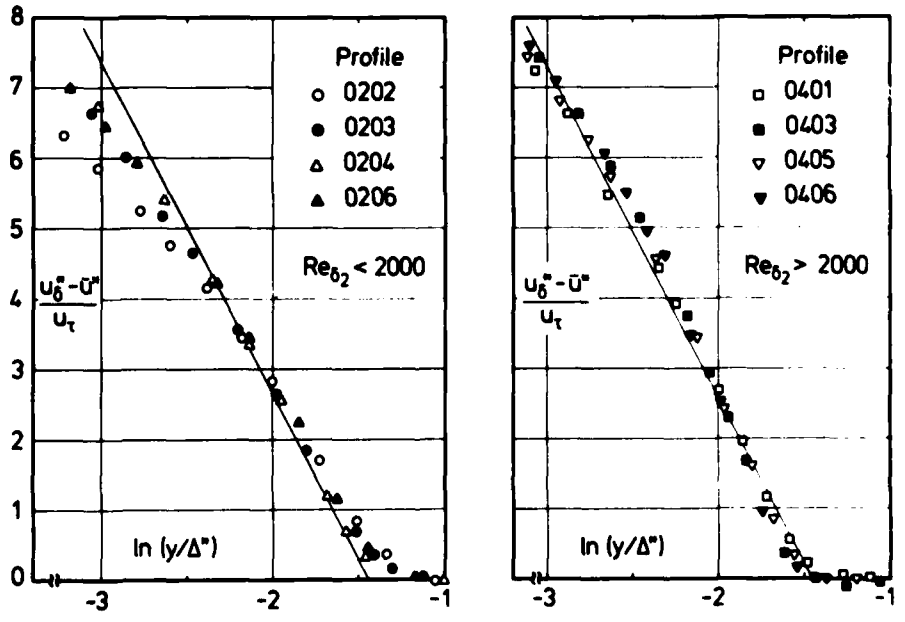

Fig. 4.4.11 Outer law for a compressible boundary layer (adiabatic wall, zero pressure gradient). Hastings & Sawyer (1970).

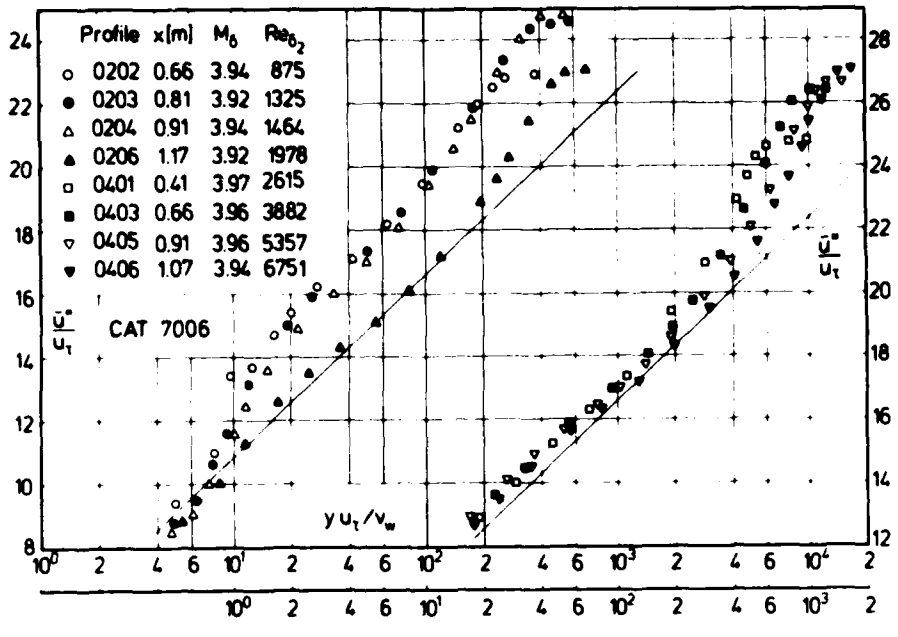

Fig. 4.4.12 Law of the wall for a compressible boundary layer (adiabatic wall, zero pressure gradient, transition effects). Hastings & Sawyer (1970).

numbers the boundary layer state was assessed by an examination of the measurements of local skin friction, velocity profiles and surface hot film signals" (Mabey 1977). A comparison of the measurements at moderate Reynolds numbers with earlier ones (cf. Figs. 4.2.1 and 4.2.2) shows that all velocity profiles lie below the log-law line for $y^+ < 200$ (Fig. 4.4.13). This is possibly due to the skin friction measurements the accuracy of which was estimated to be only 7 % (Mabey, appendix E). The values of the form parameter H_{12K} lie in the range which is characteristic of moderate to low Reynolds number boundary layers (Rotta 1962).

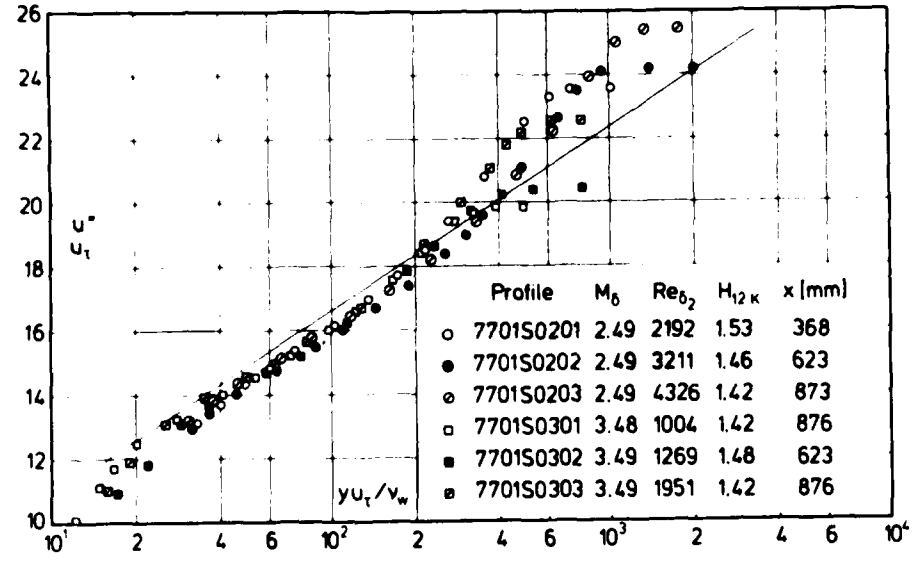

Fig. 4.4.13 Law of the wall for a compressible boundary layer (adiabatic wall, zero pressure gradient, defined origin). Mabey (1977).

A further decrease in Reynolds number - $800 \leq Re_{\delta_2} \leq 1500$ - reveals that the [illegible] velocity profiles (Fig. 4.4.14) almost vanishes, which is to be expected. Furthermore, [illegible], the measurements do not follow the logarithmic law any longer, at least quantitatively. The author does not comment on these discrepancies but hints at probe problems due to a rather thin boundary layer. The only comparable velocity profiles were measured by Coles (1953) and Stalmach (1958), and are presented as profiles 53010401/0701/1001/1301 in Fig. (4.2.5) and Fig. (4.2.10), respectively.

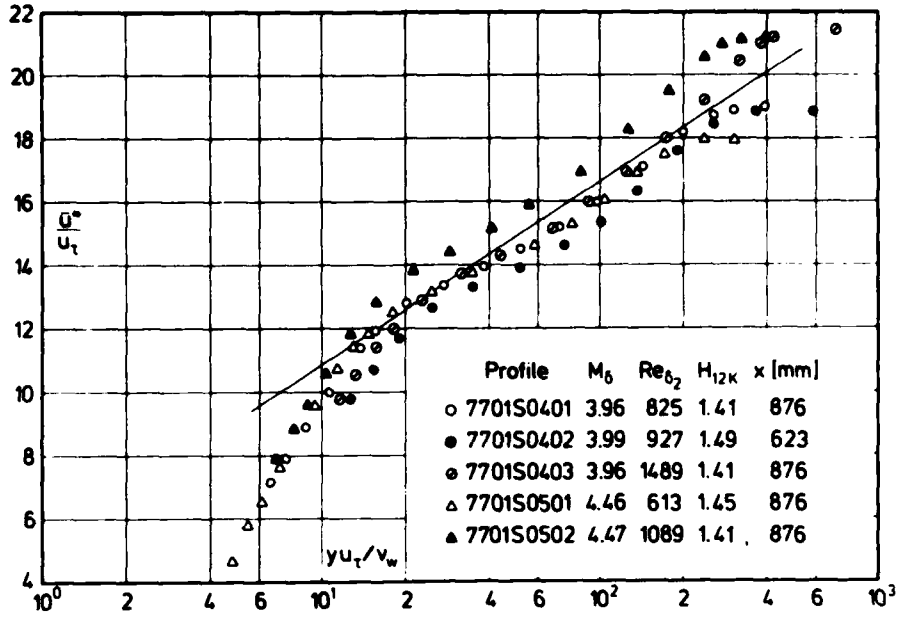

Fig. 4.4.14 Law of the wall for a compressible boundary layer (adiabatic wall, zero pressure gradient, defined origin). Mabey (1977).

Profile 53011301 especially shows a slope which differs from that of the logarithmic law, but the overall behaviour of the velocity profile fits into the framework given in § 4.2. A comparison between the outer law (eqn. 3.3.17) and the velocity measurements (Fig. 4.4.15) shows good agreement - though necessarily within a small range expected at these low Reynolds numbers (see also figures 4.2.6 and 4.3.2).

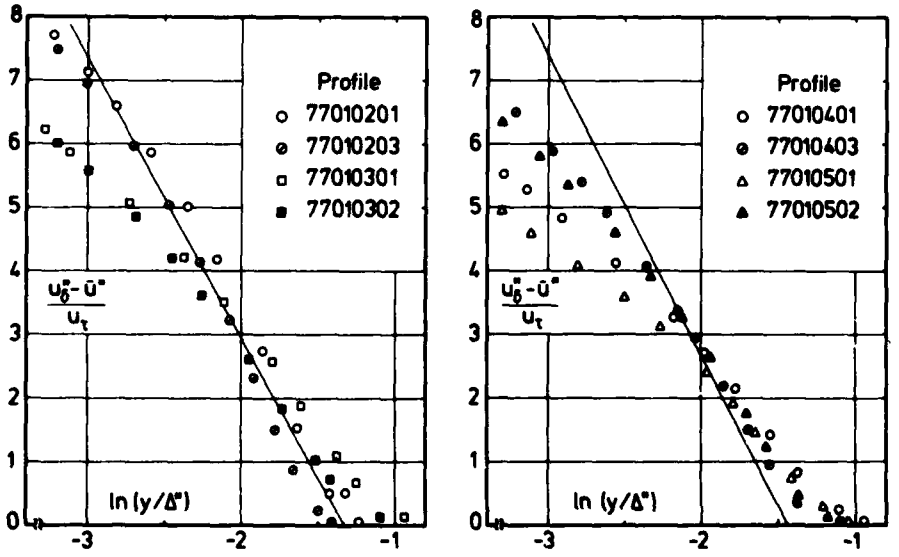

Fig. 4.4.15 Outer law for a compressible boundary layer (adiabatic wall, zero pressure gradient, defined origin). Mabey (1977).

Judging from the velocity measurements presented so far, it is easy to distinguish low Reynolds number turbulent velocity profiles from low Reynolds number transitional ones by comparing measurements with the semi-empirical relationships in the log-law region and in the outer region. Fully turbulent velocity profiles should agree both with the logarithmic law and at least - within a small range - with the outer law. Transitional velocity profiles can agree with the outer law (Fig. 4.4.11) but do not agree with the logarithmic law (Fig. 4.4.12) if the transition process has not reached the wall. Furthermore the value of H_{12K} provides a useful indicator of the state of the boundary layer - at least for boundary layers with zero pressure gradient.

It was therefore surprising to find a further category of low Reynolds number velocity profiles - $370 \leq Re_{\delta_2} \leq 640$ - shown in Figs. (4.4.16) and (4.4.17). We cannot account for profiles 7701S0601/0701 which we simply think must result from experimental error. The remaining three velocity profiles shown appear to be strongly transitional (note also the H_{12K} values), judging by a comparison with the logarithmic law (Fig. 4.4.16); but except for profile 0702 they show an outer law behaviour which resembles much more that of velocity profiles in a severe pressure gradient (see § 5). Unless a plausible explanation can be found for discrepancies as these we think it futile to look for possible low-Reynolds number effects on the constants in the logarithmic law (see § 3.3).

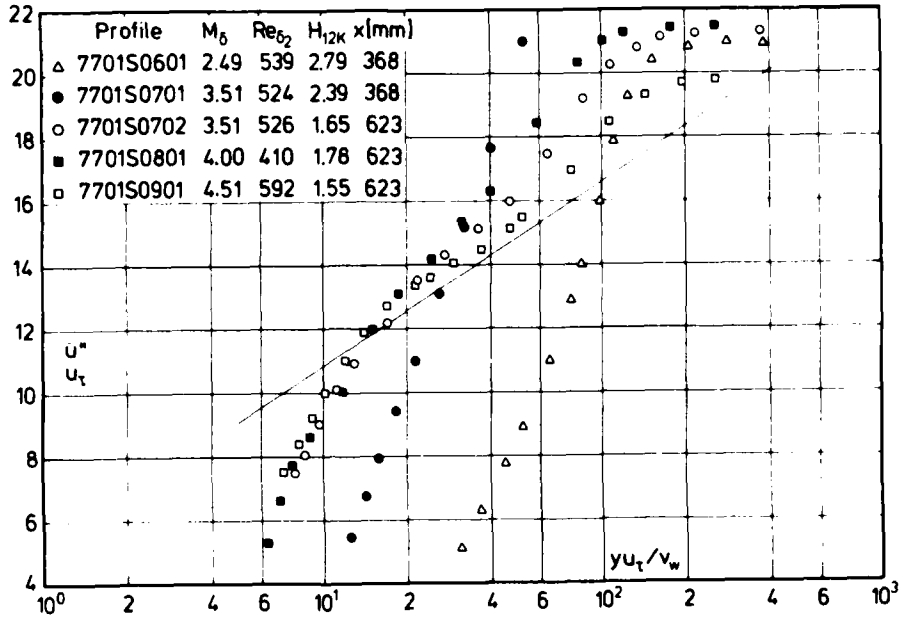

Fig. 4.4.16 Law of the wall for a compressible boundary layer at low Reynolds numbers (adiabatic wall, zero pressure gradient, defined origin). Ashey (1977)

There is a last group of low Reynolds number data which should perhaps be mentioned here. Because of confusing secondary effects they have not been introduced earlier. In general, very high Mach number boundary layers are characterised by a large value of μ_w/μ_δ, so that exceptionally low values of Re_{δ_2} are observed in flows which nevertheless have some turbulent characteristics. The extreme example is the contoured nozzle wall boundary layer studied by Kemp and Owen (CAT 7206) with Mach numbers from 19 to 45 (Figs. 5.2.13 and 5.2.14). Re_{δ_2} lies in the range 60-300, and in transformed axes the greatest value of $(y\ u_\tau/\nu)$ is about 50, while H_{12K} takes values between 2.40 and 3.10. The outer region is indeed turbulent, as was confirmed by hot-wire measurements, but the inner region is certainly still transitional (Figs. 5.2.13, 5.2.14). In view of the low values of $(y\ u_\tau/\nu_w)$ it is not surprising that there is no discernable log law. The lack of any agreement either quantitatively or qualitatively cannot be asigned solely to low Reynolds number effects however, as the layer has experienced a very strong upstream expansion in the nozzle throat, possibly even passing through a region of re-laminarisation. The local streamwise pressure gradients, and even more so, the local normal pressure gradients, are also substantial.

A somewhat similar, though not so extreme, case is described by Hill (CAT 5901). The boundary layer was

formed in a conical nozzle, and is not subject to significant pressure gradients in the region of study. The Reynolds number range (Re_{δ_2} from 130-470, Re_Θ 1000-3000) is such that re-laminarisation in the throat region is not improbable, though there is insufficient information on transition for any conclusion to be drawn. Here again the H12K values (1.8-2.5) are more characteristic of a laminar layer. The inner region has not become fully turbulent (Fig. 5.2.7) whereas the outer region shows pressure gradient effects, i.e. deviations from the outer law (Fig. 5.2.8) which conceal possible low Reynolds number effects. On the whole the outer region appears to be turbulent.

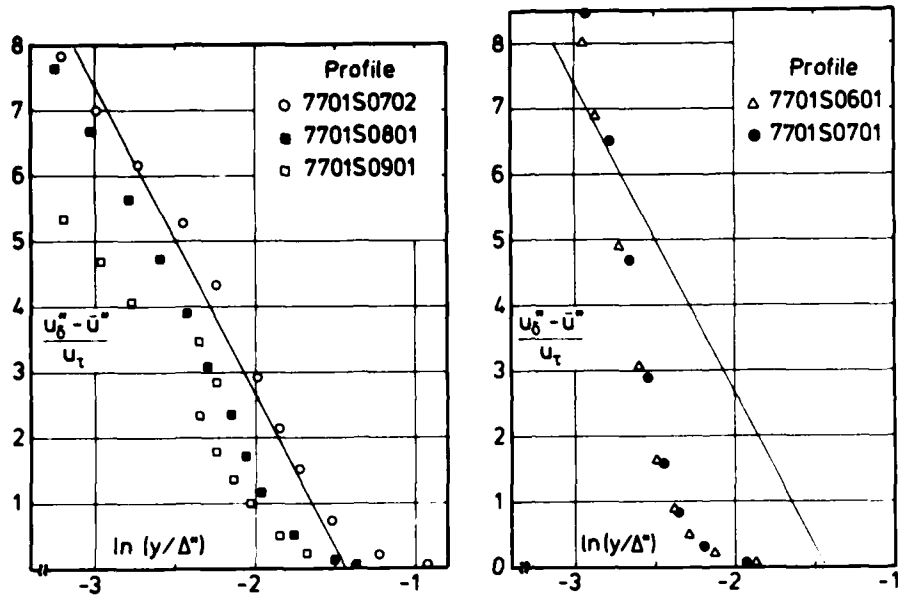

Fig. 4.4.17 Outer law for a compressible boundary layer at low Reynolds numbers (adiabatic wall, zero pressure gradient, defined origin). Mabey (1977).

4.5 Upstream history effects

A shortcoming of many of the older boundary layer calculation methods, both for subsonic and supersonic flow, lies in their inability to account for the upstream history of the boundary layer and relaxation of upstream effects downstream. One reason for this failure is the assumption that the development of a boundary layer, and here especially the distributions of turbulent shear stress $\overline{u'v'}$ and temperature transport $\overline{v'T'}$, is determined by local conditions only, via eddy coefficients of momentum and heat transfer or otherwise.

Relaxation is not used here in the strict sense of the word as it is defined, for example,in thermodynamics, but is meant to describe the transition process between two well-defined, possibly equilibrium states of the turbulence structure.

In supersonic flow these upstream effects influence the velocity and the temperature fields in different ways even for a Prandtl number of unity since their features are not similar across the layer unless there is a sufficiently long history of similar "input" conditions at the wall and in the free stream (which includes pressure gradients) (Morkovin 1960). The mode of propagation of relevant quantities in both fields is parabolic, i.e. corresponds to nearly parabolic spreading of changes in time or space from the source of a point disturbance. Local features of the temperature and velocity field depend therefore on the boundary conditions and on the upstream history unless there is a sufficiently long relaxation region.

As was shown for subsonic flow, upstream history and relaxation effects may influence the inner and the outer region of a boundary layer more or less strongly and for a different length of time. In Klebanoff & Diehl's (1952) experiment, where the boundary layer had been disturbed by a spanwise rod lying on the wall (with diameter, d, about equal to the undisturbed boundary layer thickness δ_0 at the trip position), a downstream distance of 26 δ_0 was not sufficient for the velocity profile to regain similarity. Clauser (1956) placed a much smaller trip rod with $d/\delta_0 = 0.055$ parallel to the wall and across the boundary layer, but now at distances $y/\delta_0 = 0.15$ and 0.55 from the wall. He found that the inner layer returns much more quickly to the universal inner law than the outer layer to its own equilibrium state, confirming the strong influence of upstream history and relaxation on the large eddies. One reason for this behaviour lies in the rather long lifetime of these eddies.

An experiment similar to the one by Klebanoff & Diehl but in supersonic flow was performed by Peake et al. (1971). These measurements unfortunately show a scatter larger than normal but the discrepancies between the log-law and the velocity profiles (Fig. 3.3.12) show at least qualitatively the downstream effect of the disturbance. For a more detailed discussion the reader is referred to section 3.3.4 where the effect of tripping devices on the boundary layer has already been discussed.

A further example of a supersonic boundary layer developing after a change in wall roughness will be discussed in section 4.6 (Kubota & Berg 1977).

Two further experiments which belong to this group of experiments in principle are characterized by relatively large local disturbances of the wall geometry:

Firstly the investigation of Clutter & Kaups (CAT 6401) - though an interesting and useful experiment - provides no skin friction data. This renders it impossible to compare the velocity profiles with the log-law or the outer law. Furthermore the profile measurements do not extend within the momentum deficit peak in about half the cases, so that the integral values, and Reynolds numbers based on δ_2, should be treated with reserve. The boundary layer was formed, in each case, under essentially constant pressure conditions on the nose extension which finished as a parallel cylinder of 70 mm diameter. For model (a) - for details see CAT 6401 or the original paper - the profiles were measured on the parallel section downstream of an abrupt increase in diameter which was of circular meridional section. The boundary layer was relaxing after traversing the strong shock-induced separation ahead of the junction, and reattachment to the shoulder of the center-body (series 01-04). Since both pressure and temperature measurements were performed, a comparison with the results of calculation methods of large enough sophistication should at least be possible.

The second investigation (Moore CAT 5805) dealt with the turbulent boundary layer behind a forward facing step. A further test configuration which continued the nozzle contour as a flat plate allowed a direct comparison between a "normal" tunnel wall boundary layer, and the "same boundary layer" subjected to an abrupt disturbance. Unfortunately no attempt was made to check on cross-flow effects, which are likely to be marked

in the region of the step. The data throughout do not appear to be very accurate although skin friction was measured with a miniaturized floating element balance. With the step originating at X = 0 approximately 25 mm downstream of the nozzle exit plate we have shown the development of the velocity profiles downstream from this position for both the undisturbed and the disturbed case in Fig. (4.5.1).

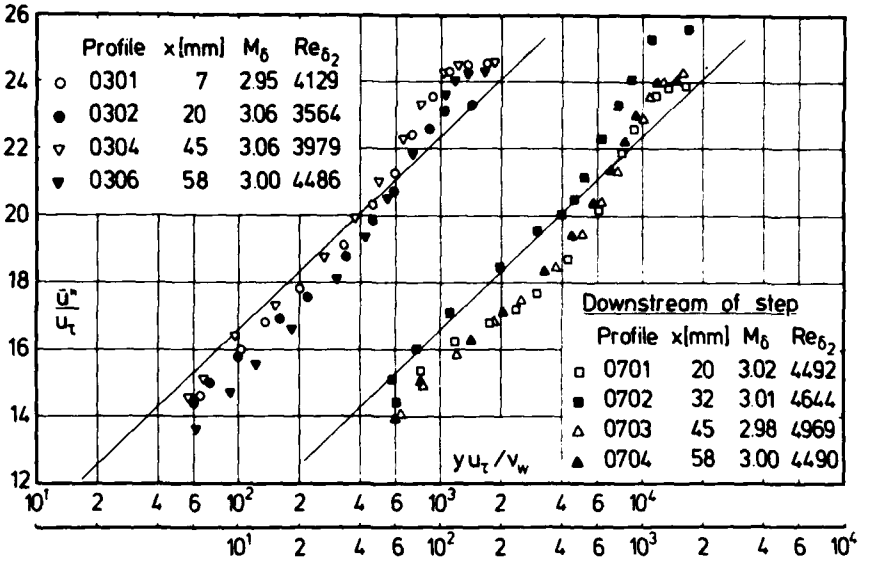

Fig. 4.5.1 Law of the wall for a compressible boundary layer (adiabatic wall, zero pressure gradient) Moore (1958).

There appears to be hardly any difference between the two series of velocity profiles (the Mach and Reynolds numbers are approximately the same in both cases). This may be due to the rather small step height, h = 2.03 mm, as compared to the displacement thickness 7 mm downstream in the undisturbed flow of 1.46 mm. The "roughness Reynolds number" $h\, u_\tau/\nu_w$ equals 67 with data from profile 0101 (see § 4.6). A comparison with other smooth wall measurements, e.g. those of Stalmach (CAT 5802), which were performed in the same tunnel and which are shown in Fig.(4.2.9), does not give an indication why Moore's velocity profiles should lie below the standard log-law curve. Agreement between the measurements and the outer law is very good as can be seen from Fig. (4.5.2).

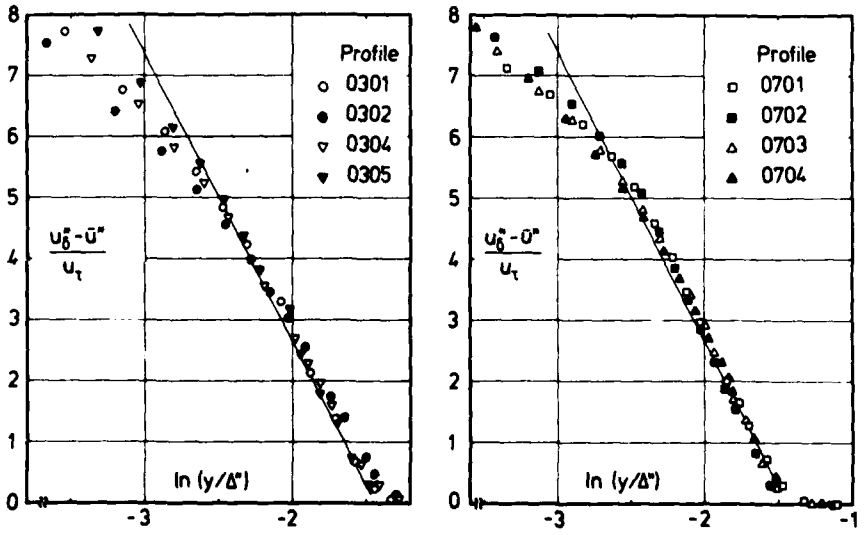

Fig. 4.5.2 Outer law for a compressible boundary layer (adiabatic wall, zero pressure gradient) Moore (1958).

This shows that pressure gradient effects from the nozzle flow upstream do not appear to play a rôle in the boundary layer region under investigation.

In this context we should draw the reader's attention to a great number of investigations which were performed in connection with tripping devices and their downstream effects. We have discussed some of Coles' velocity profiles from this point of view (Fig. 3.3.11) and wish to refer at least to Stone (1971) and to Stone & Cary (CAT 7209). A great deal of heat transfer data was obtained but only presented as a small scale graph so that it could not be used for discussion. No skin friction measurements were taken, but a comparison between measurements and velocity profiles in log-law coordinates - τ_w was calculated according to Fernholz (1971) - showed less distortion introduced by the trips than is reported by the authors. On a transformed log-law plot, no effect can be seen which could not be accounted for by the general experimental scatter.

There is still another group of experiments which it would certainly be appropriate to discuss in this section - that is, boundary layers downstream of a shock interaction. Since hardly any fully documented shock-boundary-layer interaction experiments were available when we began the data compilation (AGARDograph 223), this type of experiment was excluded. This shortcoming may be remedied, however, in a further volume and a discussion must be postponed at present.

Though Morkovin (1960) had already warned that in high speed flow "the approach to a typical equilibrium or ideal turbulent boundary layer state might be rather slow" the effects of upstream pressure gradient and/or wall temperature changes on the downstream boundary layer were "absorbed" rather slowly by the scientific community. Rotta (1965) pointed out differences between "zero-pressure gradient" temperature profiles on flat plates and on nozzle walls, a result which we hope to have confirmed by our discussion of a sufficiently large number of experiments in sections 2.5.6 and 5.1. Bushnell et al. (1969) and Bushnell & Beckwith (1969) have shown by a nonsimilar finite difference calculation that for the nozzle flow which they investigated the temperature-velocity relationship changes from a quadratic behaviour in the pressure gradient region to a linear one far downstream in the zero-pressure gradient region.*) The same authors reported that profile measurements along a straight section downstream of the nozzle exit of a Mach 6 flow indicate that a distance of the order of 60 boundary layer thicknesses may be necessary before the flow begins to revert toward a linear temperature-velocity variation. These latter measurements are probably those by Jones & Feller (CAT 7002) which were made in a cylindrical test section with a ratio of boundary layer thickness δ to radius R_z up to 0.7, so that the effect of transverse curvature may well be substantial. The data is fairly rough, and showed much scatter. Although skin friction measurements were added in a later experiment (Srokowski et al. 1976) we do not think the data reliable enough to discuss them in detail (see also editors' comments for CAT 7002 in AGARDograph 223).

There exist two interesting investigations where the upstream conditions were varied: those by Feller (1973) and Gates (1973) neither of which is documented in detail though Gates (CAT 7301) gave at least tabulated data for velocity and temperature. Feller investigated four cases at nearly the same stagnation and free-stream conditions, i.e. about the same pressure gradient history upstream of the survey station (2.39 m downstream of the throat). The four cases were: (i) settling chamber and throat insulated; (ii) settling chamber unheated, throat heated to about air stagnation temperature; (iii) settling chamber heated to air stagnation temperature, throat unheated; (iv) both settling chamber and throat heated above air stagnation temperature. Cases (i) and (iv) were already presented by Beckwith et al. (1971) and present the two extremes, (i) following the quadratic curve below $(\bar{u}/u_\delta) = 0.85$ and (iv) lying almost half way between the linear and quadratic relation for the Crocco temperature. Cases (ii) and (iii) lie between (i) and (iv). Section 2.5.6 should have shown how difficult it can be to interpret data which are plotted as Crocco temperature versus $\bar{u}/u_\delta$ but we do agree with Feller (1973) that differences between the data are due to the effects of the different upstream wall temperature distributions and that "the important factor may be some integral of the convective heat transfer from the gas to the wall in the upstream region" (see also Sturek 1971).

The experiments performed by Gates (CAT 7301) constitute another even more extensive attempt to identify the influence of pressure and temperature history effects (Fig. 4.5.3). A flat plate with a leading edge section

*) Beckwith et al. (1971) report that in the Langley M = 19 tunnel (CAT 7105) the normalized total temperatures follow a quadratic curve in the outer region and a linear relation in the inner region of the boundary layer.

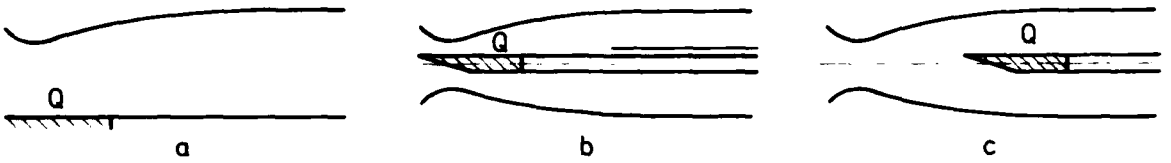

Fig. 4.5.3 Flow configurations. Gates (1973).

(a half-wedge of 10^0 included angle) which could be cooled was fixed along the tunnel centre line in that part of the test section where the pressure gradient was zero (configuration (c), series 09 and 10). The temperature distribution on the wall which provided the temperature upstream history was designed such that the wall temperature fell from 283 K at the leading edge to 91 K at X = 0.427 m, rose to 296 K at X = 1.45 m and remained constant up to 3.28 m (velocity and temperature profiles series 10). In the case which was used for comparison the wall temperature was nearly adiabatic with slight heat transfer to or from the plate (profile series 09). Since the pressure distribution was identical in both experiments any differences between the cooled and uncooled leading edge cases must therefore be ascribed to the temperature history alone. It is, however, extremely unfortunate that no skin friction measurements were provided so that upstream effects on the skin friction at the measuring stations could not be observed. A comparison between the velocity profiles and the log-law - where τ_w was calculated according to Fernholz (1971) - does not show differences between the two groups of velocity profiles (Fig. 4.5.4). Leaving aside the possible uncertainty in the

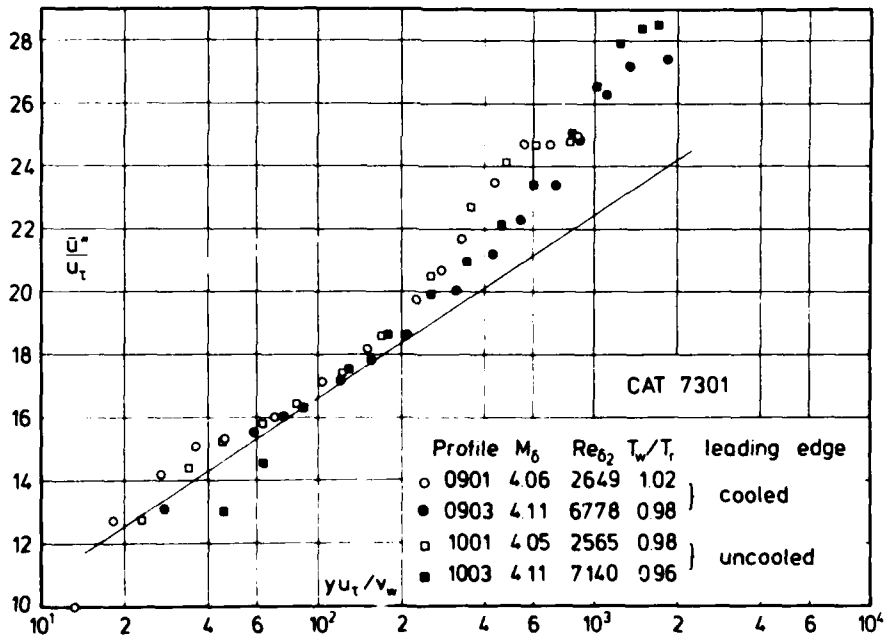

Fig. 4.5.4 Law of the wall for a compressible boundary layer (upstream temperature history, zero pressure gradient, defined origin). Gates (1973). c_f from Fernholz (1971).

determination of the skin friction which could of course change the picture, no differences between the velocity profiles can be observed which go beyond the normal scatter. As so often in NOL measurements the wake strength is larger (profiles 0903 and 1003) than in comparable cases (cf. section 3.3.3). The equivalent temperature profiles are shown in Fig. (2.5.6) and do not show upstream effects either.

An obvious gross effect of upstream heating as reported by Gates is to modify the downstream adiabatic wall temperature. For example, in the absence of any leading edge cooling the "experimental recovery factor" was about 0.88. The corresponding value with a cooled leading edge was 0.78 at the first measuring station (X = 0.914 m) relaxing to 0.86 at the most downstream station (X = 2.743 m). Similar effects were reported by Voisinet & Lee (CAT 7202).

In configuration (b) the test plate in the tunnel was extended upstream by a plate of similar construction where the leading edge was formed by a half wedge of 19^0 included angle and was 153 mm upstream of the throat (X = 0). Again the leading edge section could be cooled by liquid nitrogen. In this experiment the wall temperature fell from 277 K at X = -0.08 m to 251 K at X = -0.015 m and rose to the adiabatic wall temperature 299 K at X = 0.305 m (profile series 08). In the second experiment on this plate the wall temperature fell from 321 K at X = 0.061 m to 298 K at X = 1.14 m remaining constant from thereon (series 07). Some velocity profiles characteristic of these cases are plotted in Fig. (4.5.5). The measurements lie slightly

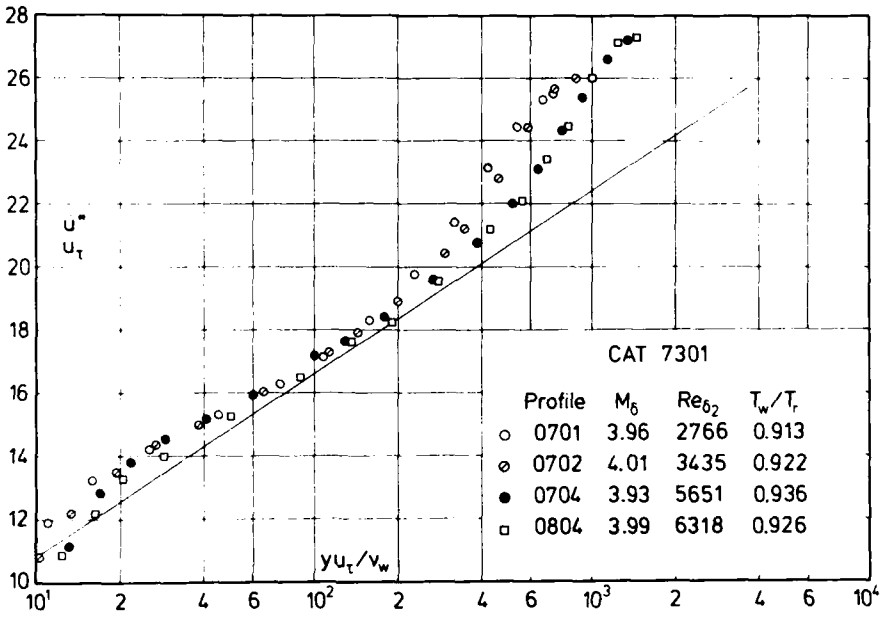

Fig. 4.5.5 Law of the wall for a compressible boundary layer with upstream temperature history (isothermal wall, zero pressure gradient, defined origin). Gates (1973).

above the log-law but they are so consistent in themselves that it is impossible to discern upstream-history effects. c_f was determined in the same way as for series 09 and 10. It is interesting to note that the severe upstream pressure history in this case does not show at all on the log-law plot.

The equivalent temperature profiles are shown in Fig. (4.5.6) and agreement with the prediction is good both for the static and for the total temperature profiles. However, attention should be drawn to the data extrapolated in the inner region by Gates himself. It is a pity that this discussion must necessarily be inconclusive because no skin friction information was provided for an investigation on this large scale.

Before we close this discussion of measurements where the boundary layer had deliberately been subjected to upstream history effects we wish to draw attention to two other large projects. Both investigations were performed in watercooled conical supersonic nozzles (Boldman et al. CAT 6901 and Back et al. CAT 7207) and had apparently clearly defined practical objectives. Although their authors provide a large amount of data, it is not sufficient to describe the upstream history effects on the downstream boundary layer, especially as no reliable skin friction data were available. The experiments were included as entries in AGARDograph 223 principally as a challenge for calculation methods.

This discussion of upstream history effects in supersonic boundary layers is not very satisfactory. This may partly be due to the fact that the "systematic" investigations performed so far do not give sufficient information or because the upstream effects were too weak, partly because these effects are hidden - and therefore not enough magnified - in experiments which had other objectives such as that of Lewis et al.(1972) (cf. Fig. 5.5.1.1 and 5.1.2) and especially those carried out in boundary layers with favourable pressure gradients (see section 5.2). In these latter cases "upstream effects" were, however, often confused with

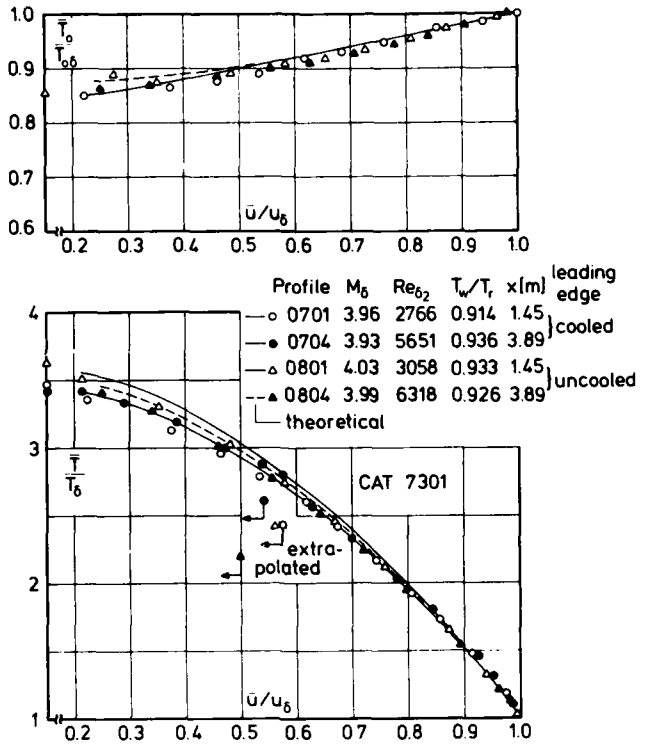

Fig. 4.5.6 Comparison between measured and theoretical temperature profiles in a boundary layer (upstream temperature history, zero pressure gradient, origin defined). Gates (1973).

combined pressure gradient and cooling effects on the temperature profiles. Deviations, for example, between measured temperatures and predictions according to the equations of table (2.5.1) probably occur simply because the validity range of these equations was exceeded (see section 5.2).

Since there exist hardly any reliable calculation methods for compressible turbulent boundary layers which can take account of the variety of upstream histories discussed above, we briefly resort to laminar boundary layer calculations to throw some light on upstream effects in a controlled manner. It is well understood that transport phenomena are radically different in laminar and turbulent flows but laminar flow calculations may at least serve as a guideline for the engineer until we have good experimental evidence for turbulent boundary layers.

Back (1970) found that favourable pressure gradient and wall cooling strongly influenced both temperature and velocity profiles over a wide range of flow velocities; this was noted for similarity solutions of the equations for laminar boundary layers. Since similarity solutions can only give a crude approximation for physically realistic compressible laminar boundary layers, Moser (1979) used a pseudo Tschebyscheff-spectral-method to calculate the development of a compressible laminar boundary layer with a wall-temperature distribution decreasing monotonically to a constant value. The numerical results are compared with the temperature-velocity relationship (eqn. 2.5.37a) using a recovery factor r = 0.85 (Walz 1966) and the velocity distribution calculated by the numerical method. Fig. 4.5.7 shows that good agreement is achieved for profiles (3.2.A) and (3.2.D), the former having hardly been influenced by the wall-temperature gradient and the latter having recovered from such a gradient. Larger discrepancies occur for profiles (3.2.B) and (3.2.C). Here eqn. (2.5.37a) does not hold since the wall is not isothermal. It is astonishing, however, that the discrepancies do not exceed 20 % in the outer region of the boundary layer and that all temperature profiles

agree in the near wall region. Note that the recovery factor as calculated by Moser was 0.787, i.e. smaller than that given above by Walz. In Fig.(4.5.7) we show therefore temperature profiles calculated according to eqn. (2.5.37a) with r = 0.787 (broken line). In this case the discrepancies are larger. Both Moser and Gates found a variable recovery factor, i.e. a function of upstream history and Mach number, but we do not think that the evidence provided for such a variation is sufficient yet.

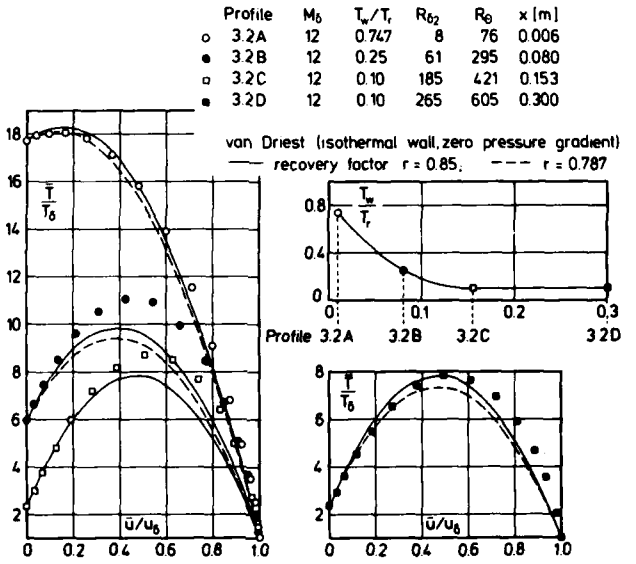

Fig. 4.5.7 Comparison between numerically calculated temperature profiles and *van Driest's analytical solution (laminar boundary layer, zero* pressure gradient, variable wall temperature, defined origin).

Further investigations using various other wall-temperature distributions are necessary before final conclusions can be drawn about the influence of variable wall temperature in the upstream region.

Fig. 4.2.17 Law of the wall for a compressible boundary layer (adiabatic wall, zero pressure gradient). Thomke (1969).

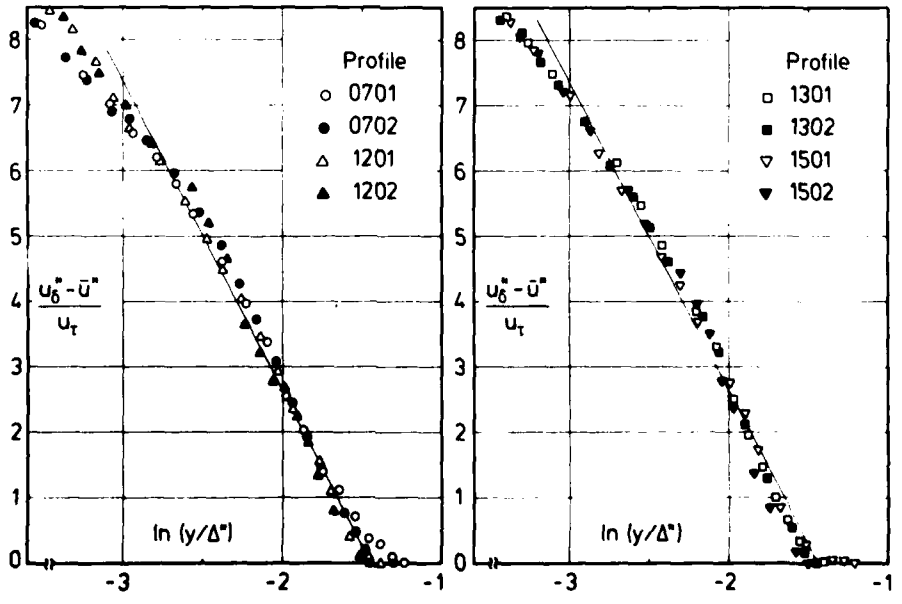

Fig. 4.2.18 Outer law for a compressible boundary layer (adiabatic wall, zero

4.6 Wall roughness

Since skin friction drag contributes a large proportion of the total drag of aerodynamic bodies cruising at supersonic speeds, the influence of surface roughness on the skin friction of a compressible turbulent boundary layer must be known. The same holds for wall heat transfer which is larger for a rough surface than for one which is aerodynamically smooth. As well as effects on the data, changes of the turbulence structure due to wall roughness are to be expected. Unfortunately there are so many possible types of roughness that even for incompressible boundary layers only a few have been investigated (for references see Schlichting 1965 and Fernholz in Bradshaw 1976). It is necessary to distinguish between two- and three-dimensional roughnesses. V-grooves and ridges such as square bars (cf. Perry et al. 1969, Antonia & Luxton 1971 for incompressible flow, and Kubota & Berg 1977 for compressible flow) are typical of the first type and sand grain roughness of the second. Such uniformly distributed roughnesses may again be divided into "closely spaced", of which sand grain roughness is typical or "widely spaced" which may in the limit be regarded as a set of more or less independent protuberances. In the first case, a single roughness scale may be sufficient to relate different sizes of sand grain roughness, for example, whereas in the second both roughness height and spacing must be taken into account. Such protuberances, single circular holes and various forward and backward facing steps were investigated as to their effect on a supersonic boundary layer by Gaudet & Winter (1973). Developments in re-entry technology and supersonic flight vehicle design have suggested the importance of two further kinds of surface roughness. One is the phenomenon of cross-hatching on heat-shield materials (e.g. Langanelli & Nestler 1969) and the other is the pattern of surface ridges or grooves with longer scale surface undulations created during the fabrication process of fiberglass wound material (Reda 1974 and Reda et al. 1975). This latter type of roughness needs, for a physical model, one or more roughness scales and at least one short and one long wavelength scale.
In contrast to the extent and complexity of the problems there is a dearth of available data, as can be seen from Table 4.6.1. Only three of the investigations listed there contain tabulated data which could be used for the data compilation (CAT 5502, 5804 and 6506), two of which deal with sand-grain roughness and one with a two-dimensional V-groove type roughness. Since Fenter & Lyons (CAT 5804) did not measure skin friction their data could not be used for a comparison with the inner or outer law of a turbulent boundary layer.

Closely spaced three-dimensional roughness

It is not astonishing to find that it is the boundary layer over the sand grain roughness covering a surface uniformly which has been investigated most thoroughly, both in low and high speed flow. Prandtl (1932) and Schlichting (1936) showed that the result of experiments by Nikuradse (1933) in which both the skin friction and the development of mean velocity profiles in a sand-roughened pipe flow had been measured also hold for incompressible boundary layers (confirmed by Hama 1954). If the roughness length scale k_r (related to the mean height of the sand grains) is made dimensionless by ν/u_τ one can distinguish between three regimes in incompressible flow. The argument holds for nominally zero pressure gradient flow, for if the shear stress in the wall region changes with y ($\partial\tau/\partial y \neq 0$) a parameter $(k_r/\tau_w)\ \partial\tau/\partial y$ must appear but its effects are unknown. According to the value of a roughness Reynolds number $k_r u_\tau/\nu_w$ one can distinguish according to Clauser (1956):

(1) Aerodynamically smooth walls ($0 \leq k_r u_\tau/\nu \leq 5$).
The roughness elements are submerged in the viscous sublayer and do not affect the boundary layer significantly. The upper limit establishes the critical permissible roughness of a surface below which the skin friction drag is the same as that for a smooth surface.

(2) An intermediate condition (often referred to as transient or transitional roughness) ($5 \leq k_r u_\tau/\nu \leq 70$). The velocity profile is affected by the roughness of the wall, and this effect is taken into account by a function f which is substituted into the law of the wall instead of the constant C in eqn. (3.2.3) where

$$f\ (k_r u_\tau/\nu) = C - \Delta\ (\tilde{u}_k/u_\tau). \qquad (4.6.1)$$

Eqn. (4.6.1) is sometimes called the Clauser form of the roughness function and is universal for the conventional sand grain roughness in pipe, duct and zero-pressure boundary layer flows.

Table 4.6.1

CAT	Author	M_δ	T_w/T_r	$Re_{\delta_2} \times 10^{-3}$	Type of roughness	k-range [mm]	P_o	T_o	c_f	Nx
	Wade (1955)	2.48	-	-	V-groove	-	-	-	-	-
(5502)	Shutts & Fenter (1955)	2.0	1	7 - 26	Sand	0.109- 0.162	CPP	iso	FEB	5
(5804)	Fenter & Lyons (1958a)	2.2 - 2.7	1	4 - 29	Sand	0.013 - 0.185	CPP	iso	-	3
	Goddard (1959)	0.7 - 4.5	1	unknown	Sand	0.0203- 0.333	FPP	iso	Drag Balance C_F	1
(6506)	Young (1965)	5	0.54-1	1.7-2.5	V-groove	0.0635- 0.381	CPP	van Driest	FEB	1
	Reda (1974) and Reda et al. (1975)	2.9	1	$Re_\Theta \cdot 10^{-3}$ 12 - 38	V-groove superimposed on wall waviness. Sand grain	-	FPP	ECP	FEB	1
	Kubota & Berg (1977)	6	≈1		Transverse square bar	0.31 - 1.25	CPP HW	ECP	FEB	10
	Voisinet (1978,1979)	2.9	1	$Re_\Theta \cdot 10^{-3}$ 2.5 - 39	Wire-mesh on surface	0.1 - 1.0	-	(?)	FEB	2

$\Delta(\bar{u}_k/u_\tau)$ in eqn. (4.6.1), the roughness induced "shift" of the outer velocity profile can be expressed according to Hama (1954) for natural roughnesses such as wrought or cast iron by

$$\Delta(\bar{u}_k/u_\tau) = (1/K)\ \ln\ [(k_r u_\tau/\nu) + 3.30] - 2.92. \qquad (4.6.2)$$

It is zero for smooth walls and depends only on the roughness Reynolds number.
The logarithmic law then reads

$$\bar{u}/u_\tau = (1/K)\ \ln\ (u_\tau y/\nu) + f\ (k_r u_\tau/\nu). \qquad (4.6.3)$$

(3) Fully developed roughness ($70 \leq k_r u_\tau/\nu$).

The velocity distribution in the log-law region is now independent of the viscosity because the characteristic Reynolds number is large. The logarithmic law of the wall simplifies to

$$\bar{u}/u_\tau = (1/K)\ \ln\ (y/k) + C_k \qquad (4.6.4)$$

where Nikuradse (1933) found C_k to be 8.5. Another form of eqn. (4.6.4) - often adopted for velocity profiles in atmospheric boundary layers - is given as

$$\bar{u}/u_\tau = (1/K)\ \ln\ (y/z_o) \qquad (4.6.5)$$

z_o being chosen so as to absorb the constant C_k. The semilogarithmic relationship between $\bar{u}/u_\tau$ and (y/k) holds only for the region close to the wall. If the reference point from which y is to be measured is not chosen correctly the region that should be linear on a semi-log plot becomes curved, and this may be used to find the origin of y (Schubauer & Tchen 1959).
Similarly, for roughness distributions other than the conventionally agreed "sand grain roughness" there may be difficulty in choosing the characteristic height k. In effect, for any repeatable roughness form, the value of k must be found experimentally as a proportion of a definable physical roughness dimension, so giving an "equivalent sand grain roughness height" k_s.
The knowledge gained in incompressible boundary layers along walls with uniformly distributed sand-grain roughness can be transferred to compressible boundary layers if the following modifications are taken into account (Goddard 1959):

(a) The kinematic viscosity ν in the roughness Reynolds number and in equations (4.6.1 to 4.6.3) must be taken as the wall value ν_w.

(b) The mean velocity $\bar{u}$ must be transformed to $\bar{u}^{++}$ according to van Driest (1951), i.e. eqn. (3.3.13.a) or as we shall do here according to eqn. (3.3.10).

(c) The upper limit for the roughness Reynolds number should be raised from 5 to 10 for an aerodynamically smooth wall.

These modifications were seen to be necessary if a velocity profile in a compressible turbulent boundary were to agree with its incompressible equivalent both in the log-law and the outer law form (see sections 3 and 4).

Goddard found for zero-pressure gradient flow along an adiabatic wall that the upper limit for an aerodynamically smooth surface was independent of Mach number for a Mach number range $0.70 \leq M\delta \leq 4.50$. The ratio of the skin friction coefficients c_{f_k}/c_{f_o} measured on a rough and a smooth wall and plotted against $k_r u_\tau/\nu_w$ remained unity up to a value of 10 of the roughness Reynolds number and followed a quadratic relationship - as given by Nikuradse for the incompressible case - from there on (Goddard Fig. 27). This result was confirmed by Reda (1974), and we present his comparison with published data in Fig. (4.6.1).

Bradshaw (1977) has observed that for large enough values of Mach and Reynolds number the flow near the top of the roughness elements must exceed M = 1 and explicit dependence on the Mach number is then to be expected.

The only tabulated data measured in a boundary layer over sand grain roughness (Shutts & Fenter 1955) are shown in Fig. (4.6.2). It is seen that the effect of roughness is to displace the velocity profile curve downward to a position essentially parallel to its original position (as had already been remarked by Nikuradse 1933). As can be seen from several evaluations of boundary layer velocity profiles over rough walls with various kinds of roughness this shift of the velocity profile $\Delta(\bar{u}_k^*/u_\tau)$ is a function only of the roughness Reynolds number (ku_τ/ν_w) (Goddard Fig. 40, Reda Fig. 19 and Kubota & Berg Fig. 18).
Kubota & Berg (1977) give a semi-empirical relationship between the velocity shift - using the velocity ratio $\Delta(\bar{u}_k/u_\tau)$ of eqn. (4.6.1):

$$\Delta\left(\frac{\bar{u}_k}{u_\tau}\right) = 3.28 - 5.70 \ln k_s^+ + 2.83 (\ln k_s^+)^2 - 0.29 (\ln k_s)^3 \qquad (4.6.6)$$

which holds for "several roughness configurations (sand grain, V-groove square bar) and Mach numbers ($0 \leq M_\delta \leq 6$)" if the roughness height k_s is chosen as the equivalent experimentally determined sand grain roughness.

Whereas eqn. (4.6.6) holds for transient and fully rough regimes a simple relationship can be derived for the fully rough regime alone. If the velocity $\bar{u}$ in eqn. (4.6.4) is substituted by $\bar{u}^*$ and if one then subtracts eqn. (4.6.4)* so obtained from eqn. (3.3.9), which holds for flow along a smooth wall, one obtains

$$\frac{\bar{u}_s^* - \bar{u}_r^*}{u_\tau} = \Delta\left(\frac{\bar{u}_k}{u_\tau}\right) = \frac{1}{K} \ln \frac{u_\tau k}{\nu_w} + C^{**} \qquad (4.6.7)$$

If this relationship is to be used for flows over walls other than covered with sand grain roughness then k must be substituted by the equivalent sand grain roughness k_s. The latter is determined from the shift of the velocity profile over the unknown roughness which is then inserted into eqns. (4.6.6) or (4.6.7). C** was found by Nikuradse to be - 3.

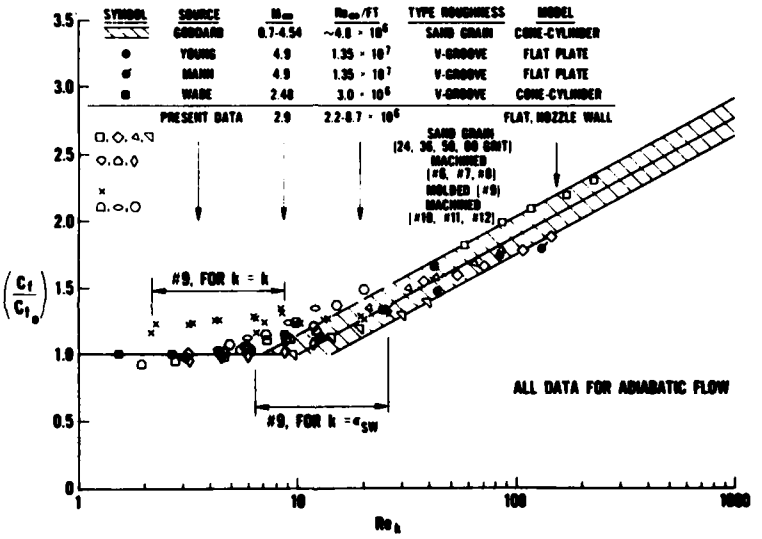

Fig. 4.6.1 Smooth-to-rough wall skin friction coefficient ratio v. roughness Reynolds number; a comparison with published data. Taken from Reda (1974)

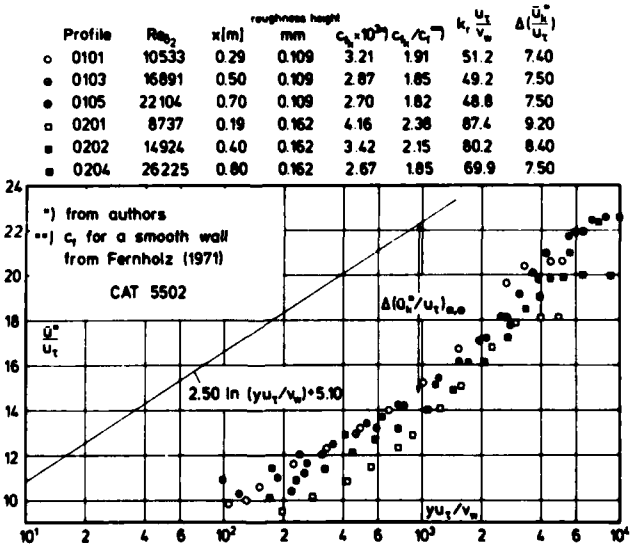

Fig. 4.6.2 Law of the wall for a compressible boundary layer (adiabatic wall, zero pressure gradient, $M_\delta = 2$, defined origin, sand-grain roughness). Shutts & Fenter (1955).

Since only a few tabulated data were available for a comparison with the above semi-empirical relationships, we have used Reda's (1974) figure 19 as our Fig. (4.6.3).

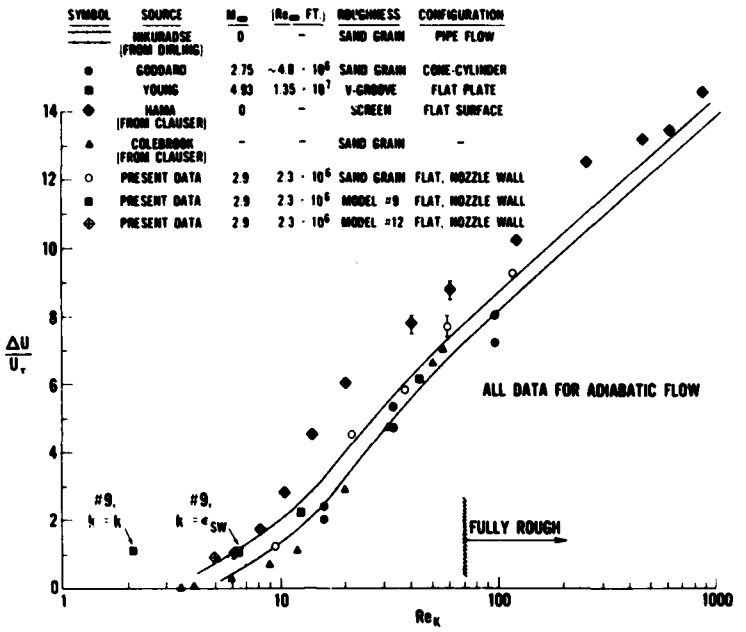

Fig. 4.6.3 Roughness induced law-of-the-wall velocity shift v. roughness Reynolds number; a comparison with published data. Taken from Reda (1974).

Fig. (4.6.4) shows the Shutts & Fenter data of Fig. (4.6.2) plotted versus the abscissa y/k. Neither these data nor those by Young (1965) agree satisfactorily with eqn. (4.6.4) if the transformed velocity $\tilde{u}^*$ is used instead of $\tilde{u}$. This may partly be due to the fact that the flow is still within the transient regime, partly that the skin friction measurements have larger errors than for boundary layers along a smooth wall. This contradicts the results found by Goddard (1959, Fig. 38).

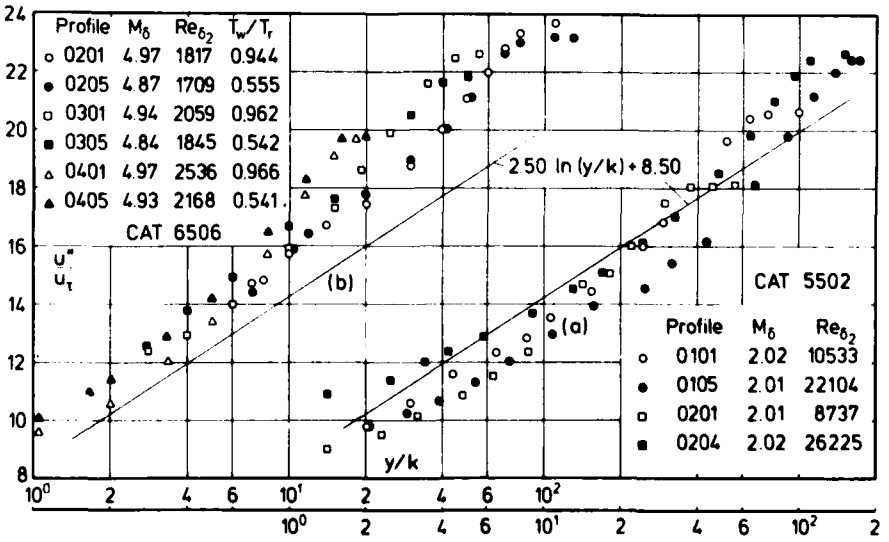

Fig. 4.6.4 Law of the wall for compressible turbulent boundary layers over rough walls (adiabatic and isothermal wall, zero pressure gradient, defined origin). Shutts & Fenter (1955) and Young (1965).

As is well known from subsonic flow measurements there is no influence of the wall roughness on the outer law as can be seen from Fig.(4.6.5).

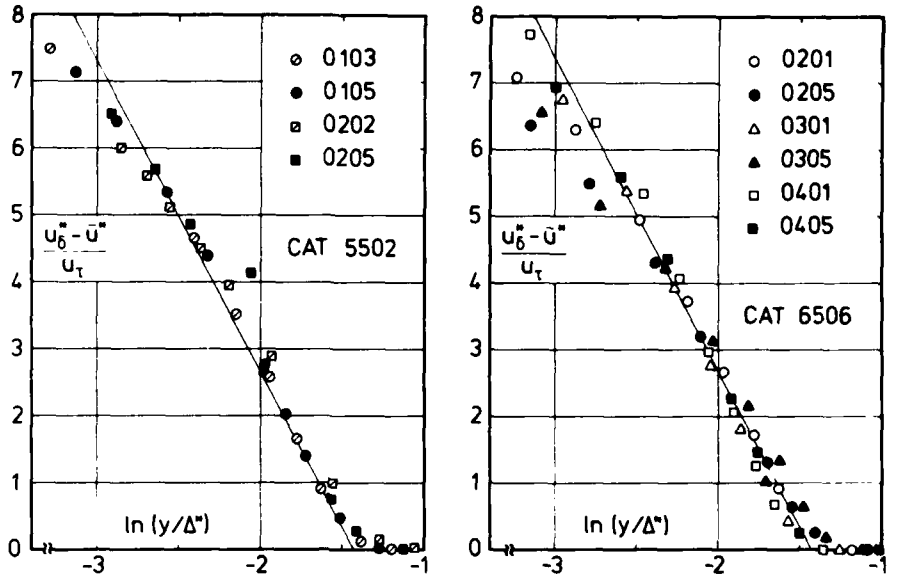

Fig. 4.6.5 Outer law for compressible turbulent boundary layers along rough walls (adiabatic and isothermal wall, zero pressure gradient, defined origin). Shutts & Fenter (1955); Young (1965).

Fenter & Lyons (CAT 5804) describe a further systematic DRL attempt to investigate the effects of distributed roughness. In these tests the boundary layer was formed on a flat plate, with an initial smooth section on which was mounted a trip. Profile measurements were then made at the downstream end of a variety of rough inserts. The absence of any shear stress measurements unfortunately reduces the value of the data greatly. (They also include one series of measurements with uniform roughness where the entire plate surface was coated with spherical beads of 0.105 mm diameter).

Two-dimensional roughness

An obvious choice for a two-dimensional roughness is the transverse V-groove or thread roughness. The chief advantage of this roughness lies in its application to bodies of revolution and several investigations have been made using such surfaces (Wade 1955, James 1959, Fenter 1960). Also, there is evidence that this type of roughness compares closely with sand grain roughness as mentioned above (Young 1965). The only experimental investigation for which tabulated data were provided in sufficient detail for a comparison with smooth wall data is that of Young (CAT 6506) who did not measure TO profiles but used the van Driest velocity transformation. The roughness pattern had a regular 90° saw tooth (V-groove) section aligned across the plate, with wave lengths of 0.127, 0.254 or 0.762 mm, and corresponding peak to trough heights of one half the wavelength. Young's measurements are distinguished in so far as both skin friction (the floating element balance was duly cooled) and heat transfer were measured and as smooth wall data were available for comparison. The latter agree very well with the logarithmic law (Fig. 4.3.1) and with the outer law (Fig. 4.3.2), irrespective of the heat transfer rate. Agreement between the rough wall data and the outer law is good as can be seen from Fig. (4.6.5.b).

The skin friction measurements show that for the smallest roughness height the increase above the smooth plate results are small. This explains the small deviation of the velocity profiles from the log-law in Fig. (4.6.6) if one takes into account additionally that measuring errors for the skin friction are likely to increase if wall roughness and heat transfer are involved. From these results one may also deduce that the smallest surface roughness used in this experiment was below the limit for the critical roughness Reynolds number. In this case the result is not affected by heat transfer - $u_\tau\, k/\nu_w$ rises from 5.2 for the

adiabatic wall to 6,6 for the cooled wall.

	Profile	M_δ	T_w/T_r	Re_{δ_2}	roughness height mm	$k\frac{u_\tau}{\nu_w}$	$\Delta(\frac{u_k}{u_\tau})$
○	0201	4.97	0.944	1817	0.0635	5.2	-
●	0205	4.87	0.555	1907	0.0635	6.6	-
△	0301	4.94	0.962	2059	0.127	11.5	1.50
▲	0305	4.84	0.542	1845	0.127	14.9	1.50
□	0401	4.97	0.967	2535	0.381	38.8	4.90
■	0405	4.93	0.541	2168	0.381	45.6	4.90

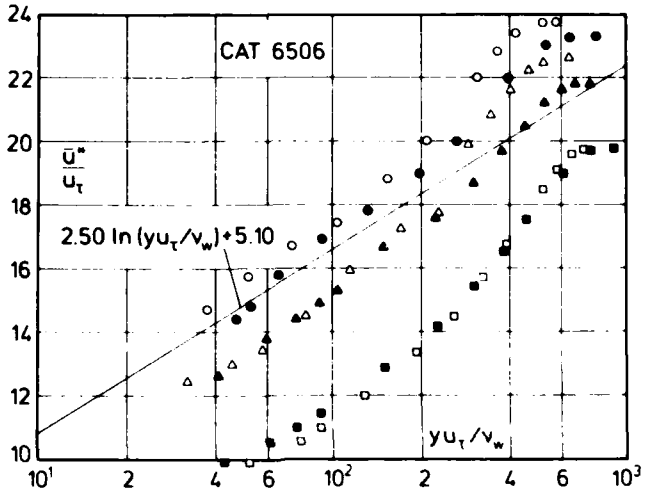

Fig. 4.6.6 Law of the wall for a compressible turbulent boundary layer (isothermal wall, zero pressure gradient, defined origin, V-groove roughness). Young (1965).

As for the larger roughness heights the expected downward shift in the velocity profiles occurs but there is hardly any difference between the cases with and without wall cooling. This means that the transformation accounts for the heat transfer as for smooth wall boundary layers described in section 4.3.

In order to complete the discussion we have also plotted some of Young's velocity profiles versus y/k (Fig. 4.6.4.b). Here we find the opposite trend to that of the Shutts & Fenter data as the measurements now lie above the Nikuradse relationship (eqn. 4.6.4), again contradicting conclusions of Goddard (1959).Since both heat transfer and skin friction were measured in this experiment we would like to quote the conclusions drawn by Young:

"With increasing roughness, heat transfer to the rough surface is increased, as is the skin friction, but to a different degree which depends on the roughness regime of the flow.
The Reynolds analogy factor, which is relatively insensitive to changes in the flow parameters, appears to remain valid as long as the roughness height is less than twice the laminar sublayer thickness. For roughness in excess of this value, the analogy factor increases directly with the roughness height until the fully rough regime is reached, after which it is probable that it increases approximately with c_f, that is, it appears that c_h may reach a relatively constant value for large roughness heights".

Another two-dimensional roughness configuration which has been studied extensively in low speed flow (e.g. Perry et al. 1969, Antonia & Luxton 1971) is the square bar type which is characterized by a height and a wavelength. If the wavelength to height ratio λ remains below a certain level quasi-stable vortices are found in the cavity in between. This type of roughness is called "d-type" (e.g. Wood & Antonia 1975). For a d-type roughness in subsonic flow little direct interaction seems to occur between the roughness and the

mean flow in the boundary layer, so that there are features similar to those of a smooth-wall boundary layer. Kubota & Berg (1977) present measurements in a compressible boundary layer over a d-type roughness ($\lambda \approx 4$) where the crests of the roughness elements were aligned with the smooth surface upstream. Roughness heights of 0.318, 0.635 and 1.27 mm were used corresponding - according to the authors - with equivalent roughness Reynolds numbers of 18, 40 and 85. Both mean flow and fluctuating flow data were acquired for several smooth-to-rough surface step changes and a single rough-to-smooth surface step change.
Since no tabulated data were available from the authors of the report we can only quote three of their conclusions:

(1) "The establishment of new equilibrium mean and fluctuating flow profiles downstream of a step change in surface roughness is accomplished in nearly the same distance (in term of boundary layer thicknesses) as in the incompressible case. The step change smooth-to-rough configuration boundary layer attains new mean flow selfsimilar profiles over some 10 δ or 20 δ_1 downstream of the step, while the fluctuation profiles reach this state some 14-16 δ or 28-32 δ_1 downstream of the step. These distances are independent of roughness height for roughnesses in the transitionally rough regime - $(k_s\ u_\tau/\nu_w) < 70$.
The step roughness change rough-to-smooth configuration produced a somewhat slower adjustment of the boundary layer some 14 δ or 28 δ_1 for mean flow equilibrium and some 20-25 δ or 40-50 δ_1 for fluctuation equilibrium.

(2) The hypersonic smooth and rough wall equilibrium profile velocity data, subsequent to a modified Van Driest transformation - modified in the sense that the $\bar{T}/T_\delta = f\ (\bar{u}/u_\delta)$ relationship was substituted by a least squares quadratic curve fit to the measured data - to "equivalent incompressible" form are well correlated by the incompressible composite law of the wall.

(3) The investigation of the rough-to-smooth step change configuration revealed the existence of very significant pressure and temperature history effects throughout the boundary layer. . . The presence of the rough surface on the nozzle wall within the expansion region was sufficient to alter the history effects but was not able to eliminate them. . . . Considerably more research is needed in this area to delineate the extent of these history effects and investigate the possibility of destroying them."

For further references on rough wall boundary layer flows the reader is referred to Fernholz (see Bradshaw "Turbulence" 1976), to Dvorak (1969) for a calculation method for incompressible flow and to Chen (1972) for a calculation method for compressible boundary layers.

5. INTERPRETATION OF MEAN FLOW DATA FOR PRESSURE GRADIENT CASES

5.1 Causes and broad effects

In section 4 it was shown that the general behaviour of a constant pressure boundary layer was, when considered as a transformed profile in relation to the wall and wake law , very similar to that of a low speed boundary layer. Departures from eqns.(3.3.9) and (3.3.17) were not generally large, and when observed could usually be ascribed to a known, if often unquantifiable, secondary factor (§§ 3.3.4, 4.2.3) or to experimental uncertainty, particularly in the determination of skin friction. This means that the van Driest transformation can cope very well with mean density gradients $\partial\bar{\rho}/\partial y$ perpendicular to a wall which may be isothermal or adiabatic if at least the pressure gradient $\partial\bar{p}/\partial x$ is zero.
It therefore seems sensible to continue a discussion of mean flow profiles on the same basis though the transformation should now take into account $\partial\bar{\rho}/\partial x$ besides $\partial\bar{\rho}/\partial y$. From subsonic experience we would expect the "constant pressure" wall law (eqn. 3.3.9) to be observed over a wide range of pressure gradients - see the figures in sections 5.2 and 5.3 - so long as the flow does not approach separation, in adverse pressure gradients, or moderate favourable pressure gradients even if far from relaminarization. We would also expect the wake function to be increased in an adverse pressure gradient and vice versa.

There are, however, distinctive features of the compressible flow. At supersonic Mach numbers the pressure changes are comparable with the total pressure, and as a result of the hyperbolic nature of the inviscid flow field, these pressure changes may be concentrated into relatively small regions. The dynamic pressure may well become very large as compared to the static pressure, so that quite small changes in flow direction may require relatively large pressure differences normal to the flow. This possibility ($p << 1/2\ \bar{\rho}\ U^2$) also leads to the possibility of turbulent Reynolds stresses in a boundary layer becoming comparable with the static pressure (Finley 1977). Finally the large proportional changes in pressure, and consequently density, lead to some features of boundary layer behaviour which appear to run counter to low speed experience - for instance a boundary layer in a strong adverse pressure gradient becomes thinner and exerts an increased shear stress on the wall (Sturek & Danberg, CAT 7101, Lewis et al. CAT 7201, Rose 1973, CAT 7306S and others). Such an effect results from the difference in the flow/unit area - velocity relationship between sub- and supersonic flow. The general tendency is for a stream tube to decrease in cross-sectional area as it slows down rather than to increase. Consequently, in an adverse pressure gradient, a boundary layer will decrease in thickness, at least until the greater part of the flow becomes subsonic, and as a result the vorticity and turbulent intensity tend to increase. The general level of Reynolds stresses

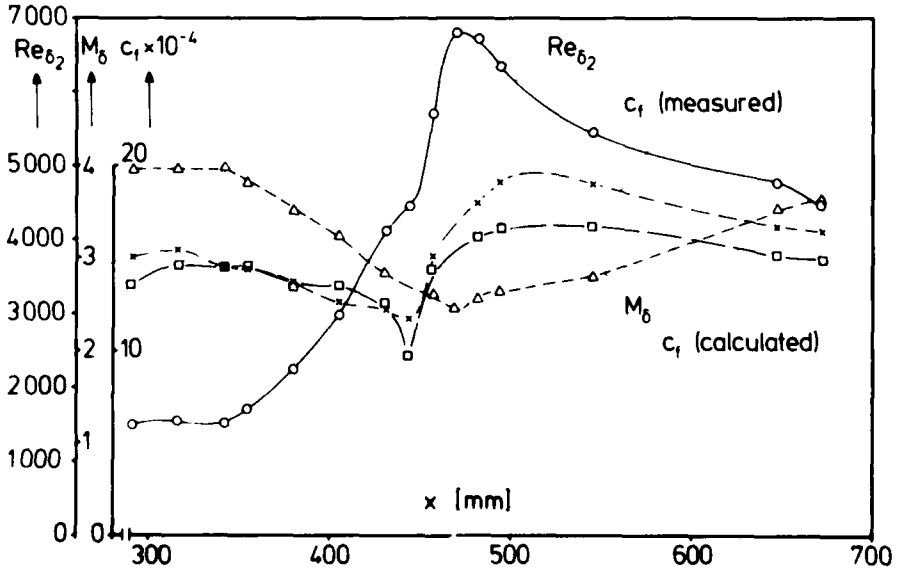

Fig. 5.1.1 Distribution of skin friction, Mach and Reynolds number in a compressible turbulent boundary layer with variable pressure gradient. Lewis et al.(1972).

therefore rises, leading to an increase in wall shear. This effect can be masked by dimensionless presentation, as the scaling quantity $\rho_\delta u_\delta^2/2$ for the skin friction coefficient also increases as the flow is decelerated. The distribution of skin friction, Mach number, and Reynolds number Re_{δ_2} in a boundary layer with varied streamwise pressure gradient (Lewis et al. 1972) is shown in Fig.(5.1.1), and the effects described above can be seen distinctly. The pressure gradients in this experiment are not severe, however, and therefore the skin friction distribution can be fairly well predicted even by a calculation method which does not hold for boundary layers with pressure gradients (Fernholz 1971).

The relevant features of the pressure fields are considered in detail in § 6 so that we here present only a brief summary. In relation to natural axes along and normal to the flow streamlines, pressure (or more strictly, normal stress) gradients along the normal can only occur as a result of streamline curvature:

$$\partial p/\partial n = -\rho u^2/R = -\gamma M^2 p/R \qquad (5.1.1)$$

where R is the radius of curvature and n and R take the same sign for concave curvature. The pressure change in a small distance such as the boundary layer thickness, δ, normal to the flow,

$$\Delta p = \delta\,(\partial p/\partial n) = \gamma M^2\ (\delta/R)\ p \qquad (5.1.2)$$

may therefore be proportionally quite large even for modest values of (δ/R) if the Mach number is high enough.

Normal pressure differences of this type, that is, associated with streamline curvature, propagate along the Mach lines of the flow and are therefore linked to the streamwise pressure gradient by

$$(\partial p/\partial n) = \mp\ \cot\mu\ (\partial p/\partial s) \qquad (5.1.3)$$

where μ is the Mach angle $\sin^{-1}(1/M)$.
The rate of change of flow direction θ is linked to the rate of change of pressure and Mach number being

$$(\partial\theta/\partial s) = \pm\ (\partial\nu/\partial s) \qquad (5.1.4)$$

where $\nu(M)$ is the Prandtl-Meyer angle. As a first estimate for the pressure variation on a curved wall, it is reasonable to replace s and n by x along the wall and y normal to it, and we refer to a flow in which the pressure gradient is associated with wall curvature as a SIMPLE WAVE FLOW. There is no rate of change of pressure along one of the families of characteristics in the free stream flow.

A flow in which equal rates of change of p, M, ν occur along both sets of characteristics has straight streamlines. In natural coordinates therefore, $\partial p/\partial n = o$. In inviscid flow, the flow along any straight wall has $\partial p/\partial n = o$, and any wave pattern will be reflected at the wall in such a way as to ensure that $\partial\theta/\partial s = o$. We refer to such a flow, with essentially straight streamlines (at least locally) as a REFLECTED WAVE FLOW. If the natural coordinates s, n are replaced by the boundary layer coordinates x, y however, an apparent normal pressure gradient will appear, as except in the trivial case of parallel flow for which $\partial p/\partial x = o$, the divergence of the streamlines (although they are straight) causes the isobar through the point (x, o) to curve away from the profile normal. For purely radial flow at a distance R_v from the vertex, the resulting apparent pressure gradient is

$$\frac{\partial p}{\partial y} = -\frac{iy}{R_v^2} \cdot \frac{\gamma M^2}{M^2-1} \cdot p \qquad (5.1.5)$$

where i is 1 for planar and 2 for conical flow, so that the pressure difference across a small distance δ, normal to the wall, is

$$\Delta p = -i\ \left(\frac{\delta}{R_v}\right)^2\ \frac{\gamma M^2}{M^2-1}\ p \qquad (5.1.6)$$

This can be seen to be fairly small for M not of order 1, $\Delta p/p$ being of order $(\delta/R_v)^2$ or less than 0.01.

We therefore expect that in reflected wave flows, $\partial p/\partial y$ will be negligible. However, although the wall on which a boundary layer is growing may be straight, the concentrated nature possible for compressible wave structures allows streamlines at quite small distances from the wall to have significant curvature

(e.g. Kussoy et al. 1978, Rose 1973, Zakkay & Wang 1972), and consequently achieve the large values of $\Delta p/p$ associated with simple wave flows. We have, in AG 223, provided an indicator of the relative importance of the simple wave element in a flow in the quantity

$$SW = (\partial\theta/\partial\nu)_n \qquad (5.1.7)$$

which should in principle be evaluated along a streamline just outside the boundary layer. This has not been found as helpful as was hoped, and it has been necessary at this stage to assign arbitrary values as

SW = 1 - flows with wall curvature and simple wave structure
(Class IIB)

SW = 0 - straight wall flows with no significant concentrated disturbances
(Class IIA)

SW = 0.5 - straight wall flows in which it is believed that the pressure gradients are strong enough to cause significant streamline curvature inside the boundary layer.
(Classified with IIB)

We would also point out the extreme case represented by the "normal pressure gradient" flows studied by Thomann (CAT 6800, series 06-09). There are no profiles available for flows of this type, but they demonstrate the existence of a class for which

SW = ∞ - curved wall flows with superposed wave structures causing circular streamlines with no streamwise property gradients, but large normal gradients.
(Class IIC)

The mean flow wall heat transfer measurements of Thomann (CAT 6800) are especially interesting as he used the identical measuring equipment for a series of flows in which all possible types of pressure gradient were observed. Of particular interest is the difference of 20 % in heat transfer rate observed for two flows on a convex surface (which is therefore not likely to be strongly affected by longitudinal vortex structures) with different strengths of pure normal pressure gradient (SW = ∞), suggesting that the strength of the normal pressure gradient element must have a significant effect on the turbulence structure. This effect has no analogue in low speed flow, since it is only on very sharp corners for which the boundary layers assumptions break down that significant normal property gradients will be observed.

Reference will be made to these various effects in the consideration of mean flow profiles and wall data below.

In accounting for large discrepancies between an experimental skin friction distribution (Zwarts 1970) and the results predicted by the Bradshaw & Ferris (1971) calculation method, Bradshaw (1974) concluded "that the mean dilatational rate of strain, div $\underline{U}$, directly affects the turbulence structure to an extent much greater than expected from the terms (in say, the Reynolds-stress transport equations) that contain the extra rate of strain explicitly. The main a priori reason for believing that compression or dilatation may have large effects on the structure of turbulent shear layers was that other extra rates of strain have been found to change the Reynolds stresses by an order of magnitude more than expected from the size of the explicit extra terms in the Reynolds-stress transport equations." Bradshaw then introduced this additional effect by modifying the transport equation in his system of equations accordingly.

As is well known from experience with calculation methods for subsonic boundary layers, every calculation procedure can be made to agree with a limited number of experiments, and so it was only a question of time before other calculation methods followed suit (e.g. Horstman 1976, 1977). Once more comparisons between calculation methods and experiments, especially in adverse pressure gradients, had been performed (Rubesin et al. 1977 and Acharya et al. 1978), it was not surprising to find that other methods could describe the experiments well even without extra compression or dilatation terms. So this effect must be considered questionable unless further evidence for its existence is brought forward.

Before we continue the analysis of mean velocity and temperature measurements, the validity range of the theoretical assumptions should be stated again and attention should be drawn to the determination of the wall shear stress and the changes of the turbulence level due to pressure gradients.

As was shown in section 2.5 the temperature-velocity relations hold for boundary layers with pressure

gradients only under the condition that the wall is adiabatic. Since the temperature distribution according to eqn.(2.5.37a) is used for the deviation of the transformed velocity $\bar{u}^*$ in the logarithmic-law and in the outer law, these relations are strictly confined to flows along an adiabatic wall if a pressure gradient is present.

Any investigation of turbulent boundary layers with pressure gradients has to deal with the basic problem of how to determine the skin friction. Floating element balances which are very reliable for zero pressure gradient flows (Winter 1977) are sensitive to pressure gradients in the streamwise direction, and the Preston tube encounters problems related to the validity of its calibration curve in pressure gradient flows, besides the problems which arise from the different calibration curves as such (a good demonstration of this dilemma is given in CAT 7102) if the flow is compressible.

Most research workers seem to have forgotten that the validity of the logarithmic law becomes at least doubtful in favourable pressure gradients if we can transfer knowledge from subsonic (Patel 1965) to supersonic flow. For a further discussion of error sources the reader is referred to Rubesin et al.(1977).

Finally attention should be drawn to the increased level of turbulence in boundary layers with adverse pressure gradients (Gootzait & Childs 1976 and Acharya et al. 1978). Again it is known from measurements in subsonic turbulent boundary layers that hot-wire signals must be corrected if the turbulence level exceeds 20 % or so, a value which will be easily exceeded in boundary layers close to separation, even in incompressible flow. Correction methods are still controversial in subsonic flows, let alone in supersonic boundary layers.

If these precautions are heeded it should be possible to discuss, and even explain, some of the discrepancies which will occur when measurements in flows with pressure gradients are compared with the logarithmic law of the wall, the outer law, and the temperature-velocity relationships which may serve as indicators of the influence or the strength of the pressure gradient.

In the following we shall discuss boundary layer measurements in flows with pressure gradients, firstly those in a favourable pressure gradient divided into (a) reflected wave - straight wall and (b) simple wave - curved wall, secondly those in an adverse pressure gradient divided in the same way.

Since the experiment of Lewis et al.(1972) includes the three cases of zero-, adverse- and favourable-pressure gradient (Fig.5.1.1), it is very well suited to serve as an example of the behaviour of velocity profiles in various pressure gradients. Sample velocity profiles are shown in log-law coordinates in Fig.(5.1.2) and in outer-law coordinates in Fig.(5.1.3). As suggested above, the strength of the wake $\Delta\ (\bar{u}^*/u_\tau)$ increases considerably in an adverse pressure gradient compared with that in a zero pressure

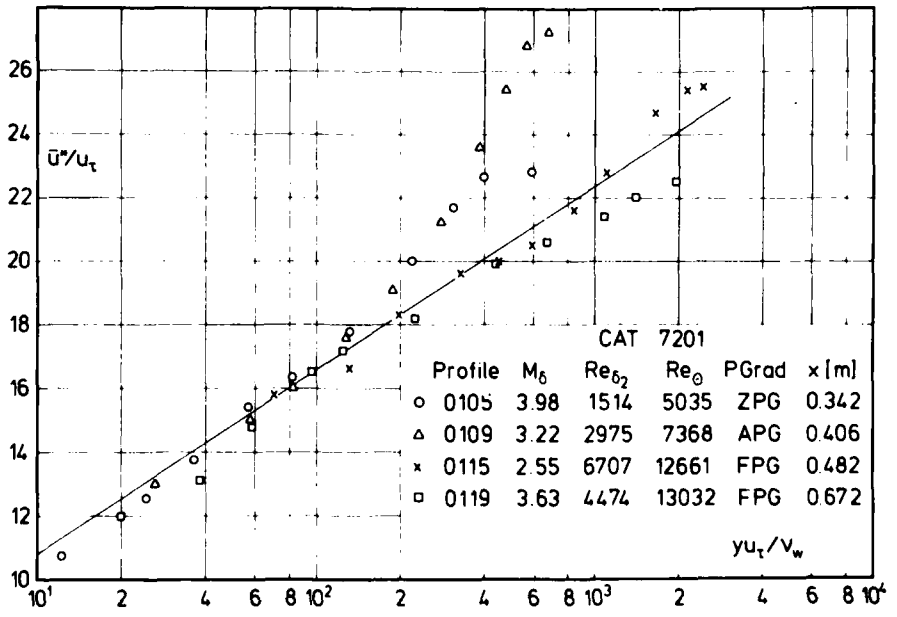

Fig. 5.1.2 Law of the wall for a compressible axisymmetric boundary layer (adiabatic wall, variable pressure gradient). Lewis et al. (1972).

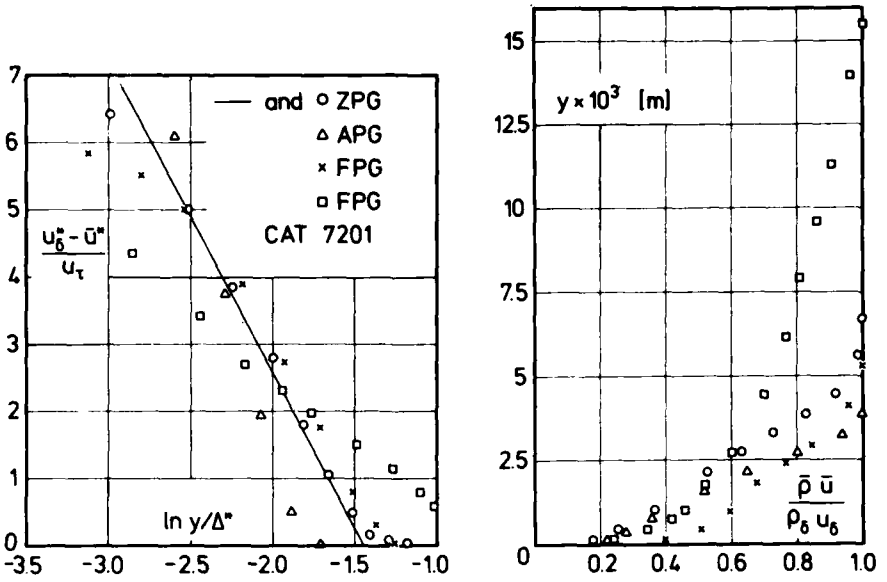

Fig. 5.1.3 Comparison of outer-law with measurements Mass flow profiles (CAT 7201)

gradient - here from approximately 2.6 to 6 - and falls to "negative" values in a favourable pressure gradient. The outer law plot shows similarly strongly characterized tendencies. The zero-pressure gradient profile (0105) agrees with the "outer law" very well. The adverse-pressure gradient profile (0109) shows a markedly steeper slope than the zero pressure gradient profile while the favourable-pressure gradient profile (0119) which is downstream of the change from adverse to favourable pressure gradient shows the reverse tendency. The other favourable-pressure gradient profile (0115) is the first profile after the change of pressure gradient, and shows by its intermediate character (as also for the wall law in Fig.5.1.2) that the nature of the profile does not depend only on the local values of the boundary conditions but also on the recent history of the boundary layer - particularly for the outer region.

In general, this behaviour of the velocity profiles is confirmed by several other cases in sections 5.2 and 5.3. This experiment may therefore serve as example of all those following except that some caution should be expressed about the determination of skin friction. Lewis et al. did not measure the wall shear stress directly but used the curve-fitting procedure of Coles & Hirst (1969) applied to equivalent incompressible velocity profiles transformed as suggested by van Driest (1951). In order to justify this procedure a calibration function for Stanton tubes was presented as evidence of consistency. Since both calibrations assume a priori the validity of the law of the wall, the good agreement of the velocity profiles with the law of the wall (Fig.5.1.2) is no independent proof of its validity, which can only be established by measuring skin friction directly, for example by a floating element balance, or, possibly, by using a range of Preston tubes down to a size small enough to qualify as a sublayer device. For compressible boundary layers the law of the wall and the outer law depend on the transformation rule for the velocity $\bar{u}^*$ which again needs a temperature - velocity relationship as given in section 2.5.4. We remarked there that eqn.(2.5.37) should only be valid for boundary layers with pressure gradients different from zero if the wall is adiabatic. It is therefore an open question how strongly the temperature profile is affected by a pressure gradient.

An inspection of Table 7.1 in AGARDograph 223 shows that there are few cases where both temperature and velocity profiles and skin friction were measured in the same experiment. Investigations which fulfill this condition and which can in principle provide evidence of the validity range of the temperature - velocity relationship are presented in Table 5.1.1 and will be discussed first.

Table 5.1.1

CAT	PG	T_o	c_f	M_δ	$Re_{\delta_2} \times 10^{-3}$	Tw/Tr
7104	APG	STP	FEB	2.4- 1.9	11 - 26	1
7101	APG	CCP,FPTP	P	3.5- 2.8	6.5 - 18.8	1
7304	FPG	ECP,FWP	FEB	3.8- 4.6	2 - 47	0.25 - 1
5901	FPG	STP	V	8 -10	0.15- 0.47	0.5
6801	FPG	STP	V	8 -11.5	0.9 - 6.8	0.3 - 0.4
7105	FPG	FWP	FEB	19.5	0.2 - 0.3	0.2
7206	FPG	STP	FEB	19 - 45	0.06- 0.13	0.35 - 0.85

A discussion of the validity of the temperature-velocity relationship in boundary layers with streamwise pressure gradients is more complicated than for the zero-pressure gradient case (cf.section 2.5.6), since none of the boundary layers has a defined origin. Therefore we cannot exclude upstream history effects. In what follows we shall adhere to the pattern of discussion already established in section 2.5.6. Fig.(5.1.4) - Waltrup & Schetz (1971) - shows a comparison of $\bar{T}/T_\delta$ as measured with the prediction of eqn.(2.5.39). Agreement between measurements and the theoretical curve is good. The right hand graph shows a comparison between the relationship $\bar{T}o/To\delta$ to $\bar{u}/u_\delta$ as here calculated from eqn.(2.5.37e) with $T_w=T_r$ and the measured values of $\bar{T}o/To\delta$. As compared with zero pressure gradient profiles, deviations between measurements and predictions are relatively large (up to 2.5 %). There is a small overshoot as is to be expected for profiles on an adiabatic wall, with a relatively more extended overshoot region as compared to the profiles in Fig.(5.1.5) for example. The measurements lie above the predicted values contrary to our findings in Figs.(2.5.1 and 2.5.4).

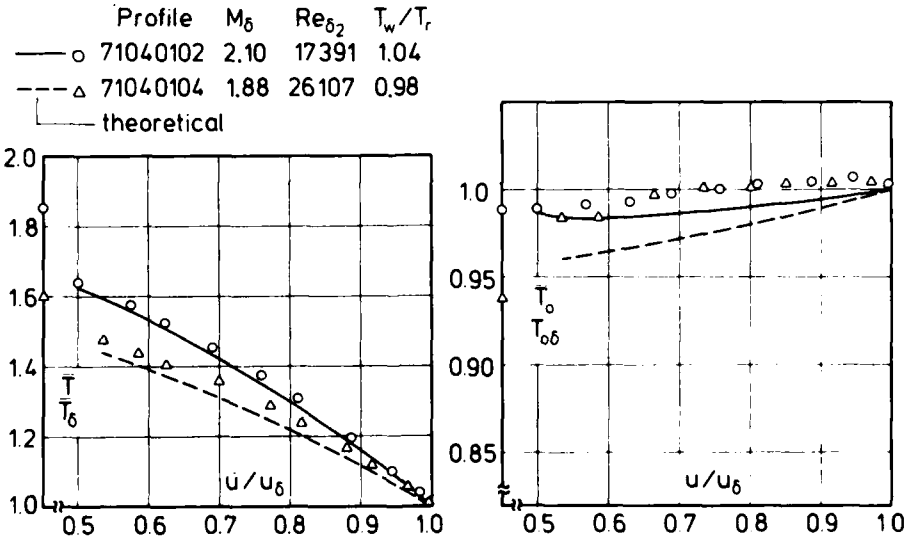

Fig. 5.1.4 Comparison between measured and theoretical temperature profiles (adverse pressure gradient, adiabatic wall, origin not defined). Waltrup & Schetz (1971).

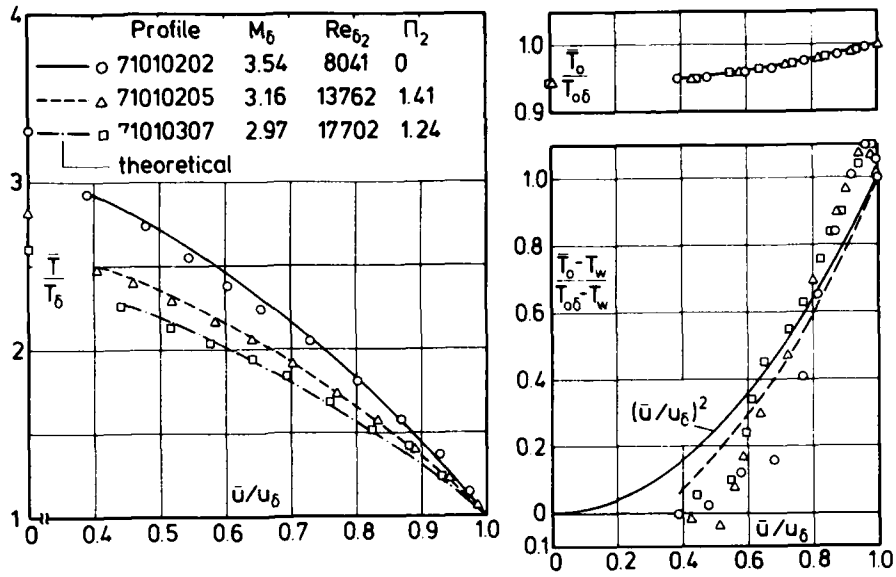

Fig. 5.1.5 Comparison between measured and theoretical temperature profiles (zero and adverse pressure gradient, adiabatic wall, origin not defined) Sturek & Danberg (1971).

The left hand graph of Fig.(5.1.5) - Sturek & Danberg (1971) - again shows good agreement between measurements and predictions, whereas large deviations again occur between the Crocco temperature function $T^* = (\bar{T}_o - T_w)/(T_{o\delta} - T_w)$ calculated from eqn.(2.5.40), using as input the experimental values of $\bar{u}/u_\delta$. The theoretical curves, all represented in the right hand figure by the dashed line, cannot be distinguished from each other but they differ from the relation $T^* = (\bar{u}/u_\delta)^2$. As we have seen already in section 2.5.6 (e.g. Fig.2.5.1), the directly measured data, shown as open symbols, apparently differ considerably from the predicted curves. We have noted above that these differences are in fact illusory.
Finally agreement between the $\bar{T}_o/T_{o\delta}$ data and the prediction is excellent, predictions and measurements being indistinguishable.
Both boundary layer experiments were performed in adverse pressure gradients (the first a reflected wave - straight wall case, the second a simple wave - curved wall case) on adiabatic walls. The following discussion is concerned with boundary layers in favourable pressure gradients on straight walls only. The first experiment is that by Voisinet & Lee (1973) and, although the cooling rate is extremely high, agreement between predictions and measurements is very good (Fig. 5.1.6). The equivalent zero-pressure gradient case

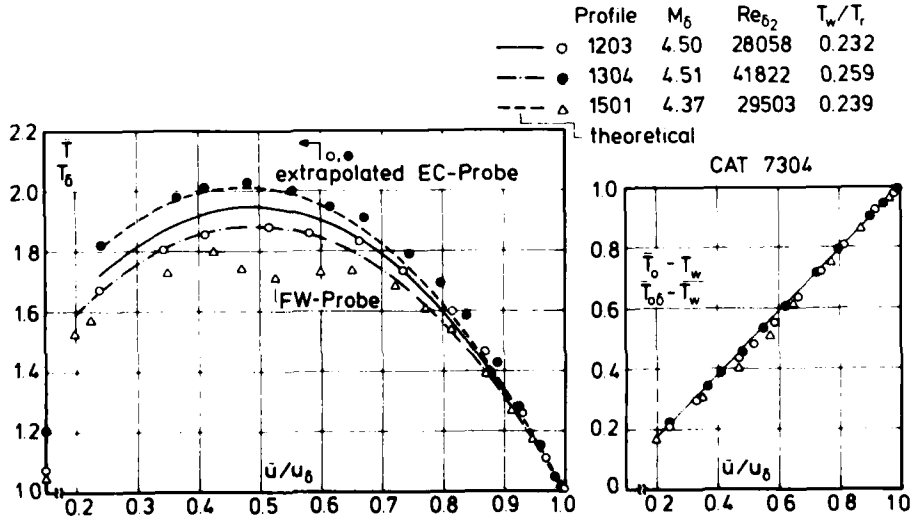

Fig. 5.1.6 Comparison between measured and theoretical temperature profiles in a boundary layer (favourable pressure gradient, isothermal wall, origin not defined) Voisinet & Lee (1973).

is shown in Fig.(2.5.18) and the resemblance to the graphs for profiles 72021103 and 1203 in Fig.(2.5.18) is striking. Again we have indicated the region where temperature measurements "had to be extrapolated due to the size of the equilibrium cone probe (ECP)". Measurements performed with a fine-wire probe (FWP) extended much more closely towards the wall but they show a dip in the temperature distribution which is probably caused by "probe-problems". The reader should note the Crocco temperature T* follows a linear relationship with $\bar{u}/u_\delta$ as in the case for a boundary layer with zero pressure gradient. It is possible that - apart from the pecularities of the NOL-tunnel - the high cooling rate has such a dominant influence that the rather moderate favourable pressure gradient is in fact too weak to affect the temperature distribution.

The next two experiments (Hill CAT 5901 and Perry & East CAT 6801) have similar geometrical arrangements since they were performed on the wall of a conical nozzle. The temperature profiles have in common that measurements and predictions differ radically from each other as far as the static temperatures are concerned (Figs. 5.1.7 and 5.1.8). Hill's boundary layer had very low Reynolds numbers and values of the

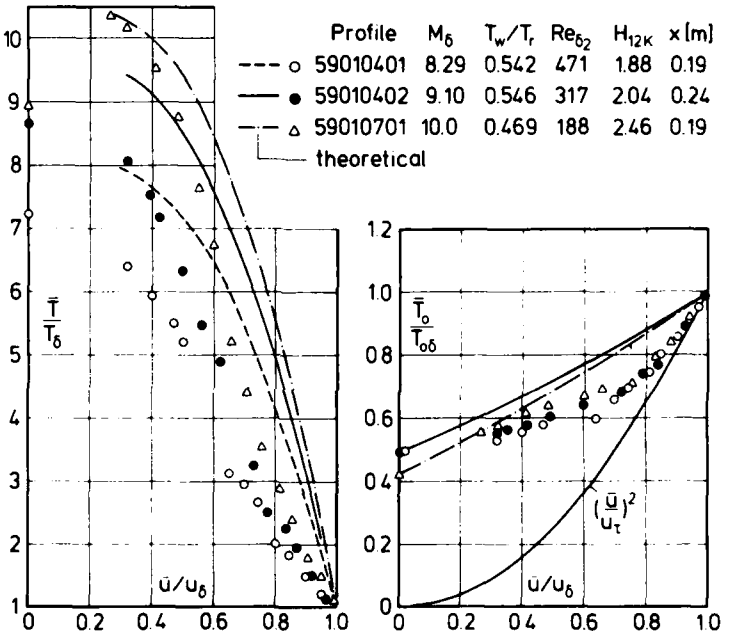

Fig. 5.1.7 Comparison between measured and theoretical temperature profiles (favourable pressure gradient, isothermal wall, origin not defined).Hill(1959)

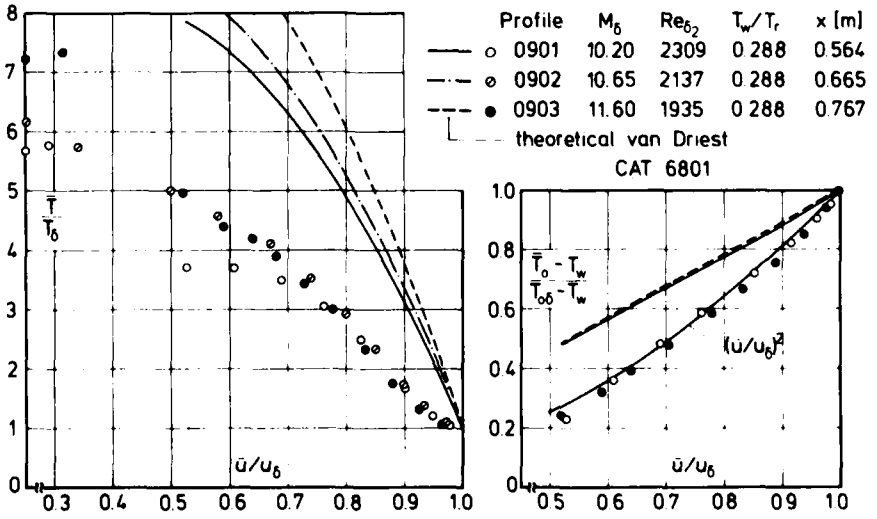

Fig. 5.1.8 Comparison between measured and theoretical temperature profiles in a boundary layer (isothermal wall, favourable pressure gradient, origin not defined). Perry & East (1968).

form parameter H_{12k} which indicate that the boundary layer may not have been far from laminar. This does not explain, however, the deviations from the predictions in Fig.(5.1.7). Since we cannot distinguish in this experiment between the influence of pressure gradient, wall cooling, and low Reynolds number, we can only accept that for one or more of these causes, the temperature-velocity relationships as given in section 2.5 do not hold any longer(see also Figs. 5.2.11 and 5.2.12).

The right hand graph of Fig.(5.1.8) reveals a most interesting phenomenon in that the measured Crocco temperature T* agrees very well with the relationship $T^* = (\bar{u}/u_\delta)^2$ but not with T* as evaluated from the measured values of $\bar{u}/u_\delta$. For this behaviour we cannot offer an explanation but must wait for further experimental evidence in similar boundary layers (cf.Figs. 5.2.13 and 5.2.14 and the associated discussion).

The final two investigations are distinguished by extremely high Mach numbers and extremely low Reynolds numbers (Beckwith et al. CAT 7105 and Kemp & OwenCAT 7206). Beckwith et al. used a fine-wire probe and a great many data points were taken. Corrections to the $\bar{T}_0$ data are perhaps more properly described as a calibration procedure. They may be summarized as amounting to finding a probe recovery factor of about 0.7 to 0.75 when the probe and its support are in a flow region where the total temperature is reasonably uniform. Conduction and radiation corrections were applied to all data, and close to the wall where the probe was at a markedly lower temperature than the support, these were large and resulted in an effective recovery factor near one.

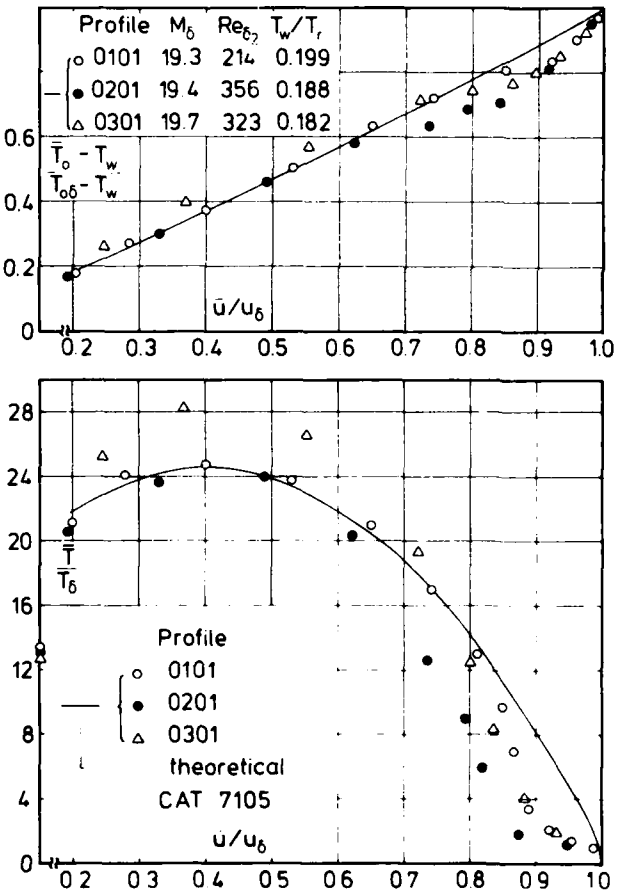

Fig. 5.1.9 Comparison between measured and theoretical temperature profiles in a boundary layer (favourable pressure gradient, isothermal wall, origin not defined). Beckwith et al. (1971).

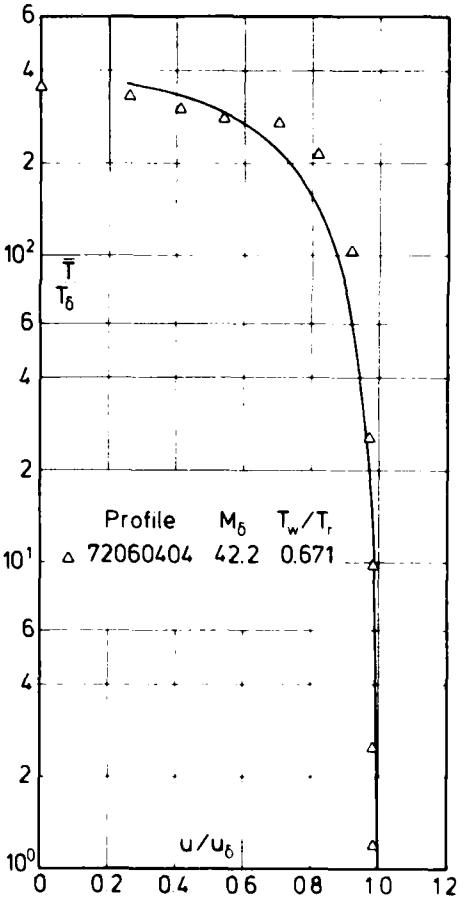

Fig. 5.1.10 Comparison between measured and theoretical temperature profiles (favourable pressure gradient, isothermal wall, origin not defined) Kemp & Owen (1972).

Fig.(5.1.9) shows fair general agreement between the measured static temperature and prediction except in the outer region. This is unusual if compared with the temperature distributions shown in section 2.5.6. The same discrepancies appear on the upper graph where T* is plotted versus $\bar{u}/u_\delta$. Again the relationship of T* to (u/u_δ) is approximately linear as opposed to quadratic and there are discrepancies in the

outer region corresponding to those in the static temperature distribution.
Fig.(5.1.10) shows the static temperature variation in a boundary layer with a Mach number M_δ = 42.2. at a moderate cooling rate. Since discrepancies are difficult to recognize on this graph in view of the axes chosen, we point out here that the apparent agreement is illusory. Actual spot values (see AGARDograph 223) depart from the curve by up to 700 %. The experiment is unique in its range so that whatever reservations we may have, we feel that the results should be presented even if the most that can be hoped for is a qualitative discussion.

Conclusions:

No experimental investigation is available for which upstream history effects on the boundary layers in a pressure gradient as discussed here can definitely be excluded. All conclusions must necessarily be tentative therefore.

The temperature-velocity relationships (2.5.39) and (2.5.40) hold for compressible boundary layers with moderate favourable and adverse pressure gradients if the wall is adiabatic. There are not enough experiments to define exactly what is meant by "moderate". In some cases the validity range may even be extended to flows with heat transfer if the wall is isothermal. There are often cases of boundary layers on isothermal walls, however, where discrepancies between measured temperature profiles and predictions are large.

More experimental investigations are necessary in boundary layers with favourable and adverse pressure gradients on isothermal walls under controlled conditions. We do not at present have any good quality data for experiments with significant streamwise wall temperature variation, let alone with a superimposed pressure gradient.

5.2 Favourable pressure gradient

5.2.1 Reflected wave - straight wall

This group (II A in AGARDograph 223) covers those flows in which a wave structure is generated somewhere else in the flow and imposed on a boundary layer flowing along a straight wall. The test layer thus passes through a "reflected wave", without significant streamline curvature.
All boundary layers discussed in this section - they are listed in Table 5.2.1 - were subject to a favourable pressure gradient in the test region. Though, particularly for the nozzle flows (CAT 5901/6801) there may have been a measure of re-laminarization in the throat, in the test region they at least show some turbulent characteristics, and are not locally in pressure gradients which might cause re-laminarization. In many cases the transition process appears imcomplete.

Table 5.2.1

CAT	M_δ	T_w/T_r	$Re_{\delta_2} \times 10^{-3}$	C_f	Origin
7201	2.4 -3.7	1.0	4.5 - 6.7	V/S	defined
7401	2.5 -3.0	1.05	6.4 - 7.8	S	not defined
7304	3.8 -4.6	0.23-1.0	2.0 -47	F	not defined
5901	8 - 10	0.5	0.15- 0.47	V	not defined
6801	8 - 11.5	0.3 -0.4	0.9 - 6.8	V	not defined

Apart from Naleid (CAT 5801) - where only one profile was measured (see Fig.5.3.8) - and Voisinet & Lee (CAT 7304) skin friction was not determined by a floating element balance (F) but only from Stanton tubes, surface fences (S) or from the velocity profiles (V). In all cases but one discussed in this section the upstream pressure gradient and/or wall temperature history could have affected the boundary layer in the text section. There was only one experiment (Lewis et al. CAT 7201) where the origin of the axisymmetric boundary layer was defined, and where the pressure-gradient distribution was known, leading from a zero via an adverse to a favourable pressure gradient.

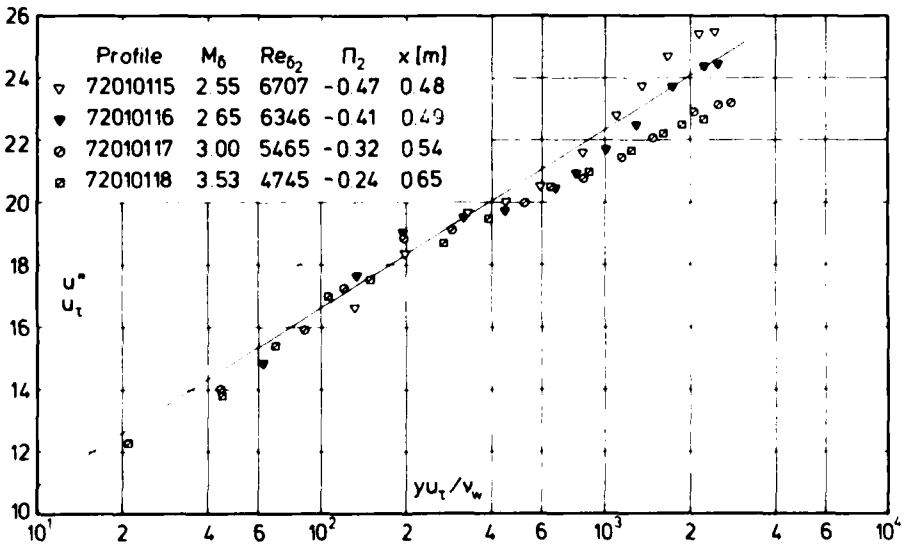

Fig. 5.2.1 Law of the wall for a compressible boundary layer (adiabatic wall, favourable pressure gradient, defined origin) Lewis et al.(1972). c_f from transformed log-law.

Transition was believed to be complete upstream of x = 0.204 m. The authors state further that heat transfer at the wall was zero within experimental accuracy. This investigation was repeated with a strongly cooled wall (Gran et al. 1974, Hahn &Lutz 1971) but the numerical data is not at present available.
Fig.(5.2.1) shows a comparison of the experimental data with the logarithmic law, revealing upstream

history effects by showing a positive wake strength for the most upstream velocity profile in the favourable pressure region (0115) and a negative wake strength further downstream as is to be expected from a mildly accelerated subsonic boundary layer (Patel 1965). Exept for profile 72010116 there is still a region where agreement with the logarithmic law is fairly good. This is not true for the outer law (Fig.5.2.2) where measurements and eqn.(3.3.17) disagree considerably because of the strong pressure gradient and history effects on the outer region of the boundary layer.

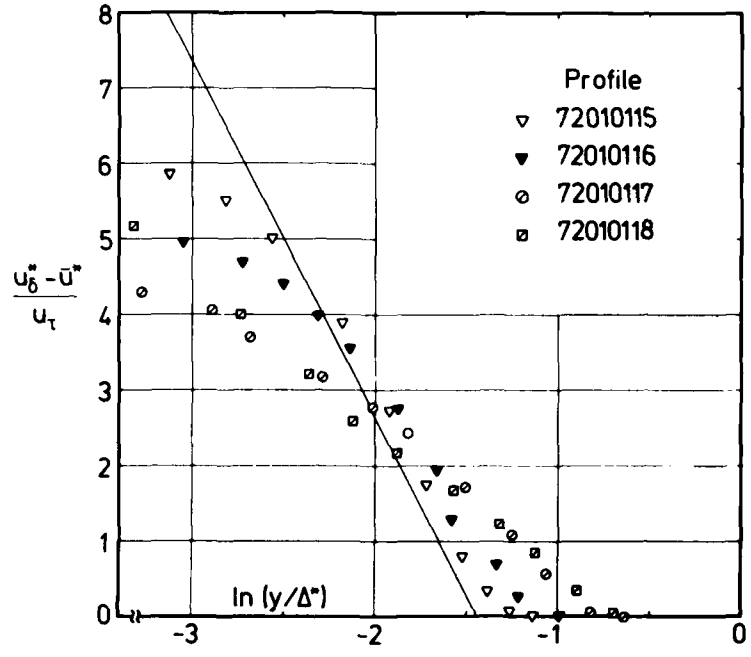

Fig. 5.2.2 Outer law for a compressible turbulent boundary layer in a favourable pressure gradient (adiabatic wall, defined origin) Lewis et al. (1972).

Thomas (CAT 7401) performed his experiment in a test boundary layer on a flat surface extending upstream into the settling chamber and facing one of a number of contoured nozzle blocks. The evidence of earlier tests (Jeromin 1966, Squire 1970) was that transition occurred well upstream, and that the velocity profiles were fully developed after experiencing the throat region expansion. The principal uncertainty here must be the question of three-dimensionality, as the length/width ration of the experimental surface is more than 5:1. Fig.(5.2.3) shows velocity profiles measured under test condition C with c_f as determined from the velocity profile slope by Thomas.

Agreement with the logarithmic law is good and there still exists a small but positive wake strength except for the most downstream profile (74010318). One explanation for this behaviour of the velocity profiles could be the small pressure gradient and the relatively short development of the boundary layer. Again there is little agreement between the measurements and the outer law (Fig. 5.2.4) though, again, there is a trend to decreasing negative slope as the boundary layer develops. As can be seen from the legend of Fig.(5.2.3) the Reynolds number R_{δ_2} falls with increasing distance downstream if the pressure gradient is favourable. It is interesting to compare the results of Thomas' experiment with a similar one in the same Reynolds number range but at higher Mach numbers by Voisinet & Lee (CAT 7304) where skin friction was determined by means of a floating element balance. The wall temperature history was carefully recorded in this experiment (TD 15 CAT 7304-A-3) showing that heat-transfer from the flow occurred in the nozzle region. As we have seen while discussing the ZPG cases of this experiment (Voisinet & Lee 1972, section 4.2, Fig.4.2.19) the measured velocity profiles (Fig. 5.2.5) lie consistently above the logarithmic law resembling the low Reynolds number profiles of Hasting & Sawyer (1970) and Watson et al.(1973) shown in Figs.(4.4.12) and (4.4.5). We therefore conclude that the transition process - delayed in any case by the favourable pressure gradient - is not complete in the inner layer. This conclusion is strengthened

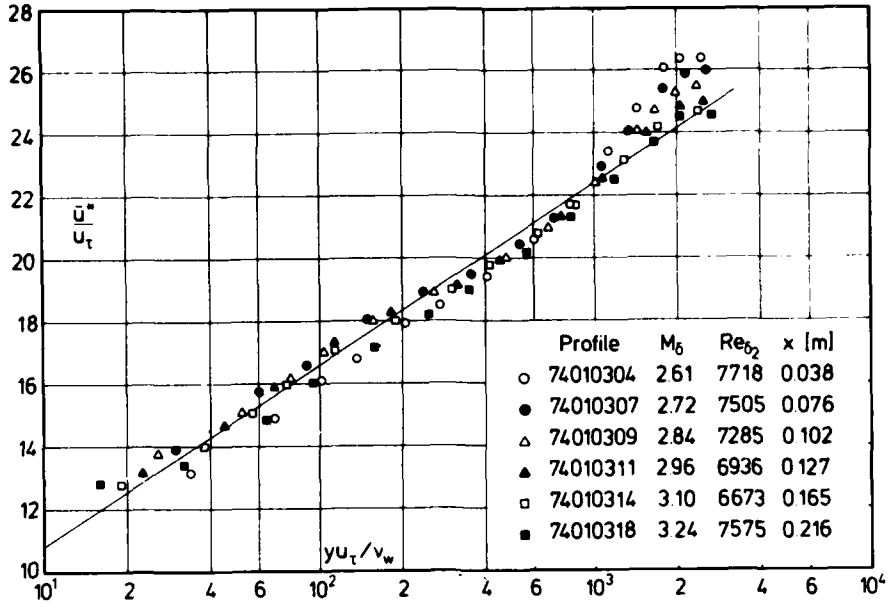

Fig. 5.2.3 Law of the wall for a compressible turbulent boundary layer (adiabatic wall, favourable pressure gradient, origin not defined). Thomas (1974). c_f from razor blade technique.

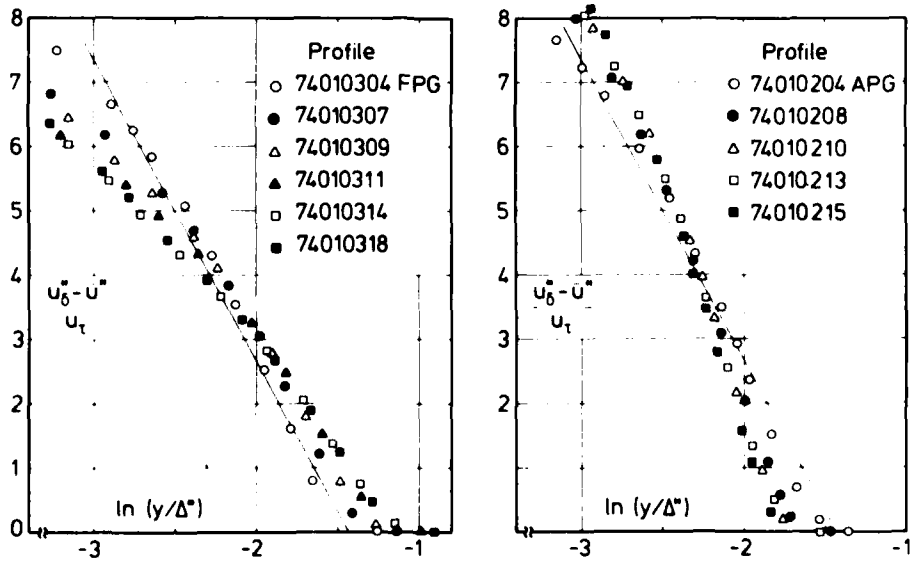

Fig. 5.2.4 Outer law for a compressible turbulent boundary layer in an adverse and favourable pressure gradient (adiabatic wall, origin not defined) Thomas (1974).

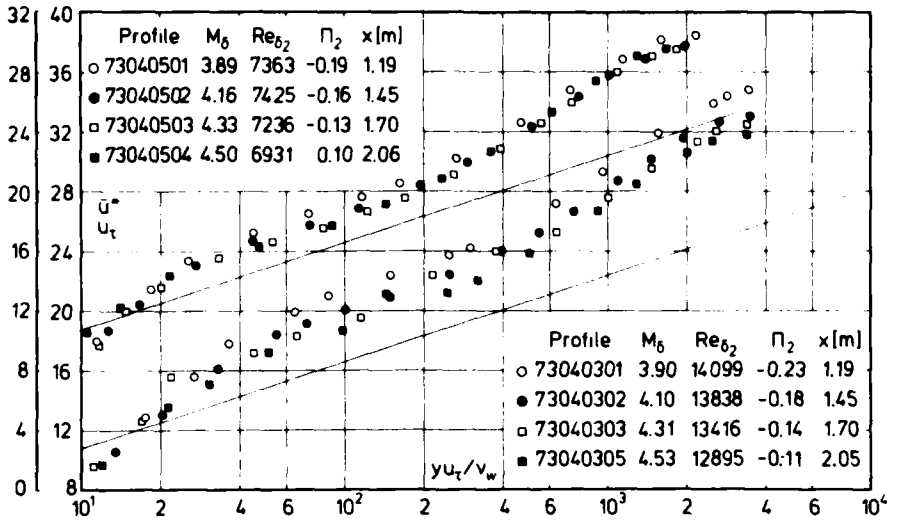

Fig. 5.2.5 Law of the wall for a compressible boundary layer (nearly adiabatic wall, favourable pressure gradient, origin not defined). Voisinet & Lee (1973). c_f from FEB.

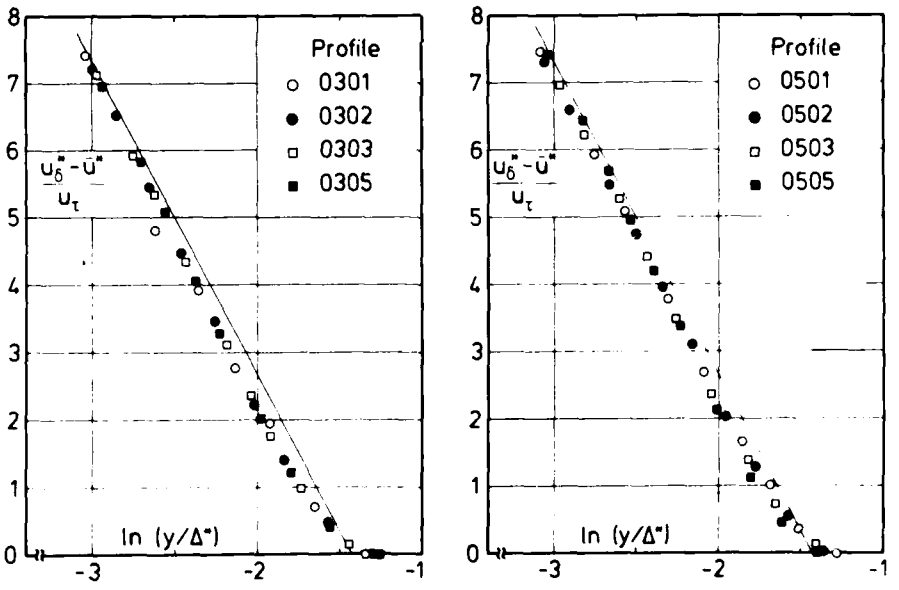

Fig. 5.2.6 Outer law for a compressible turbulent boundary layer in a favourable pressure gradient (nearly adiabatic wall, origin not defined). Voisinet & Lee (1973).

by a comparison of the measurements with the outer law (Fig.5.2.6) where transition is complete (see also Fig.4.4.11, Hasting & Sawyer). In order to explain the unexpected agreement with the outer law we must assume that the favourable pressure gradient is effectively much weaker than in the preceeding cases of Lewis et al. and of Thomas - the gradient dM_δ/dx at least is considerably smaller - which means that the velocity profiles may not differ much from those in a zero-pressure gradient.

Fig.(5.2.7) shows velocity profiles in the same boundary layer but with severe wall cooling. Although transition should be delayed even more by wall cooling, profile 73041403 lies below the logarithmic law at about the same Mach and Reynolds number as the velocity profiles in Fig.(5.2.5) along an adiabatic wall. The skin friction data for the highly cooled boundary layer were corrected by Voisinet (1977) and both the old and the corrected values are given in the legend of Fig.(5.2.7). Nevertheless the scatter in the data is rather large. The only clear tendency is that the downstream velocity profiles lie in general below the upstream ones. There is good agreement between the velocity profiles and the outer law (Fig.5.2.8), irrespective of the change in c_f. Agreement with the log law (Fig.5.2.9) and the outer law (Fig.5.2.10) is good, as would be expected in view of the low values of Π_2.

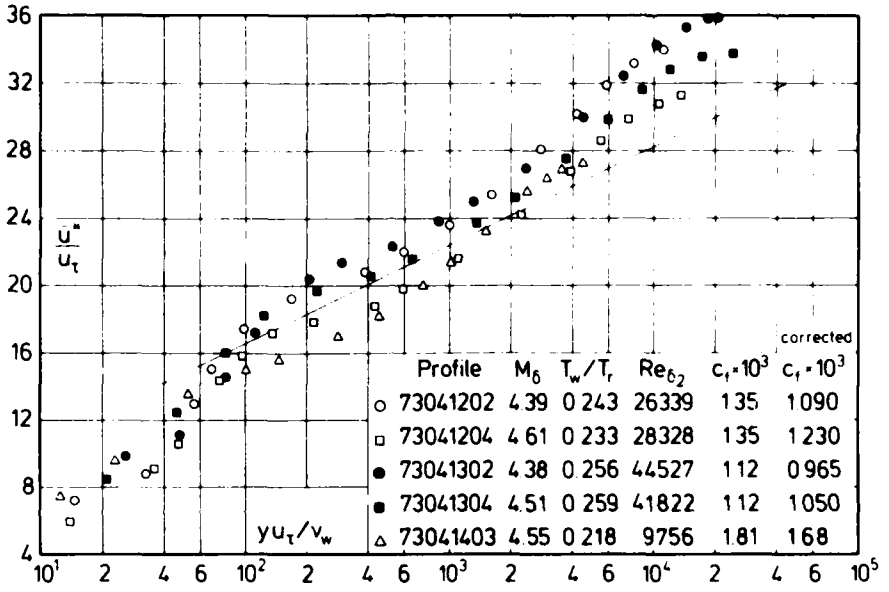

Fig. 5.2.7 Law of the wall for a compressible boundary layer (isothermal wall, favourable pressure gradient, origin not defined) Voisinet & Lee (1973). c_f from Voisinet (1977) corrected.

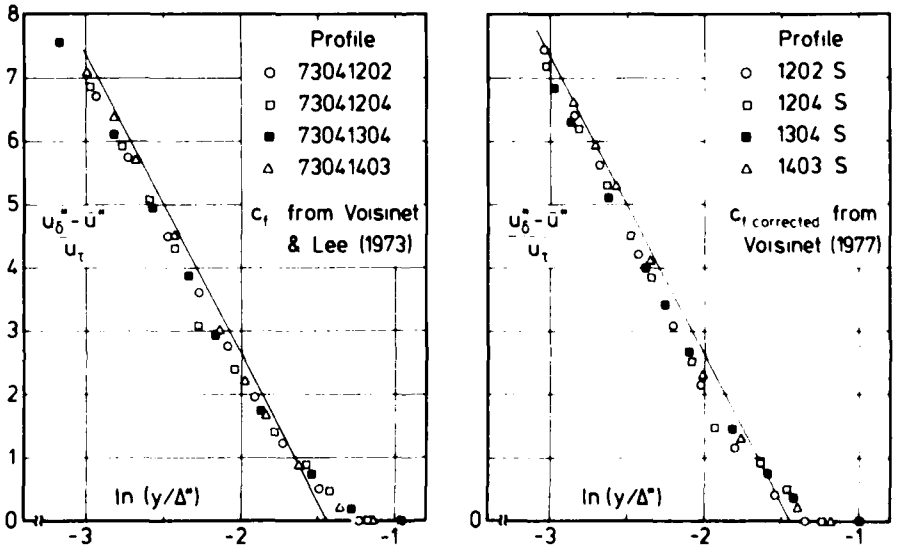

Fig. 5.2.8 Outer law for a compressible boundary layer in a favourable pressure gradient (isothermal wall, origin not defined) Voisinet & Lee (1973).

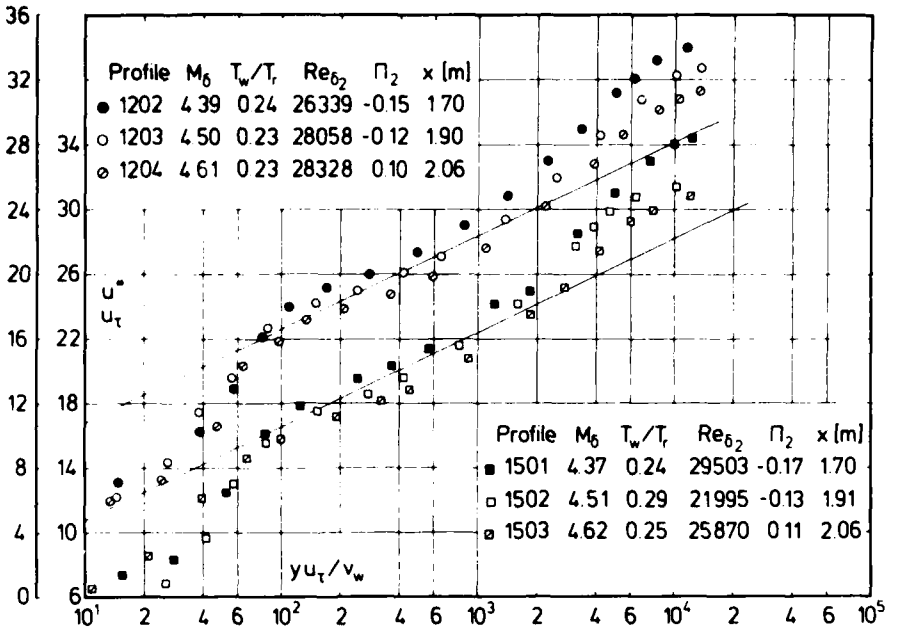

Fig. 5.2.9 Law of the wall for a compressible boundary layer (isothermal wall, favourable pressure gradient, origin not defined) Voisinet & Lee CAT 7304. c_f from Voisinet (1977) FEB.

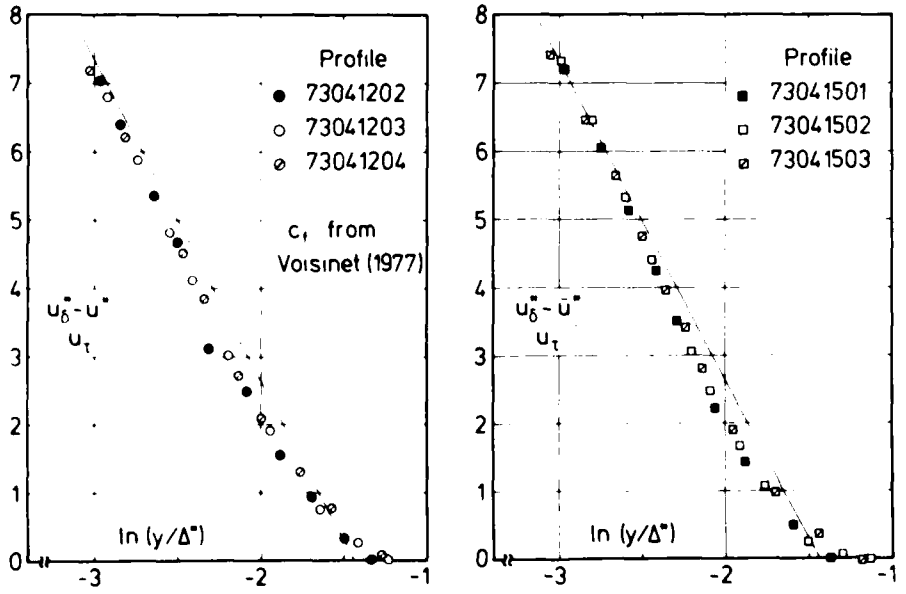

Fig. 5.2.10 Outer law for a compressible turbulent boundary layer in a favourable pressure gradient (isothermal wall, origin not defined) Voisinet & Lee (1973).

There are two further investigations of accelerated boundary layers in conical nozzles with nominally isothermal walls where the favourable pressure gradient was stronger than in the case of CAT 7304 but where the skin friction was determined from the wall slope of the velocity profile. However, the Reynolds numbers Re_{δ_2} were smaller by almost a factor 100 and the Mach number larger by a factor of 2. The velocity profiles plotted in Fig.(5.2.11) show a typical laminar/transitional behaviour (Hill CAT 5901), i.e. the inner region has in no case become fully turbulent. Comparisons should be made with Figs.(4.4.5) and

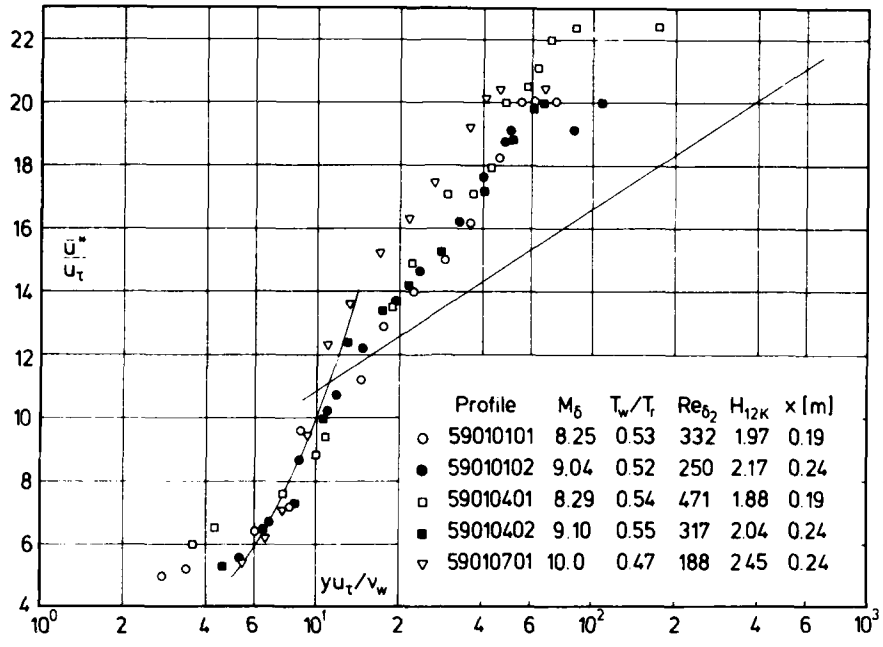

Fig. 5.2.11 Law of the wall for a compressible boundary layer (isothermal wall, favourable pressure gradient, origin not defined) Hill (1959). c_f from velocity gradient.

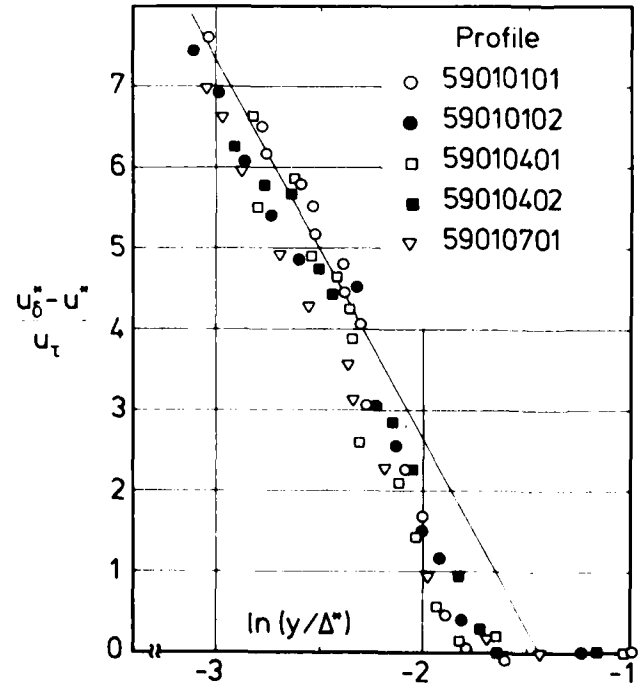

Fig. 5.2.12 Outer law for a compressible boundary layer in a favourable pressure gradient (isothermal wall, origin not defined) Hill (1959).

(4.4.8). Here again the shape parameter H_{12k} is a good indicator of the transitional behaviour of the boundary layer. The outer region (Fig. 5.2.12) reflects a low Reynolds number behaviour similar to that shown in Fig.(4.4.6) for the measurements of Watson et al.(CAT 7305) or for a boundary layer in an adverse pressure gradient and not the behaviour of a boundary layer in a favourable pressure gradient (e.g. Fig. 5.2.2).

Perry & East (CAT 6801) also made measurements in the boundary layer on the wall of a conical nozzle. An obvious practical difference from the Hill (CAT 5901) measurements is that the running time, in a given tunnel, was very short of order 10-20 ms. The instrumental difficulties were therefore more pronounced, and in fact it was only possible to obtain one datum point from each run. Velocity profiles in inner region coordinates are presented in

Figs.(5.2.13 and 14), with the author's skin friction values as deduced from the slope of the velocity profile. The Mach number range is much the same as for Hill (CAT 5901; Fig.5.2.11) and the heat transfer parameter not too disimilar. The Reynolds numbers are, however, an order of magnitude greater. The lack of agreement with the wall law is therefore surprising and superficially suggests that the boundary layer, at least in the inner region, is not yet fully turbulent. It is not even possible to discern a definite trend towards the wall law at the higher Reynolds numbers - compare series 03/09. The outer law plots (Fig. 5.2.15) also show little consistency - series 06/09 behaving much as zero pressure gradient profiles, while series 01/03 appear, if anything, to show a pattern more characteristic of adverse pressure gradient profiles (see Fig.5.3.5). Data reduction for this experiment assumes small normal pressure gradients,

	Profile	M_δ	T_w/T_r	Re_{δ_2}	Re_Θ	H_{12K}	x [m]
○	68010101	8.0	0.39	3265	13558	1.48	0.548
□	68010102	8.50	0.39	2648	12309	1.49	0.650
△	68010103	8.87	0.39	2969	14949	1.49	0.752
●	68010301	8.05	0.35	7085	26350	1.46	0.548
■	68010302	8.50	0.35	6575	27047	1.45	0.650
▲	68010303	9.05	0.35	6716	31073	1.49	0.752

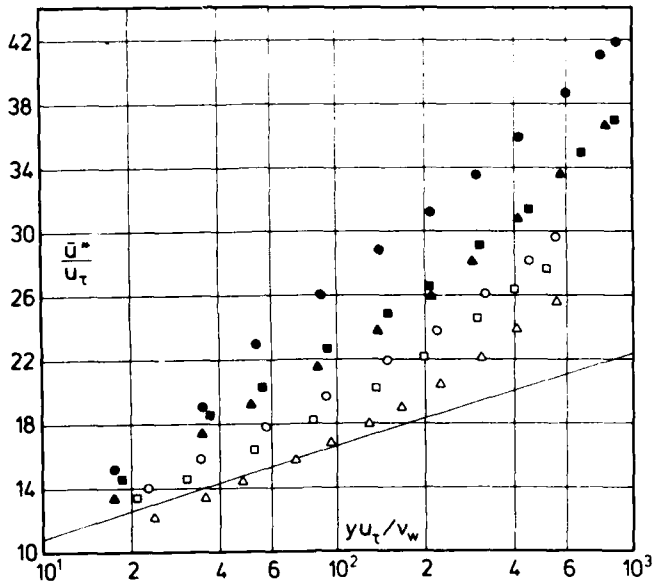

Fig. 5.2.13 Law of the wall for a compressible boundary layer in a favourable pressure gradient (isothermal wall, origin not defined. Perry & East (1968). c_f from velocity profile.

which is reasonable, and uses experimental temperature values (Fig.5.1.8) which differ markedly from the "van Driest" predicted values. It is tempting to ascribe the log law disagreement to the uncertainty in skin friction values as determined from the velocity gradient, but the variation is excessive, and there is no pattern to it. We cannot therefore draw any definite conclusions from this experiment, and must leave interpretation to wait on further knowledge while retaining a suspicion that we are once more observing the consequences of the gradual progression of transition inwards from the critical layer towards the wall - possibly retarded by the (not very strong) favourable pressure gradient. This not very strong pressure gradient and the comparison with the Hill data render it unlikely that the combination "pressure gradient and wall cooling" invalidates the temperature-velocity relationship and consequently the transformation for the velocity $\bar{u}$.

Profile	M_δ	T_w/T_r	Re_{δ_2}	Re_Θ	H_{12K}	x [m]
○ 68010601	9.90	0.316	1068	5340	1.62	0.564
□ 68010602	10.50	0.316	888	4950	1.62	0.665
△ 68010603	11.20	0.316	731	4624	1.66	0.767
● 68010901	10.20	0.288	2309	11130	1.55	0.564
■ 68010902	10.65	0.288	2137	11191	1.53	0.665
▲ 68010903	11.60	0.288	1935	11927	1.55	0.767

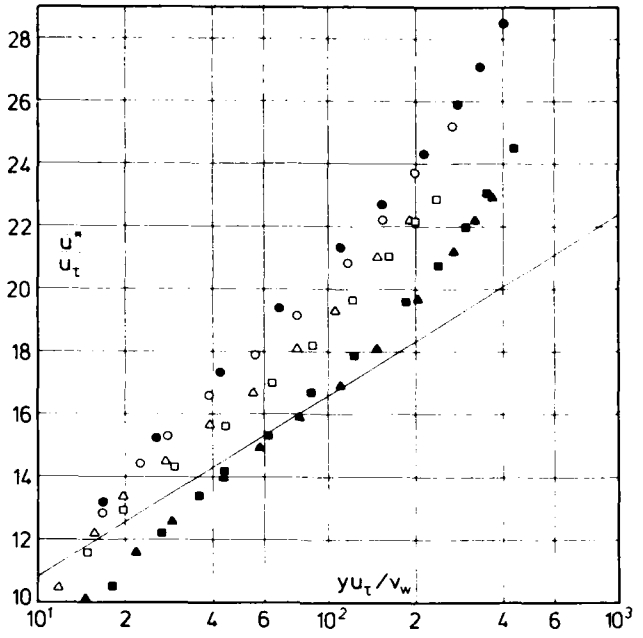

Fig. 5.2.14 Law of the wall for a compressible boundary layer in a favourable pressure gradient (isothermal wall, origin not defined. Perry & East (1968). c_f from velocity profile.

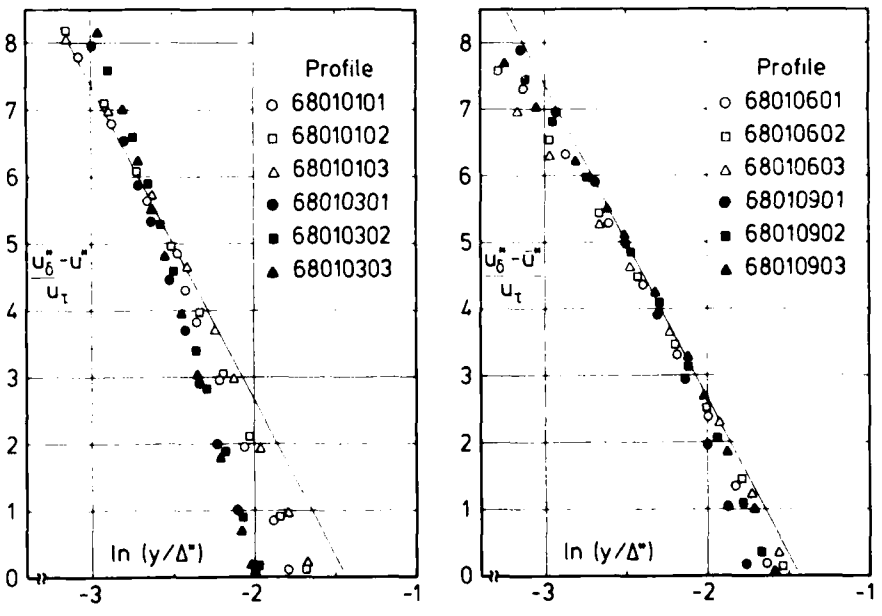

Fig. 5.2.15 Outer law for a compressible boundary layer (isothermal wall, favourable pressure gradient, origin not defined). Perry & East (1968).

5.2.2 Simple wave - curved wall

In these flows the curved streamlines require, in principle, normal pressure gradients, the significance of which increases with Mach number.

The only boundary layer experiment with a favourable pressure gradient along a curved wall (contoured nozzle) including skin friction measurements, was performed by Kemp & Owen (CAT 7206). There are two further unique features, the extremely high Mach numbers and the as extremely low Reynolds numbers. It is probably impossible at present to interpret these measurements in terms of correlations drawn directly from flat plate experience. These measurements were made in a Mach number range unmatched by any other reported experiment, and the instrumental and conceptual difficulties are such that no great emphasis should be placed ony any precise numerical value. We suppose that there were strong thermal and pressure history effects as can be seen from Fig.(5.2.16, see legend of 5.2.17). The velocity profiles are not typical

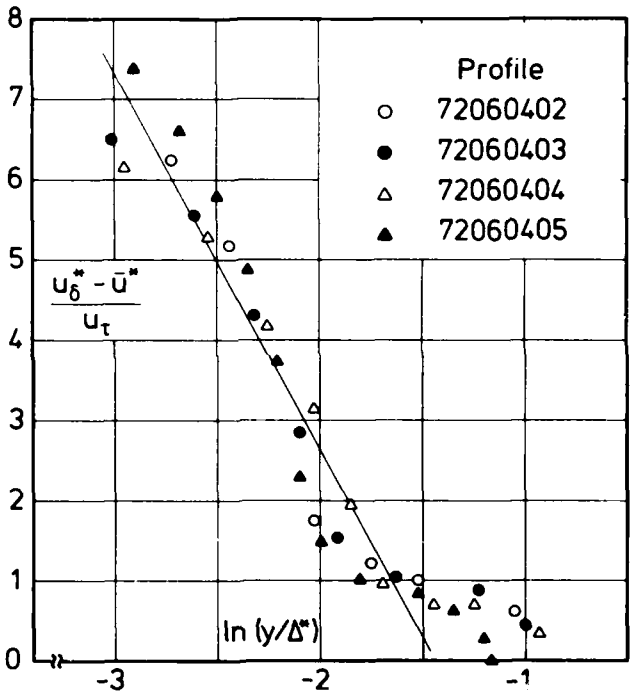

Fig. 5.2.16 Outer law for a compressible boundary layer with a favourable pressure gradient along an isothermal wall. Kemp & Owen (1972).

of those found in a favourable pressure gradient boundary layer (e.g. Figs.5.2.2 and 5.2.4). They can be compared qualitatively, however, with those of Hill (Fig.5.2.12) - except very close to the outer edge of the layer - where we also think that upstream history effects were present. As was mentioned in the editors' comment of CAT 7206 (AGARDograph 223), some scatter was introduced in the outer region of the profiles by using the authors' $\bar{T}/T_\delta$ data as an input for the profiles, so that for the outermost profile points the pressures may be up to 5 % in error from this cause alone.

The inner law plot shows a most unusual behaviour also (Fig.5.2.17). In inner region coordinates the maximum value of yu_τ/ν_w is of the order 40 and the H_{12k} value which has been shown to be a good indicator of the state of the boundary layer is characteristic of a laminar boundary layer (the Blasius profile is characterized by $H_{12k} = 2.60$).

The thickness of the viscous sublayer is very large (approximately 25 %) compared to the thickness of the

	Profile	M_δ	T_w/T_r	Re_{δ_2}	Re_Θ	H_{12K}	x[m]
○	72060402	29.4	0.665	131	6145	2.52	1.07
●	72060403	34.5	0.661	114	6154	2.46	1.63
△	72060404	42.2	0.671	63	3610	2.61	2.79
▲	72060405	43.8	0.623	65	3757	3.10	3.55

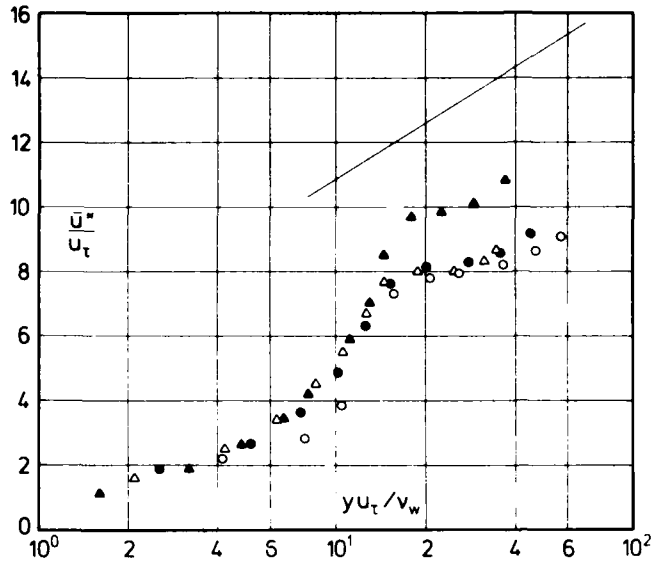

Fig. 5.2.17 Law of the wall for a compressible boundary layer with a favourable pressure gradient along an isothermal wall. Kemp & Owen (1972). c_f from FEB.

boundary layer. This, however, is to be expected for such low Reynolds numbers ($50 < Re_{\delta_2} < 180$). The differences between the two definitions of the boundary layer Reynolds number, Re_{δ_2} and Re_Θ, can be seen very clearly in this case. The discrepancies between our Reynolds number - here the comparison was made between the Re_Θ values - and those of the source arise from our choosing a different viscosity law for helium at low temperatures as stated in the introduction of AGARDograph 223.

The last experiment to be discussed in this section describes a boundary layer formed on the wall of a contoured axisymmetric nozzle. The profiles were measured at a single station near the nozzle exit and 2.08 m axially from the throat (Beckwith et al.1971). The wall temperature was kept nearly constant in the cooled part of the nozzle extending from x = 0.145 m downstream of the throat, at about 0.17_0T (330-300 K), but the high heat transfer rates in the throat region caused the wall temperature there to reach an estimated value of about 0.8 T_0.
A major topic of the source paper is probe correction procedures. In the wall region, for example, the viscous and rarefaction effects on the Pitot data involve correction factors of up to 2.14 as assessed by Beckwith et al. For a description of the data correction and evaluation procedures the reader is referred to CAT 7105 or the source paper. The authors originally determined a skin friction value from the Mach number gradient at the wall. A later paper (Harvey & Clark 1972) describes shear stress measurements made 0.20 m downstream of the profile station. These measurements were interpolated on the basis of the authors' Re_Θ values so as to give skin friction data in association with the profiles. Using transformed coordinates no log-law region exists (Fig.5.2.18). In the same way as for the velocity profiles of Kemp & Owen (Fig.5.2.17), the viscous sublayer reaches a proportion of the boundary layer thickness much larger than in the boundary layers encountered so far. Again the Reynolds number Re_{δ_2} is small. It is therefore almost astonishing to find rather good agreement with the outer law (Fig.5.2.19) which proves again that the transition process has set in but has not progressed yet towards the inner region.

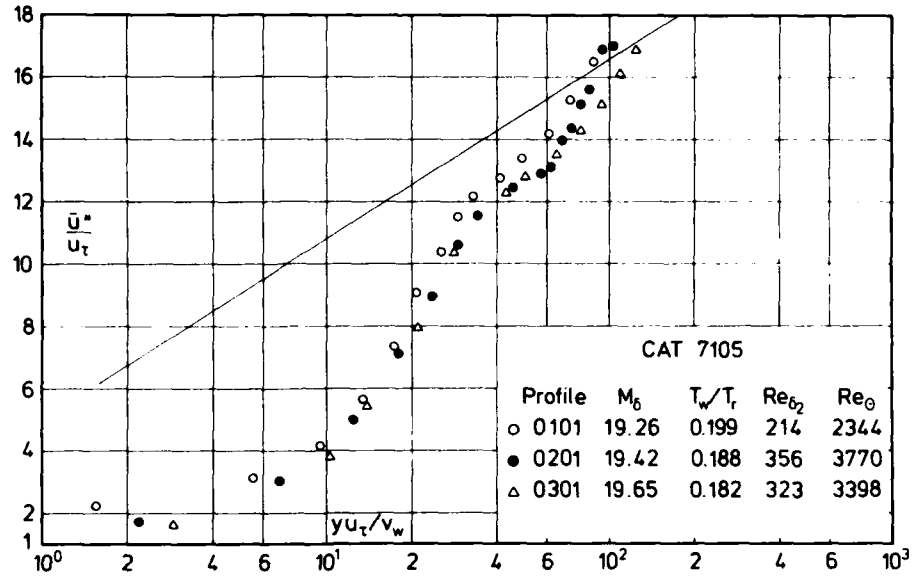

Fig. 5.2.18 Law of the wall for a compressible boundary layer (favourable pressure gradient, isothermal wall, origin not defined). Beckwith et al. (1971). c_f from FEB.

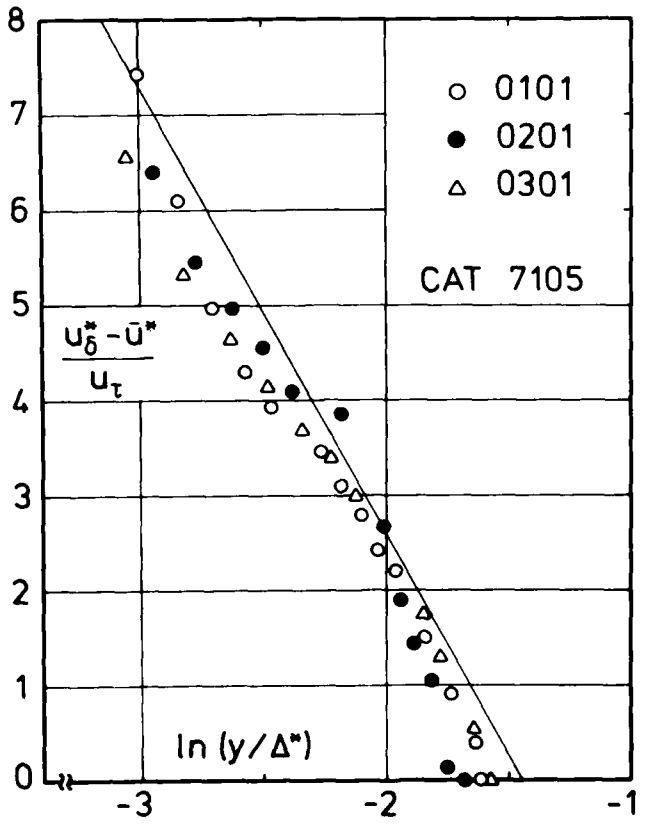

Fig. 5.2.19 Outer law for a compressible boundary layer (favourable pressure gradient, isothermal wall, origin not defined). Beckwith et al. (1971).

5.3 Adverse pressure gradient

5.3.1 Reflected wave - straight wall

We have discussed the features of the reflected wave - straight wall flow in a favourable pressure gradient in section 5.2.1. They remain unchanged in principle in an adverse pressure gradient flow. The relevant boundary layer experiments are listed in table 5.3.1 and discussed below.
None of these boundary layers approached separation, however, and only three experiments (Sturek & Danberg 1971, Kussoy et al. 1978 and Gootzait & Childs 1977) contain shear stress and/or fluctuating velocity measurements which are of great importance for the discussion of this type of flow.

Table 5.3.1

CAT	M_δ	Tw/Tr	$Re_{\delta_2} \times 10^{-3}$	c_f	Origin
7102	4 - 2	1.0	3 - 39	P	defined
7201	4 - 2.4	1.0	1.5 - 6.8	V/S	defined
7802 S	2.3 - 1.9	1.0	11 - 34	*)	not defined
5801	2	1.0	7.1 - 8.2	F/P	not defined
7104	2.4 - 1.9	1.0	11 - 26	F	not defined
7401	2.5 - 2.2	1.0	7 - 13	S	not defined
7007	4 - 3	1.0	10 - 32	P	not defined

*) embedded hot-wire

As in earlier sections we begin by a discussion of results from experiments for which the boundary layer had a defined origin, the flow was adiabatic and three-dimensionality was nominally eliminated by an axisymmetric configuration. Peake et al. (CAT 7102) made measurements on the inner surface of a hollow cylinder, with a retractable centre body on the axis which was used to impose a pressure gradient on the test layer. Preston tubes were employed to determine the wall shear stress, using a number of compressible calibration procedures, of which we have arbitrarily chosen the Hopkins & Keener (1966) TR-method. As a control check, we first present a set of zero pressure gradient profiles (series 01, Fig.5.3.1). Agreement with the log law is fairly good, but some scatter is shown in both slope and position. The outer-law-profiles are self consistent and agree fairly well with the outer law (Fig.5.3.3.b).
Series 02 (Fig.5.3.2) covers the adverse pressure gradient results, but neither the boundary conditions for the profiles nor the results, are easy to interpret. Profiles 0201, 0203 were respectively at the start and end of the adverse-pressure gradient, with 0202 in the middle. Profiles 0204-6 are in a zero-pressure gradient relaxation-flow downstream of the pressure rise. Profile 0201 is therefore, except at the wall, in an adverse longitudinal and a normal pressure gradient, and the upstream distance over which the pressure gradient has acted increases as we move out from the wall. The pressure field is as shown in the sketch, where the arrows indicate the direction of the pressure gradient, much as shown in Fig.(6.1.2) with the pressure gradient reversed. Both the departure of profile 0201 from the log law and its difference from 0101 (to which if the longitudinal wall pressure distribution alone is considered, it should be identical) may therefore be caused by adverse streamwise pressure gradients, by the pressure increase in the normal direction, or by both. Discrepancies may also, in part, spring from the resulting errors in data reduction, since the normal pressure gradient will result in the Mach number in the outer region being less than that calculated assuming constant pressure. Profile 0202 is in a region where normal pressure gradients should be negligible. For this, and the succeeding profiles, the slope of the inner region suggests that there may be errors in the skin friction values. It seems that the wake region is more pronounced than for a typical zero-pressure gradient case, if not very different from series 01 in the same experiment. Profile 03 is again subject to both longitudinal and normal pressure gradients, this time of a sense to cause the Mach numbers in the outer region to be greater than assumed. The appearance on the log law plot is again much as would be expected of a subsonic adverse pressure gradient layer.

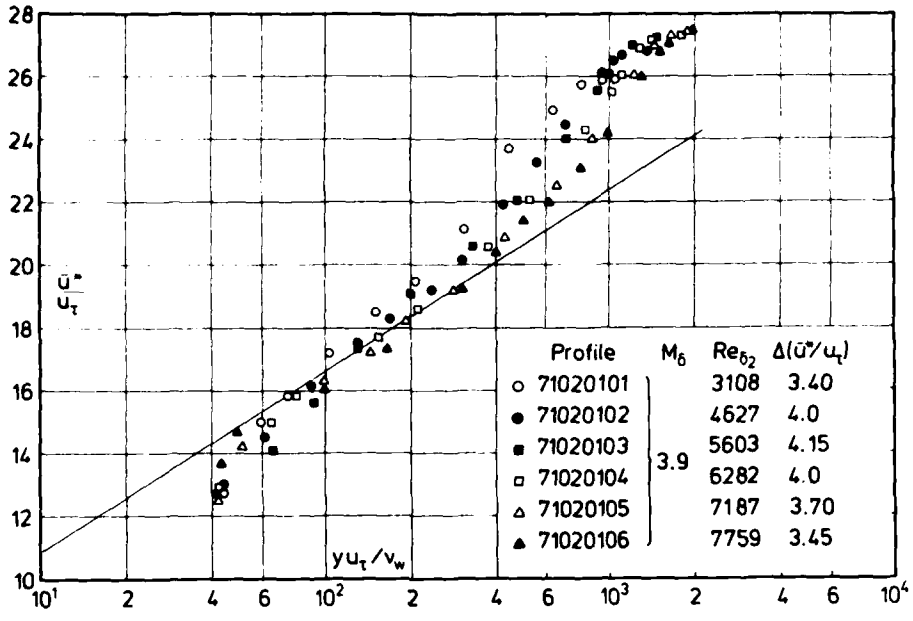

Fig. 5.3.1 Law of the wall for a compressible boundary layer (adiabatic wall, zero pressure gradient, defined origin). Peake et al. (1971).

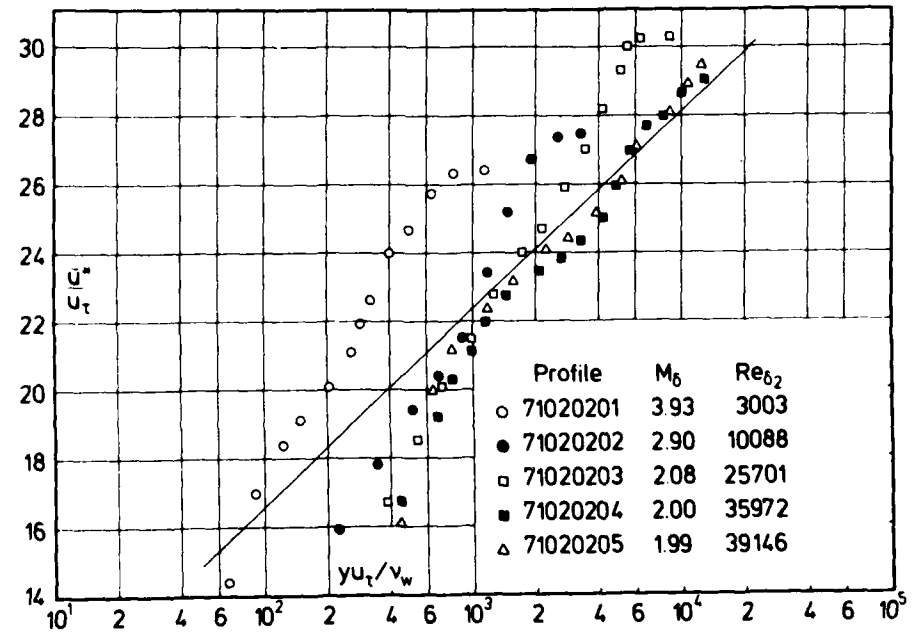

Fig. 5.3.2 Law of the wall for a compressible boundary layer (adiabatic wall, adverse pressure gradient, defined origin) Peake et al.(1971). c_f from Preston tube.

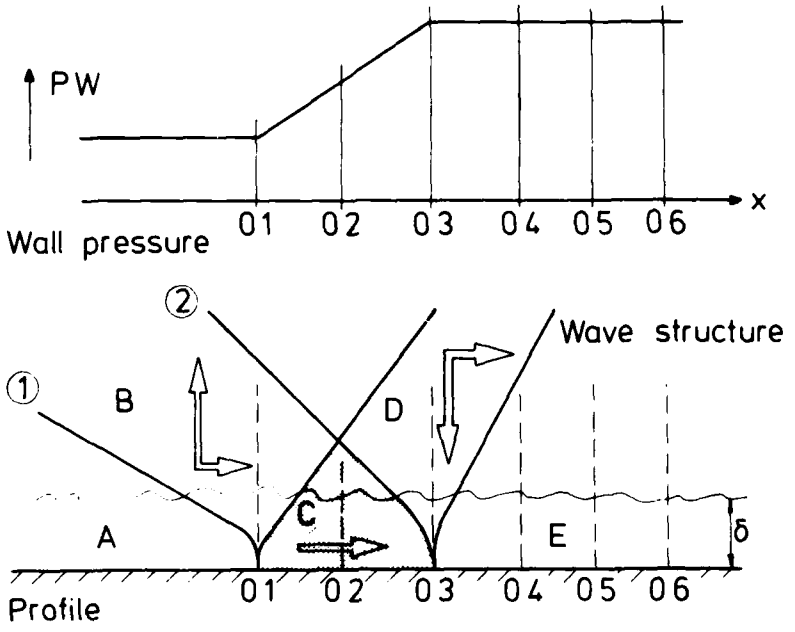

Peake et al. recalculated profile 0203 (also 0202 for which it was inappropriate) with a normal pressure gradient of double the magnitude which would be predicted by § 6.1.3 eqn. (6.1.14b) below. The calculations contain discrepancies, but would seem to indicate that Mach number and velocity values taking account of the normal pressure gradient should not differ detectably from those assuming constant pressure on the velocity profile plots. The succeeding profiles 0204, 0205, in a zero pressure gradient region, appear if anything more as expected of a favourable pressure gradient flow on the log law plot. In the outer law plot (Fig.5.3.3) 0201 shows a steeper slope and lower values in the outermost region, and this typical behaviour spreads inwards, becoming very pronounced for 0202, less so for 0203 while 0204 and 0205 in contrast to their log-law behaviour return towards the zero pressure gradient law.

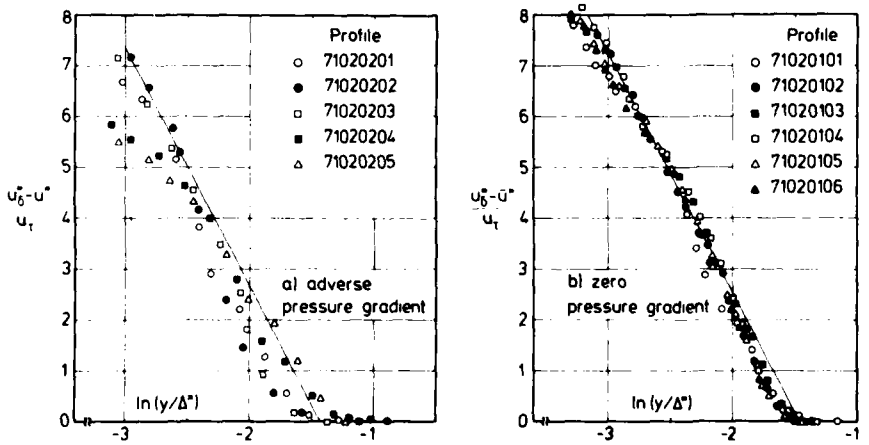

Fig. 5.3.3 Outer law for an axisymmetric compressible turbulent boundary layer (adiabatic wall, defined origin). Peake et al. (1971).

We should perhaps note here that for any flow in which the boundary layer edge lies in a simple wave region (whether in a wholly simple wave flow or as an incoming or outgoing simple wave forming part of a structure as shown in the sketch above), it may not be possible to define u_δ precisely. This should be borne in mind when inspecting any outer law plot such as Fig.(5.3.3) and its successors throughout § 5. The dependence of u on p in a free-stream flow is not very strong at high Mach numbers, so that the problem is not likely to become serious unless the normal pressure gradients are very strong, or the Mach number relatively low(see § 7).

Lewis et al.(CAT 7201) also performed tests on the inner surface of a cylinder, thus eliminating end effects, and a pressure gradient was again imposed by a centre body. There are no upstream pressure gradient effects as for the accelerated flow region of the same experiment (Fig.5.2.1), and it is astonishing how well the inner law plot (Fig.5.3.4) resembles that of velocity profiles in a moderate adverse pressure gradient boundary layer in subsonic flow. For the compressible boundary layer the skin friction values were obtained by the curve-fitting procedure of Coles & Hirst (1969) applied to equivalent incompressible velocity profiles transformed as suggested by van Driest (1951). Again the velocity profiles hardly extend into the inner region.

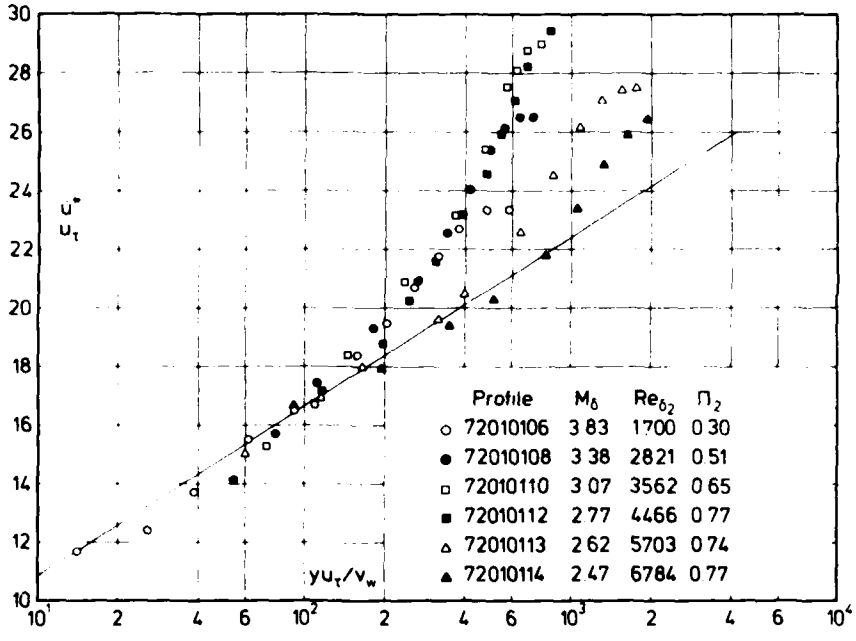

Fig. 5.3.4 Law of the wall for a compressible boundary layer (adiabatic wall, adverse pressure gradient, defined origin) Lewis et al. (1972). c_f from transformed log-law.

The development of the layer near stations 13 and 14 is particularly interesting. Here the wall pressure gradient is adverse with quite high values of Π_2. However, profiles 0113 and 0114 are moving towards the log law, after profiles 0108-0112 have shown what might be termed classic low-speed adverse-pressure gradient behaviour (Fig.5.3.4). The adverse pressure gradient stops at or just downstream of station 14, to be followed by a favourable pressure gradient, consequently the whole of profile 0114 and probably most of the outer part of 0113 are in fact in a simple wave favourable pressure gradient region. The same behaviour is visible in the outer law plot (Fig.5.3.5). Profile 0106, the first shown here and the first in the adverse pressure gradient region shows a rather weak influence of the pressure gradient, as might be expected.

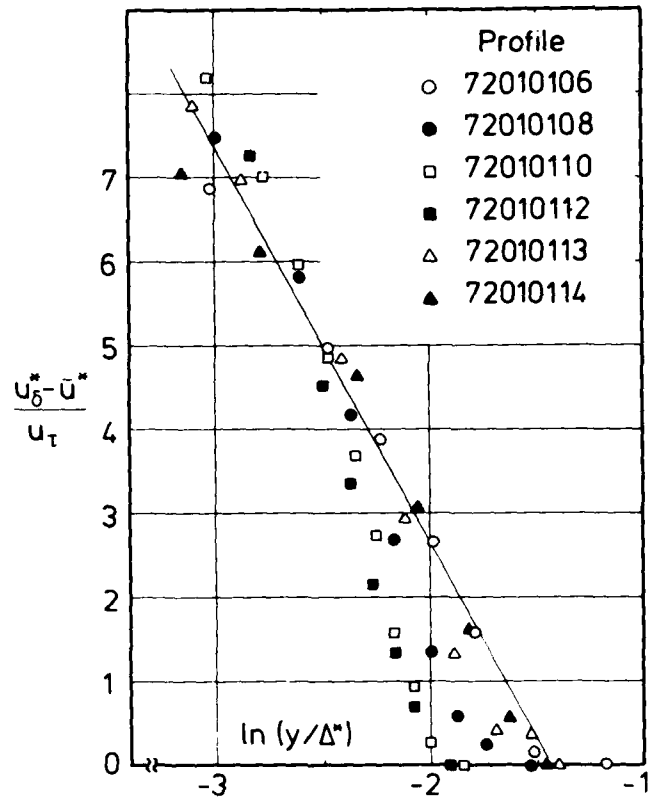

Fig. 5.3.5 Outer law for a compressible turbulent boundary layer in an adverse pressure gradient (adiabatic wall, defined origin) Lewis et al.(1972).

All other cases considered here describe boundary layers in adverse, or more complex pressure gradients for which the upstream history is not defined other than by the provision of one or more profiles in a zero pressure gradient region ahead of the imposition of the pressure gradient.
A particularly fully instrumented study is that made by Kussoy et al.(CAT 7802 S). The test boundary layer is formed on the inner surface of a cylindrical extension to an axisymmetric nozzle, and four different centre-bodies were used to impose a reflected wave pressure gradient. Two of these cases include full profile measurements, at close streamwise intervals. The wave structures produced in both cases consist of a compression followed by an expansion. In the first, more "moderate", pressure gradient of series 01, the wall pressure is initially constant, then rises as the compression reaches the wall and is reflected before continuing at a constant level to the end of the test zone. The expansion wave does not reach the wall, although the outer part of the downstream profiles (0110-0113) is affected. For the more abrupt pressure gradient of series 02 the wall pressure, after an initial constant pressure portion (0202), rises to a plateau (0210-0212) as for series 01, but the expansion wave then reaches the wall and the pressure falls markedly in the region described by the last two profiles (0213, 0214). There is evidence of a strong compression wave entering the test-region in the outer part of the last profile.

The wave structures are relatively concentrated, in that the streamwise extent - at any given value of y - is of the same order as the boundary layer thickness, so that in terms of the general flow structure illustrated in Fig.(6.1.2) and the sketch above (Peake et al., CAT 7102), the "reflected wave" region

(indicated by stippling in Fig.6.1.2) is entirely submerged in the boundary layer. The static pressure field is easily explained in terms of the wave structure, and will be discussed in § 6.2 below.

Wall law profiles are shown for series 01 and 02 in Figs.(5.3.6.a and 6b) respectively. Profiles 0102, 0104 and 0203 are only slightly, if at all, affected by the incoming wave structure and appear as typical zero-pressure gradienc profiles in both shape and position in the log-law plot. 0107 is at the start of the adverse pressure gradient as observed at the wall and 0109 at the end. The wake component is observed to increase as expected (Fig.5.3.6.a) and then decrease again for 0111 and 0113.
Numerical agreement with the log-law is, however, very poor. It is possible that the flush-mounted hot-wire skin friction gauges are influenced by the pressure gradient effects, though as sublayer devices they should be relatively unaffected. Series 02(Fig.5.3.6.b) shows the same general behaviour. The initial zero-pressure gradient profile of 0203 develops an increased wake component by 0207, at the start of the adverse-pressure gradient at the wall, which becomes increasingly exaggerated in profiles 0209 and 0210 before decreasing in 0212 and 0214, where the wall pressure gradient is favourable. Again there seems to be a strong pressure-linked effect on the skin friction values, and this discussion has been based on an inspection of the profiles individually, disregarding the downward displacement of the log law.

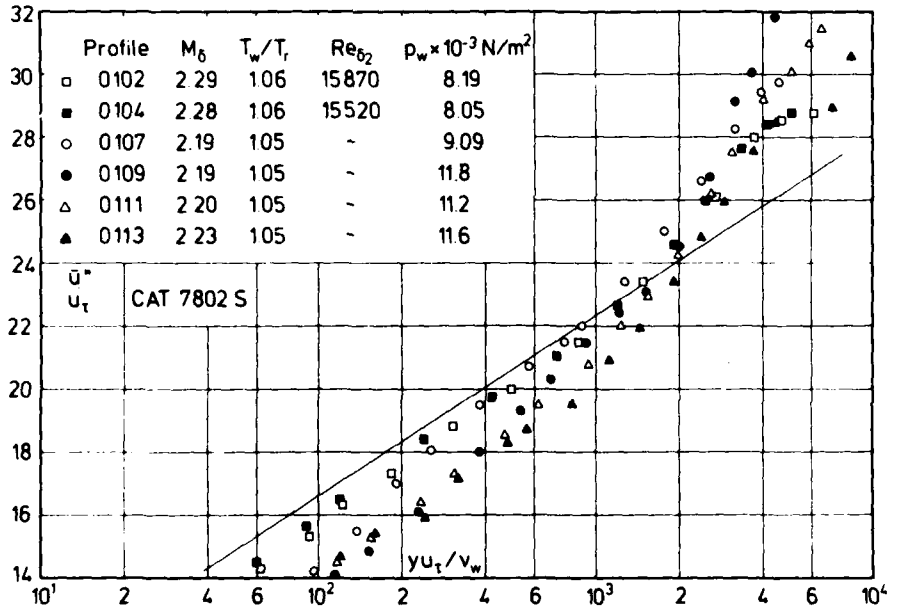

Fig. 5.3.6.a Law of the wall for an axisymmetric compressible turbulent boundary layer (adiabatic wall, variable pressure gradient, origin not defined). Kussoy et al.(1978). c_f from heated-wire gauge.

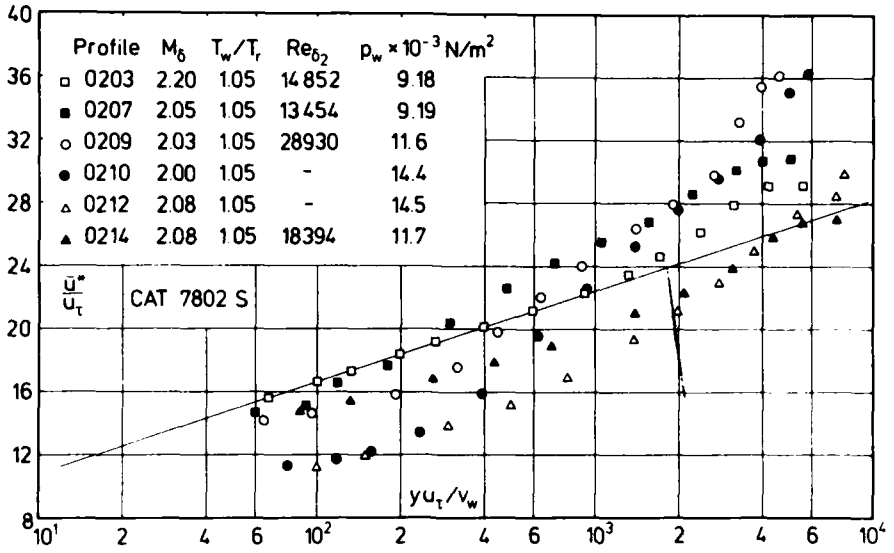

Fig. 5.3.6.b Law of the wall for an axisymmetric compressible turbulent boundary layer (adiabatic wall, variable pressure gradient, origin not defined). Kussoy et al.(1978). c_f from heated-wire gauge.

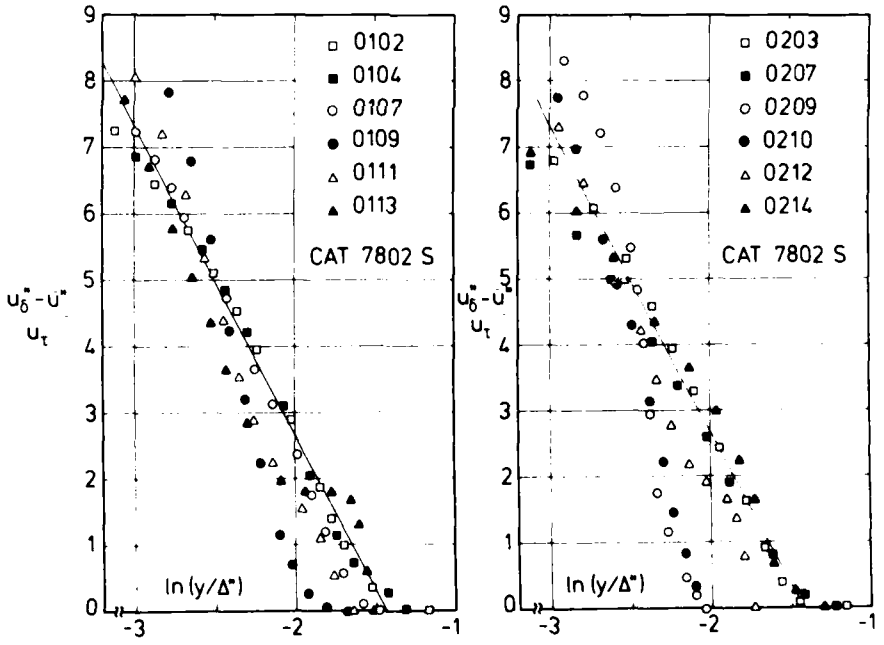

Fig. 5.3.7 Outer law for an axisymmetric compressible turbulent boundary layer (adiabatic wall, variable pressure gradient, origin not defined). Kussoy et al.(1978). c_f from heated-wire gauge.

In the outer region plots (Fig.5.3.7) there seems to be a slightly greater delay before the influence of the pressure gradient is made apparent. For series 01, profiles 01, 04 and 07 agree well with the zero-pressure gradient law. Profile 0109, however, shows very strong adverse pressure gradient characteristics, which are progressively relaxed in profiles 0111 and 0113, though with a very peculiar kink in the inner law plot (Fig.5.3.6.a). This may possibly be a result of the penetration of the outgoing compression wave by the incoming expansion wave.

For series 02, profiles 03 and 07 agree with the zero-pressure gradient law though 07 is not fully typical in the inner region - in the log-law plot, Fig.(5.3.6.b) the shape of this profile is also a little odd. Profiles 0209 and 0210, respectively in the middle and towards the end of the adverse-pressure region as measured at the wall, show a very strong adverse-pressure gradient behaviour, with 0210 tending very slightly to return towards the zero-pressure gradient line. Profile 0212, at the end of the wall zero-pressure gradient region, and affected in its outer region by the incoming expansion wave - it shows a point of inflection which it is tempting to compare with the kink in 0113 - is well back towards the zero-pressure gradient line while 0214 is tending to lie on the other side as it begins to develop favourable-pressure gradient characteristics (cf. Fig.5.2.4) .

The picture generally is confused by the uncertainty in the skin friction measurements, which should not affect the outer law plot very strongly, and by the inevitable complexity of a flow field with superposed wave structures.
In the remaining cases, either static pressure was not measured, or the pressure gradients were not strong enough for it to become necessary to analyze the flow in such detail.

Naleid's experiment (1958) represents an early attempt to determine the influence of pressure gradients on skin friction and on the Preston tube calibration. The profiles presented were measured at the same station on the floor of a wind tunnel in different mild pressure gradients with approximately the same edge state. The skin friction values associated with these velocity profiles were measured directly with a floating element balance. We only show a comparison of the measurements with the logarithmic law (Fig.5.3.8), since the pressure gradient has little effect either in the log-law region or in the outer region in this case.

Waltrup & Schetz (1971) performed their investigation on the bottom nozzle block and test section wall of a wind tunnel. Pressure gradients were imposed by three ramps of the full tunnel width which were mounted in the centre of the tunnel . The test boundary layer had undergone a largely two-dimensional expansion in the nozzle . Spark schlieren photographs clearly established, however, that the boundary layer was turbulent.

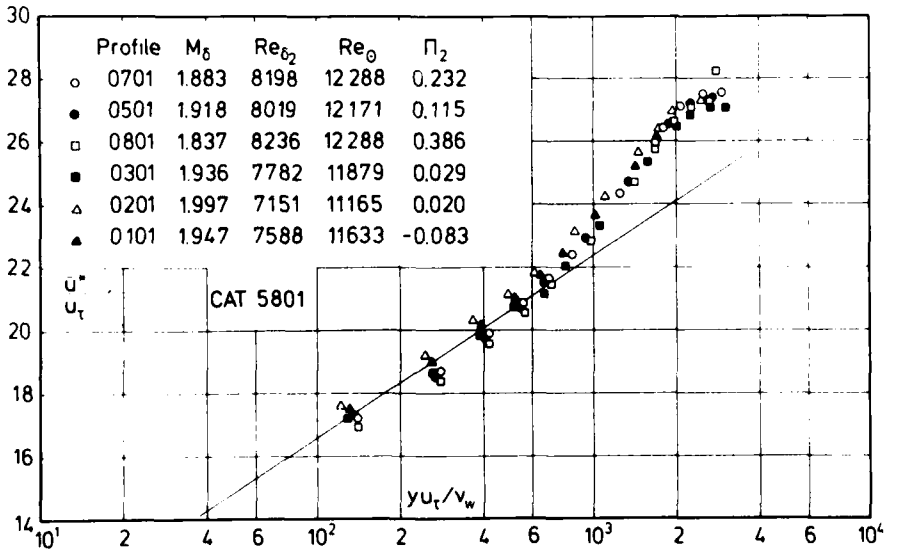

Fig. 5.3.8 Law of the wall for a compressible boundary layer (adiabatic wall, adverse pressure gradient, origin not defined). Naleid(1958). c_f from FEB.

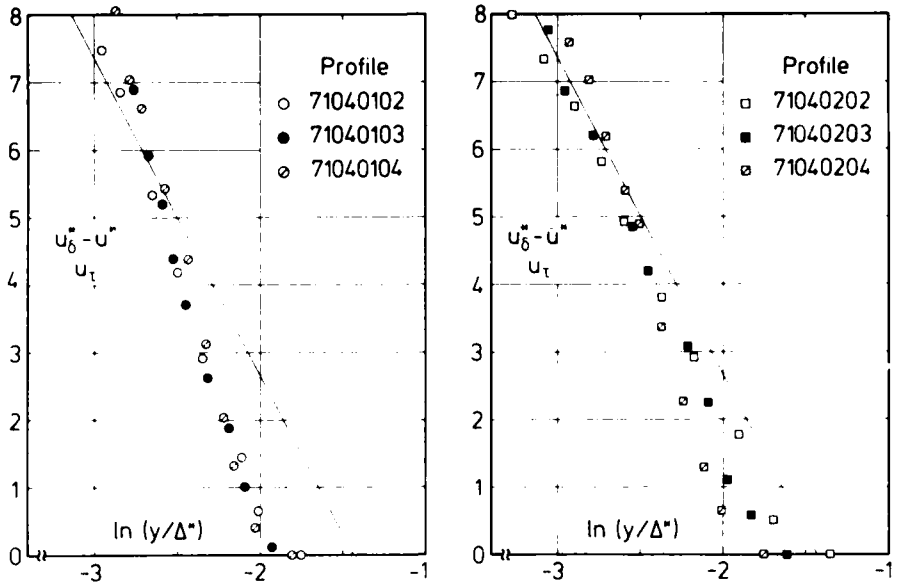

Fig. 5.3.9 Outer law for a compressible turbulent boundary layer in an adverse pressure gradient (adiabatic wall, origin not defined) Waltrup & Schetz (1971).

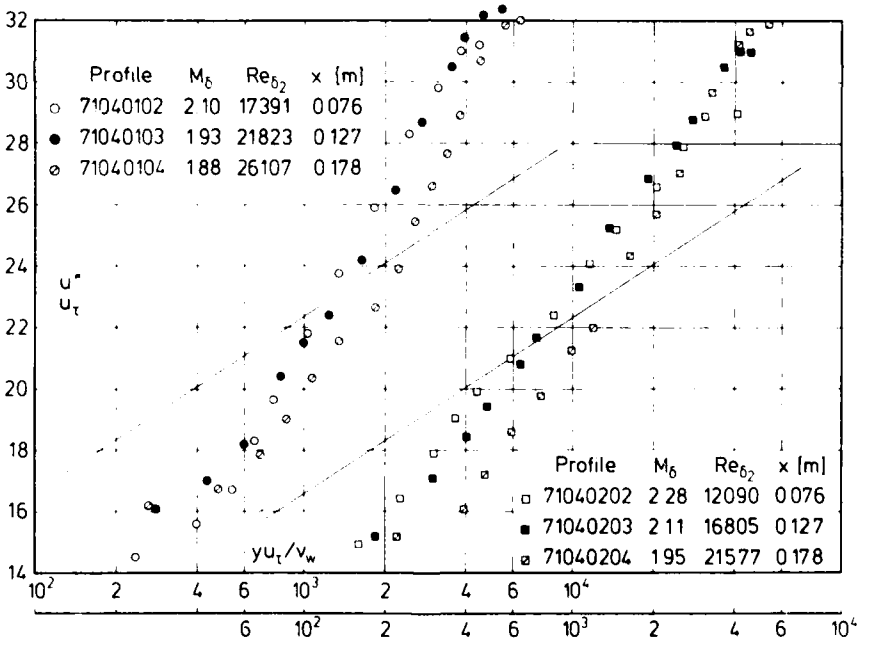

Fig. 5.3.10 Law of the wall for a compressible boundary layer (adiabatic wall, adverse pressure gradient, origin not defined) Waltrup & Schetz (1971). c_f from FEB. Two different pressure gradient developments.

The profiles presented consist of three sets - two of which are shown in Figs.(5.3.9 and 5.3.10) - each representing the development of the layer under a different pressure gradient. The outer law plot shows the adverse pressure gradient behaviour of the velocity profiles (Fig.5.3.9) whereas the velocity profiles do not apparently exhibit a log-law region in Fig.(5.3.10). It is possible that this is a consequence of using a moment sensitive (i.e. pivoted) balance in a relatively strong pressure gradient so that a moment is produced by the pressure field on the face of the balance element (parallel-flexure balances are not

sensitive to pressure gradient induced error - see Winter 1977). The pressure gradient was not strong enough to cause separation in the boundary layer, so that a distinguishable log-law region should exist.

Thomas(1974) has investigated boundary layers in favourable (Figs.5.2.3 and 5.2.4) and adverse pressure gradients on a flat surface facing one of a number of contoured nozzle blocks. For the zero pressure gradient experiment in the same test section the reader is referred to Jeromin(1966). As mentioned in section 5.2 the principal uncertainty here must be the question of three-dimensionality, as the length to width ratio of the experimental surface is over 5:1. The profiles are given in fine detail as can be seen from Fig.(5.3.11) where agreement between measurements and the logarithmic law is very good. The profiles

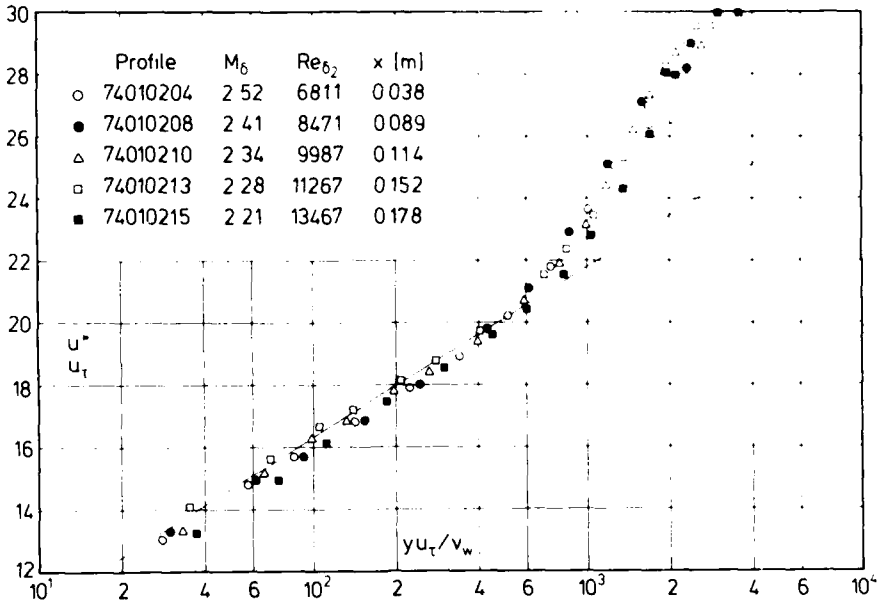

Fig. 5.3.11 Law of the wall for a compressible turbulent boundary layer (adiabatic wall, adverse pressure gradient, origin not defined) Thomas (1974). c_f from razor blade technique.

show a long linear region and values for the wake strength (Δ ($\bar{u}^*/u_\tau$) $\sim$ 5.5) which are considerably higher than most results for zero-pressure gradient boundary layers in the same Reynolds number range (cf. Figs. 3.3.4 and 3.3.6). This is in agreement with results obtained in subsonic boundary layers. The wall shear stress was estimated using the razor-blade technique after Smith et al.(1962) and the sensors were calibrated against the Spalding & Chi (1964) skin friction correlation for boundary layers in zero pressure gradient flows. Although one may have reservations about this calibration method, the results as seen in Fig.(5.3.11) are convincing. Fig.(5.3.12) shows a comparison between the outer law and the measurements, which cross the theoretical curve with a greater negative slope - as expected for velocity profiles in an adverse pressure gradient.

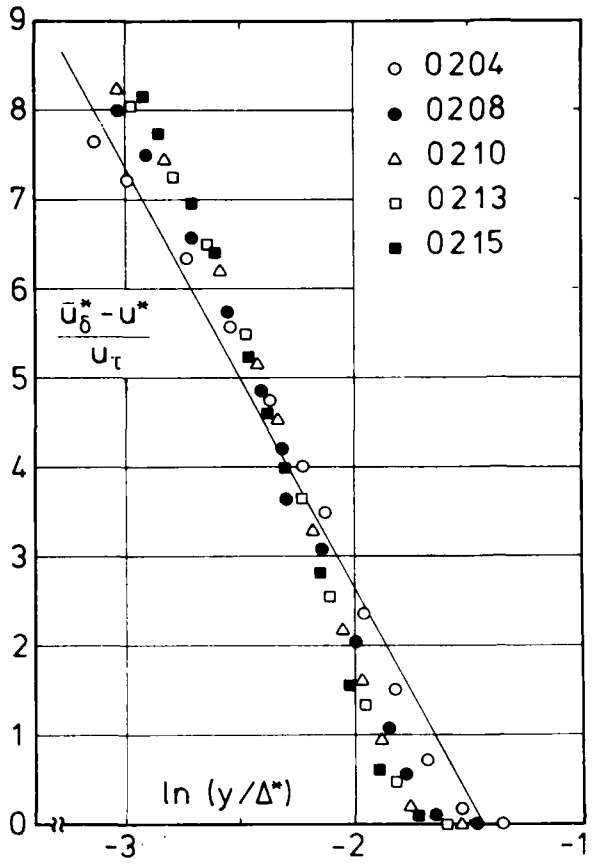

Fig. 5.3.12 Outer law for a compressible boundary layer (adiabatic wall, adverse pressure gradient, origin not defined). Thomas (1974). c_f from razor blade technique.

The last experiment in this group is that of Zwarts (1970). The test boundary layer was formed on the floor of the 0.127 m square wind tunnel and the test section started about 0.75 m downstream of the nozzle throat. A contoured splitter plate was designed by the method of characteristics to give a Mach number distribution on the tunnel floor such that the initial flow at M_δ = 4 passed through a constant Mach number gradient falling to M_δ = 3 over a distance of 0.15 m, followed by a second region of constant Mach number flow. Surface flow visualization tests showed that there was considerable flow convergence in the adverse pressure gradient region due to inflow from the tunnel sidewalls. Preston tube measurements at stations 38.1 mm to either side of the centre line showed differences in skin friction of up to 10 % from the centre line value. The author offers skin friction values deduced from several calibration functions (data evaluated from the Hopkins & Keener method (1966) which gives the smallest c_f values were selected here). Agreement of the velocity profiles with

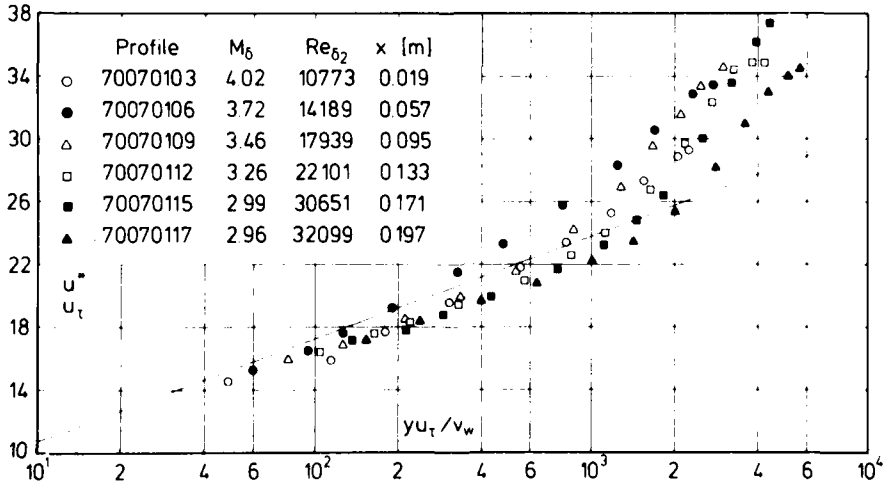

Fig. 5.3.13 Law of the wall for a compressible boundary layer (adiabatic wall, adverse pressure gradient, origin not defined) Zwarts (1970). c_f from Preston tube.

the logarithmic law is fair, all profiles lying low which means that the skin friction velocity is still too high (Fig.5.3.13) if agreement with the log-law should be reached.
The outer law plot (Fig.5.3.14) is typical, if more pronounced than Fig.(5.3.12) of an adverse pressure gradient boundary layer. Profile 0117 is in a near zero-pressure gradient but shows adverse-pressure gradient characteristics inherited from the upstream flow, though it is relaxing towards the zero-pressure gradient curve.

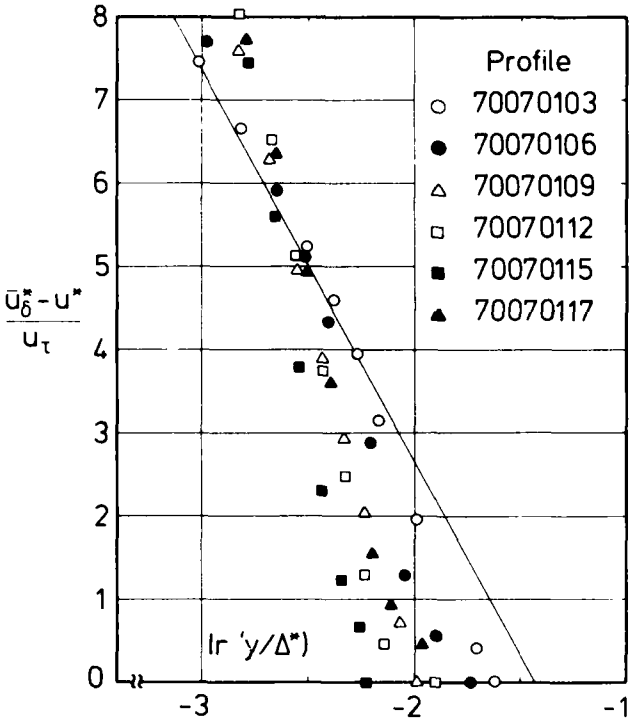

Fig. 5.3.14 Outer law for a compressible turbulent boundary layer in an adverse pressure gradient (adiabatic wall, origin not defined) Zwarts (1970).

5.3.2. Simple wave - curved wall

This section deals with pressure gradient cases in which the pressure gradient is the result of streamline curvature. This is associated with a "simple wave" which may either be generated in the test-zone itself, and propagate downstream, or may be generated elsewhere and be propagated downstream so as to strike the test-zone. The curved mean flow of the simple wave cases is associated with normal pressure gradients, which at high Mach numbers become very large. There is very little available information on what effect this may have on the turbulent structure (CAT 7101 contains the only measurements of fluctuating quantities), but the effects are unlikely to be negligible. There are relatively few available accounts of simple wave flows, and this is especially unfortunate as the boundary layers on a hypervelocity vehicle will always experience locally-generated simple wave structures. The typical adverse pressure gradient case is the flow approaching an inlet where a concave surface gives rise to a generated simple compression wave. From among the three reported simple wave compression tests, Clutter & Kaups (CAT 6401), Stroud & Miller (CAT 6503) and Sturek & Danberg (CAT 7101) only the last one provides sufficient data to allow it to be used in our normal scheme of comparisons.

The boundary layer experiment performed by Sturek & Danberg (1971) took place on a ramp forming a continuation of the flat test wall opposite a flexible plate nozzle. The test section extended 0.56 m downstream from the nozzle exit plane and the curved ramp started with a faired step at x = 0.305 m. The test zone included a zero pressure gradient region before the ramp followed by a simple wave isentropic compression. Oil flow visualisation did not show appreciable divergence of the streamlines near the centre line, but streamlines near the side walls diverged considerably. The main portion of the data consists of three

sets of eight profiles, each set for a different reservoir pressure. In each case (series 02 and 03 are discussed here) three zero pressure gradient stations were followed by five on the curved ramp. The wall shear stress was determined using a Preston tube and the Yanta et al.(1969) calibration curve. The velocity profiles are plotted in inner law coordinates in Figs.(5.3.15) and (5.3.16) with the adverse pressure

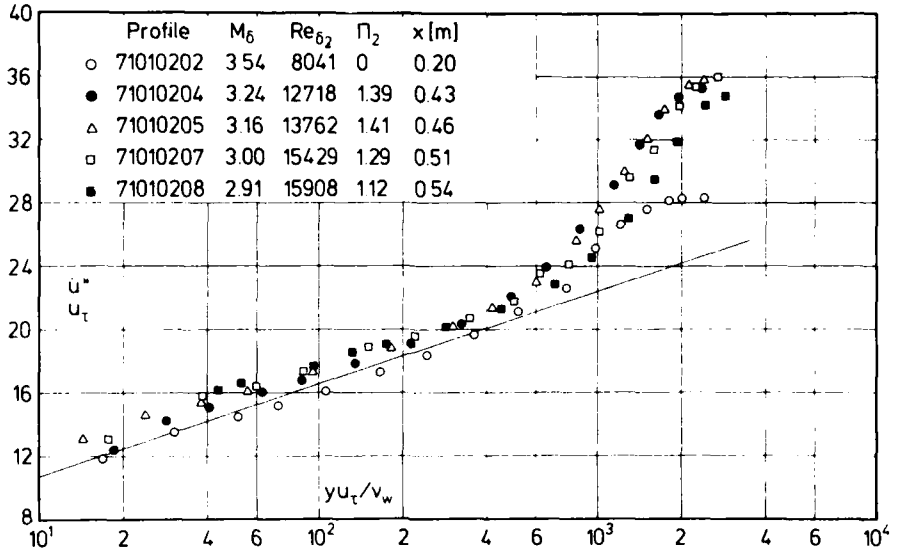

Fig. 5.3.15 Law of the wall for a compressible boundary layer (adiabatic wall, adverse pressure gradient, origin not defined). Sturek & Danberg (1971). c_f from Preston tube.

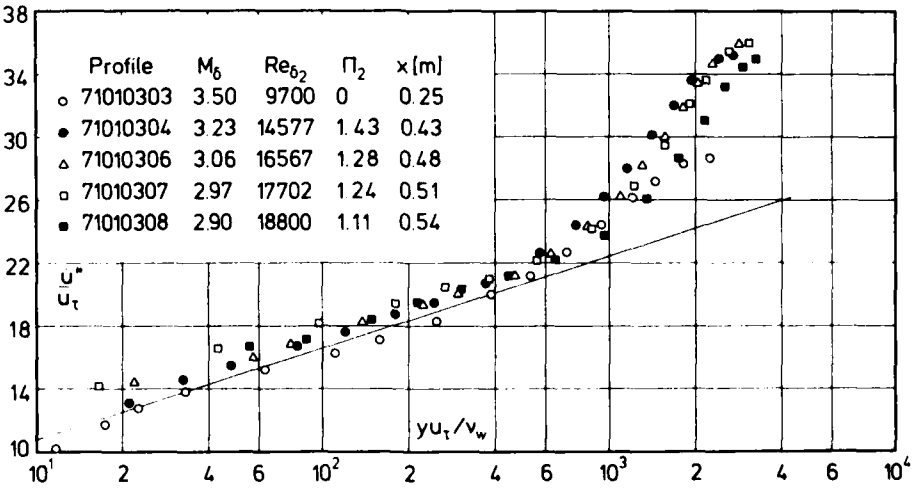

Fig. 5.3.16 Law of the wall for a compressible boundary layer (adiabatic wall, adverse pressure gradient, origin not defined). Sturek & Danberg (1971). c_f from Preston tube.

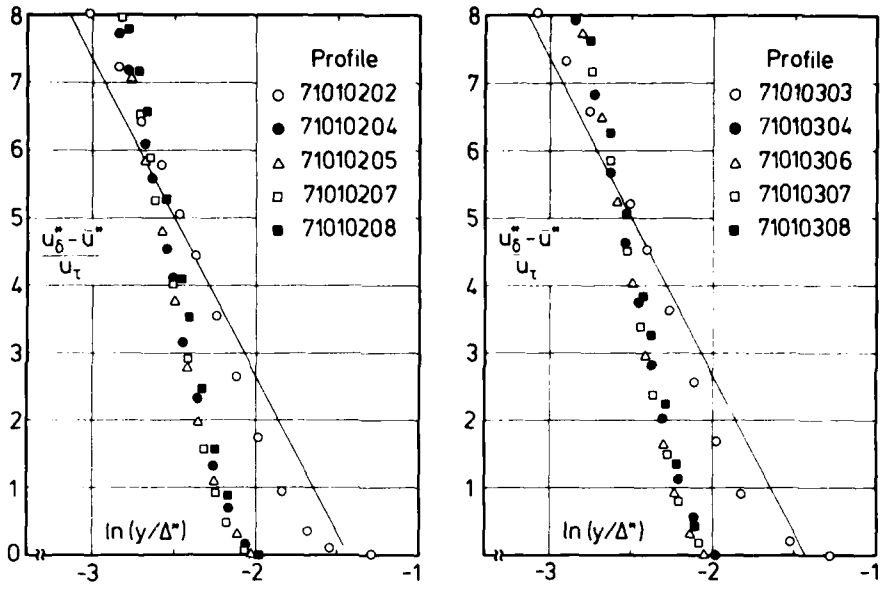

Fig. 5.3.17 Outer law for a compressible turbulent boundary layer in an adverse pressure gradient (adiabatic wall, origin not defined). Sturek & Danberg (1971).

gradient profiles lying above the logarithmic law (although within the normal scatter band) whereas the zero pressure gradient profile lies slightly below the log law. The wake strength is much larger than for the profiles in Fig.(5.3.11) but so is the pressure gradient parameter Π_2. This behaviour of the velocity profiles in a moderate adverse pressure gradient is confirmed by the outer law plot shown in Fig.(5.3.17).

Finally we show two sets of profiles measured on a waisted body by Winter et al.(CAT 7004). In addition to the simple wave pressure gradient induced by longitudinal curvature there are probably strong convergence and divergence effects resulting from the large proportional change in transverse curvature (the value of δ/R is not so high as to make transverse curvature itself a dominating feature).
Skin friction was determined by the razor blade technique. The profiles appear to have little or no systematic relationship to the wall law (Figs.5.3.18 and 19) and it is only possible to say that the flow is so complex, with history effects, simple wave pressure gradient, and convergence - divergence all superimposed, that it would not be profitable to assign the large differences observed to any one of these.
We have the same difficulty in arriving at any conclusions when inspecting the outer region profiles (Figs.5.3.20 and 21) but nevertheless present them for information.

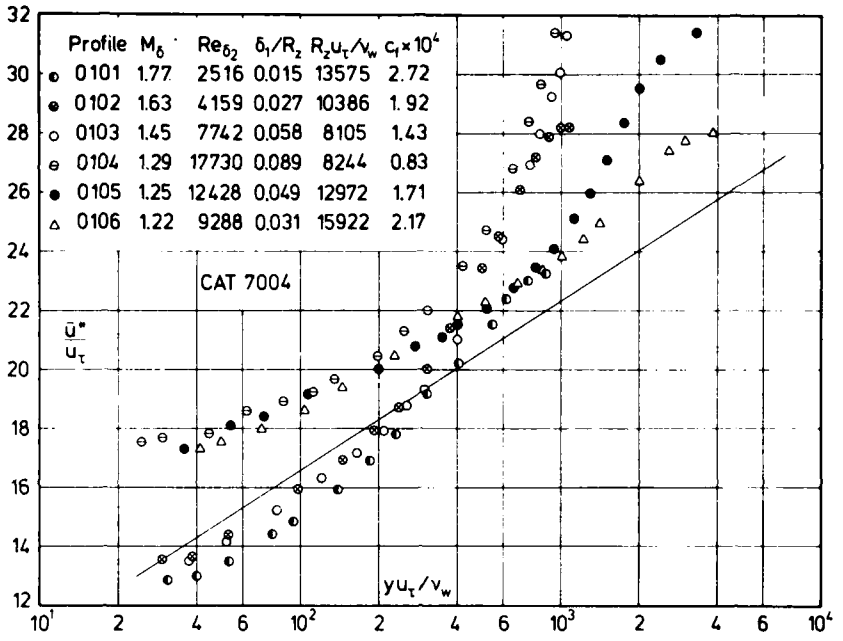

Fig. 5.3.18 Law of the wall for an axisymmetric compressible boundary layer (adiabatic wall, variable pressure gradient, defined origin). Winter et al.(1970).

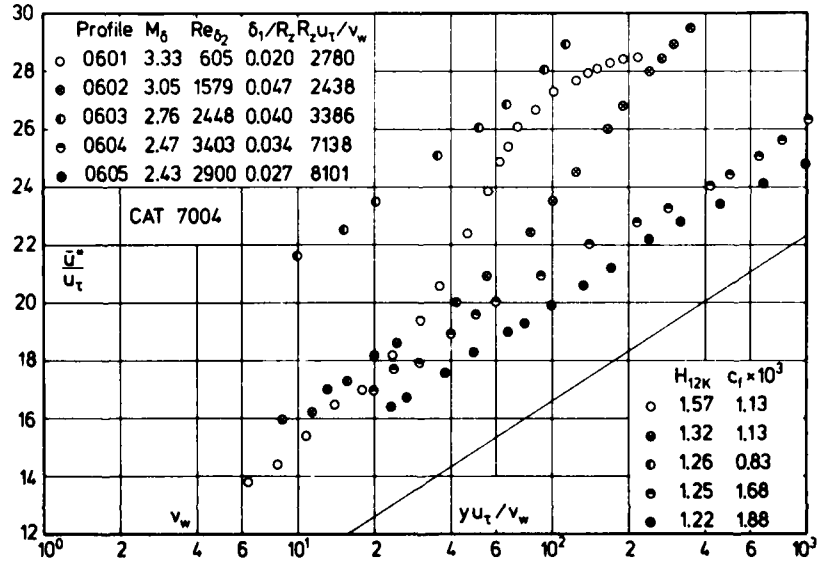

Fig. 5.3.19 Law of the wall for an axisymmetric boundary layer (adiabatic wall, variable pressure gradient, defined origin). Winter et al. (1970).

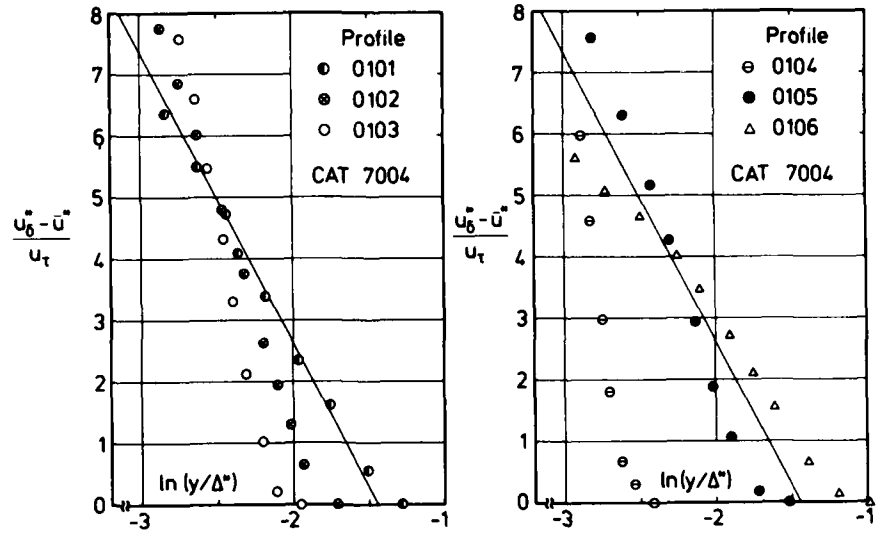

Fig. 5.3.20 Outer law for an axisymmetric compressible boundary layer (adiabatic wall, variable pressure gradient, defined origin). Winter et al.(1970).

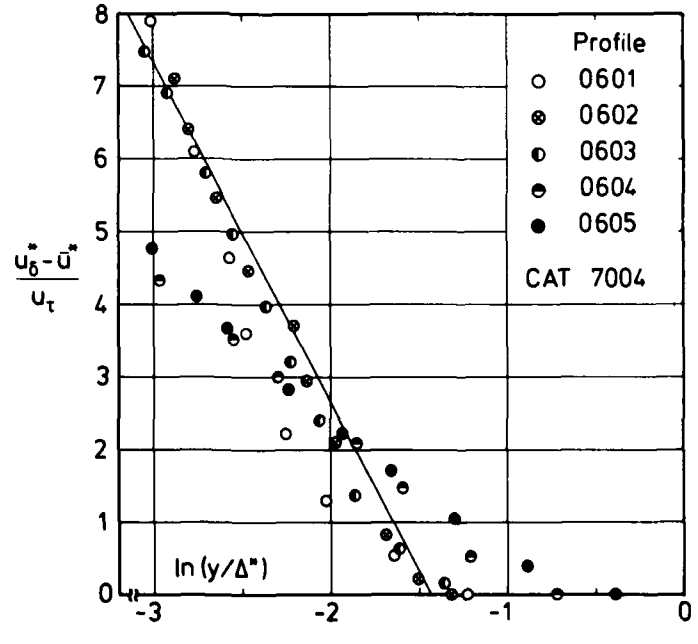

Fig. 5.3.21 Outer law for an axisymmetric compressible boundary layer (adiabatic wall, variable pressure gradient, defined origin). Winter et al.(1970).

5.4 Conclusions

a) We have discussed the results of about fourteen experiments in pressure gradients and compared the profiles to the inner and outer laws for the zero-pressure gradient case. The picture which results is somewhat confusing, so that any conclusions here are only tentative.

b) The law of the wall in transformed coordinates does hold for flows with moderate favourable and adverse pressure gradients on adiabatic walls. We have not examined flows close to separation or re-laminarization.

c) The law of the wall in transformed coordinates would seem to apply erratically to flows on cooled isothermal walls in moderate pressure gradients. The cases with substantial disagreement appear to be associated with Reynolds numbers $Re_{\delta 2}$ below 2000, in some cases ranging below 400. The experiment of Perry & East is, even among these cases, of a special kind.

d) For all experiments with Mach numbers above about 5 in accelerated flows, the nozzle wall studies, the $Re_{\delta 2}$ values were low, in some cases very low indeed. The boundary layers studied were not fully turbulent and displayed transitional characteristics.

e) The outer law as specified by eqn.(3.3.17) provides a useful indicator of pressure gradient effects. In a favourable pressure gradient the negative slope on our usual plot becomes less, giving values which lie above the zero pressure gradient curve in the outer region. In contrast, the data for an adverse pressure gradient show a greater negative slope with values below the zero pressure gradient law in the outer region.

f) Wall shear stress values should be regarded with suspicion, as the extent to which zero pressure gradient Preston tube calibrations may be used has yet to be established, and floating element balances operating on the moment principle are subject to errors which are not in general allowed for (Winter 1977).

g) Measurements are needed in adverse pressure gradients with heat transfer for a cooled isothermal wall, and for all pressure gradients with wall temperature varied in a controlled manner.

6. NORMAL PRESSURE GRADIENTS

We have, at various points above (§§ 2.3, 5.1) remarked that in compressible flows quite large pressure gradients may be observed normal to the wall on which a boundary layer has formed. In this section we attempt to predict the likely occurrence and magnitude of such pressure variations by an examination of the root causes. We will first consider the pressure field in various types of ideal flow, and then see in what way 'inviscid' flow features are modified by the presence of the boundary layer. At hypersonic speeds we will further note that Reynolds stresses may become significant compared to the mean static pressure, while the boundary layer itself may well induce relatively large changes in the free stream flow. Together, the various normal pressure gradient effects can cause serious difficulties in the interpretation of results, both directly by their effect on pressure and density values, and less obviously through the difficulty found in specifying reference qualities.

6.1 Normal Pressure gradients in ideal flow

In this section, and elsewhere throughout this report excepting § 6.3,distinction will be made between "pressure" and "normal stress". (In all cases, what is referred to as a pressure gradient should actually be more strictly called a normal stress gradient.) Outside the boundary layer, the "pressure gradients" are uniquely related to the local fluid accelerations. In natural coordinates for a steady flow

$$(\partial\bar{p}/\partial s) = -\bar{\rho}\,\bar{u}(\partial\bar{u}/\partial s) \tag{6.1.1}$$

and

$$(\partial\bar{p}/\partial n) = -\bar{\rho}\,\bar{u}^2/R \tag{6.1.2}$$

where $\bar{u}$ is the velocity and s the distance along the streamline, n is distance measured normal to the streamline, and R is the radius of curvature (n and R taking the same sign for concave curvature).

At high speeds the static pressure $\bar{p}$ becomes small compared to $\bar{\rho}\,\bar{u}^2$ or the total pressure $\bar{p}_0$, and $(\partial\bar{p}/\partial n)$ (eqn. 6.1.2) may become relatively large even for large values of R. If $(\partial\bar{p}/\partial n)$ is taken as constant over a small distance, such as the boundary layer thickness δ, in the n direction, the pressure difference is given approximately by

$$\frac{\Delta\bar{p}}{\bar{p}} \simeq \frac{\delta}{\bar{p}}\frac{\partial\bar{p}}{\partial n} = -\gamma M^2\left(\frac{\delta}{R}\right) \tag{6.1.3}$$

and it is easy to see how, even at modest Mach numbers, significant changes in pressure can occur across a boundary layer on a curved wall. As an example, consider the ramp flow studied by Sturek & Danberg (CAT 7101) where a 20% static pressure variation is found across the boundary layer with an edge Mach number of about 3.

In natural coordinates a transverse pressure gradient occurs only in a curved flow. The quantities required to determine it are, however, not generally available - for instance it is difficult to imagine a simple way of measuring R - while the direct measurement of $\bar{p}$ in the flow field is often extremely difficult. It is particularly helpful therefore to relate the transverse pressure gradients to the longitudinal gradients, as on the wall streamline it is relatively simple to measure the latter. It is also helpful to generalize this relation in attempting to account for - or exclude - certain secondary effects.

In all sections below, we define the "normal pressure gradient" in local cartesian coordinates as the variation of pressure along the local, straight, normal y to the surface on which the boundary layer is growing, x being the coordinate along the surface in the stream direction. Then since $\bar{p}$ is a function of x and y only

$$\left(\frac{\partial\bar{p}}{\partial y}\right)_x \left(\frac{\partial y}{\partial x}\right)_{\bar{p}} \left(\frac{\partial x}{\partial\bar{p}}\right)_y = -1 \tag{6.1.4}$$

and any attempt to link the normal pressure gradient $(\partial\bar{p}/\partial y)$ to the streamwise pressure gradient $(\partial\bar{p}/\partial x)$

may be reduced to an attempt to trace the isobars $(\partial y/\partial x)_{\bar{p}}$.

6.1.1 The simple wave

Any flow in which changes of property are found along only one of the two families of characteristics (Mach lines) will be described as a simple wave flow. Such a wave structure is generated when a flow, hitherto uniform, flows over a cruved wall and the isobars are then formed by the downstream running family of characteristics (we assume here that these do not coalesce to form a shock). A streamline of such a "generated" simple wave can in principle be replaced by a solid wall, and its curvature will then be such as to cancel the wave structure which approaches it from upstream. The isobars are thus the family of characteristics approaching from upstream. For a simple wave flow, therefore, close to the wall along which x is measured,

$$(\partial\bar{p}/\partial y) = \mp \cot\mu \left(\frac{\partial\bar{p}}{\partial x}\right) \qquad (6.1.5)$$

where μ is the Mach angle and the -sign refers to a generated wave, the + sign to be cancelled wave (Fig. 6.1.1).

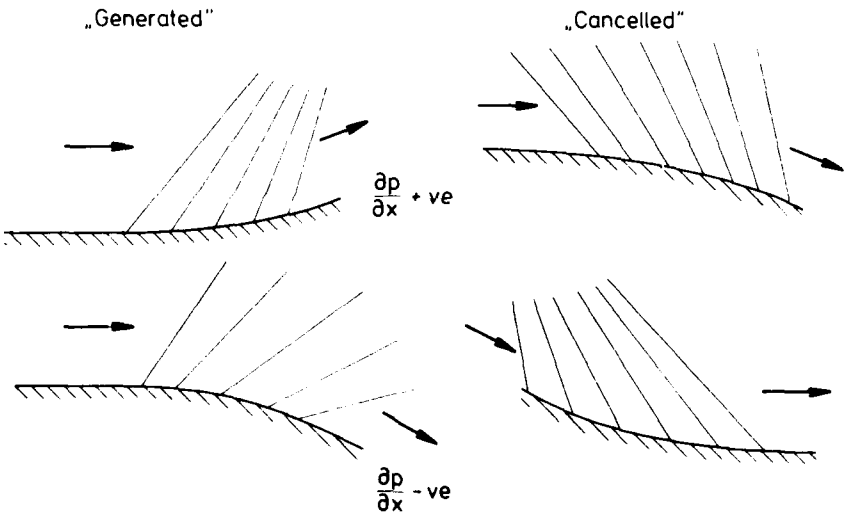

Fig. 6.1.1 Relationship between pressure gradient and curvature for "generated" and "cancelled" simple waves. Boundary layer effects not represented.

A generated wave is formed, for example, by the first curved ramp or centre body of a supersonic engine intake, while the designer of the "bell" or downstream divergent portion of a contoured nozzle will aim to exactly cancel the wave structure generated in the throat region.

Equation 6.1.5 may be rearranged to give the "ideal flow" normal pressure gradient as

$$(\partial\bar{p}/\partial y) = \mp (M^2-1)^{\frac{1}{2}} (\partial\bar{p}/\partial x) \rightarrow \mp M \frac{\partial\bar{p}}{\partial x} \qquad (6.1.6)$$

or

$$\frac{1}{\bar{p}} \frac{\partial\bar{p}}{\partial y} = \cdot \frac{(M^2-1)^{\frac{1}{2}}}{M} \frac{\gamma M^2}{1 + \frac{\gamma-1}{2} M^2} \frac{\partial M}{\partial x} \rightarrow + \frac{2\gamma}{\gamma-1} \frac{\partial M}{\partial x} \qquad (6.1.7)$$

where the high Mach number limit is indicated by the arrow. If it is assumed that the flow direction and curvature near the wall do not vary too rapidly, eqns. (6.1.5 - 6) allow $(\partial\bar{p}/\partial y)$ to be estimated from the pressure variation along the wall.

We emphasize that eqns. (6.1.5 - 7) apply only to a simple wave flow characterised by streamline curvature. The direction of flow changes in accordance with

$$\frac{1}{R} \doteq \frac{\partial\theta}{\partial s} = \pm \frac{\partial\nu}{\partial s} \qquad (6.1.8)$$

where θ is the flow direction and ν is the Prandtl-Meyer angle. Streamwise property gradients may also occur without change of direction, as described in the next section, and eqns. (6.1.5 - 8) do not apply to these "reflected wave" structures.

6.1.2 The reflected wave

If the rates of change of properties are equal along both sets of characteristics, the streamline deflection θ in eqn. (6.1.8) due to one set exactly opposes that resulting from the other end and the streamline remains a straight line. This streamline could be replaced by a straight wall, when the two sets of characteristics are represented by the approaching wave structure together with its reflection at the wall. We will refer to such a region of superposed wave structures as a "reflected wave". As an example, consider the simple wave structure and its reflection shown in Fig.(6.1.2). Within the region ABC the transverse components of the two simple waves oppose each other, and to the first order cancel out.

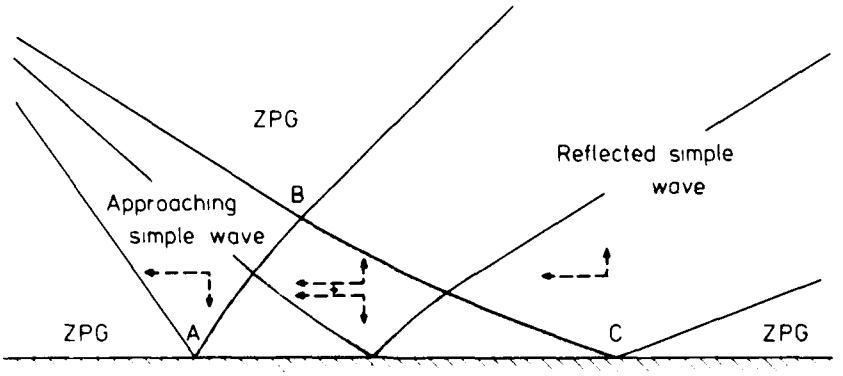

Fig. 6.1.2 Reflection of a simple wave structure at a straight wall. The boundary of the region defined here as a "reflected wave" is indicated by stippling. Boundary layer effects not represented.

A "pure" reflected wave as defined in these terms would be produced in a radial "source flow", for which the streamlines are straight and all originate from the vertex, or virtual origin of the flow (Fig. 6.1.3). The isobars are circles centred on the vertex so that

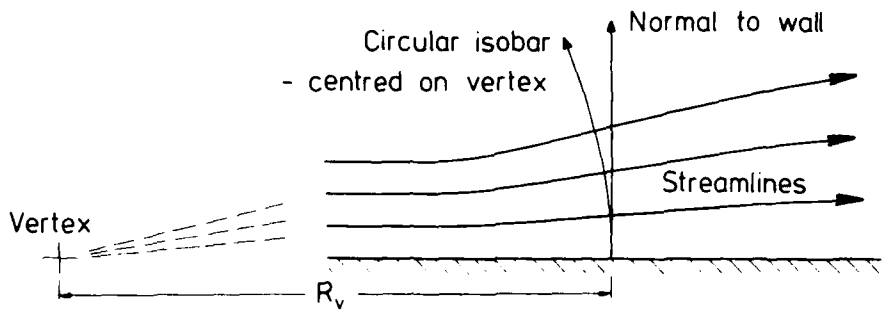

Fig. 6.1.3 Departure of the isobar from the profile normal in a region of local radial flow. Boundary layer effects not represented.

$$(\partial x/\partial y)_{\bar{p}} = - y/R_v \tag{6.1.9}$$

where R_v is the distance from the vertex. Thus for such a flow

$$(\partial \bar{p}/\partial y) = \frac{y}{R_v} (\partial \bar{p}/\partial x) \tag{6.1.10}$$

and substituting the isentropic flow relations

$$\frac{1}{\bar{p}} \frac{\partial \bar{p}}{\partial y} = - \frac{iy}{R_v^2} \frac{\gamma M^2}{M^2-1} \rightarrow - \frac{i\gamma y}{R_v^2} \tag{6.1.11}$$

where i is 1 for planar and 2 for conical flow, while the arrow again indicates the high Mach number limit.

Other forms in which the distance from the vertex is eliminated, so as to give $(\partial \bar{p}/\partial y)$ in terms of local quantities only, are

$$\frac{1}{\bar{p}} \frac{\partial \bar{p}}{\partial y} = - \frac{y}{i} \frac{M^2-1}{\gamma M^2} \left(\frac{1}{\bar{p}} \frac{\partial \bar{p}}{\partial x}\right)^2 \rightarrow \frac{-y}{i} \left(\frac{1}{\bar{p}} \frac{\partial \bar{p}}{\partial x}\right)^2 \tag{6.1.12}$$

or

$$\frac{1}{\bar{p}} \frac{\partial \bar{p}}{\partial y} = - \frac{y}{i} \frac{\gamma(M^2-1)}{\left(1 + \frac{\gamma-1}{2} M^2\right)^2} \left(\frac{\partial M}{\partial x}\right)^2 \rightarrow \frac{-4\gamma y}{i(\gamma-1)^2} \left(\frac{1}{M} \frac{\partial M}{\partial x}\right)^2 \tag{6.1.13}$$

This apparent pressure gradient arises essentially from the increasing divergence of the isobar from the "straight" profile normal, as y increases (Fig. 6.1.3). In a true radial flow of the type leading to eqn. 6.1.11, it can be seen that only small pressure differences across a boundary layer could result. A typical layer growth rate is of the order of 10^{-1} radian so that from eqn. (6.1.11) the proportional

change in pressure ($\Delta\bar{p}/\bar{p}$) is about 10^{-2}. It is however, possible to impose a concentrated wave structure on to a thick boundary layer in such a way that the local virtual R_v is very much less in relation to δ than for the true source flow. An estimate of the "reflected wave" contribution can then be made from eqns. (6.1.12) or (6.1.13). In general the detailed distribution of pressure in the imposed wave structure will not produce an exact cancellation of the simple wave element throughout the region of interaction - exact cancellation is imposed only at the wall - so that such a concentrated wave structure may well induce substantial streamline curvature quite close to the wall (e.g. Zakkay & Wang, CAT 7208, Rose, CAT 7306S, Kussoy et al., CAT 7802S). Where curvature is pronounced, the pressure changes associated with it will always dominate the "apparent" gradients associated with a fully cancelled structure.

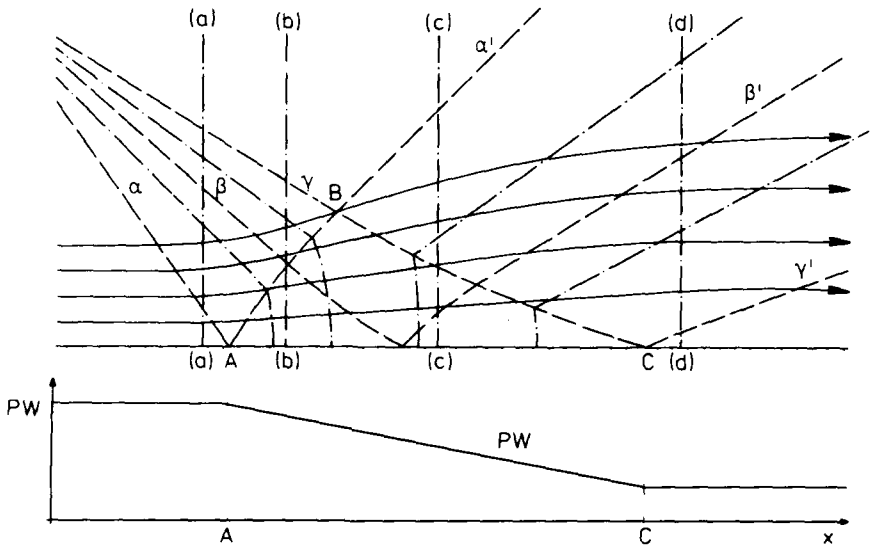

Fig. 6.1.4 Streamline and isobars for the reflection of a simple wave expansion at a straight wall:- (a)-(d), representative profile normals —·— ;α-γ, characteristics, and their reflections α'-γ' — — ; isobars —·— and streamlines ——. Boundary layer effects not represented.

6.1.3 Changes in pressure gradient

Figure (6.1.4) shows the characteristics of Fig. (6.1.2) together with the associated streamline pattern. It is assumed that the wave structure is such that within ABC cancellation is complete. In the simple wave regions the characteristics are straight and the streamlines curved, while in the reflected wave region the opposite is true. The inclination of the isobars to the normal is low in ABC, changing abruptly at the boundary to take up the inclination of the characteristics in the simple wave region. Any traverse which is completed within ABC will show only the relatively small normal pressure changes associated with the local radial flow, while any traverse penetrating the simple wave regions will show the much greater gradients associated with curvature. It is therefore possible to make a traverse in a region where both ($\partial\bar{p}/\partial x$) and ($\partial\bar{p}/\partial y$) are zero near the wall - such as traverse (a) - which will at quite small values of y start to show a large normal pressure gradient. Reference to Fig. (6.1.2) shows how within ABC the streamwise components of the pressure gradient reinforce while the transverse components cancel. It can be seen therefore, that the normal pressure gradient on the profile normal (a), associated with the change from zero pressure gradient to the reflected pressure gradient from A to C, has one half of the magnitude of a simple wave producing the streamwise pressure gradient which is found along the wall just after A. That is, where SW denotes a simple wave and RW a reflected wave.

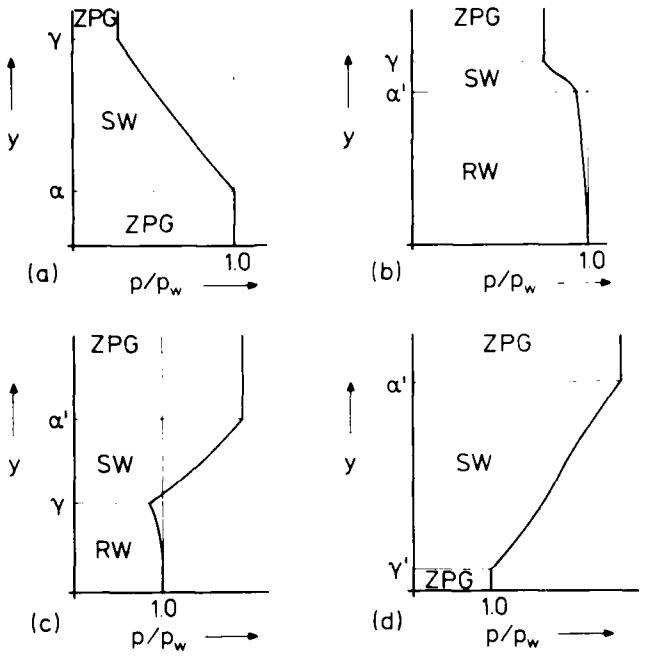

Fig. 6.1.5 Schematic static pressure profiles at various streamline stations for a simple wave expansion. Not to scale. Profile normals (a)-(d) and characteristics α-γ,α'-γ' as in Fig. (6.1.4). Boundary layer effects not represented.

$$\left(\frac{\partial \bar{p}}{\partial y}\right)_{(a),SW} = \frac{1}{2} \cot \mu_A \left(\frac{\partial \bar{p}}{\partial x}\right)_A \text{(Along AC, RW)} \qquad (6.1.14a)$$

while the corresponding relationship at the downstream end, profile normal (d), is

$$\left(\frac{\partial \bar{p}}{\partial y}\right)_{(d),SW} = -\frac{1}{2} \cot \mu_C \left(\frac{\partial \bar{p}}{\partial x}\right)_C \text{(Along AC, RW)} \qquad (6.1.14b)$$

Figure (6.1.5) shows, qualitatively, the variation of static pressure on the four profile normals (a) - (d) of Fig. (6.1.4), in relation to the leading (α) and trailing (γ) characteristics of the incoming wave pattern and the outgoing wave (α', γ').

6.1.4 Concentrated disturbances

The discussion in § 6.1.3 above is based on the behaviour of wave structures which are large compared with a transverse characteristic dimension such as the boundary layer thickness. In test facilities concentrated disturbances of small scale are often present, caused by minor imperfections in the construction of the apparatus. Figure 6.1.6 shows how such changes of characteristic dimension very much less than the transverse dimension δ may give rise to pressure differences across the boundary layer up to double the size of the original disturbance. Special care should be taken in interpreting data from sources in which flow uniformity is specified in terms of Mach number, as for isentropic flow and an unreflected disturbance

$$\frac{\Delta \bar{p}}{\bar{p}} = -\frac{\gamma M^2}{\left(1 + \frac{\gamma-1}{2} M^2\right)} \frac{\Delta M}{M} \to \frac{-2\gamma}{\gamma-1} \frac{\Delta M}{M} \qquad (6.1.15)$$

so that a 1% discrepancy in M might give rise to a pressure difference of up to 14% across the boundary

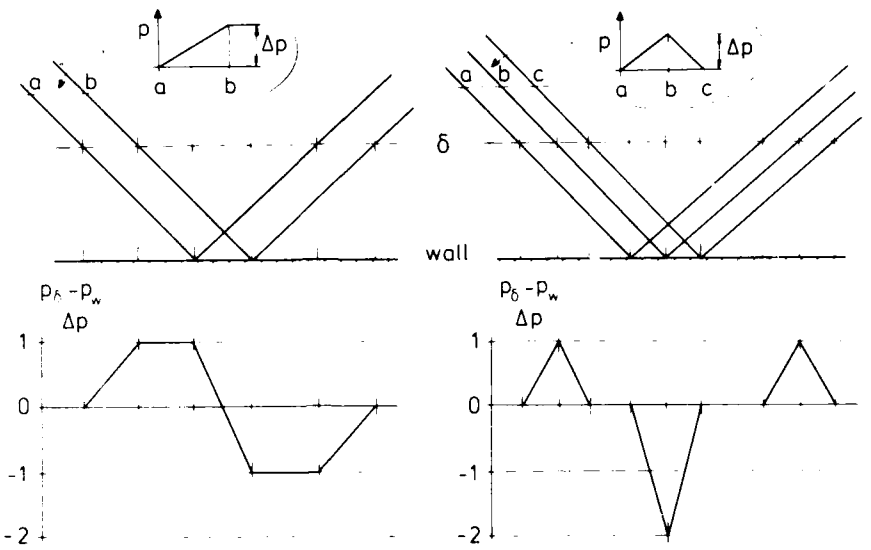

Fig. 6.1.6 Normal pressure differences across a 'boundary layer' (viscous effects not represented) caused by concentrated disturbances

layer at high M.

6.1.5 The "pure" normal pressure gradient

In § 6.1.1 we examined the normal pressure changes associated with a curved flow such that the streamwise rate of variation of Prandtl Meyer angle ν was equal to the rate of change of direction θ (eqn. 6.1.8). In § 6.1.2 the gradients associated with a compound wave structure such that the changes in θ cancelled while those in ν reinforced were assessed. It is also possible to superpose two wave structures in such a way that the changes in ν oppose while those in θ reinforce. The result is a "pure" normal pressure gradient flow with streamlines along which properties are invariant - as for instance at a free-jet boundary. It is important to recognise therefore that the absence of a longitudinal pressure gradient does not guarantee the absence of a normal pressure gradient. A special case of this type, for which an exact solution is possible (Bickley, in Howarth 1953, p. 158), is the "compressible free vortex", with circular streamlines. Equation 6.1.2, with the isentropic flow relations, gives the result

$$(r/r^*)^2 = 2(1 + \frac{\gamma-1}{2} M^2)/(\gamma+1)M^2 \qquad (6.1.16)$$

where r^* is the radius at which $M = .$ [As M tends to infinity, there is a minimum possible radius at which $(r/r^*)^2 = (\gamma-1/(\gamma+1).]$ Some of the flows studied by Thomann (CAT 6800) have domains of this type, and such investigations are potentially of great value in that they should allow the isolation of the effects of curvature and of normal pressure gradients. Attempts to set up and study such boundary layers have been made or are projected by Müller (1973 - Fig. 6.1.7) and Horton (1978).

6.2 Modifications to the ideal flow pattern caused by the boundary layer

The estimates of normal pressure gradients and differences in § 6.1 above assume that the flow is acted on by normal stresses only. If the isobars are to be traced through a boundary layer, it is necessary to examine the influence of shear stresses. We may then predict the resulting changes in the wave pattern

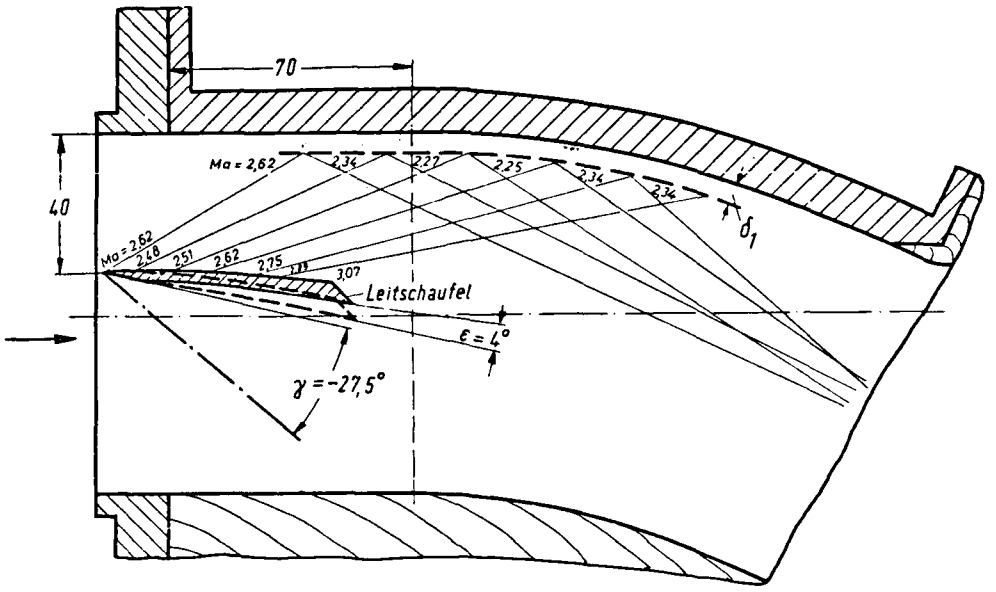

Fig. 6.1.7 Experimental arrangement intended to produce constant pressure along the displacement surface of a boundary layer (Facsimile from Müller, 1973)

as a whole, and so the likely pressure variations. The 'history' of all parts of the boundary layer can then be described.

6.2.1 Isobars in the boundary layer

In any boundary layer the velocity at small distances from the wall is low, so that in this region centripetal accelerations ($\overline{\rho}\ \overline{u}^2/R$) become negligible. The limiting tendency for any isobar must therefore be that it approach the wall normally, whether the wall is straight, when it would do so in any case, or curved, when in inviscid flow at high Mach numbers it would not (§ 6.1.1). As the isobar leaves the wall however, the velocity and, to a lesser extent, the density tend to their free stream values very rapidly (Figs. 2.1 1., 2.1.2) so that the isobar inclination soon approaches the ideal or free stream value.

A valuable discussion of the local behaviour of the isobars in rotational flow is given by Myring & Young (1968). Large isobar inclinations to the normal and hence large normal pressure differences are associated with curved, simple wave flows. For such a flow, Myring and Young showed that the effects of inherited vorticity and local shear stress are relatively small, and opposed in such a way that the isobar follows the local Mach line very closely. This conclusion perhaps needs modification at low Mach numbers ($M^2 < 2$), but in the high Mach number flows for which normal pressure gradient effects are marked, the low Mach number region lies close to the wall where the specific mass flow is very small. Even for a relatively low speed ($M_\delta \sim 3$) flow such as Sturek & Danberg (CAT 7101 - see § 6.2.2) the $M^2 = 2$ point lies closer to the wall than $\delta_1/2$.

Myring and Young find in a reflected wave that the isobar will pass closely through the successive intersections of equally stepped right and left running Mach lines, and so will be very nearly normal to the wall, as in ideal flow.

Since the local Mach lines curve towards the wall the effect of the boundary layer is to shift the effective generation, cancellation or reflection of any wave structure slightly upstream, and to reduce the pressure differences expected across the region occupied by the boundary layer from the values which would be predicted from ideal flow considerations alone. In this respect the effect is much the same as would be observed if the actual wall and boundary layer were to be replaced by an extension of the free stream flow into the outer part of the space occupied by the boundary layer with generation, cancellation or reflection of any wave structure at a stream surface corresponding to the displacement surface of the boundary layer.

The displacement surface here is to be interpreted as a stream surface of the free stream extended into the space in reality occupied by the boundary layer. The extension should take into account all wave structures in the free stream up- and down-stream of the station under consideration, and all such stream surfaces are in principle determinate if sufficient details of the free stream flow are known. The displacement surface then marks the inner boundary of an ideal mass flow equal to that of the original free stream and boundary layer. In general it will not be possible to determine the displacement surface directly, and practical approximations are discussed in § 7 below.

The isobars of a simple wave flow, therefore, are Mach lines of the free stream outside the boundary layer. As an isobar is followed into the boundary layer its inclination to the wall increases as the Mach number falls. If it is assumed to follow the local Mach line throughout the boundary layer, it will eventually become normal to a surface on which M = 1. This surface will, for modest to high free stream Mach numbers, lie very close to the wall - for the Sturek & Danberg (CAT 7101) flow described below, at y-values less than $\delta_1/20$. The subsonic flow between this M = 1 surface and the wall is relatively slow and of low density (the specific momentum flux for the Sturek & Danberg case at M = 1 is 10% of the boundary layer edge value, while at higher Mach numbers it is an even lower proportion) so that this portion of the curved flow can support only very small pressure differences and the isobar continues to the wall effectively normally.

6.2.2 Measurements of the static pressure field in a simple-wave flow

The behaviour described at the end of the previous section is best illustrated by a practical numerical example. There are very few flows for which static pressure measurements have been made at sufficiently close intervals for the pressure field to be properly described. The only fully documented simple wave case is the flow on a two dimensional ramp described by Sturek & Danberg (CAT 7101 - Fig. 6.2.1). A full description is given in AGARDograph 223, the essential feature being that a relatively thick boundary layer was grown under ZPG conditions (profiles 01-03- the original flow direction is shown by the arrow marked U_0) before passing on to a curved concave ramp (profiles 04-08). The static pressure field on the ramp, shown to scale in Fig. (6.2.1), is deduced entirely from measurements on the profile normals marked 04 - 08, and so depends partly on subjective factors introduced when cross-plotting and interpolating. The original data are however smooth and provided at close intervals, so that it is unlikely that substantial error has been introduced. The isobars are shown as the right-running set of curved Mach lines. The separation between the M=1 surface and the wall is of order 1% of the boundary layer thickness and could scarcely be shown at this scale. Also shown is a single left-running Mach line, while extrapolations of this and the right running Mach line or isobar which meets it at the wall are shown as reflected at the displacement surface. In the following section (§ 7) it will be shown that the δ_1 surface can not in fact be determined precisely. The surface shown here is a smoothed curve sketched through the "D STAR" values which represent the best estimate we can make. The essential difficulty lies in the requirement for values corresponding to an extension of the free stream flow into the boundary layer region as far as the δ_1 surface. The figure can not therefore show more than the plausibility of the general mechanism discussed above. It would however be very difficult to introduce a substantial change in the pattern shown while using the original data, and in succeeding sections we will describe the flow in terms of wave structures interacting with the displacement surface - which inevitably they affect as a result of the bulk compression and expansion resulting from their associated pressure changes.

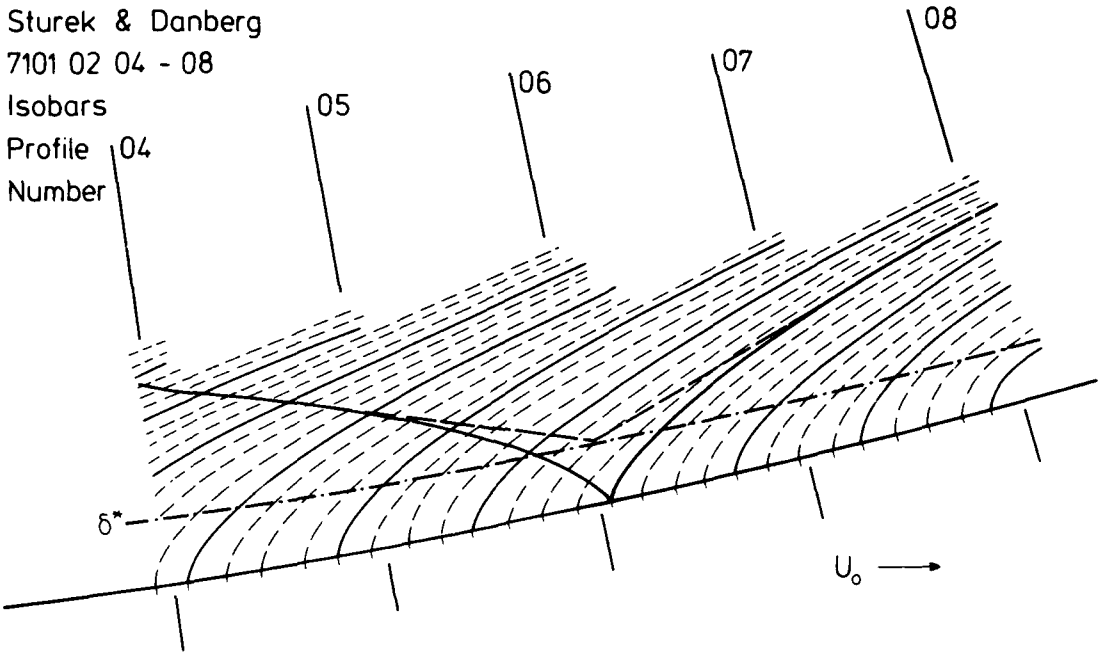

Fig. 6.2.1 Isobars for the flow on a curved planar ramp (Sturek & Danberg 1971). The pressure data are interpolated from the static pressure profiles CAT 7101 0104-8. The left running lines are a local incoming Mach Line (——) and an extrapolation of a corresponding free stream characteristic (— —).

6.2.3 Static pressure field measurement in a reflected wave flow

Kussoy et al (1978-CAT 7802S) provide detailed measurements in a reflected wave adverse pressure gradient flow. For the fully instrumented studies, two contoured centre-bodies were successively mounted on the axis of a cylindrical test section and traversed along the axis so as to permit measurements at up to 14 stations relative to the wave structure, using a single station traverse gear mounted in the test surface. In consequence there is some slight but systematic variation of the boundary layer entering the wave structure, and the 'reference', or 'first-' profiles of each set, which were measured with the centre bodies retracted, are not strictly part of each series. The pressure gradients were not so great as to cause positive pressure waves to coalesce into shock waves anywhere in the test zone, nor did separation occur. The data have already been discussed briefly above (Figs. 5.3.6, 5.3.7).

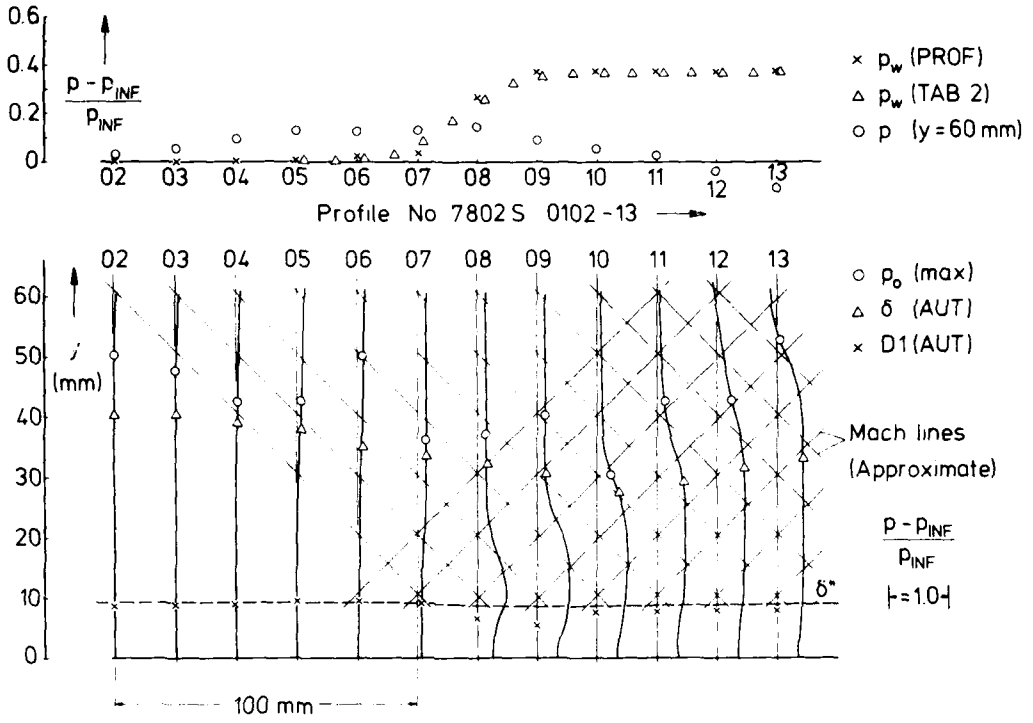

Fig. 6.2.2 Static pressure profiles for a straight wall adverse pressure gradient flow. (Kussoy et al., 1978 CAT 780S 0102-0113). Lower: profiles with (x), authors' δ_1 point; (– –), δ* (§ 7) displacement surface; (△), authors' boundary layer edge; (O), position of p_0 peak. Upper: longitudinal static pressure variation, (x), at wall from profile data; (△) at wall from pressure runs (authors' table 2); (O), at y = 60 mm, outside the boundary edge.

The static pressure fields are shown in the form of profile measurements in Figs. (6.2.2, 6.2.3). In each case the static pressure distribution in the flow direction at the wall (y = 0) is shown, as also are values for y = 60 mm corresponding to a traverse well outside the boundary layer. There are two values for p_w, depending on whether data are taken from wall pressure runs (labelled "Tab. 2") or from the profile runs. The differences are not great. In each case the wave structure produced by the centre body consists of a compression wave followed by an expansion. An incoming wave at y = 60 mm leads the wall pressure change that it causes by about 120 mm.

For series 01 the start and finish of the incoming compression can be detected in the static pressure profiles, as can the outgoing reflected wave which, however, initially appears more concentrated and stronger than might be expected (see the "bulge" in the inner part of profiles 0108 and 0109). For the later profiles the general shape of the static pressure distribution is as expected if allowance is made for the arrival of the incoming expansion wave in the outer part of the layer

from profile 0109 on. A light grid has been sketched in to show the approximate direction of the Mach lines, along which changes will propagate. Two values for the displacement surface are shown, one for D STAR calculated allowing for varying static pressure as suggested in § 7 below, the other representing the authors' δ_1 values calculated as for a zero pressure gradient case. It is interesting that for both series 01 and 02, the conventional expression suggests a marked dip in the displacement surface in the zone where the incoming pressure wave approached the wall. If this were in fact present, an expansion - compression - expansion wave would propagate outwards from the affected area. There is little sign of any such structure either in the static pressure profiles, or in the wall pressure variation.

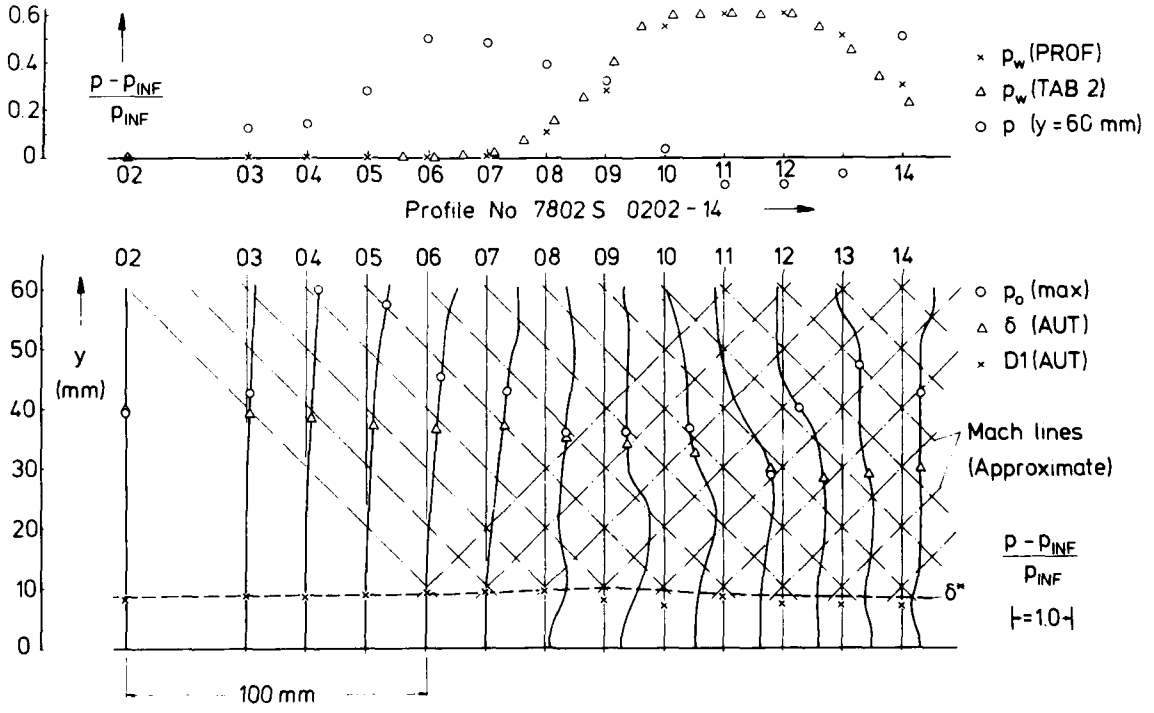

Fig. 6.2.3 Static pressure profiles for a straight-wall adverse pressure gradient flow. (Kussoy et al., 1978, CAT 7802S 0202 - 0214). Legend - as for Fig. 6.2.2.

It is evident from the foregoing that any attempt at accounting for pressure history effects in the velocity profiles, as in § 5, must taken into consideration the history of the particular part of the layer under discussion. In a wave structure whose dimensions are comparable with the boundary layer thickness, the past history of the inner and outer layers may be very different.

An inspection of the pressure field of series 02 (Fig. 6.2.3) makes this point even more clearly. Here the compression wave is stronger than in series 01, and is followed more rapidly by a stronger expansion wave. Consequently the pressure at a point in the boundary layer may be either above or below the wall pressure, while the local upstream history will consist first of a pressure rise, corresponding to the incoming compression wave, on which is superposed in any order, and with any degree of overlap, compression by the outgoing reflected wave and expansion to the incoming rarefaction wave. The pressure changes can again be seen to follow the (approximate) Mach line grid, and there is again a localised dip in the authors' δ_1 value where the compression wave reaches the wall. The D STAR (§ 7) value if anything shows the reverse tendency. Both here and to a lesser extent for series 01 (Fig. 6.2.2) the wall pressure seems a little low in relation to the general pressure level in the inner part of the boundary layer in a way which is not explained easily in terms of the wave structure. The observed pressure variation suggests that there is a weak outgoing expansion wave in this region, or alternatively that the probes are affected by the wall and the wave structure so as to give a slightly high reading when close to the wall.

The static pressure distributions shown in Figs (6.2.2) and (6.2.3) demonstrate how complicated the local pressure history may become, even with a relatively simple applied wave structure.

6.3 Reynolds stresses

The turbulent kinetic energy level in the boundary layer is closely related to the level of the Reynolds stresses. Of these, the shear stress in the inner fully turbulent region is approximately equal to the wall shear stress. As the Mach number rises, the skin friction coefficient c_f at a given value of $Re_{\delta 2}$ and T_w/T_r falls, by a factor of about 5 as M goes from 0.5 to 7 in a zero pressure gradient layer without heat transfer. The typical Reynolds stresses $\overline{\rho}\,\overline{u'v'}$, $\overline{\rho}\,\overline{v'^2}$ etc. are therefore falling in relation to the free stream dynamic pressure $\frac{1}{2}\rho u_e^2$. The static pressure, however, falls even more rapidly since

$$\overline{q}_e = \tfrac{1}{2}\overline{\rho}\overline{u}_e^2 = \tfrac{1}{2}M_e^2\overline{p}_e \qquad (6.3.1)$$

(the ratio $\overline{p}_e/\overline{q}_e$ falls from M = 0.5 to M = 7 by a factor of 200) so that at high Mach numbers the Reynolds stresses may become of the same order as the mean static pressure.

6.3.1 Normal stresses in hypersonic nozzle boundary layers

The normal stress acting in the y direction is composed essentially of contributions from the mean static pressure and from the normal Reynolds stress $\overline{\rho}\,\overline{v'^2}$, viscous normal stresses being negligible. Equation (6.1.2) should therefore be modified, in general, to read, writing $\overline{\sigma}$ for the total normal stress

$$\partial\overline{\sigma}/\partial n = (\partial/\partial n)(\overline{p} + \overline{\rho}\,\overline{v'^2}) = -\overline{\rho}\,\overline{u}^2/R \qquad (6.3.2)$$

from which it may be seen that a significant Reynolds stress will cause a local dip in the static pressure as compared to the value which would be predicted from a momentum balance for the mean flow alone.

In zero-pressure-gradient cases the Mach number has not generally been sufficiently high for the Reynolds stress contribution to be significant, and in any case experimentalists tend to assume that there is no pressure variation in the normal direction. Apparently anomalous observations in hypersonic nozzle wall boundary layers can be explained if the Reynolds stress is assumed to play a significant part (Finley, 1977 and below). A nozzle wall boundary layer experiences strong normal pressure gradients as a result of wall curvature, so that it can become difficult to differentiate between the various contributions to the static pressure field.

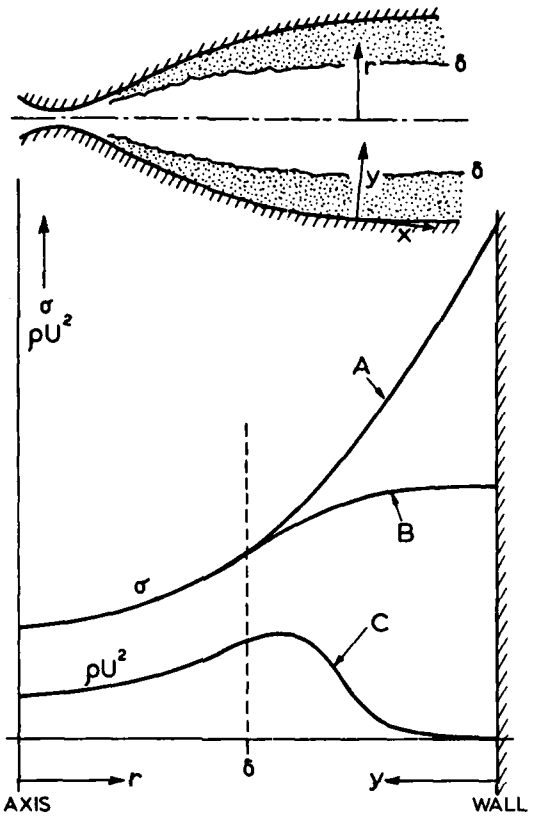

Fig. 6.3.1 Variation of normal stress σ in a contoured hypersonic nozzle.
Curve A: Normal stress as it would be determined for inviscid flow by a characteristics calculation starting from the pressure distribution on the axis
Curve B: Normal stress distribution as modified by retardation in the boundary layer.
Curve C: Specific momentum flux distribution showing the fall which occurs in the boundary layer

Figure (6.3.1) shows the normal stress ($\overline{\sigma}$) variation in a hypersonic nozzle. Curve A represents the 'ideal flow' distribution which would be determined by a characteristics calculation proceeding from the pressure distribution on the axis. In the absence of retardation by the boundary layer, the specific momentum flux $\overline{\rho}\ \overline{u}^2$ would vary in a similar manner, but, as discussed in § 6.2 above, not only does the velocity fall as the wall is approached but also, especially in a hypersonic layer, the density falls very rapidly, so that the actual specific momentum flux is distributed more as shown in curve C. The rate of change of normal stress as predicted by eqn. (6.3.2) therefore falls off as the wall is approached giving a variation of the form shown as curve B, which has zero slope at the wall.

Static pressure measurement at very high Mach numbers is formidably difficult, so that no great emphasis should be placed on exact numerical values. However, Figs. (6.3.2) and (6.3.3), drawn from measurements in nozzle wall boundary layers at Mach numbers of order 20, show measured static pressure distributions which dip noticeably below normal stress distributions predicted from eqn. (6.3.2). The stress values (curves B1, B2, B) were determined using the tabulated values of $\overline{\rho}$, $\overline{u}$ for Beckwith et al., CAT 7105, and Fischer et al., CAT 7001, with the assumption that R could be treated as constant through the boundary

layer, and requiring the curve to pass through the reported pressure values at the wall and the boundary layer edge. In Fig. (6.3.2) curve D2 represents values obtained from corrected static probe measurements. Curve D in Fig. (6.3.3) is the authors' representation of measured values as used for convenience in data reduction. There are inevitable inconsistencies in any analysis of this data resulting from the variety of assumptions which may be incorporated. The figures show however that in both these cases there is a dip in the static pressure distribution of order 0.4 - 0.5 $\bar{p}_w$, the dip being greatest in the zone where turbulent mixing is very intense. We therefore presume that this is a Reynolds stress effect.

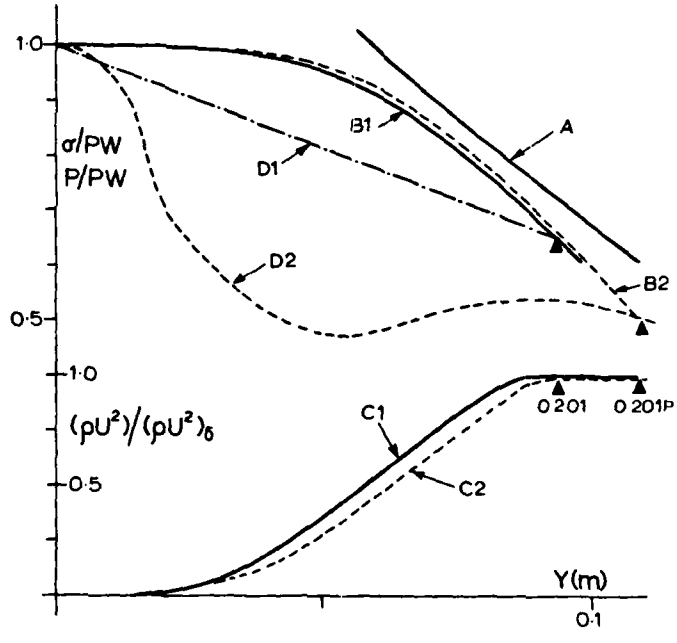

Fig. 6.3.2 Normal stress and static pressure observed in a M = 20 nozzle boundary layer (Beckwith et al. 1971, CAT 7105 0201, 0201P).
Curve A: σ/p_w as calculated for inviscid flow by Beckwith et al.
Curves B1, B2: σ/p_w as modified by the boundary layer. Calculated from eqn. (6.3.2) assuming constant R and using the data as tabulated for: (B1, 0201), the linear static pressure distribution assumed by the authors (D1) and (B2,0201P) the authors' measured static pressure distribution (D2).
Curves C1, C2: Specific momentum flux distributions used to calculate B1(C1) and B2(C2).
Curves D1, D2: Static pressure distributions as assumed by the authors for data reduction (D1) and as obtained from corrected static probe measurements (D2).
▲ : Assumed boundary layer edge points.

6.3.2 Scaling of Reynolds stresses

If we assume that the peak values of the various Reynolds stresses will to the first order bear a fixed relationship, we may use these results to estimate the likely magnitude of a Reynolds-stress-induced static-pressure dip in other flow cases. We take the wall shear stress as typical of turbulent stresses and write, ignoring any dependence on pressure gradient for the time being,

$$\Delta\bar{p}(\text{max.}) = (\bar{\sigma} - \bar{p})\text{max.} = (\bar{\rho}\,\overline{v'^2})\text{max.} = 2k\tau_w = k\gamma\, p_e M_e^2 c_f \qquad (6.3.3)$$

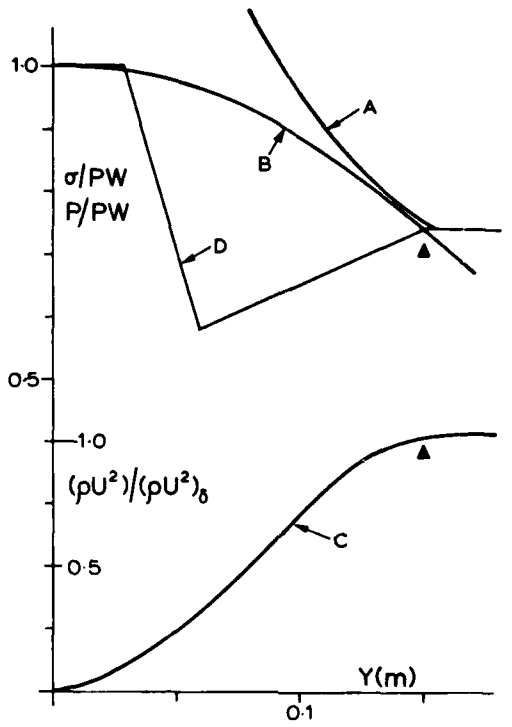

Fig. 6.3.3 Normal stress and static pressure observed in a M = 22 nozzle boundary layer. (Fischer et al. 1970, CAT 7001 0104).
Curve A : σ/p_w for inviscid flow (D.M. Bushnell, private communication)
Curve B,C,D: as for (Fig. 6.3.2), all referring to the authors' representation of the static pressure distribution (D).

There are no fully measured profiles of the type that we require to evaluate k, but static pressure was measured in the two cases shown above in Figs.(6.3.2, 6.3.3). A wall shear stress value in the same facility used by Beckwith et al. and under closely matched conditions was measured by Harvey & Clark (1972). With the profile 0201P shown in Fig. (6.3.2) this gives a value of 3.14 for k as defined in eqn. (6.3.3). There is no corresponding wall stress value for the profile measured by Fischer et al. (1970, Fig. 6.3.3), though they do provide an estimate for c_f based on the limiting slope of the velocity profile. This gives a value for k of 3.8. It is extremely difficult either to measure a shear stress value, or to estimate it from the profile at these Mach numbers ($M \sim 20$) so that these results only permit us to estimate k as roughly 3, preference being given to the Beckwith et al. (1971) result since it uses a measured c_f value, while the set of straight lines used by Fischer et al. (1970) unduly emphasizes the peak difference (see Fig. 6.3.4 below). The numerical values given here differ slightly from those given in Finley (1977) due to differences in the choice of scaling values for p_δ and c_f. Those presented here are consistent internally with the tables in AGARDograph 223.

It is tempting to go further and attempt to deduce the distribution of the Reynolds stress contribution $\overline{\rho}$ through the boundary layer. In Fig. (6.3.4), $(\Delta\overline{p}/\gamma p_\delta M_\delta{}^2 c_f)$ as suggested by eqn. 6.3.3 is plotted against y/δ. The δ value is inevitably very imprecise (see § 7) since we are here dealing with flows strongly affected by normal pressure gradients. The peak value of $(\Delta\overline{p}/\gamma p_\delta M_\delta{}^2 c_f)$ is the value of k as defined in eqn. 6.3.3, and the 'peakiness' of the Fischer et al. representation of the static pressure distribution obviously gives rise to a misleading value. With these reservations the two distributions

are in surprisingly good agreement.

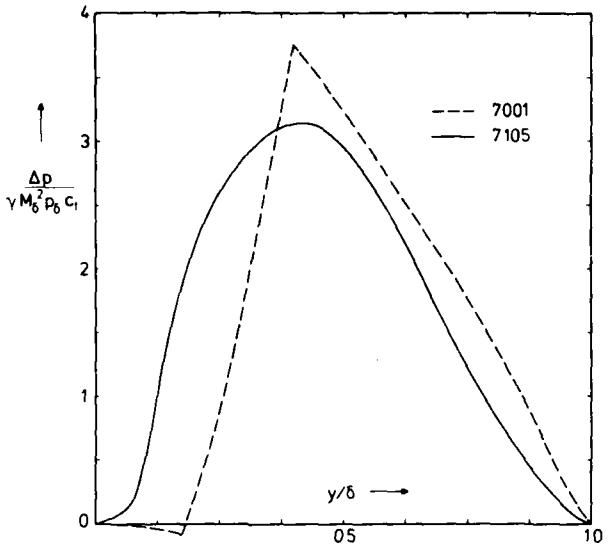

Fig. 6.3.4 Pressure drop due to Reynolds stress scaled according to eqn. (6.3.3). Values from Beckwith et al., CAT 7105, (——— , δ = 112 mm) Representation of values from Fischer et al., CAT 7001, (– – – –, δ = 152 mm).

If there is in fact an element of universality in this Reynolds stress distribution, then it may be used to predict the static pressure variation in cases where measurements were incomplete. As an example, we show in Fig. (6.3.5) a possible reconstruction of the static pressure profile at M_δ = 44.6 for a case studied by Kemp & Owen (CAT 7206). This is an extreme example and has been chosen to illustrate a number of secondary points. If the difference $(\overline{\sigma} - \overline{p})$ is dependent on the intensity of turbulent fluctuations, then it should take a peak value at or near the y-position corresponding to peak fluctuations. Accordingly this figure has been constructed by using the authors' data, reduced assuming a linear static variation between a Pitot-derived value at the boundary layer edge and the wall value (curve D1), to construct the normal stress variation (curve B) as for Figures (6.3.2, 6.3.3). The $\Delta\overline{p}$ variation has then been applied taking account of the turbulent fluctuations measured with a hot film and shown in Fig. 28 of Kemp & Owen (1972). These show the peak as occurring at $y/\delta \approx 0.8$, and also show a significant fluctuation level in the free stream. The inner part of the distribution, again guided by Fig. 28 of CAT 7206, has been assumed to start at the point at which the specific momentum flux becomes significant (curve C). The uncertainties are numerous, beginning perhaps with some question as to the meaning of static pressure under these circumstances. If static pressure readings were to be taken in such a flow, there would be in addition to all the calibration uncertainties relating to steady flow mentioned by Beckwith et al. (CAT 7105), the question of the likely response of a probe in a flow with such high implied fluctuation levels. It seems probable that the original results used to construct Fig. (6.3.4) are also so affected.

6.3.3 Reynolds stresses in straight-wall flows

The effect of Reynolds stresses is most pronounced at high Mach number. The data based used for § 6.3.2 consists therefore of the two nozzle wall boundary layer cases available with more or less full profile information. The influence of wall curvature on the static pressure field is thus comparable in magnitude, if different in form, to that of Reynolds stresses. We therefore look at the Reynolds stress

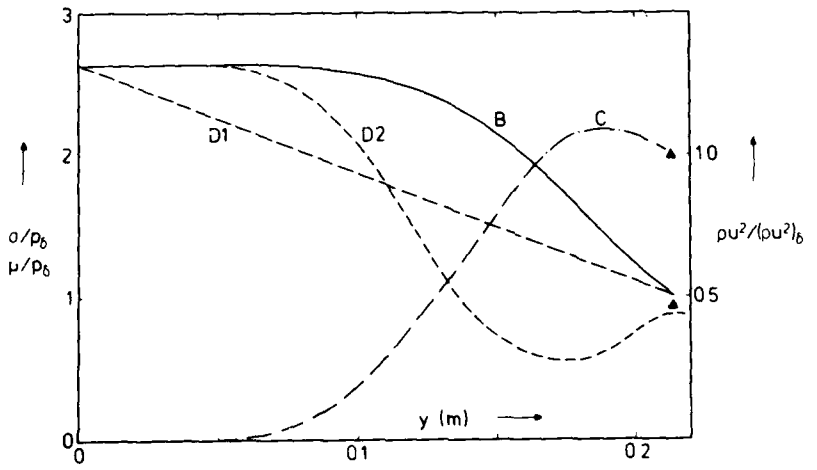

Fig. 6.3.5 Reconstruction of static pressure profile (D2) for a hypersonic nozzle wall boundary layer. (Kemp & Owen CAT 7206 0604, M = 44.6, $Re_{\delta 2}$ = 81, Re_θ = 4800, TW/TR = 0.65). D1, static pressure assumed by authors; B, normal stress distribution; C, specific momentum flux. Compare Figs. (6.3.2) & (6.3.3).

effects likely to be associated with straight wall flows. Eqn. (6.3.2) shows that for a straight wall zero longitudinal pressure gradient flow, no difference in static pressure should be observed across the boundary layer as a whole, and for moderate reflected wave flows the argument of § 6.1.2 would also suggest only small pressure differences. In table (6.3.1) an estimate is given of the likely pressure dip which might be found in a range of typical straight wall boundary layers if the quantitative estimate of § 6.3.2 is assumed to hold over the full Mach number range. Unfortunately there are very few cases in which a static pressure distribution was measured - usually experimentalists who took account of possible static pressure variations were satisfied if a Pitot-derived free stream pressure matched the wall pressure. The $(\Delta\bar{p}/p_\delta)$ values predicted are in many cases substantial, though the significance of the variation, and its susceptibility to measurement, remain uncertain. The key experiments would appear to be the NOL boundary layer channel studies of Voisinet & Lee (CAT 7202/7304) for which static pressure profiles were detailed and precise enough, if the probes used response appropriately, to detect the pressure dips of 5-8% predicted. No such dip is apparent in the reported results. It remains difficult however to account for the observations of Beckwith et al. (CAT 7105) and Fischer et al. (CAT 7001) other than by invoking the Reynolds stress mechanism. In § 6.4.2 we discuss the straight wall measurements of Laderman & Demetriades (1974, CAT 7403). It is suggested there that there is a boundary-layer-induced simple wave generated at the displacement surface which accounts for the overall pressure difference $(p_w - p_\delta)$ observed. If this is accepted, a normal stress distribution may be sketched in on the same basis as for the curves B above, and a Reynolds stress dip of about 0.13 p_δ becomes apparent (source Fig. 5). The prediction in table (6.3.1) is 0.15 p_δ. This result would seem to give very good agreement with the above, but does depend on the basic wave structure being as assumed.

Table 6.3.1. Possible Reynolds stress induced pressure dips in straight-wall boundary layers.

CAT	Author	M	$Re_{\delta 2} \times 10^{-3}$	T_w/T_r	$C_f \times 10^4$	$(\Delta p/p_\delta)_{max}$	Comment
5301 0201	Coles	1.98	4.36	1.0	21.8	0.036	ZPG. See remarks on longitudinal pressure variations in para. 6.4.1.
0901		3.70	2.73	1.0	13.8	0.079	
1201		4.54	1.29	1.0	13.1	0.114	
6502 0103	Moore/ Harkness	2.67	360	1.0	8.62	0.026	ZPG
6702 0401	Danberg	6.46	0.38	0.64	15.6	0.273	ZPG. Static pressure data were measured but discarded. See para. 6.4.1.
0801		6.34	1.07	0.86	9.92	0.167	
7102 0106	Peake et al	3.90	7.76	1.0	10.3	0.066	ZPG case, series 01.
7104 0102	Waltrup/ Schetz	2.10	17.4	1.0	13.4	0.025	Reflected wave APG. Static pressure profile measured. See para. 6.4.4. small dip found.
7202 0101	Voisinet/	4.75	1.56	0.93	8.90	0.084	ZPG. Static pressure profile measured. No dip found.
0305	Lee	4.80	13.3	0.91	5.55	0.054	
7203 1001	Hopkins/	7.47	15.5	0.36	7.33	0.172	ZPG.
1201	Keener	7.39	4.53	0.46	7.14	0.164	
7205 0102	Horstman/ Owen	7.20	2.10	0.50	8.50	0.185	ZPG. Hotwire data available at M=6.7.
7302 0914	Winter/ Gaudet	2.21	46.5	1.0	12.9	0.026	ZPG.
7304 0101	Voisinet/	3.85	2.28	0.94	12.4	0.077	Reflected wave, FPG. Static pressure profile measured. No dip found.
0305	Lee	4.53	65.8	0.95	6.58	0.057	
7305 0303	Watson et al	9.80	0.44	1.0	3.78	0.182	ZPG. See para. 6.4.2.
0504		10.3	1.55	1.0	2.40	0.028	
7402 0101	Mabey et al	2.49	3.10	1.0	18.5	0.048	ZPG.
0303		2.50	9.09	1.0	15.6	0.041	
1601		4.50	1.08	1.0	13.7	0.116	
1805		4.49	6.81	1.0	8.8	0.075	
7403 0101	Laderman/ Demetriades	9.37	6.52	0.42	4.06	0.150	Nominal ZPG. See para. 6.3.4, 6.4.2. Static pressure measured, large difference found. Hotwire data available.

6.3.4 Inferences drawn from fluctuation measurements

Any attempt at estimating the effect of Reynolds stresses more directly is inhibited by the general uncertainty as to flucutation levels in hypersonic boundary layers. As the Mach number rises there is a general tendency for the turbulent intensity in terms of local mean flow quantities to rise. This must imply an element of doubt in the interpretation of any hot wire/hot film results. For modest Mach numbers there is some evidence (if much disputed) that the application of Morkovin's hypothesis in the form of the "coordinate stretching density factor" (see Owen et al., 1975, Figure 10; Laderman & Demetriades, 1974, Figure 16) may correlate the data. In essence this amounts to the assumption that stress distributions, as opposed to fluctuation velocity components, will remain substantially invariate with Mach number. To apply this argument to a Mach number range beyond M = 5 is perhaps a little rash, but information as to the individual components of turbulent intensity is not available so that one has little option. The hot wire is presumed to respond to specific mass flow and to total temperature fluctuations, and the reduction of such data from cross wires to yield Reynolds stresses in flows with significant pressure and density fluctuations is essentially controversial.

Direct observation of the $\overline{v'^2}$ component is limited to the laser observations of Johnson & Rose (1975) at M = 2.9. At this Mach number, Morkovin's hypothesis might be expected to apply, so that the results should perhaps be expected to scale to low speed results. On the whole (source, Figures 1,2) this is the case. This implies a peak value for the y-component normal stress of about double the wall shear stress. The values incidentially agree quite well with hot-wire derived values, with the hot wire values on the whole lying higher.

We are here attempting to compare results obtained at Mach 20 with results obtained at "modest" Mach numbers, so that intermediate results are of crucial importance. Owen et al. (1975) report hot-wire-derived results at M = 6.7 (source, figure 10) which suggest $\bar{\rho}\ \overline{u'^2}$ values of order τ_w as compared with values reported by Kistler (1958) and Morkovin & Phinney (1958) of roughly twice τ_w (CAT 5803). $\bar{\rho}\ \overline{v'^2}$ values are possibly, at high Mach number, rather greater than $\bar{\rho}\ \overline{u'^2}$ values. Laderman & Demetriades (1973, 1974, CAT 7403) originally reported substantially lower fluctuation levels at M = 9.4. They have since reappraised their data in the light of relatively low speed experiments (M = 3, CAT 7702S) so that the shear stress profiles achieve better agreement with the limiting value at the wall (Laderman & Demetriades, 1979). As part of this reappraisal, requiring substantial changes in modal analysis, they note that $\overline{v'^2}$ values are "quite a bit" higher than $\overline{u'^2}$ values. The crucial point is the degree of correlation between u' and v', as the normal stresses may be substantially greater than the shear stresses if the correlation level is low. The value of $\bar{\rho}\ \overline{v'^2}/\tau_w$ predicted by eqn. (6.3.3) using the data of CAT 7105 and CAT 7001 is about 6. If "quite a bit" (see above) encompasses a ratio of about 1.5, this is feasible. More precisely, they include data for $[(\overline{v'^2})/u_\delta^2]^{\frac{1}{2}}$ at $(y/\delta) = 0.5$ over the whole Mach number range 0 to 10. The graph (source Figure 14) suggests a near constant value of 0.04. If this is used directly in eqn. (6.3.3), it gives a value for $\Delta\bar{p}/p_\delta$ of about 0.18, in good agreement with the estimates above.

Any approach other than a simplistic correlation must be a little hopeful, as the local turbulence levels (as opposed to turbulence levels referenced to free stream mean quantities) may be very high indeed. Hot wire or hot film derived values therefore need to be evaluated with extreme caution. Extreme hypersonic results are few, but Fischer et al. (1971, CAT 7001) report mass flow fluctuations of 50% referred to local mean values at M = 20, while Kemp & Owen (CAT 7206) report peak values at M = 38 of 80%. Referred to freestream mean flow quantities, the fluctuation levels, respectively 10% and 5%, do not seem too large. It would be a brave man however who placed too much credence in any numerical hot-wire/hot-film result obtained in such flows.

6.4 Boundary layer induced pressure gradients - anomalous cases

Setting aside the question of possible Reynolds stress induced local pressure drops, the main proposition of §§ 6.1, 6.2 is that significant normal pressure gradients will only be observed in connection with streamline curvature. At high speeds the curvature required is not great, and may therefore be associated as much with the curvature of the boundary layer displacement surface as with the curvature, if not great, of the wall on which the boundary layer is growing.

6.4.1 Normal pressure gradients in straight walls

A boundary layer growing on a straight wall will not in general develop so as to have a displacement thickness which increases linearly with distance from the leading edge. In general it will not even increase monotonically in a zero pressure gradient flow, since the change in shape factor at transition implies that with a momentum thickness which of necessity increases monotonically, there is very likely to be a local reduction in displacement thickness. The tendency for flows which have not developed the very thick sublayers (and so displacement thicknesses) characteristic of hypersonic boundary layers will be for the displacement surface to be initially convex with an increasing radius of curvature as the laminar layer develops, as for a low speed layer, to pass through a concave region associated with transition, and then to develop into a very slightly convex surface in the full turbulent region. The radii of curvature involved are very large, so that at low speeds pressure variations associated with displacement surface curvature will be negligible. However, as the Mach number rises there may come a stage at which the simple wave structure generated at the displacement surface causes detectable longi-

tudinal and normal static pressure gradients. The linkage between longitudinal and normal pressure gradients characteristic of simple wave flows (eqns. 6.1.5 - 6.1.7) implies that the resulting normal gradient is likely to be noticeably greater than the longitudinal gradient.

Coles (1953 - CAT 5301) found static pressure variations along his flat plate of about 5%. The plate was very carefully constructed, and so effectively flat, and the empty tunnel static pressure variations did not exceed 1%. He therefore attributed this variation to boundary layer induced effects. Since any incoming disturbance is relatively small, this conclusion implies a simple wave structure originating from the displacement surface with a radius of curvature in the range 100 δ to 600 δ. Danberg (1964, Figure 10) noted differences between freestream static and wall static pressure of up to 10% at low values of x, falling downstream. His boundary layer measurements covered an $Re_{\delta 2}$ range of about 300 - 1700, and so covered the transitional region. The curvature of the displacement surface required is about 500 δ. In the case of Danberg (tabulated as CAT 6702) there are four successive stations so that overtly it should be possible to look for the appropriate displacement surface curvature. The precision of δ_1 determination called for would however be several orders of magnitude greater than can in fact be accomplished in an experiment, so that the mechanism cannot be confirmed. For fully developed turbulent layers on straight walls in nominally zero pressure gradient conditions, boundary layer induced pressure gradients should be very small so long as the boundary layer growth follows the general pattern of a low speed layer. Where a static pressure determination has been made for high Reynolds number cases, the authors have in general remarked that no significant difference between wall and free stream pressure was found (Stalmach, 1958, Pitot determination; Sturek & Danberg, 1972, Pitot and static determination; Voisinet & Lee, 1972, Pitot and static, everywhere except station 1 which was, away from the wall, in the last part of the nozzle expansion - as profile d in Fig. 6.1.4, Fig. 6.1.5; Horstmann & Owen, 1972, Pitot; Watson et al., 1973, Pitot - but see below). This is also the general observation in flows with not-too-strong reflected wave pressure gradients. (Lobb et al., 1955, Pitot; Naleid, 1958, Pitot; Hill, 1959, Pitot; Pasiuk et al., 1965, Pitot; Waltrup & Schetz, 1971, Pitot and static - but with a dip - see below; Voisinet & Lee, 1973, Pitot and static; Thomas, 1974, Pitot and static).

The references cited here are those in which some specific comment was made. For the majority of straight wall cases, the authors have assumed that the static pressure was constant, usually not even considering it necessary to say so.

Significant static pressure differences across boundary layers on straight walls are noted by experimenters working with strong pressure gradients (Zakkay & Wang, 1972, Kussoy et al., 1978; Gopinath & East 1975: various of those working with shock-boundary layer interactions) but there remain anomalous cases.

6.4.2 Anomalous cases

While numerical agreement may be somewhat vague, the great majority of observed normal pressure gradients can be explained by appeal to one or other of the mechanisms discussed in § 6.1, with some reference to § 6.3. There remain however a few cases which do not overtly fall into any of the groups suggested above. Of these the most important are the measurements made by Laderman & Demetriades (1972b, 1974, CAT 7403). A single profile was studied in detail (PT2, T0, P profiles) on a flat tunnel wall at $M = 9.37$, $T_w/T_r = 0.4$, $Re_{\delta 2} = 6500$. As a straight wall, high Reynolds number ($Re_\Delta = 37{,}000$) zero longitudinal pressure gradient case therefore we would expect no static pressure differences across the layer, while there might possibly be (Table 6.3.1) a 15% pressure dip in the layer as a result of the action of Reynolds stresses. The actual observation is of a 40% pressure difference across the layer, as established by Pitot measurements, the detailed static distribution, after corrections applied to give agreement in the free stream, being of the general type sketched in Figs (6.3.2, 6.3.5) above, with a "Reynolds stress dip" of about $0.13p_\Delta$ occurring in the range $0 < y/\delta < 0.4$. This suggests that the displacement surface is locally concave to the free stream. The authors do however report a longitudinal wall pressure gradient of 25 per metre. Further detail of the wall pressure distribution, which is strongly Reynolds number dependent, is reported in McRonald (1975). There is a minimum in wall pressure upstream of the survey station, which moves further upstream as the total pressure and so characteristic Reynolds number falls. The tunnel calibration reports (Laufer et al. 1967) however show no corresponding longitudinal pressure gradients on the centre line. Consequently the pressure gradient developing along the tunnel wall cannot

AD-A087 704 ADVISORY GROUP FOR AEROSPACE RESEARCH AND DEVELOPMENT--ETC F/G 20/4
A CRITICAL COMMENTARY ON MEAN FLOW DATA FOR TWO-DIMENSIONAL COM--ETC(U)
MAY 80 H H FERNHOLZ, P J FINLEY

UNCLASSIFIED AGARD-AG-253 NL

3 OF 3

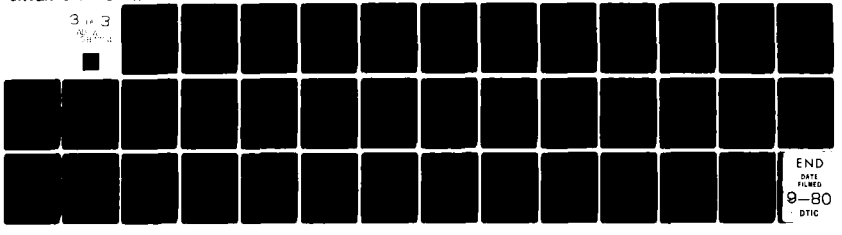

END
DATE FILMED
9-80
DTIC

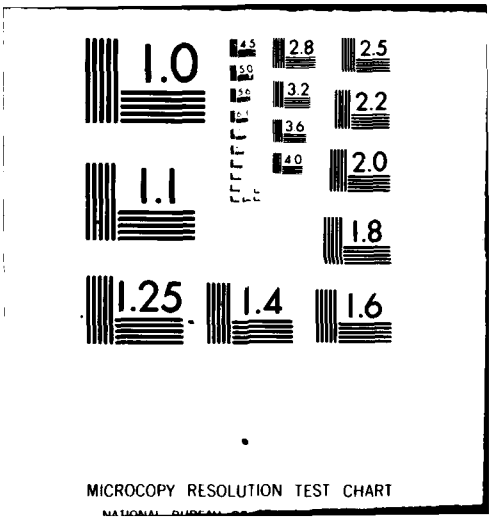
1.0
1.1
1.25
1.4
1.6
1.8
2.0
2.2
2.5
2.8
3.2
3.6
4.0
4.5
5.0
5.6
6.3
7.1
MICROCOPY RESOLUTION TEST CHART

be the result of an incoming pressure gradient reflected at the wall, and must be a simple wave structure originating at the wall as a result of boundary layer growth.

If we assume that there is a simple wave structure, then the transverse and longitudinal pressure gradients are linked by eqn. (6.1.6)

$$\Delta p(y)/p \simeq \bar{+}M(\delta/\Delta x)\Delta p(x)/p \qquad (6.4.1)$$

which with the values δ = 0.15 m, Δx = 1 m and $(\partial p/\partial x)$ = 25%/m gives an estimate for the pressure difference across the layer of 35%, as compared with the 40% reported.

This explanation implies that the displacement surface is concave, with a radius of about 300 δ, in contrast to the very slightly convex displacement surface which would be expected for a low speed layer. In turn this implies that the boundary layers on a parallel sided duct will compress the free stream flow well before the boundary layer itself has reached the axis, and this in turn implies a more rapid axial compression than would be predicted from any crude one-dimensional Fanno line approach. There is insuffient experimental information from long parallel sided ducts at high Mach number to allow us to say at what Mach number this hypothetical displacement surface concavity becomes significant, how soon it follows on from transition, or if there is generally a convex displacement region soon after transition. The only apparently comparable measurements are those of Watson et al CAT 7305, which were made at M ≃ 10, but at much lower Reynolds number on a flat plate. For any flat plate, however sharp edged, at this Mach number, there is a strong leading edge shock-boundary-layer interaction giving a shock wave of noticeable curvature near x = 0. In consequence the 'free stream flow' or more properly the boundary layer exterior flow has noticeable vorticity. It is therefore very difficult to decide, from Pitot measurements, whether there is or is not a static pressure difference across the boundary layer. If the greater total pressure loss associated with the more steeply inclined part of the leading edge shock is not sufficiently allowed for - and it is difficult to predict the details of the viscous interaction - a straight application of the normal shock relation to the Pitot reading will give an over-estimate of the static pressure, and vice-versa. Watson (1978) presents (source pp 13/14, Fig. 9) details of the flow field calculated assuming that static pressure variation across the boundary layer could be neglected. The calculated flow field implies a 'low speed' type of δ_1 variation - initially convex, concave in the transition region, and convex in the fully turbulent region. The associated static pressure variations would be $\partial p/\partial y > 0, < 0, > 0$, and clearly an iterative calculation would be possible. Combined with the uncertainty of the influence of significant exterior flow vorticity, it is unlikely that quantitative results would be particularly helpful - it is only possible to say that the assumption $p_w/p_d = 1$ is a convenient first approximation which is certainly incorrect.

The results of Watson (1978) and Watson et al. (1973, CAT 7305) are not so much anomalous as uncertain. There remain however a number of experiments displaying, to a greater or lesser extent, inexplicable features. The most significant of these is the conical nozzle flow studied by Backx (1975) reported also as Backx & Richards (1976). For this straight wall flow at M = 15 and 20, $T_w/T_r \simeq 0.15$ and $R_\theta \times 10^{-3}$ = 35 and 25, the wall static pressure was observed to be up to 80% greater than the free stream pressure as determined from Pitot measurements. This difference is very much greater than can be accounted for by the basic reflected wave mechanism (§ 6.1.2). While experimental error is always possible at these Mach numbers, it is very unlikely that Pitot and wall static measurements could be in error by this amount, so that an alternative explanation must be sought. Backx (1975) considered the question at some length in the light of estimated values of various terms in the y-momentum equation, without being able to account for a pressure difference of more than 20%. In common with many discussions of the time, the possible Reynolds stress contribution is confused with the possible effects of streamline curvature. If the latter is the cause of the observed pressure difference, the flow must, in the boundary layer, be of simple wave character. Any such argument can only be very tentative, since it amounts to the suggestion that a displacement surface concavity of the type suggested in connection with the Laderman & Demetriades case (CAT 7403) is developing, and causing a compression at the wall which outweighs the source flow expansion of the conical nozzle. The observation of conical flow in the core of the nozzle (Slechten, quoted by Backx, 1975) does not eliminate this possibility, as a wave structure developing at

the wall at Mach 15-20 would require about 10 diameters to reach the centre line. The displacement surface curvature required is of order 500δ and so would not be likely to be detected by any boundary layer calculation, which would be more concerned with the growth of δ_1 and unlikely to give a precision which would allow of a curvature estimate.

Peterson (1974) and Peterson & George (1975) report hypersonic (M = 14) contoured nozzle wall measurements, which as expected show p_w greater than p_δ. The original measurements were made with a calibrated "cone-static" probe with static holes on the face of a 10^o half angle cone. The measurements have been repeated using a conventional low-speed type of static probe (CCP, static holes, 16d downstream of shoulder of conical nose, Peterson, private communication, 1978, and CAT 7405S). There are substantial differences in the detail static pressure distributions recorded. The arguments for accepting one set of results rather than the other will not be rehearsed here, but both sets of data include points near the wall for which $\overline{p} > p_w$, the original data showing more scatter. This feature cannot be accounted for by the mechanisms discussed here, except possibly by a localised disturbance, and must be attributed to uncertainty in instrumental response to highly turbulent flows or to possible wall interactions. In other respects a curved-wall normal stress distribution with a 'Reynolds-stress dip' accounts well for the observed pressure variation.

Pfeiffer & Will (1973, CAT 7307S) give profiles measured on an extension to a conical nozzle. This was either 'unheated' when the wall temperature remained substantially constant and equal to that in the nozzle ($T_w/T_r \simeq 0.5$), or 'heated' to a temperature of the same order as the free stream total temperature. The general tendency is for the pressure to rise from the wall to the freestream, with a localised rise near the wall. These results appear to contradict every suggestion made above. The difference ($p_\delta - p_w$) increases downstream, reaching a maximum of about 0.5 p_δ in both cases if the wall static value is taken (the probe data do not reach quite such low values). The overall difference is small for the first station, but the localised rise close to the wall is about 0.2 - 0.3 p_δ. This can only be accounted for, if real, by a localised disturbance. Otherwise it implies a negative (!) value of $\overline{\rho}\,\overline{v'^2}$, or, more realistically, instrumental error. Details of the probe configuration and correction procedure are not available, and it may be that the data are in fact uncorrected. The overall difference is much less likely to be in error, but implies a convex displacement surface with a radius of order 400 δ.

Finally, we remark the static pressure dip of about 4-6% observed by Waltrup & Schetz (CAT 7104) in the outer part of the boundary layer in straight wall flows at M = 2. This is 2-3 times the dip which would be predicted from the Reynolds stress estimate of § 6.3 above; and raises the question of possible pressure gradient effects, as the data base used in § 6.3 was obtained in favourable pressure gradient flows, while Waltrup & Schetz (1971) were studying adverse pressure gradients. Since the first station in each case corresponds to a zero pressure gradient flow and there is no trend with downstream distance as the adverse pressure gradient takes effect, it seems more likely that any discrepancy is the result of the general uncertainty of probe response in highly turbulent flows.

6.5 General comment on the interpretation of experimental data

Taken at face value, the correlations of static pressure difference across boundary layers as presented by Fischer et al. (1970, 71) and Kemp & Owen (1972) should have as independent variable not the Mach number but a group of the general nature ($\gamma M_\delta^2/R$), where R is an appropriate mean streamline radius of curvature. Since they report the overall difference across the layer the Reynolds stress dip should not affect the correlation. We reproduce figure 9 of Kemp & Owen (1972) as Fig. (6.5.1), with some additions. The legend is as in the original, but several of the sources may be found in AGARDograph 223. We have not ourselves obtained data for some of the cases quoted. The level of correlation obtained implies a 4:1 range in the value of ($\gamma\delta/R$) which seems not improbable for hypersonic contoured nozzle data. The 'anomalous case' data however also fall broadly within this band, implying that displacement surface curvature may be of the same order even on a straight surface. For instance, the value of R(wall)/δ for CAT 7105 (Figure 6.3.2 above) is about 300, which may be compared with the straight-wall (R/δ) values of 100-600 deduced in § 6.4. The wall geometry ceases therefore to be the obvious controlling feature in hypersonic flows, with the associated low local unit Reynolds numbers, and it is

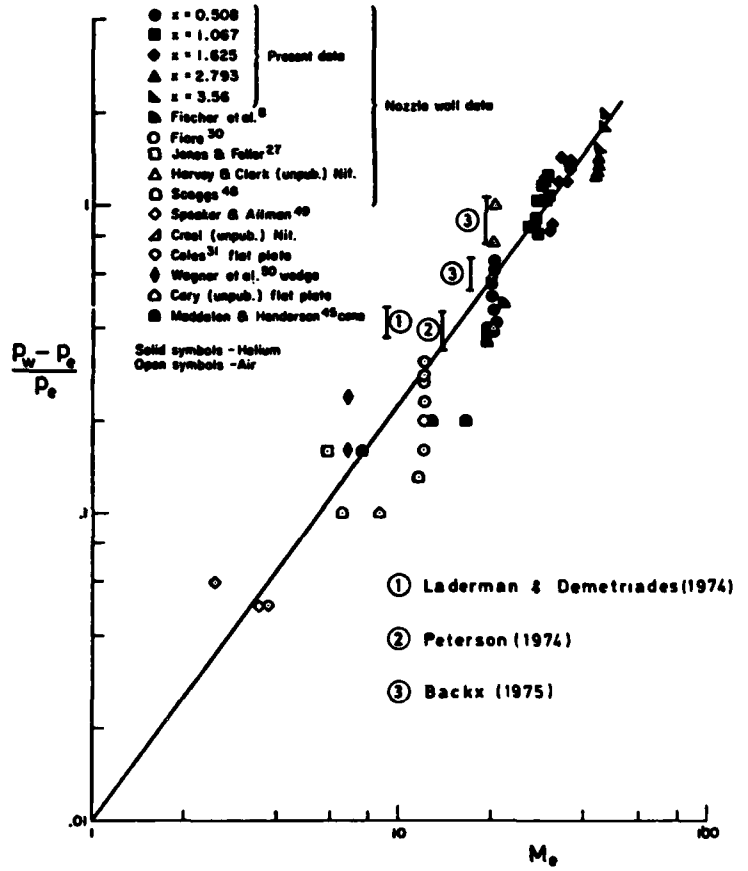

Fig. 6.5.1 Overall static pressure differences across boundary layers. Facsimile from Kemp & Owen (1972) with additions.

easy to visualise, for example, a nozzle running in an off-design condition such that the displacement surface corresponded to the boundary of a free jet. There would then be only a very small, possibly zero, gradient of p_w, while $\partial p/\partial y$ in the boundary layer could be quite large. An observer whose interest lay in the quality of the flow in the test core would however consider the flow reasonably uniform, since he would be observing a domain covering stationary (minimum) values of p as a function of both x and y.

It may be possible (see for instance Beckwith et al., 1971) to make and calibrate static probes which can be used accurately in the Mach and Reynolds number ranges in question in steady flow, and away from solid walls. The effect of a solid wall, or at least the point at which static pressure results should be discarded because of wall proximity, can in part be inferred by observing any change in wall pressure caused by the approach of the probe. It seems unlikely however that the steady flow calibrations can be expected to hold very closely in regions of very high turbulent intensity. The calibration corrections are often very large (of order 2:1) so that the possibility of non-linear interaction between various factors needs to be taken very seriously.

The analysis of the sections above provides a number of flow models which separately or together allow static pressure data which, at high Mach numbers, are likely to be rather dubious, to be fitted to a curve of the right type. The static pressure data on their own will always be inadequate. To provide a proper outer limit, Pitot data should always be taken for a substantial distance outside the boundary layer. Unless there are significant entropy gradients in the outside flow, this will allow a fit, not only to the static pressure level at the boundary layer edge, but also to the likely level of normal stress gradients to be expected. A streamwise Pitot survey is also very valuable as it will reveal the presence of any concentrated disturbances. The wall pressure should be measured not only at the profile station, but at fairly close intervals for a region upstream and downstream. The wall pressure gradient is a

significant datum in any attempt at constructing the wave pattern, and is one of the easiest and cheapest sets of data to obtain. The normal stress gradient at the wall is zero, and the distribution between p_w with zero gradient and p_δ with a known gradient is then fairly closely constrained. The detail distribution may be refined by using the profile data to determine the distribution of specific momentum flux as in § 6.3.1, and is not very sensitive to small changes in the profile input. The static pressure distribution as measured may then be compared to the normal stress distribution in the light of the probable effect of Reynolds stresses as predicted in § 6.3.2 and the consistency of the whole assessed. At high Mach numbers it is not wise to predict from the wall curvature as such, since, as remarked above, the contribution to $(\gamma\delta/R)$ from displacement effects may well be the same order as that from the wall curvature, so that it is better to work from the profile information itself where possible.

A boundary layer calculation may give the value of δ_1 within a few percent without giving any precision in a value of $\partial^2\delta_1/\partial x^2$, so that it is as yet not reasonable to expect calculation methods to give any reliable prediction for boundary layer induced normal pressure gradient effects.

6.6 Conclusions

(a) Normal pressure gradients are primarily associated with streamline curvature.
(b) At high Mach numbers the minimum radii of curvature required to give significant normal pressure gradients may well be very large - of order 500 δ.
(c) Significant streamline curvature may occur within the boundary layer as the result of the reflection of an incoming wave structure even though the wall be straight.
(d) Significant streamline curvature may well be induced by the variation of boundary layer displacement thickness in the absence of any incoming wave structure and of any wall curvature.
(e) A pressure dip will be superposed on the normal stress distribution associated with streamline curvature because the normal stress is the sum of a static pressure contribution and a Reynolds stress contribution which may well, at hypersonic Mach numbers, be of the same order.
(f) The presence or absence of significant normal pressure gradients cannot be inferred from the longitudinal (wall) static pressure distribution alone. The link between longitudinal and normal pressure variations depends strongly on the wave structure involved.
(g) The above conclusions are with few exceptions qualitatively supported by the available experimental evidence. Some of the arguments put forward in connection with boundary layer induced pressure gradients are however speculative, and would be clarified by experiments in which the flow outside the boundary layer was studied in rather greater detail than is usual.
(h) Exact quantitative results at hypersonic Mach numbers probably cannot be hoped for, as the response of available static probes in the intensely turbulent part of the boundary layer is problematic even when they have been calibrated in steady flow over an appropriate Mach and Reynolds number range.

7. BOUNDARY LAYER LENGTH SCALES

7.1 The 'physical' boundary layer thickness

The flow on any surface supporting a tubulent boundary layer is, in principle, easily divided into that region affected by vorticity and turbulence, the boundary layer itself, and the region further out which is in most laboratory cases irrotational, the free stream or exterior flow. Unfortunately, even in the simplest possible case with a uniform free stream, there is no clear practical boundary between the two regions since the flow properties in the boundary layer approach their free stream values asymptotically. The majority of practical boundary layer thickness definitions are based on a small measured difference between flow in the outer part of the boundary layer and the free stream (the simplest being δ_{995}, the distance from the surface at which the velocity reaches 0.995 of the free stream value). The combination of a small property decrement (e.g. 0.005 u_e) and the very small gradients causes the resulting boundary layer thickness value to be very sensitive to the accuracy of measurement. At high Mach numbers, the approach of properties to their free stream values becomes even more gradual, and the difficulty is compounded by the likely presence of normal pressure gradients, so that the limiting tendency is not to a set of constant values, but for most properties to a free stream value which itself has a variation in the y-direction.

The determination of a boundary layer thickness δ is of importance for two main purposes. Firstly, a scaling length is required when property distributions in different cases are to be compared, particularly for the variation of turbulence quantities. Secondly, there is need to know where the boundary layer edge is - or at least when a position may safely be assumed to be outside it. Experimentally we wish to know how far out a traverse needs to continue, and for various practical applications it is very important to know when boundary layers growing on opposed surfaces will begin to interact directly. The second factor is also of importance since for many purposes, both in the theoretical treatment and in the documentation of experimental work, scaling values of the flow properties are required, and these are usually taken, in principle, to correspond to the flow just outside the boundary layer.

7.1.1 The boundary layer edge state or 'D-state'

We have throughout the earlier sections of this volume, and its predecessor AGARDograph 223, referred to the boundary layer 'delta' properties ρ_δ, u_δ etc. and used them in theoretical sections and for the formation of Reynolds numbers, integral thicknesses etc. without so far enquiring too closely how they might be determined. A formal approach follows defining terms used in the rest of this section.

The reservoir or R-state In an experimental facility the R-state is the state of fluid from the settling chamber brought reversibly and adiabatically to rest. In flight it is the state of fluid unaffected by the presence of the vehicle brought reversibly and adiabatically to rest relative to the vehicle. The R-state is therefore not a function of position.

The exterior flow or E-state The state of fluid at any point outside the boundary layer is referred to as an E-state. In general the E-state is a function of position, being dependent on the static pressure field in the test zone or generated by the vehicle. Many laboratory flows are shock-free so that the stagnation properties of an E-state are those of the R-state, and so not functions of position. In free flight and in laboratory tests with shock waves in the free stream there will generally be free-stream entropy or total pressure gradients which will cause the stagnation E-state to be a function of position also.

The boundary layer edge or D-state The D-state at a particular station is defined as a state in the outer part of the boundary layer which is specified by some artibrary criterion of departure from a neighbouring E-state.

The R-, E-, and D- states are all actual physically observable states and in principle directly measurable. The R-state is easily, accurately and precisely measured with very simple probes. For the majority of experimental cases in which free stream entropy gradients are negligible, R-state measurements therefore also provide good values for the stagnation properties of the E-states. In such cases a Pitot survey will straightforwardly determine the Mach number and static pressure distribution for all points known to lie outside the boundary layer, with some possible difficulties arising from real gas effects at very high

Mach numbers. Where entropy gradients are present in the free stream, a static property must be measured directly. While troublesome, this will usually be possible with for example a static probe, as the influence of fluctuations should be negligible, so that a probe can be calibrated directly in an appropriate Mach and Reynolds number range.

The D-state however is arbitrarily defined, and usually not too carefully. The D-state lies inside the boundary layer, but is intended to occur 'at the outer edge' of the layer, so that the D-state properties are representative of the local E-state while differing from them slightly as a result of the application of the chosen criterion of difference. If a specification of the D-state is to be at all precise, it is clearly necessary to have available accurate, precise, values for both the outer region 'profile data' and for the local E-state. The most common criteria applied are of the type $u = 0.995\ u_e$ in which the chosen difference is usually much smaller than accuracy of measurement and often less than experimental scatter. Since the boundary layer thickness is then defined as the y-value at which the D-state occurs, and since the property gradients in this region may be very small, it is apparent that even if the precision with which the states in question are estimated is much increased by some averaging or curve fitting procedure, no very precise value for δ can be hoped for on this basis.

7.1.2 Property based boundary layer edge criteria for zero normal pressure gradient cases

If the velocity variation along a profile normal is the result of boundary layer action alone, then a criterion based on a property decrement such as the $0.995\ u_e$ one cited above is in principle straightforward to apply, since u_e and other exterior flow properties are constant. Because it is perhaps the most familiar from low speed studies, the $0.995\ u_e$ criterion initially appears very attractive. However as the Mach number rises, the velocity gradient in the outer part of the layer becomes progressively less and less, so that although the $0.995\ u_e$ criterion will give a usable set of values for the D-state, any estimate of the value of δ becomes increasingly imprecise and indeed unrepeatable. Other properties, such as ρ, M, p_{t2} and possibly in very strong heat transfer cases, T_o may approach their free stream values more abruptly and at greater y-values, and so provide decrement criteria which are more suitable, or at least more precise in the value for δ which they yield. There is some evidence that values so derived also bear a relationship to the point at which turbulence levels reach the free stream value (Laderman & Demetriades, 1979, measurements on a cone at M = 7.1. Revision of Laderman, 1976). The abruptness with which the various flow properties approach the free stream values is perhaps best assessed by an examination of the isentropic and normal shock equations in small difference or error form. For small departures from a local prevailing level

$$\frac{dp_o}{p_o} - \frac{dp}{p} = \frac{\gamma M^2}{1 + \frac{\gamma-1}{2} M^2} \frac{dM}{M} \rightarrow \frac{2\gamma}{\gamma-1} \frac{dM}{M}, \qquad (7.1.1)$$

$$\frac{dp_{t2}}{p_{t2}} - \frac{dp}{p} = \frac{2\,(2M - 1)}{2\gamma M^2 - (\gamma-1)} \frac{dM}{M} \rightarrow 2 \frac{dM}{M}, \qquad (7.1.2)$$

and, eliminating (dM/M),

$$\frac{dp_{t2}}{p_{t2}} = \frac{2(2M^2-1)(1 + \frac{\gamma-1}{2} M^2)}{M^2[2\gamma M - (\gamma-1)]} \frac{dp_o}{p_o} + \frac{2(M^2-1)^2}{M^2[2\gamma M - (\gamma-1)]} \frac{dp}{p} \rightarrow \frac{\gamma-1}{\gamma} \frac{dp_o}{p_o} + \frac{1}{\gamma} \frac{dp}{p} \qquad (7.1.3)$$

where the arrows indicate the high Mach number limit, and the static pressure terms are retained for later use.

If the velocity is to be related to the pressure changes it is necessary to incorporate the energy equation to allow for possible changes in the total temperature:

$$\frac{dp_o}{p_o} - \frac{dp}{p} = \gamma M^2 \left(\frac{du}{u} - \frac{1}{2} \frac{dT_o}{T_o}\right) \qquad (7.1.4)$$

The total temperature term is usually smaller than the velocity term, though not always negligible, and may take either sign. We will initially assume that the flow may be treated, at least in this region, as isoenergetic - i.e. T_o is taken as constant, partly for simplicity, and partly because we have not found a case in which the general conclusions which follow are affected.

For a layer with no normal pressure gradient in isoenergetic flow of a diatomic gas, eqns. (7.1.1 - 7.1.4) give the ratios shown in table (7.1.1).

Table 7.1.1 Relationships between small property changes (γ = 1.4, p, T_o, constant)

Mach number Ratio:	2	4	6	10	∞
$(dp_o/p_o)/(dM/M)$	3.11	5.33	6.15	6.67	7
$(dp_{t2}/p_{t2})/(dM/M)$	1.81	1.95	1.98	1.99	2
$(dp_o/p_o)/(dp_{t2}/p_{t2})$	1.72	2.73	3.11	3.35	3.5
$(dp_o/p_o)/(du/u)$	5.6	22.4	50.4	140	∞
$(dp_{t2}/p_{t2})/(du/u)$	3.26	8.21	16.2	41.8	∞

It can be seen the relationships between small changes in p_o, p_{t2} and M are not strongly dependent on Mach number, while the small velocity changes become less and less sensitive to changes in these variables as the Mach number rises. The 0.995 u_e criterion would correspond to p_{t2} values ranging from 0.984 p_{t2e} at M = 2 to about 0.79 p_{t2e} at M = 10 (though precise numerical values should no longer be taken from small difference equations when the decrement in question is of the order of 20%).

In Fig. (7.1.1) we show experimental values of various flow properties near the boundary layer edge for a profile measured by Horstman & Owen (CAT 7205) with M_e = 7.2. The authors' D-state was defined as the point at which p_o/p_{or} = 0.99, and property values are normalised to this state. The very gradual limiting tendency of u/u_δ, in comparison to the rapid change in p_{t2} and p_o, derived from the Pitot measurements, is very marked, and suggests that the most readily applied criterion will be based directly on p_{t2} measurements, or, as the authors have done here and as is recommended below, on a derived p_o value.

Fig. (7.1.1) shows that this case, for which T_w/T_r was about 0.5, the variation of T_o was also very gradual, and for this reason alone would therefore not be likely to provide a useful decrement criterion. In addition since T_o values are frequently observed to "overshoot" the free stream value, and so display a very gradual fall from values $T_o > T_{o\delta}$ to $T_o = T_{o\delta}$, we reject any further serious consideration of a T_o criterion.

7.1.3 Other criteria for zero normal pressure gradient cases

The property decrement criteria are the most commonly employed, but many others have been proposed. The most obvious is the use of the photographic image in a schlieren or shadowgraph picture. If not significantly affected by refraction (and a properly focused schlieren system should not be while shadowgraph pictures inherently are) this approach will lead to high values of δ, as the image will show the peaks or outermost movements of the eddies present averaged in some manner along the light path and over the time of exposure.

A variety of plotting methods have been put forward, the general aim being to obtain a δ value from a reasonably well conditioned intersection of curves or lines rather than from the almost "grazing" intersection implicit in the use of a small property decrement. These all rely on the free stream properties being accurately known and truly constant. Kistler (CAT 5803) used for δ the y-value at which an extrapolation of the semi-logarithmic portion of his velocity profile reached the free stream velocity. This procedure yields a relatively precise value for δ if the E-states are accurately known, but in common with many other methods requires a fairly complete data reduction before it can be applied. A number of

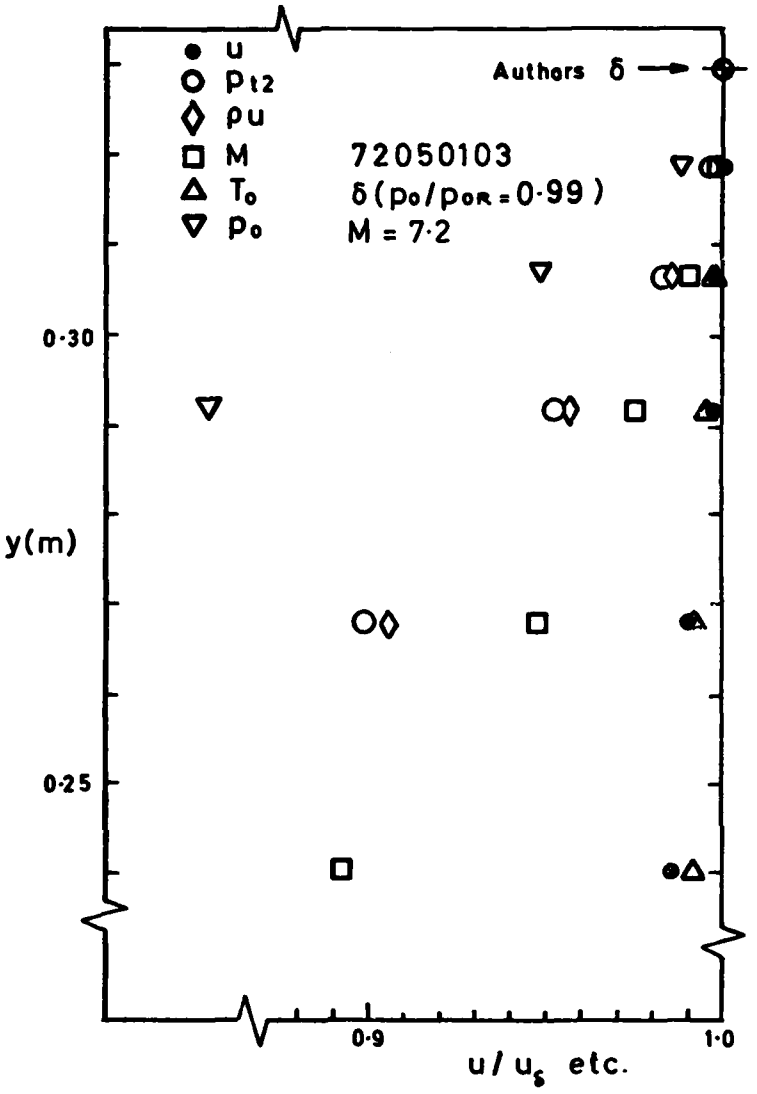

Fig. 7.1.1 Variation of boundary layer flow properties near the boundary layer edge (Horstman & Owen, CAT 7205 0103)

authors (Peterson, 1969; Winter et al., 1970, inter alia) have noted that in many profiles there is a substantial region in which p_{t2} appears to vary linearly with distance from the wall. An extrapolation of this linear variation to meet the free stream value then provides a well conditioned intersection and a precise δ-value. A study of the application of this criterion (Hill, 1976) showed that the δ value was typically a little greater than the value using a 0.995 u_e criterion, but less than the "Kistler" value obtained from the semi-log plot. However, as the Mach number rises the linear portion found up to about Mach 4 increasingly becomes curved, so that the method can no longer be used. Peterson (1969) also gives examples of the application of a method due originally to Schlichting. The outer region is assumed to behave generally as a wake and leads to a prediction (Schlichting, 1968) that

$$[1 - (u/u_\delta)]^{1/2} \propto [1 - (y/\delta)^{3/2}] \qquad (7.1.5)$$

The intercept on the y-axis of a plot of $[1 - (u/u_\delta)]^{1/2}$ should then yield a value for $\delta^{3/2}$. In practice the variation is not linear over the whole outer region so that an element of subjective judgement is required in deciding the range to be treated as linear. Again, it is not a convenient procedure unless data reduction is already complete. Peterson (1969) discusses the question generally, and a further examination has been made by Hill (1976).

Selection of an explicit criterion may be avoided if it is assumed that the relevant portion of the profile is properly described by a wall-and-wake law (eqns. 3.2.5, 3.2.6), so that the value of δ may be obtained from a statistical fit to the experimental data points, either in the original physical variables or after transformation to "equivalent incompressible form" (eqn. 3.3.10). The validity of this procedure must depend on how closely the profile does in fact follow the wall-and-wake law, and on the form of the wake law assumed. It has the advantage of removing subjective judgement as a factor except in the need for a decision as to how near to the (as yet unknown) δ-value one should include data points, since most wake laws do not properly represent the outermost part of the layer. This difficulty may be overcome by using a more complex wake- or divergence-function (see the various forms of eqn. 3.2.6 and Bull, 1969) but the additional complication is probably not worthwhile

If fluctuation measurements are available, a boundary layer edge or characteristic thickness may be defined in relation to these. Definition 'by approach to the free stream fluctuation level' cannot be very precise, as the fluctuation level measurements can never be very accurate. The availability of conditional sampling techniques however makes possible a definition in terms of the 50% intermittency point, as suggested and initially applied by Laderman & Demetriades (CAT 7403). This proposal is attractive as it provides a well conditioned intersection and should be universally applicable. It should also relate properly to the physical process of turbulent mixing in the boundary layer. The 50% intermittency point lies well within the δ-value as defined by the other criteria discussed above, but this is not of itself a disadvantage if the δ-value is defined as a suitable multiple of the y-value at 50% intermittency.

Finally, the problems of choosing an edge criterion may be avoided by using a suitable integral thickness. If there is in fact any universal similarity in the inner and outer regions of the transformed velocity profiles of zero pressure gradient boundary layers, then the defect-integral thickness Δ^* defined in eqn. (3.3.16) should bear a nearly fixed proportion to the physical boundary layer thickness δ, however that may be defined. Acceptance of eqn. (3.3.17) as a description of the outer region gives $\Delta^*/\delta = 4.18$. This corresponds to taking δ as defined by the intersection of eqn. (3.3.17) with the (y/Δ^*) axis in the outer region plots presented in § 4 above, and the validity of the procedure depends on the quality of the fit near the point of intersection. The intersection itself is well conditioned, and, as an integral thickness, Δ^* is precisely determined.

7.1.4 Boundary layer thickness in the presence of normal pressure gradients

When the free stream wave structure is such as to imply significant normal pressure gradients, properties such as M, T, p, ρ, u vary as a result of the free stream pressure field as well as the action of turbulent mixing in the boundary layer. Almost any criterion based on these 'static' properties therefore becomes unworkable, as the gradients in the free stream are finite, while the gradients due to the boundary layer alone are tending to zero. The pressure field induced variation will always therefore become greater than the shear-induced variation at sufficiently large y. Criteria based on a property decrement are particularly difficult to apply, since the decrement is a difference from a quantity which is itself a function of position, and probably experimentally, and so imprecisely, defined.

In a normal pressure gradient case it is always possible to find at least one property which reaches a maximum near the boundary layer edge, and the position of this maximum may be used to define a δ-value. As an example, consider the Pitot pressure profile for a flow with negative $(\partial p/\partial y)$ such as Sturek & Danberg, CAT 7101. As the wall is approached from the free stream, p_{t2} initially rises as the Mach number falls at constant p_o. With a further approach to the wall, p_o begins to fall rapidly as a result of viscous action and the rise in p_{t2} associated with rising static pressure is outweighed by the fall due to the drop in p_o. This approach is not to be encouraged, as it is evident that, other things being equal, a δ-value obtained from a property maximum will occur relatively closer to the wall in a strong normal pressure gradient than in a weak one. The requirement is for comparison with a property which does not vary in the free stream.

In the majority of laboratory cases the free stream total pressure p_{oe} and total temperature T_{oe} may be treated as constant, so that in principle these properties provide a proper base for a boundary edge criterion. The total temperature, however, is not suitable in practice, firstly because it shows a very

gradual approach to the free stream value, and secondly because of the possibility of a 'total temperature overshoot' (see § 7.1.2 and Fig. 7.1.1). A criterion based on p_o, on the other hand, is very attractive. Of the various possible properties it approaches the free stream value the most abruptly (eqns. 7.1.1 - 7.1.4, table 7.1.1 and Fig. 7.1.1) so that a p_o criterion is overtly the most distinct possible. Unfortunately, p_o cannot be measured directly and must instead be found as a combination of experimental Pitot and static tube measurements. The appropriate combination of errors, using eqn. (7.1.3) would seem, at first sight, to counter the advantage of rapid approach to the free stream value exactly. This is not in fact the case, since experimentally one is, or should be, looking for differences between sets of readings taken with the same instruments, so that systematic error should cancel, while random error can be reduced to any desired degree by increasing the number of readings. In principle, the edge criterion should be made by comparison of p_{oe} and p_{or} but at high Mach numbers when for systematic error

$$\frac{dp_o}{p_o} = \frac{\gamma}{\gamma-1}\frac{dp_{t2}}{p_{t2}} - \frac{1}{\gamma-1}\frac{dp}{p} \qquad (7.1.3)$$

the error in (dp/p) is likely to be so large that such an approach will be unhelpful. Instead, the Pitot and static measurements should extend into the exterior flow until there is no systematic trend visible in the p_o value, which may then be usefully compared to the value of p_{or} to give a check on the static pressure value rather than an edge criterion.

Where, in AGARDograph 223 and its successor, we have received profile data which allow us to calculate p_o at points well out into the free stream, we have in general observed that readings are sufficiently precise and repeatable to allow the use of a 1% p_o decrement as a sensible edge criterion. Scatter in p_o is usually small - so small in fact that we have not infrequently avoided making a judgement of the D-state by taking the highest recorded p_o value as the boundary layer edge, at least for initial numerical processing (e.g. Figs. 6.2.2, 6.2.3).

Our experience therefore leads us to recommend that the boundary layer edge state, and the boundary layer edge, be taken at a point where

$$(p_{oe} - p_{od}) = 0.01(p_{oe} - p_w) \qquad (7.1.6)$$

which at high Mach numbers corresponds very closely to $(p_{od}/p_{oe}) = 0.99$, and at low speeds reduces to the common 0.995 u_e criterion.

This criterion should also be applied in zero-normal-pressure-gradient cases, when if the normal pressure gradient is truly negligible, it may be replaced by a directly measured p_{t2} criterion calculated from eqn. (7.1.3) - or, approximately, following table 7.1.1, a 1/3% p_{t2} decrement. To eliminate systematic error the measurements should always extend into the free stream and to allow other workers to apply their own criteria when they wish, the experimental values obtained outside the D-point should be included in any data presentation.

7.2 Integral thicknesses

In the previous section we emphasised the arbitrary nature of the definition of the physical boundary layer thickness δ, and the consequent lack of precision in any numerical value which may be obtained. Suitably defined 'integral thicknesses' do not suffer this disadvantage, since with proper formulation such as that discussed below, the integrands in the defining equations all tend to zero at large y so that the values of the integrals are not sensitive to the choice of δ. A precisely determined length scale is desirable, the object being to use it both as a scaling length for property distributions through the boundary layer and also in the formation of Reynolds numbers when looking for overall similarity rules and empirical projections of data. With the exception of the Rotta-Clauser outer law defect thickness Δ (eqn. 3.3.16), the defining integrals for the usual 'thicknesses' δ_1, δ_2, δ_3 etc., include velocities measured relative to the wall, so that the ratio of any one thickness to any other is Reynolds number dependent. None of these integral thicknesses therefore serves as a scaling length for property distributions even in incompressible flow, so that there is even less reason to attempt any such scaling in compressible cases. The

usual choice of scaling length for Reynolds number formation, δ_2, follows principally from the importance of the momentum defect in the momentum integral equation, and has no special justification in similarity terms. The choice is in essence arbitrary,and if $Re_{\delta 2}$ or Re_θ (see eqns. 2.3.5, 2.3.6) are used as the specifying variable in a data presentation, the ratios of δ_1, δ_3 etc. to δ_2 are implicitly a part of that presentation - as in principle, though not usually in practice, should be the technically desirable relationship to the length of boundary layer development x.

The integral thicknesses are notionally defined so as to represent in convenient form 'deficits' of mass flow, momentum, kinetic energy etc., in the real boundary layer as compared to a reference flow which is representative of the exterior flow extending inwards to the wall for the displacement thickness, and, for the others, to the displacement surface. The integral thicknesses therefore have, in principle, straightforward physical interpretations. When a boundary layer does not experience a significant normal pressure gradient, the E-states are functions of x only and the calculation and interpretation of δ_1, δ_2 etc., present no complications. We see below however that if the physical significance of the quantities called 'displacement thickness', 'momentum thickness' etc. is to be retained in flows with normal pressure gradients, it is necessary to change the usual 'constant E-state' formulation of the integrals to take account of the fact that the E-states are functions of y. As an obvious point, if δ_2 were to be calculated for planar flow from the usual equation

$$\delta_2 = \int_0^\delta \frac{\rho u}{\rho_\delta u_\delta} \left(1 - \frac{u}{u_\delta}\right) \qquad (7.2.1,2.3.8)$$

it is apparent that the value of δ_2 so determined is a function of δ, since ρ_δ and u_δ depend on the choice of D-state. We will see below that eqn. (7.2.1) can only give a value of δ_2 representing the supposed momentum deficit $\rho_\delta u_\delta{}^2 \delta_2$ by chance. A proper formulation of the integral thicknesses will be seen to require inconvenient procedures, so that in addition to a correct presentation we will consider various possible approximations.

7.3 The displacement surface

A technically important result of the growth of the boundary layer is the change induced in the free stream flow, by comparison with some equivalent ideal flow in which viscous effects do not develop. At high Mach numbers the 'displacement effect' may be very large - consider for instance the boundary layer induced pressure gradients discussed in § 6.4, above, or, more directly, the large values of displacement thickness found in hypersonic nozzles (δ_1 is about $0.25R_z$ for CAT 70010104, examined below) so that it is of some importance to assess the effect correctly. Here we require that the comparison be made with an ideal inviscid flow which has the same free stream as that actually observed outside the boundary layer for all $y > \delta$. The ideal flow must extend into the space in fact occupied by the real, viscous, boundary layer flow, and we require, in principle, that this reference flow should be in every particular an extension of the actual free stream flow. If the free stream is supersonic the reference flow is determinate, and could be calculated by the method of characteristics from experimental information describing a sufficient extent of the free stream up- and downstream of the profile normal (Fig. 7.3.1). The displacement surface is then a stream-surface of the reference flow such that the mass flow between the displacement surface and any chosen surface in the free-stream is the same as that in the real viscous flow between the wall and the chosen free-stream stream-surface. The wall is not in general a stream-surface of the reference flow, since the displacement surface is not in general a stream-surface of the real flow. The reference flow is not uniquely determined when the free stream is subsonic, or when an extension of a supersonic free stream indicates that the Mach number in the reference flow will locally become subsonic for $y > \delta^*$ (see below).

7.3.1 Displacement thickness in flows with normal pressure gradients

In this section we will denote a 'properly defined' displacement thickness by δ^*, in contrast to a 'usually defined' thickness δ_1 (eqns. 7.2.1, 2.3.8) or various improperly defined quantities specified by eqns. (7.4.1 - 3). A mass balance between the real flow (ρ,u etc.) and the reference flow (ρ',u' etc.) then requires

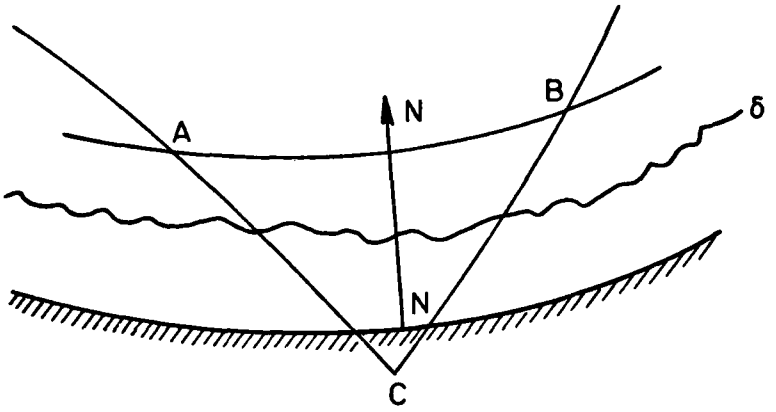

Fig. 7.3.1 Uniqueness of the reference flow. AB is a line in the free stream along which properties are known. AC and BC are right- and left-running characteristics of the free stream flow. All properties in the domain of determinancy ABC are then known so that values along the profile normal NN may be calculated.

$$\int_0^h \rho u(R_z + y\cos\alpha)dy = \int_{\delta^*}^h \rho' u'(R_z + y\cos\alpha)dy, \tag{7.3.1}$$

where h is a value of y greater than δ, R_z is the transverse curvature of the wall, defined positive for boundary layers on the exterior of an axisymmetric body and α is the inclination of the wall to the axis. The form of eqn. (7.3.1) shows that values of ρ', u', for $y < \delta^*$ do not affect the result, so that a calculation of the reference flow does not need to extend to the wall. By the same token, approximate reference flows discussed below need only be accurate representations for $y > \delta^*$. We will in general assume that $\cos\alpha$ may be taken as one, and rewrite eqn. (7.3.1) for convenience in processing data as

$$\int_0^{\delta^*} \rho' u'(1 + \frac{y}{R_z})dy = \int_0^{\delta} (\rho' u' - \rho u)(1 + \frac{y}{R_z})dy \tag{7.3.2}$$

Since, in a flow with normal pressure gradients, ρ' and u' are functions of y, it is necessary to solve for δ^* as a limit in the full form of eqn. (7.3.2).

7.3.2 Displacement thickness in flows with no normal pressure gradient - importance of transverse curvature

If normal pressure gradients are negligible, ρ',u' are constant and may be set equal to ρ_δ,u_δ. Eqn (7.3.2) then reduces to

$$\delta^* + \frac{\delta^{*2}}{2R_z} = \int_0^{\delta} (1 - \frac{\rho u}{\rho_\delta u_\delta})(1 + \frac{y}{R_z})dy \tag{7.3.3}$$

which is the proper form of the defining equation for δ_1, now equal to δ^*, for axisymmetric flow. Data sources by no means always make it clear how far the defining equations for integral thicknesses have taken account of transverse curvature, so that it is advisable to assess its importance. A thorough general treatment for zero normal pressure gradient cases (though this condition is not explicitly stated) is given by Hokenson (1977). We therefore restrict comment here to some general observations. It is apparent that the evaluation of the integral will be inaccurate if (y/R_z) is omitted when (δ/R_z) is significant compared to one at the desired level of accuracy. In general, though not always, source papers have recognized this. In hypersonic flows especially, (δ^*/R_z) may take relatively high values (e.g. 0.25 for CAT 7001), and it is then important to include the $(\delta^{*2}/2R_z)$ term. This is usually not done, the only case in AG223 for which full account of transverse curvature was taken by the original authors being Kemp & Owen (CAT 7206), who however did not in this allow for the very strong normal pressure gradients in

their experiment (see Fig. 6.3.5). In all except the most exceptional circumstances (Richmond 1957, CAT 5701S) the other integral thicknesses δ_2, δ_3 etc. are small compared to R_z so that the quadratic term on the left of equations su h as (7.3.3) - see eqns. (7.5.4) below - may be ignored safely. It will usually only be significant for the determination of the displacement thickness.

7.4 Reference flows, and improper formulations

The reference flow as defined in § 7.3 above is in principle determinate and straight-forwardly, if laboriously, calculable. It is unusual in practice to have a set of values which have been calculated as an extension of the neighbouring experimental free stream flow field. Values are sometimes given for nozzle flows (corresponding to the curves labelled A in Figs. 6.3.1 - 6.3.3) but not necessarily for the exact flow conditions at which the boundary layer measurements were taken. Often the 'theoretical' curves are also calculated in advance, using a predicted displacement surface before the measurements are in fact obtained. This is perhaps the cause of the failure of curves A and B or D to agree at the boundary layer edge in Fig. (6.3.2), and to a lesser extent in Fig. (6.3.3).

7.4.1 Choice of reference flow

To solve eqn. (7.3.2) the reference flow properties ρ',u' must be known. We examine below the effect of three levels of representation of the reference flow:

(a) "Characteristics based". For a profile measured in a nozzle by Fischer et al. (CAT 70010104) we have a characteristics determination of the inviscid flow field, starting from the pressure distribution on the axis (D.M. Bushnell, private communication). This is in reasonably good agreement with experimental values at the boundary layer edge (Fig. 6.3.3), and extends in as far as $y = \delta^*$.

(b) "Linear extention". The reference flow is approximated by a linear projection of the free stream properties into the boundary layer space. This was done graphically as a best eye-estimate. The procedure is relatively convenient, as all the integrands which result are simple polynomials. The linear extension is clearly the obvious first approximation, and in the outer part of the layer will only depart gradually from the 'correct' characteristics values.

(c) "Pressure based". Both the characteristics-based and the linear extension reference flow require that a separate input of reference flow data be made, in addition to the boundary layer measurements. A device which has been commonly employed, and which we adopted in AGARDograph 223, is to calculate a reference flow assumed to be given by an isentropic extension from the free stream total pressure p_{oe} (or failing that, $p_{o\delta}$) to the local experimental value of the static pressure.

The requirement is for good prediction of the reference flow for $y > \delta^*$ (which has yet to be determined). The extent to which the estimates based on linear extension and the local static pressure are likely to provide a good estimate may be assessed from Fig. (7.4.1), based on Figs. (6.3.2, 6.3.3). The linear extension of pressure, as a typical property, will evidently be a good approximation to the characteristic solution. The local measured static pressure is however markedly lower throughout, in particular for hypersonic nozzle flows as a consequence of the "Reynolds stress dip". Regrettably it is apparent, for a flow of the type chosen as an example here, as also for the additional case considered in the numerical experiment below, that the difference between the local static pressure as measured and any static pressure deduced as a reasonable extension of the exterior flow field is large enough to suggest that serious error will result if the pressure based reference flow is adopted for calculation purposes. Therefore, despite its convenience, this approach should probably be abandoned.

(P. Bradshaw, private communication, points out that a boundary layer calculation which did not allow for $\partial p/\partial y$ would probably use as a boundary condition a 'pseudo-velocity' calculated from p_{oe} and p_w - that is pressure, velocity and density used as 'free stream values' would in fact be the wall states of the pressure based reference flow. Figs. (6.3.2, 6.3.3) perhaps indicate that this would be imprudent for a flow with strong $\partial p/\partial y$ though the approach provides a very useful starting point for the calculation of flows such as shock-boundary-layer interactions).

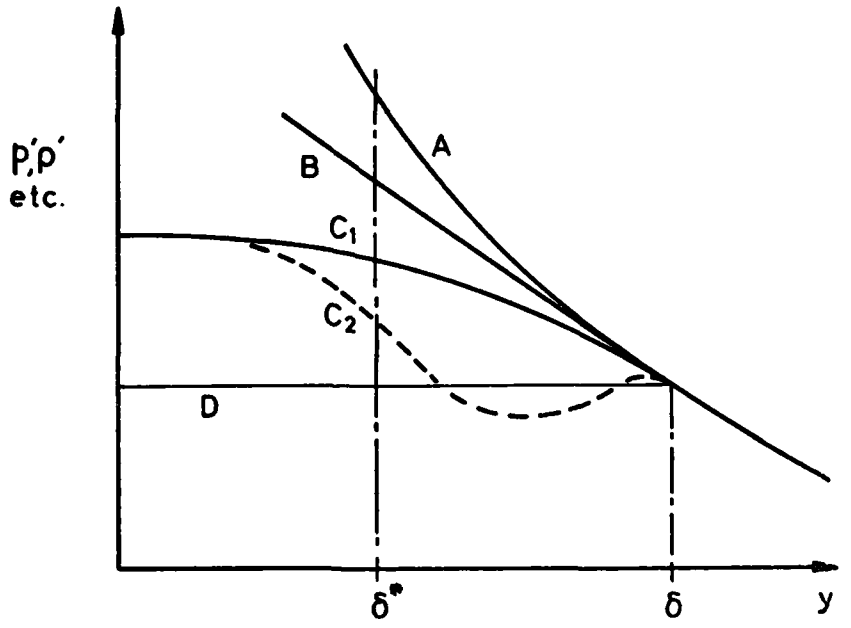

Fig. 7.4.1 Sketch to illustrate different levels of approximation to the reference flow.
A - 'characteristics' or exact value,
B - 'linear extension',
C - 'pressure based',
D - 'constant reference flow'.
The experimental variation shown as C_1 is typical of flow at modest supersonic Mach numbers. In a hypersonic nozzle the 'Reynolds stress dip' (§ 6.3) will give a variation such as the broken line of C_2.

7.4.2 Effect of reference flow variations: Improper formulations

In table (7.4.1) we compare values of δ^* for two profiles (Fischer et al., 7001 0104, the nozzle flow discussed above, and, as representative of flows at lower Mach number, Sturek & Danberg, 7101 0205, measured

Table 7.4.1 Values of displacement thickness (δ^*) and related integral quantities

	Quantity	Reference flow	Eqn.	Values	
	Profile no.	-	-	7001 0104	7101 0205
	M_δ	-	-	21.6	3.16
	p_w/p	-	-	1.35	1.21
1	δ^*(m)	Characteristics	(7.3.2)	7.73×10^{-2}	-
2	δ^*(m)	Linear extension	(7.3.2)	7.57 "	8.31×10^{-3}
3	δ^*(m)	Pressure based	(7.3.2)	6.91 "	7.68 "
4	δ_{1p}(m)	Pressure based	(7.4.1)	7.00 "	7.77 "
5	$\delta_{1(pw)}$(m)	Pressure based	(7.4.2)	7.67 "	8.68 "
6	$\delta_{1(p\delta)}$(m)	Pressure based	(7.4.3)	6.22 "	7.61 "
7	δ_1(m)	Constant, δ values	(7.3.3)	7.31 "	6.80 "

Rows 1 - 3: "properly defined" with differing estimates of the reference flow.
3 - 5: comparison between "properly defined" δ^*(row 3) and improperly defined quantities (rows 4 -6) with the same reference flow.
7: conventional definition.

on a planar ramp). The first three rows give properly defined values of δ^*, with differing estimates of the reference flow. These are succeeded by three improperly defined quantities which have been suggested by various authors attempting to handle the problem of a non-constant reference flow. (As examples,

see McLafferty & Barber, 1959, 1962; Kepler & O'Brien, 1962; Voisinet & Lee, 1972, CAT 7202, 1973, CAT 7304. These authors used a pressure based reference flow and $\delta_{1(pw)}$ as defined in eqn. 7.4.2. Hoydysh & Zakkay, 1969, give complicated definitions which are equivalent to $\delta_{1(pw)}$ and $\delta_{1(p\delta)}$, eqns. 7.4.2, 7.4.3. The definitions adopted by Stroud & Miller, 1966, CAT 6503 are similar. Clutter & Kaups, 1964, CAT 6401, used an 'inviscid' reference flow calculated from the model wall pressure distribution which was then shifted into agreement at the boundary layer edge, with $\delta_{1(p\delta)}$ as defined in eqn.(7.4.3). Finally, in row 7 we give the usual δ_1 value, which may be regarded either as incorrectly formulated, or as an extreme example of a badly estimated reference flow (ρ',u' equal to ρ_δ,u_δ, which are functions of δ). The comparisons form two groups. Variations between row 1, 2, 3 and possibly 7 show the effect of inaccurate estimation of the reference flow. Variations between rows 3, 4, 5 and 6 result from different formulations all using the same (pressure based) reference flow, indicated by writing ρ',u' as ρ_p,u_p. The improperly defined quantities are given by eqns.(7.4.1-7.4.3):

$$\delta_{1p} + \frac{\delta_{1p}^2}{2R_z} = \int_0^\delta (1 - \frac{\rho u}{\rho_p u_p})(1 + \frac{y}{R_z})dy \qquad (7.4.1)$$

This quantity was proposed because of its similarity to the conventional δ_1 and is attractive since no scaling quantities are required, while it is independent of δ if the D-point is taken sufficiently far out.

$$[\delta_{1(pw)} + \frac{\delta_{1(pw)}^2}{2R_z}] (\rho u)_{pw} = \int_0^\delta (\rho_p u_p - \rho u)(1 + \frac{y}{R_z})dy. \qquad (7.4.2)$$

This quantity, as used for instance by Voisinet & Lee (1972, 1973), has the advantage that the scaling quantities ρ_{pw}, u_{pw} do not depend on the choice of D point, so that the value of $\delta_{1(pw)}$ is again independent of δ if δ is sufficiently large. In contrast $\delta_{1(p\delta)}$ below is, through the influence of changes in the D-state, dependent on the choice of D point. It is included as more directly comparable with the conventional δ_1, definition of eqns. (7.2.1, 7.3.3)

$$[\delta_{1(p\delta)} + \frac{\delta_{1(p\delta)}^2}{2R_z}]\rho_\delta u_\delta = \int_0^\delta (\rho_p u_p - \rho u)(1 + \frac{y}{R_z})dy \qquad (7.4.3)$$

The three δ^* values of rows 1-3 clearly demonstrate the influence of the reference flow assumption. (The first row is blank for 7101 0205 as we do not have details of a characteristics calculation). Both flows are on concave walls so that the pressure, and so density and specific mass flow values, fall progressively from the characteristics solution to the pressure based assumption. Row 7, for 7001 0104, gives a higher value again, as would be expected since the Reynolds stress dip causes the static pressure over most of the range $\delta^* < y < \delta$ to be less than the boundary layer edge value, p_δ. For 7101 0205, the row 7 value is the lowest as at the (relatively) low Mach number, the Reynolds stress dip is small or negligible (and was not detected) so that the experimental static pressure distribution is of the form of curve B in Figs. (6.3.2, 6.3.3) and so everywhere above p_δ. (Excepting the Reynolds stress dip, these trends would be reversed for flow over a convex surface).

We cannot claim that the value given in row 1 is accurate in absolute terms, but the differences between rows should be representative. Numerically, at 10% from row 1 to row 3 for 7001 0104 and 22% from row 2 to row 7 for 7101 0205 the differences are appreciable. The technical significance depends on the actual displacement thickness values. For 7001 0104 δ^*/R_z is 0.25 and the difference in δ^* values is, at 7 mm, greater than any conceivable fabrication error. The difference suggests that very refined characteristic calculations for nozzles may well not be justified. For 7101 0205, the difference, at 1.5 mm, is also large compared with likely fabrication errors or the precision of inviscid flow field calculations. Errors resulting from the improper calculation of the reference flow are therefore significant.

As compared with a 'usual' δ_1 determination with constant reference flow, or the pressure-based value, the linear extension appears to give a reasonable approximation (within 2%). It would obviously be fairly straightforward to use a higher order polynomial extrapolation of the free stream propery variation so as to refine this approach, and in the absence of a characteristic calculation and possibly for any extension of these ideas to lower speed flows for which the reference flow is not in principle uniquely determined, this would appear to be the most promising method of estimating a proper δ^* value, if high

accuracy is required. A curve fitting procedure would also eliminate the element of subjective judgement present in the calculations of table 7.4.1.

The improperly defined quantities of rows 4-6 should be compared to the correctly defined but inaccurately determined δ^* value of row 3, as all use the same reference flow. The quantities δ_{1p} and $\delta_{1(pw)}$ are insensitive to choice of δ and the agreement between δ^* (row 3) and δ_{1p} appears to be good. This must be regarded as an empirical agreement which may exist for concave wall flows, as we do not have any convex wall data with sufficient detail for a useful comparison. Any general analytical estimate of the difference between δ^* and δ_{1p} or an equivalent quantity using a better reference flow is intractable since δ^* is found by solution of eqn. (7.3.2) for δ^* as the limit of a definite integral. The difference between $\delta_{1(pw)}$ and δ^* with the same reference flow is unacceptably large - 10% or more - so that this formulation is unlikely to be useful. The row 6 quantity $\delta_{1(p\delta)}$ takes an arbitrary value depending on the choice of a δ value, and like the 'usual' δ_1 of row 7 should be discarded for this reason alone. In a concave wall flow such as the two examples treated here, as the chosen value of δ increased δ_1 would fall continuously while $\delta_{1(p\delta)}$ would rise. The arbitrary nature of $\delta_{1(p_\delta)}$ is particularly clearly illustrated by the values obtained for the nozzle flow reported by Kemp & Owen (CAT 7206). For 10 cases out of 29, $\delta_{1(ps)}$ as defined by eqn. (7.4.3) is found to take a complex value (shown as NOT REAL in the print-out in AGARDograph 223).

In conclusion, the error resulting from an inaccurately assessed reference flow would seem, on an empirical basis, to be much greater than the error resulting from a choice of certain improperly defined quantities, such as δ_{1p} with a better reference flow, which may be more straightforwardly determined.

7.5 Defect thicknesses

The displacement thickness δ^* is a quantity which has direct physical significance in its own right. Particularly at hypersonic speeds, when it may achieve relatively large values and so modify the exterior flow to a substantial extent, there is a need to evaluate it properly and as accurately as possible. The momentum thickness, whether in its 'usual' formulation as δ_2 (eqn. 2.3.4), or properly defined as θ below (eqn. 7.5.5) has no such direct physical significance, but rather provides (at least in flows without normal pressure gradients) a convenient way of describing the accumulated friction effect of the boundary layer. It appears in the momentum integral equation in just this way - the integral equation itself being a convenient shorthand for a control surface momentum balance. If only because of its importance in the momentum integral equation, the momentum defect thickness is also, conventionally, the most favoured reference length for the formation of Reynolds numbers intended to correlate experimental data. The factors which affect a proper definition of the momentum thickness apply equally to the other defect thicknesses, such as δ_3, δ_4 etc., each integral quantity having value only in so far as it actually describes the defect of the flow property (specific momentum, kinetic energy, total enthalpy etc.) resulting from the presence of the boundary layer. Our initial development is therefore in general terms.

7.5.1 General formulation for a property defect

We require a value for the defect of a convected property q (specific momentum, kinetic energy, total enthalpy as appropriate) in the real boundary layer as compared with the value for the same mass flow of fluid in the ideal or reference flow, which must therefore be evaluated from the displacement thickness outwards. The defect should be described accurately, and a proper formulation will be insensitive to the choice of D-state or δ-point. A proper defining equation for the deficit of the property q is then, following the arguments of § 7.3,

$$\frac{(\text{deficit of } q)}{2\pi R_z} = \int_{\delta^*}^{h} \rho' u' q' \left(1 + \frac{y\cos\alpha}{R_z}\right) dy - \int_{0}^{h} \rho u q \left(1 + \frac{y\cos\alpha}{R_z}\right) dy \qquad (7.5.1)$$

in which it can again be seen that reference flow values for $y < \delta^*$ do not influence the result. In calculation it is again convenient to rearrange eqn. (7.5.1) as (once more setting $\cos\alpha = 1$):

$$\frac{(\text{deficit of } q)}{2\pi R_z} = \int_{0}^{\delta} (\rho' u' q' - \rho u q)\left(1 + \frac{y}{R_z}\right) dy - \int_{0}^{\delta^*} \rho' u' q' \left(1 + \frac{y}{R_z}\right) dy \qquad (7.5.2)$$

The subsequent definition of a defect thickness in terms of the property deficit is essentially arbitrary, as it is necessary to choose representative scaling values for ρ, u and q. The natural extension of low speed practice is to define a deficit annulus adjacent to the wall and δ_q in depth, where δ_q is the desired defect thickness. Then

$$\frac{(\text{deficit of q})}{2\pi R_z} = \int_0^{\delta_q} (\rho' u' q')_{\text{scale}} (1 + \frac{y}{R_z}) dy \qquad (7.5.3)$$

where $(\rho' u' q')_{\text{scale}}$ is the chosen scaling flux per unit area of the convected property q, and is essentially defined in terms of an arbitrary chosen state of the reference flow.

For flows with no normal pressure gradient in which ρ',u',q' are constant and may be evaluated at the D-state, eqns. (7.5.1 - 7.5.3) then give

$$\delta_q + \frac{\delta_q^2}{2R_z} = \int_0^{\delta} \frac{\rho u}{\rho_\delta u_\delta} (1 - \frac{q}{q_\delta})(1 + \frac{y}{R_z}) dy \qquad (7.5.4)$$

which can be seen to reduce to the 'usual' definition for a planar flow. As remarked in § 7.3.2 above, the defect thicknesses are nearly always very small compared to R_z so that the quadratic term $(\delta_q^2/2R_z)$ may usually be dropped safely.

7.5.2 Momentum defect thickness

We take the momentum defect thickness as a typical integral quantity of this class, and will not discuss the other possibilities further. If it is desired to describe the momentum defect as a thickness, a scaling value for (ρu^2) must be chosen, and the value of the thickness which results will be in inverse proportion to this scaling value. Ideally the scaling value should be taken at a fixed state with physical significance in the reference flow, but the only value which suggests itself on this basis is a value calculated at $y = \delta^*$, which would in practice be inconvenient. A fixed value may be obtained by choosing $(\rho u^2)_{pw}$, the value for the pressure-based reference flow at the wall. This state however is not a state of a reasonable extension of the free stream flow field, and so not attractive, although it is in fact numerically not too different from the values of a characteristic based or linear extended reference flow at $y = \delta^*$ (see Figs. 6.3.2, 6.3.3). The choice is arbitrary, and for our convenience, since many of the necessary integral quantities are tabulated in AGARDograph 223, the scaling quantity used here is $(\rho u^2)_\delta$. Recognising that the value of a properly defined momentum defect thickness will then depend on the choice of D-state we may then recast eqns. (7.5.1)-(7.5.3) to give

$$\theta = \frac{(\text{momentum deficit})}{2\pi R_z \rho_\delta u_\delta^2} = \int_{\delta^*}^{\delta} \frac{\rho' u'^2}{\rho_\delta u_\delta^2} (1 + \frac{y}{R_z}) dy + \delta_2 + \frac{\delta_1^2}{2R_z} + \delta_1 + \frac{\delta_1^2}{2R_z} - \delta - \frac{\delta^2}{2R_z} \qquad (7.5.5)$$

where δ_1,δ_2 are the 'usual' displacement and momentum defect thicknesses evaluated with a constant reference flow corresponding to the D-state. The formulation for the momentum deficit (as opposed to the value of θ) is not sensitive to the choice of D-point so long as the same value of δ is used for all the integrals.

7.5.3 Choice of reference flow

It is apparent that the value of the momentum deficit and of θ as found from eqn. (7.5.5) will depend on the reference flow values used. Once δ has been chosen, the only term affected is the integral at the start of the right hand side of (7.5.5). Unfortunately, the (positive) value of this integral is very nearly the same as the (negative) sum of the remaining terms, so that the value of θ, and so the momentum deficit, is found as the difference of two large quantities of nearly the same magnitude. The value is therefore very sensitive to the determination of the reference flow, so much so that in any flow with significant normal pressure gradients, it may be wise to say that the momentum deficit cannot be sensibly determined unless unusually precise and accurate information for the reference flow is available. In table (7.5.1) we give, in rows 1-3, values for θ calculated using the same data as for the δ^* comparison of table (7.4.1).

In row 2, calculated using the linear extension reference flow, the integral term in eqn. (7.5.5) is about

Table 7.5.1 Values of momentum thickness θ and related integral quantities

	Quantity	Reference flow	Scaling	Eqn.	Values	
	Profile no.	-	-	-	7001 0104	7101 0205
	M_δ	-	-	-	21.6	3.16
	P_w/P_δ	-	-	-	1.35	1.21
	Defect thicknesses (mm):					
1	θ	Characteristics	$(\rho,u)_\delta$	(7.5.5)	2.46	-
2	θ	Linear extension	$(\rho,u)_\delta$	(7.5.5)	2.33	1.50
3	θ	Pressure based	$(\rho,u)_\delta$	(7.5.5)	0.18	1.51
4	δ_{2p}	Pressure based	$(\rho,u)_\delta$	(7.5.6)	0.23	1.37
5	$\delta_{2(pw)}$	Pressure based	$(\rho,u)_{pw}$	(7.5.7)	0.21	1.35
6	$\delta_{2(p\delta)}$	Pressure based	$(\rho,u)_\delta$	(7.5.8)	0.25	1.52
7	δ_2	Constant,δ values	$(\rho,u)_\delta$	(7.5.4)	0.24	1.62

Rows 1 - 3: "properly defined" with differing estimates of the reference flow.
3 - 5: comparison between 'properly defined' θ (row 3) and improperly defined quantities (rows 4 - 6) with the same reference flow.
7: conventional definition.

20 times θ for 7001 0104, and 8 times θ for 7101 0205, so that the absolute values of θ given here should not be expected to be very accurate even within the framework of the assumptions used to calculate them. The trends however should be representative, and consequently the fact that a properly determined θ value using a reasonable extension of the free stream (rows 1, 2) can, as for 7001 0104, be 10 times as large as a value using the customary constant reference flow (row 7) or the convenient pressure based variable reference flow which has been much used in the past (row 3) is very disturbing. The difference is not so marked for the relatively low Mach number case 7101 0205, though it would not be safe to assume that reasonable agreement is ensured by lower Mach numbers.

It is evidently important that any 'proper' scheme for calculating the integral thicknesses should be self consistent. The δ^* value used in determining θ must be calculated using the same reference flow - the general sensitivity of the calculation is further displayed by a fall in θ (row 2) for 7001 0104 from 2.33 mm to 0.82 mm if the δ^* value obtained from the characteristics calculation is used in eqn. (7.5.5) instead of the self-consistent linear extension value. The corresponding change in δ^* values is 2½%. Thus a δ^* value may well be found with acceptable accuracy for the specification of displacement effect while a higher order of accuracy in δ^* is required if a proper θ value is to be calculated.

7.5.4 Improper formulations

In rows 4, 5, 6 of table (7.5.1) we also present various integral quantities related to the momentum thickness. These are δ_2-type quantities related to the δ_1-type quantities defined in eqns. (7.4.1 - 7.4.3) with the same supposed advantages and disadvantages in formulation. They originate in the works cited at the start of § 7.4.2.

$$\delta_{2p} + \frac{\delta_{2p}^2}{2R_z} = \int_0^\delta \frac{\rho u}{\rho_p u_p}\left(1 - \frac{u}{u_p}\right)\left(1 + \frac{y}{R_z}\right)dy \qquad (7.5.6)$$

$$\left[\delta_{2(pw)} + \frac{\delta_{2(pw)}^2}{2R_z}\right](\rho u^2)_{pw} = \int_0^\delta \rho u(u_p - u)\left(1 + \frac{y}{R_z}\right)dy \qquad (7.5.7)$$

$$\left[\delta_{2(p\ )} + \frac{\delta_{2(p\delta)}^2}{2R_z}\right](\rho u^2)_\delta = \int_0^\delta \rho u(u_p - u)\left(1 + \frac{y}{R_z}\right)dy \qquad (7.5.8)$$

The deficit value appearing in eqns. (7.5.7, 7.5.8) is the same, the difference between $\delta_{2(pw)}$ and $\delta_{2(p\delta)}$ merely reflecting the difference between the scaling values used. Rows [illegible] the same reference flow, and except for row 5, the same scaling quantities. The results of our [illegible]ition again suggest that the choice of a proper reference flow is far more important than the choice [illegible]ormulation, though the modest level of agreement in rows 3, 4 and 6 should be considered to contain a measure of coincidence. The final row, 7, again provides the 'usual' value for comparison, either with rows 1-3, as an example of a badly estimated reference flow, or as a further case of improper formulation. For this case alone is the actual deficit obtained dependent on the choice of D-point.

7.6 Discussion

The analysis above shows that the momentum defect thickness is, as by the same token, would be the other property defect thicknesses, very sensitive to the accuracy of determination of the reference flow. In tables (7.4.1) and (7.5.1), row 1 represents a best estimate of the appropriate reference flow and row 2 a sensible first approximation. In rows 3 to 6 a convenient but inaccurate method of calculation is used, while a 'conventional' value is given in row 7 (this 'conventional' value is in a sense properly defined, but with an exceedingly inaccurate reference flow). The results show that while acceptable estimates can be made for the displacement thickness, a properly defined momentum thickness can only be determined in the presence of normal pressure gradients if enough measurements are made in the free stream to allow a refined estimate, or a proper characteristics calculation, of an appropriate reference flow as discussed in § 7.2.1 above.

Any agreement between a properly defined value of θ using a good estimate for the reference flow and one or more of the improperly defined quantities in rows 4-7 must be regarded as coincidental. This leaves the question of whether the very large difference between the best estimate of row 1 for 7001 0104 and rows 4-7 is significant. The characteristics solution used does not agree exactly at the boundary layer edge, so that there is some systematic error. The reference flows used for row 1 and 2 do however differ quite noticeably, while row 2 appears as quite a good approximation when plotted out. It seems likely then that the difference is real, and numerically, with a factor of 10, it is most marked. Whether it is exactly calculated or not, the mere fact that so large a variation can result from choosing a proper as opposed to an improper definition must, for flows with significant normal pressure gradients, throw in doubt any correlations based on Reynolds numbers using θ as a reference length. In the absence of firm reference flow values which agree with experimental data at the edge of the boundary layer, the numerical results are inevitably erratic. Agreement at the D-state for profile 7001 0104 was quite good for both the characteristics solution and the eye-estimated linear extension. For profile 7101 0205, the linear extension was based on the free stream measurements, but did not agree at the D-point which was retained at the $(\rho u)_{max}$ point as for AGARDograph 223. This introduces yet a further variable requiring exploration. The range of variation is not however so marked in this case.

7.7 Conclusions

(a) Special care is required in arriving at values for all boundary layer thickness scales in flows with significant normal pressure gradients.

(b) The physical boundary layer thickness is best defined in terms of a total pressure criterion, or possibly in relation to percentage intermittency.

(c) The integral thicknesses cannot be evaluated properly without information which allows a precise determination of a reference flow which is in all particulars a reasonable extension of the potential flow outside the boundary layer.

(d) The displacement thickness δ^* can probably be determined with reasonable accuracy even with an approximate reference flow.

(e) The value of the momentum defect thickness θ, as properly representative of the momentum deficit of the boundary layer, is exceedingly sensitive to accuracy in the reference flow.

(f) Reference flow information is generally inadequate for the determination of a proper θ-value.

(g) Consequently correlations of data, for flows with normal pressure gradients, which are based on Re_θ should be examined closely.

(h) The arguments above once more emphasise a requirement for experimental observations to extend well into the free stream.

REFERENCES

Acharya M. 1977 Effects of compressibility on boundary layer turbulence. AIAA J. 15, 303-305 and AIAA Paper 76-334.

Acharya M. 1978 On the measurement of turbulent fluctuations in high speed flows using hot wires and hot films. NASA TM 78535.

Acharya M., Kussoy M.I., Horstman C.C. 1978 Reynolds number and pressure gradient effects on compressible turbulent boundary layers. AIAA Paper 78-199. See also Kussoy, Horstman, Acharya. Finally AIAA J. 16, 1217-1218.

Ackermann G. 1942 Plattenthermometer in Strömung mit großer Geschwindigkeit und turbulenter Grenzschicht. Forschung auf dem Gebiet des Ingenieurwesens 13, 226-234.

Adams J.C., Hodge B.K. 1977 The calculation of compressible, transitional, turbulent and relaminarizational boundary layers over smooth and rough surfaces using an extended mixing length hypothesis. AIAA Paper 77-682.

Adcock J.B., Peterson J.B., McRee D.J. 1965 Experimental investigation of a turbulent boundary layer at Mach 6, high Reynolds numbers and zero heat transfer. NASA TN D-2907, (CAT 6501).

Allen J.M. 1970 Experimental Preston tube and law-of-the-wall study of turbulent skin friction on axisymmetric bodies at supersonic speeds. NASA TN D-5660, (CAT 7005).

Allen J.M. 1972 Pitot probe displacement in a supersonic turbulent boundary layer. NASA TN D-6759, (CAT 7303).

Allen J.M. 1973a Evaluation of compressible flow Preston tube evaluations. NASA TN D-7190, (CAT 7303).

Allen J.M. 1973b Evaluation of Preston tube calibration equations in supersonic flow. AIAA J. 11, 1461-1463.

Allen J.M. 1974a Effects of Mach number on Pitot probe displacement in a turbulent boundary layer. NASA TN D-7466.

Allen J.M. 1974b Reply by author to P. Bradshaw and K. Unsworth (Evaluation of Preston tube calibration equations in supersonic flow). AIAA J. 12, 1295-1296.

Allen J.M. 1975 Influence of probe geometry on Pitot probe displacement in supersonic turbulent flow. AIAA J. 13, 949-950.

Allen J.M. 1976 Systematic study of error sources in supersonic skin friction balance measurements. NASA TN D-8291.

Allen J.M. 1977a Experimental study of error sources in skin friction balance measurements. Trans ASME Ser. I 99, 197-204.

Allen J.M. 1977b Re-evaluation of compressible flow Preston tube calibrations. NASA TM X-3488.

Allen J.M. 1977c Re-evaluation of compressible flow Preston tube calibrations. J. Fluids Engrg. 99, 197.

Antonia, R.A., Luxton R.E. 1971 The response of a turbulent boundary layer to a step change in surface roughness. Pt. 1 Smooth to rough. J. Fluid Mech. 48, 721-761.

Back L.H. 1970 Acceleration and cooling effects in laminar boundary layers - subsonic, transonic and supersonic speeds. AIAA J. 8, 794-802.

Back L.H., Massier P.F., Cuffel R.F. 1967 Flow phenomena and convective heat transfer in a conical supersonic nozzle. J. Spacecraft & Rockets 4, 1040-1047.

Back L.H., Cuffel R.F., Massier P.F. 1969a Laminarization of a turbulent boundary layer in nozzle flow. AIAA J. 7, 730-733.

Back L.H., Cuffel R.F., Massier P.F. 1969b Laminar, transition and turbulent boundary layer heat transfer measurements with wall cooling in turbulent airflow through a tube. Trans. Am. Soc. Mech. Engrs. Ser. C, 91, 477-487.

Back L.H., Cuffel R.F., Massier P.F. 1970a Laminarization of a turbulent boundary layer in nozzle flow - boundary layer and heat transfer measurements with wall cooling. Trans. Am. Soc. Mech. Engrs. Ser. C, 92, 333-344.

Back L.H., Cuffel R.F., Massier P.F. 1970b Experimental convective heat transfer and pressure distributions and boundary layer thicknesses through a variable cross sectional area channel. 4th Int. Heat Transfer Conf. Versailles, 2.

Back L.H., Cuffel R.F. 1970 Relationship between temperature and velocity profiles in a turbulent boundary layer along a supersonic nozzle with heat transfer. AIAA J. 8, 2067-2069.

Back L.H., Cuffel R.F. 1971 Turbulent boundary layer and heat transfer measurements along a convergent-divergent nozzle. Trans. Am. Soc. Mech. Engrs., Ser. C, 93, 397-407.

Back L.H., Cuffel R.F. 1972 Turbulent boundary layer measurements along a supersonic nozzle with and without wall cooling. Trans. Am. Soc. Mech. Engrs., Ser. C, 94, 242-243, (CAT 7207).

Backx E. 1973 Measurements in the Mach 15 turbulent boundary layer on the wall of the longshot conical nozzle. Von Karman Institute. Preprint 73-01.

Backx E. 1975 A study of the turbulent boundary layer at Mach 15 and 19.8 on the wall of a conical nozzle. Ph. D. thesis Catholic Univ. Leuven.

Backx E., Richards B.E. 1976 A high Mach number turbulent boundary layer study. AIAA J. 14, 1159-1161.

Bartlett R.P., Edwards A.J., Harvey J.K., Hillier R. 1979a Pitot pressure and total temperature profile measurements in a hypersonic, turbulent boundary layer at M = 9. I.C. Aero Rep. 79-01.

Bartlett R.P., Edwards A.J., Hillier R. 1979b Development and calibration of a total temperature probe for the Imperial College Aeronautics Dept. Gun Tunnel. I.C. Aero Rep. 79-02.

Beckwith I.E. 1970 Recent advances in research on compressible turbulent boundary layers. In Analytical Methods in Aircraft Aerodynamics. NASA SP 228, 355-416.

Beckwith I.E., Harvey W.D., Clark F.L. 1971 Comparisons of turbulent boundary layer measurements at Mach number 19.5 with theory and an assessment of probe errors. NASA TN D-6192, (CAT 7105).

Berg D.E. 1977 Surface roughness effects on the hypersonic turbulent boundary layer. CALTECH Pasadena Ph. D. thesis. Univ. Microfilms 77-17260. See also Kubota & Berg.

Bertram M.H., Neal L. 1965 Recent experiments in hypersonic turbulent boundary layers. NASA TM X-56335.

Bertram M.H., Cary A.M., Whitehead A.H. 1968 Experiments with hypersonic turbulent boundary layers on flat plates and delta wings. AGARD Hypersonic Boundary Layers and Flow Fields. Conf. Proc. 30.

Boldman D.R., Schmidt J.F., Fortini A. 1966 Turbulence, heat transfer and boundary layer measurements in a conical nozzle with a controlled inlet velocity profile. NASA TN D-3221.

Boldman D.R., Schmidt J.F., Ehlers R.C. 1967 Effect of uncooled inlet length and nozzle convergence angle on the turbulent boundary layer and heat transfer in conical nozzles operating with air. Trans. Am. Soc. Mech. Engrs. Ser. G 89, 341-350.

Boldman, D.R., Neumann H.E., Schmidt J.F. 1967b Heat transfer in 30^{o} and 60^{o} half-angle of convergence nozzles with various diameter uncooled pipe inlets. NASA TN D-4177.

Boldman D.R., Schmidt J.F., Gallagher A.K. 1968 Laminarization of a turbulent boundary layer as observed from heat-transfer and boundary layer measurements in conical nozzles. NASA TN D-4788.

Boldman D.R., Schmidt J.F., Ehlers R.C. 1969 Experimental and theoretical turbulent boundary layer development in a Mach 4.4 water cooled conical nozzle. NASA TN D-5377, (CAT 6901).

Boldman D.R., Neumann H.E., Ehlers R.C. 1970 Velocity, intermittency and turbulence intensity measurements in the boundary layer of an accelerated flow. NASA TN D-6043.

Boldman D.R., Graham R.W. 1972 Heat transfer and boundary layers in conical nozzles. NASA TN D-6594.

Bradshaw P. 1974a The effect of mean compression or dilatation on the turbulence structure of supersonic boundary layers. J. Fluid Mech. 63, 449-464.

Bradshaw P. (Editor) 1976 Topics in Applied Physics, Turbulence. Springer V. Berlin.

Bradshaw P. 1977a Compressible turbulent shear layers. Ann. Rev. Fluid Mech. 9, 33-54.

Bradshaw P. 1977b An improved van Driest skin-friction formula for compressible turbulent boundary layers. AIAA J. 15, 212-214.

Bradshaw P., Ferris D.H. 1971 Calculation of boundary layer development using the turbulent energy equation: compressible flow or adiabatic walls. J.Fluid Mech. 46, 83-110.

Bradshaw P., Unsworth K. 1973 A note on Preston tube calibrations in compressible flow. I.C. Aero. Rep. 73-07.

Bradshaw P., Unsworth, K. 1974 Comment on "Evaluation of Preston tube calibration equations in supersonic flow". AIAA J. 12, 1293-1295.

Brederode de V., Bradshaw P. 1978 Influence of side walls on the turbulent center-plane boundary layer in a square duct. J. Fluids Engrg. 100, 91-96.

Bruno J.R., Yanta W.J., Risher D.B. 1969 Balance for measuring skin friction in the presence of heat transfer. NOL TR 69-56.

Bull M.K. 1969 Velocity profiles of turbulent boundary layers. J. Roy. Aeronaut. Soc. 73, 143-147.

Busemann A. 1931 Gasdynamik in Handbuch der Experimentalphysik. Bd IV, 1. Eds. Wien-Harms. Akad. Verlagsgesellschaft, Leipzig.

Busemann A. 1935 Gasströmung mit laminarer Grenzschicht entlang einer Platte. ZAMM 15, 23-25.

Bushnell D.M., Johnson C.B., Harvey W.D., Feller W.V. 1969 Comparison of prediction methods and studies of relaxation in hypersonic turbulent nozzle-wall boundary layers. NASA TN D-5433.

Bushnell D.M., Beckwith I.E. 1969 Calculation of nonequilibrium hypersonic turbulent boundary layers and comparisons with experimental data. AIAA Paper 69-684.

Bushnell D.M., Cary A.M.Jr., Harris J.E. 1976 Calculation methods for compressible turbulent boundary layers.State-of-the-art 1976. NASA SP 422.

Cary A.M. 1970a Turbulent boundary layer heat transfer and transition measurements with surface cooling at Mach 6. NASA TN D-5863.

Cary A.M. 1970b Summary of available information on Reynolds analogy for zero-pressure-gradient, compressible turbulent boundary layer flow. NASA TN D-5560.

Cary A.M., Bertram M.H. 1974 Engineering prediction of turbulent skin friction and heat transfer in high-speed flow. NASA TN D-7507.

Cebeci T., Smith A.M.O. 1974 Analysis of turbulent boundary layers. Academic Press, New York.

Chapman D.R., Kester R.H. 1953 Measurements of turbulent skin friction on cylinders in axial flow at subsonic and supersonic velocities. J. Aero. Sci. 20, 441-448.

Chen K.K. 1972 Compressible turbulent boundary layer heat transfer to rough surfaces under arbitrary pressure gradient. AIAA J. 10, 623-629 (1972) and AIAA Paper 71-166, 1-10.

Chew Y.T., Squire L.C. 1979 The boundary layer development downstream of a shock interaction at an expansion corner. J.F.M. (to be published).

Chew Y.T. 1979 Shock wave and boundary layer interaction in the presence of an expansion corner. Aero. Quart. XXX, 506-527.

Clauser F.H. 1956 The turbulent boundary layer. Advances in Applied Mechanics Vol. IV, New York 1-56.

Clutter D.W., Kaups K. 1964 Wind-tunnel investigation of turbulent boundary layers on axially symmetric bodies at supersonic speeds. Douglas Aircraft Rept. LB 31425, AD 435111, (CAT 6401).

Cohen N.B. 1959 A method for computing turbulent heat transfer in the presence of a streamwise pressure gradient for bodies in high-speed flow. NASA Memo. 1-2-59L.

Colburn A.P. 1933 A method of correlating forced convection heat transfer data and a comparison with fluid friction. Trans. AICh. Engrs. 29, 174-210.

Coleman G.T. 1973a A study of hypersonic boundary layers over a family of axisymmetric bodies at zero incidence: Preliminary report and data tabulation. Imp. Col. Aero. Rep. 73-06.

Coleman G.T. 1973b Hypersonic turbulent boundary layer studies. Ph.D. thesis, Univ. of London.

Coleman G.T., Osborne C., Stollery J.L. 1973 Heat transfer from a hypersonic turbulent boundary layer on a flat plate. J. Fluid. Mech. 60, 257-272.

Coles D. 1953 Measurements in the boundary layer on a smooth flat plate in supersonic flow.
I. The problem of the turbulent boundary layer.
II. Instrumentation and experimental techniques at the Jet Propulsion Laboratory.
III. Measurements in a flat plate boundary layer at the Jet Propulsion Laboratory.
J.P.L. Cal. Inst. Tech. Rep.Nos. 20-69, 20-70, 20-71, (CAT 5301).

Coles D. 1954 Measurement of turbulent friction on a smooth flat plate in supersonic flow. J. Aeronaut. Sci. 21, 433-448, (CAT 5301).

Coles D. 1956 The law of the wake in the turbulent boundary layer. J. Fluid Mech. 1, 191-226.

Coles D. 1964 The turbulent boundary layer in a compressible fluid. Phys. Fluids 7, 1403-1423.

Coles D.E., Hirst E.A. 1969 Proceedings Computation of Turbulent Boundary Layers - 1968 AFOSR-IFP Stanford Conference. Volume II Compiled Data. Stanford Univ., Stanford, USA.

Crocco L. 1932 Sulla trasmissione del calore da una lamina piana a un fluido scorrente ad alta velocità. L'Aerotecnica 12, 181-197.

Crocco L. 1946 Lo strato laminare nei gas. Ministero della Difesa-Aeronautica,Roma.Monografie Scientifiche di Aeronautica 3. Transl. in Aerophys. Lab. North Amer. Aviation Rept.AL-684; 1948

Crocco L. 1963 Transformations of the compressible turbulent boundary layer with heat exchange. AIAA J. 1, 2723-2731.

Danberg J.E. 1960 Measurements of the characteristics of the compressible turbulent boundary layer with air injection. NAVORD Rep. 6683.

Danberg J.E. 1961 The equlilibrium temperature probe, a device for measuring temperatures in hypersonic layers NOLTR 61-2.

Danberg J.E. 1964 Characteristics of the turbulent boundary layer with heat and mass transfer at M = 6.7. NOLTR 64-99.

Danberg J.E. 1967 Characteristics of the turbulent boundary layer with heat and mass transfer: Data tabulation. NOLTR 67-6, (CAT 6702).

Danberg J.E. 1971 A re-evaluation of zero pressure gradient compressible turbulent boundary layer measurements. CPP 93-71 (AGARD)

Demetriades A. 1960 An experiment on the stability of hypersonic laminar boundary layers. J. Fluid Mech. 7, 385-396.

Dhawan S. 1953 Direct measurement of skin friction. NACA Rep. 1121.

van Driest E.R. 1951 Turbulent boundary layer in compressible fluids. J. Aeronaut. Sci.18, 145-160.

van Driest E.R. 1954 The laminar boundary layer with variable fluid properties. Presented at the 1954 Meeting of the Heat Transfer and Fluid Mechanics Institute, Berkeley.

van Driest E.R. 1955 The turbulent boundary layer with variable Prandtl number in "50 Jahre Grenzschichtforschung". Ed. H. Görtler, Vieweg Verlag Braunschweig.

van Driest E.R. 1956 The problem of aerodynamic heating. Aeronaut. Eng. Review 15, 26-41.

Dunn D.W., Lin C.C. 1955 On the stability of the laminar boundary layer in a compressible fluid. J. Aero. Sci. 22, 455.

Dvorak F.A. 1969 Calculation of turbulent boundary layers on rough surfaces in pressure gradients. AIAA J. 7, 1752-1759.

East R.A., Perry J.H. 1967 A short time response stagnation temperature probe. Aeronaut. Res. Council C.P. 909.

Eaton C.J. et al. 1968 Experimental studies at Mach numbers of 3.4 and 5 of turbulent boundary layer heat transfer in two-dimensional flow with pressure gradient. BAC GW Div. Rep. ST 2310.

Economos C. 1970 A modified form of the Coles-compressibility transformation. AIAA J. 8, 2284-2286.

Economos C., Boccio J. 1970 An investigation of the high speed turbulent boundary layer with heat transfer and arbitrary pressure gradient. NASA CR 1679 and 1680.

Fallis W.B. 1952 Heat transfer in the transitional and turbulent boundary layers of a flat plate at supersonic speeds. UTIA Rep. 19. Inst. Aerophys. Univ. Toronto.

Favre A. 1964 The Mechanics of Turbulence. Gordon & Breach, New York.

Favre A. 1965 Equation des gaz turbulents compressibles. J. Mécanique 4, 361-421.

Favre A. 1971 Equations statistiques aux fluctuations turbulents dans les écoulements compressibles, cas des vitesses et des temperatures. Compt. Rend. Acad. Sci. Paris, Ser. A 273, 1087.

Feller W.V. 1973 Effects of upstream wall temperatures on hypersonic tunnel wall boundary-layer profile measurements. AIAA J. 11, 556-558.

Fenter F.W. 1958 An investigation of the threshold value of surface roughness at supersonic speeds. Rep. No. DRL-416, CM-919.

Fenter F.W. 1959 The turbulent boundary layer on uniformly rough surfaces at supersonic speeds. Rep. DRL-437.

Fenter F.W. 1960 The turbulent boundary layer on uniformly rough surfaces at supersonic speeds. Rep. No. DRL-468, CM-941 (this reference given in Young (1965) and in AG 223 is probably incorrect and should read Fenter (1959) as above. See source catalogue in Vol. III).

Fenter F.W., Stalmach D.J. 1957 The measurement of local turbulent skin friction at supersonic speeds by means of surface impact pressure probes. Rep. No. DRL-392, CM-878.

Fenter F.W., Lyons W.C. 1958 An experimental investigation of the effects of several types of surface roughness on turbulent boundary layer characteristics at supersonic speeds. Rep. No. DRL-411, AD 657 134, (CAT 5804).

Fernholz H. 1964 Three-dimensional disturbances in a two-dimensional incompressible turbulent boundary layer. Aero. Res. Council R + M 3368 (London).

Fernholz H. 1969 Geschwindigkeitsprofile, Temperaturprofile und halbempirische Gesetze in kompressiblen turbulenten Grenzschichten bei konstantem Druck. Ing. Arch. 38, 311-328.

Fernholz H. 1971 Ein halbempirisches Gesetz für die Wandreibung in kompressiblen turbulenten Grenzschichten bei isothermer und adiabater Wand. ZAMM 51, T 148-149.

Fernholz H. 1972 Departures from a fully developed turbulent velocity profile on a flat plate in compressible boundary layers. Fluid Dynamics Transactions Vol. 6, Pt. II, 151-177.

Fernholz H.H., Finley P.J. 1976 A critical compilation of compressible turbulent boundary layer data. Von Karman Institute for Fluid Dynamics, Lecture Series 86.

Fernholz H.H., Finley P.J. 1977 A critical compilation of compressible turbulent boundary layer data. AGARD AG-223.

Finley P.J. 1966 Velocity measurements in a thin turbulent water layer. La Houille Blanche 6, 713-721.

Finley P.J. 1977 Static pressure in hypersonic nozzle boundary layers. AIAA J. 15, 878-881.

Fischer M.C. 1972 Spreading of a turbulent disturbance. AIAA J. 10, 957-959.

Fischer M.C., Maddalon D.V., Weinstein L.M., Wagner R.D. 1970 Boundary layer surveys on a nozzle wall at M_∞= 20, including hot-wire fluctuation measurements. AIAA Paper 70-746, (CAT 7001).

Fischer M.C., Maddalon D.V., Weinstein L.M., Wagner R.D. 1971 Boundary layer Pitot and hot-wire surveys at M_∞= 20. AIAA J. 9, 826-834.

Fischer M.C., Maddalon D.V. 1971 Experimental laminar, transitional and turbulent boundary layer profiles on a wedge at local Mach number 6.5 and comparison with theory. NASA TN D-6462, (CAT 7103).

Fischer M.C., Weinstein L.M. 1972 Cone transitional boundary layer structure at M_e = 14. AIAA J. 10, 699-701.

Gates D.F. 1973a Measurements of upstream history effects in compressible turbulent boundary layers. NOL TR 73-152, (CAT 7301).

Gates D.F. 1973b An experimental investigation of the effect of upstream conditions on the downstream characteristics of compressible turbulent boundary layers - using supersonic half nozzle and conventional flat plate. Ph.D. thesis Univ. Maryland, Univ. Microfilms 73-23731.

Gates D.F., Allen R.W. 1974 Experimental measurements of upstream history effects in supersonic turbulent flow. Proc. 1974 Heat Transfer and Fluid Mechanics Institute, 330-347.

Gaudet L., Winter K.G. 1973 Measurements of the drag of some characteristic aircraft excrescences immersed in turbulent boundary layers. RAE Tech. Memo Aero. 1538.

Goddard F.E. 1959 Effect of uniformly distributed roughness on turbulent skin friction drag at supersonic speeds. J. Aeronaut. Sci. 26, 1-15 and J.P.L. Rep. 20-113 (1957).

Gootzait E., Childs M.E. 1974 Mean and fluctuating flow measurements in axisymmetric supersonic boundary layer flow subjected to distributed adverse pressure gradients. NASA-CR-139435.

Gootzait E., Childs M.E. 1977 Turbulence measurements in axisymmetric supersonic boundary layer flow in adverse pressure gradients. AIAA Paper 77-129.

Gopinath R., East R.A. 1973 The effect of adverse pressure gradient on the hypersonic turbulent boundary layer on a nozzle wall at high rates of heat transfer. A.A.S.U. Report 326. Univ. Southampton.

Gran R.L., Lewis J.E., Kubota T. 1974 The effect of wall cooling on a compressible turbulent boundary layer. J. Fluid Mech. 66, 507-528.

Green J.E., Coleman G.T. 1973 An exploratory study of shear stress induced pressures in inclined surface slots beneath a turbulent boundary layer. RAE Tech. Memo Aero. 1513.

Haase W., Gauler H.F., Thiele F. 1973 Ein Vergleich numerischer Integrationsverfahren bei konstanter und variabler Schrittweite. Interner Bericht No. 13, Lehrstuhl f. Oberschall-technik, Techn. Univ. Berlin.

Hahn J.S. 1970 Experimental investigation of adiabatic wall turbulent boundary layers with pressure gradient at Mach number 4. USA AEDC TR 70-31.

Hahn J.S., Lutz R.G. 1971 Turbulent boundary layers with pressure gradient and heat transfer at Mach number 4. AEDC TR 71-3 (AD 8791364).

Hama F.R. 1954 Boundary layer characteristics for smooth and rough surfaces. Trans. Soc. Nav. Architects Marine Engrs. 62, 333-358.

Harvey W.D., Clark F.L. 1972 Measurement of skin friction on the wall of a hypersonic nozzle. AIAA J. 10, 1256-1258.

Hastings R.C., Sawyer W.G. 1970 Turbulent boundary layers on a large flat plate at M = 4. RAE Techn. Rep. 70040 and R + M 3678, (CAT 7006).

Heronimus G.A. 1966 Hypersonic shock tunnel experiments on the W7 flat plate model-expansion side, turbulent flow and leading edge transpiration data. Cornell Aeronaut.Lab.Inc. Cal Rep. AA-1952-Y2.

Hill F.K. 1956 Boundary layer measurements in hypersonic flow. J. Aeron. Sci. 23, 35-42

Hill F.K. 1959a Turbulent boundary layer measurements at Mach numbers from 8 to 10. Phys. Fluids 2, 778-680, (CAT 5901).

Hill F.K. 1959b Skin friction and heat transfer measurements at Mach numbers from 8 to 10 in turbulent boundary layers. Appendix II, Bumblebee Aerodyn. Panel T.G.-14-37, Vol. I. Phys. Lab. Johns Hopkins Univ. p. 15-26.

Hill M. 1976 Examination of boundary layer edge criteria. Project report, Dept. Aeronaut. Imperial College London.

Hinze J.O. 1959 Turbulence. McGraw Hill, New York.

Hodge B.K., Adams J.C. 1978 The calculation of compressible transitional, turbulent and relaminarizational boundary layers over smooth and rough surfaces using an extended mixing length hypothesis. AEDC pp. 1-103. See also Adams & Hodge.

Hokenson G.J. 1977 Consistent integral thickness utilization for boundary layers with transverse curvature. AIAA J. 15, 597-600.

Holden M.S. 1972 An experimental investigation of turbulent boundary layers at high Mach number. NASA CR-112147.

Hopkins E.J., Keener E.R. 1966 Study of surface Pitots for measuring turbulent skin friction at supersonic Mach numbers - adiabatic wall. NASA TN D 3478, (CAT 6601).

Hopkins E.J., Rubesin M.W., Inouye M., Keener E.R., Mateer G.C., Polek T.E. 1969 Summary and correlation of skin friction and heat transfer data for a hypersonic turbulent boundary layer on simple shapes. NASA TN D-5089.

Hopkins E.J., Keener E.R., Dwyer H.A. 1971 Turbulent skin friction and boundary layer profiles measured on nonadiabatic flat plates at hypersonic Mach numbers. AIAA Paper 71-167.

Hopkins E.J., Inouye M. 1971 An evaluation of theories for predicting turbulent skin friction and heat transfer on flat plates at supersonic and hypersonic Mach numbers. AIAA J. 9, 993-1003.

Hopkins E.J., Keener E.R., Polek T.E., Dwyer H.A. 1972 Hypersonic turbulent skin friction and boundary layer profiles on nonadiabatic flat plates. AIAA J. 10, 40-48.

Hopkins E.J., Keener E.R. 1972 Pressure gradient effects on hypersonic turbulent skin friction and boundary layer profiles. AIAA J. 10, 1141-1142 and AIAA Paper 72-215, (CAT 7203).

Hornung H.G. 1966 A survey of compressible flow boundary layers - theory and experiment. Australian ARC Rep. ACA 67.

Horstman C.C. 1977 A turbulence model for nonequilibrium adverse pressure gradient flows. AIAA J. 15, 131-132 and AIAA Paper 76-412.

Horstman C.C., Owen F.K. 1972 Turbulent properties of a compressible boundary layer. AIAA J. 10, 1418-1424, (CAT 7205).

Horstman C.C., Kussoy M.I., Lanfranco M.J. 1978 An evaluation of several compressible turbulent boundary layer models: Effect of pressure gradient and Reynolds number. AIAA Paper 78-1160.

Hovstadius G. 1977a A mass flow probe for measurement in high enthalpy supersonic boundary layers. Sweden FFA-128.

Hovstadius G. 1977b A combined probe for measurement of mass flow, stagnation temperature, and stagnation pressure in supersonic boundary layers. Sweden FFA-129.

Howarth L. (Ed.) 1953 Modern Developments in Fluid Dynamics. Oxford, Clarendon Press.

Huffman G.D., Bradshaw P. 1972 A note on von Kármán's constant in low Reynolds number turbulent flow. J. Fluid Mech. 53, 45-60.

Hughes T. 1973 Some heat transfer measurements in compressible turbulent boundary layers. Aeronaut. J. 77, 94-98.

Jackson M.W., Czarnecki K.R., Monta W.J. 1965 Turbulent skin friction at high Reynolds numbers and low supersonic velocities. NASA TN D-2687, (CAT 6505).

James C.S. 1959 Boundary layer transition on hollow cylinders in supersonic free flight as affected by Mach number and a screwthread type of surface roughness. NASA Memo 1-20-59A.

Jeromin L.O.F. 1966 Compressible turbulent boundary layer with fluid injection. Ph. D. thesis Cambridge, (CAT 6602).

Jeromin L.O.F. 1968 An experimental investigation of the compressible turbulent boundary layer with air injection. Aeronaut. Res. Council, R. + M. No. 3526.

Johnson D.A., Rose W.C. 1975 Laser velocimeter and hot-wire anemometer comparisons in a supersonic boundary layer. AIAA J. 13, 512-515.

Johnson D.A., Rose W.C. 1976 Turbulence measurements in a transonic boundary layer and free-shear layer using laser velocimetry and hot-wire anemometry techniques. AIAA Paper 76-399.

Jones R.A., Feller W.V. 1970 Preliminary surveys of the wall boundary layer in a Mach 6 axisymmetric tunnel. NASA TN D-5620, (CAT 7002).

Kârmân Th.v. 1935 The problem of resistance in compressible fluids. Reale Accademia d'Italia, V Convegno della Fondazione Allessandro Volta, Rome, p. 226-290.

Kârmân Th.v., Tsien H.S. 1938 Boundary layer in compressible fluids. J. Aeronaut. Sci.5,227-232.

Keener E.R., Hopkins E.J. 1969 Use of Preston tubes for measuring hypersonic turbulent skin friction. AIAA Paper 69-345.

Keener E.R., Hopkins E.J. 1971 Accuracy of Pitot pressure rakes for turbulent boundary layer measurements in supersonic flow. NASA TN D-6229.

Keener E.R., Hopkins E.J. 1972 Turbulent boundary layer velocity profiles on a nonadiabatic flat plate at Mach number 6.5. NASA TN D-6907, (CAT 7204).

Keener E.R., Polek T.E. 1972 Measurements of Reynolds analogy for a hypersonic turbulent boundary layer on a nonadiabatic flat plate. AIAA J. 10, 845-846.

Kelnhofer Wm.J. 1970 Wall temperature effects on subsonic gas flows. DLR-FB 70-66.

Kemp J.H., Owen F.K. 1972 Experimental study of nozzle wall boundary layers at Mach numbers 20 to 47. NASA TN D-6965, (CAT 7206).

Kendall J.M. 1971 JPL Experimental investigations. Proceedings Boundary Layer Transition Workshop Vol. IV Aerospace Corp. San Bernardino, Calif.

Kendall J.M. 1975 Wind tunnel experiments relating to supersonic and hypersonic boundary layer transition. AIAA J. 13, 290-299.

Keyes F.G. 1952 The heat conductivity, viscosity, specific heat and Prandtl numbers for thirteen gases. Project Squid TR No. 37. M.I.T. Cambridge, Mass.

Kistler A.L. 1958 Fluctuation measurements in supersonic turbulent boundary layers. Ballistic Research Laboratories, Rep. 1052 and Phys. Fluids 2, 1959, (CAT 5803).

Klebanoff P.S., Diehl Z.W. 1952 Some features of artificially thickened fully developed turbulent boundary layers with zero pressure gradient. NACA R-1110.

Klebanoff P.S., Tidstrom K.D. 1959 Evolution of amplified waves leading to transition in a boundary layer with zero pressure gradient. NASA TN D-195.

Kline S.J. et al. (Editors) 1968 Proceedings Computation of turbulent boundary layers - 1968 AFOSR-IFP-Stanford Conference, Vol I.

Korkegi R.H. 1954 Transition studies and skin friction measurements on an insulated flat plate at a hypersonic Mach number. GALCIT Memo. No. 17.

Korkegi R.H. 1956 Transition studies and skin friction measurements on an insulated flat plate at a hypersonic Mach number. J. Aeronaut. Sci. 23, 97-107 and 192.

Kovasznay L.S.G. 1950 The hot-wire anemometer in supersonic flow. J. Aeronaut. Sci. 17, 565.

Kovasznay L.S.G. 1953a Development of turbulence measuring equipment. NACA TN 2839.

Kovasznay L.S.G. 1953b Turbulence in supersonic flow. J. Aeronaut. Sci. 20, 657-674, 682.

Kubota T., Berg D.E. 1977 Surface roughness effects on the hypersonic turbulent boundary layer. CALTECH AD A 042141. See also Berg (1977).

Küster H.J. 1972 Ein Integralverfahren zur Berechnung zweidimensionaler kompressibler turbulenter Grenzschichten mit Druckgradient und Wärmeübergang auf der Basis einer Kompressibilitäts-transformation. Dissertation T.U. Berlin.

Kussoy M.I., Horstman C.C., Acharya M. 1978 An experimental documentation of pressure gradient and Reynolds number effects on compressible turbulent boundary layers. NASA TM 78488.

Laderman A.J. 1976 New measurements of turbulent shear stresses in hypersonic boundary layers. AIAA J. 14, 1286-1292.

Laderman A.J. 1978a Effect of wall temperature on a supersonic turbulent boundary layer. AIAA J. 16, 723-730.

Laderman A.J. 1978b Pressure gradient effects on supersonic boundary layer turbulence. Ford Aerospace & Communications Corp. Aeronautics Div. Rep. No. U-6467. Newport Beach, Calif.

Laderman A.J. 1979 Adverse pressure gradient effects on supersonic boundary layer turbulence. AIAA Paper 79-1563.

Laderman A.J., Demetriades A. 1972a Turbulence measurements in the hypersonic boundary layer over a cooled wall. Philco Ford. Corp. Publ. U-5079.

Laderman A.J., Demetriades A. 1972b Measurements of the mean and turbulent flow in a cooled-wall boundary layer at Mach 9.37. AIAA Paper 72-73.

Laderman A.J., Demetriades A. 1974 Mean and fluctuating flow measurements in the hypersonic boundary layer over a cooled wall. J. Fluid Mech. 63, 121-144, (CAT 7403).

Laderman A.J., Demetriades A. 1977 Investigation of the structure of a cooled wall turbulent supersonic boundary layer. Aeronutronics Publ. No. U-6370.

Laderman A.J., Demetriades A. 1979 Turbulent shear stresses in compressible boundary layers. AIAA J. 17, 736-744.

LaGraff J.E. 1972 Observations of hypersonic boundary layer transitior using hot wire anemometry. AIAA J. 10, 762-769. And Ph.D. thesis Oxford University 1970.

Langanelli A.L., Nestler D.E. 1969 Surface ablation patterns: A phenomenological study. AIAA J. 7, 1319-1325.

Laufer J., Vrebalovich T. 1960 Stability and transition of a supersonic laminar boundary layer on an insulated flat plate. J. Fluid Mech. 9, 257-299.

Laufer J. 1969 Thoughts on compressible turbulent boundary layers. Rand Corporation RM-5946-PR, Santa Monica.

Lee R.E., Yanta W.J., Leonas A,C. 1968 Velocity profile, skin friction balance and heat transfer measurements of the turbulent boundary layer at Mach 5. Proc. 1968 Heat Transfer and Fluid Mechanics Institute.

Lewis J.E., Gran R.L., Kubota T. 1972 An experiment on the adiabatic compressible turbulent boundary layer in adverse and favourable pressure gradients. J. Fluid Mech. 51, 657-672, (CAT 7201).

Lewis C.H., Miner E.W., Anderson E.C. 1972 Effects of strong axial pressure gradients on turbulent boundary layer flows. Virginia Polytech. Blacksburg Va., AGARD CP 93/R 21.

Libby P.A., Visich M. 1959 The law of the wake in compressible turbulent boundary layers. J. Aero/Space Sci. 26, 541-542.

Lin C.C. (Editor) 1959 Turbulent Flows and Heat Transfer. Vol. V, High speed aerodynamics and jet propulsion. Princeton University Press. Princeton, New Jersey.

Lobb R.K., Winkler E.M., Persh J. 1955 Experimental investigation of turbulent boundary layers in hypersonic flow. NOL NAVORD Report 3880, (CAT 5503).

Mabey D.G. 1965 Boundary layer transition measurements using a surface hot film downstream of distributed roughness at Mach numbers from 1.3 to 4. J. Roy. Aeronaut. Soc. 69, 96-100.

Mabey D.G. 1977 Some observations on the wake component of the velocity profiles of turbulent boundary layers at subsonic and supersonic speeds. RAE TR 77-004.

Mabey D.G., Meier H.U., Sawyer W.G. 1974 Experimental and theoretical studies of the boundary layer on a flat plate at Mach numbers from 2.5 to 4.5. RAE TR 74127, (CAT 7402).

Mabey D.G., Gaudet L. 1975 Performance of small skin friction balances at supersonic speeds. J. Aircraft 12, 819-825.

Mabey D.G., Sawyer W.G. 1976 Experimental studies of the boundary layer on a flat plate at Mach numbers from 2.5 to 4.5. ARC R+M 3784.

Mack L.M. 1954 An experimental investigation of the temperature recovery factor. Rept. 20-80 Jet Propulsion Lab., Pasadena.

Mack L.M. 1971 Progress in compressible boundary layer stability computations. Proc. Boundary Layer Transition Workshop. Vol. IV Aerospace Corp., San Bernardino, Calif.

Mack L.M. 1975 Linear stability theory and the problem of supersonic boundary layer transition. AIAA J. 13, 278-289.

Mc Ronald A.D. 1975 Measurements of density and temperature in a hypersonic turbulent boundary layer using the electron beam fluorescence technique. Ph.D. thesis Univ. S.California.

Maise G., McDonald H. 1968 Mixing length and kinematic eddy viscosity in a compressible boundary layer. AIAA J. 6, 73-80.

Martellucci A., Langanelli A.L., Hahn J. 1974 Hypersonic turbulent boundary layer characteristics with mass transfer. SAMSO TR 74 112 also as GE RSD Doc. 74 SD 2039.

Marvin J.G. 1977 Turbulence modeling for compressible flows. NASA TM X-73, 188.

Mathews D.C., Childs M.E. 1970 Use of Coles' universal wake function for compressible turbulent boundary layers. J.Aircraft 7, 137-140.

Maurer F., Petersen J.C., Pfeifer H.J., Haertig J. 1975 Messung von Geschwindigkeitsprofilen in einem Überschallwindkanal mittels Laser-Doppler-Verfahren. BMFT-FB W 75-15.

Maurer F., Petersen J.C. 1975 Messungen der Geschwindigkeitsprofile turbulenter Überschall-grenzschichten mit dem Laser-Doppler-Velocimeter im Vergleich zu Ergebnissen mit einer kombinierten Druck-Temperatur-Sonde. Abhandl. Aerodyn. Inst. der RWTH Aachen, H.22, 254-259.

Meier H.U. 1968 Eine kombinierte Sonde für Temperatur- und Druckmessungen in Grenzschichten bei kompressiblen Strömungen. AVA Göttingen 68 G 03.

Meier H.U. 1969b A combined probe for temperature and pressure measurements in boundary layers in compressible flow. AIAA J. 7, 529-530.

Meier H.U. 1970a Experimentelle und theoretische Untersuchungen von turbulenten Grenzschichten bei Überschallströmung. M.P.I. Mitteilungen Nr. 49, (CAT 7003).

Meier H.U. 1977 Measuring techniques for compressible turbulent boundary layers. DLR-FB 77-49.

Meier H.U., Rotta J.C. 1970 Experimental and theoretical investigations of temperature distributions in supersonic boundary layers. AIAA Paper 70-744.

Meier H.U., Rotta J.C. 1971 Temperature distributions in supersonic turbulent boundary layers. AIAA J. 9, 2149-2156.

Meier H.U., Lee R.E., Voisinet R.L. 1974 Vergleichsmessungen mit einer Danberg-Temperatursonde und einer kombinierten Druck-Temperatur-Sonde in turbulenten Grenzschichten bei Überschallanströmung. ZfW 22, 1-10 and ICIASF (1973).

Michel R. 1977 Prediction of the onset and development of boundary layer transition. ESA TT-414.

Mikulla V., Horstman C.C. 1976 Turbulence measurements in hypersonic shock-wave boundary layer interaction flows. AIAA J. 14, 568-575.

Monta W.J., Czarnecki K.R., Deveikis W.D. 1968 Drag due to two-dimensional roughness in a turbulent boundary layer at Mach 3 with and without heat transfer. NASA TN D-4746.

Moore D.R. 1958 An experimental investigation of the turbulent boundary layer behind a forward-facing step in supersonic flow. Rep. DRL-425 , CF-2707, AD 655 462, (CAT 5805).

Moore D.R., Harkness J. 1965 Experimental investigations of the compressible turbulent boundary layer at very high Reynolds numbers. AIAA J. 3, 631-638, (CAT 6502).

Morkovin M.V. 1956 Fluctuations and hot-wire anemometry in compressible flows. AGARDograph No. 24.

Morkovin M.V. 1960 The structure of supersonic turbulent boundary layers. AGARD Wind Tunnel and Model Testing Panel.

Morkovin M.V. 1962 Effects of compressibility on turbulent flows. In: Mechanique de la Turbulence. Editions du Centre Nat. de la Rech. Sci.(See also Favre).

Morkovin M.V. 1967 Signal interpretation in high speed anemometry. Proc. Int. Symp. Hot-Wire Anemometry, Univ. Maryland, 38-51

Morkovin M.V. 1969 Critical evaluation of transition from laminar to turbulent shear layers with emphasis on hypersonically traveling bodies. Tech. Rep. AFFDL-TR-68-149.

Morkovin M.V., Phinney R.E. 1958 Extended applications of hot-wire anemometry to high speed turbulent boundary layers. Dept. Aeronaut. The Johns Hopkins Univ. ASTIA AD-158-279.

Morkovin M.V., Kline S.J. 1968 Calculation of incompressible turbulent boundary layers. A review of the AFOSR-IFP Stanford 1968 Conference. NASA SP 216 pp. 2.1-2.13.

Moser H.A. 1979 Berechnung der kompressiblen laminaren Grenzschichtströmung mit Druckgradient und veränderlicher Wandtemperatur mit einem Pseudo-Tschebyscheff-Spektralverfahren. Dissertation T.U. Berlin.

Myring D.E., Young A.D. 1968 The isobars in boundary layers at supersonic speeds. Aeronaut. Quart. 19, 105-126.

Naleid J.F. 1958 Experimental investigation of the impact pressure probe method of measuring local skin friction at supersonic speeds in the presence of an adverse pressure gradient. Report No. DRL-432, CF-2739, (CAT 5801).

Neal L. 1966 A study of the pressure, heat transfer, and skin friction on sharp and blunt flat plates at Mach 6.8. NASA TN D-3312.

Neubert W. 1974 Zähigkeit und Recovery-Faktor von Helium für Temperaturen von $0{,}4^{o}$ bis 400^{o} K. Studienarbeit Hermann-Föttinger-Institut für Thermo- und Fluiddynamik,T.U. Berlin.

Nikuradse J. 1932 Gesetzmäßigkeit der turbulenten Strömung in glatten Rohren. Forsch. Arb. Ingenieurwesen, Heft 356.

Nikuradse J. 1933 Strömungsgesetze in rauhen Rohren. Forsch. Arb. Ingenieurwesen, Heft 361 and NACA TM 1292 (1950)

Nothwang G.J. 1957 An evaluation of four experimental methods for measuring mean properties of a supersonic turbulent boundary layer. NACA Rep. 1320.

Owen F.K. 1969 Fluctuation measurements in compressible boundary layers. Ph.D. thesis Oxford Univ. and ARC 31228.

Owen F.K. 1970a Transition experiments on a flat plate at subsonic and supersonic speeds. AIAA J. 8, 518-523.

Owen F.K. 1970b Fluctuation and transition measurements in compressible boundary layers. AIAA Paper 70-745.

Owen F.K., Horstman C.C. 1972a Hypersonic transitional boundary layers. AIAA J. 10, 769-775.

Owen F.K., Horstman C.C. 1972b On the structure of hypersonic turbulent boundary layers. J. Fluid Mech., 53, 611-636.

Owen F.K., Horstman C.C., Kussoy M.I. 1975 Mean and fluctuating flow measurements of a fully developed, non-adiabatic hypersonic boundary layer. J. Fluid Mech. 70, 393-413.

Pasiuk L., Hastings G.M., Chatham R. 1965 Experimental Reynolds analogy factor for a compressible turbulent boundary layer with a pressure gradient. NOL TR 64-200, (CAT 6504).

Patel V.C. 1965 Calibration of the Preston tube and limitations on its use in pressure gradients. J. Fluid Mech. 23, 185-208.

Patel V.C., Head M.R. 1969 Some observations on skin friction and velocity profiles in fully developed pipe and channel flows. J. Fluid Mech. 38, 181-201.

Peake D.J., Brakmann G., Romeskie J.M. 1971 Comparisons between some high Reynolds number turbulent boundary layer experiments at Mach 4 and various recent calculation procedures. Nat. Res. Council of Canada and AGARD CP-93-71 Paper 11, (CAT 7102).

Perry A.E., Schofield W.H., Joubert P.N. 1969 Rough wall turbulent boundary layers. J. Fluid Mech. 37, 383-413.

Perry J.H., East R.A. 1968 Experimental measurements of cold wall turbulent hypersonic boundary layers. AGARD CP No. 30, (CAT 6801).

Perry J.H. 1968 An experimental study of the turbulent boundary layer at high Mach number and high wall heat transfer. Ph.D. thesis Univ. Southampton.

Peterson C.W. 1974 Pressure and temperature measurements in a cold wall hypersonic turbulent boundary layer. Proc. 1974 Heat Transfer and Fluid Mech. Inst., 105-121.

Peterson C.W., George O.L. 1974 Wind tunnel pressure probes: New calibrations for new geometries and flow environments. AIAA Paper 74-635 and AIAA J. 13, 1263-1264 (1975).

Peterson J.B. 1969 Boundary layer velocity profiles downstream of three-dimensional transition trips on a flat plate at Mach 3 and 4. NASA TN D 5523.

Pfeiffer H., Will H. 1973 Profile measurement in hypersonic turbulent boundary layers with heat transfer. Euromech Colloquium 43, Göttingen.

Potter J.L., Whitfield J.D. 1962 Effects of slight nose bluntness and roughness on boundary layer transition in supersonic flows. J. Fluid Mech. 12, 501-532.

Prandtl L. 1932 Zur turbulenten Strömung in Rohren und längs Platten. Ergebnisse der AVA Göttingen (Oldenbourg Verlag, München) 4, 18-29.

Reda D.C. 1974 Compressible turbulent skin friction on rough and rough/wavy walls in adiabatic flow. NOL TR 74-34.

Reda D.C., Ketter F.C., Fan C. 1975 Compressible turbulent skin friction on rough and rough wavy walls in adiabatic flow. AIAA J. 13, 553-555.

Rose W.C. 1973 The behaviour of a compressible turbulent boundary layer in a shock-wave induced adverse pressure gradient. NASA TN D-7092 (and Ph.D. thesis Univ. Washington 1972).

Rotta J.C. 1950 Ober die Theorie der turbulenten Grenzschichten. Mitt. M.P.I. f. Strömungsforschung, Göttingen Ber. 1 and NACA TM 1344 (1953).

Rotta J.C. 1959 Über den Einfluß der Machschen Zahl und des Wärmeüberganges auf das Wandgesetz turbulenter Strömung. Z.F.W. 7, 264-274.

Rotta J.C. 1960 Turbulent boundary layers with heat transfer in compressible flow. AGARD Rep. 281.

Rotta J.C. 1962 Turbulent boundary layers in incompressible flow. In Progress in Aeronautical Sciences, Vol. 2, Pergamon Press.

Rotta J.C. 1964a Temperaturverteilungen in der turbulenten Grenzschicht an der ebenen Platte. Int. J. Heat Mass Transfer 7, 215-228.

Rotta J.C. 1964b A review of experimental temperature distribution in supersonic and hypersonic turbulent boundary layers with heat transfer. AVA 64 A 10, Göttingen.

Rotta J.C. 1965 Heat transfer and temperature distribution in turbulent boundary layers at supersonic and hypersonic flow. AGARDograph 97, 35-63.

Rubesin M.W., Rose W.C. 1973 The turbulent mean flow, Reynolds stress and heat flux equations in mass-averaged dependent variables. NASA Tech. Memo X-62248.

Rubesin M.W., Crisalli A.J., Horstman C.C., Acharya M. 1977 A critique of some recent second order closure models for compressible boundary layers. AIAA Paper 77-128.

Rudy D.H., Weinstein L.M. 1970 Investigation of turbulent recovery factor in hypersonic Helium flow. AIAA J. 8, 2286-2287.

Saffman P.G. 1977 Problems and progress in the theory of turbulence. Structure and Mechanisms of Turbulence Vol. II, p. 273. Ed. H. Fiedler, Springer Verlag Berlin.

Samuels R.D., Peterson J.B., Adcock J.B. 1967 Experimental investigation of the turbulent boundary layer at a Mach number of 6 with heat transfer at high Reynolds numbers. NASA TN D-3858, (CAT 6701).

Schlichting H. 1936 *Experimentelle Untersuchungen zum* Rauhigkeitsproblem. Ing. Archiv 7,1 and NACA TM 823.

Schlichting H. 1965 Grenzschichttheorie. Braun Verlag Karlsruhe,and Boundary Layer Theory, 6th English Edition 1968.

Schubauer G.B., Tchen C.M. 1959 In Turbulent Flows and Heat Transfer . Ed. C.C.Lin. Princeton University Press, Princeton New Jersey.

Schultz D.L., Jones T.V. 1973 Heat transfer measurements in short duration hypersonic facilities. AGARDograph 165.

Shang J.S. 1973 Computations of hypersonic turbulent boundary layers with heat transfer. AIAA Paper 73-699.

Shoulberg, R.H., Hill J.A.F., Rivas M.R. 1952 An experimental determination of flat plate recovery factors for Mach numbers between 1.90 and 3.14. M.I.T. Naval Supersonic Lab.,1952, Rep.36.

Shoulberg R.H., Hill, J.A.F., Rivas M.R. 1954 An experimental determination of flat plate recovery factors for Mach numbers between 1,90 and 3,14. J. Aeronaut. Sci. 21, 763-771.

Shoulberg R.H., Kendal R.E. et al. 1953 An experimental investigation of flat plate heat transfer coefficients at Mach numbers of 2; 2,5; and 3,0 for a surface temperature to stream total temperature ratio of 1,18. M.I.T. Naval Supersonic Lab. Rep. No. 39.

Shutts W.H., Hartwig W.H., Weiler J.E. 1955 Final report on turbulent boundary layer and skin friction measurements on a smooth thermally insulated flat plate at supersonic speeds. Report No. DRL-364, CM-823, (CAT 5501).

Shutts W.H., Fenter F.W. 1955 Turbulent boundary layer and skin friction measurements on an artificially roughened thermally insulated flat plat at supersonic speeds. Report No. DRL-366, CM-837, AD 409935, (CAT 5502).

Smith K.G., Gaudet L., Winter K.G. 1962 The use of surface Pitot tubes as skin friction meters at supersonic speeds. Aeronaut. Res. Council R + M 3351.

Smits, A.J., Young S.T.B., Bradshaw P. 1979a The effects of short regions of high surface curvature on turbulent boundary layers. J. Fluid Mech. 94, 209-242.

Smits, A.J., Eaton J.A., Bradshaw P. 1979b The response of a turbulent boundary layer to lateral divergence. J. Fluid Mech. 94, 243-268.

Spalding D.B., Chi S.W. 1964 The drag of a compressible turbulent boundary layer on a smooth flat plate with and without heat transfer. J. Fluid Mech. 18, 117-143.

Squire H.B. 1942 Heat transfer calculation for aerofoils. Brit. Aeronaut. Res. Council Rept. and Mem. 1986.

Squire L.C. 1970 Further experimental investigation of compressible turbulent boundary layers with air injection. ARC R + M 3627.

Squire L.C. 1971 Eddy viscosity distributions in compressible turbulent boundary layers with injection. Aeronaut. Quart. XXIII, 169-182.

Squire L.C., Thomas G.D., Marriott P.G. 1977 Compressible turbulent boundary layers with injection. AIAA J. 15, 425-427.

Srokowski A.J., Howard F.G., Feller W.V. 1976 Direct measurements at Mach 6 of turbulent skin friction reduction by injection from single and multiple flush slots. AIAA Paper 76-178.

Stalmach C.J. 1958 Experimental investigation of the surface impact probe method of measuring local skin friction at supersonic speeds. Univ. of Texas, DRL-410, CF 2675, (CAT 5802).

Stewartson K. 1964 The Theory of Laminar Boundary Layers In Compressible Fluids. Oxford Univ. Press.

Stone D.R. 1971 The effect of discrete jets used as a boundary layer trip on transition, heat transfer and the downstream flow field at Mach numbers of 6.0 and 8.5. M.Sc. thesis North Carolina State Univ.

Stone D.R., Cary A.M. 1972 Discrete sonic jets used as boundary layer trips at Mach numbers of 6 and 8.5.NASA TN D-6802, (CAT 7209).

Stroud J.F., Miller L.D. 1965 An experimental and analytical investigation of hypersonic inlet boundary layers. Lockheed-California Co. Burbank LR-18803 and AFFDL-TR-65-123 Vol. I and II, (CAT 6503).

Stroud J.F., Miller L.D. 1966 Hypersonic inlet boundary layer research. J. Aircraft 3, 548-554.

Sturek W.B. 1970 An experimental investigation of the supersonic turbulent boundary layer in a moderate adverse pressure gradient Pt. 1. A detailed description of the experiment and tabulation. Ballistic Research Labs. Aberdeen Proving Grounds, Md. BRL Report 1543.

Sturek W.B. 1971 Ph.D. thesis Univ. of Delaware, Newark, Del.

Sturek W.B. 1973a Calculation of turbulent shear stress in supersonic turbulent boundary layer zero and adverse pressure gradient flow. AIAA Paper 73-166.

Sturek W.B. 1973b Wall heat transfer effects on supersonic nozzle wall boundary layer temperature profiles. Ballistic Res. Lab. Memorandum Rep. No. 2328.

Sturek W.B. 1974 Turbulent boundary layer shear stress distribution for compressible adverse pressure gradient flow. AIAA J. 12, 375-376.

Sturek W.B., Danberg J.E. 1971a Experimental measurements of the supersonic turbulent boundary layer in a region of moderate adverse pressure gradient. AIAA Paper 71-162.

Sturek W.B., Danberg J.E. 1971b Supersonic turbulent boundary layer in an adverse pressure gradient. Univ. Delaware T.R. No. 141, (CAT 7101).

Sturek W.B., Danberg J.E. 1971c The supersonic turbulent boundary layer in an adverse pressure gradient - experiment and data analysis. AGARD CCP-93-71.

Sturek W.B., Danberg J.E. 1972a Supersonic turbulent boundary layer in adverse pressure gradient. Pt. I: The experiment. AIAA J. 10, 475-480.

Sturek W.B., Danberg J.E. 1972b Supersonic turbulent boundary layer in adverse pressure gradient. Pt. II: Data analysis. AIAA J. 10, 630-636.

Sun C.C., Childs M.E. 1973 *A modified wall-wake velocity profile for turbulent compressible* boundary layers. J. Aircraft 10, 381-383.

Sun C.C., Childs M.E. 1976 A wall-wake velocity profile for compressible nonadiabatic flows. AIAA J. 14, 820-822.

Thomann H. 1967a Heat transfer measurements at M = 7.17 - first step of a comparison between tunnel test and free flight. FFA Rep. 110.

Thomann H. 1967b Heat transfer in a turbulent boundary layer with a pressure gradient normal to the flow. FFA - 113.

Thomann H. 1968 Effect of streamwise wall curvature on heat transfer in a turbulent boundary layer. J. Fluid Mech. 33, 282-292, (CAT 6800).

Thomann H. 1969 See Drougge G, Thomann H.: Measurements of heat transfer in a highly cooled turbulent boundary layer at M = 4.6 and 7. FFA AU-120-4.

Thomas C.D. 1974 Compressible turbulent boundary layers with combined air injection and pressure gradient. ARC R + M 3779 and Ph. D. thesis Cambridge 1973, (CAT 7401).

Thomke G.J. 1969 Boundary layer skin friction characteristics in the supersonic test section of the Douglas Aerophysics Laboratory 4 ft Trisonic Wind Tunnel. McDonnell-Douglas Astronautics Co. Santa Monica, (CAT 6903). (Unpublished private communication).

Townsend A.A. 1960 Equilibrium layers and wall turbulence. J. Fluid Mech. 11, 97-120

Vas I.E., Settles G.S., Bogdonoff S.M. 1976 An experimental study of the compressible turbulent boundary layer over a wide range of Reynolds number. Princeton University report (CAT 7601).

Voisinet R.L.P. 1977 Temperature-step effects on direct measurement of skin-friction drag. NSWC NOL TR 77-7.

Voisinet R.L.P. 1978 Influence of surface roughness and mass transfer on turbulent boundary layer flow. DEA-Meeting 1978.

Voisinet R.L.P. 1979 Combined influence of roughness and mass transfer on turbulent skin friction at Mach 2.9. AIAA Paper 79-0003.

Voisinet L.P., Lee R.E. 1972 Measurements of a Mach 4.9 zero pressure gradient turbulent boundary layer with heat transfer. NOL TR 72-232, (CAT 7202).

Voisinet L.P., Lee R.E. 1973 Measurements of a supersonic favourable-pressure-gradient turbulent boundary layer with heat transfer - Part 1 - Data compilation. NOL TR 73-224, (CAT 7304).

Voisinet R.L.P., Lee R.E., Meier H.U. 1974 Comparative measurements of total temperature in a supersonic turbulent boundary layer using a conical equilibrium and combined temperature-pressure probe. NOL TR 74-10.

Wade J.H.T. 1955 An experimental investigation of the effects of surface roughness on the drag of a cone-cylinder model at a Mach number of 2.48. Univ. Toronto. UTIAS Rep. 34.

Wallace J.E. 1967 Hypersonic turbulent boundary layer studies at cold wall conditions. Proc. 1967 Heat Transfer and Fluid Mech. Inst., 427-451.

Waltrup P.J., Schetz J.A. 1971 An experimental investigation of a compressible turbulent boundary layer subjected to a systematic variation of adverse pressure gradients. Virginia Polytechnic Institute VPI-E-71-18, (CAT 7104).

Waltrup P.J., Schetz J.A. 1973 Supersonic turbulent boundary layer subjected to adverse pressure gradients. AIAA J. 11, 50-58.

Walz A. 1956 Theorie und Praxis der Berechnung von Strömungsgrenzschichten. Habilitationsschrift T.H. Karlsruhe.

Walz A. 1959 Compressible turbulent boundary layers with heat transfer and pressure gradient in flow direction. J. Research Nat. Bureau of Standards. Vol. 63B, 53-70.

Walz A. 1966 Strömungs- und Temperaturgrenzschichten. Verlag G. Braun Karlsruhe.

Watson R.D., Harris J.E., Anders J.B. 1973 Measurements in a transitional/turbulent Mach 10 boundary layer at high Reynolds numbers. AIAA Paper 73-165, (CAT 7305).

Weiler J.E., Hartwig W.H. 1952 The direct measurement of local skin friction coefficient. DRL Report 295 CF-1747.

Westkaemper J.C. 1959 An experimental evaluation of the insulated mass technique of measuring heat transfer at high velocities. Report No. DRL-439, CF-2765.

Westkaemper J.C. 1963 Step temperature effects on direct measurements of drag. AIAA J. 1, 1708-1710.

Whitfield D.L., High M.D. 1977 Velocity-temperature relations in turbulent boundary layers with non-unity Prandtl numbers. AIAA J. 15, 431-434 and AIAA Paper 76-411.

Willmarth W.W. 1975 Structure of turbulence in boundary layers,in"Advances in Applied Mechanics" Academic Press, New York, pp. 159-254.

Wilson D.M. 1969 A correlation of heat-transfer and skin friction data and an experimental Reynolds analogy factor for highly cooled turbulent boundary layers at Mach 5.0. NOLTR-69-51.

Winkler E.M. 1954 Stagnation temperature probes for use at high supersonic speeds and evaluated temperatures. NAVORD Rep. 3834.

Winkler E.M. 1961 Investigation of flat plate hypersonic turbulent boundary layer with heat transfer. Trans. Am. Soc. Mech. Engrs. Ser. E, 83, 323-329, (CAT 5902).

Winkler E.M., Cha M.H. 1959 Investigation of flat plate hypersonic turbulent boundary layer with heat transfer at a Mach number of 5.2. NOL NAVORD Rep. 6631, (CAT 5902).

Winter K.G. 1976 Notes on the measurement of aerodynamic heat transfer in model testing facilities. RAE TM Aero 1657.

Winter K.G. 1977 An outline of the techniques available for the measurement of skin friction in turbulent boundary layers. Progr. Aerospace Sci. 18, 1-57.

Winter K.G., Smith K.G., Rotta J.C. 1965 Turbulent boundary layer studies on a waisted body of revolution in subsonic and supersonic flow. AGARDograph 97, 1, 933-962.

Winter K.G., Smith K.G., Gaudet L. 1965 Measurements of turbulent skin friction at high Reynolds numbers at Mach numbers of 0.2 and 2.2. AGARDograph 97, 1, 97-124.

Winter K.G., Gaudet L. 1968 Some recent work on compressible turbulent boundary layers and excrescence drag. NASA SP 216, 15.1 - 15.25.

Winter K.G., Gaudet L. 1970 Turbulent boundary-layer studies at high Reynolds numbers at Mach numbers between 0.2 and 2.8. RAE TR 70251.

Winter K.G., Rotta J.C., Smith K.G. 1970 Studies of the turbulent boundary layer on a waisted body of revolution in subsonic and supersonic flow. ARC R + M 3633 (supersedes RAE TR 6815 (1968)), (CAT 7004).

Winter K.G., Gaudet L. 1973 Turbulent boundary-layer studies at high Reynolds numbers at Mach numbers between 0.2 and 2.8. ARC R + M 3712, (CAT 7302). Supersedes RAE Rep. 70251 (1970).

Wood D.H., Antonia R.A. 1975 Measurements in a turbulent boundary layer over a d-type surface roughness. Aeronaut. Quart. 26, 202.

Yanta W.J., Brott D.L., Lee R.L. 1969 An experimental investigation of the Preston probe including effects of heat transfer, compressibility and favourable pressure gradient. AIAA Paper 69-648.

Young A.D. 1951 The equations of motion and energy and the velocity profile of a turbulent boundary layer in a compressible fluid. The College of Aeronautics Cranfield Rep. 42. (See also "Modern Developments in Fluid Dynamics" Ed. L. Howarth (1953), Oxford Clarendon Press.

Young F.L. 1965 Experimental investigation of the effects of surface roughness on compressible turbulent boundary layer skin friction and heat transfer. Univ. Texas Report ORL-532, AD 621 085, (CAT 6506).

Zakkay V., Wang C.R. 1972 Turbulent boundary layer in an adverse pressure gradient without effect of wall curvature. NASA CR-112247, (CAT 7208).

Zwarts F. 1970 Compressible turbulent boundary layers. Ph.D. thesis, Mc Gill Univ. Dept. Mech. Eng., (CAT 7007).

Additional references

Horton A.P. 1978 Reported as CC 767 in the CAARC yearbook 1978, ARC, London.

Hoydysh W.G., Zakkay V. 1969 An experimental investigation of hypersonic turbulent boundary layers in adverse pressure gradient. AIAA J. 7, 105-116.

Kepler C.E., O'Brien R.L. 1962 Supersonic turbulent boundary layer growth over cooled walls in adverse pressure gradients. United Aircraft Corp. Aero. Syst. Div. ASD-TDR-62-87.

McLafferty G.H., Barber R.E. 1959 Turbulent boundary layer characteristics in supersonic stream having adverse pressure gradients. United Aircraft Co., East Hartford Rep. R 1285, II, 1-124.

McLafferty G.H., Barber R.E. 1962 The effect of adverse pressure gradients on the characteristics of turbulent boundary layers in supersonic streams. J. Aerospace Sci. 29, 1-10.

Müller J. 1973 Untersuchungen der turbulenten Grenzschicht an einer Konkav gekrümmten Wand bei Uberschallstromung. AVA-Bericht IB 251-73 A21.

Richmond R.L. 1957 Experimental investigation of thick axially symmetric boundary layers on cylinders at subsonic and supersonic speeds. Guggenheim Aeronaut. Lab. CALTECH. Hyp. Res. Prog. Memo. 39.

REPORT DOCUMENTATION PAGE

1. Recipient's Reference	2. Originator's Reference	3. Further Reference	4. Security Classification of Document
	AGARD-AG-253	ISBN 92-835-1362-2	UNCLASSIFIED

5. Originator Advisory Group for Aerospace Research and Development
North Atlantic Treaty Organization
7 rue Ancelle, 92200 Neuilly sur Seine, France

6. Title A CRITICAL COMMENTARY ON MEAN FLOW DATA FOR TWO-DIMENSIONAL COMPRESSIBLE TURBULENT BOUNDARY LAYERS

7. Presented at

8. Author(s)/Editor(s)	9. Date
H.H.Fernholz and P.J.Finley	May 1980
10. Author's/Editor's Address	**11. Pages**
See Flyleaf	228

12. Distribution Statement This document is distributed in accordance with AGARD policies and regulations, which are outlined on the Outside Back Covers of all AGARD publications.

13. Keywords/Descriptors

Turbulent boundary layer	Two dimensional flow
Boundary layer flow	Turbulent flow
Compressible flow	Flow distribution

14. Abstract

This volume presents a discussion of mean flow profile data for compressible boundary layers. In AGARDograph 223, (Fernholz and Finley, 1977) the predecessor of this volume, data were presented for nominally two-dimensional flows for which mean flow profile data were available in tabular form. Data for 59 experimental boundary layer studies were given, with a brief introduction. Comment and discussion were reserved for this volume, AGARDograph 253. Suitable cross-references are given to relate the discussion in this volume to the earlier publication.

The commentary in this volume includes discussion of the theoretical basis for interpretation of measurements, concepts from low-speed studies, interpretation of mean flow data with and without pressure gradient. The causes of normal pressure gradients are described, so as to allow an estimation of their magnitude, and their influence on boundary layer scale lengths. A third volume is planned in this series, which will include additional data, some of which is discussed here.

This work was sponsored by the Fluid Dynamics Panel of AGARD.

AGARDograph No.253
Advisory Group for Aerospace Research and Development, NATO
A CRITICAL COMMENTARY ON MEAN FLOW DATA FOR TWO-DIMENSIONAL COMPRESSIBLE TURBULENT BOUNDARY LAYERS
by H.H.Fernholz and P.J.Finley
Published May 1980
228 pages

This volume presents a discussion of mean flow profile data for compressible boundary layers. In AGARDograph 223, (Fernholz and Finley, 1977) the predecessor of this volume, data were presented for nominally two-dimensional flows for which mean flow profile data were available in tabular form. Data for

P.T.O.

AGARD-AG-253

Turbulent boundary layer
Boundary layer flow
Compressible flow
Two dimensional flow
Turbulent flow
Flow distribution

AGARDograph No.253
Advisory Group for Aerospace Research and Development, NATO
A CRITICAL COMMENTARY ON MEAN FLOW DATA FOR TWO-DIMENSIONAL COMPRESSIBLE TURBULENT BOUNDARY LAYERS
by H.H.Fernholz and P.J.Finley
Published May 1980
228 pages

This volume presents a discussion of mean flow profile data for compressible boundary layers. In AGARDograph 223, (Fernholz and Finley, 1977) the predecessor of this volume, data were presented for nominally two-dimensional flows for which mean flow profile data were available in tabular form. Data for

P.T.O.

AGARD-AG-253

Turbulent boundary layer
Boundary layer flow
Compressible flow
Two dimensional flow
Turbulent flow
Flow distribution

AGARDograph No.253
Advisory Group for Aerospace Research and Development, NATO
A CRITICAL COMMENTARY ON MEAN FLOW DATA FOR TWO-DIMENSIONAL COMPRESSIBLE TURBULENT BOUNDARY LAYERS
by H.H.Fernholz and P.J.Finley
Published May 1980
228 pages

This volume presents a discussion of mean flow profile data for compressible boundary layers. In AGARDograph 223, (Fernholz and Finley, 1977) the predecessor of this volume, data were presented for nominally two-dimensional flows for which mean flow profile data were available in tabular form. Data for

P.T.O.

AGARD-AG-253

Turbulent boundary layer
Boundary layer flow
Compressible flow
Two dimensional flow
Turbulent flow
Flow distribution

AGARDograph No.253
Advisory Group for Aerospace Research and Development, NATO
A CRITICAL COMMENTARY ON MEAN FLOW DATA FOR TWO-DIMENSIONAL COMPRESSIBLE TURBULENT BOUNDARY LAYERS
by H.H.Fernholz and P.J.Finley
Published May 1980
228 pages

This volume presents a discussion of mean flow profile data for compressible boundary layers. In AGARDograph 223, (Fernholz and Finley, 1977) the predecessor of this volume, data were presented for nominally two-dimensional flows for which mean flow profile data were available in tabular form. Data for

P.T.O.

AGARD-AG-253

Turbulent boundary layer
Boundary layer flow
Compressible flow
Two dimensional flow
Turbulent flow
Flow distribution

59 experimental boundary layer studies were given, with a brief introduction. Comment and discussion were reserved for this volume, AGARDograph 253. Suitable cross-references are given to relate the discussion in this volume to the earlier publication.

The commentary in this volume includes discussion of the theoretical basis for interpretation of measurements, concepts from low-speed studies, interpretation of mean flow data with and without pressure gradient. The causes of normal pressure gradients are described, so as to allow an estimation of their magnitude, and their influence on boundary layer scale lengths. A third volume is planned in this series, which will include additional data, some of which is discussed here.

This work was sponsored by the Fluid Dynamics Panel of AGARD.

ISBN 92-835-1362-2

59 experimental boundary layer studies were given, with a brief introduction. Comment and discussion were reserved for this volume, AGARDograph 253. Suitable cross-references are given to relate the discussion in this volume to the earlier publication.

The commentary in this volume includes discussion of the theoretical basis for interpretation of measurements, concepts from low-speed studies, interpretation of mean flow data with and without pressure gradient. The causes of normal pressure gradients are described, so as to allow an estimation of their magnitude, and their influence on boundary layer scale lengths. A third volume is planned in this series, which will include additional data, some of which is discussed here.

This work was sponsored by the Fluid Dynamics Panel of AGARD.

ISBN 92-835-1362-2

59 experimental boundary layer studies were given, with a brief introduction. Comment and discussion were reserved for this volume, AGARDograph 253. Suitable cross-references are given to relate the discussion in this volume to the earlier publication.

The commentary in this volume includes discussion of the theoretical basis for interpretation of measurements, concepts from low-speed studies, interpretation of mean flow data with and without pressure gradient. The causes of normal pressure gradients are described, so as to allow an estimation of their magnitude, and their influence on boundary layer scale lengths. A third volume is planned in this series, which will include additional data, some of which is discussed here.

This work was sponsored by the Fluid Dynamics Panel of AGARD.

ISBN 92-835-1362-2

59 experimental boundary layer studies were given, with a brief introduction. Comment and discussion were reserved for this volume, AGARDograph 253. Suitable cross-references are given to relate the discussion in this volume to the earlier publication.

The commentary in this volume includes discussion of the theoretical basis for interpretation of measurements, concepts from low-speed studies, interpretation of mean flow data with and without pressure gradient. The causes of normal pressure gradients are described, so as to allow an estimation of their magnitude, and their influence on boundary layer scale lengths. A third volume is planned in this series, which will include additional data, some of which is discussed here.

This work was sponsored by the Fluid Dynamics Panel of AGARD.

ISBN 92-835-1362-2